

# UNCLASSIFIED

AD NUMBER	
AD395844	
CLASSIFICATION CHANGES	
TO:	UNCLASSIFIED
FROM:	CONFIDENTIAL
LIMITATION CHANGES	
TO: Approved for public release; distribution is unlimited.	
FROM: Distribution authorized to U.S. Gov't. agencies and their contractors; Administrative/Operational Use; JAN 1969. Other requests shall be referred to Director, Air Force Rocket Propulsion Lab., Attn: RPPR/STINFO. Edwards AFB, CA 93523.	
AUTHORITY	
31 Jan 1981, DoD 5200.10 Group-4 ; AFPRL ltr 5 Feb 1986	

THIS PAGE IS UNCLASSIFIED

THIS REPORT HAS BEEN DELIMITED  
AND CLEARED FOR PUBLIC RELEASE  
UNDER DOD DIRECTIVE 5200.20 AND  
NO RESTRICTIONS ARE IMPOSED UPON  
ITS USE AND DISCLOSURE,

DISTRIBUTION STATEMENT A

APPROVED FOR PUBLIC RELEASE;  
DISTRIBUTION UNLIMITED,

BEST COPY  
AVAILABLE

AD 395 844

AUTHORITY:

AFRPL

1rr 5 Feb 86



# **SECURITY**

---

# **MARKING**

**The classified or limited status of this report applies to each page, unless otherwise marked.**

**Separate page printouts MUST be marked accordingly.**

---

THIS DOCUMENT CONTAINS INFORMATION AFFECTING THE NATIONAL DEFENSE OF THE UNITED STATES WITHIN THE MEANING OF THE ESPIONAGE LAWS, TITLE 18, U.S.C., SECTIONS 793 AND 794. THE TRANSMISSION OR THE REVELATION OF ITS CONTENTS IN ANY MANNER TO AN UNAUTHORIZED PERSON IS PROHIBITED BY LAW.

NOTICE: When government or other drawings, specifications or other data are used for any purpose other than in connection with a definitely related government procurement operation, the U.S. Government thereby incurs no responsibility, nor any obligation whatsoever; and the fact that the Government may have formulated, furnished, or in any way supplied the said drawings, specifications, or other data is not to be regarded by implication or otherwise as in any manner licensing the holder or any other person or corporation, or conveying any rights or permission to manufacture, use or sell any patented invention that may in any way be related thereto.



**CONFIDENTIAL**

AFRPL-TR-69-2

AD 395844

(TITLE UNCLASSIFIED)  
DEVELOPMENT AND DEMONSTRATION OF  
ABLATIVE THRUST CHAMBER ASSEMBLIES  
USING  $\text{LF}_2/\text{N}_2\text{H}_4$  BLEND PROPELLANTS

Final Report

Contract No. FO4611-67-C-0003

Robert C. Schindler and Harold V. Kiser

Aerojet-General Corporation

TECHNICAL REPORT

January 1969

GROUP 4

DOWNGRADED AT 3 YEAR INTERVALS DECLASSIFIED AFTER 12 YEARS

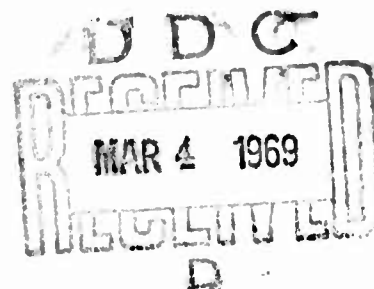
In addition to security requirements which must be met, this document is subject to special export controls and each transmittal to foreign governments or foreign nationals may be made only with prior approval of AFRPL (RPPR/STINFO), Edwards, California 93523.

This material contains information affecting the national defense of the United States within the meaning of the Espionage Laws, Title 18, U.S.C. Section 793 or 794. The transmission or revelation of which in any manner to an unauthorized person is prohibited by law.

AIR FORCE ROCKET PROPULSION LABORATORY  
Research and Technology Division  
Air Force Systems Command  
Edwards, California

1083

**CONFIDENTIAL**



**CONFIDENTIAL**

"When U. S. Government drawings, specifications, or other data are used for any purpose other than a definitely related Government procurement operation, the Government thereby incurs no responsibility or any obligation whatsoever, and the fact that the Government may have formulated, furnished, or in any way supplied the said drawings, specifications, or other data, is not to be regarded by implication or otherwise, or in any manner licensing the holder or any other person or corporation, or conveying any rights or permission to manufacture, use, or sell any patented invention that may in any way be related thereto."

**CONFIDENTIAL**

(This page is Unclassified)

**CONFIDENTIAL**

AFRPL-TR-69-2

(TITLE UNCLASSIFIED)  
DEVELOPMENT AND DEMONSTRATION OF  
ABLATIVE THRUST CHAMBER ASSEMBLIES  
USING  $\text{LF}_2/\text{N}_2\text{H}_4$  BLEND PROPELLANTS

Final Report

Robert C. Schindler and Harold V. Kiser

In addition to security requirements which must be met, this document is subject to special export controls and each transmittal to foreign governments or foreign nationals may be made only with prior approval of AFRPL (RPPR/STINFO), Edwards, California 93523.

GROUP 4

DOWNGRADED AT 3 YEAR INTERVALS DECLASSIFIED AFTER 12 YEARS

This material contains information affecting the national defense of the United States within the meaning of the Espionage Laws, Title 18, U.S.C. Section 793 or 794. The transmission or revelation of which in any manner to an unauthorized person is prohibited by law.

AIR FORCE ROCKET PROPULSION LABORATORY  
Research and Technology Division  
Air Force Systems Command  
Edwards, California

1083

**CONFIDENTIAL**

**UNCLASSIFIED**

FOREWORD

This report is the second and final report on this program, and summarizes thrust chamber assemblies using  $\text{LF}_2/\text{N}_2\text{H}_4$  blend propellants. The first report, AFRPL-TR-67-52, describes the design philosophy of the initial components. The work was accomplished by the Aerojet-General Corporation, Liquid Rocket Operations, Sacramento, California, under Contract FO4611-67-C-0003 for the Air Force Rocket Propulsion Laboratory, Edwards AFB, California. The report spans the complete contractual period from 1 September 1966 through 19 August 1968. The Air Force Project Engineer was Mr. L. Tepe, RPRRE.

The principal contributors to this project were:

Mr. C. W. Williams, Program Manager  
Mr. R. C. Schindler, Project Engineering Manager  
Mr. H. V. Kiser, Project Engineer  
Messrs. D. L. Kors and L. B. Bassham, Performance Analysis  
Messrs. J. M. McBride and R. A. Hewitt, Stability Analysis  
Messrs. L. Schoenman and R. W. Michel, Thermal Analysis  
Messrs. G. R. James and P. J. Krusi, Structural Analysis  
Messrs. R. S. Simonsen and G. W. Hooper, Test Facilities

This report contains data items which are unclassified when singularly presented; however, should they be collectively presented, such items can compromise a classified data set as per Air Force Regulation 205-1, para. 3-5.b.(4).

This technical report has been reviewed and is approved.

L. Tepe, RPRRE

**UNCLASSIFIED**

ABSTRACT

The "Development and Demonstration of Ablative Thrust Chamber Assemblies Using  $\text{LF}_2/\text{N}_2\text{H}_4$  Blend Propellants," Contract F04611-67-C-0003, was a comprehensive exploratory development effort which included the design, fabrication, and testing of injectors, ablative thrust chambers, and a radiation-cooled divergent nozzle extension. It was conducted in three phases over a 25 month period. The design study was accomplished in Phase I while Phases II and III consisted of evaluations of thrust chamber assemblies which utilized non-damped and acoustically-damped injectors, respectively.

A single injector body configuration was used throughout the program. It incorporated triplet-type elements in a flat-faced, nickel body without baffles. Injector durability was demonstrated with a single unit which accumulated over 846 sec of testing. It was determined that maximum performance could be achieved with stable operation by using acoustic resonators built into the chamber wall.

Two different composite ablative chamber configurations were evaluated. One had a precharred fibrous graphite throat insert with uncharred ablative materials both upstream and downstream of the throat. The other had a precharred fibrous graphite liner which extended from the injector to a station downstream of the throat. The latter configuration failed during testing as a result of local buckling of the liner. A throat insert design unit was tested six times at vacuum conditions for a total duration of 605 sec. An acoustic resonator was incorporated in a second throat insert chamber configuration and tested three times for a duration of 160 sec.

A radiation-cooled columbium nozzle was tested at vacuum conditions for an accumulated duration of 233 sec. This nozzle was used to evaluate three different thermal barrier coatings.

The forty tests conducted in the program provided verification of the analytical methods applied in the chamber design, supplemented existing technology, and provided previously unavailable materials information. This demonstration of the two ablative chamber designs provided ample evidence that adequate technology is available to develop space engines using an interhalogen oxidizer.

TABLE OF CONTENTS

	<u>Page</u>
I. <u>INTRODUCTION</u>	1
II. <u>SUMMARY</u>	2
III. <u>CONCLUSIONS AND RECOMMENDATIONS</u>	4
A. CONCLUSIONS	4
B. RECOMMENDATIONS	5
1. <u>High-Temperature Material Properties</u>	5
2. <u>Improved Acoustic Resonator</u>	5
3. <u>Flightweight Long-Duration Ablative Chamber</u>	5
IV. <u>DESIGN AND FABRICATION</u>	6
A. INJECTORS	6
1. <u>Material Selection</u>	6
2. <u>Description of Selected Design</u>	9
a. Injector Body	9
b. Injector Patterns	9
c. Instrumentation	18
3. <u>Thermal Predictions</u>	20
4. <u>Thermal Accumulator</u>	22
5. <u>Structures</u>	26
6. <u>Fabrication</u>	30
B. UNCOOLED THRUST CHAMBERS	32
1. <u>Standard Design</u>	32
2. <u>Acoustic Resonator Design</u>	36
C. WATER-COOLED COMBUSTION CHAMBER ASSEMBLY	38
1. <u>Description</u>	38
a. ATJ Graphite-Lined Combustion Chamber Assembly	38
(1) Throat Region	40
(2) Chamber Section	40
(3) Structural Analysis	41

TABLE OF CONTENTS (cont.)

	<u>Page</u>
b. Composite Ablative-Lined Combustion Chamber Assembly	42
2. <u>Fabrication</u>	44
D. ABLATIVE THRUST CHAMBERS	46
1. <u>Material Selection</u>	46
a. Selection Criteria	47
b. Material Controls	51
2. <u>Thrust Chamber Descriptions</u>	51
a. Thrust Chamber Design No. 1	51
b. Thrust Chamber Design No. 2	57
3. <u>Thermal Analysis</u>	60
4. <u>Fabrication</u>	62
5. <u>Rework of S/N 001 Chamber</u>	63
a. Requirement and Material Selection	63
b. Description	63
c. Fabrication	63
E. NOZZLE EXTENSION	66
1. <u>Design, Description, and Analysis</u>	66
2. <u>Materials and Protective Coatings</u>	68
3. <u>Fabrication</u>	70
V. <u>TESTING</u>	71
A. FACILITIES AND PROCEDURES	71
1. <u>Facilities</u>	71
2. <u>Facility Operational Procedures</u>	72
a. Cleanliness	72
b. Safety	72
3. <u>Thrust Chamber Assembly Operational Procedures</u>	72
a. Thrust Chamber Valves	72
b. Injector-Chamber Assembly	73
c. Sequence of Test Operations	75

TABLE OF CONTENTS (cont.)

	<u>Page</u>
B. THRUST CHAMBER ASSEMBLY TESTING	78
1. <u>Phase II Testing</u>	78
2. <u>Phase III Testing</u>	105
VI. <u>TEST RESULTS</u>	120
A. COMBUSTION STABILITY	120
1. <u>Stability Summary</u>	120
2. <u>Method of Injector Pattern Evaluation</u>	139
3. <u>Method of Damper Evaluation and Analytical Results</u>	141
B. PERFORMANCE ANALYSIS	149
1. <u>Method of Analysis</u>	151
a. Kinetic Loss	151
b. Boundary Layer Loss, BLL	152
c. Divergence Loss, CDL	152
d. Mixture Ratio Distribution Loss, MRD	152
e. Energy Release Loss, ERL	154
f. Performance Interaction	155
2. <u>Sea-Level Test Results</u>	156
a. Injector S/N T <sup>2</sup>	156
b. Injector S/N 2	156
c. Injector S/N 2, Mod 1	158
d. Injector S/N 2, Mod 2	158
e. Injector S/N 2, Mod 3	158
f. Injector S/N 6	159
g. Injector S/N 7	159
3. <u>Altitude Test Results</u>	160
4. <u>Design Condition Extrapolation</u>	163
a. Injector S/N 7	163
b. Injector S/N 2, Mod 3	167
c. Injector S/N 6	167



TABLE OF CONTENTS (cont.)

	<u>Page</u>
d. Injector S/N 2, Mod 2	167
e. Injector S/N 2, Mod 1	169
f. Injector S/N 2	169
g. Injector S/N T <sup>2</sup>	169
h. Injector Performance Correlation	169
i. Optimum Injector Performance	171
(1) Pressure Drop	171
(2) Wall Compatibility	171
(3) Nozzle Redesign	173
C. COMPATIBILITY	174
1. <u>Description of Compatibility Analytical Models</u>	174
a. Gas Dynamic Model	174
b. Spray Fan Characterization Model	175
2. <u>Analysis of Test Results</u>	175
a. Injector S/N 2, Mod 3	175
b. Injector S/N 6	179
c. Injector S/N 7	185
3. <u>Optimum Compatibility</u>	188
D. THERMAL ANALYSIS	190
1. <u>Uncooled Steel Chambers</u>	190
2. <u>Cooled Chambers</u>	193
3. <u>Ablative Chambers</u>	193
a. Chamber S/N 002	193
b. Chamber S/N 001	195
c. Chamber S/N 003	195
4. <u>Injectors</u>	197
5. <u>Simulant Thermal Accumulator</u>	200

# UNCLASSIFIED

## TABLE OF CONTENTS (cont.)

	<u>Page</u>
E. <b>STRUCTURAL ANALYSIS</b>	200
1. <u>Method of Analysis</u>	202
a.    Finite Element Program E11401	202
b.    Finite Element Program E11405	202
2. <u>Analysis Results</u>	203
a.    Ablative Chamber S/N 001	203
b.    Ablative Chamber S/N 002	203
c.    Ablative Chamber S/N 003	203
VII. <u>FLIGHT CONFIGURATION</u>	208
A.    DESCRIPTION	208
B.    THERMAL ANALYSIS OF ABLATIVE CHAMBER	210
C.    PERFORMANCE	211

## APPENDICES

I. <u>AEROJET-GENERAL SUBSCALE TESTING (PRE-PROPOSAL INVESTIGATION)</u>	215
A.    INTRODUCTION	216
B.    PERFORMANCE RESULTS	216
C.    FUEL ORIFICE EROSION	216
II. <u>ACOUSTIC DAMPER ANALYSIS, DESIGN AND METHODS</u>	226
A.    ACOUSTIC DAMPER ANALYSIS	227
1. <u>Introduction</u>	227
2. <u>Discussion of Analysis Used</u>	227
3. <u>Historical Approach to Acoustic Damper Analysis</u>	228
4. <u>Recent Modifications to the Historical Approach</u>	231
5. <u>Anomalies of Absorption Coefficient Approach</u>	232
6. <u>Generalized Liner Analysis</u>	234
7. <u>IFAR Damper Analysis</u>	240

UNCLASSIFIED

# UNCLASSIFIED

## APPENDICES (cont.)

	<u>Page</u>
B. BASIS OF METHODS FOR STABILITY ANALYSIS	247
1. <u>Description of Analytical Model</u>	247
2. <u>Analytical Assumptions</u>	248
3. <u>Injector Patterns</u>	250
4. <u>Results Versus Predictions</u>	253
III. <u>METHOD OF CONDUCTING A THERMAL DESIGN ANALYSIS</u>	254
A. INTRODUCTION	255
B. ABLATIVE CHAMBER ANALYSIS	255
C. INJECTOR ANALYSIS	256
D. SYSTEM ANALYSIS	257
IV. <u>FABRICATION CONTROL OF ABLATIVE CHAMBERS</u>	258
V. <u>TEST FACILITIES AND TEST OPERATIONAL PROCEDURES</u>	263
A. FACILITIES	264
1. <u>Test Facility J-2</u>	264
2. <u>Test Facility J-4</u>	266
B. CLEANLINESS	266
1. <u>Initial Cleaning</u>	266
2. <u>Passivation</u>	269
C. SAFETY	269
1. <u>Personnel Protection</u>	269
a. Fluorine Storage and Transfer	270
b. Test Firing	271
c. Check Lists	271
2. <u>Transfer of Fluorine</u>	273
3. <u>Fluorine Disposal</u>	273
4. <u>Exhaust Products Control</u>	273
D. INSTRUMENTATION	275
E. TEST DATA ACQUISITION	278
1. <u>Digital Test Data Acquisition and Processing</u>	278
2. <u>Digital Data</u>	278

x

UNCLASSIFIED

# UNCLASSIFIED

## APPENDICES (cont.)

	<u>Page</u>
VI. <u>METALLURGICAL EXAMINATION OF COLUMBIUM NOZZLE EXTENSION, P/N 1131920-9</u>	279
A. SUMMARY	280
B. INVESTIGATION AND RESULTS	282
1. <u>Bend Test</u>	282
2. <u>Microhardness Traverse</u>	282
3. <u>Metallographic Examination</u>	282
C. DISCUSSION	282
D. RECOMMENDATIONS	287
E. CONCLUSIONS	287
VII. <u>POST-TEST ANALYSES OF ABLATIVE CHAMBER S/N 002</u>	289
A. INTRODUCTION	290
B. SUMMARY	293
C. DISCUSSION	293
1. <u>Dimension and Weight</u>	293
2. <u>Visual Inspection</u>	295
a. Throat Profile	295
b. Full-Length Cross-Section	295
c. Profile of Maximum Regression	295
d. Segment 195-Degrees to 270-Degrees	303
e. Segment 270-Degrees to 45-Degrees	303
f. Segment 90-Degrees to 195-Degrees	303
g. Radial Ring, Segment 6-in. from Forward End of Chamber	303
h. Photomicrographs of AGCarb-101 and Carbon/Phenolic Back-Up	305
3. <u>Density Comparisons</u>	305
4. <u>Regression and Char Profile</u>	311
5. <u>Decomposition Gas Effects</u>	311
6. <u>Performance of Materials</u>	313
D. CONCLUSIONS	314

APPENDICES (cont.)

	<u>Page</u>
VIII. <u>HIPERKINETIC NOZZLE DESIGN, <math>LF_2/N_2H_4</math> BLEND</u>	315
A. SUMMARY	316
B. TECHNICAL DISCUSSION	316
1. <u>Method of Approach</u>	316
a. Potential Performance Improvement	317
b. Method of Contour Adjustment	320
2. <u>Analytical Results</u>	320
a. Design Constraints	320
b. Hiperkinetic Nozzle Contour	320
c. Performance Comparison	321
d. Effect of Design Constraints	321
Bibliography	326

NOMENCLATURE

$A_{\text{element}}$	Injector area of spray fan, in. <sup>2</sup>
$A_{\text{fuel}}$	Injector area of fuel rich spray fan, in. <sup>2</sup>
$A_f$	Area of acoustic liner face surface, ft <sup>2</sup>
$A_{f1}$	Area at which frozen chemical composition occurs, in. <sup>2</sup>
$A_o$	Area of acoustic liner orifice cross section, ft <sup>2</sup>
$A_t$	Area of combustion chamber throat, in. <sup>2</sup>
$A_{vn}$	Pressure sensitive coefficient
$\alpha$	Thermal expansion coefficient, in./in. °F
$B$	<u>Rate of change of equilibrium composition</u> Kinetic rate of change in composition
BL	Boundary layer
BLL	Boundary layer loss
BP	Boiling point
BTU	British thermal unit
$C$	Speed of sound, ft/sec
$c^*$	Characteristic exhaust velocity, ft/sec
C-D	Curvature - Divergence
CDL	Curvature divergence loss
$C_2F_2$	Di Fluoro Acetylene
$CLF_3$	Chlorine trifluoride
CN	Cyanide
CO	Carbon nonoxide
$C_p$	Specific heat, pressure Btu/lbm °F
$C_s$	Stagnation chamber gas speed of sound, ft/sec
CSM	Combustion Stability Monitor
$d$	Acoustic liner orifice diameter, ft
$d_f$	Fuel orifice diameter, ft
$E$	Modulus of elasticity, psi
$e$	Base of natural logarithm
ERE	Energy release efficiency
ERL	Energy release loss

NOMENCLATURE (cont.)

$^{\circ}\text{F}$	Degree fahrenheit
$F_o$	Force function, lbf
$F_v$	Thrust vacuum, lb
FCN	Fluorine cyanide
FFC	Fuel film cooling
FS	Factor of safety
$FS_1$	Fire switch on
$FS_2$	Fire switch off
FT	Feet
$f$	Coefficient of friction
$f_1$	Frequency, $\text{sec}^{-1}$
$f_o$	Acoustic liner resonant frequency without mean gas flow, $\text{sec}^{-1}$
$\text{GF}_2$	Gaseous fluorine
$g$	Gravitational constant, $32 \text{ ft/sec}^2$
$\text{gr/cm}^3$	Grams per cubic centimeter
$H_{pq}$	Normalizing factor in eigenfunction expansion
$H_{f \text{ effective}}$	Heat of formation of combustion species at resulting combustion value
$H_{f \text{ reference}}$	Heat of formation of combustion species at reference value
HF	Hydrogen fluoride
$\text{H}_2\text{O}$	Water
$h$	Index denoting solutions in the radial direction
$h_{\text{fusion}}$	Heat of fusion, Btu/lbm
ID	Inside diameter
INJ	Injector
$I_{sp}$	Specific impulse, lb-sec/lbm
$I_{sp \text{ meas}}$	Specific impulse calculated from thrust and propellant weight flow measurements, sec
$I_{sp(O/F)}$	Specific impulse at valve mixture ratio, lb-sec/lbm
$I_{sp(O/F)v}$	Specific impulse at vaporized mixture ratio, lb-sec/lbm

NOMENCLATURE (cont.)

$I_{spPre}$	Specific impulse predicted, lb-sec/lbm
$I_{spTheo}$	One dimensional isentropic expansional specific impulse at valve mixture ratio
$I_{spv}$	One dimensional specific impulse at vaporized propellant
in.	inch
in. <sup>3</sup>	Cubic inch
$J_v$	Bessel function of the first kind of order $v$
$j$	$\sqrt{-1}$ , indicates an imaginary number
ksi	Thousands of pounds per square inch
$k$	Thermal conductivity, Btu/in. sec °F
$k_1$	Spring constant, lbf/ft
$L$	Backing distance of acoustic liner cavity, ft
$L_Q$	Length of quarter wave tube, ft
$L^*$	Chamber characteristic length, in.
$LF_2$	Liquid fluorine
$LN_2$	Liquid nitrogen
$l$	Effective length of orifice, ft
lb	Pound
lbf	Pounds force
lbm	Pounds mass
$M_c$	Mean chamber Mach number at entrance to nozzle
MHF-3	Mixed hydrazine fuel 3
Mod	Modification
MMH	Monomethyl hydrazine
MP	Melting point
MR	Mixture ratio
MRD	Mixture ratio distribution loss
MS	Margin of safety
$m$	Mass, lbm sec <sup>2</sup> /ft



NOMENCLATURE (con't.)

n	Pressure interaction index of Crocco theory
$N_2H_4$	Hydrazine
OD	Outside diameter
ODIE	One dimensional isentropic expansion
ODK	One dimensional kinetic
O/F	Oxidizer to fuel ratio
P	Pressure, lb/in. <sup>2</sup>
$P_c$	Chamber pressure, psia
PCRF	Critical pressure of fuel, psi
PCRO	Critical pressure of oxidizer, psi
$P_f$	Pressure at which frozen chemical composition occurs, psi
$P_{fJ}$	Fuel manifold pressure, psia
$P_i$	Local injector acoustic pressure oscillation, psi
$P_{vh}$	Axial dependant factor of perturbation pressure
P/N	Part number
PoJ	Oxidizer manifold pressure, psia
PPM	Parts per million
psi	Pounds per square inch
°R	Degree Rankine
R	Radial dependant factor of perturbation pressure
R'	First derivative of R
R''	Second derivative of R
$R_{vh}$	Same as R except v and h identify acoustic mode
r	Radial distance from centerline of chamber, ft
$r_1$	Damping constant lb-sec/ft <sup>5</sup>
$r_c$	Radius of chamber, ft
$S_{vh,v}$	Separation constants
sec	second
S/N	Serial number
SPL	Sound pressure level in decibels, dB

NOMENCLATURE (cont.)

T	Admittance coefficient
$T_2$	Temperature of gas in acoustic liner cavity, °R
$T_B$	Bulk temperature, °F
$T_c$	Temperature of gas in combustion chamber, °R
1T	First tangential acoustic mode of the chamber
2T	Second tangential acoustic mode of the chamber
t	Time, sec
$t_1$	Acoustic liner orifice thickness, ft
U	Axial dependent factor of perturbation axial velocity
u	Mean chamber gas velocity, ft/sec
$\bar{u}$	Nondimensionalized mean chamber gas velocity, $\frac{u}{c_s}$
$u'$	Nondimensional axial perturbation of gas velocity
V	Volume of acoustic liner cavity, ft <sup>3</sup>
$V_1$	Velocity, ft/sec
$V_o$	Volume of acoustic liner orifice, ft <sup>3</sup>
$v_o$	Injector oxidizer orifice velocity, ft/sec
$v_f$	Injector fuel orifice velocity, ft/sec
$W_f$	Fuel flow rate, lb/sec
$W_o$	Oxidizer flow rate, lb/sec
$\dot{w}_t$	Total propellant flowrate, lbm/sec
$\dot{w}_v$	Vaporized propellants flowrate, lbm/sec
x	Distance in x direction, ft
$\dot{x}$	Velocity in x direction, ft/sec
$\ddot{x}$	Acceleration, ft/sec <sup>2</sup>
$Y_r$	Nondimensional Holmholtz resonator admittance
$Y_{nt}$	Nondimensional intrinsic combustion admittance
$Y_v$	Bessel function of the second order of v
Z	Axial length, inch
A, B, D, E, $A_{vh}$	Constants determined by boundary conditions
$\alpha$	absorption coefficient

NOMENCLATURE (cont.)

$\alpha_1$	Thermal diffusivity, in. <sup>2</sup> /sec
$\gamma$	Ratio of specific heats
$\Delta$	Amount difference
$\Delta_{nl}$	Nonlinear SPL correction factor, ft
$\delta$	Damping rate, dB/sec
$\epsilon$	Expansion ratio (area of nozzle exit divided by area of chamber throat)
$\epsilon_1$	Strain, in per in.
$\eta_{DIV}$	Divergence loss efficiency
$\theta$	Angular distance around perimeter of chamber, radian
$\theta_n$	Nozzle exit angle with relation to axis, measured in degrees
$\bar{\theta}$	Acoustic resistance ratio of acoustic liner orifices
$\mu$	Gas viscosity, lb/sec-ft
$\pi$	Ratio of circumference to diameter of circle (3.1416)
$\rho$	Gas density lbm-sec <sup>2</sup> /ft <sup>4</sup>
$\rho_1$	Density, lb/in. <sup>3</sup>
$\bar{\rho}$	Nondimensional mean chamber gas density, $\rho/\rho_s$
$\rho'$	Nondimensional perturbation of gas density
$\rho_i$	Injector propellant injection density lbm/ft <sup>2</sup>
$\rho_s$	Stagnation chamber gas density lbm-ft <sup>4</sup> /sec <sup>2</sup>
$\Sigma$	Summation
$\sigma$	Ratio of acoustic liner orifice area to injector face area
$\sigma_1$	Calculated stress, psi
$\tau$	Sensitive time lag of combustion, sec
$\tau_1$	Shear stress, psi
$\phi$	Heat flux
$\phi_{BO}$	Burn out heat flux
$\bar{\chi}$	Acoustic reactance ratio of acoustic liner orifices
$\omega$	Angular frequency, $2\pi f$ , sec <sup>-1</sup>
$\omega_d$	Angular frequency with damping, sec <sup>-1</sup>
$\omega_n$	Undamped natural frequency, sec <sup>-1</sup>

NOMENCLATURE (cont.)

$\Omega$	Nondimensional angular frequency, $\omega r_c/c$
$( )_i$	$i$ th stream tube
$\mathcal{H}$	Angular dependant factor of perturbation pressure
$\mathcal{H}''$	Second derivative of $\mathcal{H}$
$\mathcal{H}_v$	Same as $\mathcal{H}$ except, $v$ identifies tangential component of acoustic mode
$\nabla$	Del operator
$>$	greater than
$<$	less than

**UNCLASSIFIED**

LIST OF TABLES

<u>No.</u>	<u>Title</u>	<u>Page</u>
I	Ablative Thrust Chamber Assembly Design Criteria	7
II	Design Duty Cycle	7
III	Material Selection Summary	8
IV	Comparison of Candidate Inorganic Materials	25
V	LF <sub>2</sub> /N <sub>2</sub> H <sub>4</sub> Injector Stress Summary	31
VI	Thermal Analysis of the Water-Cooled Nickel Nozzle	40
VII	Thermal Conditions for the Water-Cooled Chamber Section	41
VIII	Properties of Selected Ablative Chamber Materials	52
IX	Test Data Summary (3 sheets)	79
X	Stability Test History of Injector S/N 7	125
XI	Summary of Injector, Orifice, and Stability Data	140
XII	Altitude Hiperkinetic Nozzle Performance	150
XIII	Test Results Performance Summary	157
XIV	Comparison of Altitude Test Results with Predictions	161
XV	Performance Comparison between S/N 7 and S/N 2, Mod 3 Injectors	165
XVI	Effect of Design Variables for Reducing Pressure Drop upon Performance	172.
XVII	AGCarb-101 Material Properties	206
XVIII	Component Densities and Fabric Orientation	262
XIX	Products of Combustion (Shifting Equilibrium)	270
XX	Microhardness Survey of Various Areas of Nozzle Extension, P/N 1131920-9	283
XXI	Hiperkinetic Nozzle Coordinates	322
XXII	Comparison of the LF <sub>2</sub> -N <sub>2</sub> H <sub>4</sub> Blend Program Nozzle Design	325

# UNCLASSIFIED

## LIST OF FIGURES

<u>No.</u>	<u>Title</u>	<u>Page</u>
1	Injector Body Configuration	10
2	Thermal Accumulator	11
3	Injector S/N 2, 158-Element Pattern	13
4	Injector S/N T <sup>2</sup> , 215-Element Pattern	14
5	Injector S/N 2, Mod 3, 68-Element Pattern	16
6	Injector S/N 6, 68-Element Pattern	17
7	Injector S/N 7, 344-Element Pattern	19
8	Predicted Maximum Injector Face Temperatures and Heat Flux into the Coolant	21
9	Predicted Post-Fire Injector Temperature Response	23
10	Predicted Post-Fire Injector Temperature Response with Thermal Accumulator	27
11	Structural Properties of Nickel 200	28
12	Fluorine Injector Stress Layout	29
13	Standard Uncooled Steel Combustion Chamber Assembly	33
14	Temperature Profile Comparison of 1018 Steel and 347 Stainless Steel vs Various Wall Thicknesses at the Throat	34
15	Temperature Transient Comparison between 347 Stainless Steel and 1018 Steel in the Chamber Region	35
16	Acoustically-Damped Uncooled Steel Chamber	37
17	Water-Cooled Combustion Chamber Assembly	39
18	Ablative-Lined Chamber Section	43
19	Segmented Liner Concept	45
20	FM 5064 Ablative Thrust Chamber Showing Badly-Eroded Throat Region (LF <sub>2</sub> /N <sub>2</sub> Blend Propellants)	48
21	8000 lb Thrust Radiation-Cooled AGCarb-101 Thrust Chamber (P/N 1129696)	50
22	S/N 001 and S/N 002 Ablative Thrust Chambers (2 sheets)	53
23	Thermocouple Probe	56
24	Disassembled Thermocouple Probe	58

# UNCLASSIFIED

## LIST OF FIGURES (cont.)

<u>No.</u>	<u>Title</u>	<u>Page</u>
25	S/N 003 Ablative Thrust Chamber	59
26	Predicted Throat Temperature for Design Duty Cycle (2 sheets)	61
27	S/N 001 Ablative Thrust Chamber	64
28	Installation of Acoustic Liner into S/N 001 Ablative Thrust Chamber	65
29	Thrust Chamber Nozzle Extension Section	67
30	Nozzle Thermal Analysis, Comparison with Apollo	69
31	Uncooled Steel Chamber Test Installation	74
32	Typical Start Transient	76
33	Typical Shutdown Transient	77
34	Pre-Test View of Injector S/N T <sup>2</sup>	82
35	Post-Test View of Injector S/N T <sup>2</sup> (2.7 sec Duration)	83
36	Post-Test (No. 009) View of Steel Chamber with S/N 2, Mod 1 Injector	85
37	Post-Test (No. -017) View of S/N 2, Mod 2 Injector	86
38	Post-Test (No. -017) View of Forward End of Steel Chamber Tested with S/N 2, Mod 2 Injector	87
39	Water-Cooled Chamber Test Installation	89
40	Ablative Liner in Water-Cooled Chamber Tested with S/N 2, Mod 3 Injector after 100 sec of Testing	90
41	Nozzle Extension and Ablative Chamber S/N 002 Test Installation	91
42	Post-Test (No. -002) View of Damaged Nozzle Section	92
43	View of Damaged Throat Insert, Ablative Chamber S/N 002	94
44	Delaminated Section of Throat Insert, Ablative Chamber S/N 002	95
45	Post-Test View of Ablative Chamber S/N 002 after 606 sec of Testing	97
46	Post-Test View of Ablative Chamber S/N 002 after 606 sec of Testing	98
47	Post-Test View of Ablative Chamber S/N 002 after 606 sec of Testing	99

# UNCLASSIFIED

## LIST OF FIGURES (cont.)

<u>No.</u>	<u>Title</u>	<u>Page</u>
48	Post-Test View of Ablative Chamber S/N 002 after 606 sec of Testing	100
49	Throat Radius Change vs Time, Ablative Chamber S/N 002	101
50	Injector S/N 2, Mod 3 after 803.25 sec of Testing	102
51	Ablative Chamber S/N 003 Test Installation	104
52	Damaged Flame Liner, Ablative Chamber S/N 003	106
53	Post-Test (No. -007) View of Forward End of Ablative Chamber S/N 003	107
54	Post-Test (No. -025) View of Steel Chamber with Acoustic Resonator	108
55	Close-Up of Steel Chamber with Acoustic Resonator after Test No. -025	109
56	Condition of Fusible Wires Following Test No. -024	111
57	Condition of Fusible Wires Following Test No. -025	112
58	Ablative Chamber S/N 001 with Acoustic Resonator	113
59	Ablative Chamber S/N 001 after 161 sec of Testing	114
60	Post-Test View of Outer Diameter Surface of Resonator Flame Liner	115
61	Post-Test View of Resonator Cavities	117
62	Post-Test View of Single-Row, Acoustically-Damped Steel Chamber	118
63	Post-Test View of Two-Row/Single-Cavity, Acoustically-Damped Steel Chamber	119
64	Spectral Analysis Showing Instabilities in Tests No. -007 and No. -010	122
65	Spectral Analysis Showing Noise Level in Tests No. -007 and No. -013	123
66	Sample Pressure Transducer Oscillograph Trace, Test No. -024	124
67	Spectral Analysis Showing Noise Level in Test No. -024, 9-Row 3-Cavity Resonator	127
68	Spectral Analysis Showing Instability in Test No. -026, Undamped Steel Chamber	128



# UNCLASSIFIED

## LIST OF FIGURES (cont.)

<u>No.</u>	<u>Title</u>	<u>Page</u>
69	Post-Test (No. -025) View of Uncooled Nine-Row/Three-Cavity Damper	129
70	Single-Row Damper	130
71	Spectral Analysis Showing Instability in Test No. -028, 1-Row 1-Cavity Acoustic Resonator	131
72	Spectral Analysis, Test No. -029, 2-Row 1-Cavity Acoustic Resonator	132
73	Spectral Analysis, Test No. -030, 2-Row 1-Cavity Acoustic Resonator	133
74	Instrumentation Locations, All Chambers	135
75	Thermocouple Temperature Traces vs Time, Test No. -025	136
76	Theoretical Gas Velocity vs Chamber Length	138
77	Liner Absorption Coefficient vs Frequency at 2000°R and 4000°R	142
78	Absorption vs Frequency, Predicted and Actual	144
79	Cylindrical Acoustic Analysis	145
80	IFAR $n/\tau$ Plot	147
81	Kinetic and Shifting Equilibrium Comparison	153
82	Comparison of Altitude Test Results with Predictions over a Range of Mixture Ratios	162
83	Performance Characteristics of Injectors Tested Using the Mass Defect Model and the 36.2 Hiperkinetic Nozzle	164
84	Comparison between Mass Defect and Enthalpy Defect Scaling Techniques for Injector S/N 7	166
85	Mass Defect Scaling Techniques for Injector S/N 2, Mod 3	168
86	Performance vs Number of Elements	170
87	Spray Fan Characterization	176
88	Compatibility Characterization, Injector S/N 2, Mod 3	177
89	Graphite Phenolic Chamber after 50 sec of Testing with Injector S/N 2, Mod 3	180
90	Graphite Phenolic Chamber after 202 sec of Testing with Injector S/N 2, Mod 3	181

# UNCLASSIFIED

## LIST OF FIGURES (cont.)

<u>No.</u>	<u>Title</u>	<u>Page</u>
91	End View of Graphite Phenolic Chamber Section Tested with Injector S/N 2, Mod 3	182
92	Axial Section of Graphite Phenolic Chamber Tested with Injector S/N 2, Mod 3	183
93	Compatibility Characterization, Injector S/N 6	184
94	Injector S/N 6, Post-Test View	186
95	Compatibility Characterization, Injector S/N 7	187
96	Injector S/N 7 after 5 sec of Testing	189
97	Location of Uncooled Steel Chamber Instrumentation	191
98	Typical Uncooled Steel Chamber Wall Responses with Injector S/N 6	192
99	Location of Thermal Instrumentation on Ablative Chamber S/N 002	194
100	Analytical vs Measured Temperature Responses Tests No. -001 through -004 (2 sheets)	196
101	Injector Instrumentation	198
102	Comparison between Measured and Predicted Backplate Cooldown	199
103	Predicted vs Measured Responses, Thermal Accumulator	201
104	Materials and Temperatures, Ablative Chamber S/N 001	204
105	AGCarb-101 Throat Insert, Gas-Side Surface Stresses	205
106	Conceptual Design of Flightweight Thrust Chamber Assembly	209
107	Predicted Throat Temperature for Design Duty Cycle (2 sheets)	212
108	8000 lb $F_2$ /BA 1014 Injector	218
109	Single Element Pentad Injector	219
110	Like-on-Like Doublet Element	220
111	Four-Element Triplet Injector at 39 sec	221
112	Four-Element Triplet Injector at 183 sec	222
113	Post-Test View of Subscale Aluminum Injector	224
114	Subscale Nickel Injector after 619 sec of Testing	225
115	Mechanical Analogy of Acoustic Resonator	229

# UNCLASSIFIED

## LIST OF FIGURES (cont.)

<u>No.</u>	<u>Title</u>	<u>Page</u>
116	Liner Model	235
117	Non-Dimensional Chamber Response Function vs Frequency for a 2800 Hz	237
118	Non-Dimensional Chamber Response Function for a Rough 9.45-in. Chamber Wall	238
119	Frequency Depression of First and Second Tangential Modes as a Function of Cavity Temperature	239
120	Fuel Controlling Stability Correlation, Hypergolic	241
121	Oxidizer Controlling Stability Correlation, Hypergolic	242
122	The Effect of Oxidizer Orifice Diameter upon n, Hypergolic	249
123	Injector S/N 2, Mod 3 n/ $\tau$ Plot	251
124	Effect of Injection Distribution Upon Stability	252
125	Test Stand J-2 Plumbing Schematic	265
126	Test Stand J-4 Complex	267
127	Test Stand J-4 Plumbing Schematic	268
128	Test Stand J-2 Exhaust Scrubber	274
129	High Temperature Sensing Probe	277
130	Locations of Specimens	281
131	Photomicrographs of "A" Specimens Taken from Nozzle Extension	284
132	Photomicrographs of "B" Specimens Taken from Nozzle Extension	285
133	Photomicrographs of "C" Specimens Taken from Nozzle Extension	286
134	Ablative Thrust Chamber with Throat Insert, P/N 1131021-19	291
135	Chamber Erosion Characteristics	292
136	Throat Profile Showing Irregular Regression Pattern at Minimum Throat Diameter	296
137	Cross-Section at 90-Degrees	297
138	Heavy Regression in Chamber and Throat Near 195-Degrees	298
139	Regression Patterns in the 95-Degree to 195-Degree Segment	299

# UNCLASSIFIED

## LIST OF FIGURES (cont.)

<u>No.</u>	<u>Title</u>	<u>Page</u>
140	Segment 195-Degrees to 270-Degrees	300
141	Segment 270-Degrees to 45-Degrees	301
142	Segment 90-Degrees to 195-Degrees	302
143	Radial Cross-Section 6-in. from Forward End	304
144	Throat and Throat Back-Up Showing Location of Density Specimens and Photomicrograph Specimens	306
145	Photomicrograph of Throat Back-Up Char Structure Showing Separation	307
146	Photomicrograph of Throat AGCarb-101 Showing Pyrolytic Deposition in a Separation	308
147	Photomicrograph of Throat Showing Pyrolytic Deposition in a Separated Area	309
148	Photomicrograph of AGCarb-101 Throat of Chamber S/N 003 Showing Separation	310
149	Regression and Char Profile for Chamber S/N 002 Taken at the 90-Degree Cross-Section	312
150	Effect of Nozzle Contour on the Freezing Point Location	318
151	Effect of the Freezing Point Location on the Kinetic Performance Loss	319

**CONFIDENTIAL**

## SECTION I

INTRODUCTION

This 25-month program was entitled "Development and Demonstration of Ablative Thrust Chamber Assemblies Using  $\text{LF}_2/\text{N}_2\text{H}_4$  Blend Propellants" (Contract F04611-67-C-0003). Its major objective was to demonstrate the performance capability of a pressure-fed ablative thrust chamber assembly using the indicated propellant combination for possible use in an uprated Transtage vehicle.

The development effort was accomplished in three phases. Phase I included the analytical activities needed to design hardware that would be tested during the ensuing two phases. In Phase II, the designs were refined, the components fabricated, and component testing was accomplished at both sea level and simulated altitude conditions. Phase III was originally designed to demonstrate performance of the injector, chamber, and nozzle assembly. Problems developed, during Phase II, resulting in a redirection of Phase III to investigate acoustic liner durability and the achievement of improved performance and dynamic stability.

The success of the program was dependent upon the development and demonstration of technology which would provide solutions for each of the following development problems:

- Injector and thrust chamber durability
- Performance
- Stability

The thrust chamber assemblies tested during this program provided adequate demonstrations of technical maturity in each of these areas.

Current analytical technology was applied for the performance, stability, and thermal design of the units tested. Testing was designed to serve a three-fold purpose in addition to a successful thrust chamber assembly demonstration. The test results permitted verification of the analytical methods, provided data to fill existing technology voids, and provided previously unavailable materials information. Suitable instrumentation was utilized throughout the test program to obtain thermal and stability data as well as to provide the specific test objective information.

**CONFIDENTIAL**

(This page is Unclassified)

# CONFIDENTIAL

## SECTION II

### SUMMARY

(U) The capabilities of advanced thrust chamber assembly designs for use in upper stage propulsion systems were investigated in this Fluorine Thrust Chamber Assembly program within the constraints of the propellants selected and the requirement for ablative thrust chambers. All of the thrust chamber assemblies in this effort were designed to satisfy both the envelope and duty cycle requirements of the Transtage Engine.

(U) In view of the development nature of the program, appropriate hardware was designed to permit an evaluation of injectors before they were tested in ablative chambers designed for extended duration capability. Uncooled steel thrust chambers were used to obtain performance, stability, and thermal data. One of these units included acoustic dampers as well as the instrumentation needed to measure damper cavity pressures and temperatures.

(U) After injectors had been tested with successful results in the uncooled chambers, they were tested in a thrust chamber having a water-cooled throat. The upstream portion of this chamber contained either an ablative or a graphite liner. This water-cooled hardware permitted injector evaluation tests of longer duration while providing materials compatibility data.

(U) Problems had been anticipated and were experienced in trying to optimize system performance, stability, compatibility and injector durability. These were largely overcome as follows:

- (U) - Injector durability was attained at the outset by using nickel as the injector material; however, unanticipated problems were encountered in fabricating nickel parts.
- (U) - Stability proved to be a more significant problem than was anticipated. It was decided to make injector pattern changes rather than to use baffles to obtain stable operation. This resulted in a trade-off between performance and stability, but maximum performance was obtained after the acoustic dampers were introduced.
- (C) - Although the first injector (S/N T<sup>2</sup>) achieved the design performance level, it was unstable during repeated tests. Pattern changes were undertaken on subsequent unstable units to improve stability, but they resulted in a reduced performance level. Injector S/N 7, which was designed to operate with acoustic dampers, exceeded the contract performance goal.

CONFIDENTIAL

# CONFIDENTIAL

(C) - This injector attained an altitude performance of 372.7 sec and an ability to recover from perturbations that were 1.6 times the chamber pressure (induced by a 20-grain pulse gun).

(U) Thrust chamber durability was found to be very good despite the reduction in injector compatibility caused by pattern changes made to achieve stable operation.

(U) Two thrust chamber design concepts were evolved. The first design included a "hard" throat insert of precharred fibrous graphite (AGCarb-101), which demonstrated good durability. This material was utilized as the full-length "hard" liner of the second thrust chamber design. Two of the throat insert designs were built; one was intended for sea-level tests while the other was configured for use with a radiation-cooled columbium nozzle extension which was tested at simulated altitude conditions. An acoustic resonator was evaluated in the sea-level thrust chamber with the hard throat.

(U) The radiation-cooled columbium nozzle, which extended from an area ratio of 7.5:1 to 9.5:1 was coated with three different chemical barriers covering separate sections. This permitted a coating evaluation to be accomplished while altitude performance data were obtained for the purpose of assessing kinetic losses.

(U) Forty test firings were made during the course of the program. Ten of these were at simulated vacuum conditions while the remaining 30 were made at sea level. The longest single test duration was 202.8 sec which was performed at vacuum conditions (ablativ chamber S/N 002 with the AGCarb-101 throat insert).

(U) Two of three different ablativ thrust chamber assemblies were successfully demonstrated. The first (ablativ chamber S/N 002 with injector S/N 2, Mod 3) was that which existed at the end of the Phase II testing while the second design (ablativ chamber S/N 001 with injector S/N 7) was test evaluated during Phase III iteration. The following is a summary of both designs in context with the contractual requirements:

	Thrust Chamber Assemblies			
	Phase II		Phase III	
	Required	Demonstrated	Required	Demonstrated
Thrust, lb	7000	7000	7000	7000
Specific Impulse, sec	370	356.4	370	372.7
Duration Capability, sec	600	605	600	160
Stability Characteristics	Inherently Stable	Inherently Stable	Dynamically Stable	Dynamically Stable

CONFIDENTIAL



# CONFIDENTIAL

## SECTION III

### CONCLUSIONS AND RECOMMENDATIONS

The demonstration of ablative thrust chamber assembly S/N 002 with injector S/N 2, Mod 3, at the conclusion of Phase II and ablative thrust chamber S/N 001 with injector S/N 7, at the conclusion of Phase III, provided ample evidence that injector and thrust chamber technology is available for development of space engines using an interhalogen oxidizer. The specific conclusions and recommendations, based upon the results from this program, follow.

#### A. CONCLUSIONS

1. Thermal loads to the injector face can be adequately predicted and acceptably measured.
2. Existing heat transfer analytical methods and the available material property data are adequate for the design of ablative thrust chambers utilizing graphitic materials.
3. Performance analysis methods allow sufficient accuracy in predicting injector performance.
4. Injector stability characteristics can be accurately predicted and should be heeded.
5. Injector patterns can be designed so that they provide desired performance and compatibility characteristics.
6. The attainment of stable combustion in an injector/chamber assembly can be divorced from injector pattern design by utilizing acoustic dampers.
7. Single and double peripheral raw acoustic resonators coupled with a common cavity perform well when they are properly tuned.
8. The one-row resonator offers the better heat transfer characteristics.
9. Facility technology is sufficiently advanced so that the use of interhalogen oxidizers imposes only minimal hazard, cost, and scheduling impact upon development testing.

**CONFIDENTIAL**

(This page is Unclassified)



## B. RECOMMENDATIONS

There are three general areas that merit further data compilation and/or development; high-temperature material properties, the acoustic resonator, and a flightweight, long-duration ablative chamber. Completion of these items would provide a technological base suitable for initiation of an engine development program.

1. High-Temperature Material Properties

Currently, the material suppliers provide only limited data, which makes it necessary to assume thermal and structural properties. Material characterizations usually are for flat stock. The effect of thermal and chemical environment upon specific materials normally are not available or predictable. These data must be deduced from test results rather than being measured under controlled conditions.

It is recommended that a program be undertaken to fill these technological voids by characterizing component materials in the anticipated environments (chemical and operating temperatures) using actual lay-up angles and cylindrical shapes.

2. Improved Acoustic Resonator

Orifice erosion was experienced with the acoustic resonators developed in this program as a result of both recirculation through the resonator cavities and chemical attack of the resonator material.

It is recommended that an appropriate acoustic resonator improvement program be undertaken to improve resonator wall durability. Various potential solutions include the use of film cooling to control chemistry at the resonator wall, the regenerative cooling of the wall, incorporation of the resonator as an integral part of the injector, and baffling of resonator cavities to reduce recirculation.

3. Flightweight, Long-Duration Ablative Chamber

It is recommended that a flightweight ablative chamber test program be undertaken for the following purposes:

- Verification of an improved acoustic resonator
- Verification of the capability of a thin-walled ablative chamber
- Evaluation of an improved throat insert design

# UNCLASSIFIED

## SECTION IV

### DESIGN AND FABRICATION

Prudent selection of preliminary design concepts, the performance of associated analytical tasks, and the creation of detailed component designs to be fabricated and tested is basic in a successfully conducted program. The design effort was directly concerned with the creation of detailed component designs for subsequent developmental testing during Phases II and III. The approach used in evolving these detailed designs included a comprehensive survey of existing literature that was pertinent to the testing of fluorine ablative thrust chamber assembly components and the formulation of preliminary component designs. These preliminary designs were then analyzed in terms of thermodynamic, structural, and chemical compatibility requirements. Their interactions were identified and analyzed in context with a thrust chamber assembly as well as complete propulsion systems. Because the achievement of the required thrust chamber assembly performance values was to be accomplished by iteration during component testing, all of the components were designed to collect meaningful data as well as to facilitate any necessary redesign should initial performance be less than desired. The use of this development concept resulted in flight-type designs rather than those that were flight-weight.

Tables I and II are listings of the criteria applied in the analyses as well as the design of the liquid fluorine/hydrazine blend ablative thrust chamber assembly (TCA).

#### A. INJECTORS

The program called for the development of an injector that was stable, high performing, and compatible with an ablative chamber. In addition, the injector body, the injector/chamber interface, and any propellant valve had to be maintained at acceptable temperatures during restart duty cycles.

Recognizing the unlikelihood that the first injector unit tested would satisfy all of the specified requirements, the basic design selected provided a capability for varying the orifice pattern while utilizing identical components up to the actual time that the orifices were drilled.

A thermal accumulator was evolved to satisfy the temperature requirements for the restart duty cycles.

##### 1. Material Selection

Nickel 200 (nickel containing less than 1% impurities) was selected as the injector material because it exhibited high thermal conductivity, strength at elevated temperatures, compatibility with halogen

# CONFIDENTIAL

TABLE I

## ABLATIVE THRUST CHAMBER ASSEMBLY DESIGN CRITERIA (U)

(C)	Propellants	LF <sub>2</sub> /N <sub>2</sub> H <sub>4</sub> Blend*
	Thrust	7000 - 8000 lb
	Chamber Pressure	100 psia
	Duration Capability (Encompassing six starts)	600 sec
	Feed Pressure (Valve Inlet):	
	Fuel	155 psia
	Oxidizer	155 psia
	Mixture Ratio (W <sub>O</sub> /W <sub>F</sub> )	1.9:1
	Outside Skin Temperature	600°F (maximum)
	Propellant Weight Flow	18.94 lb/sec
	Specific Impulse	370 sec
	Thrust Chamber Assembly:	
	Length	81.6-in. (maximum)
	Nozzle Skirt Diameter	47.1-in. (maximum)

TABLE II

## DESIGN DUTY CYCLE

(U)	<u>Firing Duration (sec)</u>	<u>Off-Time (min)</u>
	315	
	9	240
	5	35
	61	14
	100	41
	110	10

\*BA 1014: Weight by Percentage, 66.7 N<sub>2</sub>H<sub>4</sub>, 24.0 MMH, and 9.3 H<sub>2</sub>O  
(4 moles N<sub>2</sub>H<sub>4</sub>, 1 mole MMH, and 1 mole H<sub>2</sub>O).

# CONFIDENTIAL

oxidizers, and resistance to fuel orifice "bellmouthing." Table III is a summary of candidate material characteristics, which provides a comparison of the significant properties of nickel, aluminum, and stainless steel.

TABLE III  
MATERIAL SELECTION SUMMARY

<u>Characteristics</u>	<u>Candidate Materials</u>		
	<u>Aluminum</u>	<u>Stainless Steel</u>	<u>Nickel A</u>
Maximum Material Operating Temperature	700°F	1700°R	1700°F
Kindling Temperature in GF <sub>2</sub>	1000+°F	1400°F	2400°F
Reported Fuel Orifice Erosion	Numerous	Some	None
Density, lb/in. <sup>3</sup>	0.1	0.3	0.3
Cost, \$/lb	1.00	0.66	5.00
Machinability	Excellent	Good	Fair
Estimated Injector Weight, lb	20	40	40

The high kindling temperature and thermal conductivity of nickel plus experience from other programs were primary determinants for selecting nickel over aluminum and stainless steel. Nickel had a history of successful use in injectors, chambers, and nozzles that were subjected to both fluorine and ClF<sub>3</sub> at chamber pressures reaching 1000 psia. Further, nickel can be welded to itself or to stainless steel and it can be brazed.

The overriding consideration in selecting Nickel 200 was the need for achieving an extended injector duration capability early in the Phase II test program with minimum development.

Until recently, the fuel orifice "bellmouthing" phenomenon (fuel orifice deteriorating at the discharge end resulting in a "bellmouth" appearance) was the most formidable obstacle to injector long-duration capability. Aerojet-General conducted a pre-proposal investigation wherein identical subscale aluminum, and nickel injectors were tested at 100 psia using LF<sub>2</sub> and BA1014 fuel. It was demonstrated that fuel orifice "bellmouthing" did not occur with the use of nickel at the conditions imposed. No difficulties were experienced in fabricating any of the subscale injector components although drilling of the fuel manifolds into the injector body became a problem with the full-scale components. The data obtained from the subscale test program are included as Appendix I.

**CONFIDENTIAL**

(This page is Unclassified)

# UNCLASSIFIED

Lithium, which has low weight, high specific heat, high latent heat of fusion, and a low melting temperature, was selected as being most suitable for the thermal accumulator. Lithium is highly toxic and spontaneously combustible with water; therefore, the use of a lithium simulant was found to be desirable. The simulant selected was solder (ASTM B-32-60T), which was both low cost and low hazard. A detailed discussion of the accumulator is provided in Section IV,A,4.

## 2. Description of Selected Design

### a. Injector Body

A single injector manifold design was selected for use throughout the entire program. This permitted early fabrication of the injector bodies, manifold covers, and inlet lines, which was committed to assembly as new orifice patterns were selected.

The basic injector is shown on Figure No. 1. It was 9.340-in. in diameter, flat-faced, and without baffles. The oxidizer manifold inlet was located on the injector axis. Oxidizer was flooded over the back surface of the injector and fed through axially-directed showerhead orifices. The fuel was fed from an annular manifold on the back surface of the injector through drilled holes into a peripheral manifold located at the injector face. This manifold then fed a network of distribution passages that were drilled parallel to the injector face with the fuel orifices intersecting these passages.

Heat-soak to the injector also was investigated because there was concern that radiation and conduction from the hot walls of the chamber liner during coast periods, following shutdown, would result in overheating the injector. This could cause the blended hydrazine fuel to undergo monopropellant decomposition at restart. A thermal accumulator, which would accept the heat-soak from the thrust chamber following shutdown, was conceived to maintain the injector and valve at temperatures below the fuel decomposition threshold.

One injector, S/N 6, incorporated the thermal accumulator (see Figure No. 2), which consisted of a cavity at the back of the injector. This cavity was filled with solder that was confined by a steel cover-plate. Several chromel-alumel thermocouples were positioned in the cavity at various depths.

### b. Injector Patterns

Three injector patterns were finalized at the outset of the program. The F-O-F triplet element was selected as the primary element type in all three patterns. The triplet element provides good atomization which results in high performance. The patterns were suited to the same drilled, manifold injector body.

UNCLASSIFIED

UNCLASSIFIED

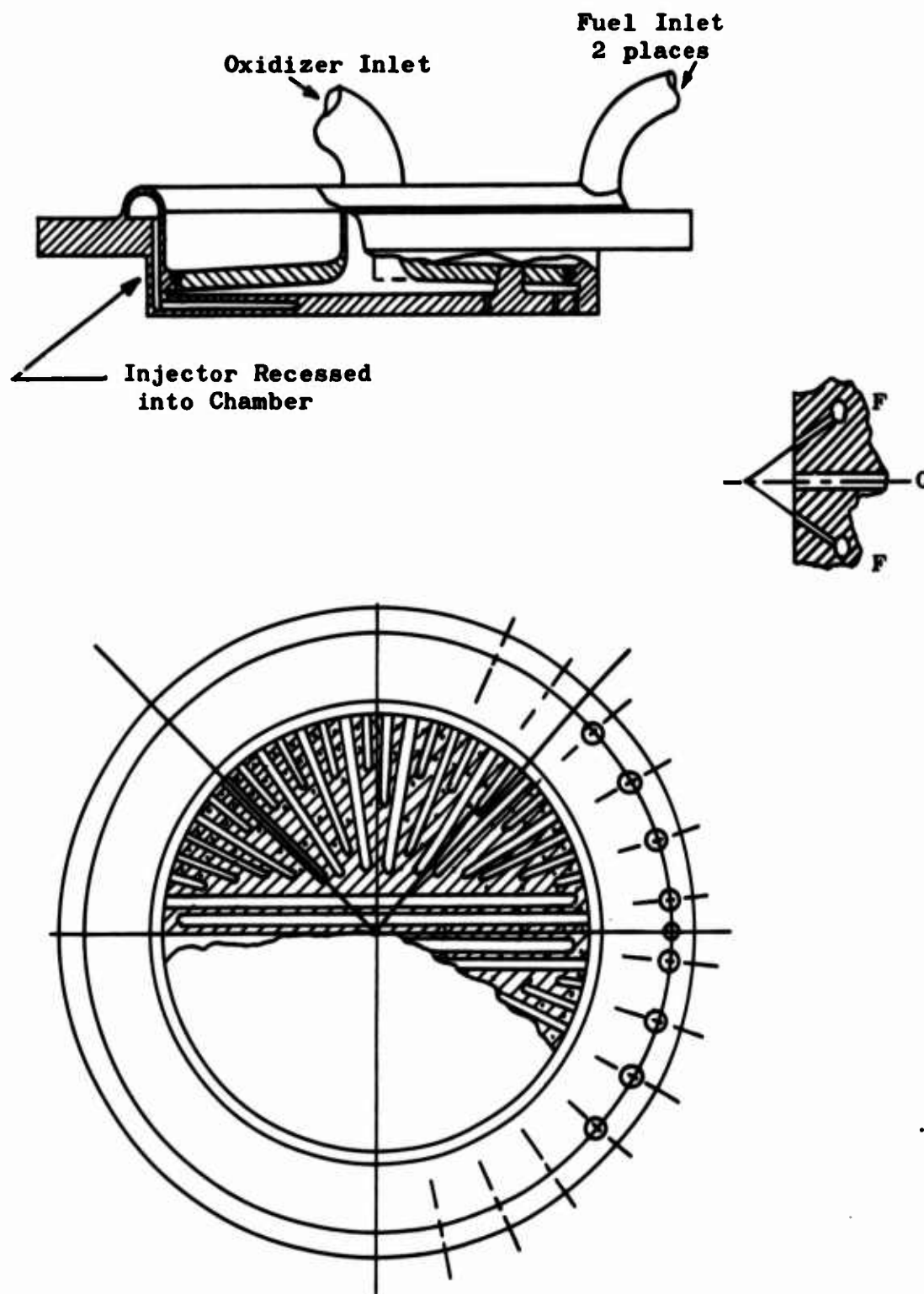


Figure 1. Injector Body Configuration

UNCLASSIFIED

UNCLASSIFIED

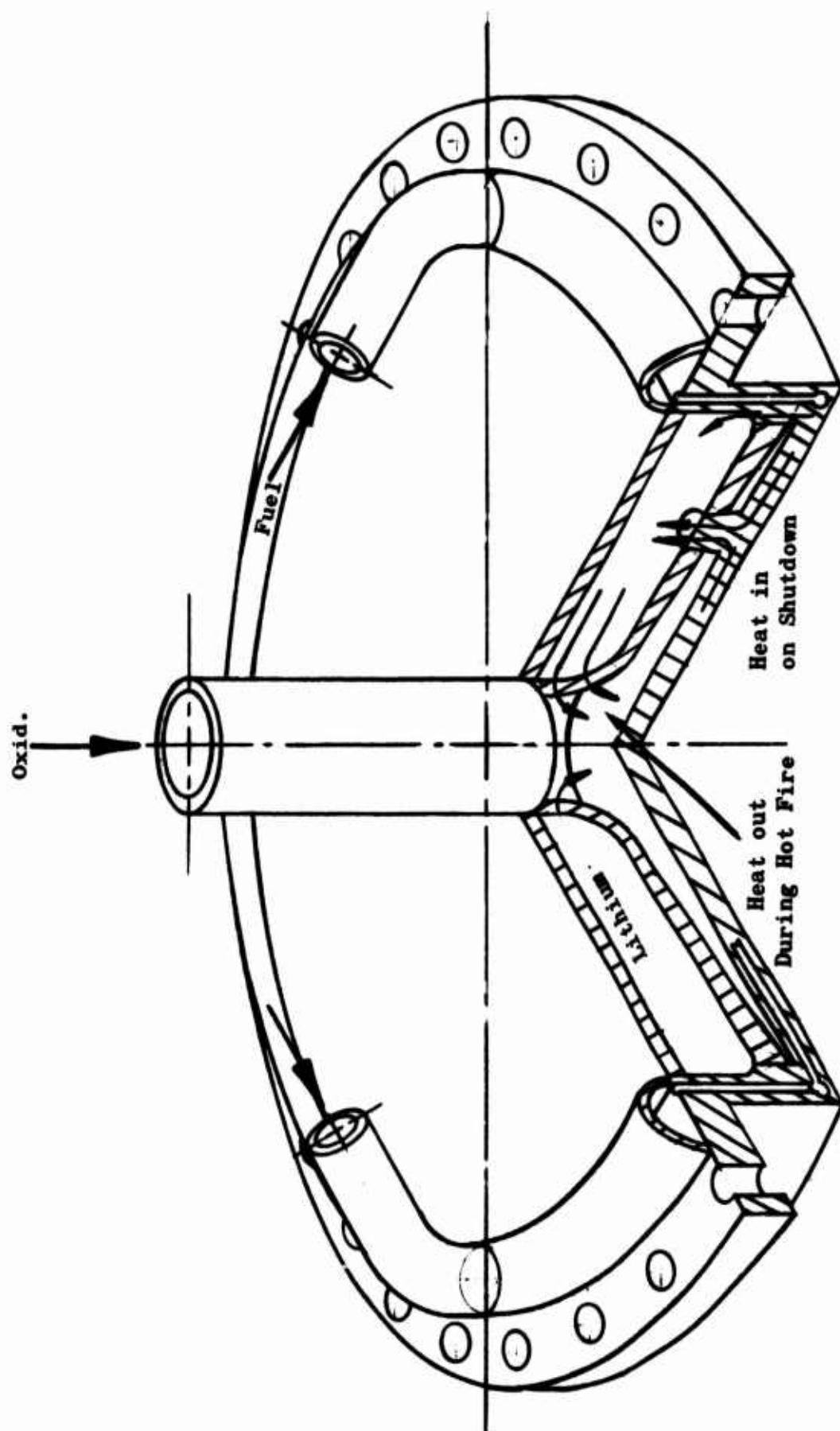


Figure 2. Thermal Accumulator

UNCLASSIFIED



# UNCLASSIFIED

All of the injector patterns were designed to have a constant mixture ratio (2.3) and flat radial mass density in the central core to achieve good performance and chamber compatibility. A mixture ratio of 1.0 and a fuel-rich barrier were utilized near the chamber wall. The designs were selected to provide a low gas side-wall temperature without chemically erosive, oxidizer-rich "cross-winds." These criteria were consistent with minimum mixture ratio distribution (MRD) performance loss and good chamber compatibility as calculated by stream tube and compatibility analyses verified by Apollo and Transtage testing.

## (1) Coarse Pattern

The coarse pattern consisted of 158 elements consisting of 60 folded triplet peripheral elements, 10 pentads (four-fuel-on-one-oxidizer) and 88 in-line triplets (see Figure No. 3). The impingement heights on the in-line triplets were 0.25-in. Initially, this pattern was expected to provide a high stability rating. Subsequent testing showed that a further reduction in element quantity was necessary to achieve stable operation.

## (2) Intermediate Pattern

The intermediate pattern was made up of 215 elements, all of which were in-line triplets except for the peripheral elements and the 10 pentads (see Figure No. 4). The impingement heights on the in-line triplet elements were staggered at 0.268-in. and 1.0-in. while the pentads were 0.280-in. high.

## (3) Fine Pattern

The fine pattern consisted of 298 elements, all of which were in-line triplets except for the peripheral folded triplets. This pattern was selected because it offered a high performance potential as well as the best predicted chamber compatibility. The impingement heights of the in-line triplets were staggered at 0.268-in. and 1.0-in. The folded triplet impingement height was also 0.268-in.

A coarse pattern injector (S/N 2) and an intermediate pattern injector (S/N T<sup>2</sup>) were fabricated. It was decided to delay manufacture of a fine pattern design until the results of tests with injectors S/N 2 and S/N T<sup>2</sup> could be evaluated. S/N T<sup>2</sup> injector was made from aluminum to avoid delays caused by difficulties experienced in drilling the fuel feed passages in the nickel units. There was a high incidence of unstable operation as discussed in Section VI, A with both of these units. This along with concurrent problems in drilling nickel injector blanks led to the decision to modify the pattern of injector S/N 2 rather than fabricate new units at the time.

UNCLASSIFIED



UNCLASSIFIED

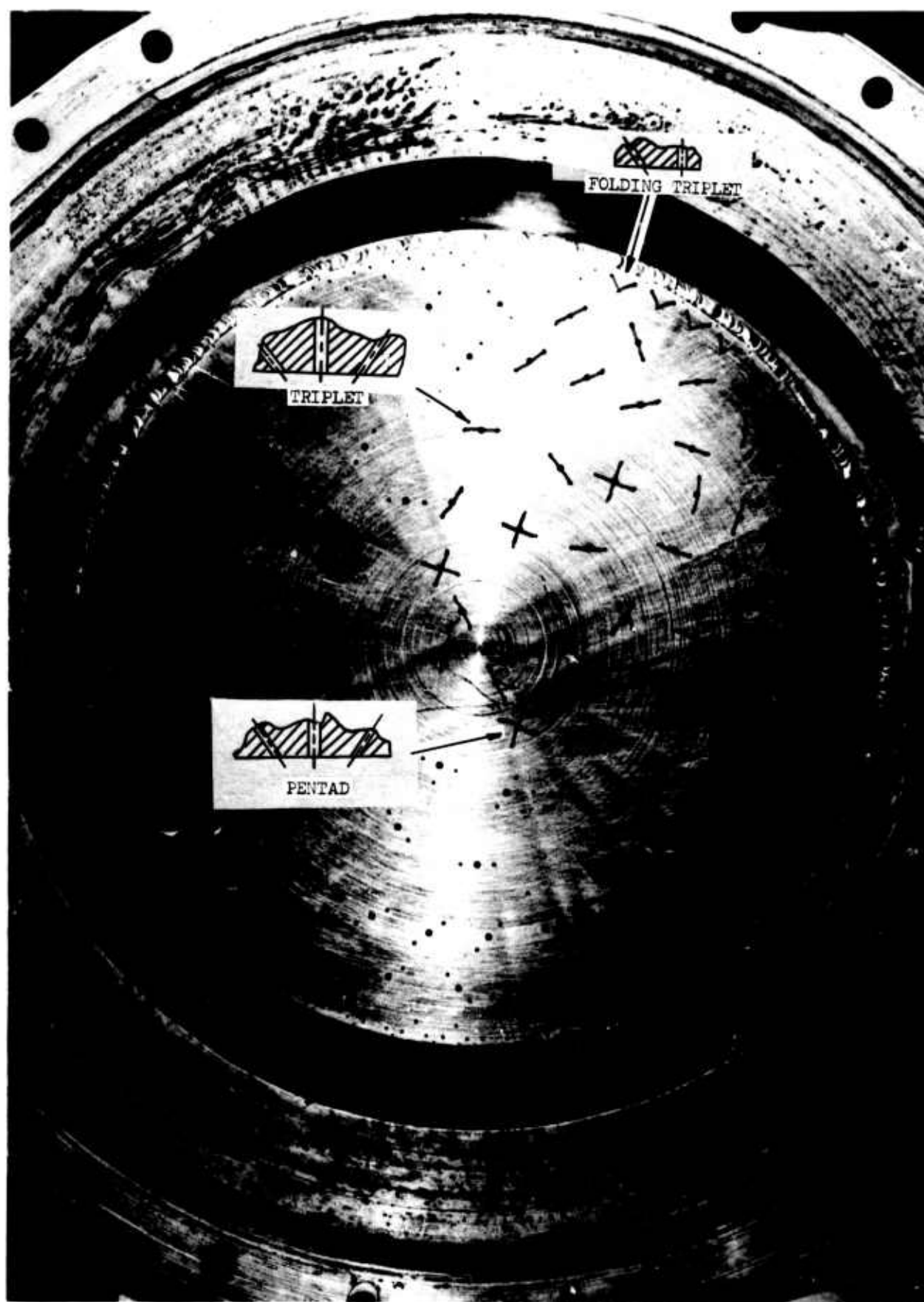


Figure 3. Injector S/N 2, 158-Element Pattern

Page 13

UNCLASSIFIED

UNCLASSIFIED

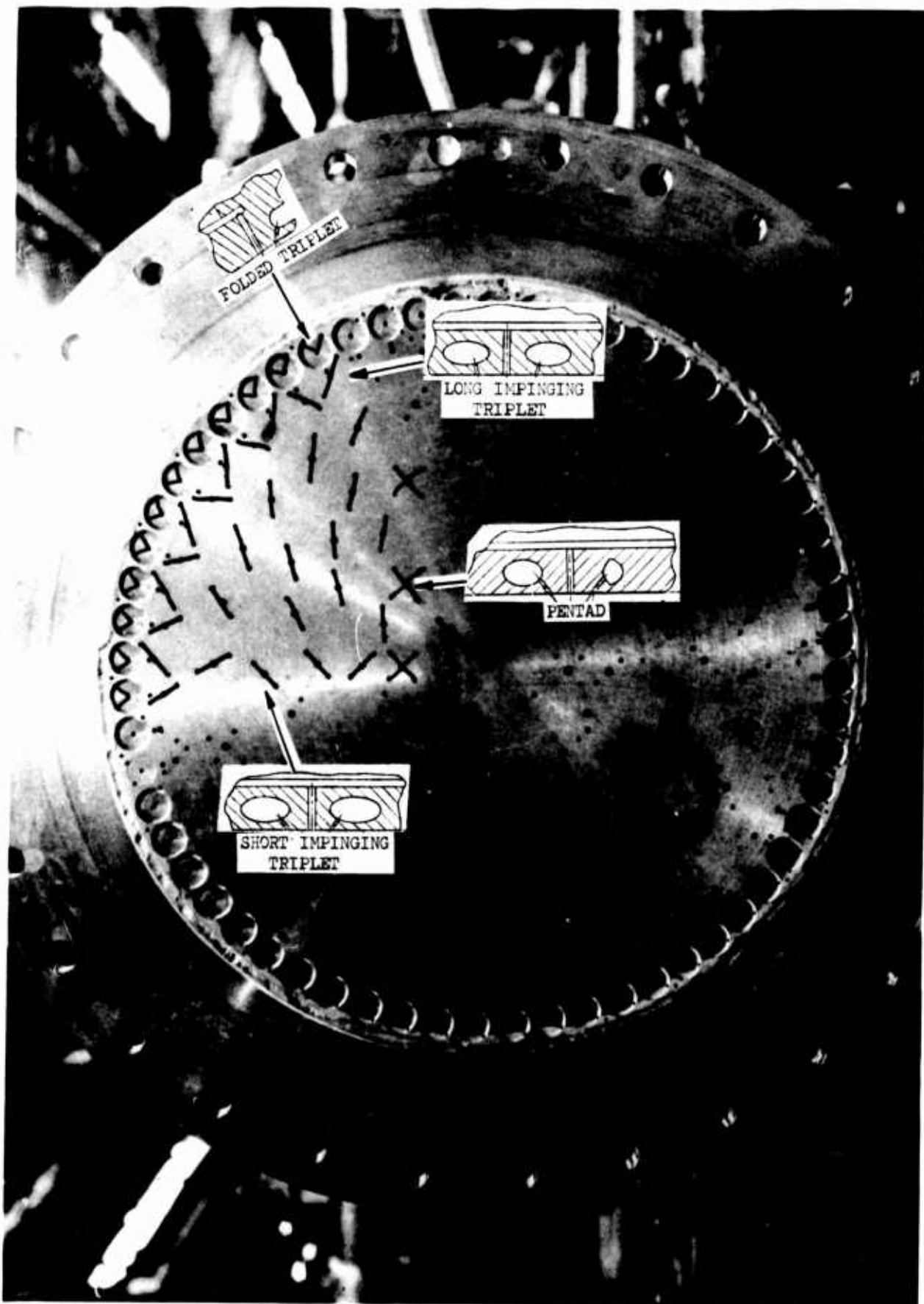


Figure 4. Injector S/N T<sup>2</sup>, 215-Element Pattern

Page 14

UNCLASSIFIED

## UNCLASSIFIED

The 158-element pattern drilled in injector S/N 2 was modified three times. Emphasis was placed upon stability attainment; the number of pattern elements was reduced in each modification.

The first modification consisted of reducing the number of elements to 98. There were 68 core triplets and 30 long-impinging (2.0-in.), unlike-doublet elements at the periphery. This pattern, which was designated as S/N 2, Mod 1 proved to be unstable.

The second modification consisted of eliminating the 30 very long-impinging unlike-doublet elements. This resulted in the 68-element design, designated as S/N 2, Mod 2. It was stable in all tests; however, it exceeded the design pressure drop requirements.

The pattern in the third modification was the same as that of S/N 2, Mod 2 except the orifice diameters were enlarged to reduce the injector pressure drop, which had increased as the result of reducing the number of elements in the previous modifications. Fuel film-cooling orifices were added in selected areas at the periphery to correct the oxidizer burn spots noted on a steel chamber following testing with the previous version. This coolant flow was approximately 2%. The third modification, designated S/N 2, Mod 3, is shown on Figure No. 5 and was stable on all tests.

Chamber streaking occurred with the injector S/N 2, Mod 3 pattern. Therefore, another 68 element pattern was designed to overcome this poor combustion chamber compatibility while retaining the stability and performance characteristics of S/N 2, Mod 3. This pattern, which is shown on Figure No. 6, was similar to that of S/N 2, Mod 3 except for the long-impinging elements which were situated closer toward the center of the pattern. Also, it had 10% fuel film-cooling. The pattern was used for injector S/N 6.

An all-new pattern was designed for injector S/N 7, which was evaluated during the Phase III testing. This design was directed toward attaining an altitude specific impulse of 370 sec and eliminating thrust chamber streaking. Stability had a minimal pattern influence because it was expected that damping would be provided by a separate acoustic resonator array on the chamber wall.

In the design of S/N 7, triplet-type elements were used to avoid the possibility of introducing new, unpredictable influences upon performance stability and compatibility with an element type change. Therefore, only the number of elements, their size, and their location were major variables.

A uniform mixture ratio and propellant distribution over the injector face along with a uniform weight flow per element were considered as being the most suitable design. This would result in minimal gas dynamic forces acting upon the chamber wall while avoiding a concentration of

## UNCLASSIFIED

UNCLASSIFIED

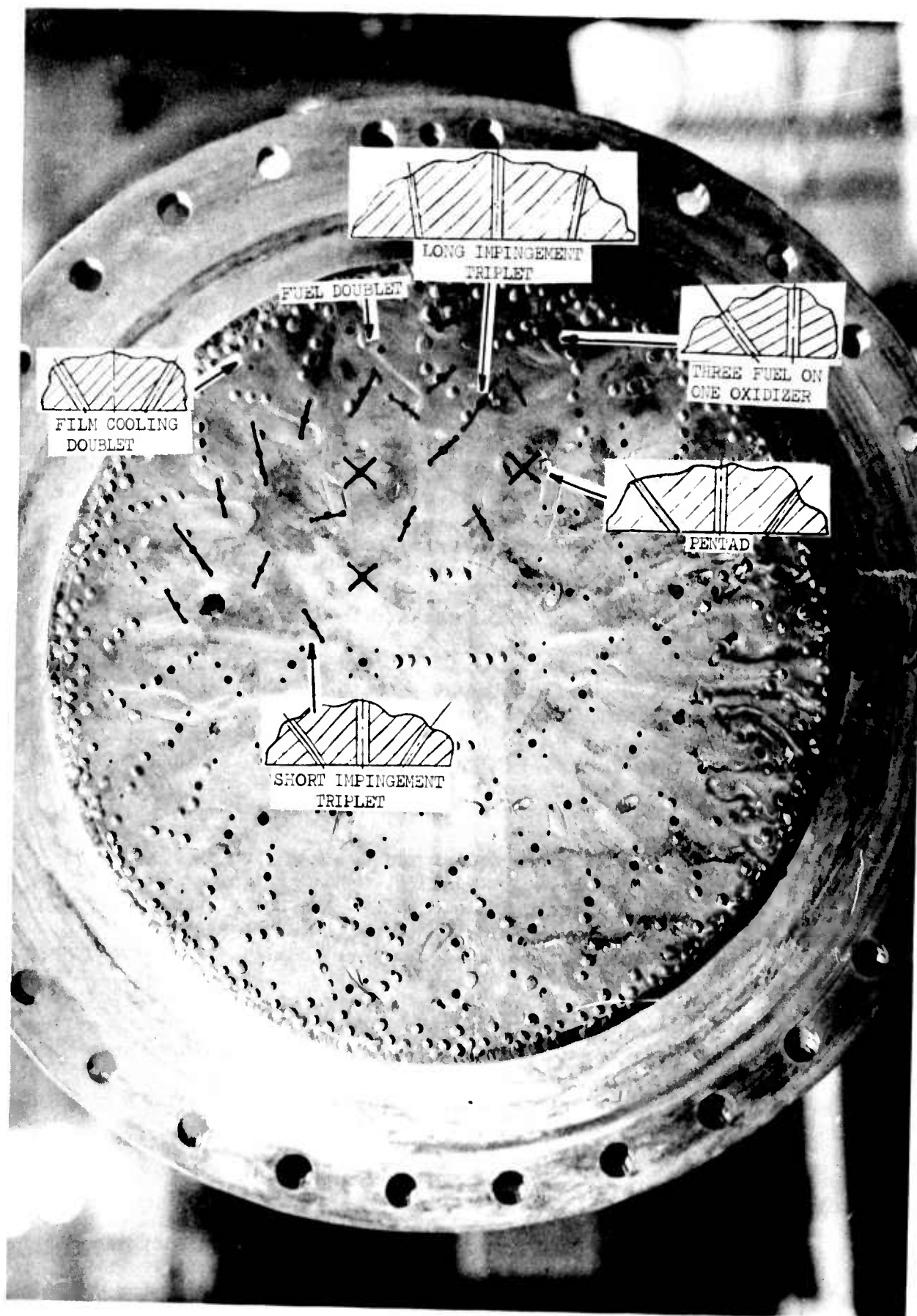


Figure 5. Injector S/N 2, Mod 3, 68-Element Pattern

UNCLASSIFIED



UNCLASSIFIED

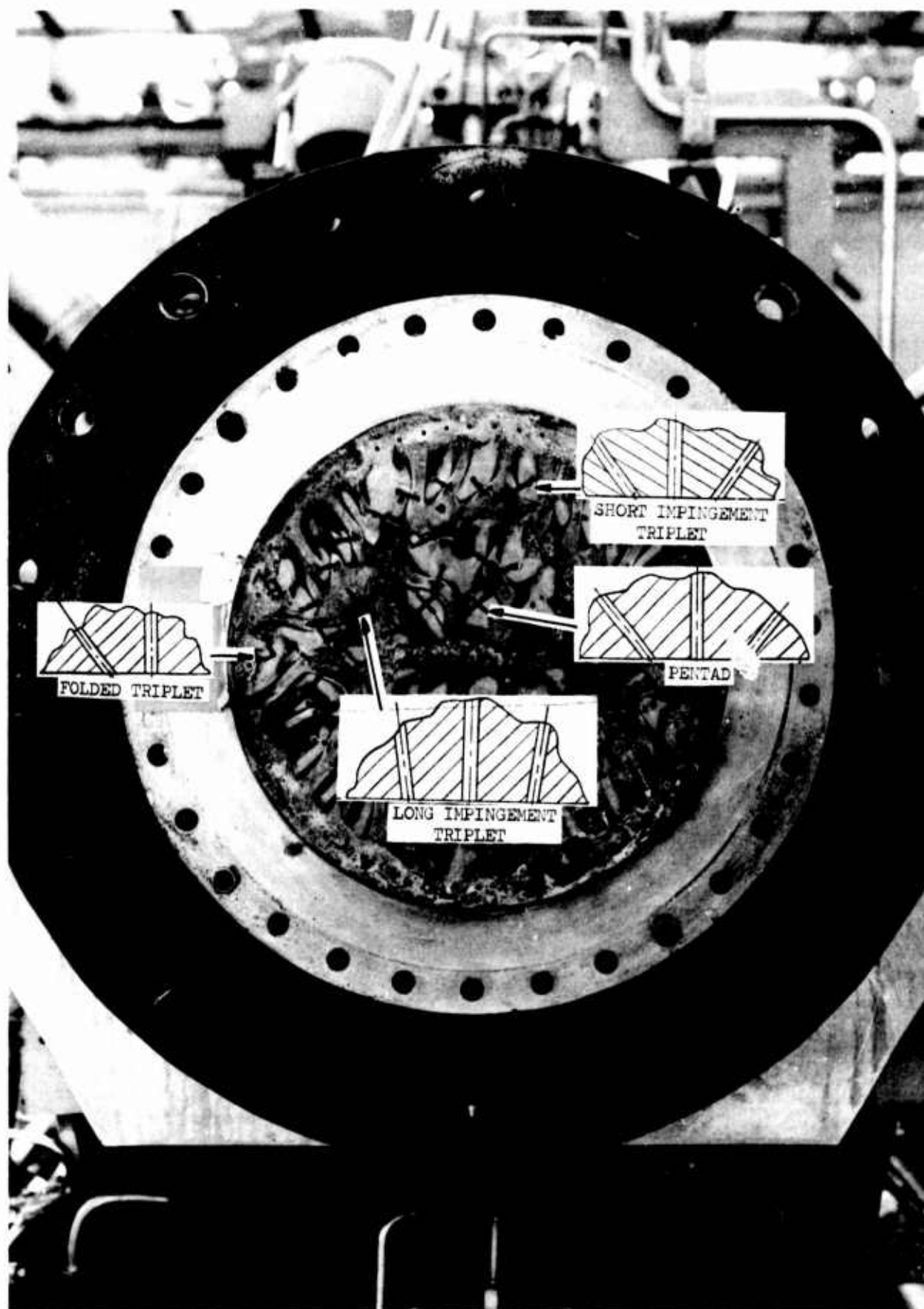


Figure 6. Injector S/N 6, 68-Element Pattern

Page 17

UNCLASSIFIED

## UNCLASSIFIED

either fuel or oxidizer. The total number of elements evolved from a study directed toward achieving their most uniform placement and having a minimum orifice diameter of 0.016-in.

A modified Priem Vaporization Model was utilized for a performance analysis and it was found that approximately 200 elements would be needed to achieve the target performance. This number of elements was increased to 344 because of compatibility considerations and to attain the maximum performance margin. Thus, a fine pattern without fuel film cooling was selected for the S/N 7 injector (see Figure No. 7). The orifice diameters were 0.020-in. for the fuel and 0.035-in. for the oxidizer. All 344 elements were fuel-oxidizer-fuel type triplets with a vacuum thrust of 20.0 lb per element.

Analysis showed that this new pattern had the same stability characteristics as the 215-element injector, S/N T<sup>2</sup>. Using fuel orifice correlations, it was predicted to be unstable in a first tangential mode. Injector S/N T<sup>2</sup> was unstable in a first tangential mode during two of its three tests.

### c. Instrumentation

The thermal analysis indicated that an injector face temperature of up to 1300°F could be experienced, which appeared to be satisfactory because of the high kindling temperature of Nickel 200 in a fluorine atmosphere. However, to actually measure face temperatures, chromel-alumel thermocouples were installed in 0.010-in. diameter holes drilled through support posts at mid-radius. All fourteen of these posts were integral with the injector body which extended through the oxidizer cover. They were designed to provide a heat path to the thermal accumulator and a structural tie between the face-plate and the oxidizer cover.

The thermocouple junctions were silver-soldered flush with the injector face. Four thermocouples of this type were installed in each injector except the aluminum one, S/N T<sup>2</sup>, which did not have support posts. In subsequent testing, these thermocouples were found to be useful for monitoring stability as well as providing design data.

Two pressure taps, located 180-degrees apart, were installed in drilled-through support posts to provide chamber pressure data. Two fuel manifold pressure taps, located 180-degrees apart, were placed in the fuel torus at the base of each fuel inlet. Oxidizer manifold pressure was measured by a single pressure tap positioned near the oxidizer inlet.

A thermocouple fitting was installed on the oxidizer inlet line near the back cover of the injector. This provided for a more accurate determination of the density of the fluorine entering the injector than could be obtained at the flowmeters which were located several feet upstream.

UNCLASSIFIED

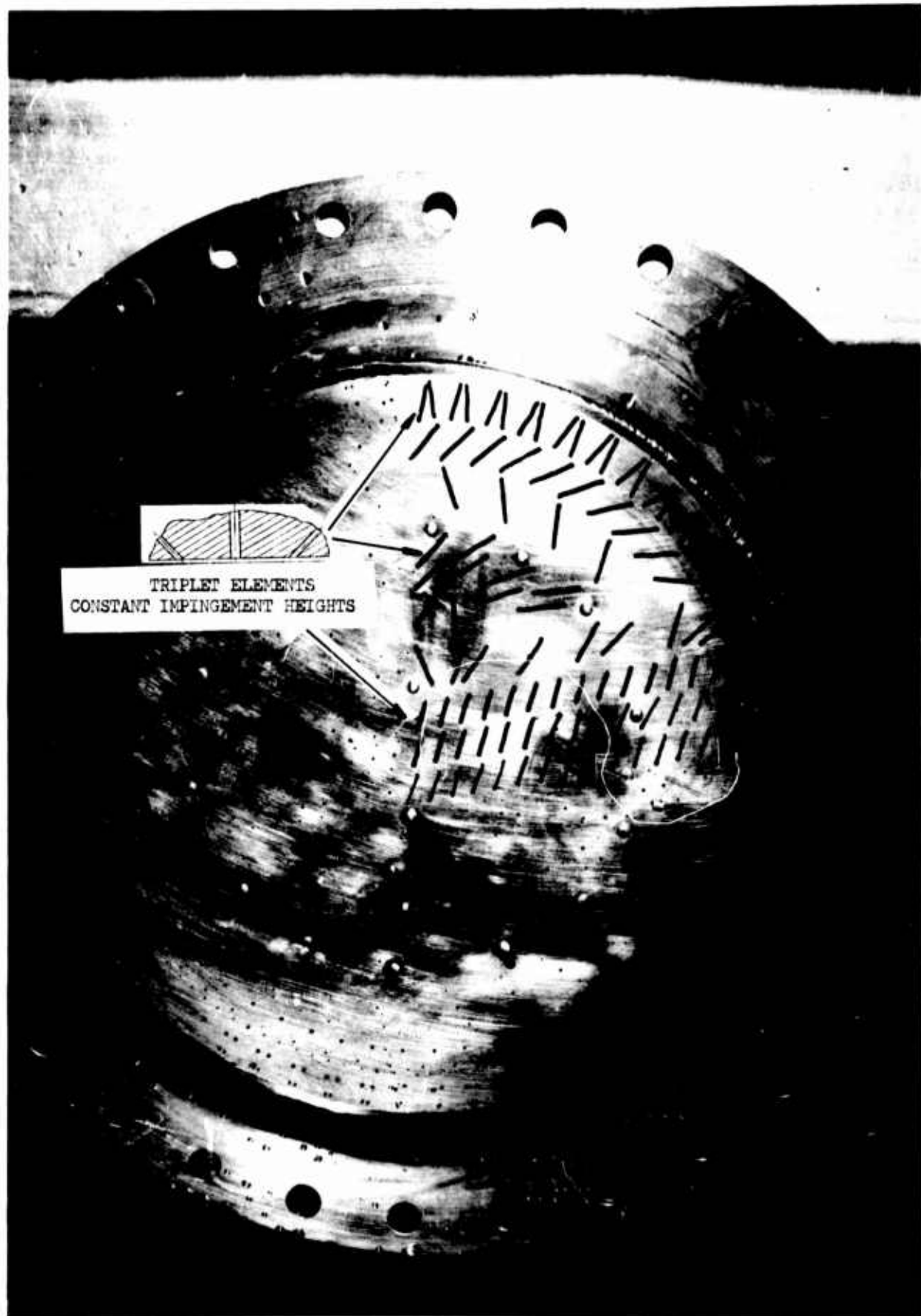


Figure 7. Injector S/N 7, 344-Element Pattern

UNCLASSIFIED

# UNCLASSIFIED

## 3. Thermal Predictions

Injector thermal analysis considered three heat transfer modes; conduction, radiation, and convection. Convection and radiation from the combustion products combine with radiation from the chamber wall to heat the injector face while it is cooled by convection to the liquid propellants. Heat is transferred from the hot side to the coolant by means of conduction through the injector face.

The analyses of these transfer modes offered varying degrees of difficulty. Conduction was relatively simple despite its being multi-dimensional. Radiation was more difficult because the temperature profile of the radiation source (largely the hot chamber wall) was not measured. Radiation comprised approximately 25% of the heat load on the face of the injector during firing. The major part of this heat load was attributed to convection from the combustion products.

Gas-side convection was the greatest uncertainty. Little information was available in the existing literature because of the broad divergencies occurring with individual injectors, which result from variation of mass flux, orifice characteristics, element type, element location, and impingement distance. The approach used was to express the convective film coefficient as a fraction of the chamber wall coefficient. Typically, this is in a range of 0.2 to 0.8 (i.e., a variation factor of 4). For design purposes, a factor of 0.8 was considered to be appropriately conservative.

The selected injector was cooled primarily by fuel flow in the cross-drilled channels. Nucleate boiling on the hot side of the channel and conventional turbulent convection on the cooler side were predicted. The fuel channel diameter, spacing, and distance from the gas-side was established by means of two-dimensional conduction studies using the Thermal Network Analyzer Computer Program. It was found that the fuel velocity was relatively unimportant in promoting good heat transfer because the high heat fluxes accompanying nucleate boiling precluded much of a temperature drop between the fuel channel surface and the coolant saturation temperature. Analytical results for the channel diameter, spacing, and distance from the face are plotted on Figure No. 8. Based upon these results as well as practical design considerations, the fuel channel diameters selected ranged from 0.17-in. to 0.25-in., the distance from the channel centerlines to the gas-side varied from 0.15-in. to 0.19-in., and the maximum centerline-to-centerline distance was 0.6-in. The predicted maximum face temperature was 1300°F and the maximum heat flux into the fuel was predicted as 4.5 Btu/in.<sup>2</sup> sec.

The predicted heat flux was high from the aspect of coolant burnout heat flux. An empirical comparison was made between the selected design and the successfully tested subscale units of similar design, to verify the acceptability of this high heat flux and/or the conservative assumptions of the analysis. The comparison showed the ratio of fuel wetted surface area



UNCLASSIFIED

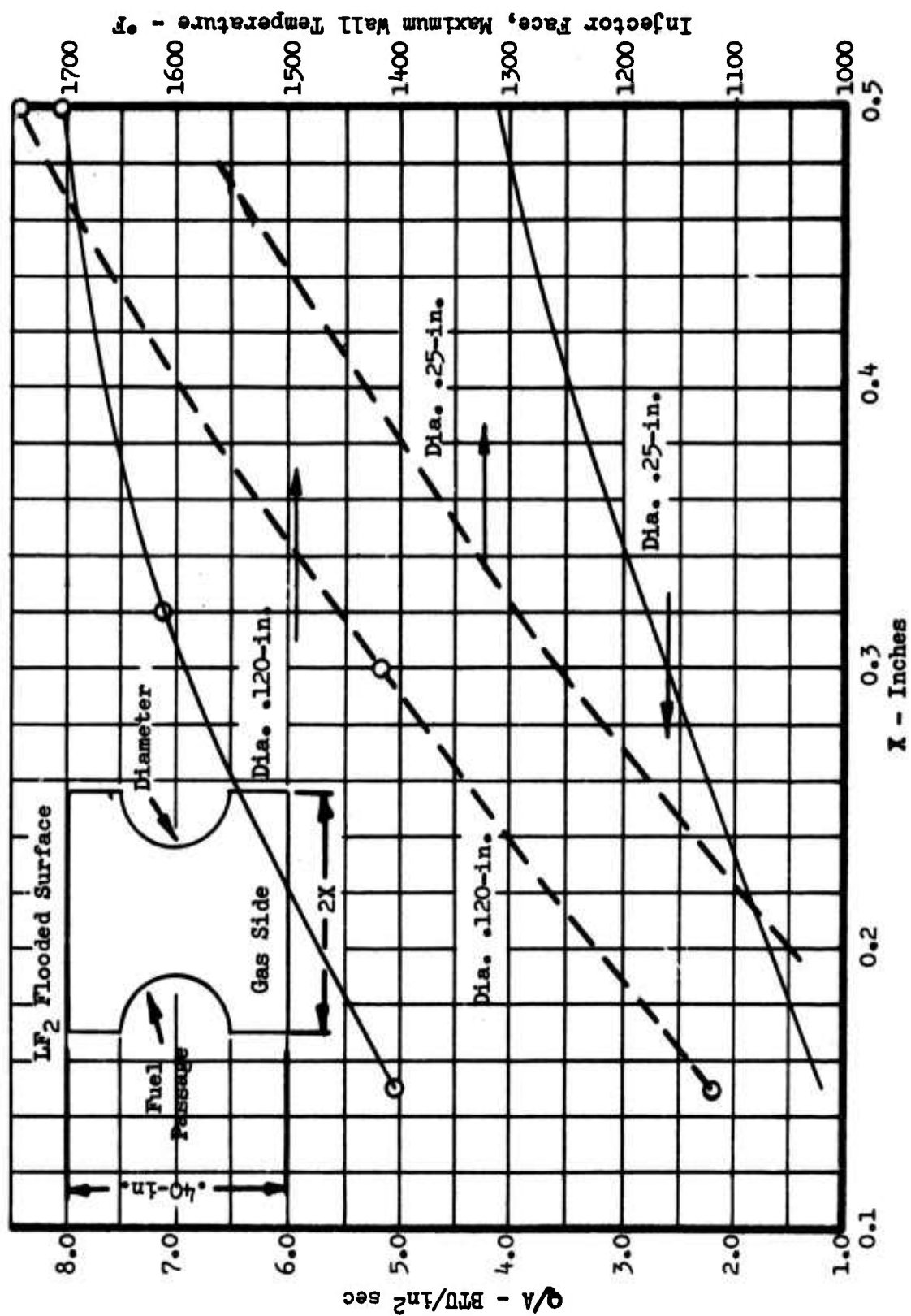


Figure 8. Predicted Maximum Injector Face Temperatures and Heat Flux into the Coolant

UNCLASSIFIED

UNCLASSIFIED

to injector face area of the full-scale design was 8% greater than it was for the subscale design (1.3 as compared to 1.2). The subscale unit operated satisfactorily without any fuel burnout; therefore, it was indicated that the full-scale unit had been provided with a slightly greater margin of safety.

#### 4. Thermal Accumulator

The thermal accumulator (see Figure No. 2) was a rechargeable heat-sink. It was designed to limit the post-fire temperature rise of the injector so that the engine could be restarted after a short coast period without any danger of fuel detonation. It was analytically predicted that the average temperature of the injector (without thermal accumulator) would be approximately 600°F at the time of restart following the shortest coast period of the design duty cycle. This 10 min coast period follows a 100 sec firing. The predicted response is shown on Figure No. 9.

The accumulator, which is located on the back of the injector, is cooled during engine firing by transferring its sensible energy content into the oxidizer flow stream. Following a firing, it soaks up the injector face heat load caused by radiation and conduction from the ablative chamber.

The analytically predicted high post-fire injector temperatures resulted from an excessive net heat input to the injector; therefore, several design approaches were considered to remedy this. The three general areas of consideration were lowering the gross heat input, increasing the gross heat loss, and enlarging the thermal capacitance of the injector.

The first option involved a reduction of the radiant heat load from the chamber by either maintaining low chamber wall temperatures during firing through the application of massive film cooling or by ensuring a low injector face heat absorption. Both of these possibilities were considered to be unrealistic. Similarly, the second option was found to be unfeasible because it involved increasing the radiation losses from the injector backplate. Even if it radiated as a black body, the backplate could not disperse the predicted load.

Increasing the capacitance, the third option, appeared to be the best solution despite it resulting in a heavier weight injector. Both active and passive systems were considered. The active systems included regenerative as well as non-regenerative cooling by means of fuel or an auxiliary fluid flow while the passive systems were comprised of high specific heat or phase-changing materials that would absorb heat.

The active systems would have required additional circuitry, including a valve and pump, and were eliminated because they would have imposed an inherent reduction in reliability. The approach of the passive system with the phase-changing materials was selected as being most advantageous from the weight aspect. This selection offered two possible alternatives; a closed system or a pressure sensitive vent system. The closed

UNCLASSIFIED

UNCLASSIFIED

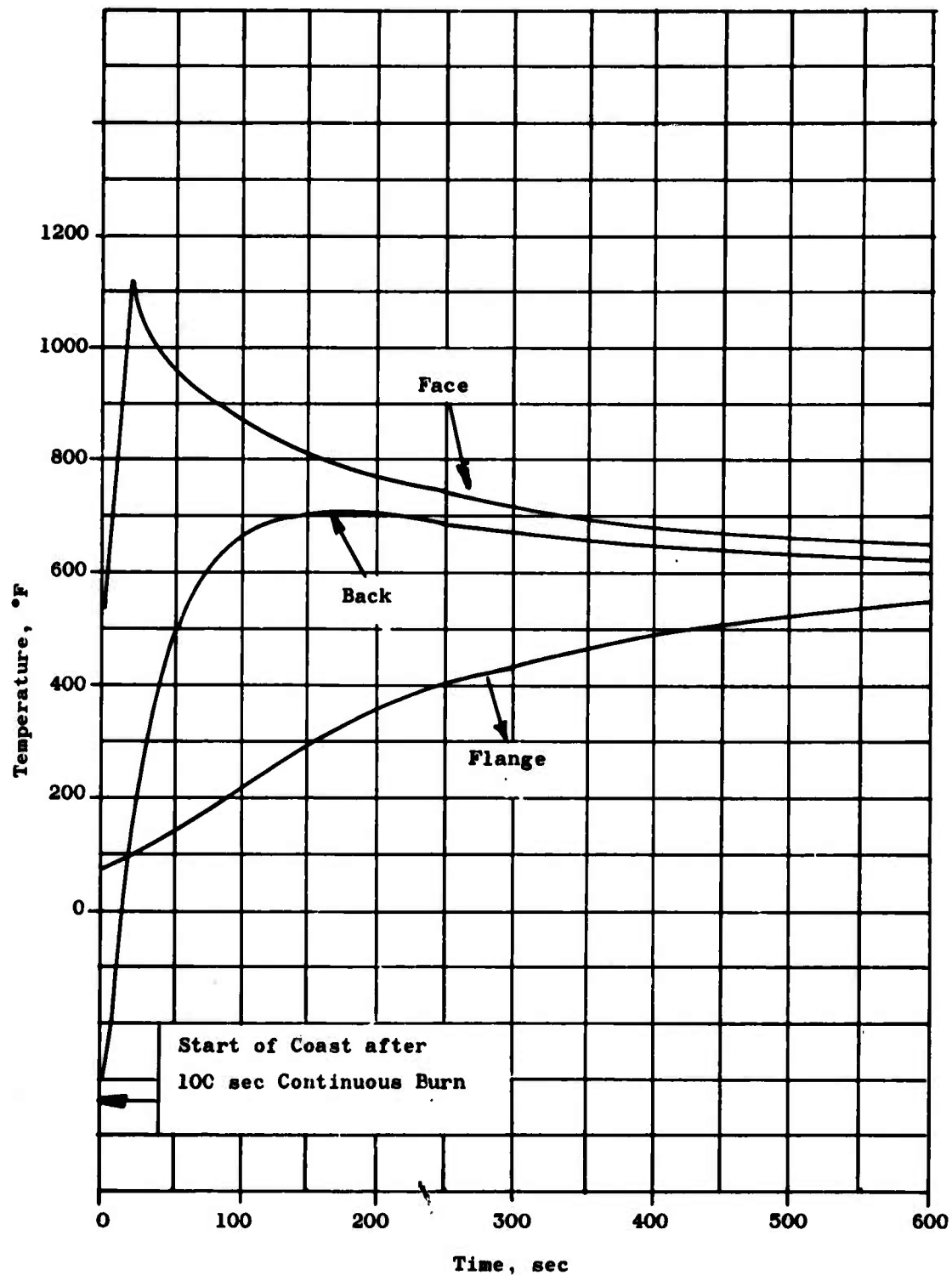


Figure 9. Predicted Post-Fire Injector Temperature Response

UNCLASSIFIED

## UNCLASSIFIED

system would contain a material which melts as the injector is heated during the coast period and then resolidifies during firing. In the pressure sensitive vent system, a subliming material or one that melts and subsequently vaporized would be used.

The closed system was selected as being the simpler and more reliable approach. The criteria established for material selection were as follows:

- a lightweight accumulator
- a high specific heat and heat of fusion material
- a high material density for packaging purposes
- chemical compatibility with nickel and stainless steel
- low thermal expansion characteristics
- high thermal conductivity to minimize response times

The inorganic candidate materials selected are listed on Table IV. Most are elemental metals, only a few of which have sufficiently low melting points to enhance the sensible energy capacity by the heat of fusion. Organic materials also were considered. Generally, these materials have high specific heats, but are limited by their low conduction and diffusion potential. In addition, they melt and boil at low temperatures. These materials were not included in the design analyses because of the limited information available regarding their thermal properties and physical behavior.

Lithium was found to be the best metallic material for this application. It has a high heat of fusion at a relatively low melting temperature, a high specific heat, and relatively good thermal conductivity. However, lithium is highly toxic and spontaneously combustible with water. These handling problems could be overcome in a flight development program. In view of the objectives and scope of this program, it was found that the use of a lithium simulant would be more desirable. Solder, 50Pb/50 Sn, was an acceptable substitute.

Some uncertainties were introduced into the early analytical efforts by the oxidizer heat transfer characteristics. Therefore, appropriate instrumentation was located on the injector backplate during firings to provide data that could be used to infer the oxidizer heat transfer coefficient.

Uncertainty also existed regarding the radiant heat load imposed upon the injector face from the chamber following a firing. This resulted from the difficulty in predicting the wall temperature profile over the length of the chamber (it cannot be measured) and uncertainty regarding thermal absorption by the injector face.

UNCLASSIFIED

# UNCLASSIFIED

TABLE IV

## COMPARISON OF CANDIDATE INORGANIC MATERIALS

Material	$\frac{k}{\text{Btu/in. sec}^\circ\text{F}}$	$\frac{\rho}{\text{lb/in.}^3}$	$\frac{C_p}{\text{Btu/lbm } ^\circ\text{F}}$	$\frac{\alpha_1}{\text{in.}^2/\text{sec}}$	$\frac{\mu}{\text{in./in.}^\circ\text{F} \times 10^6}$	$\frac{MP}{^\circ\text{F}}$	$\frac{h_{\text{fusion}}}{\text{Btu/lbm}}$	$\frac{BP}{^\circ\text{F}}$
Ag	0.00540	0.378	0.055	0.260	10.9	1770		
Al	0.00210	0.098	0.214	0.100	13.7	1220		
Be	0.00269	0.065	0.390	0.086	6.4	2340		
C	0.00146	0.081	0.170	0.105	1.5	7000		
Cd	0.00120	0.312	0.055	0.070	13.3	610	234.0	767
Cu	0.00555	0.322	0.090	0.192	9.8	1980		
Fe	0.00095	0.284	0.105	0.030	10.4	2800		
Li	0.00090	0.019	0.780	0.060	31.1	354	179.0	2490
Mo	0.00186	0.367	0.062	0.081	3.1	4760		
Na	0.00115	0.033	0.330	0.105	34.6	208	49.6	1620
Ni	0.00086	0.321	0.105	0.020	9.2	2650		
Pb	0.00049	0.408	0.028	0.004	16.3	620	10.6	2850
Sn	0.00090	0.263	0.061	0.056	13.0	450	26.0	4100
50Pb/50Sn	0.00062	0.320	0.048	0.044	13.0	361-421	23.0	
Zn	0.00150	0.258	0.092	0.064	19.3	787		

NOTES: C = graphite

50Pb/50Sn = solder

Material properties evaluated at room temperature

Heats of fusion and boiling points given for potential phase-changing candidates only

## UNCLASSIFIED

The predicted post-fire injector (face, back, and flange) temperature response with the thermal accumulator is shown on Figure No. 10. These predictions are for the period following a 100 sec firing and reflect initial temperature levels. The effect of utilizing a thermal accumulator is to lower the average temperature from approximately 600°F to 400°F, which is an acceptable level for engine restart.

### 5. Structures

Stress analyses of the basic injector design were performed to verify that adequate margins existed for the anticipated pressure and thermal stresses. It was established that the margins were satisfactory where yield was a necessary criterion. Also, it was found that induced stresses above the yield point of the nickel still permitted a 10,000 thermal fatigue cycle life. The stress-strain properties of nickel that were used in the analyses are shown on Figure No. 11.

The average temperature used for the injector face was approximately 300°F less than the maximum predicted in the thermal analysis. The fuel passage drill spacing resulted in locally high temperatures where the material section was greatest. Because these "highest temperature" isotherms (1300°F) occurred in the radial sectors only and affected a very small percentage of the total injector cross-section, they had an insignificant affect upon injector strength. Figure No. 12 shows the estimated average temperature in each of the selected finite elements as well as the computer model zone mapping. Analyses were accomplished using a finite element computer program, which is applied to obtain displacements and stresses within plane or axisymmetric solids with linear or non-linear material properties. The continuous body is replaced by a system of elements with triangular or quadrilateral cross-section. In the finite element approximation, the continuous structure is replaced by a system of elements that are interconnected at joints or nodal points. Equilibrium equations, in terms of unknown nodal point displacements, are developed at each nodal point. A solution of this set of equations constitutes a solution for the system.

The analysis was performed considering operation thermal gradients and pressure loads in the injector with the injector flange fixed against rotation. Second order plastic deformation or stress relieving also was considered when pertinent.

As shown on Figure No. 12, the typical stress levels were 5,700 psi for the injector face, 15,000 psi for the oxidizer cover plate, and 7,000 psi for the injector/chamber flange. The highest stress level of 33,683 psi, which is shown at the intersection of the face plate and back cover manifold, was in the plastic range but remained acceptable upon the basis of cycle life calculations. In the other areas that exceed the material yield strength, the condition was not considered detrimental because

UNCLASSIFIED



UNCLASSIFIED

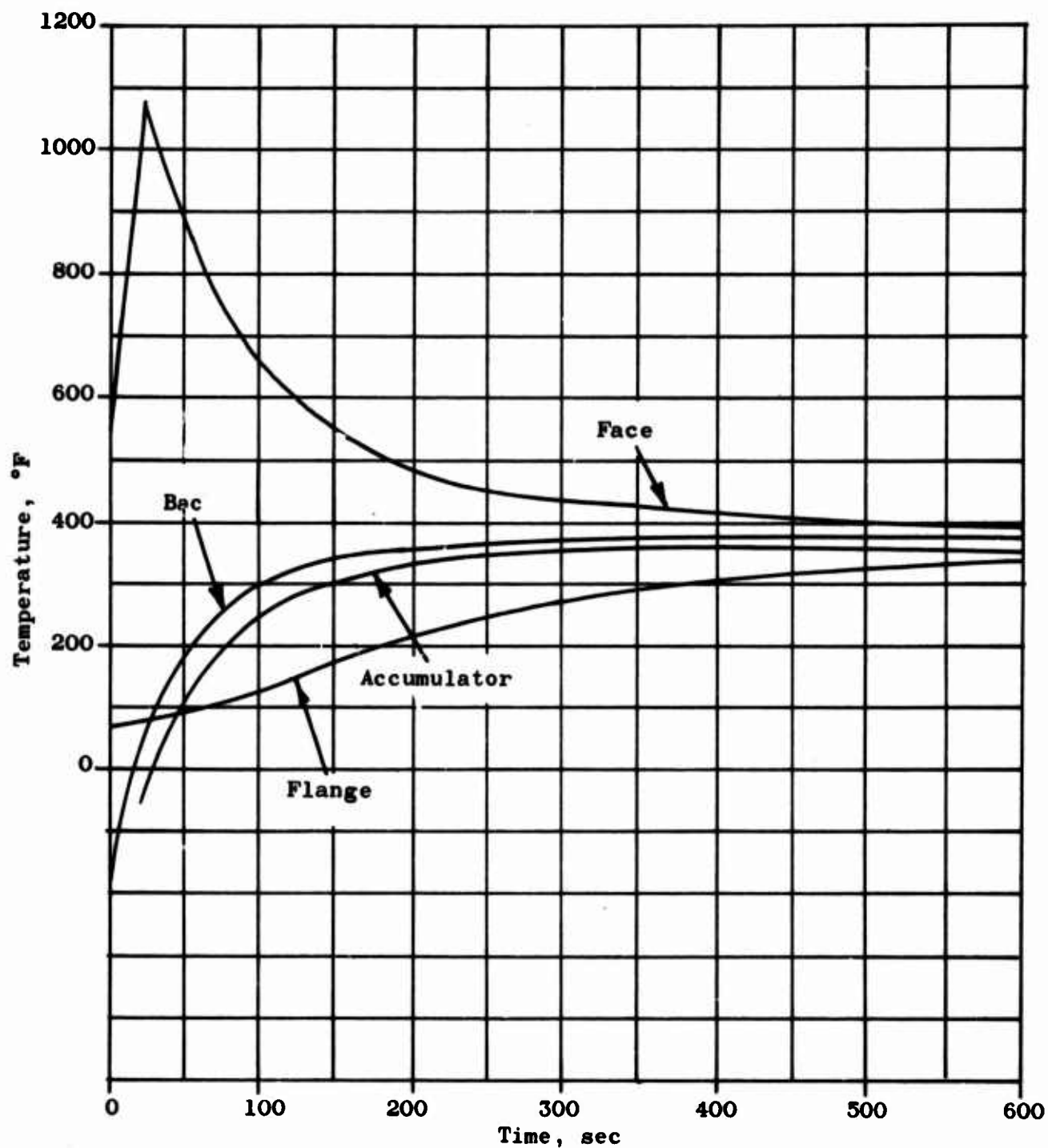


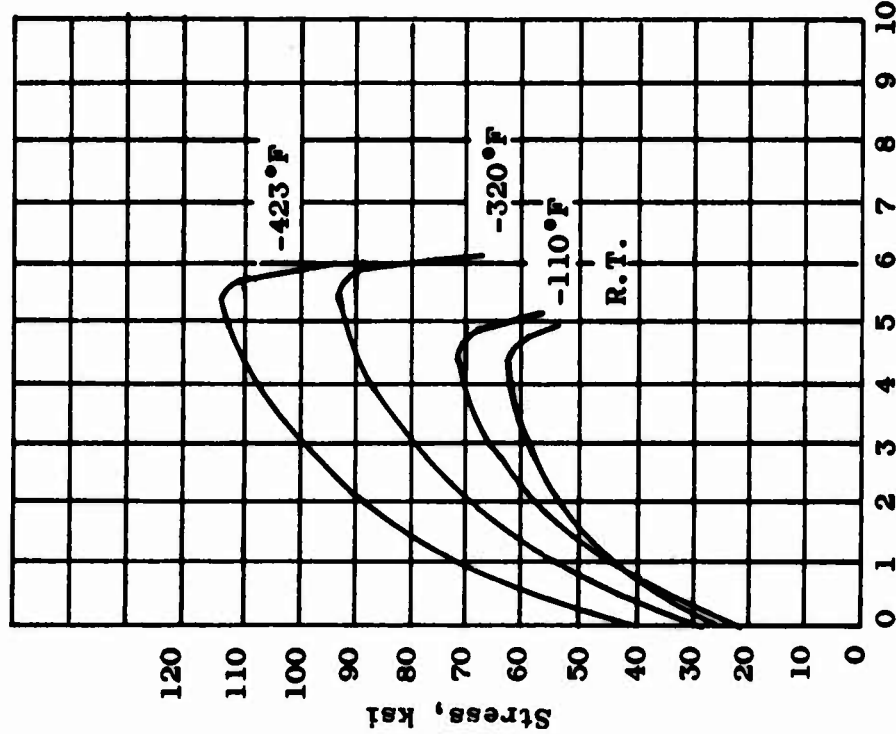
Figure 10. Predicted Post-Fire Injector Temperature Response with Thermal Accumulator

UNCLASSIFIED

UNCLASSIFIED

ANNEALED NICKEL 200

ANNEALED NICKEL 200



\*International  
Nickel Company

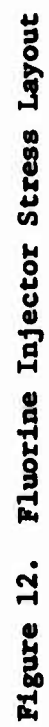
TEMP°F	F <sub>TU</sub>	F <sub>TY</sub> 2%	ELONG %	E (10 <sup>6</sup> )
R.T.	67	21.5	47	30
200	66.5	22.3	46	29.6
300	66.7	31.7	44.5	29.1
400	66.5	30.2	44.0	28.6
500	67.5	19.6	45	28
600	66.2	20.2	47.0	27.4
650	62.0	18.1	47.0	
700	52.5	17.0	61.5	26.9
800	44.0	16.5	65.0	26.2
900	37.0	15.0	66.0	25.6
1000	31.5	13.5	69.0	25.0
1100	26.5	11.5	72.0	24.3
1200	21.5	10.0	76.0	23.7
1400	14.0	7.0	89.0	

Figure 11. Structural Properties of Nickel 200

UNCLASSIFIED



**UNCLASSIFIED**



UNCLASSIFIED

only localized yielding would occur and under realistic load cycling conditions, some yielding was acceptable. Low cycle fatigue analysis indicated the injector could endure approximately 10,000 cycles as shown on Table V.

#### 6. Fabrication

It was anticipated that the accurate positioning of the drilled manifolds would require development of both tooling and tape controls for the numerically-programmed machine used for this drilling. An aluminum injector body was fabricated and used for this tooling checkout. After X-ray inspection showed that all of the drilled manifolds were correctly positioned, the drilling of the Nickel 200 blanks was undertaken. These nickel blanks proved difficult to drill despite nickel specimens having been previously drilled to evaluate the effects of drill feed and speed.

As a result of the delays encountered in drilling the nickel, the aluminum injector body used for the tooling checkout was completed as a test injector. Aluminum covers were made and the unit was used for test firings. This injector was designated as S/N T<sup>2</sup> ("Tool-Try Injector").

At the outset of the program, it was decided that rework would not be attempted on patterns in completed injectors. There was too high a risk of potential unpredictable effects upon stability and performance as a result of welding and redrilling orifices. However, the delays encountered in developing satisfactory drilling techniques for nickel altered this original decision and the pattern of injector S/N 2 was modified.

The following criteria were applied to all pattern modifications:

(a) Each orifice was separately welded closed. This precluded any weld from bridging a fuel orifice and an oxidizer orifice, which could have resulted in an inter-manifold leakage path if the weld were porous.

(b) Welds were not machined. In this way, the welded area remained clearly identified and would not be inadvertently drilled. Also, the thickness of the weld material was not reduced.

(c) The new orifices were located in unwelded areas apart from the old "welded" orifices to ensure that the entry condition for each new orifice was predictable.

(d) Injectors were back-flushed, water-flowed, and passivated following rework, all of which was necessary for fluorine service.

The effectiveness of these criteria is evident from the three modifications accomplished on injector S/N 2. This unit accumulated 846.6 sec of operation in 25 tests. Then, it was "loaned" to another program and tested four times for an additional 95.0 sec.

UNCLASSIFIED

TABLE V

LF /N<sub>2</sub>H<sub>4</sub> INJECTOR STRESS SUMMARY  
(Reference Figure No. 16)

14 Post Configuration

Plastic	A.	Flange-injector radius	$\sigma_1$ MAX = 42,415 psi @ 0°F max tensile
	B.	Oxidizer inlet radius	$\tau_1$ MAX = 16,900 psi @ 0°F max shear
	C.	Inside face oxidizer channel	$\sigma_1$ MAX = 38,713 psi @ 1000°F max compression
Elastic	A.	Flange-Injector radius	$\sigma_1$ MAX = 164,690 psi max tensile
	B.	Oxidizer inlet radius	$\tau_1$ MAX = 56,100 psi max shear
	C.	Inside face oxidizer channel	$\sigma_1$ MAX = 165,690 psi max compression

Low cycle fatigue analysis indicates that the injector can endure approximately 10,000 cycles.

Effective Strain and Stress (Based on Plastic Analysis)

A.	Flange-injector radius	$\epsilon = 0.061$ in./in. $\sigma_1$ EFF = 26,086 psi max tensile
B.	Oxidizer inlet radius	$\epsilon = 0.14597$ in./in. $\tau_1$ EFF = 33,683 psi max shear
C.	Inside face oxidizer channel	$\epsilon = 0.12419$ in./in. $\sigma_1$ EFF = 16,586 psi max compression

## B. UNCOOLED THRUST CHAMBERS

Uncooled steel thrust chambers were designed and fabricated to permit evaluation of injector performance, stability, and heat flux. Two types, with identical internal contours, were used during the test program. Phase II was directed toward the development of a high performing and inherently stable injector while Phase III was oriented toward evolving a high performing injector demonstrating dynamic stability. Therefore, a smooth wall chamber was used during Phase II while an acoustic resonator was incorporated into the design for Phase III.

1. Standard Design

The standard uncooled thrust chamber, shown on Figure No. 13, was designed with the same internal combustion chamber configuration as the prototype ablative chambers. This chamber had an expansion ratio of 1.65 and a divergent half-angle of 15-degrees. The combustion chamber-to-injector interface was a flanged and bolted joint which was the same as that used in the development of ablative combustion chambers. The injector-to-chamber joint was sealed with a silicone O-ring. The injector piloted into the chamber 1.5-in. to protect the forward end of the ablative chamber from hot gases. The uncooled thrust chambers were fabricated from mild steel rather than stainless steel because the mild steel offered a reduction in hardware cost as well as improved thermal characteristics. The units had provision for thermocouple pins, pulse-guns, and Photocon high-frequency pressure transducers.

The thermocouples were used to identify chamber thermal environment and the effect of film coolant variations. Five Photocon pressure transducers were appropriately located to permit the detection and identification of high-frequency instability. The pulse gun ports allowed the use of a pyrotechnic charge to perturbate the combustion process for an evaluation of resistance to instability.

A heat transfer analysis was conducted to determine the effect of chamber wall thickness material and test duration upon the gas-side and back-side wall temperatures. The results of this study are summarized on Figures No. 14 and 15. The data from this analysis served as the basis for selecting a mild steel chamber wall thickness of 0.75-in.

The small loads induced by the proof (150 psia) and leak pressures yielded a margin of safety much greater than two<sup>(1)</sup> because the uncooled combustion chamber wall thickness was selected upon the basis of heat transfer rather than stress. Although thermal stresses occurring during a test firing exceed the elastic limit of the mild steel, the life of the combustion chamber was predicted to be in excess of 9,000 short-duration, hot-firing test cycles.

---


$$(1) \text{ M.S.} = \frac{F_{TY}}{\sigma_1 (\text{Factor of Safety})} - 1 = 10$$

UNCLASSIFIED

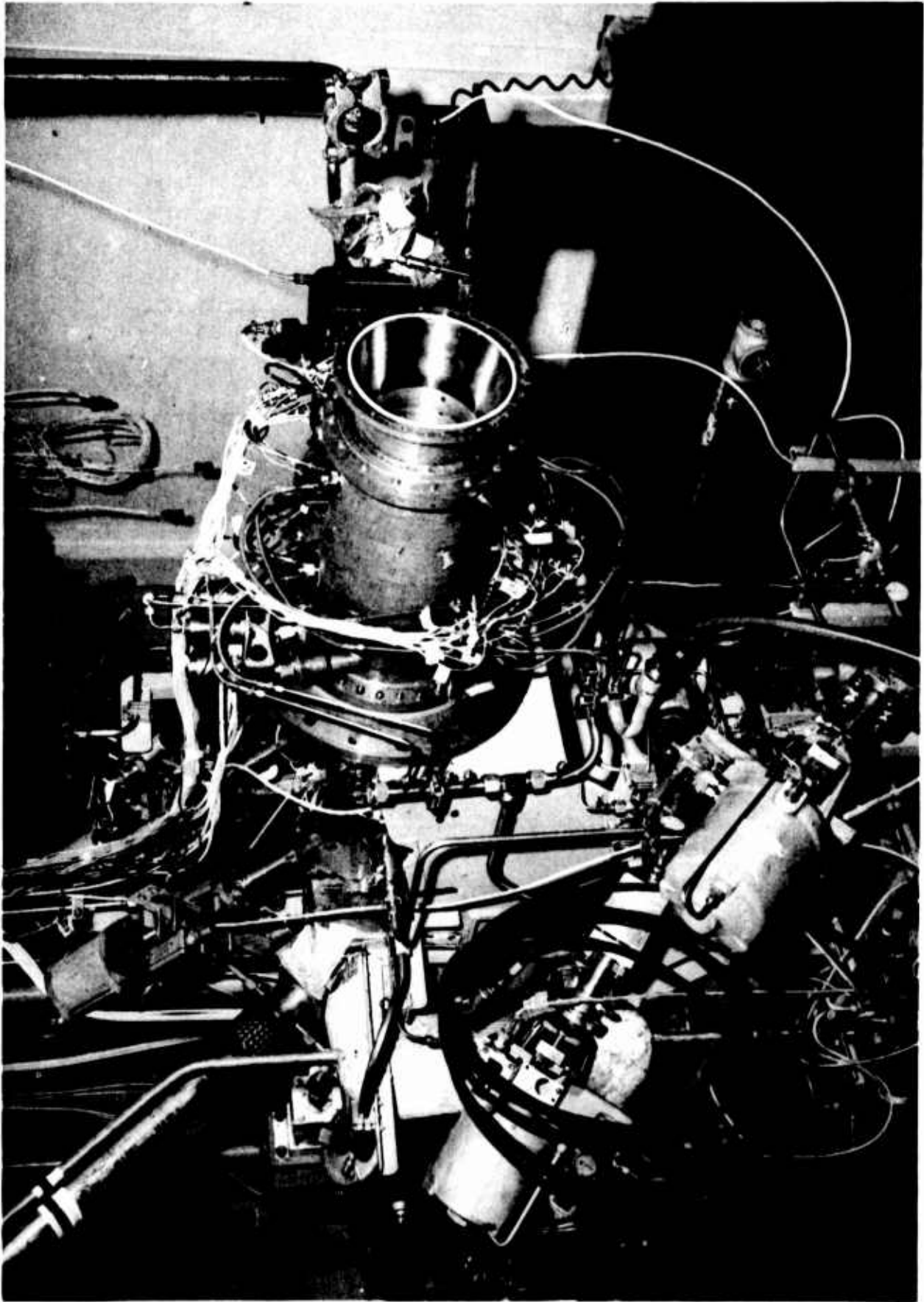


Figure 13. Standard Uncooled Steel Combustion Chamber Assembly

Page 33

UNCLASSIFIED

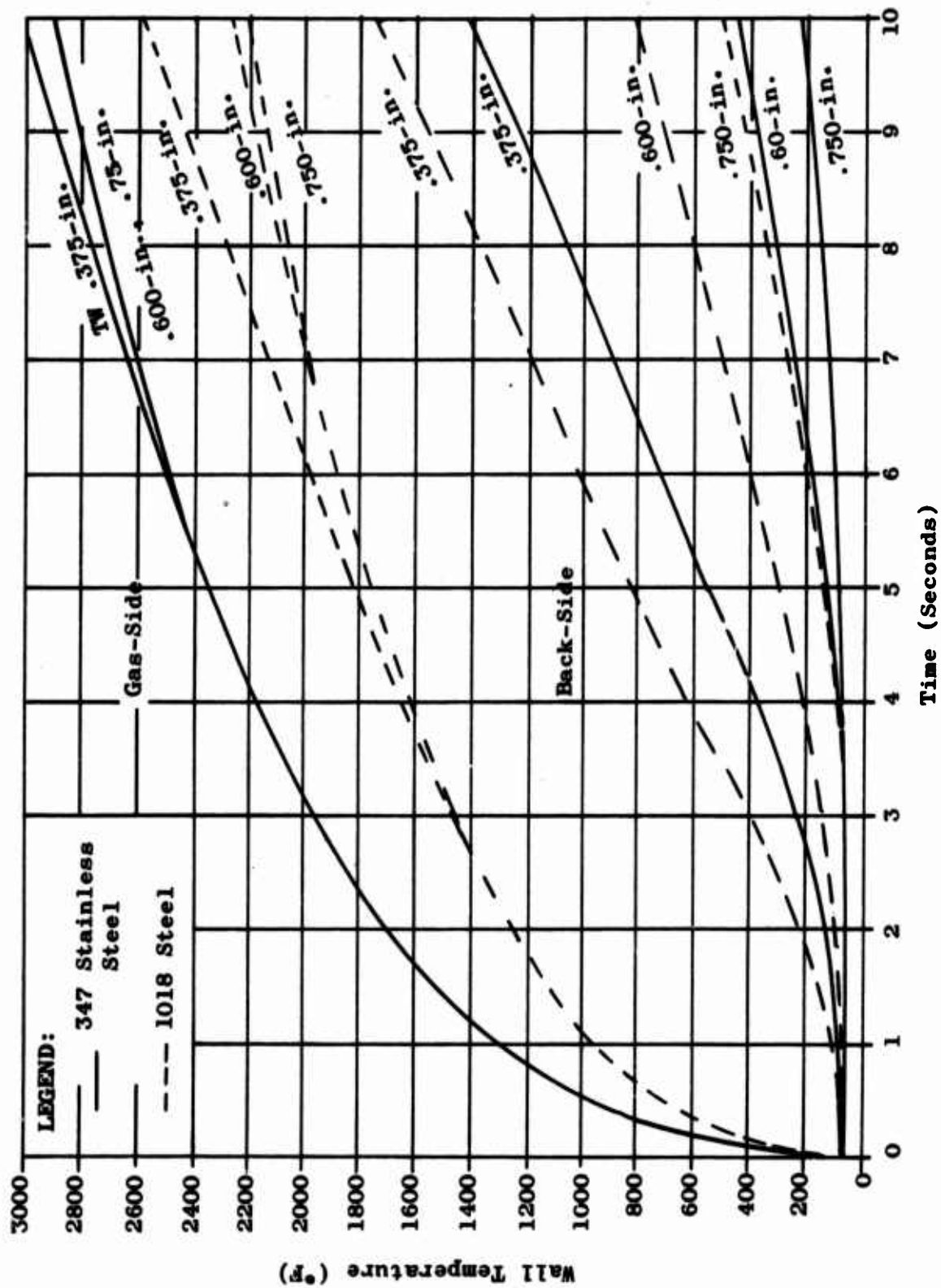


Figure 14. Temperature Profile Comparison of 1018 Steel and 347 Stainless Steel vs Various Wall Thicknesses at the Throat



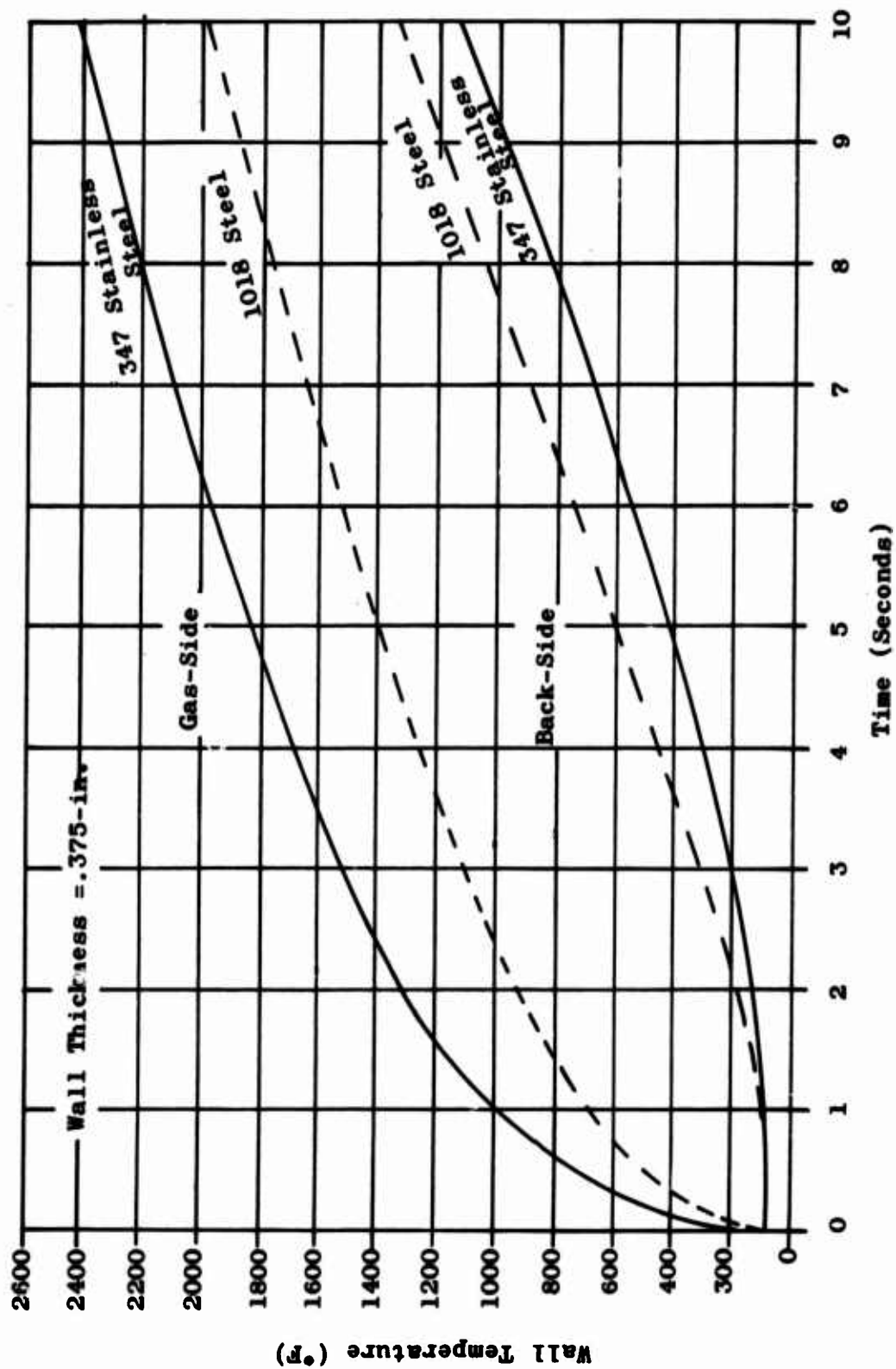


Figure 15. Temperature Transient Comparison between 347 Stainless Steel and 1018 Steel in the Chamber Region

## 2. Acoustic Resonator Design

The forward end of the thrust chamber design shown on Figure No. 13 was modified to incorporate a three-cavity, nine-row acoustic resonator, the design of which was based upon the information presented in Appendix II. This modified chamber design is shown on Figure No. 16.

Two photocon high-frequency pressure transducer bosses were located in the resonator cavity nearest the injector. These were in addition to the three bosses located at the start of the convergence section.

Obtaining resonator cavity gas temperatures was desirable to verify thermal predictions for the design of the acoustic resonators to be used in the ablative chambers. Two problem areas existed in measuring the temperature of the products of combustion in the resonating cavities. First, there was the anticipated operating temperature which would be in excess of 3000°F. Chromel-alumel thermocouples fail at approximately 2500°F. Secondly, there was the highly corrosive property of the fluorinated combustion product.

Two solutions were identified; either a tungsten/tungsten-rhenium thermocouple or an iridium/iridium rhodium thermocouple could be used. Although attacked by the combustion products, these thermocouples would be satisfactory for a single test of short or medium duration. With a gas temperature of 3500°F, the corrosion rate of the tungsten was approximately 2.5 mils/sec. The iridium/iridium rhodium thermocouples were made from more noble metals and therefore, would have a much lower corrosion rate resulting in a greater life expectancy.

The second approach was to place fusible wires, each having a different melting temperature, in the resonator cavities. Post-fire examination of these wires for evidence of melting would provide an approximation of the resonating cavity temperature. Three fusible wire materials were selected; one was a 300 series stainless steel having a melting point of approximately 2600°F while the other two were in the platinum family of noble metals. They were platinum which melts at 3224°F and rhodium which melts at 3571°F. One wire from each of the selected materials was mounted on the end of a 0.25-in. diameter stainless steel rod to form a temperature sensor, which was designed to fit into a standard thermocouple boss.

To permit verification of the fusible temperature sensor operation, provisions also were made for the installation of an iridium/iridium rhodium thermocouple in the same cavities as the temperature sensors.



UNCLASSIFIED

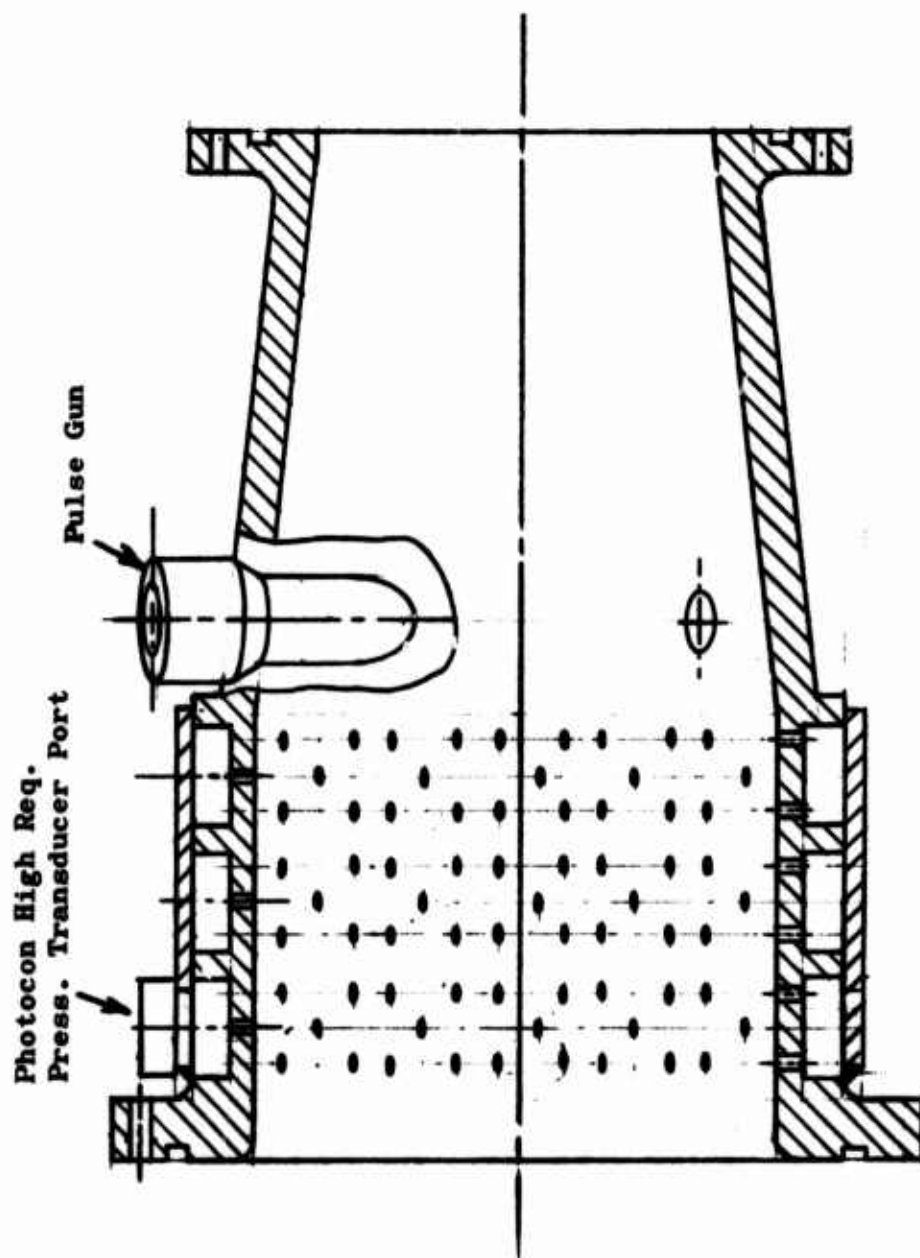


Figure 16. Acoustically-Damped Uncooled Steel Chamber

UNCLASSIFIED

## C. WATER-COOLED COMBUSTION CHAMBER ASSEMBLY

A water-cooled thrust chamber was designed for the evaluation of thrust chamber ablative materials, injector durability testing, and performance assessment.

It consisted of a water-cooled nozzle which matched either an ablative-lined or a graphite-lined cylindrical combustion chamber.

The materials evaluation and the injector durability testing were thought to require a thrust chamber less costly than an all-ablative unit which could be tested for durations of hundred of seconds. The graphite or ablative inserts would identify injector streaking. Their high gas-side wall temperatures would maximize injector heat load. The extended duration would ensure steady-state operation and verify the performance obtained with the uncooled steel units.

1. Description

## a. ATJ Graphite-Lined Thrust Chamber Assembly

The water-cooled combustion chamber assembly, which is shown on Figure No. 17, consisted of two major items; a water-cooled nozzle assembly and a water-cooled, cylindrical combustion chamber containing a graphite liner. The internal contour of the unit was the same as that of the uncooled steel and ablative thrust chambers. The exhaust nozzle expanded to a 1.65:1 area ratio with a nozzle half-angle of 15-degrees.

The water-cooled combustion chamber assembly was instrumented for coolant water temperatures and pressures.

The water-cooled nozzle assembly consisted of a housing, a nickel nozzle, and a split aluminum shroud which directed coolant flow over the nickel nozzle at the required velocities. The nickel nozzle was designed for easy replacement.

The water-cooled, cylindrical combustion chamber assembly consisted of an external housing and nickel sleeve which contained a graphite insert. The housing and graphite liner shell were the boundaries of a water coolant circuit designed to protect the housing from the residual heat of the graphite. The unit was designed for easy replacement of the graphite liner.

Thermal design of the coolant circuits of the throat region and chamber section ensured that the nickel wall temperature did not exceed 1000°F and that burnout heat flux ratios were less than 0.5.

UNCLASSIFIED

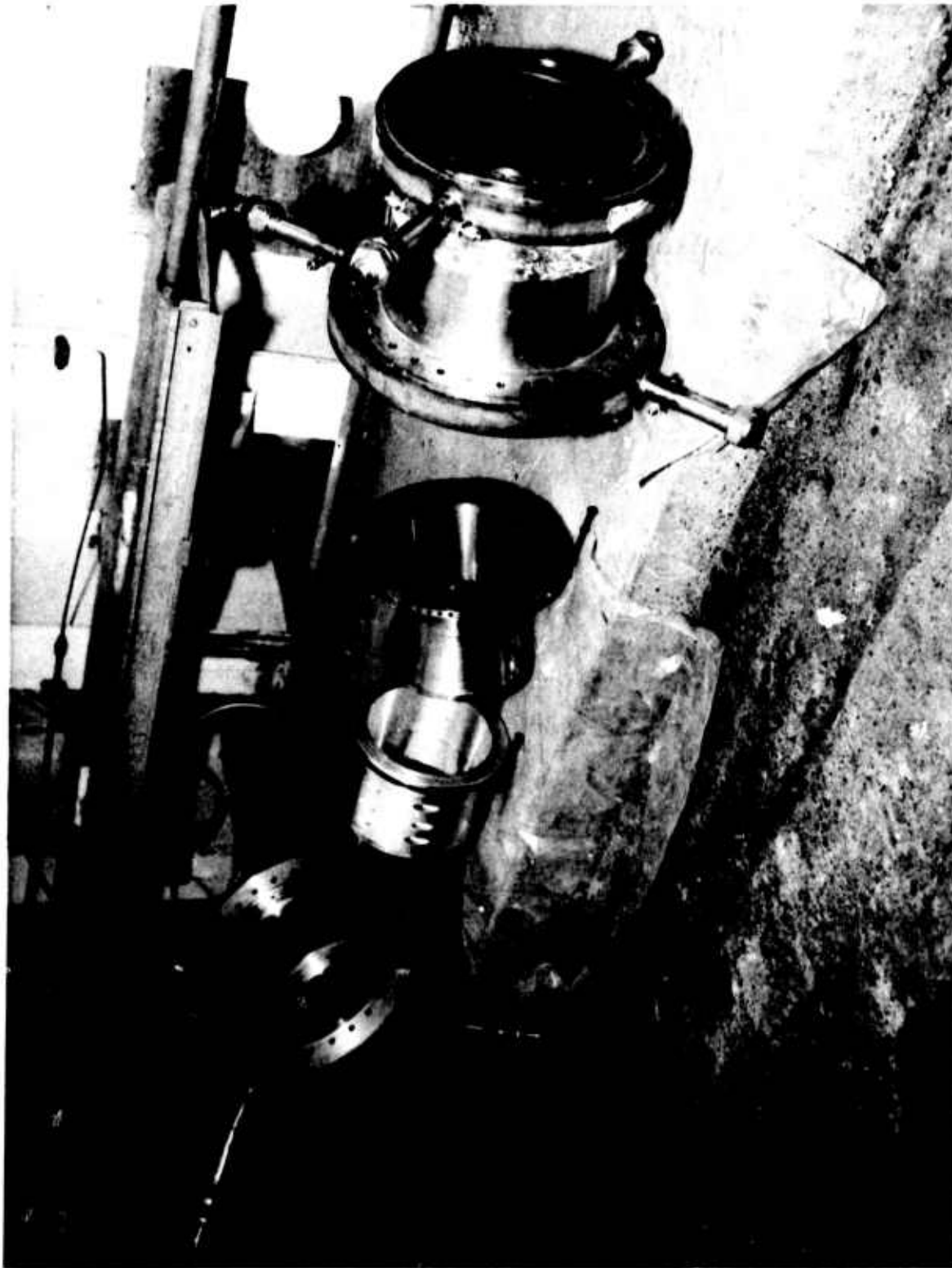


Figure 17. Water-Cooled Combustion Chamber Assembly

UNCLASSIFIED

## (1) Throat Region

A 0.150-in. thick nickel wall, a water velocity of 50 ft/sec, a bulk temperature of 100°F, and water pressure of 250 psia were selected as reasonable values for the throat region. These values served as the basis for wall temperatures, heat fluxes, and burnout heat fluxes which were calculated and found to meet the desired limits. Predictions of the bulk temperature rise, coolant flow rates, and pressure are summarized in Table VI.

TABLE VI

## THERMAL ANALYSIS OF THE WATER-COOLED NICKEL NOZZLE

Gas-Side Wall Temperature	840°F
Liquid-Side Wall Temperature	200°F
Heat Flux ( $\phi$ )	2.9 Btu/in. <sup>2</sup> sec
Burnout Heat Flux Ratio ( $\phi/\phi_{BO}$ )	0.20 Btu/in. <sup>2</sup> sec*
Estimated Bulk Temperature Rise	20°F
Coolant Water Flow Rate Requirement	45 lb/sec
Estimated Maximum Pressure Drop	70 psi**
Recommended Inlet Pressure	>300 psia

\* $V_1 = 50$  ft/sec,  $P = 250$  psia,  $T_B = (100 + 20)$  °F

\*\*Includes 40 psi for exit and entrance losses.

## (2) Chamber Section

The ATJ graphite liner in the chamber section had a minimum thickness of 0.86-in. to provide surface temperatures near the injector which were similar to those expected in the ablative chambers. It was contained in a 0.150-in. nickel sleeve and the flow passage was a continuous spiral channel having approximate dimensions of 0.75-in. wide by 0.25-in. deep and 16-ft long. Water pressure was 250 psia and velocity 37.5 ft/sec. Operating parameters are presented in Table VII.

TABLE VII

## THERMAL CONDITIONS FOR THE WATER-COOLED CHAMBER SECTION

Liner Wall Temperature (one-inch)	2400°F
Maximum Nickel Temperature	680°F
Heat Flux ( $\phi$ )	1.4 Btu/in. <sup>2</sup> sec
Burnout Heat Flux ( $\phi_{BO}$ )	7.4 Btu/in. <sup>2</sup> sec*
Burnout Heat Flux Ratio ( $\phi/\phi_{BO}$ )	0.19
Estimated Bulk Temperature Rise	145°F
Coolant Water Requirement	3 lb/sec
Estimated Pressure Drop	120 psi**
Recommended Inlet Pressure	350 psia

\*V<sub>1</sub> = 37.5 ft/sec, P = 250 psia, T<sub>B</sub> = (100 + 145) °F

\*\*Includes 25 psi for exit and entrance losses.

## (3) Structural Analysis

The stress analysis of the water-cooled combustion zone assembly indicated that the chamber housing would have a 1.73 margin of safety at proof pressures<sup>(2)</sup>. The liner assembly consisted of a graphite liner contained in a cooled, nickel sleeve with a clearance ranging from 0.001-in. to 0.004-in. Neglecting the rigidity supplied by the graphite liner, the cooled stainless steel retaining sleeve was marginal with respect to buckling stability at coolant jacket proof pressures. An analysis was conducted to determine the stresses in the graphite liner and the steel sleeve during steady-state operation. Based upon the most adverse condition of zero clearance between the graphite and the sleeve, there would be a 15,000 psi tension load in the steel sleeve and a 250 psi compression load in the graphite during operation.

---

(2) Margin of Safety is defined as:  $M.S. = \frac{F_{TY}}{\sigma_1 \times FS} - 1$

A margin of safety of zero represents an adequate structural design.

Nickel was selected for the cooled nozzle in preference to stainless steel or aluminum because of its strength at high temperature and its high thermal conductivity. A stress analysis of the nickel nozzle indicated that it would not have collapsed under the proof pressure conditions or under shutdown conditions at the conclusion of a hot firing. This analysis showed the nozzle to have a 0.42 margin of safety at shutdown. High thermal stresses were predicted in the nozzle during firing. Actual testing showed some dimensional distortion which did not affect the unit's operation.

b. Composite Ablative-Lined Combustion Chamber Assembly

The ablative chamber section of the water-cooled thrust chamber assembly was interchangeable with the water-cooled ATJ graphite lined unit. It consisted of an ablative liner contained in an uncooled mild steel case. This unit matched the water-cooled nickel nozzle. The ablative lined chamber shown on Figure No. 18 was used to evaluate liner materials and injector chamber compatibility. It incorporated four thermocouples of the type used on the ablative thrust chambers. Two thermocouple locations were at the silica phenolic/graphite phenolic material interface while the other two were positioned at the steel/silica phenolic interface. This ablative-lined unit was intended to permit test evaluations that would be comparable with those obtained using the all-ablative chambers.

Thermocouple probes were designed to provide accurate char depth versus time data for the ablative chambers. They were developed and verified with the ablative combustion chamber liners prior to their installation into the all-ablative chambers.

Two combustion chamber liner designs were prepared to provide data for the later Phase II ablative chambers. One had an all-ablative liner while the other had a full-length fibrous graphite liner backed by ablative. The design shown on Figure No. 18 had a two-component wall consisting of graphite fabric-reinforced phenolic, FM 5064, which was backed with a silica fabric-reinforced phenolic, FM 5067. The FM 5064, was tape-wrapped at a 45-degree-to-centerline angle while the FM 5067 was oriented parallel to the centerline (flat wrapped). Two full-length FM 5064 liners were fabricated with one having a nominal resin content of 36% while the other had a 30% content. These liners were cut into four, 180-degree semi-cylinders and interchanged to form a bi-component, cylindrical, segmented liner. Bonding was accomplished using RTV 60 silicone rubber which was initially used successfully in the segmented liner joints of a segmented, multiple ablative chamber<sup>(3)</sup> in another program<sup>(4)</sup>.

(3) P/N 708208-29, S/N 028

(4) Contract AF 04(611)-9366, "Ablative Materials Evaluation in a Fluorinated Oxidizer Environment," September 1965

UNCLASSIFIED

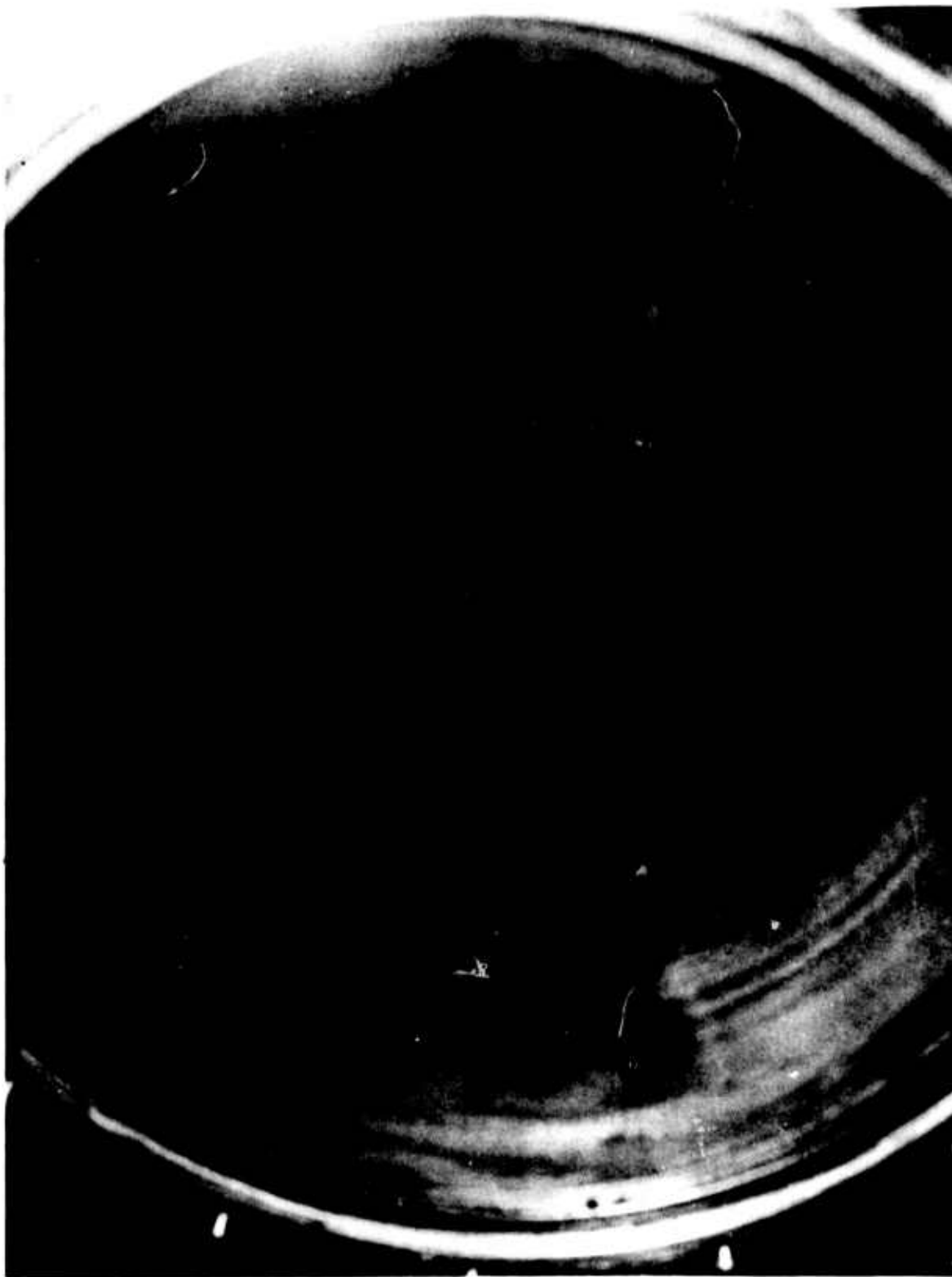


Figure 18. Ablative-Lined Chamber Section

UNCLASSIFIED



A grid of 0.067-in. diameter radial holes on 0.5-in. centers was drilled through 180-degrees (including 90-degrees of each cylindrical segment) of the reassembled liner (see Figure No. 19). The FM 5067 insulation then was wrapped over the FM 5064 with special care taken to assure that resin did not plug the drilled holes.

Thus, test firings would show if the combustion gas environment had an effect upon the silica fabric-reinforced phenolic as well as serve to establish the design criteria for ablative chambers. Testing also would permit the effect of resin content variation in the ablative liner material, FM 5064, to be ascertained. Test evaluation in another program<sup>(5)</sup> was accomplished using FM 5064 and other liner materials. Analysis of the results indicated that a resin content of 30% produced less shrinkage, lower expansion, and a higher density char. The segmented chamber design was expected to provide further data.

The second ablative liner concept was intended to anticipate the design of a full ablative thrust chamber. This unit incorporated fibrous graphite as a full-length gas-side liner. The disposition of the pyrolysis gases resulting from the ablative insulation materials was accommodated by providing escape paths for the gases. Small holes were drilled over the entire liner surface. In this design, the 0.067-in. diameter holes were drilled through the fibrous graphite material and spaced at 0.5-in. intervals over 180-degrees of the liner surface. This provided for a direct comparison to be made of the possible and actual escape paths of the pyrolysis gases.

## 2. Fabrication

The water-cooled assembly, with both the water-cooled ATJ graphite-lined chamber section and the uncooled composite ablative-lined chamber section, was fabricated without incident. In addition, a spare nozzle liner with its shroud was manufactured along with two spare ATJ graphite liners.

Two segmented ablative chamber liners, like that shown on Figure No. 18 were fabricated. One ablative section was assembled in the steel case and instrumented while the other was held as a spare. The spare was not tested.

Fabrication of the second uncooled combustion chamber design, which had a full length AGCarb-101 liner, was not completed because of a change in test program requirements. The material was subsequently used to make the acoustic resonator liner which was incorporated in the S/N 001 ablative thrust chamber tested during Phase III of the program.

(5) Contract AF 04(611)-10933, "Evaluation of Characteristics Affecting Attainment of Optimum Properties of Ablative Nozzle Components," 1966-1967

CONFIDENTIAL

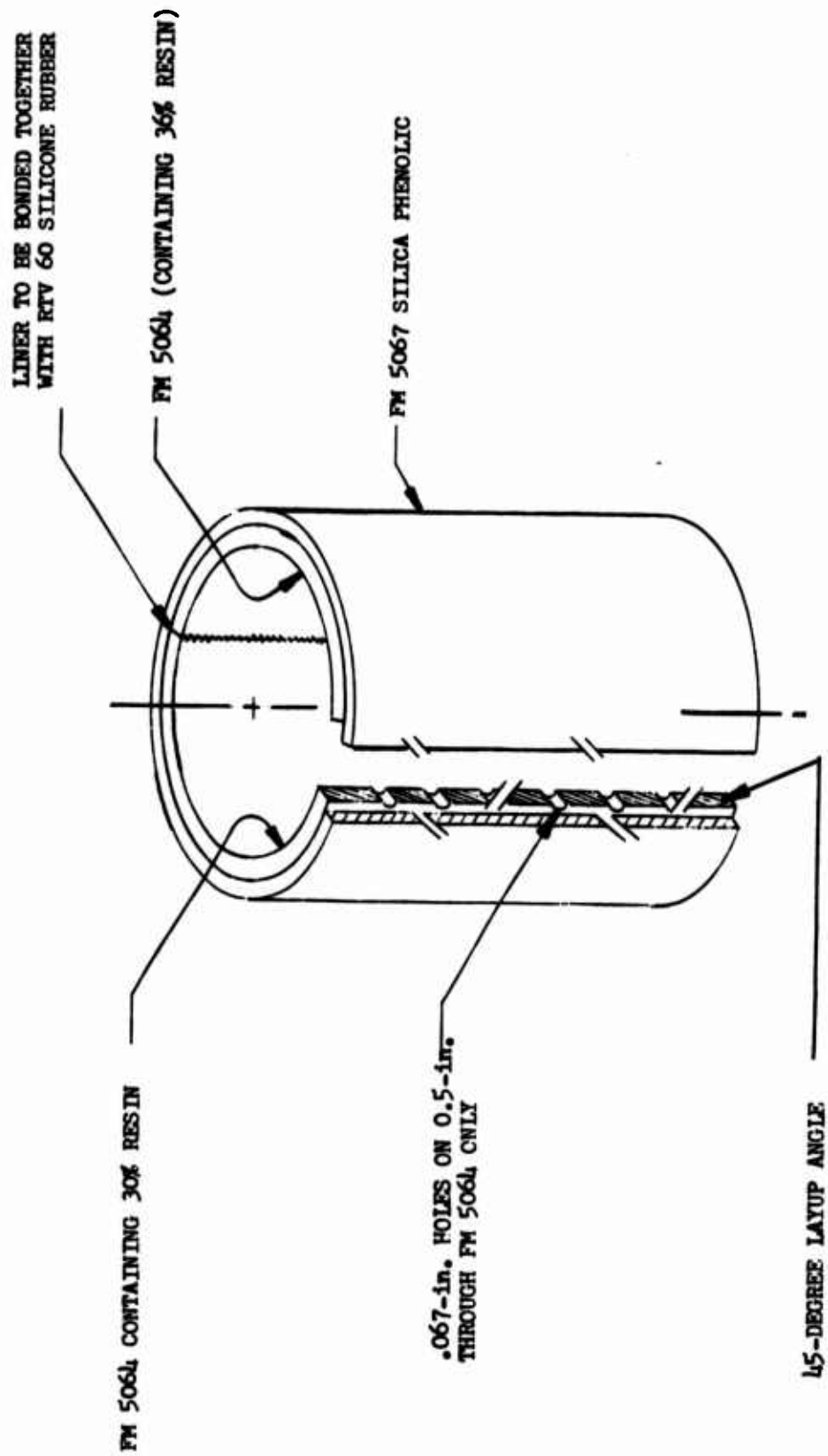


Figure 19. Segmented Liner Concept

CONFIDENTIAL

(This Page is Unclassified)

D. ABLATIVE THRUST CHAMBERS

(U) At the inception of the program, it was considered that satisfactory thrust chamber erosion characteristics would be obtained by controlling the boundary layer mixture ratio and using either a bulk graphite or a fibrous graphite composite (i.e., AGCarb-101) at the throat. The gas dynamic forces, which cause physical erosion (surface ablation), would be resisted by high shear strength, high density graphite char and pre-pyrolized graphites at the gas-side interface. The basic graphite materials had very good structural properties; therefore, the mechanical design of the ablative thrust chamber primarily was concerned with providing for the different thermal growths of the various structural elements.

(U) Evolving a chamber that was thermally optimum was more difficult. Graphite is a good thermal conductor and consequently, a poor thermal insulator, except when in one of its structurally weaker, anisotropic forms (e.g., pyrolytic and Grafoil). This necessitated a trade-off between thickness and the material selection to limit the external surface temperature to 600°F while maintaining a realistic wall thickness as well as structural adequacy. This study constituted a major portion of the ablative thrust chamber design effort.

(C) The program specified that two thrust chamber designs would be evaluated. These thrust chambers were required to retain structural integrity for an accumulated duration of 600 sec, which included five restarts. Acceptable throat erosion was calculated to allow a 14% increase in throat diameter. Any further erosion would result in exceeding the maximum thrust level. The outer surface temperature of the chamber was restricted to a maximum of 600°F.

(U) In summary, structural integrity, erosion resistance, and skin temperature control were the three basic requirements for the ablative thrust chamber design. Of the three, skin temperature proved to be the most restrictive to the design.

1. Material Selection

(U) The selection of thrust chamber materials was based upon data obtained from a comprehensive literature search and from the results of materials evaluation programs previously conducted by Aerojet-General (6), (7), (8). Carbon phenolic, graphite phenolic, and fibrous graphite materials were used in these programs to construct 3750 lb (sea-level) thrust chambers. These

(6) Contract AF 04(611)-9366, op.cit.

(7) Contract AF 04(611)-10918, "Fluorinated Oxidizers, Combustion Chamber Materials Evaluation," January 1967

(8) Aerojet-General IR&D, "Advanced Transtage Fluorine Feasibility Program," 1964

chambers were tested using fluorine and hydrazine blend propellants. Testing was accomplished at 100 psia chamber pressure<sup>(9)</sup> and 200 psia chamber pressure<sup>(10)</sup>. In all, 17 carbon and graphite materials were evaluated.

a. Selection Criteria

The following was the criteria used to select candidate liner materials:

- (1) Resistance to chemical attack by  $F_2$  and HF
- (2) Ability to withstand high temperatures
- (3) Dimensional and chemical stability
- (4) Thermal shock resistance
- (5) Low thermal conductivity
- (6) Ease of fabrication
- (7) Cost and availability

In the evaluation of the carbon and graphite materials, the most suitable materials were identified as a graphite phenolic ablative system, FM 5064, and a fibrous, pre-pyrolized, graphite composite, assigned the Aerojet-General designation of AGCarb-101. This composite is made from a graphite fabric-reinforced phenolic, FM 5228, which has been carbonized, graphitized, re-impregnated with a high coking pitch, and regraphitized.

Data showed that the graphite fabric-reinforced phenolic, FM 5064, could satisfy all of the requirements except dimensional stability at the throat region. Figure No. 20 shows an FM 5064 ablative chamber tested in an earlier materials evaluation<sup>(11)</sup>. It was operated at a chamber pressure of 200 psia producing a sea-level thrust of 3750 lb. A total test duration of 350 sec was accumulated. The throat area was badly eroded after the last test, but the cylindrical section indicated adequate durability. This data led to the conclusion that a hard, non-ablative material should be used in the throat area.

The FM 5064 material was selected as the chamber flame liner for Thrust Chamber Design No. 1. This design was applied to two units, which were fabricated using FM 5064 as an ablative liner in the chamber section. One, S/N 001, had an exit area ratio of 1.65:1 while the other, S/N 002, had an exit area ratio of 7.5:1.

Other graphite fabric-reinforced phenolics were reviewed which exhibited physical properties comparable to those of FM 5064 while being less costly. One of these was WB 8207, which had appeared satisfactory in an earlier materials evaluation program. However, it had a limited

(9) Contract AF 04(611)-9366, op. cit.

(10) Contract AF 04(611)-10918, op. cit.

(11) Fluorinated Oxidizer Thrust Chamber Materials Evaluation Program, Phase II, Contract AF 04(611)-10918, Report AFRPL-TR-66-322, 1966



Figure 20. FM 5064 Ablative Thrust Chamber Showing Badly-Eroded Throat Region (LF<sub>2</sub>/N<sub>2</sub> Blend Propellants)



test history and was eliminated from consideration as a flame liner in the chamber section. WB8207 was used as the nozzle ablative liner material because the nozzle section does not experience as severe an environment nor is it as critical to the structural integrity of the thrust as the upstream chamber section. This use of the WB8207 permitted test evaluation of an alternative and lower cost ablative liner material.

The AGCarb-101 fibrous graphite material which was selected for the throat region does not have as extensive a test history as FM 5064; however, in one thrust chamber application<sup>(12)</sup>, it demonstrated adequate structural strength as well as an erosion resistance that was superior to any other material evaluated except for the high-density bulk graphites (i.e., ATJ). In considering thermal shock sensitivity, like most composite structures, AGCarb-101 was capable of forgiving some degree of plastic strain. Therefore, it was judged to be superior to the bulk graphites. An AGCarb-101 thrust chamber tested in a previous program had been subjected to six firings using the LF<sub>2</sub>/hydrazine blend propellants. These firings resulted in an accumulated duration of 255 sec. The chamber pressure was 100 psia and the vacuum equivalent thrust was 8000 lb. The AGCarb-101 liner was free-standing and radiation-cooled from a station one-third of the way down the chamber to the exit plane (see Figure No. 21). The unit was subjected to hot starts as well as a single 150 sec test and it performed exceptionally well. After the test series, the throat radius had increased approximately 0.05-in. There was no ply delamination although the injector end of the chamber sustained some localized, streak-type erosion.

Based upon this experience AGCarb-101 was selected as the flame liner material in both Thrust Chamber Designs No. 1 and No. 2. In one application, it was used as a throat insert while in the second application, it was used as a full-length liner.

Any one of a number of carbon and silica fabric-reinforced phenolics would have been suitable pyrolyzing insulators. Carbon phenolics have a higher thermal conductivity and are satisfactory for high temperature use (i.e., insulators in contact with the flame liner). Silica phenolics have a lower conductivity but melt when exposed to temperatures in excess of 3000°F. Therefore, a two-component insulation was used. Carbon fabric-reinforced phenolic, WB8217, was selected as the high temperature insulation behind the FM 5064 ablative liner in Thrust Chamber Design No. 1, in which the throat insert was used. Silica fabric-reinforced phenolic, WB2230, was selected as the low temperature insulator.

Graphite fabric-reinforced phenolic, WB8207 rather than carbon phenolic was selected as the insulation in contact with the AGCarb-101 throat insert because it offered better dimensional stability at high temperatures even though its thermal conductivity was higher. The AGCarb-101 throat insert was mechanically locked to the backup material.

(12) Contract AF 04(611)-10918, op. cit.

UNCLASSIFIED

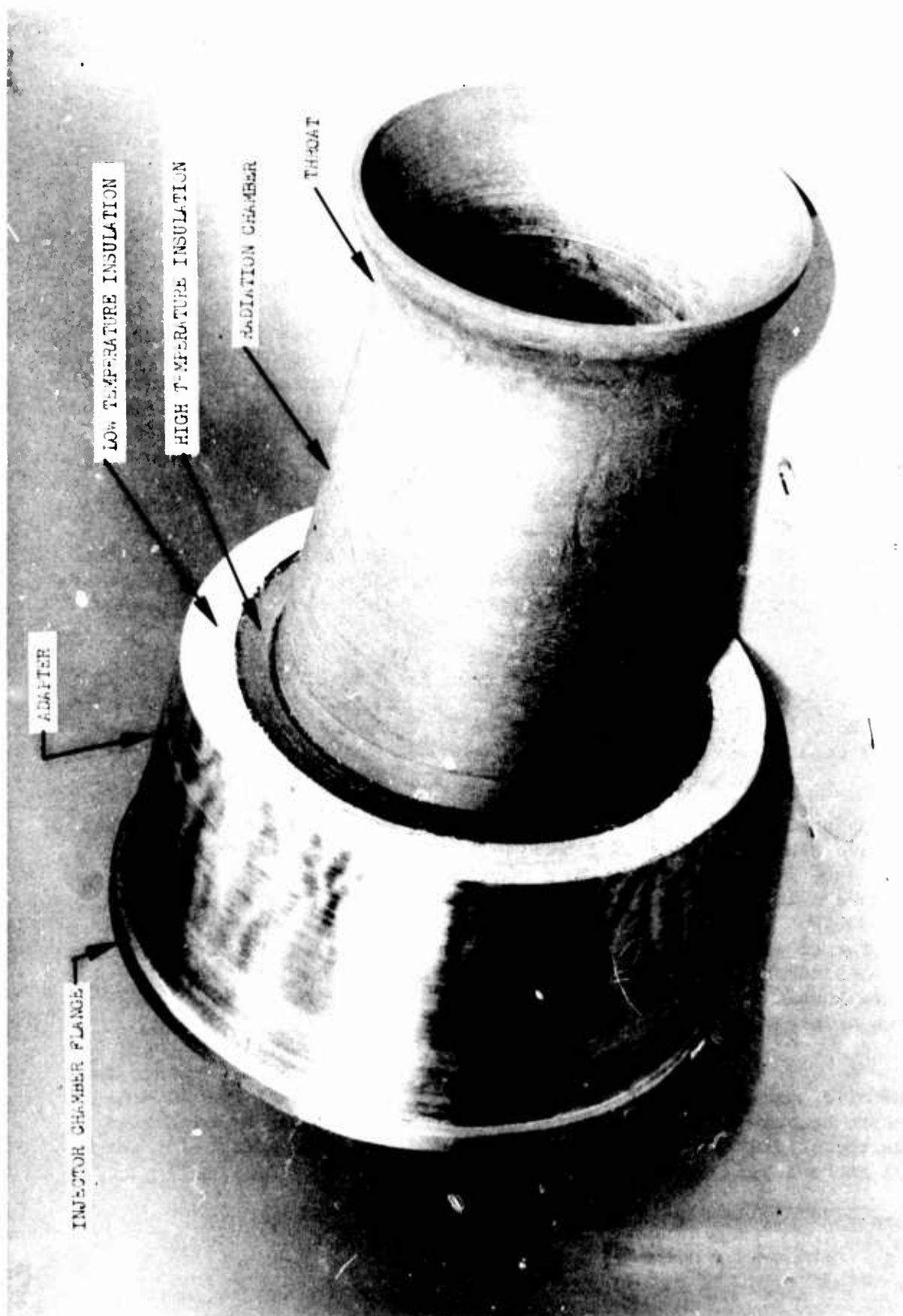


Figure 21. 8000 lb Thrust Radiation-Cooled AGCarb-101 Thrust Chamber  
(P/N 1129696)

UNCLASSIFIED



UNCLASSIFIED

The second thrust chamber design, which incorporated a full-length AGCarb-101 flame liner, also had a two-component insulation system. Material selection again was within the carbon and silica fabric-reinforced phenolic families. However, the specific materials selected differed from those of the first design because of a desire to increase the options for future material selections. Carbon fabric-reinforced phenolic, FM 5072, and silica fabric-reinforced phenolic, FM 5067, were picked for use in the high and low temperature zones, respectively.

A fiberglass structural shell was used in the number one design. This shell was attached to a low carbon steel flange at the forward end of the chamber. The second design had a full-length low carbon steel case rather than fiberglass.

The properties of the selected ablative chamber materials are listed on Table VIII.

b. Material Controls

The material properties information and recommendations from the previously conducted program<sup>(13)</sup> served as the basis for selecting the FM 5064 as well as the basic material for AGCarb-101 (FM 5228). Fabrication and material controls are further defined in Appendix IV.

All of the ablative chamber components were fabricated so that they were at least 1-1/4-in. longer than specified by the design. This excess provided control samples for laboratory evaluations as well as for the analyses of the performance variations exhibited by the completed chamber.

2. Thrust Chamber Descriptions

a. Thrust Chamber Design No. 1

This design incorporated the throat inserts and two thrust chambers were fabricated (S/N 001 and S/N 002). The chamber design is shown on Figure No. 22. The S/N 002 chamber had an exit area ratio of 7.5:1, which was reduced to 1.65:1 in the S/N 1 chamber by eliminating the ablative portion downstream of the throat insert. The description which follows is applicable to both S/N 001 and S/N 002 chambers because thermal conditions were identical and the loads were similar.

---

(13) Contract AF 04(611)-10933, op. cit.

UNCLASSIFIED

UNCLASSIFIED

TABLE VIII

## PROPERTIES OF SELECTED ABLATIVE CHAMBER MATERIALS

Physical Property*	Graphite Phenolic		Carbon Phenolic		Silica Phenolic		AGCarb-101***
	FM5064	WB8207	WB8217	FM5072	WB2230	FM5067	
Tensile Strength, psi	12,500	18,000	18,000	15,000	12,000	14,000	11,000
Tensile Modulus, $\times 10^{-6}$	3.24	2.0	2.0	2.5	2.3	2.3	1.8
Compressive Strength, psi	16,400	17,000	27,000	23,000	16,000	N/A	10,000
Compressive Strength Mod., $\times 10^{-6}$	2.24	1.7	2.0	2.6	1.2	N/A	N/A
Flexural Strength, psi	23,900	23,000	35,000	30,000	27,000	20,000	14,000
Flexural Modulus, $\times 10^{-6}$	2.02	1.95	2.9	2.2	2.9	2.6	N/A
Thermal Expansion Coefficient, in./in./°F 45° layup (max) R.T. to 300°F	5.0	4.7	6.0	3.2	5.0**	N/A	0.8
Thermal Conductivity at R.T. flatwise, Btu-in./ft <sup>2</sup> hr-°F	7.0	5.8	3.3	3.5	2.7	2.38	16.0
Compressive Strength-Flatwise, psi	49,000	N/A	42,000	N/A	N/A	52,000	N/A
Compressive Modulus, $\times 10^{-6}$	1.59	N/A	1.2	N/A	N/A	2.3	N/A
Interlaminar Shear Strength, psi	2000	1800	2000	1800	1800	1500	750
Specific Heat, Btu/lbm-°F	0.25	0.25	0.25	0.23	0.25	0.25	0.17
Specific Gravity	1.45	1.41	1.42	1.40	1.71	1.76	1.40

\*Room Temperature Unless Noted

\*\*Normal to Plys.

\*\*\*With the Plys.

UNCLASSIFIED

CONFIDENTIAL

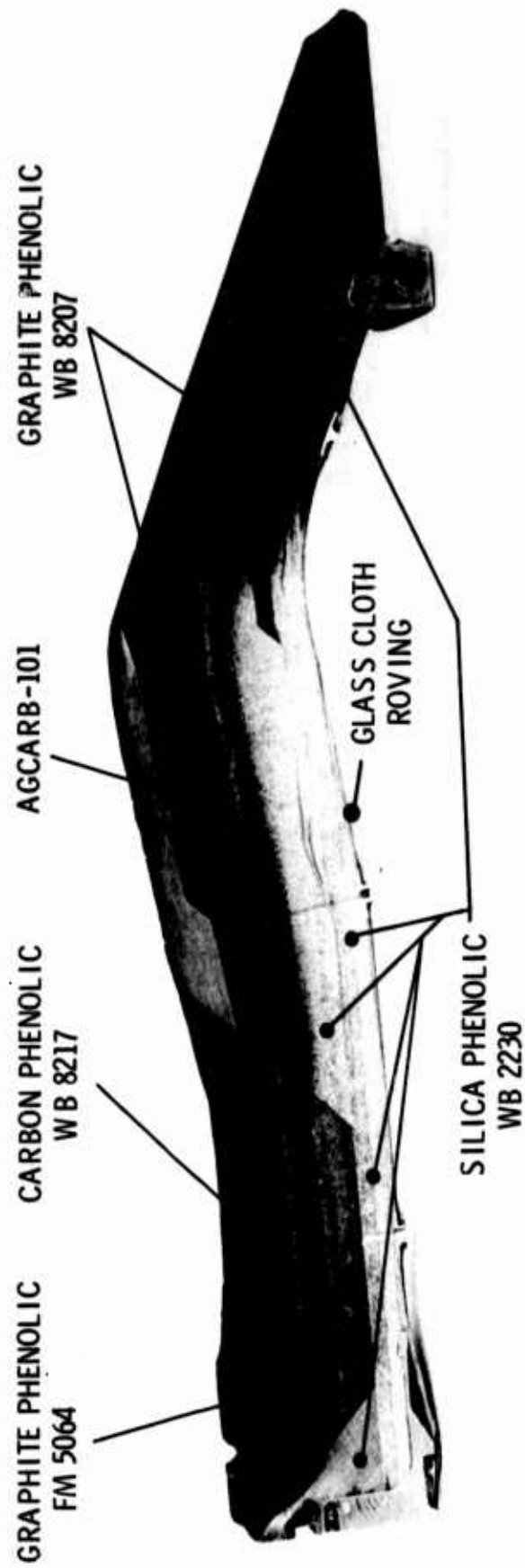


Figure 22. S/N 001 and S/N 002 Ablative Thrust Chambers

CONFIDENTIAL

# CONFIDENTIAL

(U) A three-component liner consisting of graphite phenolic (FM 5064) forward of the throat, fibrous graphite (AGCarb-101) at the throat and graphite phenolic (WB8207) downstream of the throat was utilized in the basic design. The forward flange and structural overwrap technology developed for the Block II Apollo Service Propulsion System ablative combustion chamber was applied, which assured that the structural integrity of the flange and shell were based upon a demonstrated design. The aft flange design was the same as that used for the Transtage ablative thrust chamber design.

(U) The throat insert region was a three-component, radially-stacked structure, wherein both pyrolyzing and non-pyrolyzing materials were used. At the outset it was thought that all materials backing the insert should be non-pyrolyzing to avoid gas entrapment behind the AGCarb-101 material, which had low permeability. However, subsequent analysis indicated that low permeability did not preclude "transpiration" of the pyrolysis gases and that the structural properties of the low conductivity non-pyrolyzing materials might not be adequate. Therefore, a satisfactory and probably superior thermal design of lower cost was achieved with a pyrolyzing backup to the AGCarb-101 liner. During Phase I, the study effort was directed toward the non-pyrolyzing configuration; but the elements of the analysis which are presented in the Phase I Report were equally applicable to the final design selected.

(U) Graphite, fabric-reinforced phenolic (WB8207) and silica fabric-reinforced phenolic (WB2230) were selected as high and low temperature backup insulators, to the AGCarb-101 insert. The location of the interface between the graphite fabric-reinforced phenolic and the silica fabric-reinforced phenolic at the plane of the throat was determined to be the point at which the maximum temperature was approximately 2500°F during steady-state operation.

(U) Structural integrity for the insert structure was provided by using an 8-degree taper to mechanically lock the components to each other. In addition, the forward end of the AGCarb-101 insert contained a step thickness increase with ensured axial rigidity. The low temperature silica phenolic insulation also contained a large radius step function which was overwrapped with additional silica fabric-reinforced phenolic, thereby assuring the integrity of the entire throat insert assembly.

(C) It was calculated that engine thrust would remain within specification if the throat diameter increase did not exceed 1.0-in. Therefore, the AGCarb-101 liner thickness at the throat was established at 0.6-in.

(U) The AGCarb-101 material used for the throat insert duplicated, as closely as fabrication techniques would permit, the lay-up angle (12-degrees to the chamber centerline) and graphitization cycle used in the successful radiation cooled chamber (P/N 1129696) shown in Figure No. 21(14).

(14) Report AFRPL-TR-66-322, op. cit.

# CONFIDENTIAL

# UNCLASSIFIED

The FM 5064, ablative liner, located forward of the throat insert (see Figure No. 23) was 1.46-in. thick. This thickness, coupled with the 45-degree to centerline ply orientation, was the maximum diameter that could be reliably tape wrapped. Compression molding using cut patterns was considered but abandoned because of cost considerations.

As shown on Figure No. 22, the insulation behind the FM 5064 liner was a two-component composite. Both of these insulation layers were oriented parallel to the flame surface to make maximum use of their insulative qualities. The inner and higher temperature layer (1.54-in. thick) was of carbon fabric-reinforced phenolic, WB8217, while the outer layer was silica fabric-reinforced phenolic, WB2230. The total insulation thickness was 2.4-in.

The ablative liner in the divergent nozzle section was tape wrapped graphite phenolic, WB8207. Ply orientation was 45-degrees to the flame surface and structural integrity was attained by mechanically locking the liner to the silica fabric-reinforced phenolic overwrap.

The use of the two component insulation concept was selected upon the basis of the 3000°F temperature limitation of silica and previous testing experience, wherein the vulnerability of silica-fabric phenolic insulation in contact with the fluorinated exhaust environment was demonstrated. The outer silica phenolic, WB2230, which extended as a continuous layer over the thrust chamber length also served as a structural tie for the three-liner components.

The fiberglass-structural shell was a high temperature, bi-directional composite that was approximately 0.080-in. thick. It was composed of two layers of basic reinforcements; high temperature phenolic-impregnated bi-directional (181 type weave) S-994 glass fabric and 20-end S-994 glass filament impregnated with high temperature phenolic resin. The roving was used principally as a reinforcement in the hoop direction whereas the bi-directional cloth was the principal load transferring medium along the chamber axis. The properties of 181 glass phenolic, parallel to the warp direction, at room and elevated temperatures are as follows:

	R.T.	300°F	400°F	500°F	600°F
Tensile Strength, psi, x 10 <sup>-3</sup>	45.86	40.2	40.0	38.0	33.0
Tensile Modulus, psi, x 10 <sup>-6</sup>	4.02	3.29	3.0	2.7	2.5
Flexural Strength, psi, x 10 <sup>-3</sup>	67.0	57.7	60.5	44.7	27.5
Flexural Modulus, psi, x 10 <sup>-6</sup>	3.8	3.4	3.08	2.73	2.19
Compressive Strength, psi, x 10 <sup>-3</sup>	65.8	61.6	47.5	34.6	27.7

UNCLASSIFIED

UNCLASSIFIED

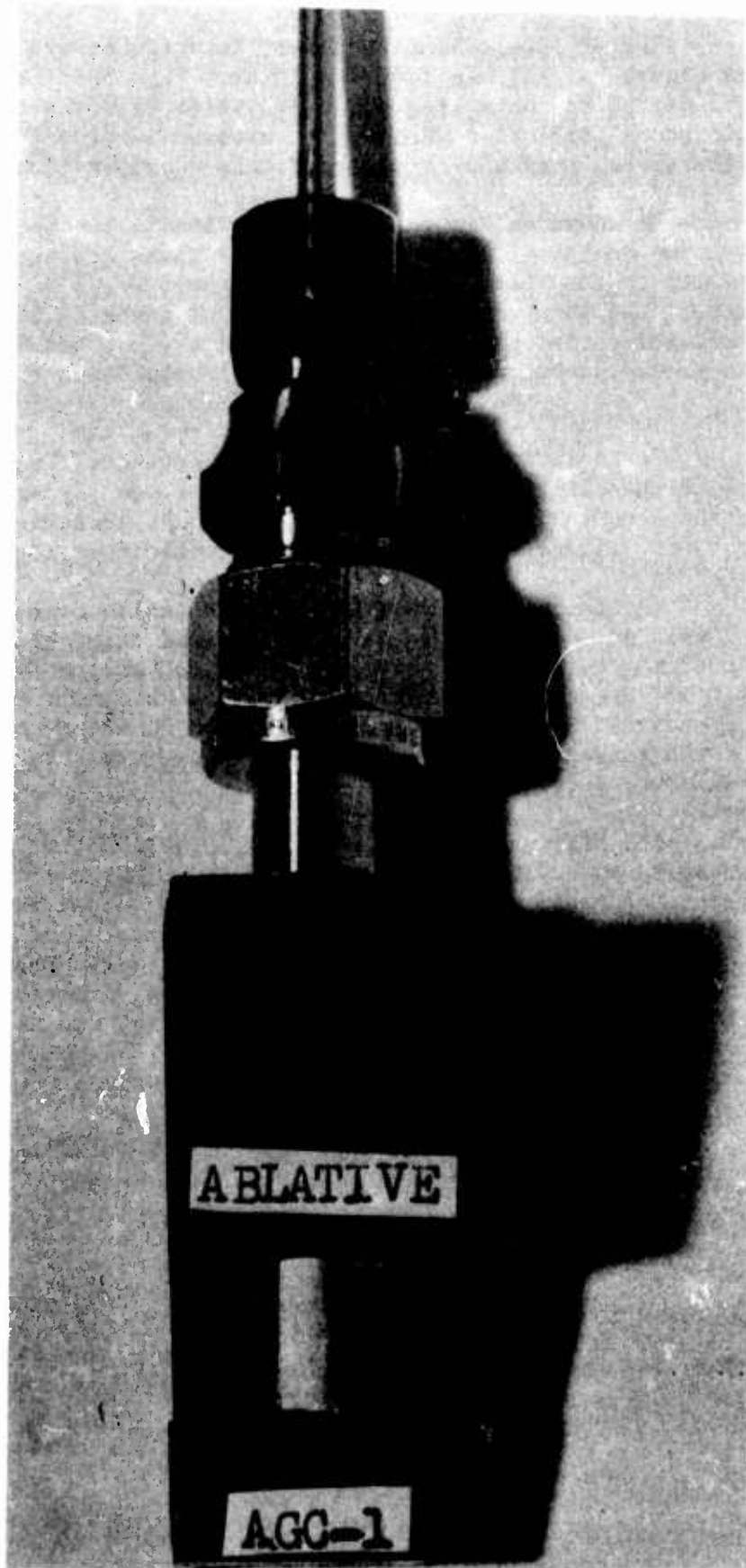


Figure 23. Thermocouple Probe

UNCLASSIFIED



# UNCLASSIFIED

The properties of the glass phenolic roving are as follows:

	<u>R.T.</u>	<u>250°F</u>	<u>500°F</u>
Tensile Strength, psi, x 10 <sup>-3</sup>	23.0	18.5	16.9
Shear Strength, psi, x 10 <sup>-3</sup>	6	3.6	2.1

The forward flange was a one-piece configuration fabricated from a low carbon steel forging (see Figure No. 22). It was based upon the test proven design of the Block II Apollo ablative chamber. Fingers were located at the lower end of the flange to mechanically lock it to the insulating material. A pocket designed into the external flange surface enabled the structural glass cloth to be mechanically locked, with the aid of glass roving, to the flange.

The aft flange, which was an integral part of the chamber, was made from silica phenolic (WB2230). The configuration of this flange was similar to that of the Transtage thrust chamber. It was a composite of the structural shell and insulating materials. The thermal analysis of the section just forward of the flange indicated a maximum char depth of approximately 2.3-in. with a peak skin temperature of approximately 500°F.

Fourteen internal thermocouples were installed in the ablative chamber as shown on Figure No. 22. Five were of the tungsten/tungsten-rhenium-type (serviceable to 4200°F) while the remainder were chromel-alumel. The tungsten/tungsten-rhenium thermocouples were located in contact with the backside of the AGCarb-101 throat insert. Photographs of the temperature measuring probe are shown as Figures No. 23 and No. 24. The installation techniques were developed and verified using the ablative liners with the water-cooled chamber before these probes were used in the all-ablative chamber.

## b. Thrust Chamber Design No. 2

This ablative thrust chamber design had a sea-level exit area ratio of 1.65:1 and one chamber was fabricated (S/N 003). It is shown on Figure No. 25. A full-length fibrous graphite (AGCarb-101) flame liner, insulated with a two-component carbon-silica fabric-reinforced phenolic system was used in this design. The entire subassembly was housed in a mild steel, thin-walled structural shell.

The design features of the AGCarb liner (lay-up angle, throat thickness, and graphitization cycle) were similar to Thrust Chamber Design No. 1. Two rows of 0.060-in. diameter holes were drilled radially through the liner (see Figure No. 25) to serve as vent holes for the pyrolysis gases generated in the surrounding insulation during test. Bleed holes were not considered necessary for Thrust Chamber Design No. 1 because of the limited throat insert length.

# UNCLASSIFIED



UNCLASSIFIED

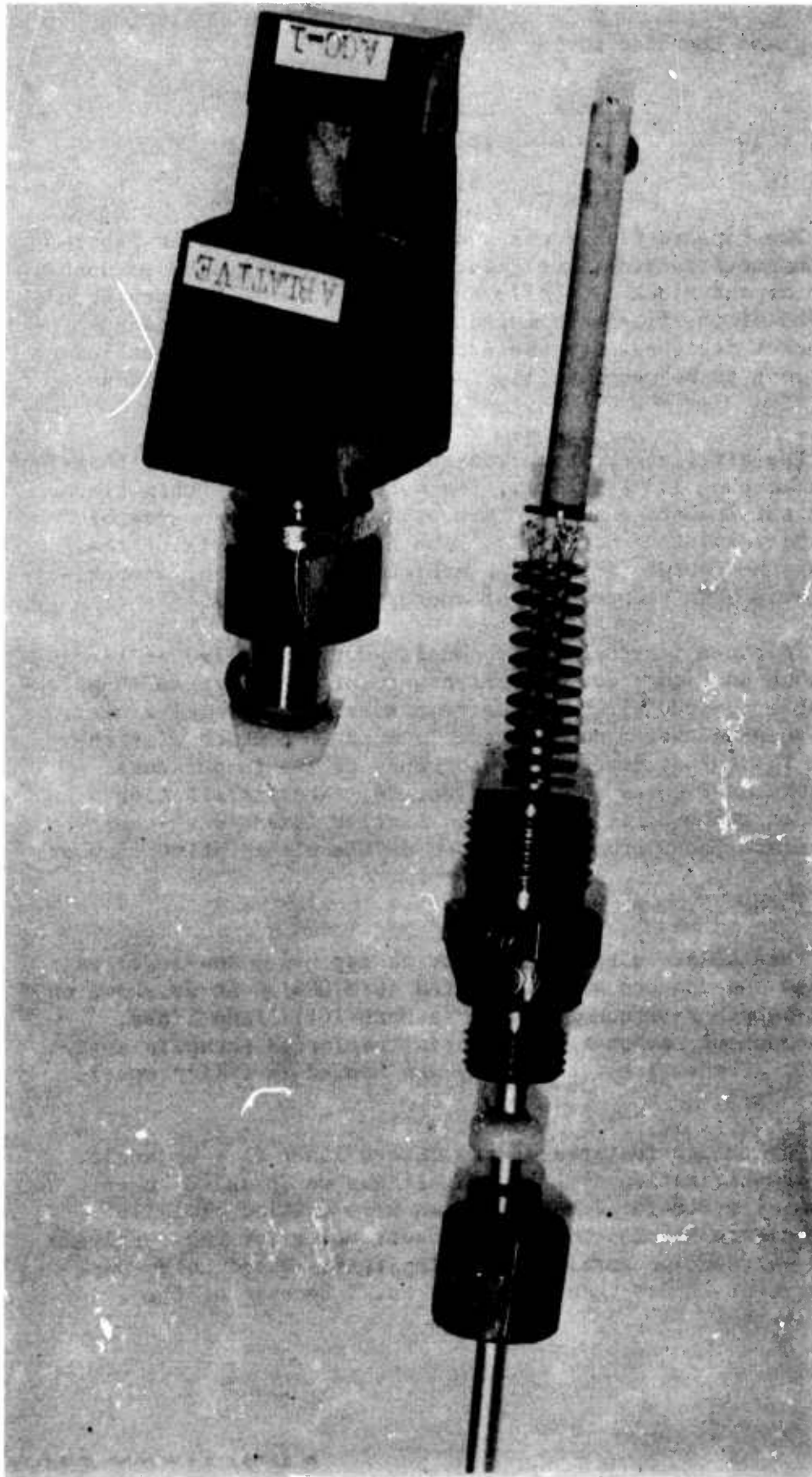
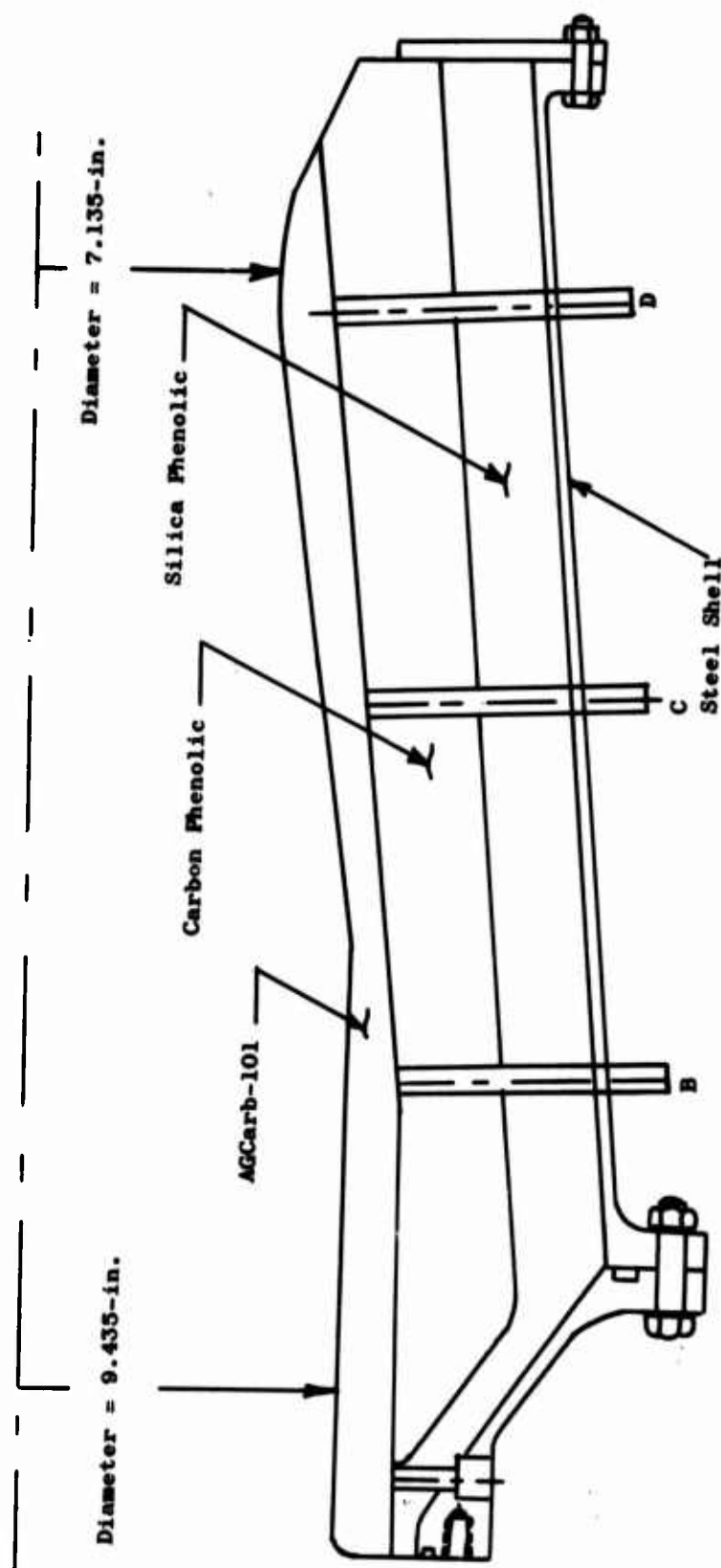


Figure 24. Disassembled Thermocouple Probe

UNCLASSIFIED

UNCLASSIFIED



<u>Thermocouple Locations</u>	
<u>Plane</u>	<u>Number</u>
A	2
B	2
C	4
D	3

Figure 25. S/N 003 Ablative Thrust Chamber

UNCLASSIFIED

UNCLASSIFIED

The high temperature insulation, FM 5072, was tape-wrapped at a 45-degree angle to the centerline of the part and the low temperature insulation, FM 5067, was flat-wrapped to maximize its insulating and structural characteristics.

The steel structural shell was a double-tapered flanged design which resulted in ease of assembly, low cost, and reliability.

All chamber components, the flame liner, both insulators, and the steel shell were designed to be fabricated as separate units. The individual components were mechanically-locked to each other with a long taper culminating at the end of the chamber. In addition, a steel retainer ring was bolted to the flanged aft end of the steel shell to restrain axial movement of the ablative composite.

Eleven internal thermocouples were installed in the ablative chamber as shown on Figure No. 25. Seven of these thermocouples were of the tungsten/tungsten-rhenium type while the remaining four were chromel-alumel. The thermocouple assembly was the same type used in the Thrust Chamber Design No. 1.

### 3. Thermal Analysis

The preliminary Thrust Chamber Design No. 1 was completed during Phase I. It was subjected to detailed one-dimensional thermal analyses to validate the dimensional assumptions. Material changes at the throat plane were subsequently incorporated into the design to reduce fabrication costs and improve structural integrity. Therefore, additional one-dimensional analyses were performed for the throat station to ensure its thermal adequacy.

The thermal model treated the char process as an equivalent, non-reversible phase change with a fixed charring temperature and heat of char. Neither dimensional ablation nor the transpiration cooling effect resulting from internal chemical reactions of pyrolysis were considered. Convective boundary conditions on the gas-side were based upon the simplified Bartz correlation for the film coefficient and the expected characteristic exhaust velocity efficiency for recovery temperature.

In general, the elevated temperature material property data (both laminate and char) were limited. Guidelines for design verification included maintaining both the silica phenolic below its melting point of 3000°F and the exterior temperature under 600°F.

The predicted temperature response for the critical restart duty cycle at the throat station of Thrust Chamber Design No. 1 is shown on Figure No. 26. The AGCarb-101 graphite phenolic interface temperature was predicted to rise to approximately 3600°F and the graphite-silica phenolic interface to approximately 1900°F. These temperatures occurred both during

UNCLASSIFIED

UNCLASSIFIED

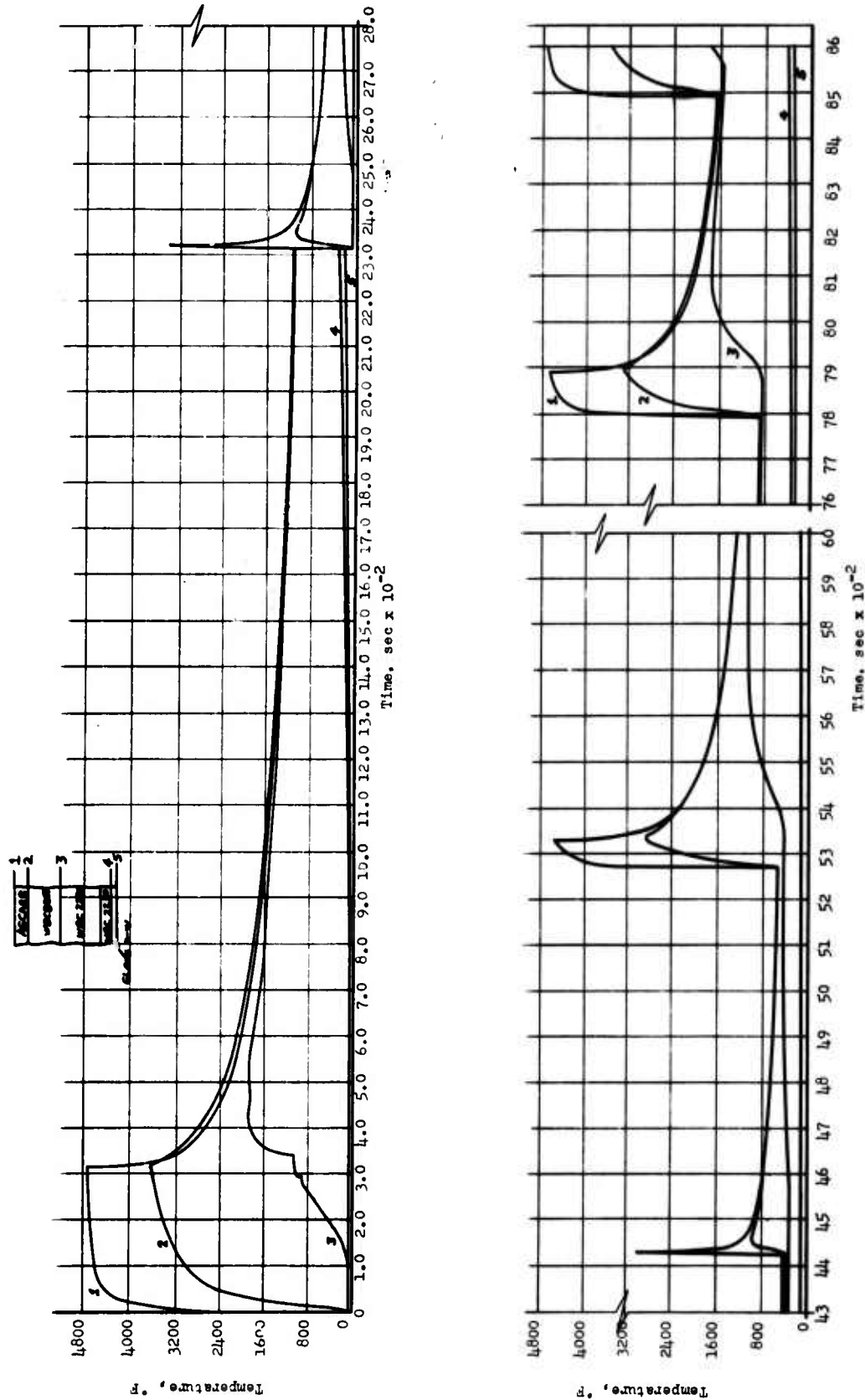


Figure 26. Predicted Throat Temperature for Design Duty Cycle

UNCLASSIFIED

UNCLASSIFIED

and shortly after the firing. The backside temperature was predicted to reach a peak value of approximately 350°F after 1.5 hours of soak following the first burn. This temperature was the maximum for the entire duty cycle. The heat inputs of subsequent firings were not as great and the low silica phenolic diffusivity prevented any rapid pulse of heat from passing through the wall to the exterior surface.

The analysis indicated that it was possible to design the chamber for the maximum exterior temperature based upon the results from the first firing (315 sec).

Thrust Chamber Design No. 2 (S/N 003) relied upon the previously discussed thermal analysis to ensure that the silica phenolic was properly located to prevent exposure to temperatures above its melting point. In addition the wall thickness at the throat approximated that of Thrust Chamber Design No. 1 to ensure that the backside surface temperature was below 600°F.

Appendix III describes a method of conducting a thermal design analysis.

#### 4. Fabrication

Ablative chambers S/N 001 and S/N 002 incorporated AGCarb-101 throat inserts. These throat inserts were fabricated and cured at 300°F at Aerojet-General, Sacramento, and then sent to the Union Carbide Corporation in Cleveland for carbonizing and graphitization.

The fabrication and assembly of the two chambers, including the final machining of the throat inserts were done at Havig Industries, Inc., Santa Fe Springs, California.

The S/N 002 chamber required repair to correct an undersize condition existing on the downstream end of the AGCarb-101 throat insert. It was found that the outside surface, below the throat, was approximately 0.125-in. undersize. The backing graphite phenolic insulation, WB8207, was increased in thickness, cured, and machined until it mated with the undersized throat insert. The repaired area was not visible and it did not affect the ensuing test series, which had a total duration of 606 sec.

The fabrication of chamber S/N 003 was accomplished at San Rafael Plastics, San Rafael, California. Graphitization of the full length AGCarb-101 liner also was conducted at Union Carbide in Cleveland. The complete manufacture of this chamber was accomplished without incident.

The fabrication details for both chamber designs are presented in Appendix IV.

UNCLASSIFIED

UNCLASSIFIED

5. Rework of S/N 001 Chamber

a. Requirement and Material Selection

An acoustically-damped ablative chamber was required in Phase III to demonstrate the long duration damping efficiency of an acoustic resonator as well as its durability in an ablative chamber. The S/N 002 thrust chamber had demonstrated the 600 sec duration required during Phase II and the similar S/N 001 unit was available for rework.

AGCarb-101 was selected as the flame surface of the resonator following its success as a throat insert in ablative chamber S/N 002. Carbonized graphite fabric-reinforced phenolic, WB8207, was selected as the material to surround the flame liner and contain the resonator cavities. Post-test analysis of the WB 8207 used as the nozzle ablative liner in chamber S/N 002 showed it to be remarkably solid with virtually no delaminations although almost completely charred. The use of these pre-charred materials would eliminate pyrolysis gases from the resonator cavities.

b. Description

The modified ablative chamber, S/N 001, shown on Figure No. 27 had an exit area ratio of 1.65:1 and the basic chamber configuration remained as previously described.

The acoustic resonator was a three-piece assembly consisting of the flame liner which was a sleeve containing nine rows of orifices, the precharred graphite phenolic housing three axial rows of resonator cavities, and a silica phenolic insulation ring. The flame liner was mechanically-locked to the carbonized sleeve which, in turn, was firmly positioned with a locking shoulder in the basic chamber. A silica phenolic, WB2230, ring insulated the forward cavity from the steel chamber flange. Figure No. 28 shows the liner being installed into the ablative thrust chamber.

The flame liner design was based upon the results from tests with chambers S/N 002 and S/N 003. Expansion gaps were provided for both axial and radial thermal growth, while the radial thickness was kept minimum. As a result, excessive compressive stresses were not allowed to develop and no cracks or delaminations were evident in the disassembled liner after testing.

A detailed discussion of the acoustic resonator design is provided as Appendix II.

c. Fabrication

Fabrication of the acoustic resonator assembly and the modifications to ablative chamber S/N 001 were accomplished without incident at San Rafael Plastics. The unmachined AGCarb-101 flame liner was available as residual material from the water-cooled chamber.

UNCLASSIFIED



UNCLASSIFIED

CHAMBER

MATERIALS: AG CARR-101 (A/C)  
GRAPHITE PHENOLIC (G/P)  
CARBON PHENOLIC (C/P)  
SILICA PHENOLIC (S/P)

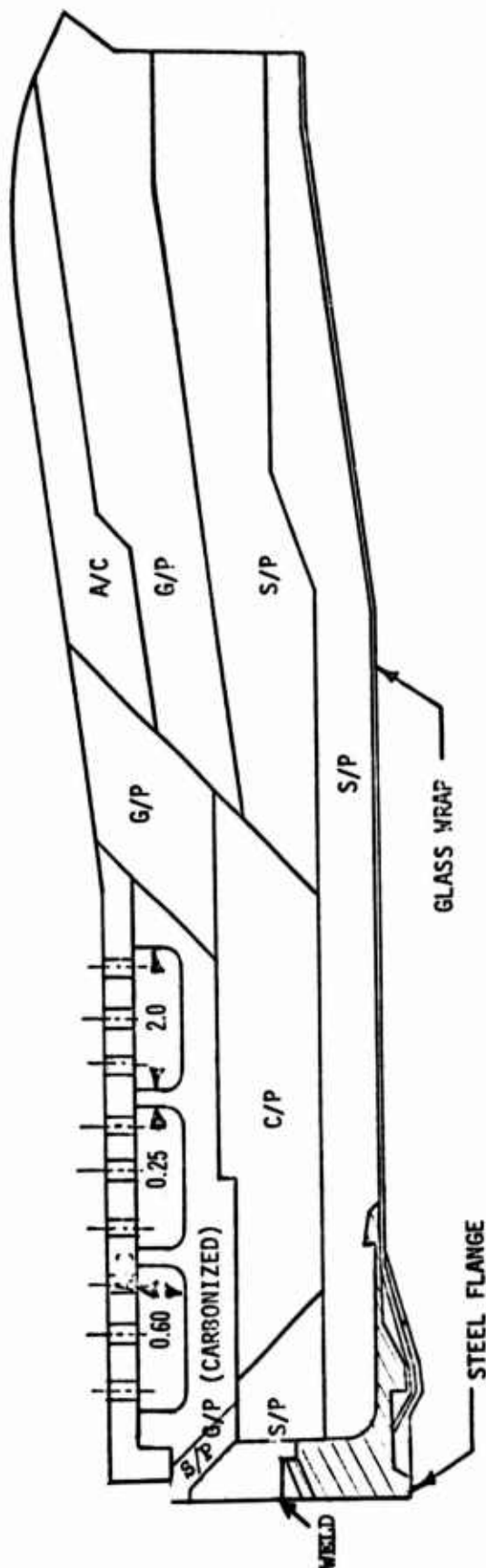


Figure 27. S/N 001 Ablative Thrust Chamber

UNCLASSIFIED



UNCLASSIFIED



Figure 28. Installation of Acoustic Liner into S/N 001 Ablative Thrust Chamber

UNCLASSIFIED

# UNCLASSIFIED

## E. NOZZLE EXTENSION

The program objective required the development of technology needed for a complete thrust chamber. This included a divergent nozzle extension which would match the ablative thrust chambers being developed. This required that a flightweight nozzle extension be designed according to the following criteria:

- radiation-cooled
- constructed of a material that was resistant to the HF, H<sub>2</sub>, and F<sub>2</sub> content of the exhaust gases
- resistant to buckling loads at temperatures from 2400°F to 2600°F
- contoured to yield the maximum thrust coefficient consistent with the contractual constraints of diameter and length

The approach used to satisfy the design requirements for the flightweight, full-size nozzle extension was the same as that for the ablative thrust chamber and injector development. Detailed design and analysis of a full-length nozzle extension were accomplished during Phase I. For the Phase II testing, a truncated nozzle was used to provide such surface area as was needed to obtain valid compatibility information. Various protective coating materials were selected for use on the shortened nozzle. The half-angle of the ablative chamber divergent nozzle and the radiator cooled extension were 25 degrees. The exit area ratio was 9.5 to 1. Testing of this unit would provide materials and performance data. It was from the assessment of kinetic performance that an optimum contour for the fully-expanded nozzle could be established.

### 1. Design, Description, and Analysis

The Phase II nozzle extension (Figure No. 29), was a 25-degree half-angle, radiation-cooled unit attaching to the S/N 002 ablative chamber (see Section IV,D,2) flange at an area ratio of 7.5:1 and terminating at an exit area ratio of 9.5:1. The ablative chamber attachment flange was in a plane which passed through area ratio 4.5:1 but an overlap in the ablative liner of the chamber made the gas-side interface at a 7.5:1 area ratio. The 7.5 to 1 station was established as being the smallest diameter at which nozzle temperatures were compatible with the use of columbium. It was consistent with the objective of evolving the lightest weight thrust chamber assembly.

The 9.5 to 1 nozzle was divided into three, 120-degree circumferential sections, each with a different coating. The base structural material was 0.030-in. thick, C-103 columbium, which was selected because of its excellent performance in both the Transtage and Apollo engine applications.

UNCLASSIFIED

UNCLASSIFIED

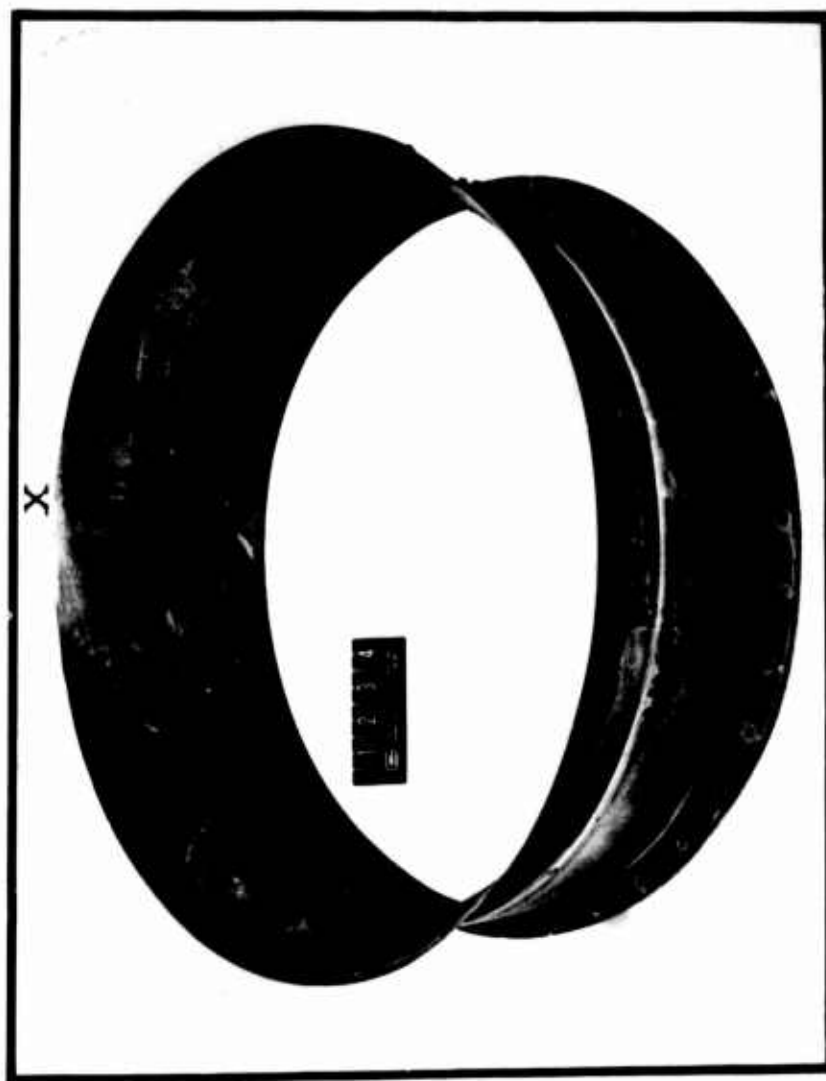


Figure 29. Thrust Chamber Nozzle Extension Section

UNCLASSIFIED

# UNCLASSIFIED

Thermal analysis of the nozzle extension yielded results which compared favorably with the predicted and actual temperatures experienced with the Apollo nozzle extension. These data are shown on Figure No. 30. The actual measured temperature of the Apollo nozzle at the transition area ratio was 2200°F, or 190°F below the predicted temperatures. The difference between the measured and actual temperature was attributable to out-gassing of the ablative chamber liner. The predicted temperature for the fluorine/nozzle extension was 2530°F. It was estimated that the steady-state wall temperature at the ablative-to-radiation transition would be approximately 2400°F because the fluorine nozzle also would benefit from out-gassing of the ablative chamber.

## 2. Materials and Protective Coatings

Extensive experience with nozzle extensions for both the Apollo Service Module and the Transtage engines had shown that C-103 columbium was satisfactory for this type of application. The thermal shock resistance properties of columbium are excellent as demonstrated in more than 100 starts of a single extension in the Transtage Program. The excellent forming and welding properties of the C-103 columbium also were demonstrated at Aerojet-General and their nozzle suppliers. However, unprotected columbium is subject to severe oxidation and nitrogen contamination when exposed to air at temperatures above 1800°F. Hydrogen embrittlement also can occur if the H or H<sub>2</sub> mole fraction of the exhaust gases is high. The exhaust products of the fluorine/hydrazine blend contain a large amount of HF and free fluorine; therefore, barrier coatings must be used to prevent the columbium from attack by these exhaust products. The HF will attack columbium to form columbium pentafluorine (CbF<sub>5</sub>) which has a melting point of 161.5°F and an approximate boiling point of 428°F. While the actual rate of attack is unknown, available data indicated it would be high. Previous work<sup>(15)</sup> indicated that an aluminide coating would provide effective protection against the effects of a fluorinated exhaust atmosphere. Therefore, the following three coatings were selected for evaluation with the test nozzle extension:

- Lunite 2<sup>(16)</sup>; an aluminide diffusion coating (final cure: 1800°F to 1900°F) similar to the NAA-85 coating used on the columbium portion of the Apollo skirt
- Lunite 3<sup>(17)</sup>; a hafnium-tantalum coating (final cure: 1800°F to 1900°F)
- A nickel aluminide ceramic plasma sprayed coating<sup>(18)</sup>

(15) Contract AF 04(611)-8183, "Maneuvering Satellite Propulsion System Demonstration," Bell Aerosystems, December 1965

(16) Product of the Vac-Hyd Processing Corp.

(17) Product of the Vac-Hyd Processing Corp.

(18) Formulation of the Tri-Metals Co.

UNCLASSIFIED

UNCLASSIFIED

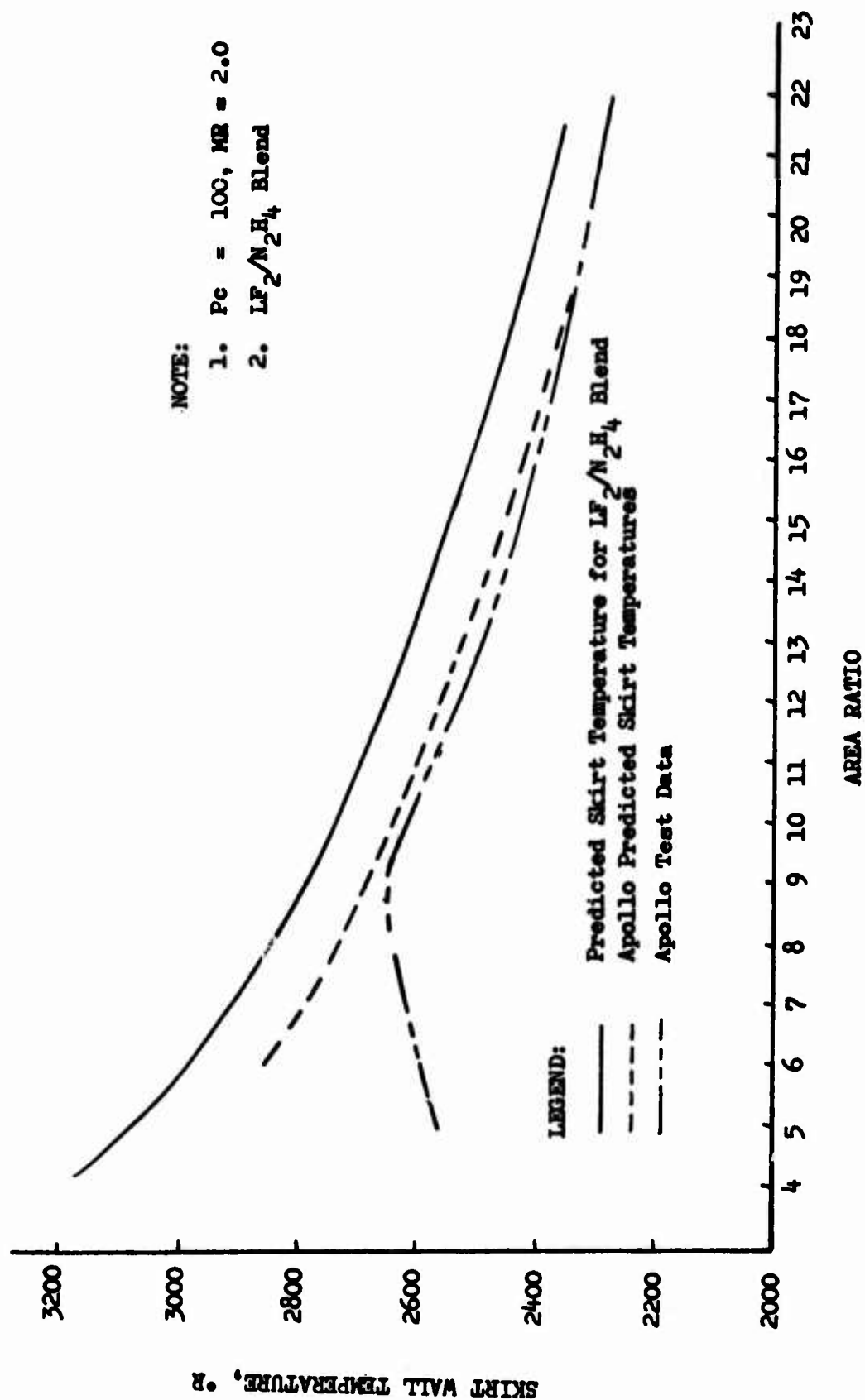


Figure 30. Nozzle Thermal Analysis, Comparison with Apollo

UNCLASSIFIED

## UNCLASSIFIED

Due to sequential coating application procedures, potential interactions between the three candidate coatings existed and were investigated with the following results(19):

- A definite possibility of a reaction existed between the aluminum in the Lunite 2 and the tantalum in the Lunite 3 during the cure cycle if they share a common cure cycle.
- A possibility existed that the nickel in the plasma spray coating and the tantalum of the Lunite 3 could combine to form a nickel-tantalum eutectic during engine test firings. This eutectic, which has a melting point of approximately 2500°F, possibly could be washed away leaving the substrate unprotected. This condition would exist at the interface or overlap of the two coatings only.
- There should be no gross interaction between the different coatings with the true conditions of the individual coatings being most valid midway between the coating interfaces.
- An uncoated columbium substrate would be subjected to attack by the HF as well as contamination (i.e., by nitrogen, hydrogen, and water vapor) during an engine firing.

Consequently, it was planned that the Lunite 2 and Lunite 3 coatings would be processed separately and that the post-test analysis samples would be taken midway between the coating interfaces.

### 3. Fabrication

One short, coated columbium nozzle extension was manufactured and the unit instrumented with chromel-alumel thermocouples to sense skin temperatures. Post-test analyses showed that the spinning process used to form the part resulted in undersize thickness in a sharp radius area.

---

(19) Information from the Battelle Memorial Institute, Columbus, Ohio

UNCLASSIFIED



# UNCLASSIFIED

## SECTION V

### TESTING

Injector-chamber testing is the verification of component designs for which there is no satisfactory substitute. The following were critical to the success of the pre-planned test program:

- Facility
- Facility Operational Procedures
- Thrust Chamber Assembly Operational Procedures

The test facility was capable of providing accurately measured performance data that could be meaningfully interpreted and evaluated. In order to effectively utilize the facility, operational procedures were developed which provided the basis for consistent system cleanliness and personnel safety. Equally important were the thrust chamber assembly operating procedures which defined component cleanliness, their assembly and sequence of test events, such as, opening and closing valve times, propellant leads and nitrogen purges.

The program objective, as initially stated, was to demonstrate the performance capability of a pressure-fed ablative thrust chamber assembly. Testing was initiated during Phase II and completed at the end of Phase III with the attainment of the program objectives. A total of 40 tests (30 sea level and 10 simulated altitude) was conducted during the program.

#### A. FACILITIES AND PROCEDURES

A detailed description of the test facilities and the test operational procedures is included as Appendix V.

##### 1. Facilities

All of the testing was accomplished in Test Area J of the Aerojet-General Sacramento Facility. Two test stands were used: Test Stand J-2, the sea-level facility, and Test Stand J-4, the simulated altitude facility. The liquid fluorine tankage capacity limited tests at Test Stand J-2 to durations of approximately 50 sec while the simulated altitude testing at Test Stand J-4 was limited by the steam supply only to durations of approximately 200 sec. At Test Stand J-2, the exhaust products were vented to atmosphere while a water scrubber was used to control them at Test Stand J-4.

All of the thirty tests with the uncooled steel chambers and the water-cooled chambers were conducted at Test Stand J-2. These included injector checkout, compatibility, and acoustic resonator pulse tests. The ten long duration, simulated altitude tests with the ablative combustion chambers were conducted at Test Stand J-4.



# UNCLASSIFIED

## 2. Facility Operational Procedures

### a. Cleanliness

The success of the test program was directly related to the cleanliness of all circuitry (facility and injector) exposed to LF<sub>2</sub>. The 40 program tests were conducted without any fires, line failures, or seal failures. A two-step cleaning procedure, which consisted of removing foreign matter followed by passivation, was applied to the injector, pressure transducer lines, transducers, thermocouples, valves and all of the other components that came into contact with LF<sub>2</sub>.

The run lines were cleaned and passivated when the facility was initially activated. When not in use, they were capped and pressurized with dry helium. After a component was replaced or the line circuitry was interrupted, the run line was repassivated. The injector was recleaned and repassivated whenever it was removed from the test site. The passivation procedure is briefly described in Appendix V.

### b. Safety

Personnel safety was the prime consideration in connection with the movement of fluorine or its products of combustion. All operations were conducted in accordance with published checklists. At any time that LF<sub>2</sub> was flowed, Test Area J was restricted to all personnel not in the control room, where the number was limited to the quantity of available breathing air packs.

Tests were conducted only under the established, favorable meteorological conditions. Pre-test as well as post-test movement of waste fluorine, primarily the bleeds and vents, was remotely controlled from the control room and this waste fluorine was discharged into a charcoal pit and burned. The reaction products of carbon tetrafluoride were vented directly into the atmosphere.

## 3. Thrust Chamber Assembly Operational Procedures

### a. Thrust Chamber Valves

The program did not include the development of propellant valves suitable for LF<sub>2</sub> use. However, Aerojet-General had previously obtained excellent results using a modified Annin valve<sup>(20)</sup>. The design specifications for these previously used valves were such that by adjusting the stroke and replacing the valve seat they were usable with either oxidizer or fuel. A copper seat was used with fluorine and a teflon seat was used with fuel. The following are the specified design features:

(20) Aerojet-General IR&D, "Advanced Transtage Fluorine Feasibility Program," 1964

UNCLASSIFIED

## UNCLASSIFIED

- (1) Type--special "Y" body
- (2) Annin P/N--A-4065
- (3) Size--1 in.
- (4) Pressure rating--1500 psi
- (5) Actuation system--pneumatic or hydraulic position controlled (gaseous nitrogen used)
- (6) Actuation pressure--500 psig
- (7) Opening time--up to 1.5 sec (approximately 0.3 sec used)
- (8) Closing time--up to 0.25 sec used
- (9) Valve bodies bored for LN<sub>2</sub> coolant passages
- (10) Percentage type valve plug
- (11) Marker to denote oxidizer or fuel setting
- (12) Less than 100 psi drop
- (13) Normally closed
- (14) Interface to use small tongue-groove flange, 1500 psi ASA rating with tongue on valve.

The valves operated trouble-free throughout the entire test program. They were treated as part of the test stand equipment and were never removed with the injector-chamber assembly.

### b. Injector-Chamber Assembly

Following passivation, the injector was assembled to the thrust chamber and installed on the test stand as an assembly. Silicone rubber O-rings were used between the injector and combustion chamber. "Zinc Chromate Putty" was used as a filler between the injector and the inside diameter of the chamber. Soft aluminum crush washers were used between the injector propellant inlet lines and the thrust chamber valves. The silicone rubber O-rings were reused while new aluminum crush washers were installed during each assembly. No seal leakages were encountered during any of the tests.

The thrust ring, which is shown on Figure No. 31 (Test No. -024 set-up), was bolted to the injector during the assembly of the injector to the chamber. Then, an outer bolt circle was used to mount the complete assembly to the test stand. No problems were encountered during the assembly of the thrust chamber assembly or its placement into the test stand.

UNCLASSIFIED

UNCLASSIFIED

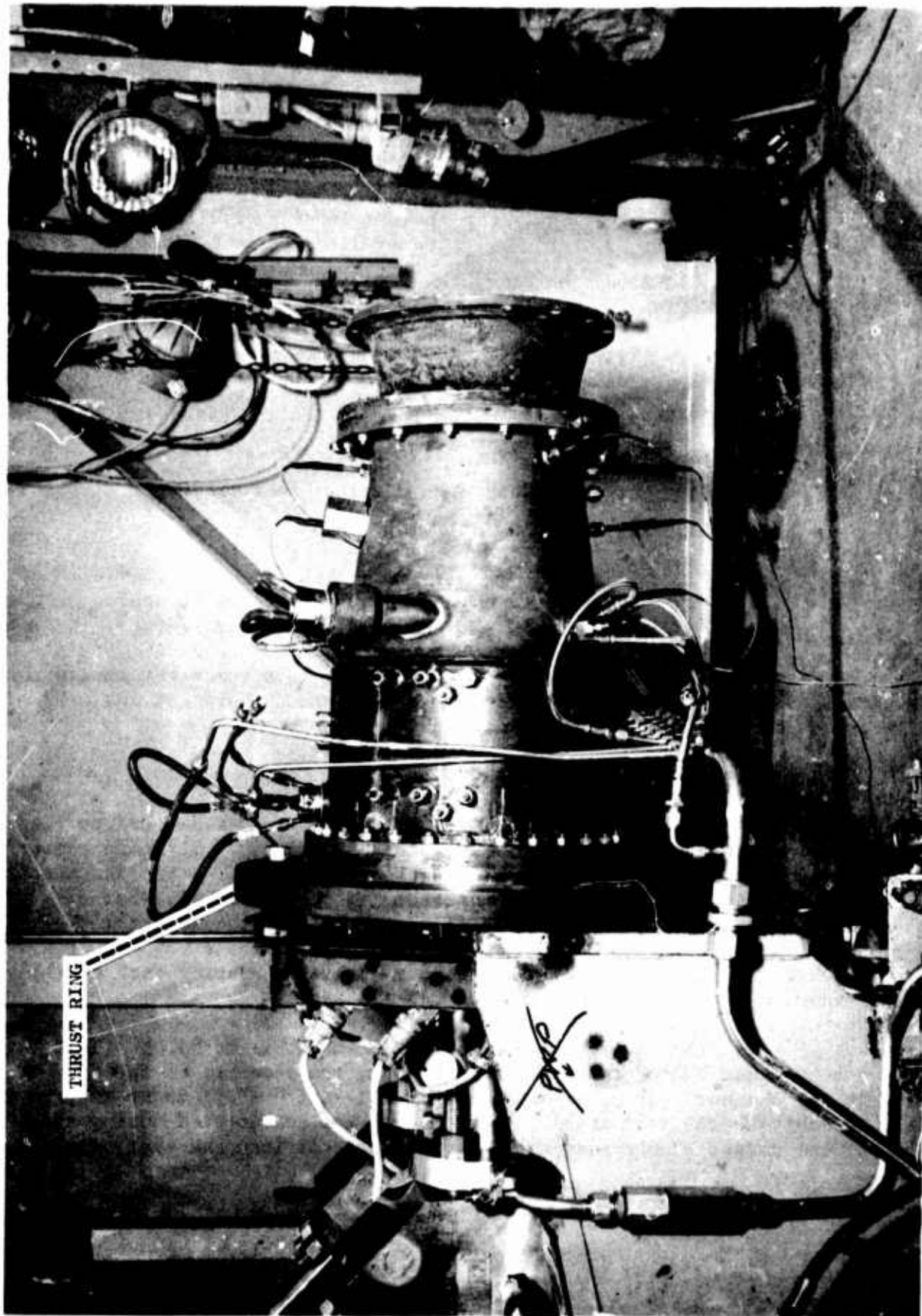


Figure 31. Uncooled Steel Chamber Test Installation

UNCLASSIFIED

# UNCLASSIFIED

## c. Sequence of Test Operations

The test sequence as indicated in Figure No. 32 was designed to provide a slow ignition with a gradual rise in chamber pressure to steady-state operation. For this reason, the "percentage-type plug" ® was used in the thrust chamber valves. The plug was machined to allow an ever-increasing flow rate with respect to valve stem travel.

Based upon the experiences in a previously conducted, trouble-free  $\text{LF}_2$  program<sup>(21)</sup>, the valves were timed to open in approximately 0.3 sec and were sequenced to provide an oxidizer lead of the propellants into the combustion chamber. The start and shutdown transients of a typical test are shown on Figures No. 32 and No. 33, respectively. The start transient record indicated that the equivalent of approximately 1.86 in.<sup>3</sup> (21.2 in.<sup>3</sup> within the oxidizer manifold between the valve and injector face) of liquid fluorine had passed through the thrust chamber valve at the time of ignition. Initially, as a result of uninsulated injector manifolding and lower pressure, the fluorine flashed to a gas and proceeded to flow into the chamber. At the same time, fuel entered and ignition was immediate. The slow rise of the chamber pressure, which started with the initial rise in fuel manifold injector pressure, can be seen on Figure No. 32. The initial fluorine flow was gaseous for approximately 0.3 sec after ignition ( $\text{FS}_1 + 0.83$  sec), at which time steady-state conditions were reached. The length of time required to achieve steady-state pressure conditions varied from test to test. The time was dependent upon the temperature of the fluorine upstream of the thrust chamber valves following the pre-test fluorine bleed of the run line (maximum time of 0.5 sec for a temperature of  $-290^\circ\text{F}$  and a minimum time of 0.15 sec for a temperature of  $-300^\circ\text{F}$ ).

Gaseous nitrogen purges entered through each injector propellant inlet flange and were used in both injector manifolds. The purge valves were opened during the test stand arming sequence, approximately 1 to 2 min prior to  $\text{FS}_1$  and were signaled to close at  $\text{FS}_1$ . It can be seen on Figure No. 32 when the nitrogen stopped flowing by noting the decay of both the fuel and the oxidizer injector pressures after  $\text{FS}_1$  and prior to ignition.

The gaseous nitrogen purges again were applied at the termination of a test with the purge valves being sequenced to open simultaneously with the electrical signal to close the thrust chamber valves. The purge valves were closed manually several minutes after the test was completed.

® Tradename, Annin Company  
(21) Ibid.

UNCLASSIFIED

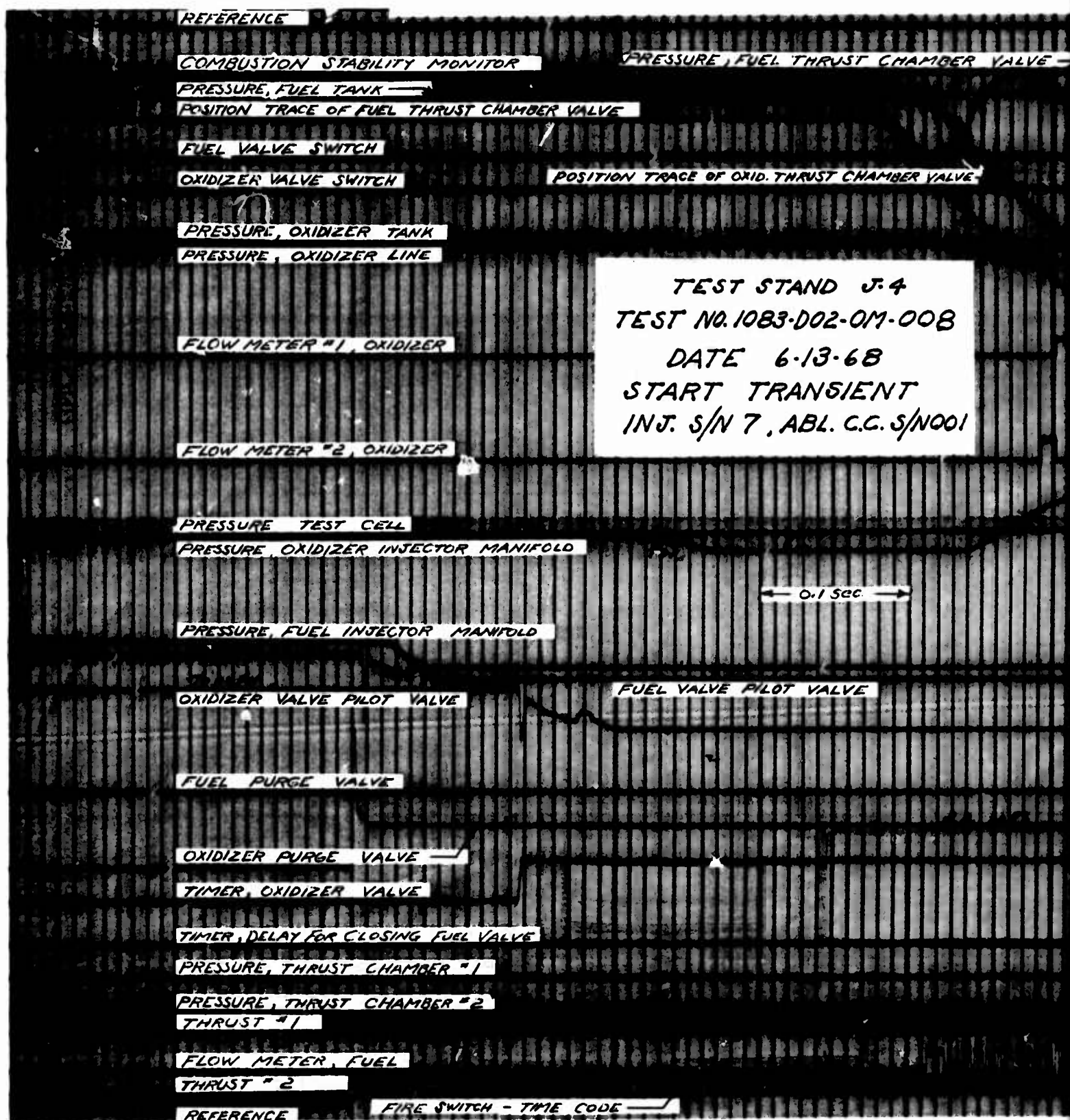


Figure 32. Typical Start Transient

UNCLASSIFIED



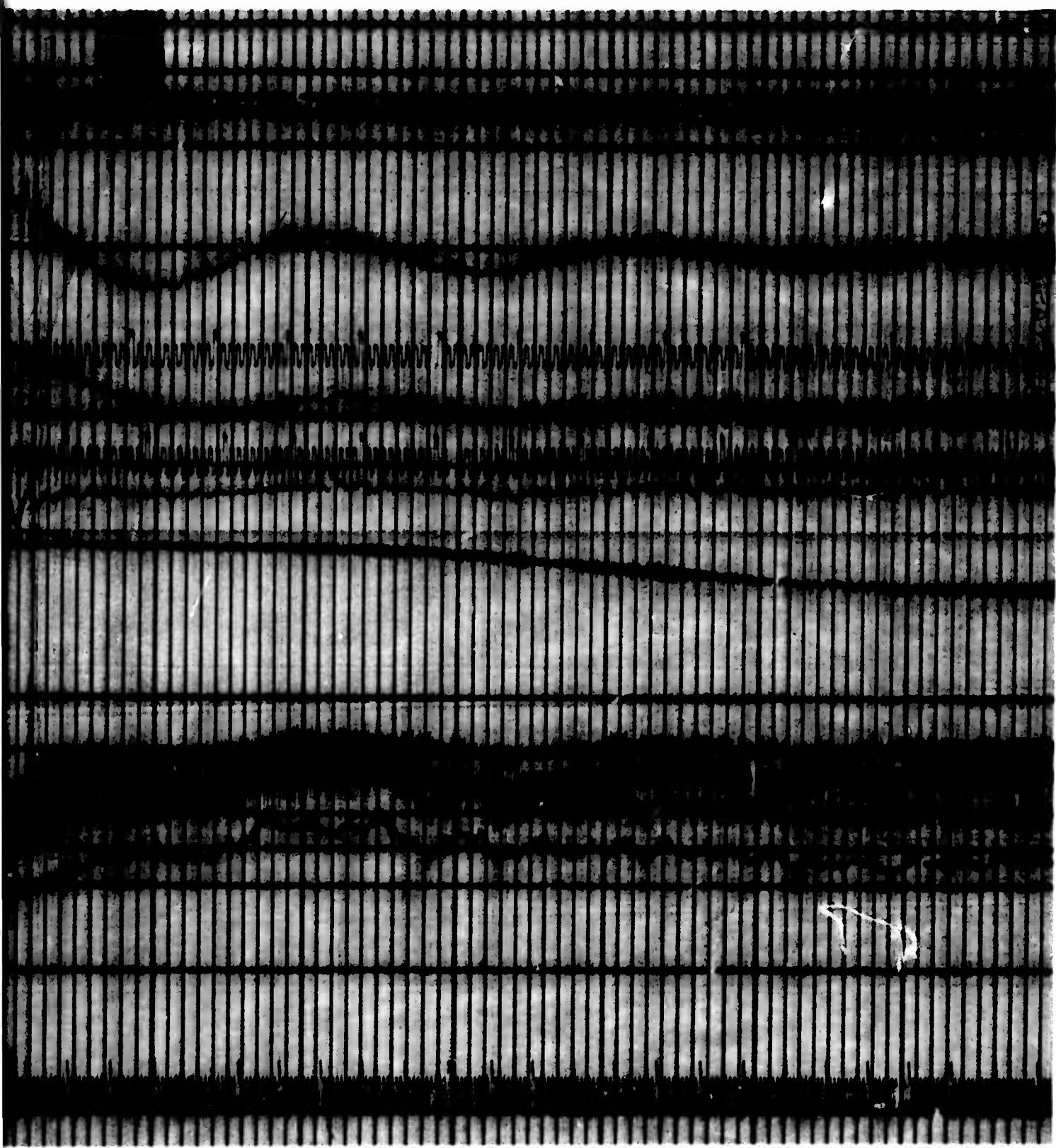
RUST CHAMBER VALVE →

ST CHAMBER VALVE

ID J-4  
72-0M-008  
3-68  
ISIENT  
L. C.C. S/N001

1 Sec →

ALVE





COMBUSTION STABILITY MONITOR

PRESSURE, FUEL TANK

THRUST CHAMBER FUEL VALVE SWITCH

PRESSURE, FUEL THRUST CHAMBER VALVE

THRUST CHAMBER OXID. VALVE SWITCH

PRESSURE, OXIDIZER TANK

PRESSURE, OXIDIZER LINE

FLOW METER #1, OXIDIZER

PRESSURE, OXID. INJ. MANIFOLD

POSITION TRACE OF OXID. THRUST CHAMBER VALVE

FLOW METER #2, OXIDIZER

POSITION TRACE OF FUEL THRUST CHAMBER VALVE

PRESSURE, FUEL, INJECTOR MANIFOLD

PRESSURE, TEST CELL

← 0.1 Sec →

THRUST CHAMBER FUEL VALVE  
PILOT VALVE

TEST STAND J-4  
TEST NO. 1083-D02-OM-008  
DATE 6-13-68  
SHUTDOWN TRANSIENT  
INJ. S/N 7, ABL. C.C. S/N 001

THRUST CHAMBER OXID. VALVE PILOT VALVE

PRESSURE, THRUST CHAMBER #1

PRESSURE, THRUST CHAMBER #2

THRUST CHAMBER FUEL PURGE VALVE

THRUST #1

THRUST CHAMBER OXID. PURGE VALVE

THRUST #2

TIMER, THRUST CHAMBER OXID. VALVE

TIMER, DELAY FOR CLOSING FUEL VALVE

FLOW METER FUEL

FIRE SWITCH - TIME CODE  
REFERENCE

CONFIDENTIAL

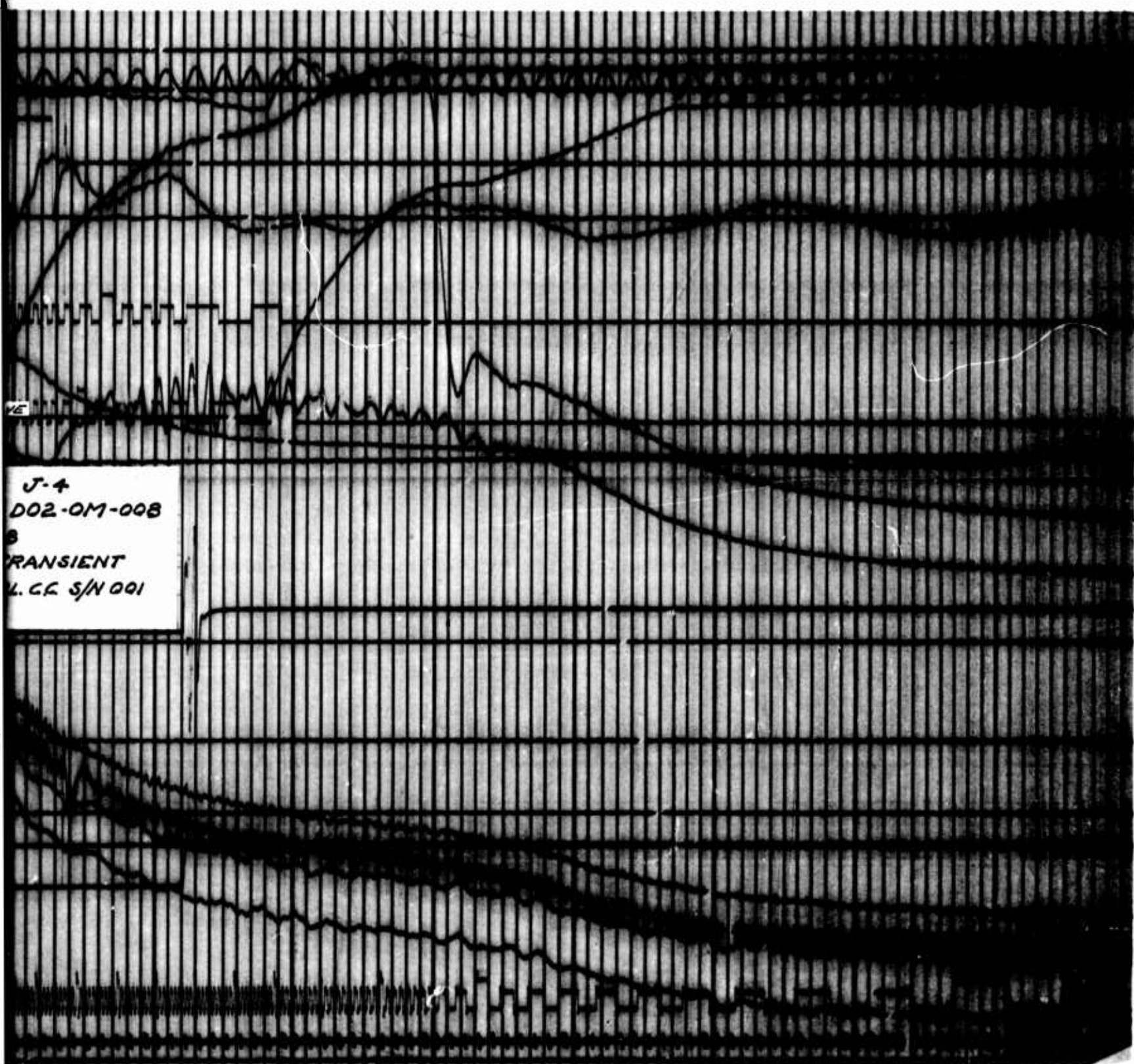


Figure 33. Typical Shutdown Transient

Page 77

CONFIDENTIAL

(This Page is Unclassified)

2

## CONFIDENTIAL

(U) The thrust chamber valves were sequenced to provide a fuel override at FS<sub>2</sub> (see Figure No. 33) to prevent oxidizer-rich gases and/or fluorine from washing over the hot ablative chamber walls. The closing time of the valves varied from under 0.1 sec to 0.25 sec. The longer closing times were utilized, without problems, to simulate the anticipated shutdown conditions of the flight-type bipropellant valve. (22)

### B. THRUST CHAMBER ASSEMBLY TESTING

(U) All of the testing was scheduled for Phase II and Phase III of the program. In Phase II testing, the injector stability and performance were evaluated using the uncooled steel thrust chambers for short duration testing. Six injector patterns in three injectors of similar designs were evaluated; three pattern iterations were conducted in one injector. Following the identification of a stable unit, more extended duration tests were undertaken to evaluate the durability and compatibility of the injector. The water-cooled nozzle with graphite and ablative-lined chambers was used in these tests.

(U) Once the injector and chamber durability was demonstrated, long duration tests were made at simulated altitude conditions using ablative thrust chambers, both with and without the radiation-cooled nozzle extension. Two ablative chambers were evaluated, one satisfactorily for six starts totaling 606 seconds.

(C) Testing during Phase III was directed toward the attainment of an altitude specific impulse of 370 seconds, the demonstration of dynamic stability and the elimination of thrust chamber streaking (improved injector-chamber compatibility).

(U) This was accomplished with one new injector having a high performance pattern and an ablative chamber reworked to incorporate an acoustic resonator. A total of ten tests was conducted during Phase III, three under simulated altitude conditions.

(U) The program test data are summarized in Table IX.

#### 1. Phase II Testing

(U) The aluminum injector (S/N T<sup>2</sup>), which incorporated 215 elements and 6% fuel film cooling, was tested three times for a total of 6.27 sec using the same uncooled steel workhorse chamber. The last two tests were unstable. Figure No. 34 is a view of the injector face before testing. As anticipated, the test durations were not sufficient to cause orifice erosion and there was no face erosion. However, the peripheral fuel manifold cover weld cracked as shown on Figure No. 35. This necessitated a weld repair after the second test. The steel chamber was undamaged.

(22) Contract AF 04(695)-197, "Transtage Development," CCN 192, "An Electro-Mechanical Bipropellant Valve for Cryogenic (Liquid Fluorine) and Storable Propellants," 1966-1967

CONFIDENTIAL

TEST

LF<sub>2</sub> / N<sub>2</sub> H<sub>4</sub> BLEND PROG

TEST NO.	DATE	INJECTOR S/N	NUMBER ELEMENTS INJ. PAT.	COMB. CHAMBER CONFIG.	POST TEST		DURATION SEC.	DATA PERIOD SEC.	M.M.	Wt LB/SEC.
					A <sub>t</sub> IN. <sup>2</sup>	€				
1083-D01-OM										
-001	2-13-67	T <sup>2</sup>	215	Uncooled Steel S/N 1	39.90	1.65	2.024	0.900 to 1.900	1.71	22.91
-002	2-14-67	T <sup>2</sup>	"	"	39.90	1.65	2.722	0.950 to 2.450	1.55	17.04
-003	2-20-67	2	158	"	39.90	1.65	2.027	0.926 to 2.027	1.57	17.14
-004	2-20-67	2	"	"	39.89	1.65	1.765	0.800 to 1.050	1.96	18.70
-005	2-22-67	2	"	"	39.89	1.65	1.695	0.900 to 1.620	1.87	18.09
-006	2-22-67	2	"	"	39.88	1.65	1.358	0.900 to 1.290	2.29	20.08
-007	5-4-67	T <sup>2</sup>	215	"	39.87	1.65	1.534	1.000 to 1.400	1.75	17.64
-008	5-5-67	2 Mod 1	98	"	39.88	1.65	1.833	1.200 to 1.700	1.77	18.18
-009	5-9-67	"	"	"	39.85	1.65	3.987	3.487 to 3.987	1.73	19.90
-010	5-10-67	"	"	"	39.82	1.65	3.047	2.500 to 2.900	1.75	20.25
-011	5-10-67	"	"	"	39.83	1.65	1.596	1.096 to 1.446	1.70	21.78
-012	5-17-67	2 Mod 2	68	"	39.83	1.65	2.014	1.514 to 2.014	2.01	17.68
-013	5-24-67	"	"	"	39.83	1.65	4.023	3.423 to 3.923	1.93	17.79
-014	5-24-67	"	"	"	39.82	1.65	4.019	3.519 to 4.019	2.26	13.22
-015	5-24-67	"	"	"	39.	1.65	4.987	4.487 to 4.987	2.00	13.50
-016	5-24-67	"	"	"	39.83	1.65	4.989	4.489 to 4.989	1.83	13.43
-017	5-24-67	"	"	"	39.78	1.65	6.033	5.533 to 6.033	2.04	13.31
-018	7-19-67	2 Mod 3	"	Water Cooled	39.92	1.65	8.416	7.916 to 8.416	1.91	18.66
-019	7-20-67	"	"	"	39.85	1.65	39.349	32.500 to 37.500	1.86	18.29

\*P<sub>0</sub> tap located on chamber wall approx. 1" below injector face



UNCLASSIFIED

TABLE IX

## TEST DATA SUMMARY

## PROGRAM TEST DATA SUMMARY

	$\dot{W}_t$ LB/SEC.	$P_c$ (face) PSIA	$P_{OJ}$ PSIA	$\Delta P_o$ PSI	$P_{fJ}$ PSIA	$\Delta P_f$ PSI	$T_{OJ}$ °F	$T_{OFM}$ °F	$T_{FFM}$ °F	$SG_o$	$SG_f$	REMARKS
1	22.91	111.3°	155	43.7	196	84.7		-252	65.3	1.406	0.986	Stable - No damage - Exhaust scrubber used - Oxidizer flowmeter invalid.
5	17.04	95.1°	132	36.9	148	52.9		-286	54.0	1.420	0.991	Unstable at $FS_1 + 2.395$ sec. - No damage - Exhaust scrubber used.
7	17.14	97	150	53.0	157	60.0		-295	70.3	1.457	0.984	Stable - No damage - Exhaust scrubber not used.
6	18.70	100.3	172	71.7	156	55.7		-289	67.3	1.433	0.985	Unstable at $FS_1 + 1.073$ sec. - No Damage.
7	18.09	98.8	161	62.2	152	53.2		-296	66.2	1.462	0.986	Unstable at $FS_1 + 1.645$ sec. - No damage..
9	20.08	97.7	165	67.3	146	48.3		-296	64.5	1.462	0.986	Unstable at $FS_1 + 1.306$ sec. - No damage.
5	17.64	97.7°	141	43.3	147	49.3	-280	-294	71.2	1.448	0.984	Unstable at $FS_1 + 1.49$ sec. - No damage
7	18.18	102.9	146	43.1	145	43.1	-287	-297	57.0	1.468	0.989	Unstable at $FS_1 + 1.79$ sec. - No damage
3	19.90	111.0	159	48.0	164	53.0	-289	-297	54.8	1.469	0.990	Stable - No damage
5	20.25	112.3	164	51.7	166	53.7	-291	-301	58.7	1.477	0.989	Unstable at $FS_1 + 2.90$ sec. - No damage
0	21.78	125	187	62.0	188	63.0	-275	-297	54.4	1.465	0.990	Unstable at $FS_1 + 1.49$ sec. - No damage
1	17.68	98.1	199	100.9	164	65.9	-308	-295	88.2	1.459	0.978	Stable - No damage
3	17.79	97.3	192	94.7	167	69.7	-280	-298	80.0	1.472	0.984	Stable - No damage
6	13.22	68.4	140	71.6	100	31.6	-278	-297	79.2	1.468	0.981	Stable - No damage
0	13.50	72.9	133	60.1	111	38.1	-279	-299	73.7	1.476	0.983	Stable - No damage
3	13.43	73.2	131	57.8	116	42.8	-280	-296	71.4	1.464	0.984	Stable - No damage
4	13.31	72.6	128	55.4	109	36.4	-288	-299	71.1	1.474	0.984	Stable - No damage
1	18.66	101.8	148	46.2	147	45.2	-313	-311	76.4	1.525	0.982	Stable - No damage - ATJ Graphite chamber liner used.
6	18.29	100.7	145	44.3	145	44.3	-305	-312	79.3	1.530	0.981	Stable - No damage - ATJ Graphite chamber liner used - Ran to $LF_2$ exhaustion

UNCLASSIFIED

TABLE IX (cont.)

LF<sub>2</sub> / N<sub>2</sub> H<sub>4</sub> BLEND PROGRAM TEST DATA

TEST NO.	DATE	INJECTOR S/N	NUMBER ELEMENTS INJ. PAT.	COMB. CHAMBER CONFIG.	POST TEST		DURATION SEC.	DATA PERIOD SEC.	M.R.	Wt LB/SEC.	P <sub>c</sub> (face) PSIA	P <sub>oJ</sub> PSIA	ΔP <sub>o</sub> PSI
					A <sub>t</sub> IN. <sup>2</sup>	ε							
1083-D01-CM													
-020	7-24-67	2 Mod 3	68	Abl. Liner and H <sub>2</sub> O Cooled Throat	39.75	1.65	50.326	42.500 to 47.500	1.86	18.38	101.7	146	44.3
-021	7-26-67	"	68	"	39.66	1.65	48.863	42.500 to 47.500	1.85	18.25	101.0	145	44.0
-022	7-27-67	"	68	"	39.55	1.65	49.894	42.500 to 47.500	1.86	18.33	101.0	145	44.0
-023	11-9-67	6	68 (W/9%FFC)	Uncooled Steel S/N 1	39.68	1.64	5.072	4.572 to 5.072	1.79	17.22	95.6	141	45.4
1083-D02-CM													
-001	9-7-67	2 Mod 3	68	Abl. S/N 2	40.2	7.44	8.544	2.000 to 8.544	1.44	16.69	93.2	143	49.8
-002	9-21-67	"	68	"	40.2	9.43	29.711	14.856 to 29.711	2.25	19.06	103.9	162	58.1
-003	11-15-67	"	68	"	41.0	7.26	194.700	194.000 to 194.500	1.83	17.73	97.1	144	46.9
-004	12-14-67	"	68	"	41.69	9.13	202.780	202.080 to 202.580	2.02	18.90	100.7	157	56.3
-005	12-19-67	"	68	"	41.69	7.26	0.8	← PREMATURE SHUT DOWN			-		
-006	12-19-67	"	68	"	42.6	7.27	170.540	169.540 to 170.540	2.04	19.02	97.5	156	58.5
-007	1-19-68	"	68	Abl. S/N 3	40.0	1.60	38.620	12.000 to 19.000	1.95	17.94	99.9	155	55.1
1083-D01-CM													
-024	5-15-68	7	344	Steel W/9 row 3 cav. resonator	39.7	1.65	2.468	1.986 to 2.486	3.10	17.77	93.7	167	73.3
-025	5-15-68	7	344	"	39.7	1.65	4.133	3.633 to 4.133	2.20	18.41	102.9	170	67.1
1083-D02-CM													
-008	6-13-68	7	344	S/N 1 abl. w/9 row 3 cav. resonator	39.87	1.65	10.820	7.500 to 8.500	1.69	16.87	95.6	160	64.4
-009	6-14-68	7	344	"	39.77	1.65	50.490	49.490 to 50.490	2.03	19.22	109.3	183	73.7
-010	6-14-68	7	344	"	39.35	1.65	100.390	99.390 to 100.390	1.97	18.66	106.7	176	69.3

UNCLASSIFIED

TABLE IX (cont.)

## PROGRAM TEST DATA SUMMARY

$\dot{W}_t$ LB/SEC.	$P_c$ (face) PSIA	$P_{oJ}$ PSIA	$\Delta P_o$ PSI	$P_{fJ}$ PSIA	$\Delta P_f$ PSI	$T_{oJ}$ °F	$T_{oFM}$ °F	$T_{fFM}$ °F	$SG_o$	$SG_f$	REMARKS
18.38	101.7	146	44.3	147	45.3	-307	-314	80.6	1.537	0.981	Stable - No damage - Ran to $LF_2$ exhaustion
18.25	101.0	145	44.0	146	45.0	-309	-314	78.7	1.536	0.981	Stable - No damage - Ran to $LF_2$ exhaustion
18.33	101.0	145	44.0	146	45.0	-311	-314	83.9	1.537	0.980	Stable - Exit end H <sub>2</sub> O cooled - Nozzle warped - Abl. liner refireable - Ran to $LF_2$ exhaustion
17.22	95.6	141	45.4	144	44.8	-303	-308	61.8	1.513	0.987	Stable - No damage
16.69	93.2	143	49.8	150	58.8	-272	-274	91.1	1.367	0.978	Stable - No damage
19.06	103.9	162	58.1	142	38.1	-300	-302	86.1	1.489	0.979	Stable - Mini-skirt failed
17.73	97.1	144	46.9	140	42.9	-299	-301	67.4	1.484	0.985	Stable - No damage visible - Streaking into throat
18.90	100.7	157	56.3	143	42.3	-299	-302	53.6	1.475	0.991	Stable - Mini-skirt cracked in sharp radius bend - Throat insert delaminated
TURE SHUTDOWN - DEFECTIVE CSM UNIT →											Stable - No damage
19.02	97.5	156	58.5	142	44.5	--	-298	52.8	1.473	0.991	Stable - Axial crack in throat insert - Streak pattern deeper
17.94	99.9	155	55.1	146	46.1	-298	-296	60.3	1.463	0.998	Stable - Chamber liner ruptured beyond repair - No injector damage
17.77	93.7	167	73.3	130	36.3	--	-300	73.0	1.481	0.983	No damage - Stable pulsed w/20 gr/ at $FS_1$ + 2.170 sec.
18.41	102.9	170	67.1	166	53.1	--	-299	71.2	1.475	0.984	Stable - No damage - Pulsed w/20 gr. at $FS_1$ + 2.168 sec.
16.87	95.6	160	64.4	175	79.4	-288	-281	76.0	1.428	0.982	Stable - No damage
19.22	109.3	183	73.7	185	75.7	-307	-307	75.7	1.509	0.982	Stable - Throat insert starting to crack axially
18.66	106.7	176	69.3	182	75.3	-306	-308	78.1	1.513	0.981	Stable - Throat insert cracked - Erosion within 3 in. of injector face

UNCLASSIFIED

2



TABLE IX (con

L F<sub>2</sub> / N<sub>2</sub> H<sub>4</sub> BLEND PROGRAM TEST

TEST NO.	DATE	INJECTOR S/N	NUMBER ELEMENTS INJ. PAT.	COMB. CHAMBER CONFIG.	POST TEST		DURATION SEC.	DATA PERIOD SEC.	M.R.	Wt LB/SEC.	P <sub>c</sub> (face) PSIA	P <sub>oJ</sub> PSIA
					A <sub>t</sub> IN. <sup>2</sup>	€						
1083-DO1-OM												
-026	6-25-68	7	344	Standard Un- cooled Steel, S/N 1	39.6	1.65	2.200	1.700 to 2.200	1.82	17.42	96.5	159
-027	6-27-68	7	344	Steel w/1 row 1 cavity re- sonator	39.8	1.64	2.486	1.986 to 2.486	1.98	18.39	104.1	170
-028	6-27-68	7	344	"	39.8	1.64	2.250	1.646 to 2.146	1.99	18.10	103.0	167
-029	6-28-68	7	344	Steel w/2 row 1 cavity re- sonator	39.8	1.64	2.300	1.659 to 2.159	2.18	18.28	102.5	168
-030	6-28-68	7	344	"	39.8	1.64	3.980	3.480 to 3.980	2.03	18.51	101.9	170

TABLE IX (cont.)PROGRAM TEST DATA SUMMARY

$\dot{W}_t$ LB/SEC.	$P_c(\text{face})$ PSIA	$P_{oJ}$ PSIA	$\Delta P_o$ PSI	$P_{fJ}$ PSIA	$\Delta P_f$ PSI	$T_{oJ}$ °F	$T_{oFM}$ °F	$T_{fFM}$ °F	$SG_o$	$SC_f$	REMARKS
17.42	96.5	159	62.5	173	76.5	--	-309	97.3	1.514	0.977	Stable until pulsed w/20 gr. at $FS_1 + 2.193$ sec. - No damage
18.39	104.1	170	65.9	179	74.9	--	-304	82.7	1.496	0.980	Stable, pulsed w/20 gr. at $FS_1 2.197$ sec. - No damage
18.10	103.0	167	64.0	175	72.0	-293	-305	82.4	1.500	0.980	Stable until pulsed w/20 gr. at $FS_1 + 2.182$ sec. - No damage
18.28	102.5	168	65.5	167	64.5	-297	-309	79.0	1.516	0.981	Stable until pulsed w/20 gr. at $FS_1 + 2.191$ sec. - No damage
18.51	101.9	170	68.1	176	74.1	-287	-311	79.4	1.523	0.981	Stable, pulsed w/20 gr. at $FS_1 + 3.800$ sec. - Some resonator hole erosion.

UNCLASSIFIED

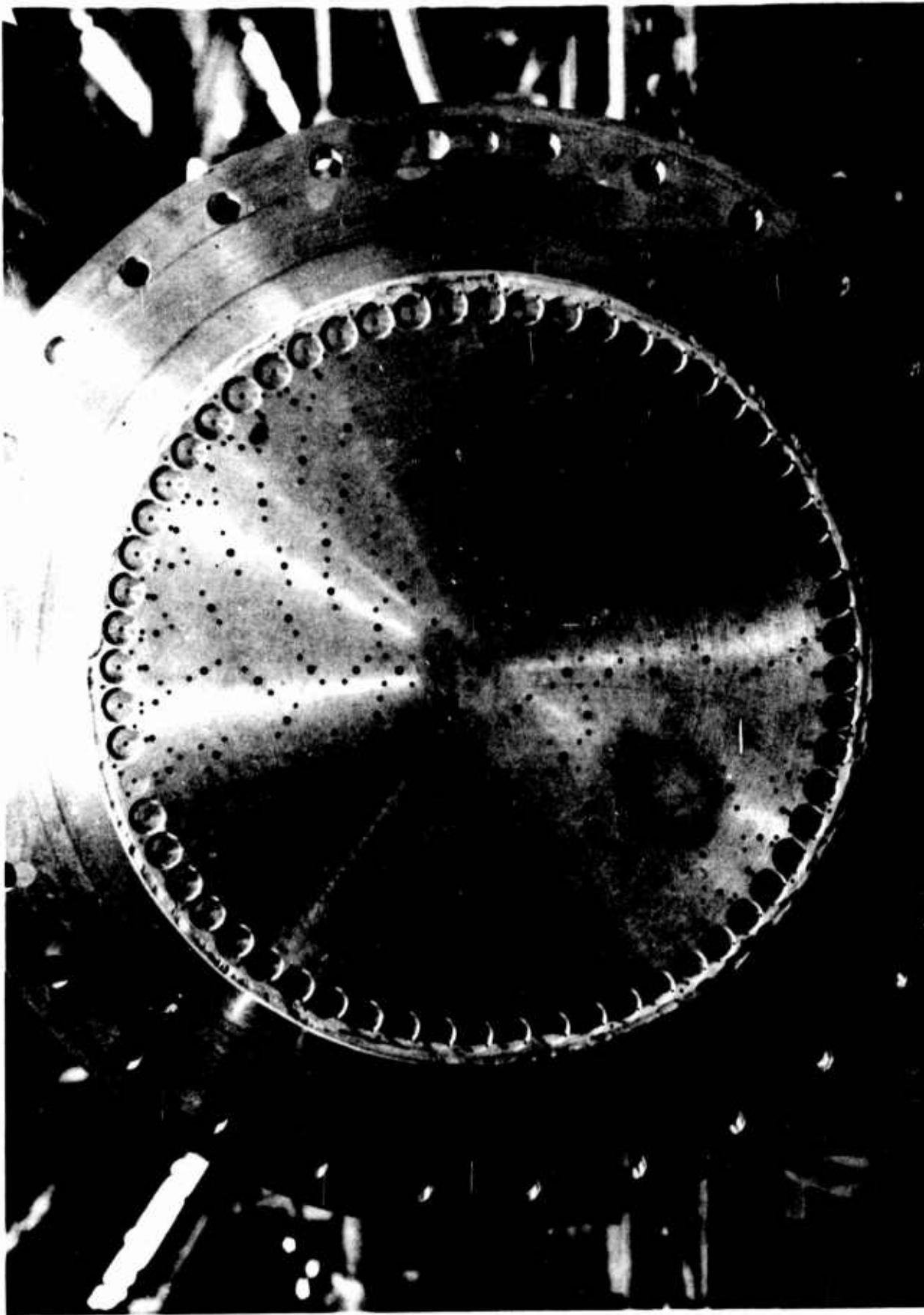


Figure 34. Pre-Test View of Injector S/N T<sup>2</sup>

UNCLASSIFIED

UNCLASSIFIED

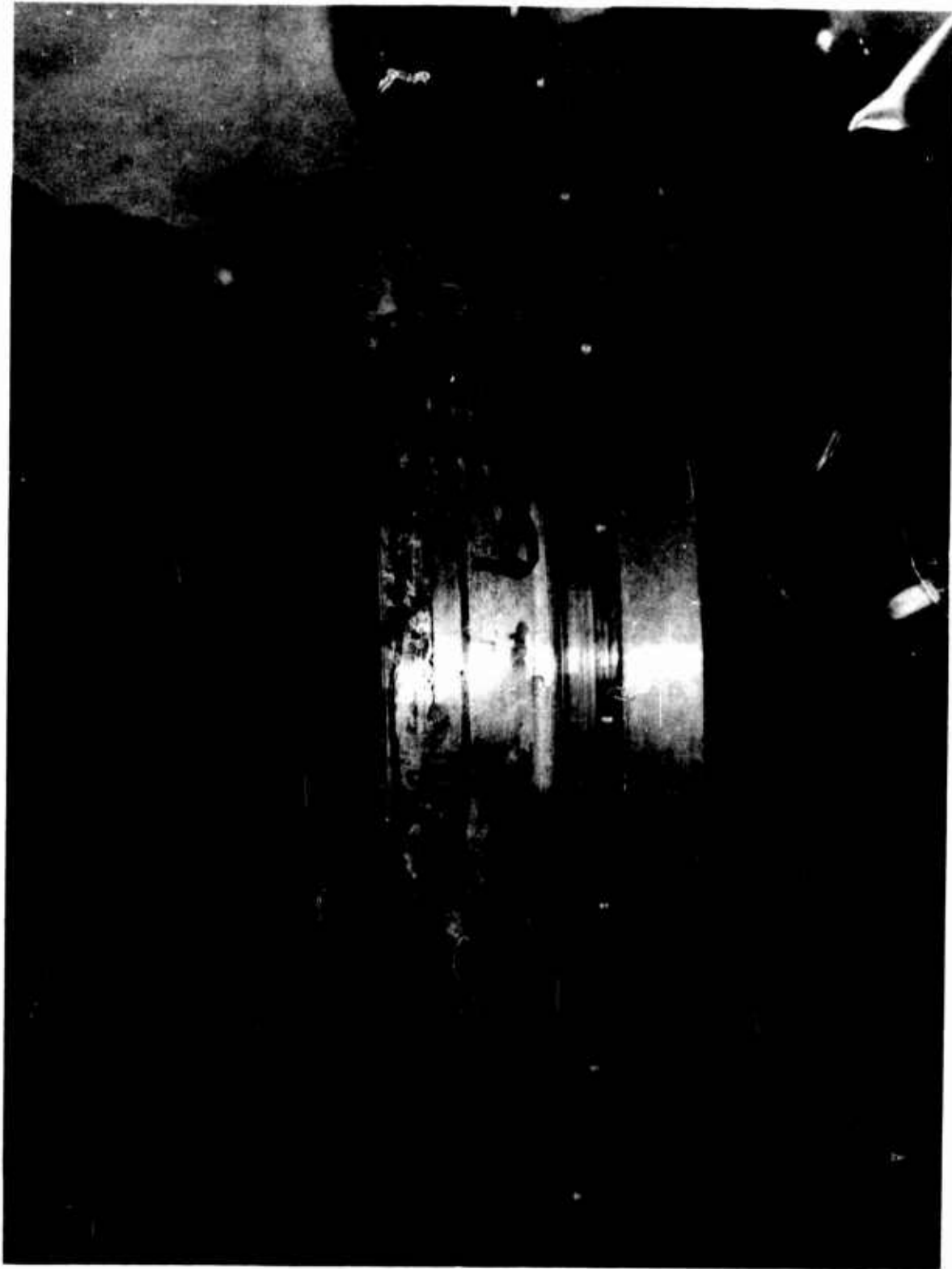


Figure 35. Post-Test View of Injector S/N T<sup>2</sup> (2.7 sec Duration)

UNCLASSIFIED

## UNCLASSIFIED

The third test was conducted to ensure that the instability which occurred during the second test was not the result of fuel loss through the cracked section. The third test also was unstable.

A combustion stability monitor (CSM) was utilized. Chamber pressure oscillations sensed by means of a high-frequency pressure transducer (Photocon) or fuel manifold pressure oscillations sensed by a Taber pressure transducer were fed to the CSM. It was set to trip and automatically terminate the test whenever peak-to-peak oscillations of 25 psi lasted for 30 millisecond at 1000 cps. A test could be terminated by the CSM within 150 millisecond after the threshold conditions were exceeded. In all instances, the time required for shutdown was sufficiently short to prevent hardware damage.

Injector S/N 2 was a nickel unit having 158 elements and 6% fuel film cooling. It was tested four times for a total of 6.85 sec. This injector was unstable during each of the last three tests, but no damage was sustained by it or the uncooled steel chamber. Chamber discolorations were quite uniform around the forward end.

Injector S/N 2, Mod 1, was the result of modifying the 158-element unit, S/N 2, into one having 98 elements including 30 long-impinging unlike-doublet elements at the periphery. It was tested four times for a total of 10.47 sec. Three of these tests were unstable but, again, no damage to either the injector or steel chamber was incurred. The chamber discolorations originating at the injector face were less uniform and some of the streaks became more pronounced (see Figure No. 36).

The injector pattern was modified further by welding the 30 peripheral elements shut and making it into a 68-element pattern which was designated as S/N 2, Mod 2. Six tests, for a total of 26.06 sec, were conducted over a range of chamber pressures and mixture ratios. All six tests were stable. Gas flow patterns marking across the injector face became well defined as well as characteristic for all of the tests made with the 68-element pattern, including S/N 2, Mod 3 (see Figure No. 37). Discolorations on the forward end of the chamber wall appeared to be non-uniform with several spots showing metal splatter (see Figure No. 38). These were located within 0.5-in. of the injector face and were less than 0.5-in. in diameter.

The modifications needed to evolve a 68-element pattern from the 158-element design resulted in an excessive injector orifice pressure drop. This was overcome by enlarging the orifice diameters and the modified unit was designated as S/N 2, Mod 3. In addition, approximately 2% fuel film cooling was added in selected areas to counter the small but well-defined chamber damage noted above.

Injector S/N 2, Mod 3, was initially tested with the water-cooled throat assembly and the cooled ATJ graphite chamber liner for durations

UNCLASSIFIED

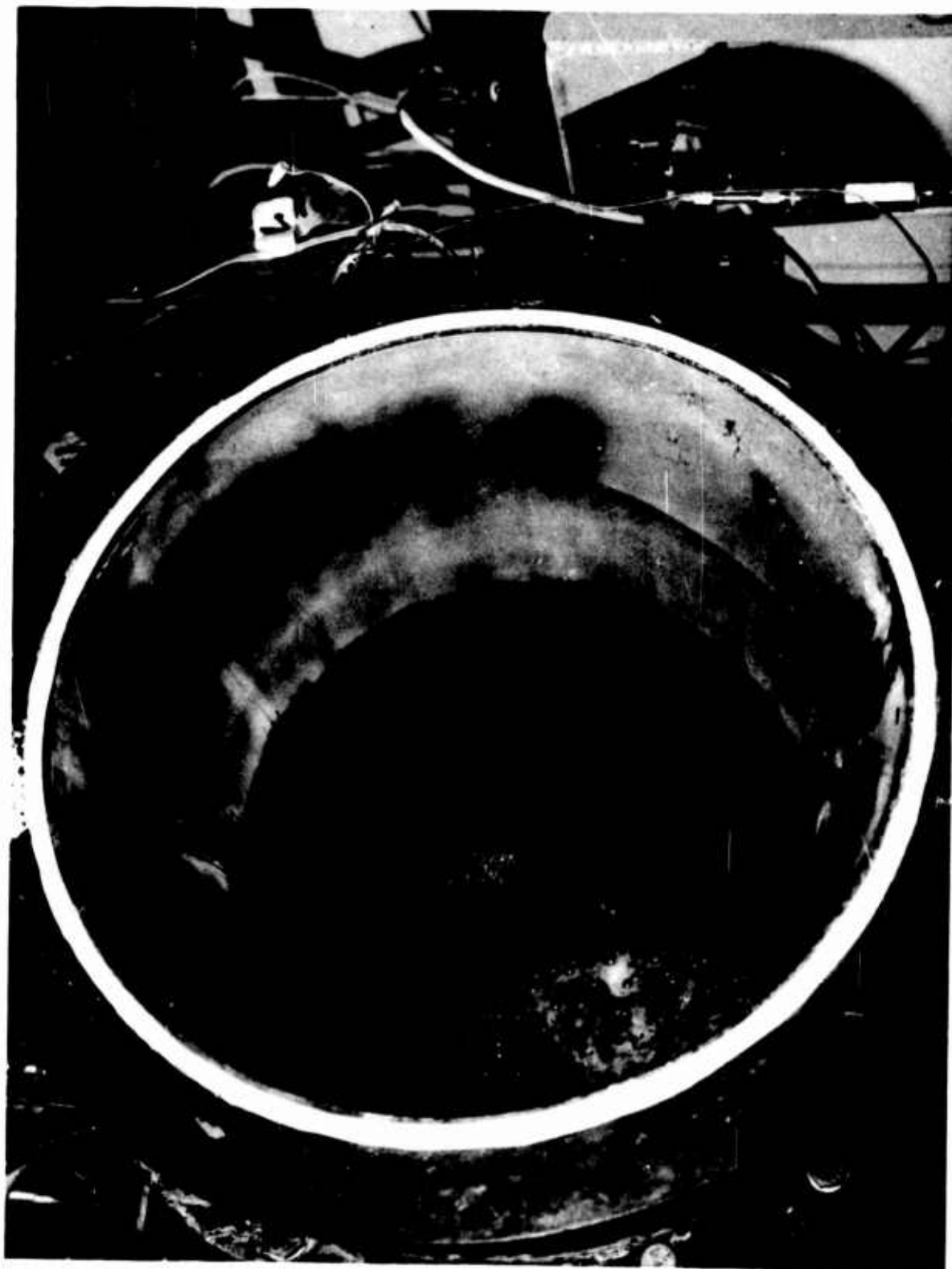


Figure 36. Post-Test (No. 009) View of Steel Chamber with S/N 2,  
Mod 1 Injector

UNCLASSIFIED

UNCLASSIFIED

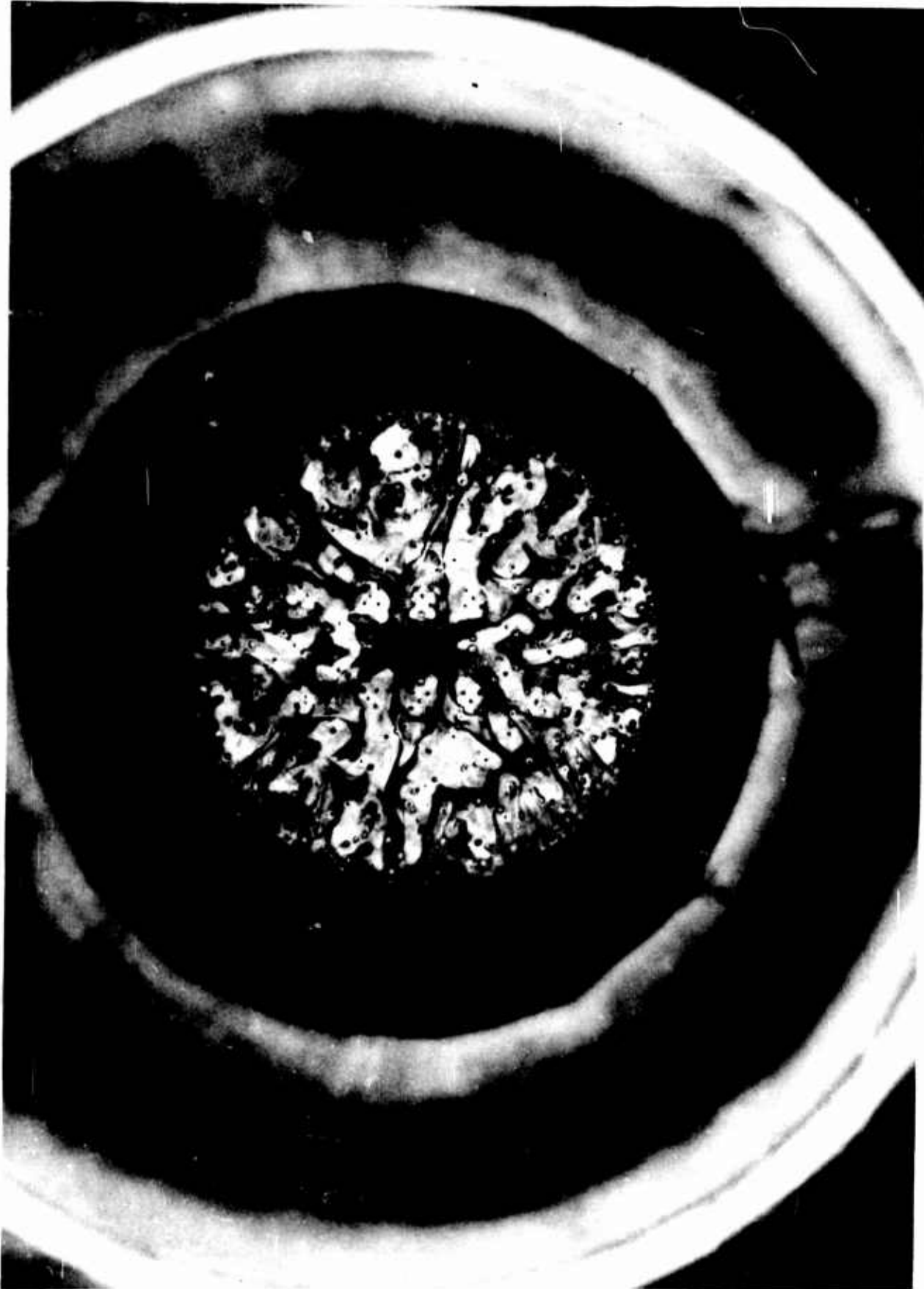


Figure 37. Post-Test (No.-017) View of S/N 2, Mod 2 Injector

UNCLASSIFIED



UNCLASSIFIED



Figure 38. Post-Test (No.-017) View of Forward End of Steel Chamber  
Tested with S/N 2, Mod 2 Injector

UNCLASSIFIED

## UNCLASSIFIED

of 8.4 sec and 39.3 sec. The test installation is shown on Figure No. 39. No erosion or damage was sustained by the throat section after the total duration of 47.77 sec. The ATJ graphite liner was slightly streaked near the injector in areas similar to those discolored on the uncooled steel chamber following tests with injector S/N 2, Mod 2.

The cooled chamber section was replaced with a segmented ablative section and tested three times for a total of 149.08 sec. The ablative-lined chamber section incorporated two specimens of graphite phenolic (FM5064) backed with silica phenolic (FM5067). The liner specimens were split axially with one having a higher resin content than the other (30% and 36%). Holes covered one half of each specimen. These holes were drilled through the graphite phenolic to expose the silica phenolic to the combustion gases. Post-test inspection revealed erosion at the forward end which matched the markings found on the previously tested ATJ graphite liner. The difference in resin content had no measurable effect upon the fluorine corrosion resistance. The lower resin content specimen (30%) had a slightly deeper char presumably as a result of its higher thermal conductivity. The condition of the ablative section after 100 sec is shown on Figure No. 40. All five tests were stable and no damage was sustained by the injector.

Injector S/N 2, Mod 3, then was assembled to ablative chamber S/N 002 and installed into Test Stand J-4 for simulated altitude tests. The assembly was tested six times for a total duration of 606.4 sec.

The first test was prematurely terminated at 8.5 sec when it became evident that the diffuser was not operating properly and hot exhaust gases were filling the test cell. Post-test examination revealed that the injector and the ablative chamber were undamaged. Appropriate replacement of damaged instrumentation and controls wiring was accomplished.

The short, radiation-cooled skirt was assembled to the ablative chamber, increasing the exit area ratio from 7.4 to 9.4 (see Figure No. 41). This skirt, which was fabricated from columbium, C-103, had been coated with three different materials to permit an evaluation of coatings under test conditions. These coatings were: nickel aluminide ceramic; Lunite 2/aluminide diffusion coating; and Lunite 3, hafnium-tantalum.

The second test also was prematurely terminated after 29.7 sec when the skirt section coated with the nickel aluminide ceramic failed. This portion of the skirt, which was a 120-degree arc, almost completely disappeared while the adjacent areas remained unaffected (see Figure No. 42). As in the first test, the injector and the ablative chamber remained undamaged.

A new columbium nozzle section was fabricated and attached with columbium rivets. This new nozzle portion was coated with Lunite 2, which appeared to have been the least affected of the original coatings.

UNCLASSIFIED

**CONFIDENTIAL**

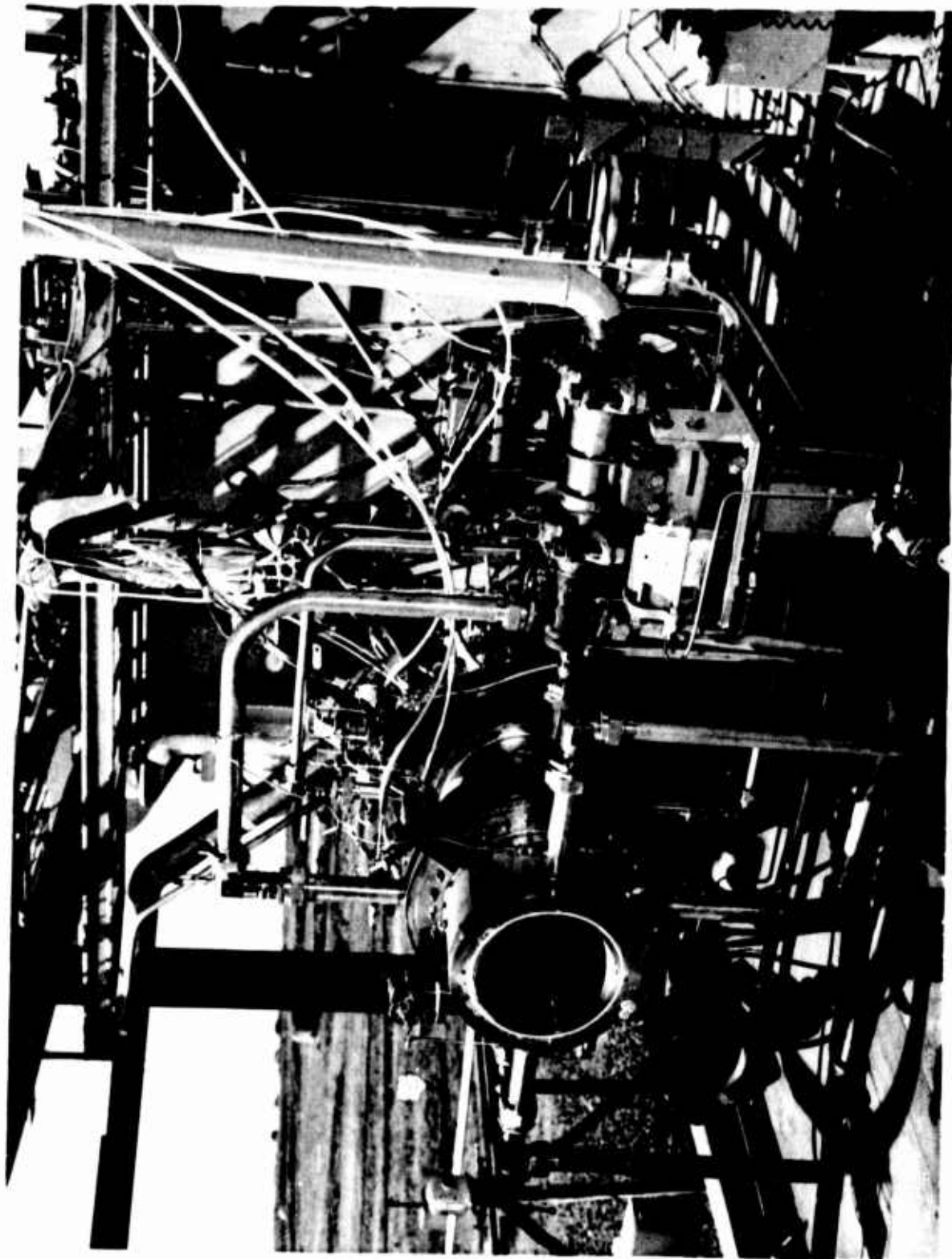


Figure 39. Water-Cooled Chamber Test Installation

Page 89

**CONFIDENTIAL**

(This Page is Unclassified)

**CONFIDENTIAL**

**Note:**

Solid Lines Denote  
Islands of Essentially  
Uneroded Areas.

Dotted Lines Denote  
Initial Development  
of Visible Streaks

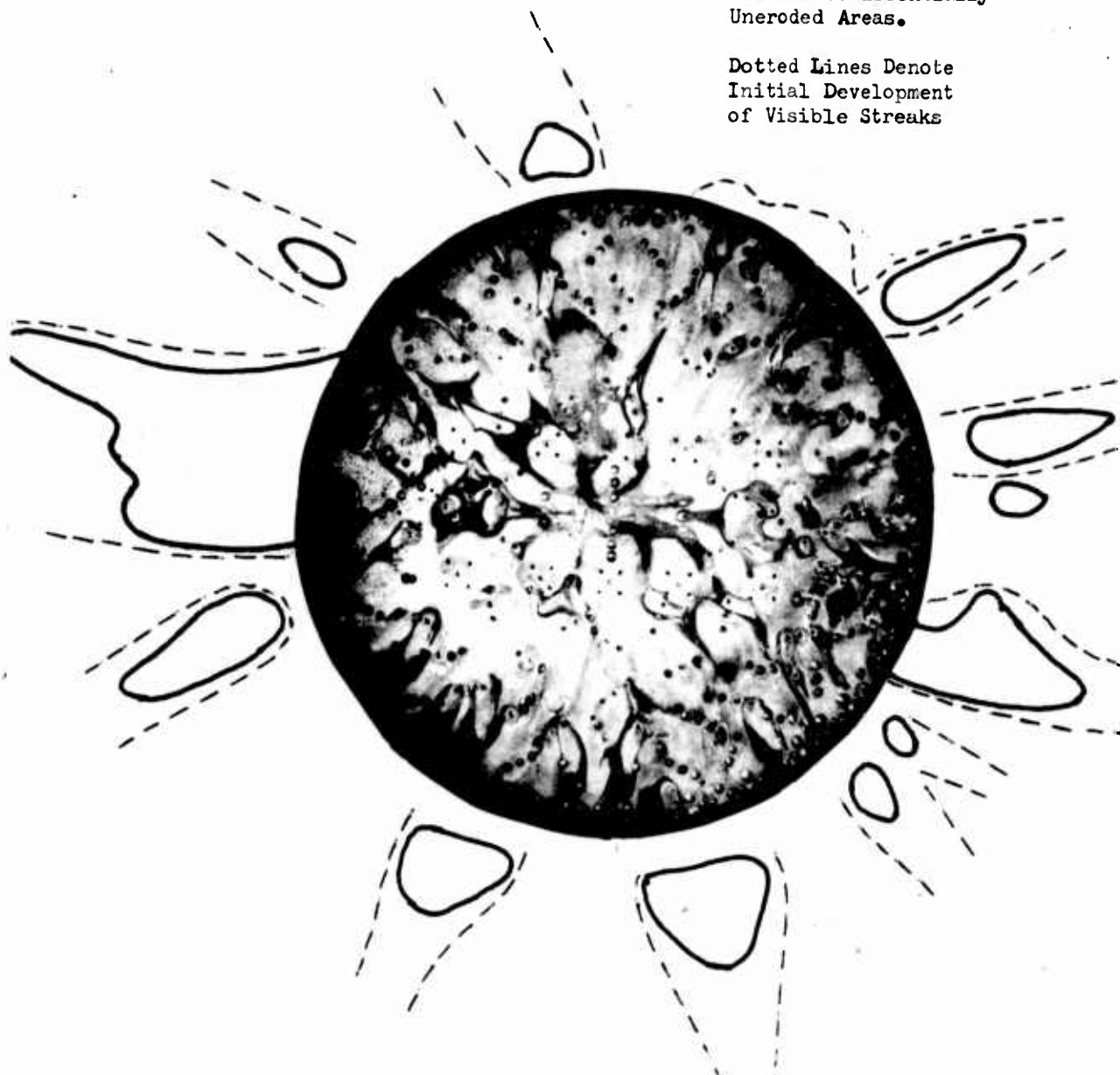


**Figure 40.** Ablative Liner in Water-Cooled Chamber Tested with S/N  
S/N 2, Mod 3 Injector after 100 sec of Testing (u)

**CONFIDENTIAL**

UNCLASSIFIED

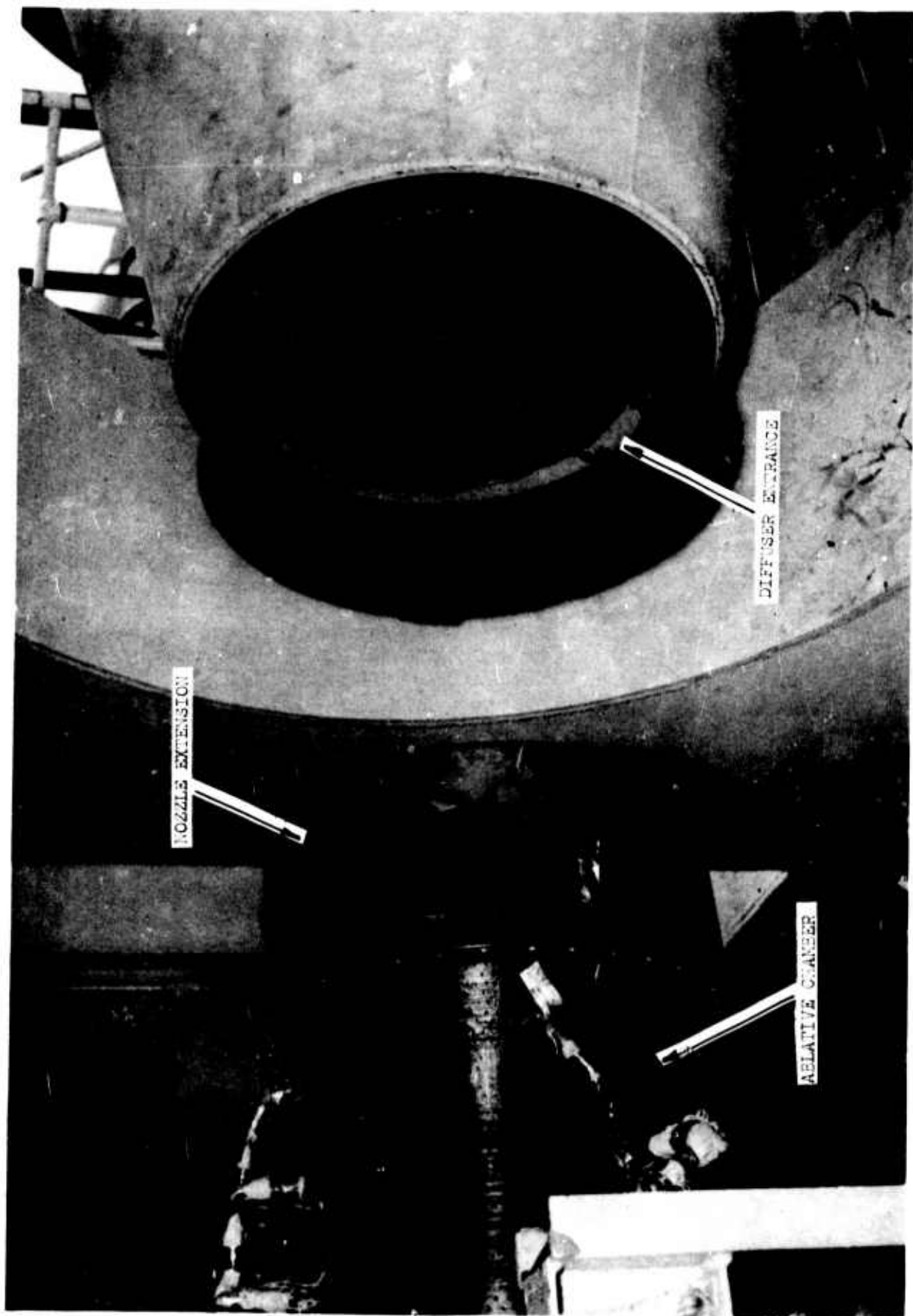


Figure 41. Nozzle Extension and Ablative Chamber S/N 002 Test Installation

UNCLASSIFIED

UNCLASSIFIED

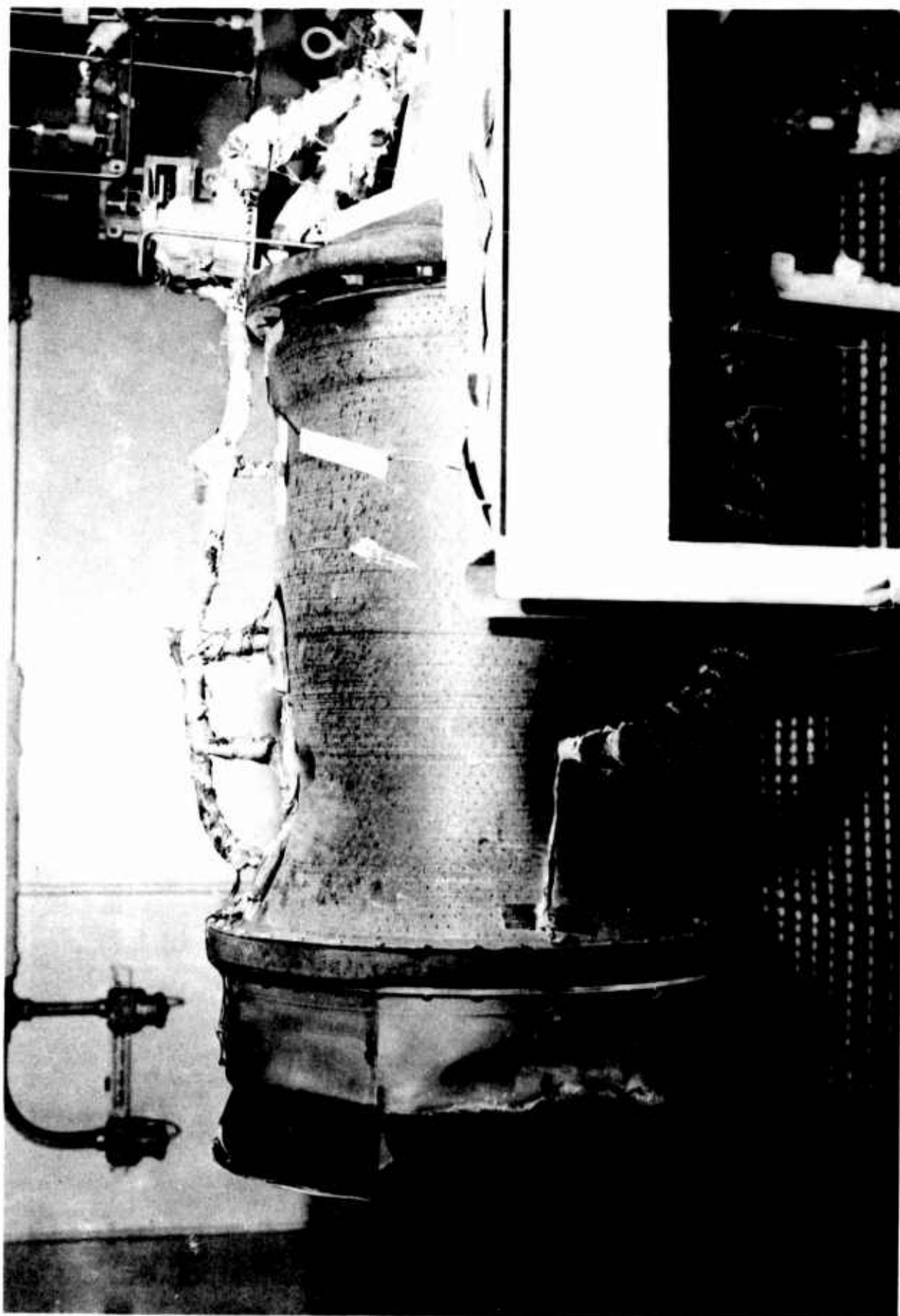


Figure 42. Post-Test (No.-002) View of Damaged Nozzle Section

UNCLASSIFIED



## CONFIDENTIAL

The injector and ablative chamber assembly without the skirt were successfully tested for 194.7 sec. This third test had been scheduled for a minimum of 150 sec, dependent upon the critical run parameters. The test was terminated when the steam supply for the ejectors was almost exhausted.

Both the injector and the ablative thrust chamber were in excellent condition. The streak pattern had started to form and partially extended to the throat. There were no delaminations or cracks in the fibrous graphite throat insert. The throat radius had increased by 0.035-in.

The fourth test, which was conducted with the repaired nozzle extension, was run without incident for a duration of 202.8 sec at a test cell pressure of approximately 0.6 psia.

No damage was sustained by the injector. The streak pattern on the ablative chamber liner became more pronounced with some streaks reaching through the throat area. An axial crack in the throat insert appeared diagonally across the plies and in the bottom of the deepest streak extending through the throat (see Figure No. 43); however, it was not serious enough to terminate testing. A delamination in the forward end of the fibrous graphite throat insert also was noted (see Figure No. 44). It appeared to be solid and was not regarded as critical to further testing.

Inspection of the columbium nozzle extension revealed that it contained a crack in the attachment area. This crack was more than a foot long which was severe enough to prevent the nozzle from being tested any further.

Metallurgical examination showed the crack to be in an area that was approximately one-half of the nominal wall thickness. This thinning was attributed to the difficulty in spinning the sharp corner at the attachment area. The lack of oxidation at the edges of the crack indicated it had occurred after shutdown.

Oxidation of the columbium on the flame side of the nozzle was more severe in the Lunite-2 coated areas. The repaired portion of the nozzle coated with Lunite-2 showed less embrittlement than the original sector. The high temperature curing of the nozzle during repair could have been detrimental to the original coating.

The outer surface of the Lunite-3 coated (hafnium-tantalum) portion of the nozzle exhibited numerous coating cracks. However, these cracks did not extend through the coating inter-metallic bond line and were not detrimental to the columbium.

The results of a metallurgical examination of the nozzle extension are presented as Appendix VI.

## CONFIDENTIAL

(This page is Unclassified)

**CONFIDENTIAL**

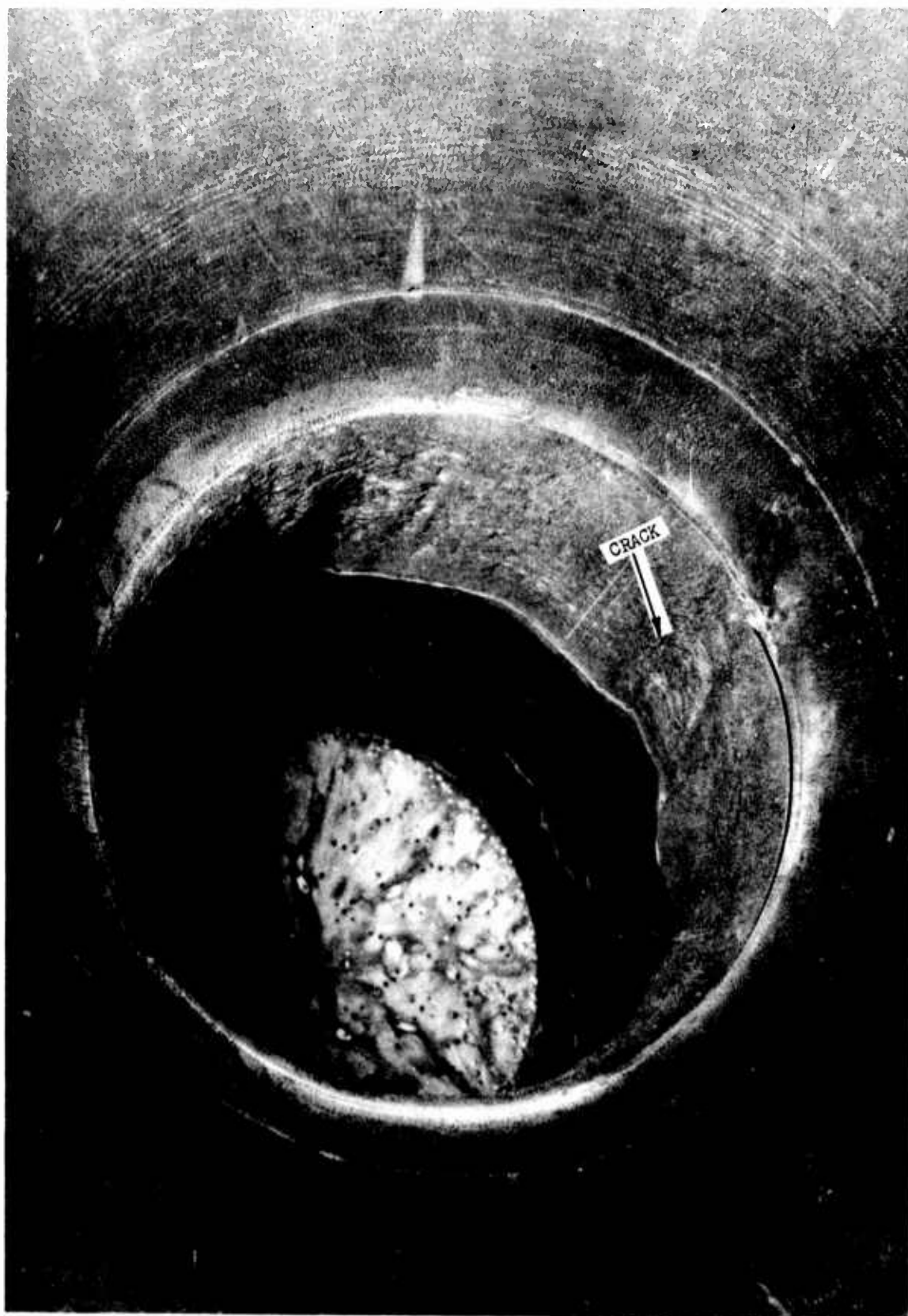


Figure 43. View of Damaged Throat Insert, Ablative Chamber S/N 002 (u)

Page 94

**CONFIDENTIAL**

**CONFIDENTIAL**



Figure 44. Delaminated Section of Throat Insert, Ablative  
Chamber S/N 002 (u)

**CONFIDENTIAL**

## CONFIDENTIAL

(U) The fifth test of the series was automatically terminated by the CSM prematurely after 0.8 sec. It was found that the CSM had been inadvertently set to identify the shutdown threshold as a frequency of less than 400 cps rather than the intended 1000 cps. This setting was corrected and the last test of the series was conducted for 170.6 sec without incident.

(C) No injector damage was noted during the post-test inspection. The condition of ablative chamber S/N 002, which had accumulated 606.4 sec of testing, is shown on Figures No. 45 through No. 48 following the last test. Operation had been satisfactory over the entire duty cycle. Major erosion, approximately 0.4-in. deep and around the entire diameter, appeared in the region adjacent to the injector and several streaks extended through the throat. Maximum streak depth at the throat was 0.5-in. and total throat area increase was approximately 6%. The radial growth in the non-streaked areas was approximately 0.12-in. Figure No. 49 is a plot of throat area increase in relationship to time. The axial crack which appeared diagonally across the plies in the fibrous graphite throat insert after the fourth test (total duration of 436 sec) remained unchanged other than an increase in width. It had no affect upon the last, 170 sec duration test. The delamination in the forward end of the fibrous graphite throat insert noted after the fourth test remained unchanged during the last test (see Figure No. 44). All of the streaks, which were characterized by smooth and rounded surfaces, had been defined within the first three tests (232.2 sec). Successive testing only deepened them.

(U) As seen on Figures No. 44 through No. 47, there was no streaking of the nozzle section of the ablative chamber. Although discolorations were evident, the surface was in excellent condition. Discolorations on the nozzle surface (see Figure No. 45) matched the locations of the major streaks within the chamber. Pyrolysis gases from the insulating material behind the throat insert appeared to have exited just downstream of the throat at a fabrication joint in the graphite phenolic. This can be seen on Figure No. 44.

(U) An in-depth, post-test analysis of S/N 002 ablative chamber is presented as Appendix VII.

(U) Injector S/N 2, Mod 3, was tested 11 times for a total of 803.25 sec without any apparent damage. Following the last test in this program, it was thoroughly cleaned and inspected. Then, this injector with the water-cooled chamber was loaned to the Aerojet-General Nuclear Rocket Operations as being a reliable unit for use in a high temperature, water penetration test program they were conducting. In the four tests conducted to date (99.0 sec), there has been no damage to either component. The condition of the cleaned face at the time injector S/N 2, Mod 3, was water-flowed is shown on Figure No. 50, where water can be seen draining from some of the orifices. Several areas of light face erosion also can be seen, but

## CONFIDENTIAL

**CONFIDENTIAL**

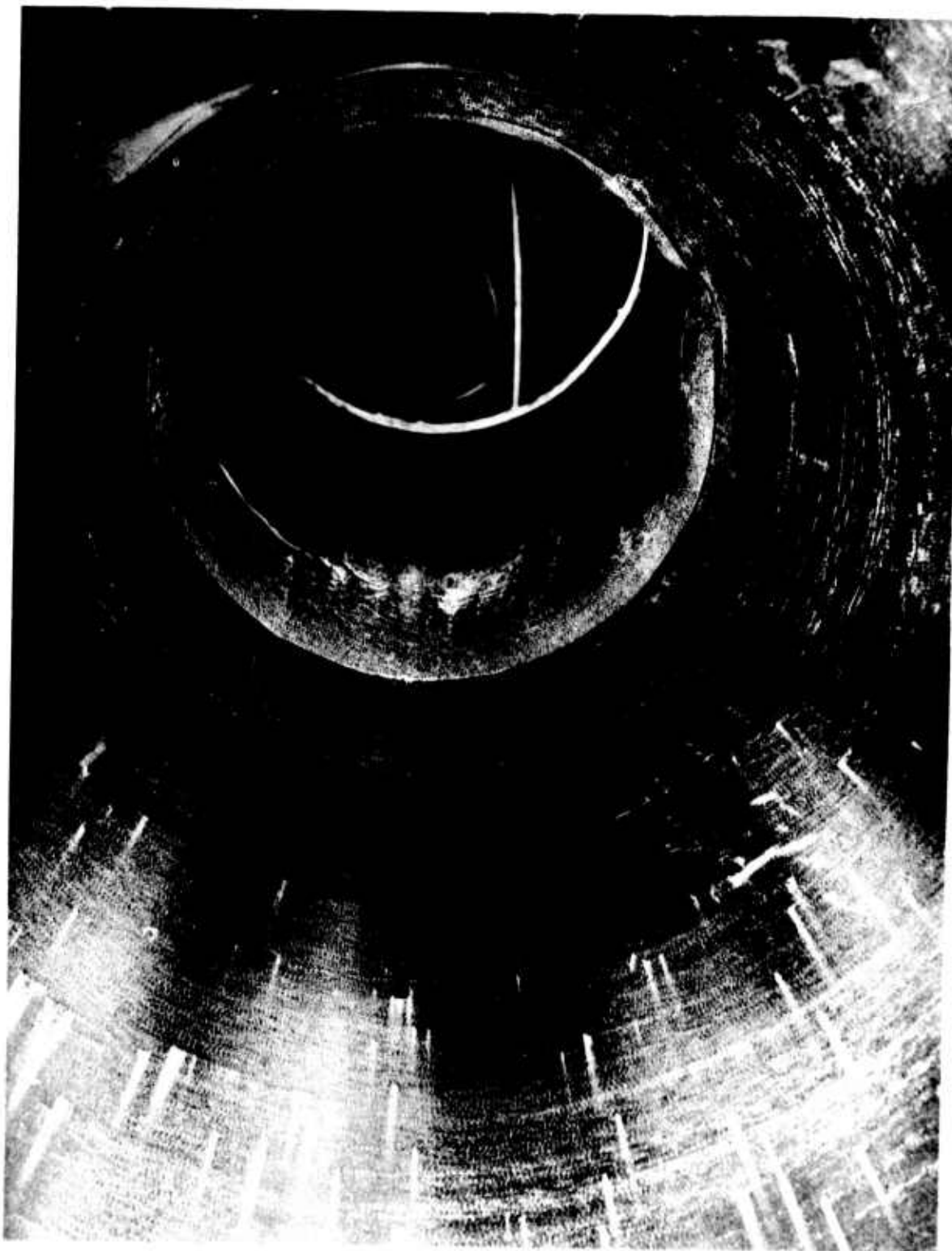


Figure 45: Post-Test View of Ablative Chamber S/N 002 after 606 sec of Testing (u)

**CONFIDENTIAL**



**CONFIDENTIAL**

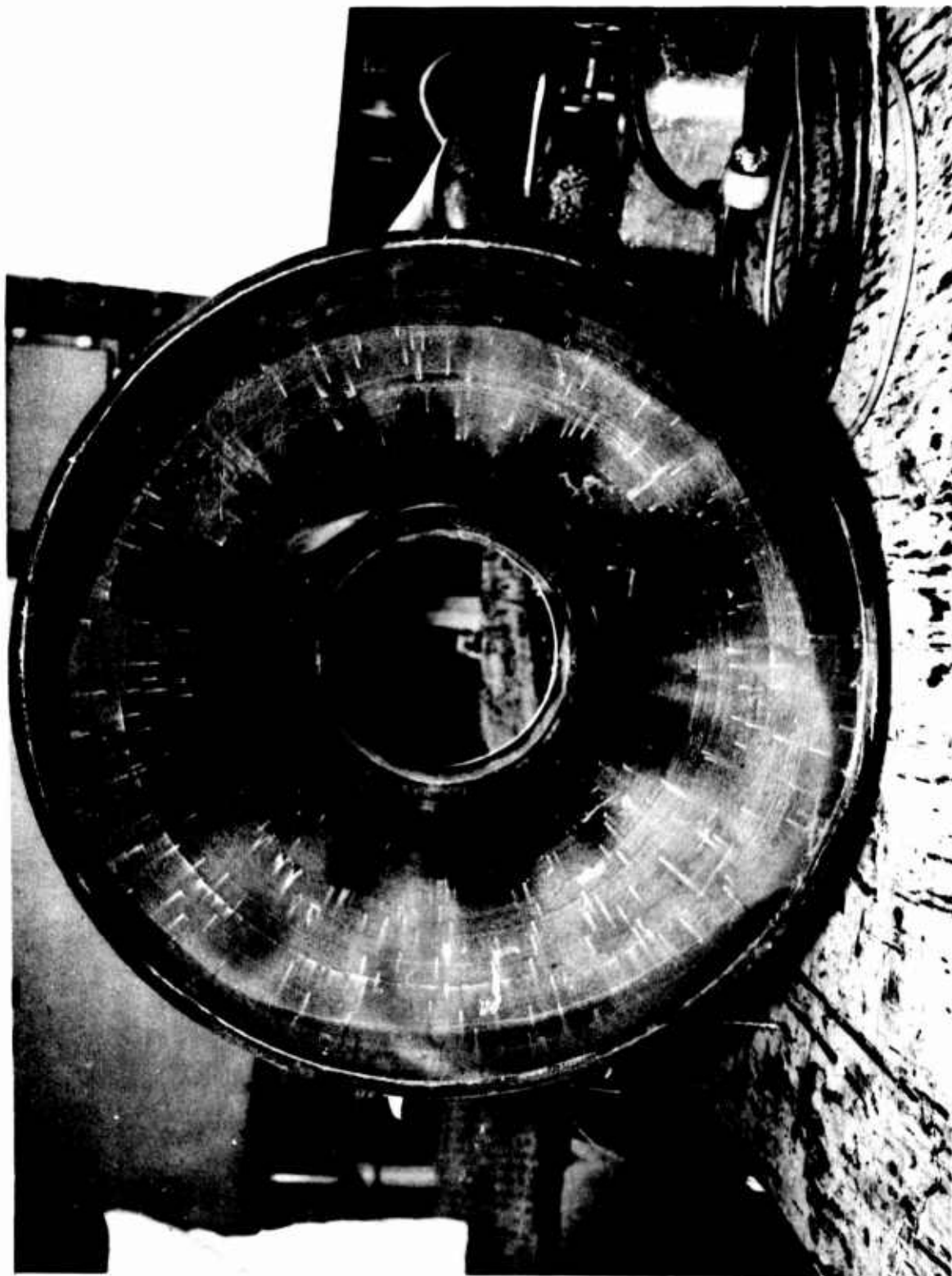


Figure 46. Post-Test View of Ablative Chamber S/N 002 after 606 sec  
of Testing (u)

**CONFIDENTIAL**



**CONFIDENTIAL**

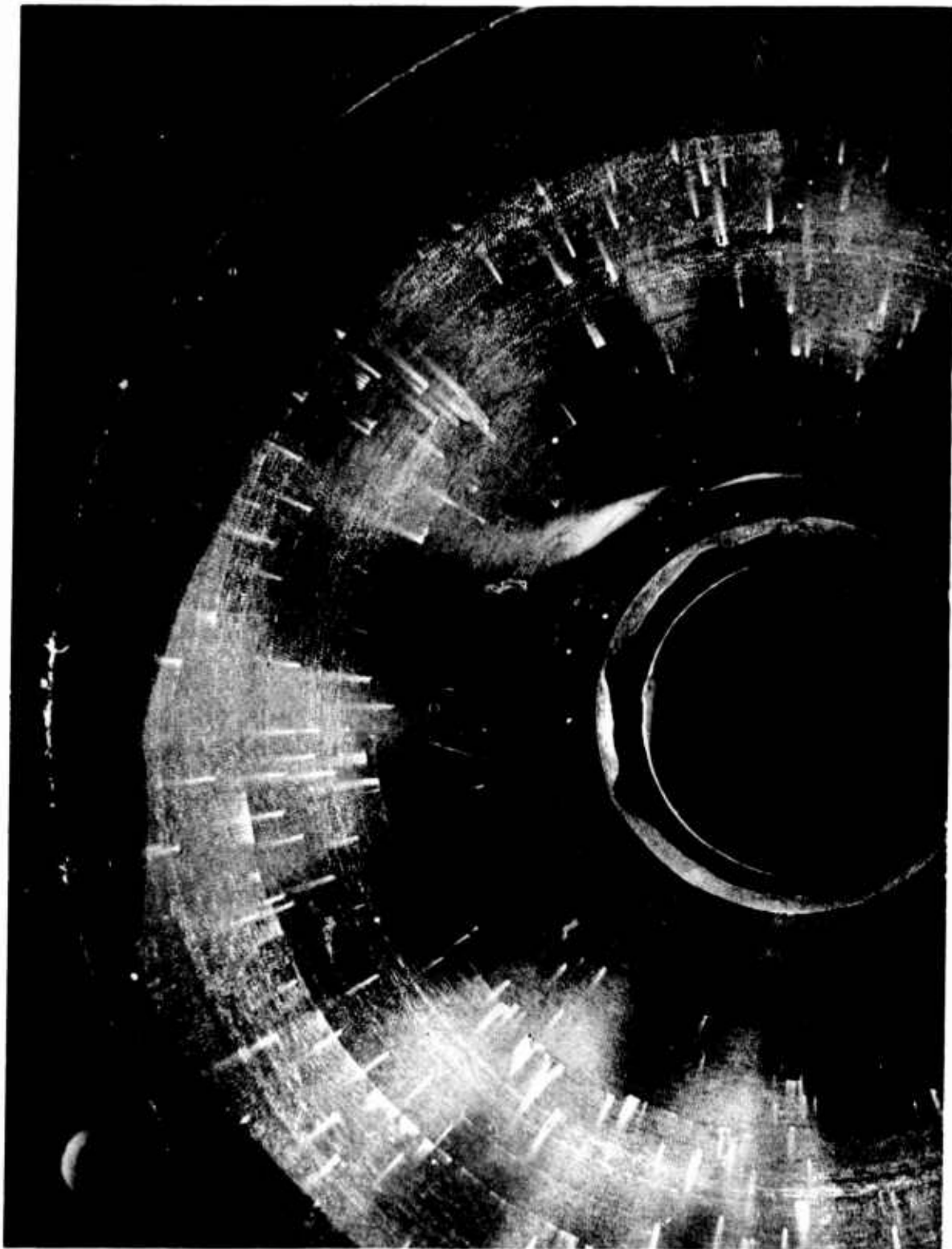


Figure 47. Post-Test View of Ablative Chamber S/N 002 after 606 sec of Testing (u)

**CONFIDENTIAL**



Figure 48. Post-Test View of Ablative Chamber S/N 002 after 606 sec  
of Testing (u)

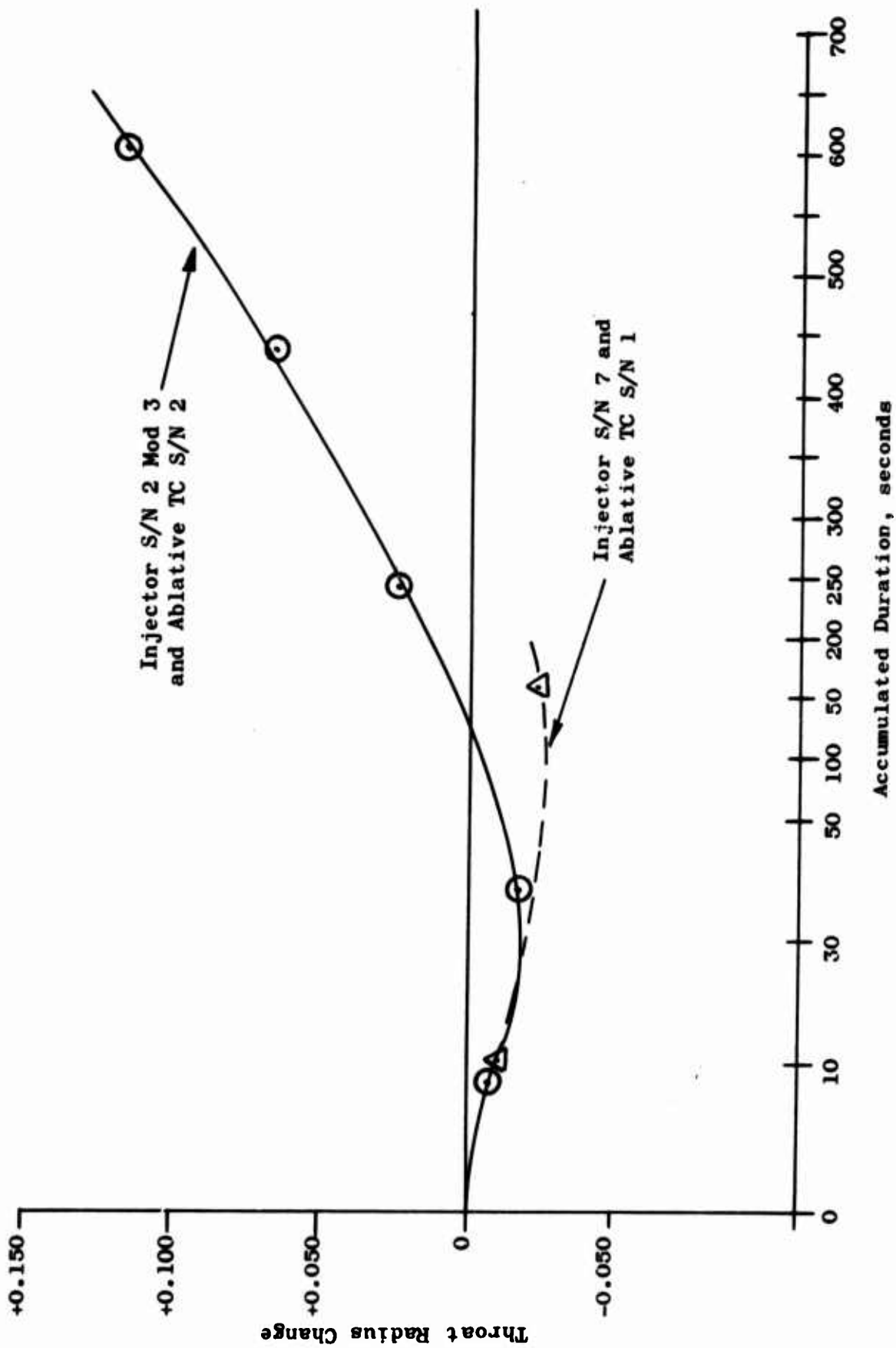


Figure 49. Throat Radius Change vs Time, Ablative Chamber S/N 002

UNCLASSIFIED

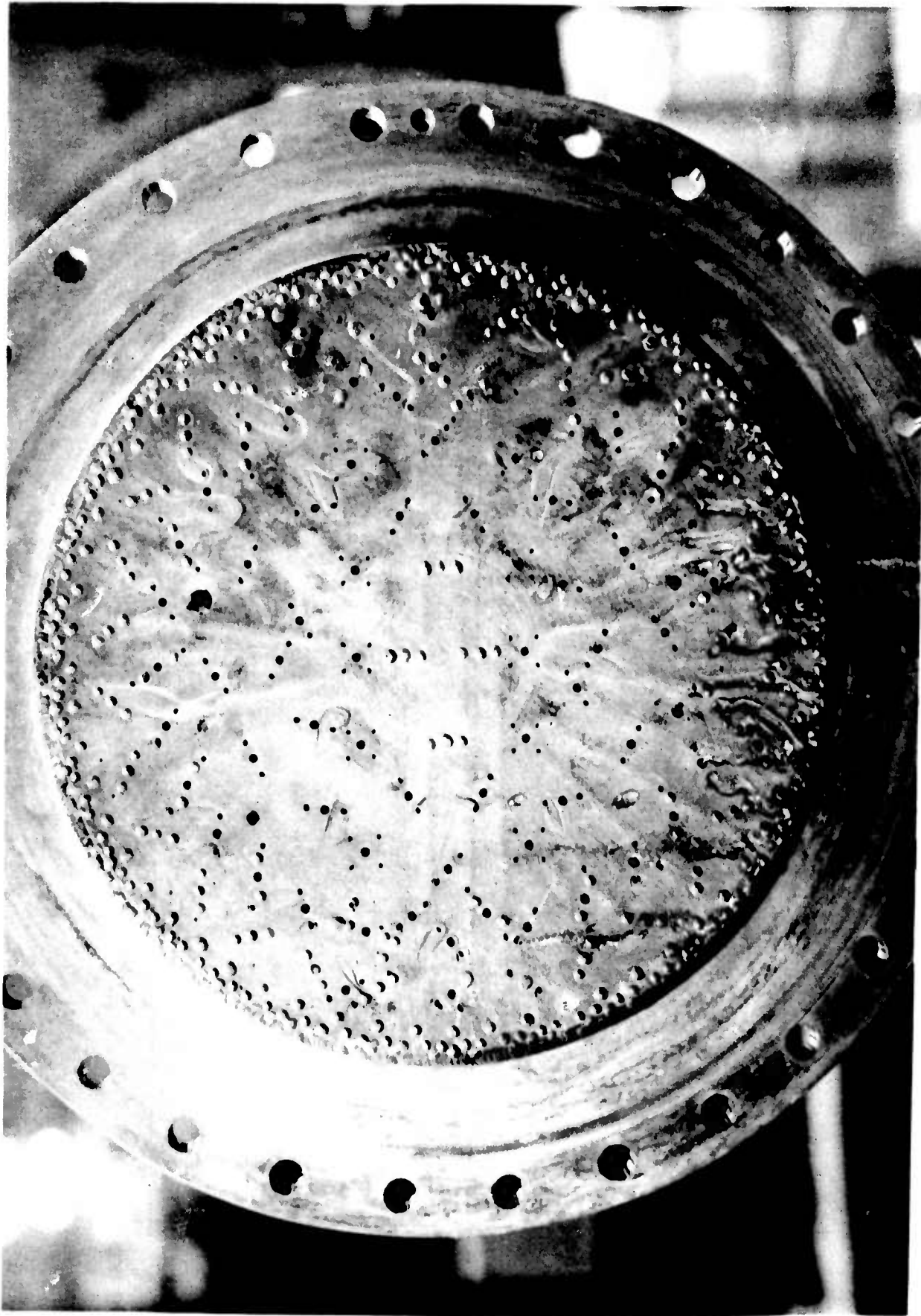


Figure 50. Injector S/N 2, Mod 3 after 803.25 sec of Testing

Page 102

UNCLASSIFIED

none are deeper than 0.010-in. This hydrotest was accomplished to inspect the orifice flow characteristics; there were no visible effects from the test history of the injector. The following is a summary of the program test history for injector S/N 2:

<u>Injector Designation</u>	<u>Pattern No. of Elements</u>	<u>No. Tests</u>	<u>Accumulated Duration (sec)</u>
S/N 2	158	4	6.85
S/N 2, Mod 1	98	4	10.47
S/N 2, Mod 2	68	6	26.06
S/N 2, Mod 3	68	11	803.25
(2% FFC and lower pressure drop)		—	—
Total		25	846.63

Injector S/N 6 was the last one to be evaluated during Phase II. It was similar to S/N 2, Mod 3, in that it had 68 staggered impingement height triplet elements, but the long impinging elements were situated closer toward the center of the face and there was 9% fuel film cooling. In addition, S/N 6 contained a thermal accumulator, which consisted of a solder filled cavity on the back of the injector, to accept the heat-soak from the ablative chamber following shutdown.

Injector S/N 6 was initially and successfully tested in the uncooled steel "workhorse" thrust chamber for a duration of 5.07 sec. No damage was sustained by either the injector or the combustion chamber. Streaking at the forward end of the combustion chamber was less pronounced than with injector S/N 2, Mod 3. Then, S/N 6 injector was installed into the ablative thrust chamber S/N 003 for a duty cycle demonstration. Thrust chamber S/N 003 contained a full-length, fibrous graphite liner insulated with carbon and silica phenolic, all encased in a steel structural container.

This testing was programmed to be a 2000 sec duty cycle, including both "on" (600 sec) and "coast" (1400 sec) periods. Although the thrust chamber was equipped with a sea-level expansion nozzle, the test was conducted in the Test Stand J-4 altitude chamber to simulate a vacuum start as well as vacuum conditions during each "coast" period. The installed assembly is shown on Figure No. 51. To accomplish the testing objectives within the capabilities of the stram system, it was planned to shut-off the steam ejectors during the long, steady-state "on" periods.

A hot gas blowback into the test cell occurred when the steam ejector valve was closed to conserve steam during the first 315 sec "on" period. This hot gas blowback resulted in a premature shutdown at 38.62 sec.

UNCLASSIFIED

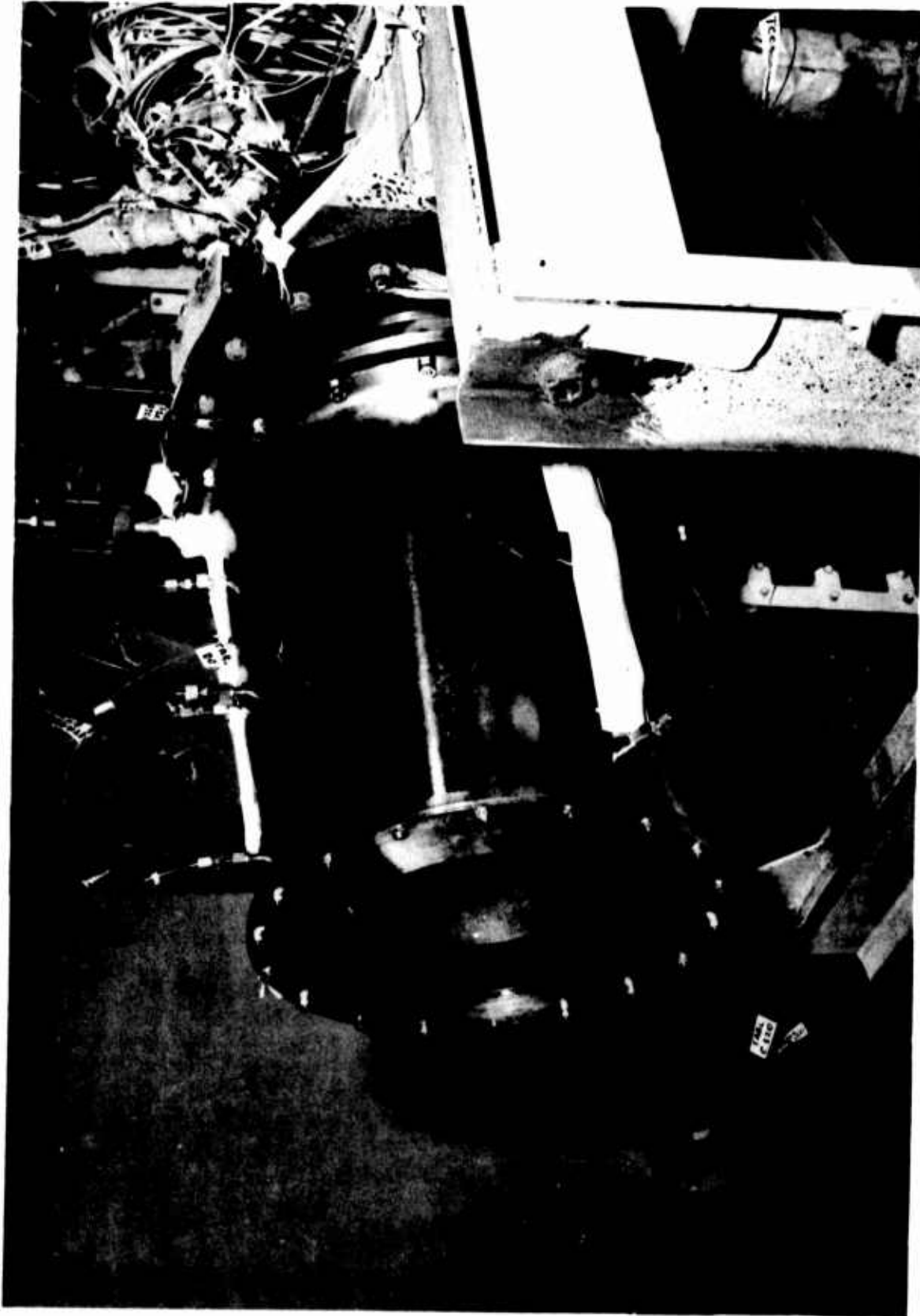


Figure 51. Ablative Chamber S/N 003 Test Installation

UNCLASSIFIED



**CONFIDENTIAL**

A post-test inspection revealed damage to the chamber instrumentation. In addition, the full-length, fibrous graphite liner had buckled at the convergent nozzle and throat area (see Figure No. 52). Thermocouple data indicated that at the time of shutdown, the gas-side temperature of the liner was approximately 400°F adjacent to the injector and 4200°F at the throat station. There was no evidence of liner streaking or erosion at either the injector end or in the throat. The injector was undamaged. The testing was terminated and the chamber disassembled for detailed examination.

Inspection of the liner disclosed several areas where the graphite-phenolic tape used in its construction had been deeply wrinkled during fabrication. The wrinkle line was axial with the wrinkle depth increasing at the throat. Wrinkles penetrated the full liner thickness in the throat area. The rupture appeared to have originated in a wrinkle line.

In addition, the silica phenolic insulation adjacent to the steel case had moved aft approximately 0.050-in. while the fibrous graphite liner retained its original position (see Figure No. 53). Movement of the silica phenolic had been over the entire chamber length because it extended a similar distance beyond the exit end. The motion of the silica insulation apparently was caused by the axial and radial growth of the AGCarb-101 liner. The design was deficient in that it allowed the AGCarb to seat against the injector, resulting in excess loads on the AGCarb material.

## **2. Phase III Testing**

All of the ten tests made during Phase III were accomplished using injector S/N 7. The two initial tests were conducted in Test Stand J-2 using the acoustically-damped uncooled steel thrust chamber. Test durations were 2.47 sec and 4.13 sec, respectively. In both tests, 20-grain charges were used for pulsing approximately 2.2 sec after the test began. In each case, the perturbation damped out in less than 5 millisecc, which demonstrated the dynamic stability of the unit.

Post-test examination after the first test indicated that the row of resonator holes nearest the injector face had started to erode while the remaining rows of holes into the resonator cavities had discolored in varying degrees only. The holes furthest from the injector appeared to be the least affected. The erosion was aggravated as a result of the increased duration of the second test. Figure No. 54 shows the resonator area of the steel chamber following the second test. A close-up of the same area is shown on Figure No. 55. There were three rows of holes in each of the three axial cavities; the holes in the forward row within each cavity were the ones affected most of all. Inspection of the forward resonator through the high-frequency pressure transducer ports indicated that the entrance of each hole had remained unchanged. All of the erosion was on the gas-side surface of the chamber.

**CONFIDENTIAL**

(This Page is Unclassified)

**CONFIDENTIAL**

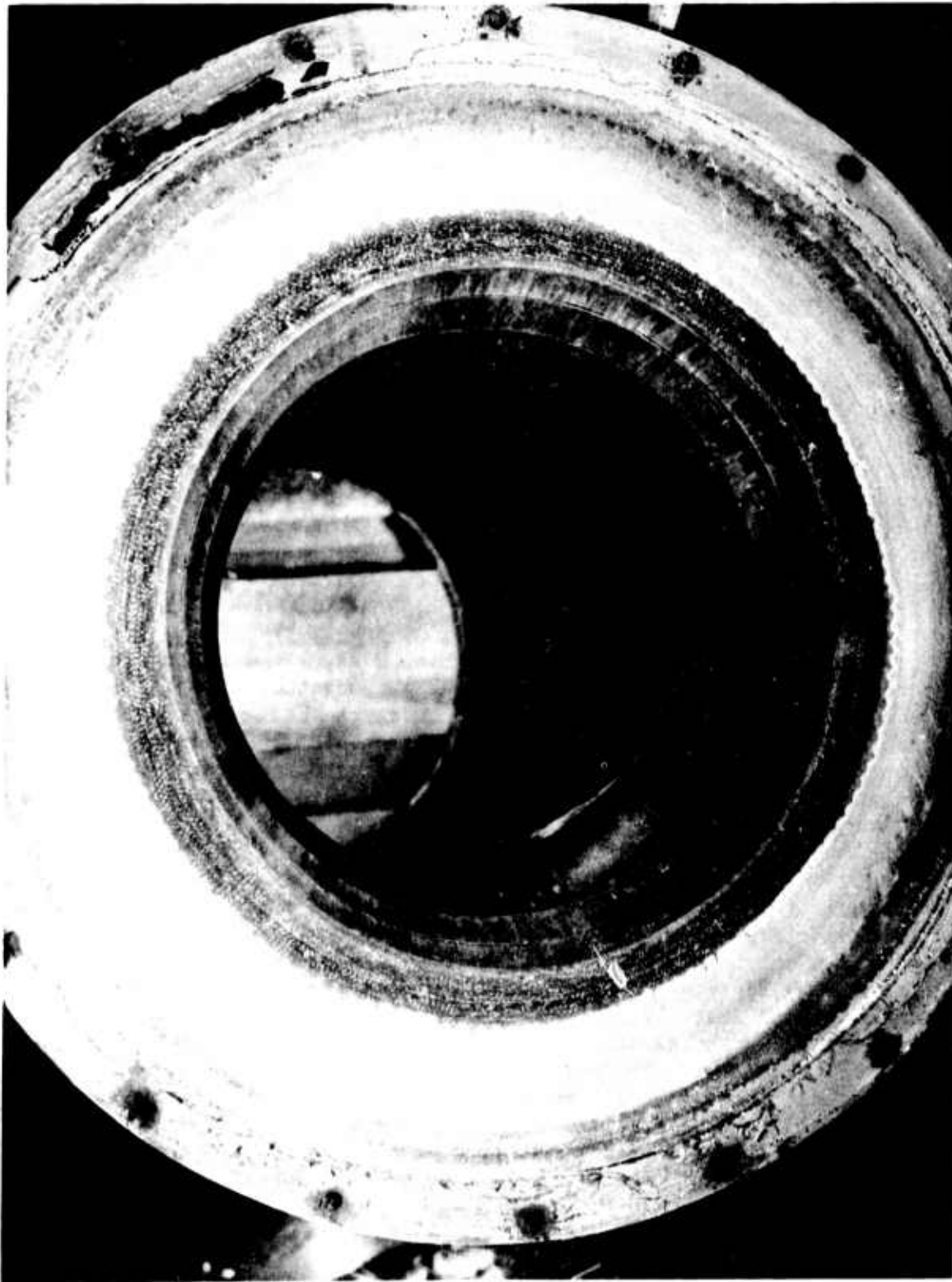


Figure 52. Damaged Flame Liner, Ablative Chamber S/N 003

**CONFIDENTIAL**

CONFIDENTIAL



Figure 53. Post-Test (No. -007) View of Forward End of Ablative Chamber  
S/N 003

CONFIDENTIAL

**CONFIDENTIAL**



Figure 54. Post-Test (No. 025) View of Steel Chamber with Acoustic Resonator (u)

**CONFIDENTIAL**

**CONFIDENTIAL**

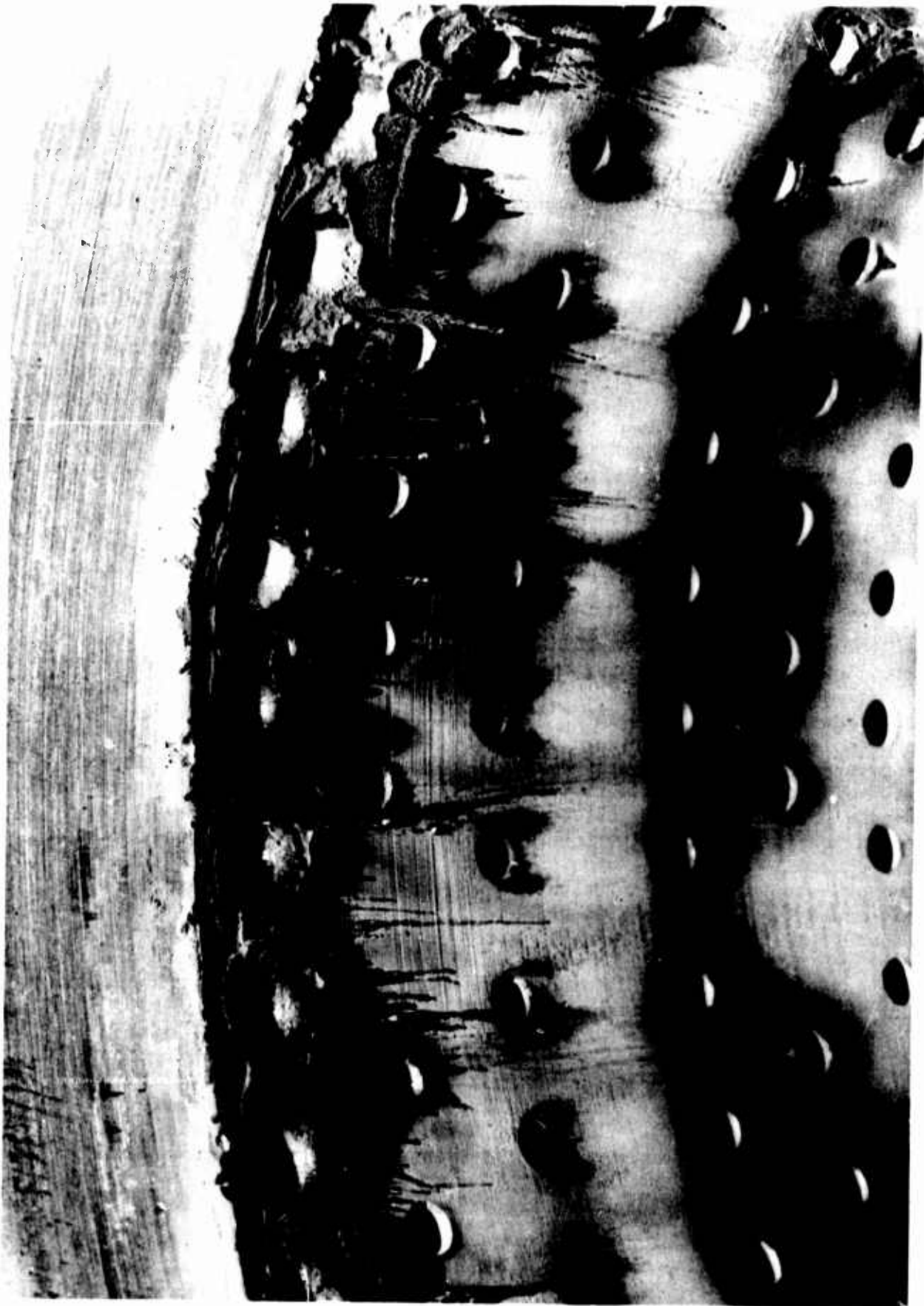


Figure 55. Close-Up of Steel Chamber with Acoustic Resonator after  
Test No. -025 (u)

**CONFIDENTIAL**



## CONFIDENTIAL

Fusible wires of 0.010-in. diameter had been installed in both the forward and aft resonator cavities to obtain hot gas temperature data. All three of the fusible wires (stainless steel, platinum, and rhodium) on each of the three pins in the forward cavity had melted, which indicated a temperature in excess of 3570° (the approximate melting temperature of rhodium). Similar fusible wires positioned in the aft cavity were virtually intact. Only one of three stainless steel wires had melted while the platinum and rhodium wires were unchanged. Thus, the aft cavity temperature apparently was near 2600°F, which is the melting temperature of stainless steel. The condition of the fusible wires following the two tests is shown on Figures No. 56 and No. 57. A single iridium/iridium rhodium thermocouple was placed in each of the two cavities adjacent to the fusible wires. The temperatures obtained from the thermocouples were within 350°F of the approximations made from the condition of the fusible wires and served to validate these estimates.

Then, injector S/N 7 was installed into S/N 001 ablative chamber, which was equipped with an acoustic liner having an identical geometry to that tested in the steel combustion chamber. The pre-test configuration of the acoustic resonator is shown on Figure No. 58. Three tests (10.82 sec, 50.49 sec, and 100.39 sec) were conducted in Test Stand J-4 under simulated altitude conditions. The combustion process was stable in each of the three tests.

Visual inspection after Test No. -010 and an accumulated duration of 161.7 sec indicated that the fibrous graphite acoustic resonator liner was seriously eroded at its forward end as shown on Figure No. 59. Testing was terminated because of the marginal liner thickness. The erosion, which was limited to the forward 3-in. of the liner, appeared to be quite uniform and in the form of short streaks ending over the second resonator cavity. The short streaks were judged to have been the result of a combination of events occurring in the outer periphery of the injector. The high vaporization rate of the fluorine resulted in an oxidizer-rich zone having a highly corrosive chemical composition. In addition, the flow through the resonator holes created a turbulent flow path which resulted in an increased erosive condition. The fibrous graphite material did not crack or delaminate. The downstream 5-in., including the second and third resonator cavities, were virtually unchanged from the pre-test condition. The graphite phenolic ablative section, which is located between the acoustic resonator liner and throat insert, also was unaffected.

The acoustic resonator liner was removed following the last test. A close inspection indicated that the first row of resonator holes was eroded in diameter but remained sharp-edged on the outer diameter of the liner (see Figure No. 60). The holes in the second and third rows, which were enlarged to a lesser extent, had developed radii on the outer diameter surface. The holes in the remaining five rows were all sharp-edged on the outer diameter side and there was virtually no diameter increase.

CONFIDENTIAL

(This page is Unclassified) -



UNCLASSIFIED

TEMPERATURE SENSORS

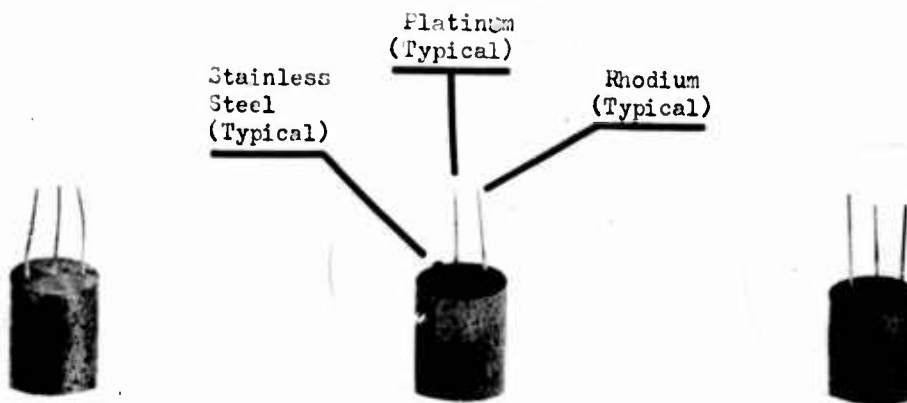
FUSEABLE WIRES

TEST 1083-001-0m-024



Forward Resonator Cavity

(Located 1st 2 inches below Injector Face)



(Located between 4.5-in. and 6.5-in. below Injector Face)

Approximate Melting Temperatures of Fusible Wires

Stainless Steel-----	2600°F
Platinum-----	3200°F
Rhodium-----	3570°F

Figure 56. Condition of Fusible Wires Following Test No. -024

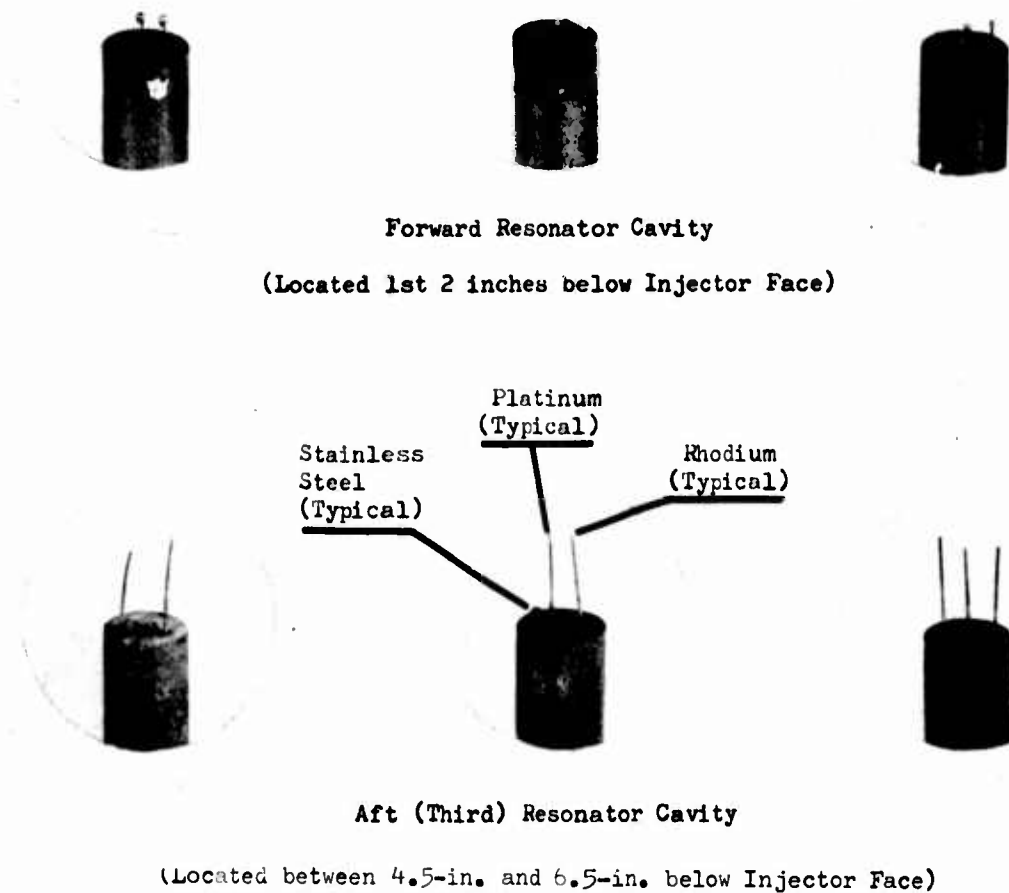
UNCLASSIFIED

UNCLASSIFIED

TEMPERATURE SENSORS

FUSEABLE WIRES

TEST 1083-001-0m-025



Approximate Melting Temperatures Fusible Wires

Stainless Steel-----	2600°F
Platinum-----	3200°F
Rhodium-----	5570°F

Figure 57. Condition of Fusible Wires Following Test No. -025

UNCLASSIFIED

**CONFIDENTIAL**

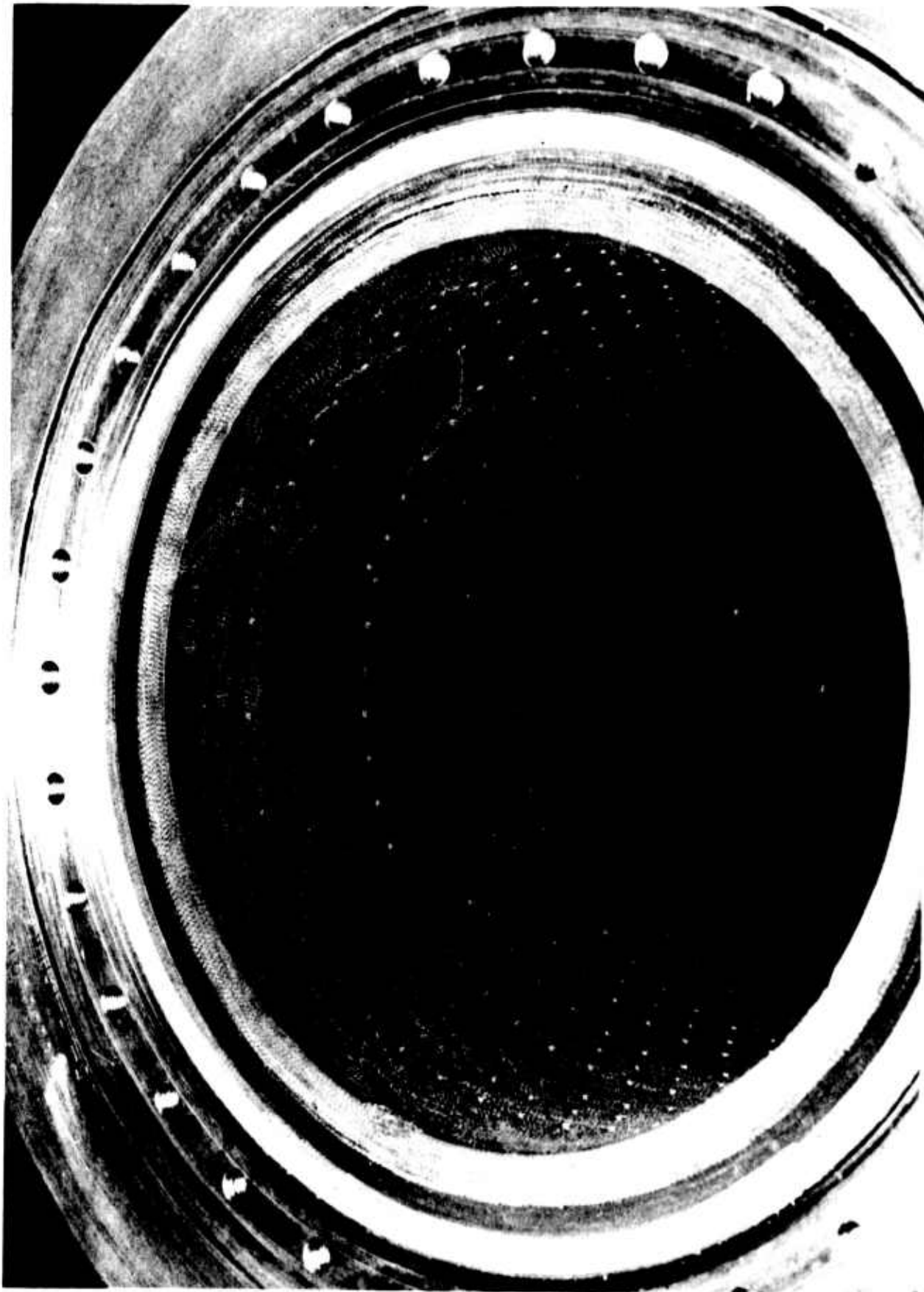


Figure 58. Ablative Chamber S/N 001 with Acoustic Resonator

Page 113

**CONFIDENTIAL**

(This Page is Unclassified)

**CONFIDENTIAL**

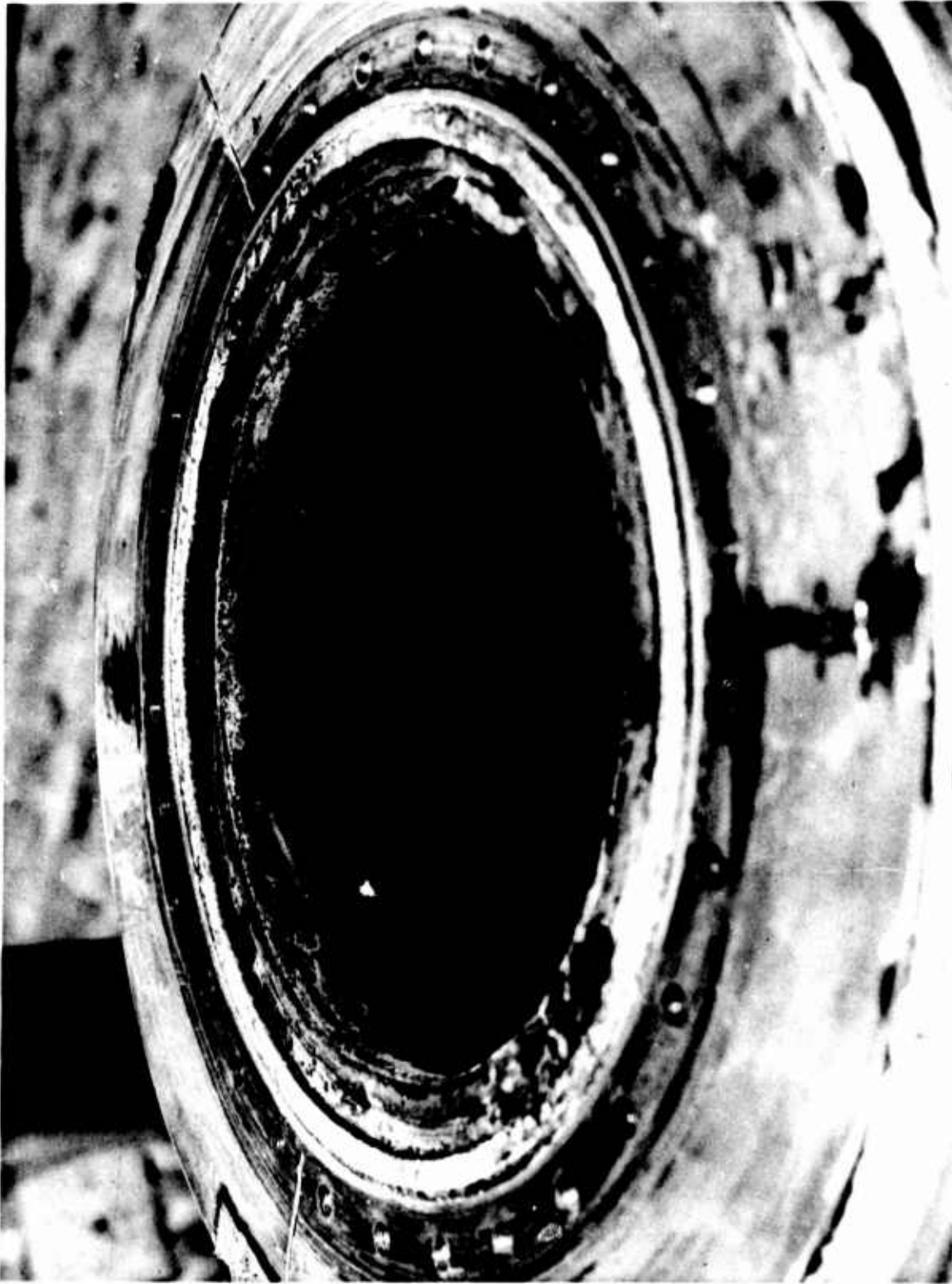


Figure 59. Ablative Chamber S/N 001 after 161 sec of Testing (u)

**CONFIDENTIAL**

**CONFIDENTIAL**

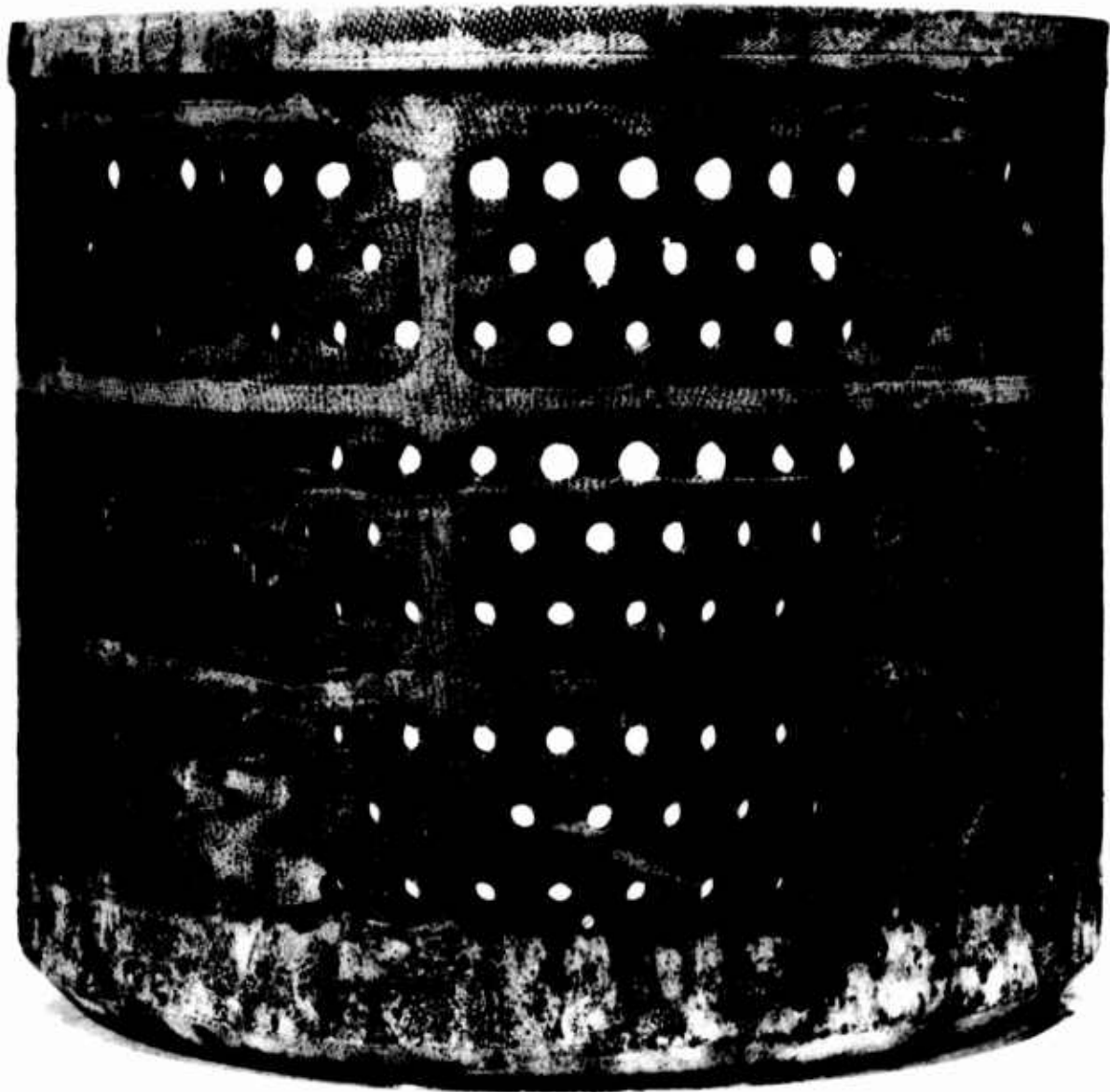


Figure 60. Post-Test View of Outer Diameter Surface of Resonator Flame Liner

**CONFIDENTIAL**

# CONFIDENTIAL

The condition of the cavity walls was excellent (see Figure No. 61). All of the surfaces were in the same condition as when they were fabricated except that the area directly behind each resonator hole in the first row was slightly rounded and depressed.

The portion of the thrust chamber downstream of the resonator showed no erosion or streaks on either the ablative or fibrous graphite materials. The throat insert had cracked axially in a manner similar to the insert of ablative chamber S/N 002. The initial evidence of cracking was noted after Test -009, which was of 50-sec duration.

Following these tests, injector S/N 7 was tested for 2.2 sec (Test No. -026) using an uncooled steel workhorse thrust chamber without acoustic dampers. A 20-grain tangential impulse gun (all pulse guns were tangentially directed) was fired approximately 2.2 sec after the test started. This triggered a first tangential mode of instability which resulted in a CSM shutdown and verified that the injector was indeed unstable. Neither the injector nor the steel combustion chamber was damaged.

The testing which followed was intended to determine if the resonator area could be reduced and the apparent hot gas recirculation could be minimized. This would potentially increase liner durability. The previously-tested steel chamber with the nine-row/three-cavity acoustic resonator was modified to a single-cavity/single-row configuration by welding all orifices closed and drilling a new first row. It was tested twice (Tests -027 and -028). The first test was repeated and stable both before and following pulsing with a 20-grain charge. This test was repeated and unstable combustion following the 20-grain pulse resulted in a CSM shutdown at 2.25 sec.

The post-test inspection revealed far less erosion of the resonator holes than with the previously-tested multiple row configuration. The gas-side of the hole entrances were rounded but not eroded excessively (see Figure No. 62). Inspection of the holes through the high-frequency pressure transducer parts indicated that their back-side was unchanged.

The acoustically damped steel chamber was reworked into a single-cavity/two-orifice row resonator configuration by drilling a second row of orifices adjacent to the first and into the same cavity. This design was tested twice. It was pulsed unstable during the first test. In the next test which was the last program test (Test No. -030), the pulse was applied at 3.8 sec and the combustion process recovered immediately.

Post-test examination revealed only minimal increase in erosion of the resonator holes nearest the injector face (see Figure No. 63). The second row of holes did not appear to be eroded. Injector S/N 7, which was used for this entire test series, showed no damage or erosion. Performance was consistent from test to test.

CONFIDENTIAL

(This Page is Unclassified)



**CONFIDENTIAL**

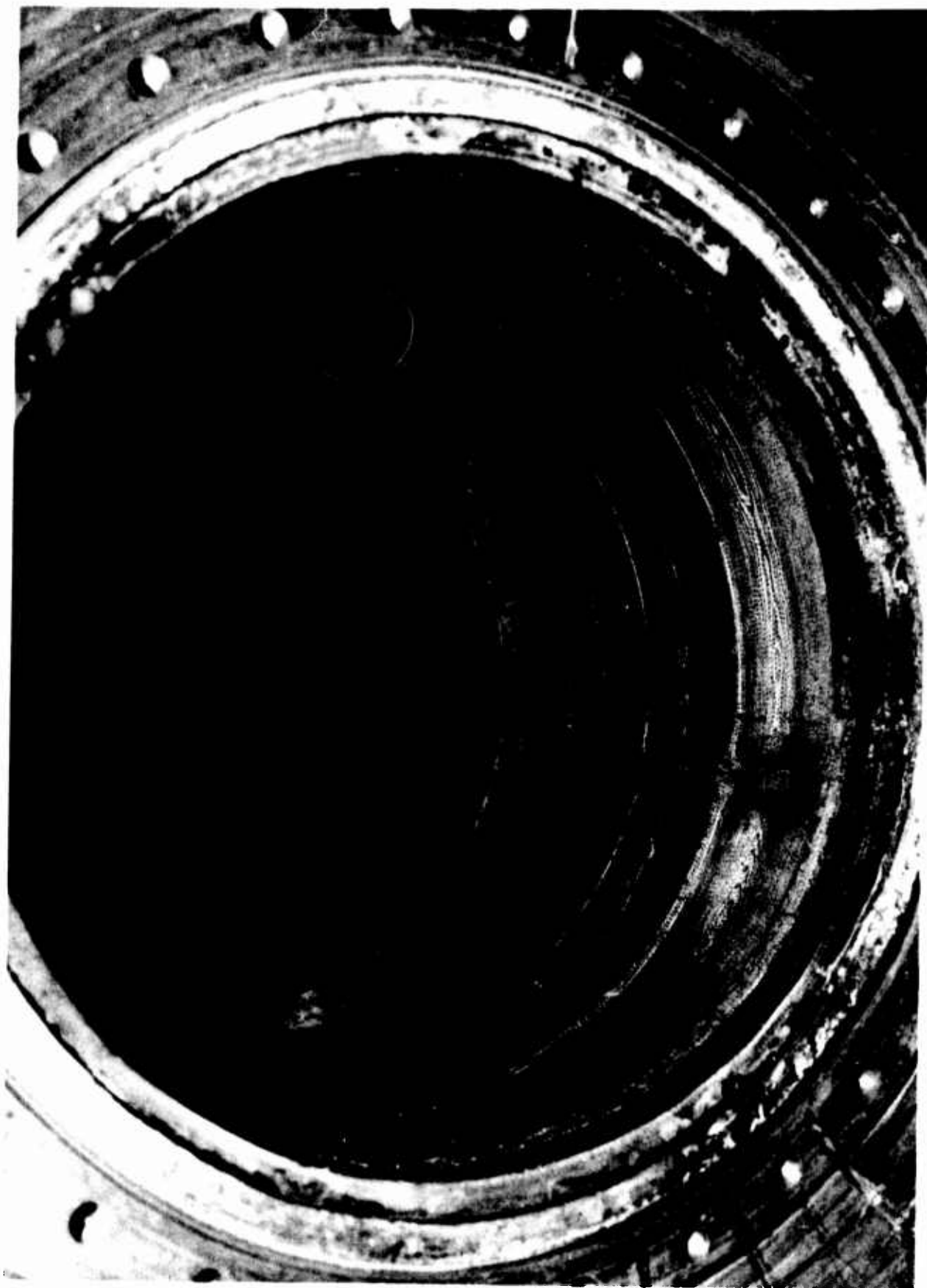


Figure 61. Post-Test View of Resonator Cavities

**CONFIDENTIAL**

**CONFIDENTIAL**

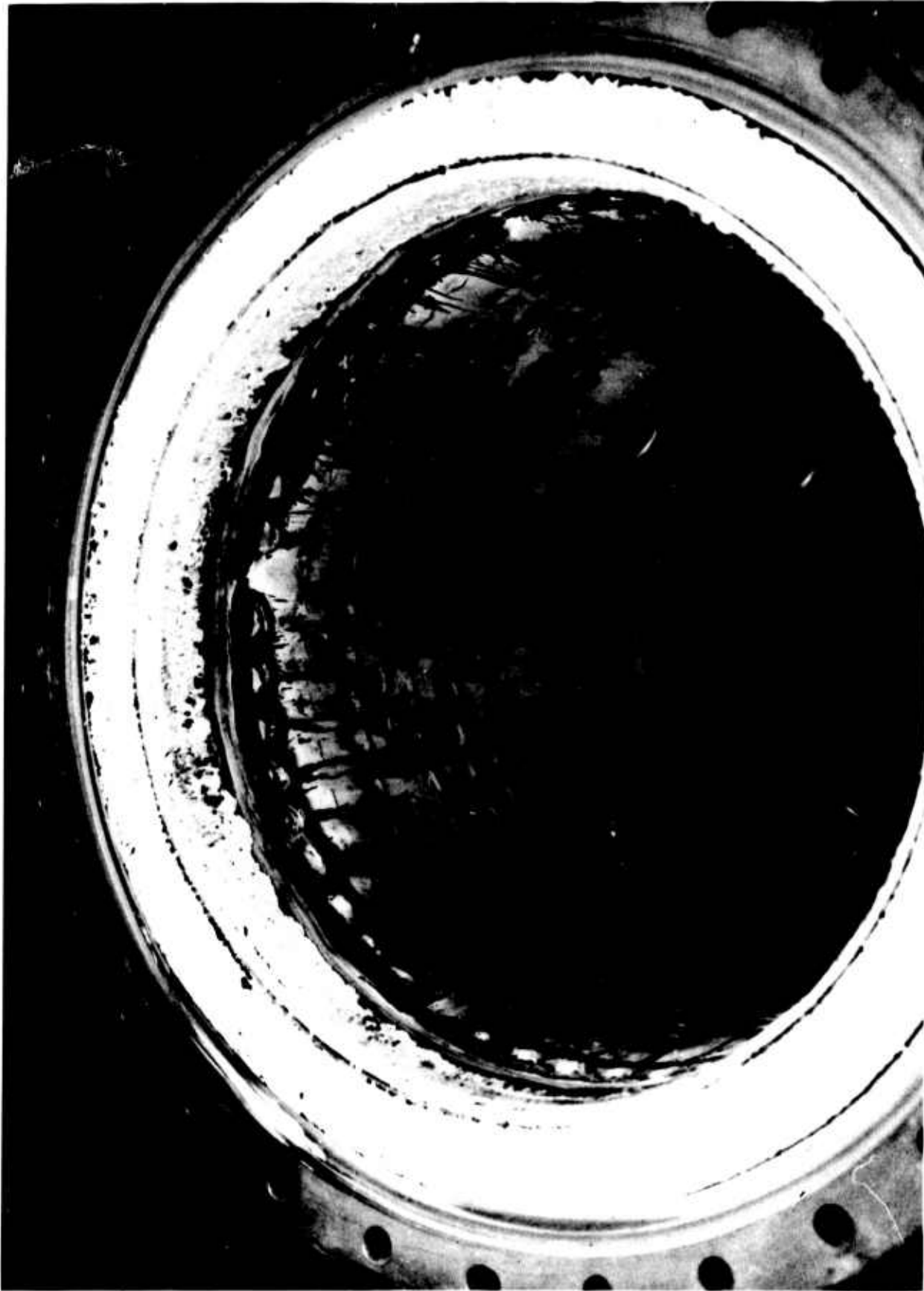


Figure 62. Post-Test View of Single-Row, Acoustically-Damped Steel Chamber

**CONFIDENTIAL**

**CONFIDENTIAL**

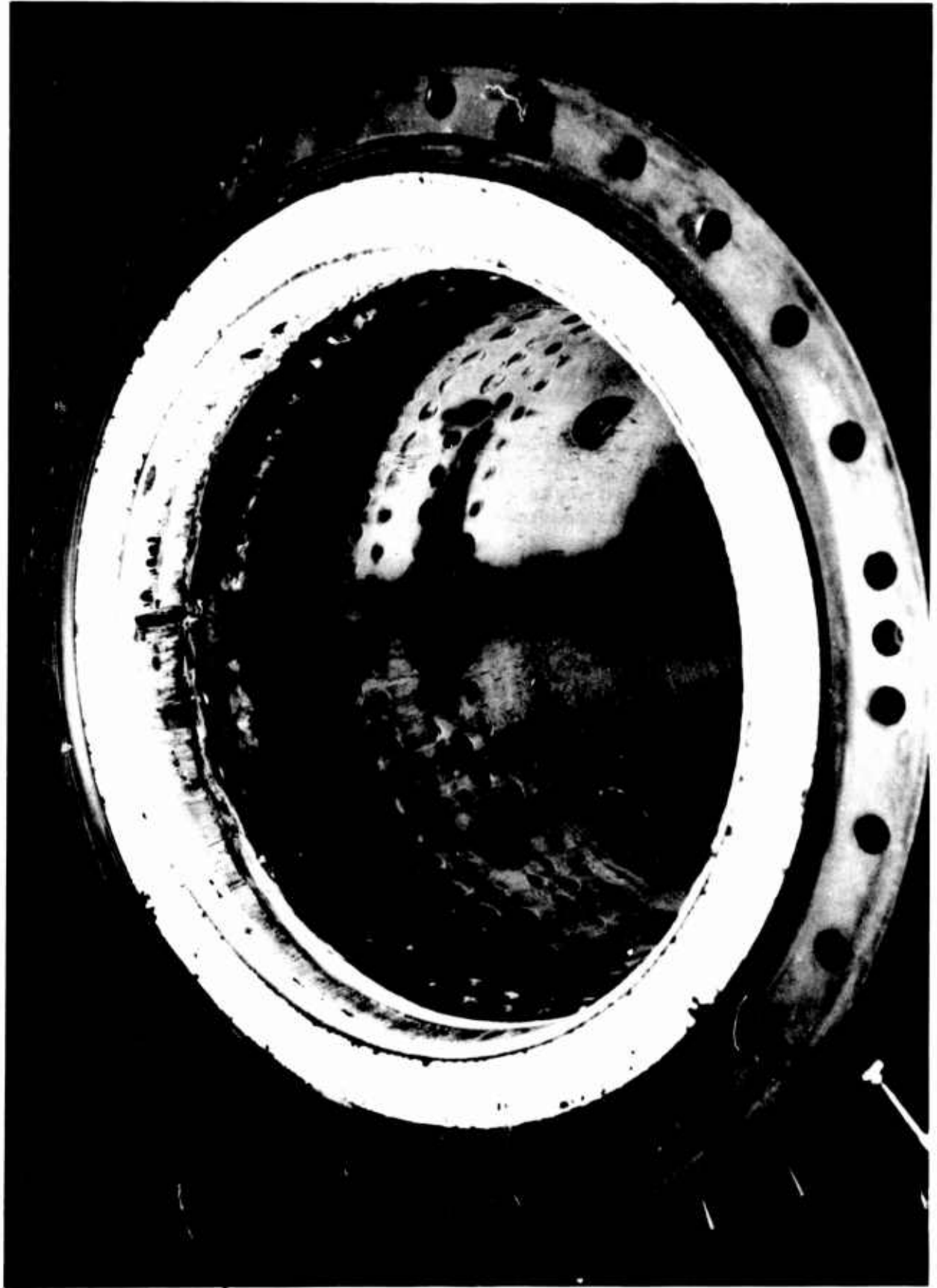


Figure 63. Post-Test View of Two-Row/Single-Cavity, Acoustically-Damped Steel Chamber

**CONFIDENTIAL**

# CONFIDENTIAL

## SECTION VI

### TEST RESULTS

The objective of the test program was to gather information both recorded and visual which would demonstrate system combustion stability, performance, injector-chamber compatibility, component durability, and thermal interactions.

Measured test data cannot always be directly compared unless identical test hardware and conditions existed. This was especially true with respect to performance. Since identical conditions for any two tests never existed, it was necessary that a performance evaluation technique be applied which would allow a direct comparison of performance values between tests. The technique used is known as the Performance Interaction Theory. It is discussed in detail as is each of the noted areas.

#### A. COMBUSTION STABILITY

The stability design study for the fluorine-hydrazine blend system required the use of existing stability correlations for different propellant combinations which were assumed to be at least qualitatively if not quantitatively similar. Although the original program approach considered the use of damping devices (i.e., injector face baffles), previous experience indicated no need for them at the outset of the program. Only the variation of the injector element parameters was considered necessary to provide stability. These parameters included the following:

- Type of elements
- Number of elements
- Orifice size
- Injection pressure drop
- Impingement angle
- Impingement distance
- Percentage of film cooling
- Mixture ratio distribution
- Mass flux distribution

Following the development of the inherently stable, 68-element injector which provided a minimum but acceptable performance, the program approach was directed toward the development of a higher performing dynamically stable thrust chamber assembly. The decision to use a chamber wall acoustic damper made it possible to configure an injector pattern where performance and compatibility were the major considerations.

#### 1. Stability Summary

The approach used to achieve combustion stability during this program was very successful. An injector which operated stable without the aid of damping devices was developed and later an acoustic damper was developed which stabilized an otherwise unstable 344 element injector. The successful

CONFIDENTIAL

(This Page is Unclassified)

# UNCLASSIFIED

68-element injector pattern was the second modification of a single injector (S/N 2, Mod 2). It differed from the previous patterns in that fewer injection elements were used and the mass flux distribution was limited to the center of the injector; there were no active elements beyond the 75% radius.

The following is a summary of the test results obtained during Phase II of the program.

Injector S/N	Pattern Description (No. of Elements)	Number of Tests Stable/Unstable		Total Duration (sec)
S/N T <sup>2</sup>	215	1	2	6.28
S/N 2, Mod 0	158	1	3	6.85
S/N 2, Mod 1	98	1	3	10.46
S/N 2, Mod 2	68 (high $\Delta P$ )	6	0	26.07
S/N 2, Mod 3	68	11	0	803.92
S/N 6	68	2	0	43.69

Spectral analysis of the 98-element and 215-element injectors during unstable operation (Test Nos. 1083-D01-OM-007 and -010) was accomplished as shown on Figure No. 64. The noise level for the 68-element and 215-element injectors operating stably during Tests No. -007 and -013 is shown on Figure No. 65.

The noise levels of the 68- and 215-element injector patterns were almost identical, however, the combustion stability of the two injectors were clearly different as indicated by test results. The 215-element pattern appeared to go unstable as the result of small chamber pressure perturbations (pops) after only a second or two of operation, while the 68-element pattern operated for hundreds of seconds and was able to withstand the occurrence of pops. The 68-element pattern may not be able to withstand all possible self induced pops but it has a greater margin of dynamic stability than the 215-element pattern. A dynamically stable injector pattern is defined as a pattern which is capable of damping any dynamic chamber pressure perturbation. Since it was not pulse tested the 68-element injector pattern has not been proven to be completely dynamically stable.

In Phase III of the program, injector S/N 7 which had 344 triplets was designed and fabricated. It was fired with an acoustic damper array in the chamber wall. A 20-grain tangential pulse gun was used to evaluate the stabilizing influence of the acoustic damper. The initial acoustic liner design tested consisted of three, axially-spaced cavities, compartmented circumferentially with five partitions. Each cavity contained three rows of 0.2-in. diameter (approximate) holes. Each cavity had a total axial length of 2.0-in. The first cavity orifice row was located 0.25-in. from the injector face. This acoustic damper design was demonstrated stable during two 20-grain tangential pulse tests when it operated for a total of 6.6 sec of testing in the acoustically-damped steel chamber. Subsequently this particular resonator design was incorporated into an ablative thrust chamber. It resulted in stable operation when tested with injector S/N 7 for a duration of 161.7 sec (see Table X). Figure No. 66 is a sample pressure transducer oscillograph trace

UNCLASSIFIED

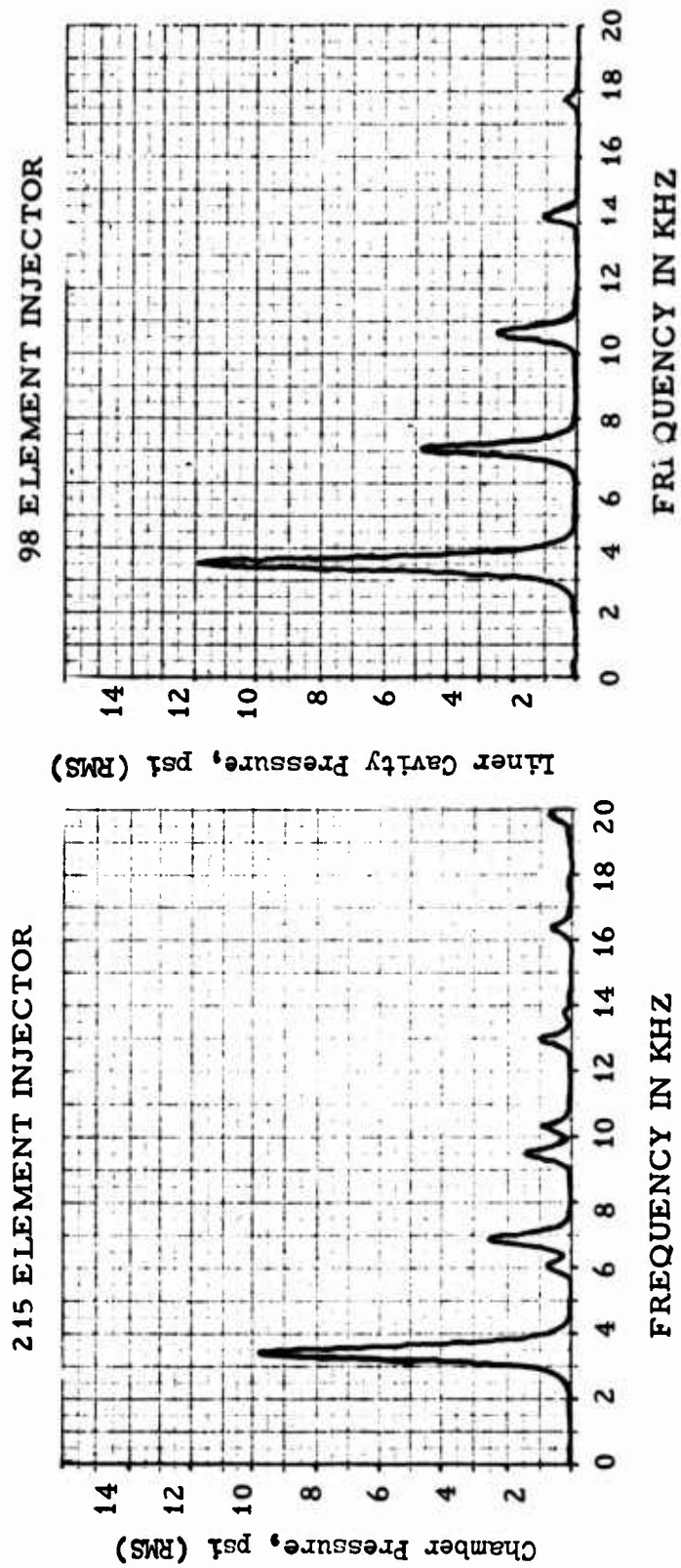
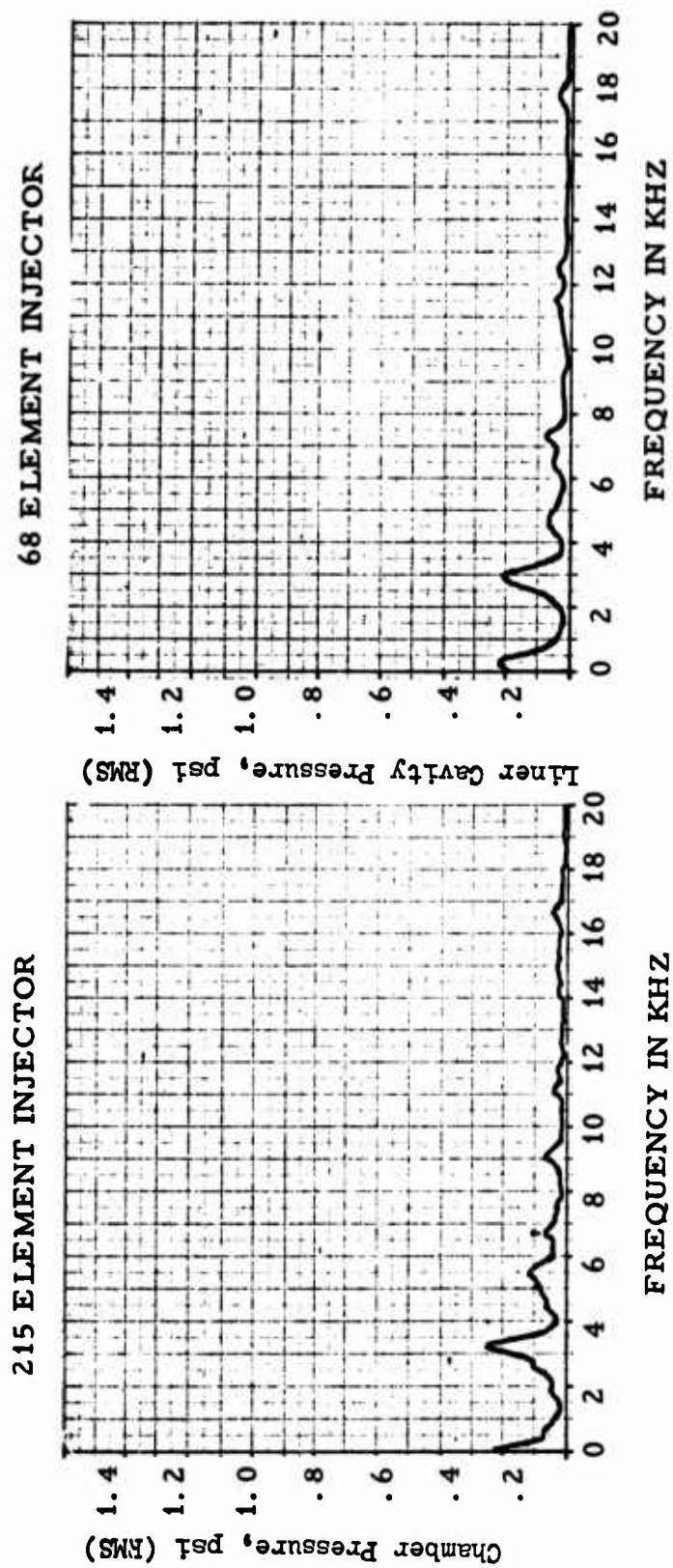


Figure 64. Spectral Analysis Showing Instabilities in Tests No. -007 and No. -010

UNCLASSIFIED



UNCLASSIFIED



UNCLASSIFIED

Figure 65. Spectral Analysis Showing Noise Level in Tests No. -007 and No. -013

UNCLASSIFIED

PULSE TEST OF SN-7 INJECTOR AND ACOUSTIC LINER (TEST 24)

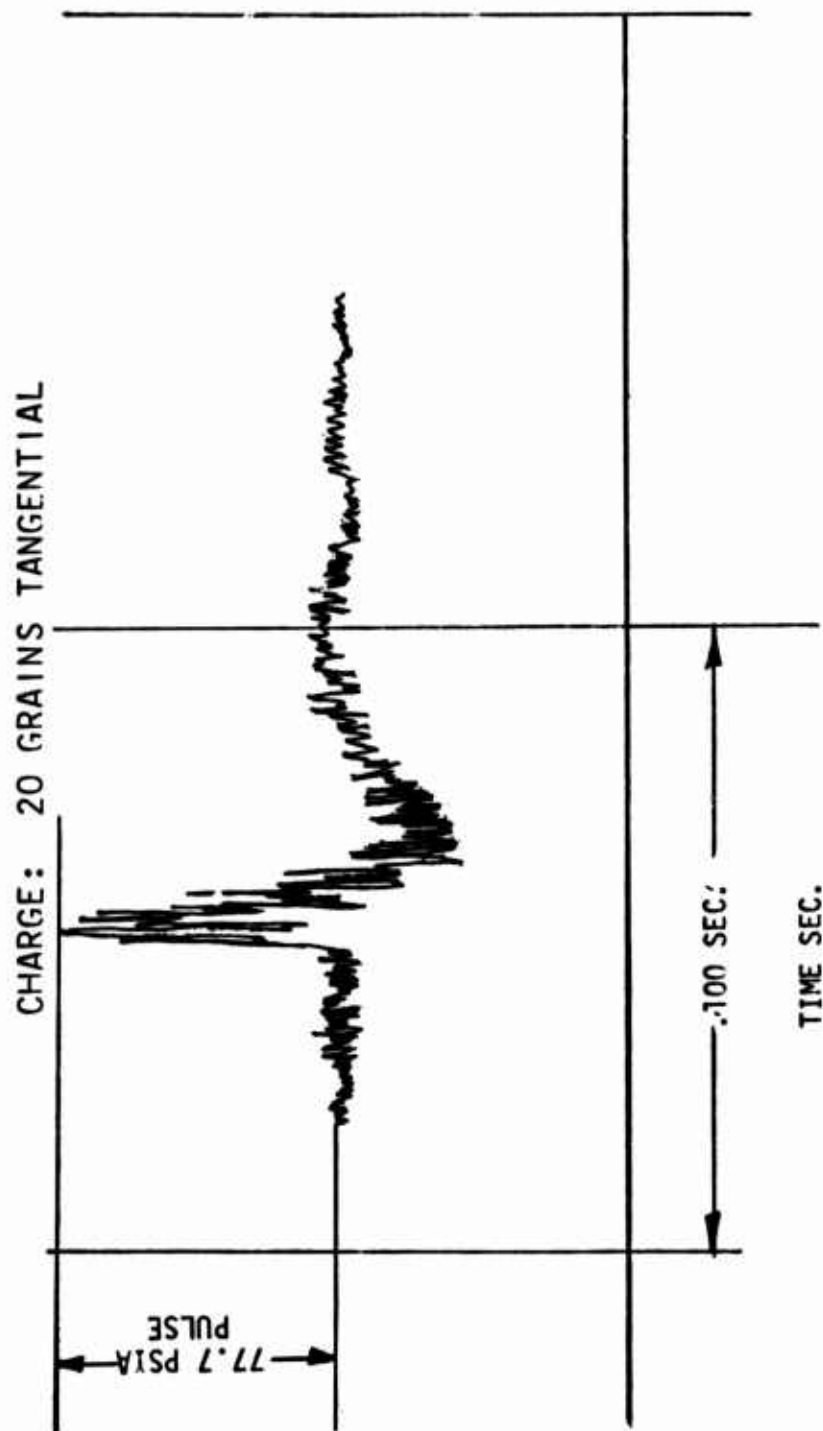


Figure 66. Sample Pressure Transducer Oscillograph Trace, Test No. -024

UNCLASSIFIED

CONFIDENTIAL

TABLE X

STABILITY  
TEST HISTORY OF INJECTOR S/N 7

Test No.	Chamber Configuration	Time of Pulse (sec)	Duration (sec)	Pulse Charge Size, Gr./Overpressure, psi	Stability
024	Uncooled steel with 9-row 3-cavity acoustic resonator	2.170	2.468	20/76	Stable
025	Same as Test 024	2.168	4.133	20/14	Stable
026	Standard uncooled steel	2.193	2.200	20/82	Unstable
027	Uncooled steel with 1-row 1-cavity acoustic resonator	2.197	2.486	20/*	Stable
028	Same as Test 027	2.182	2.250	20/82	Unstable
029	Same as Test 028 except 2nd row of orifices drilled into first resonator cavity	2.191	2.300	20/73	Unstable
030	Same as Test 028 except 2nd row of orifices drilled into first resonator cavity	3.800	3.980	20/60	Stable
008	Ablative with 9-row 3-cavity acoustic resonator	Not pulsed	10.820		Stable
009	Same as Test 008	Not pulsed	50.490		Stable
010	Same as Test 008	Not pulsed	100.390		Stable

\*Malfunction of high frequency tape recorder; however, stable pulse decay was observed on low frequency records.

CONFIDENTIAL

(This page is Unclassified)

## CONFIDENTIAL

of a 20-grain pulse from Test No. -024, where the 344-element injector was used with the steel, nine-row/three-cavity damper. A spectral analysis of the noise level obtained during this test is presented as Figure No. 67.

(C) When the 344-element injector S/N 7 was tested with the uncooled steel acoustically damped chamber (Tests No. -024 and -025) it demonstrated dynamically stable operation. The injector was then tested in the undamped steel chamber and pulsed with a 20-grain tangential pulse (Test No. -026); the combustion process became unstable. Two of the chamber pressure spectral analyses from the unstable portion of this test are presented on Figure No. 68.

(C) Although the nine-row/three-cavity acoustic damper, which is shown in Figure No. 69 after testing, was adequate for providing stability, it was subject to excessive first row orifice enlargement. This was considered to be caused by hot oxidizer rich gas circulating through the resonator cavities driven by the static pressure gradient at the chamber wall. Two modifications were undertaken; the total amount of acoustic damper surface area was reduced by closing the orifices of the second and third cavities and the original open orifice area of the first cavity placed in a single row of 0.375-in. diameter orifices. The resulting design (see Figure No. 70) was similar to the single-row acoustic dampers that had been successfully tested in an Aerojet-General sponsored program.

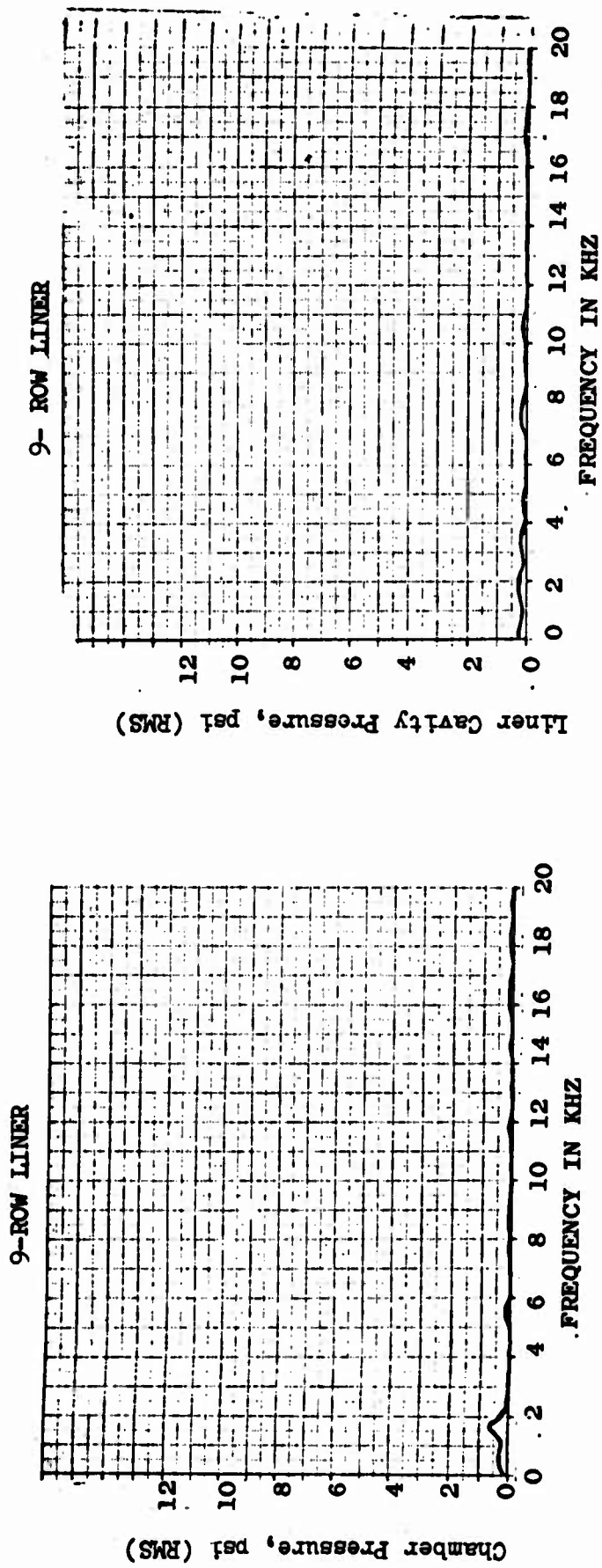
(C) This modified acoustic damper was subjected to two tests with 20-grain pulses. It demonstrated stability in the first test but became unstable following the pulse during the second test. A spectral analysis from the unstable test (No. -028) is shown on Figure No. 71. Test results showed that the system might have been stable without pulsing and that it was only marginally stable to the 20-grain pulse. The single row of holes significantly reduced hot gas flow into the resonator cavity with a consequent reduction in the cavity temperature which resulted in a resonator configuration that was not properly tuned to damp the first tangential mode at approximately 3500 cps.

(C) Another damper modification was undertaken. It was planned to drill 0.375-in. diameter orifices in the second axial cavity, but an error was made and the orifices were drilled into the first axial cavity instead (see Figure No. 63). This resulted in a design which had twice the desired open area and a design resonance frequency that was 40% above 3300 cps. Also, it offered the same disadvantage as the original dampers in allowing hot gas to flow through the liner in an axial direction. Test firings with the two-row single-cavity damper resulted in one stable and one unstable test when it was pulsed with a 20-grain tangential pulse gun. The spectral analyses of these two tests are shown on Figures No. 72 and No. 73.

(U) The instrumentation requirements for the acoustic damper evaluation consisted of the same five high-frequency instruments used for the undamped steel chamber; two were acoustic cavity pressure transducers and three were located downstream of the damper. Two sets of fusible wires were

## CONFIDENTIAL

UNCLASSIFIED



Page 127

UNCLASSIFIED

Figure 67. Spectral Analysis Showing Noise Level in Test No. -024

UNCLASSIFIED

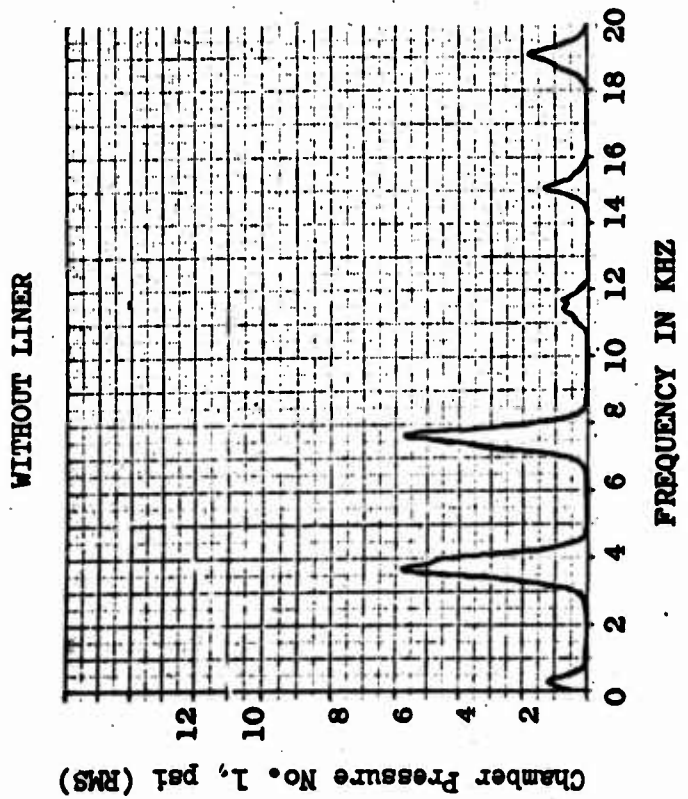
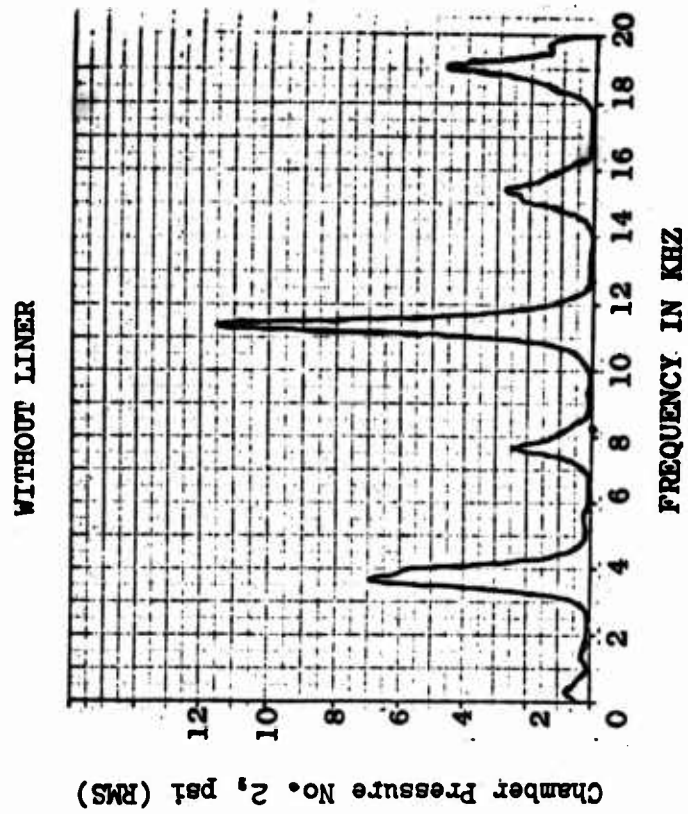


Figure 68. Spectral Analysis Showing Instability in Test No. -026

UNCLASSIFIED



CONFIDENTIAL

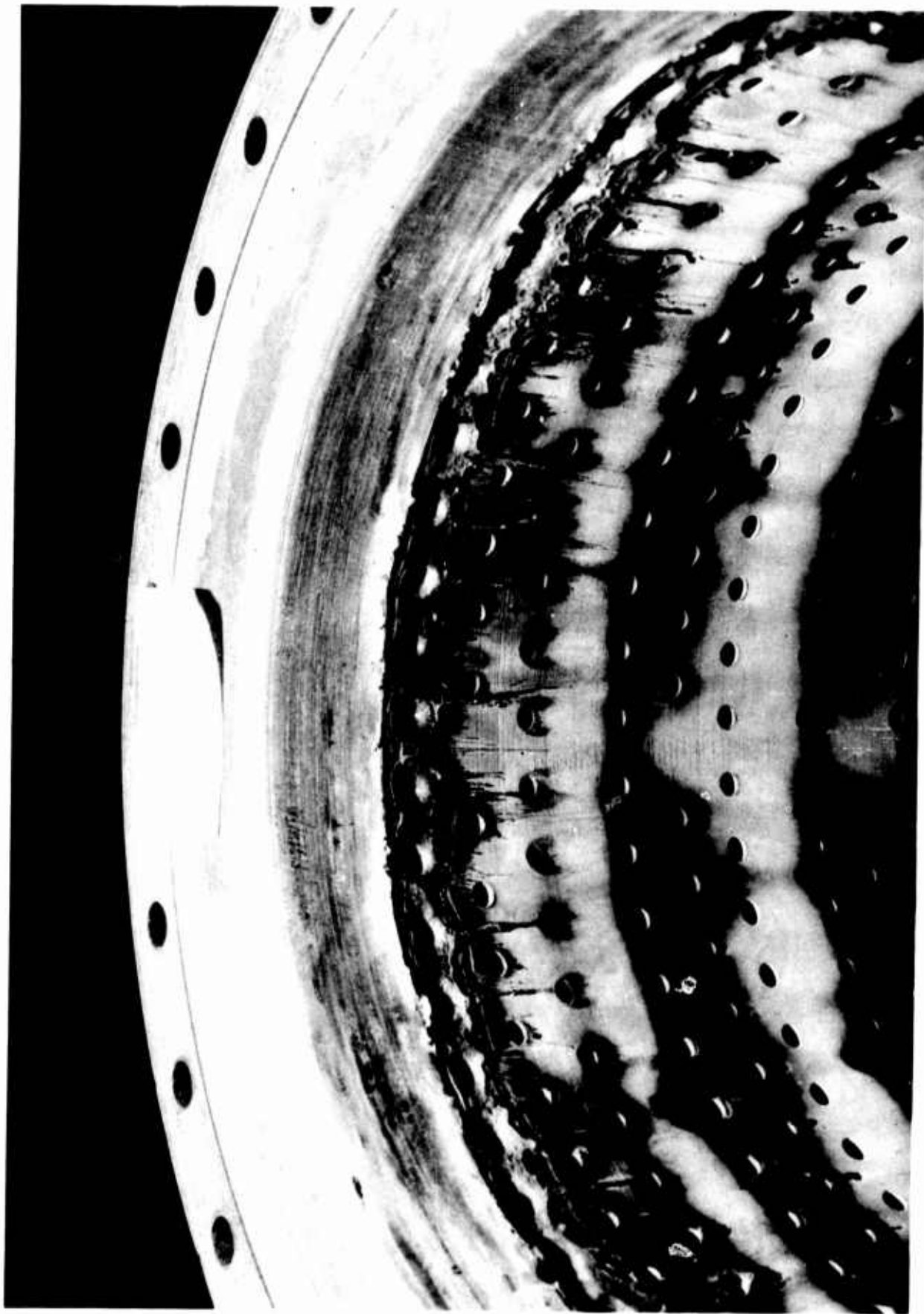


Figure 69. Post-Test (No. -025) View of Uncooled Nine-Row/Three-Cavity Damper

CONFIDENTIAL

**CONFIDENTIAL**



Figure 70. Single-Row Damper

Page 130

**CONFIDENTIAL**

(This Page is Unclassified)

UNCLASSIFIED

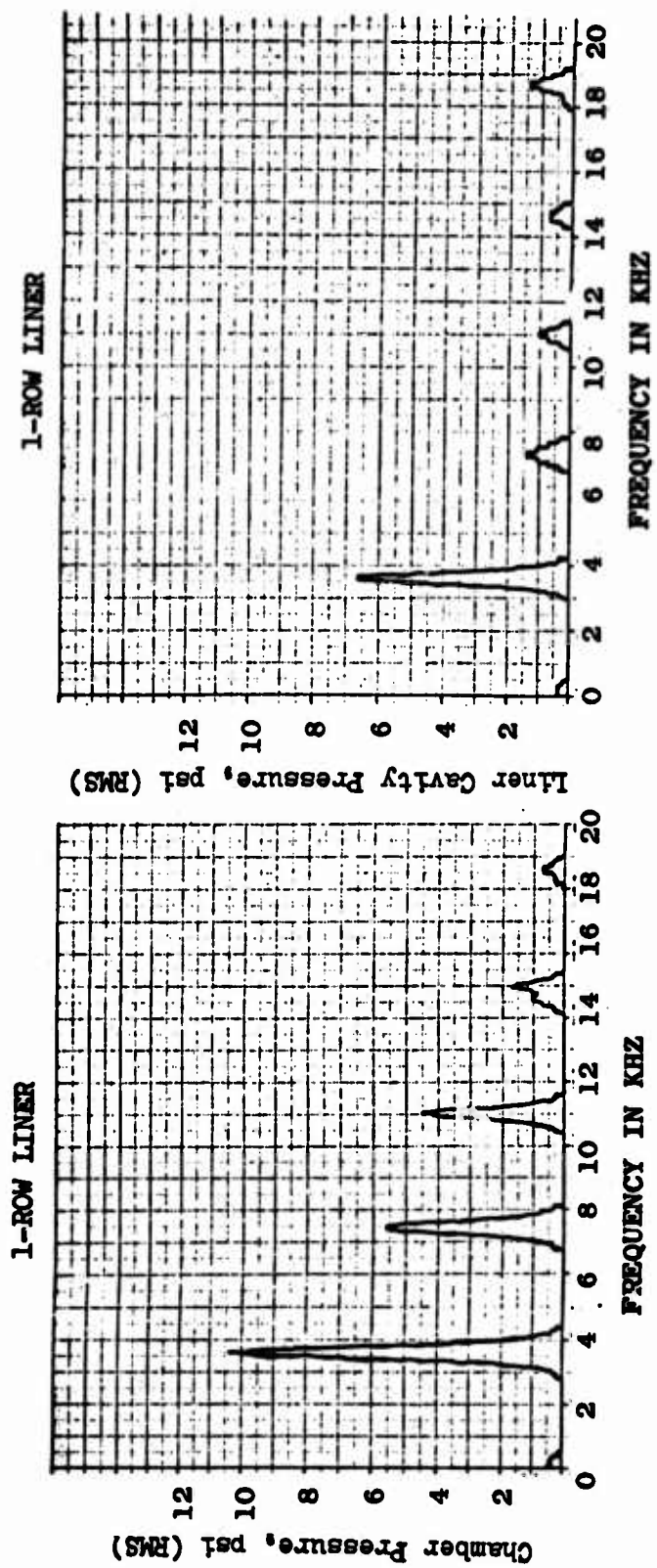


Figure 71. Spectral Analysis Showing Instability in Test No. -028

UNCLASSIFIED

UNCLASSIFIED

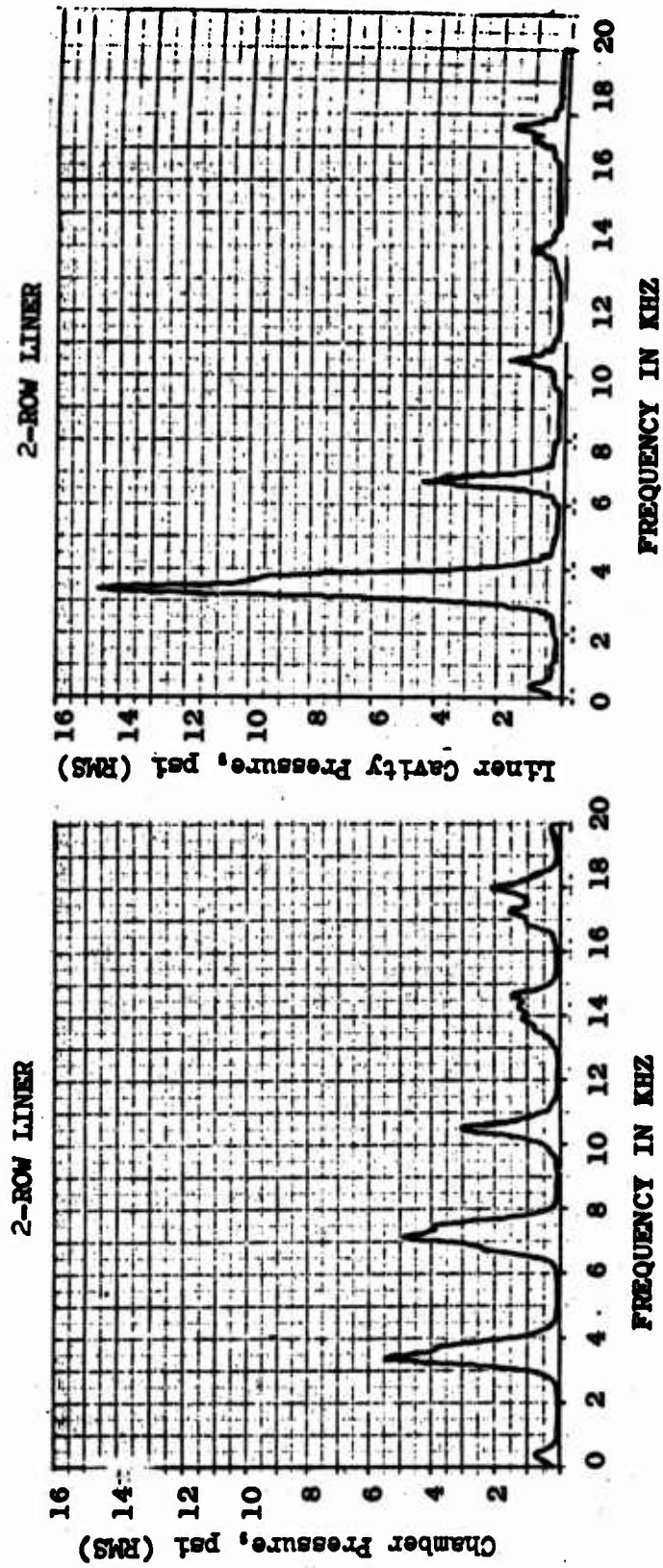


Figure 72. Spectral Analysis, Test No. -029

UNCLASSIFIED

CONFIDENTIAL

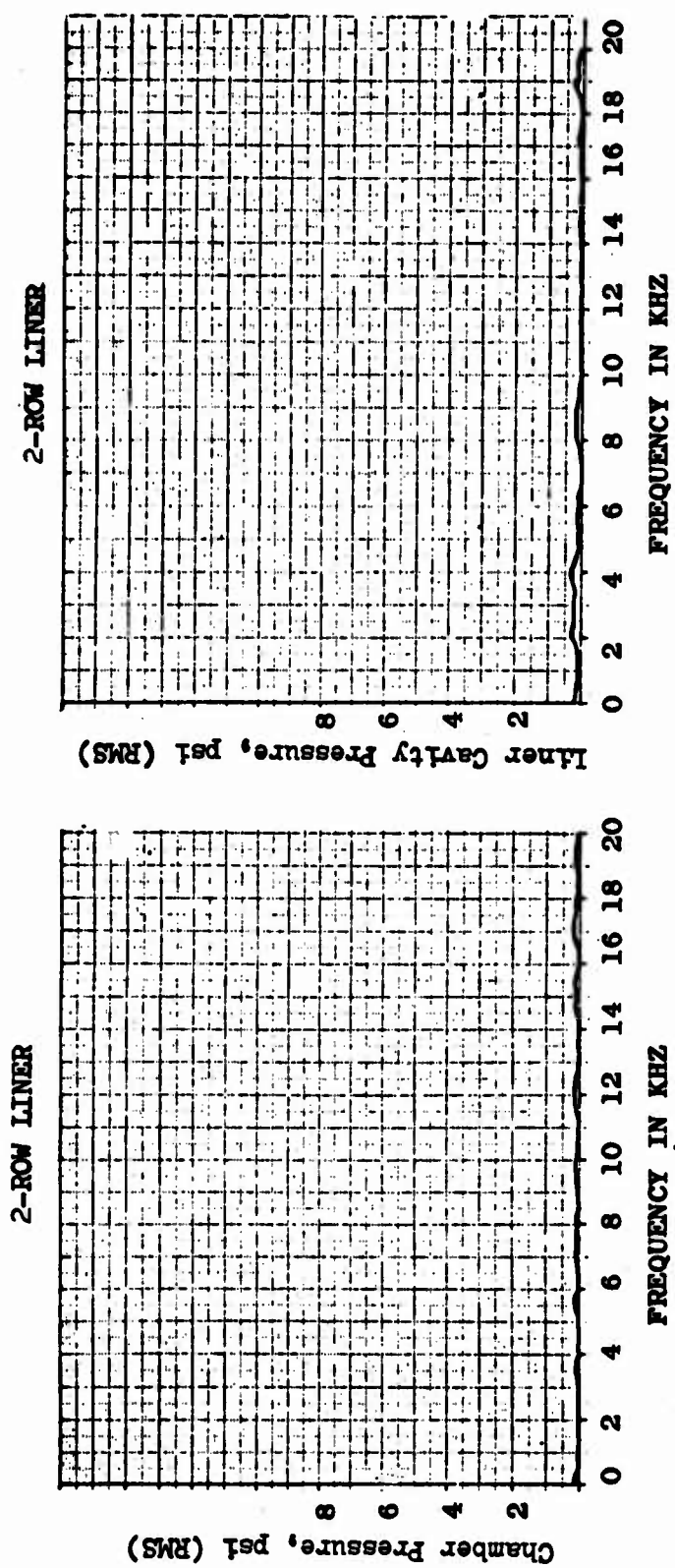


Figure 73. Spectral Analysis, Test No. -030

CONFIDENTIAL

(This Page is Unclassified)



## CONFIDENTIAL

fabricated and used to determine the temperature range occurring in the cavities. Figure No. 74 shows the specific instrumentation locations as well as the designations used.

There was a significant variation in the thermal environment of the cavities with the nine-row/three cavity damper. Fusible wires (as discussed in Section V,B,2) had been placed into the first and third cavities of the nine-row damper and only those wires in the third cavity (furthest downstream) survived the testing. These wires were reused for the single cavity dampers. The results observed from these fusible wires are presented below. All tests listed were for a 2.4 sec duration.

<u>Test No.</u>	<u>Damper</u>	<u>Cavity</u>	<u>Estimated Condition/Temperature</u>
1083-D01-OM	Orifice Rows/Cav.		
-024	3	First cavity	Completely melted - 4000°R
	3	Third cavity	Stainless steel melted > 2000°R
-027	1	First cavity	No further melting of stainless steel > 2000°R
-029	2	First cavity	Completely melted stainless steel - 4000°R

The above estimates of the first and third cavity gas temperatures were subsequently substantiated by the thermocouple data from Test No. -025 (see Figure No. 75). The thermal data show that the thermal environment of the one-row/one-cavity dampers is either cooler or approximately equal to the third axial cavity of the nine-row/three-cavity damper.

The fact that the nine-row/three-cavity damper successfully damped the tangential gun pulses suggests that a hot ( $\sim 4000^{\circ}\text{R}$ ) first cavity with an 8% open ratio is tuned accurately enough to give adequate absorption for the frequency range of interest.

The other two damper configurations were successful in damping one out of two chamber pressure pulses as shown in Table X. However, the latter configurations were significantly untuned due to a combination of either high cavity gas temperature with a high percentage open area or a low cavity gas temperature with a lower percentage open area. The low temperature ( $\sim 2000^{\circ}\text{R}$ ) of the one-row damper resulted in the resonant frequency of this damper being 30% low, while the two-row damper was 40% high, because of the 16% open area ratio and high temperatures ( $\sim 4000^{\circ}\text{R}$ ).

The effect of cavity gas temperature on the resonant frequency  $f_0$ , of the acoustic damper is reflected in the speed of sound  $c$ , of the gas in the cavity. The speed of sound of the cavity gas is proportional to the square root of the cavity gas temperature. The resonant frequency of the damper is

## CONFIDENTIAL



UNCLASSIFIED

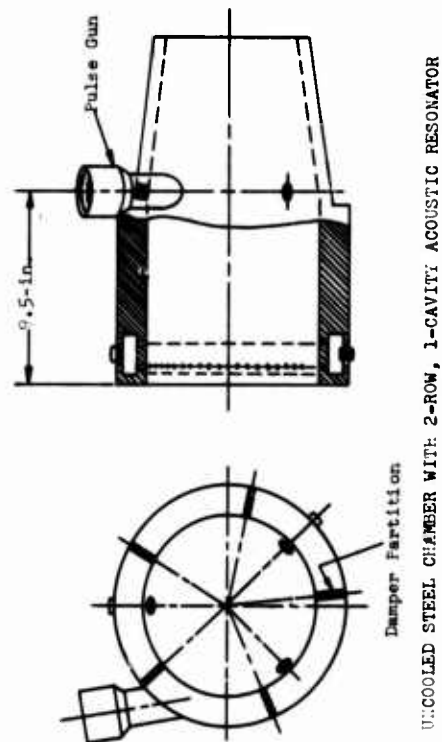
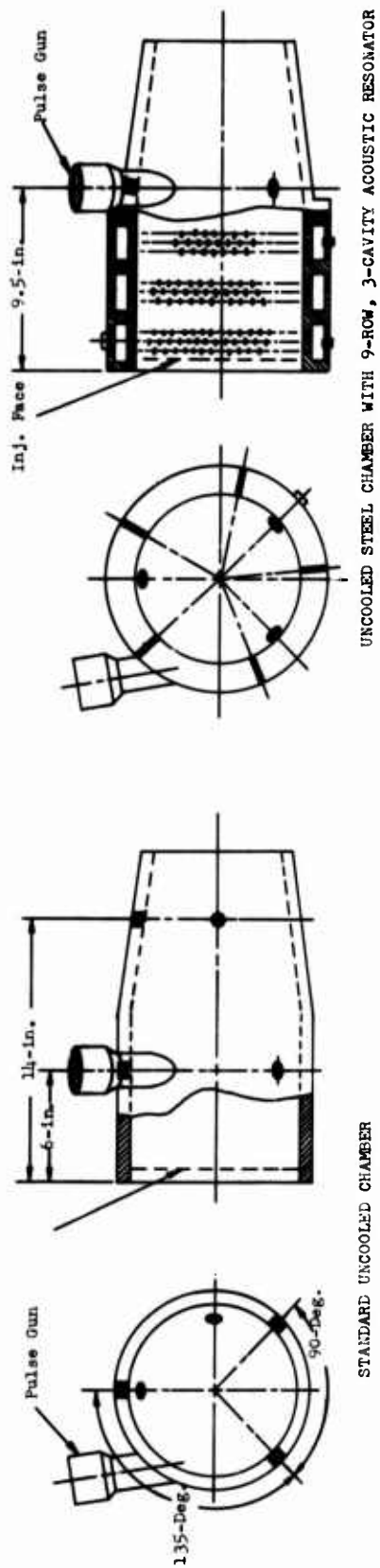


Figure 74. Instrumentation Locations, All Chambers

UNCLASSIFIED

UNCLASSIFIED

THERMOCOUPLE TEMPERATURE VS TIME, TEST 025

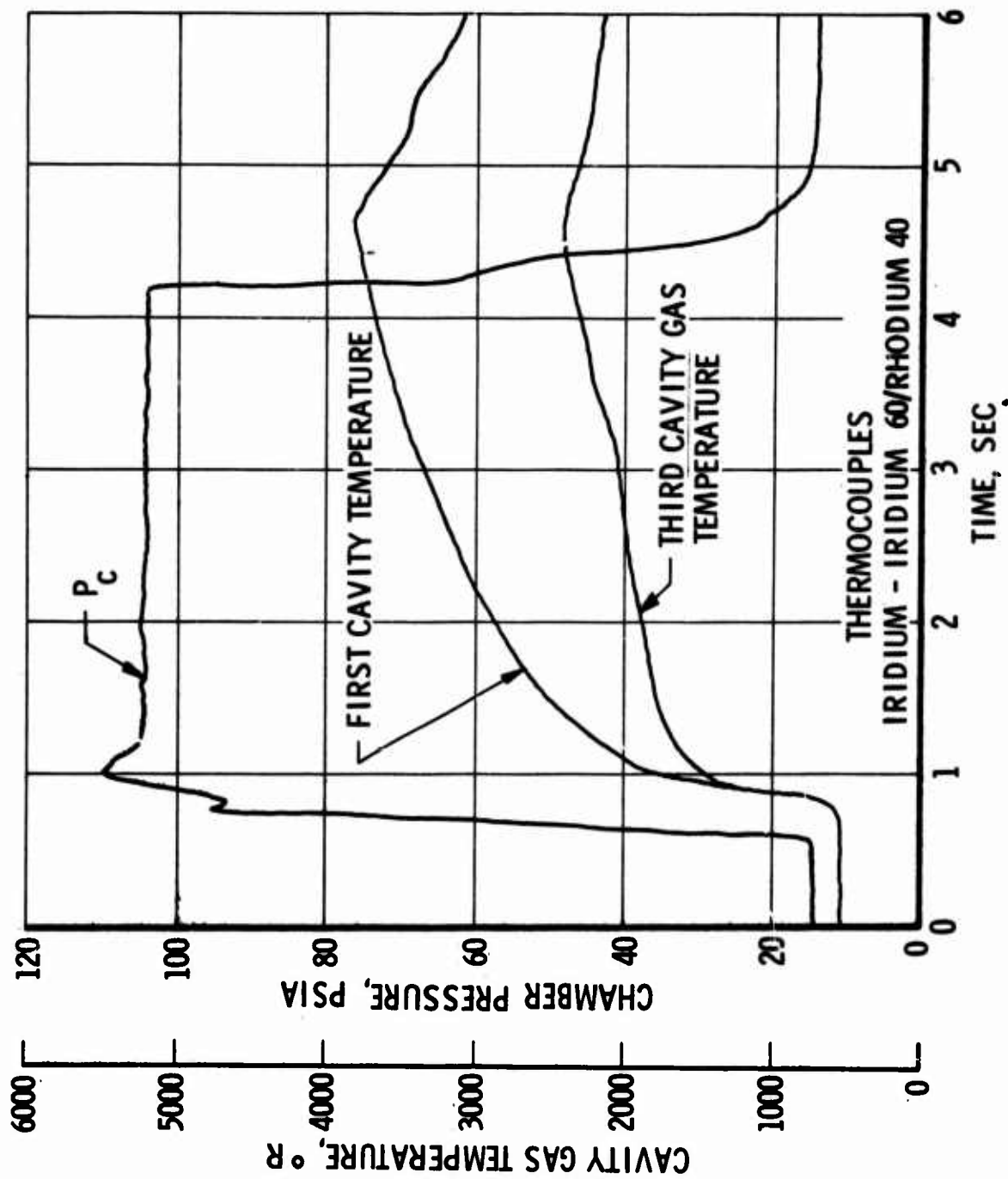


Figure 75. Thermocouple Temperature Traces vs Time, Test No. -025

UNCLASSIFIED

# UNCLASSIFIED

also related to the square root of the damper orifice open area ratio,  $\sigma$ , as shown by the Helmholtz resonant frequency equation<sup>(23)</sup>

$$f_o = \frac{c}{2\pi} \sqrt{\frac{\sigma}{Ll}} \quad \text{Equation (1)}$$

where  $l$  is the equivalent orifice thickness and  $L$  is the cavity backing distance.

If only the first cavity is considered to be significant in damping the combustion instability, a tentative conclusion can be made regarding the resonant frequency tuning of the damper. The successful damper used during Test No. -024 had an open area of about 8% and a cavity gas temperature of about 4000°R. Increasing the open area by a factor of two as mistakenly done prior to Test No. -029, or decreasing the cavity gas temperature by a factor of two resulted in only 50% successful pulse damping. This result implies that a factor of 1.414 above or below the design resonant frequency is required to cause a noticeable decrease in the damping of a given size damper. Figure No. 76 shows the theoretical percentage of vaporization converted into combusted gas velocity in relationship to chamber length for S/N 7 injector as well as a reference injector-face-acoustic-resonator system which was experimentally proven successful.

Examination of the fibrous graphite resonator tested in the ablative chamber showed that the upstream, or first, orifice row of each three-row cavity exhibited a greater orifice enlargement than did the two downstream orifice rows. This orifice enlargement was most pronounced for the first cavity. Localized erosion existed on the back wall of the cavity outboard of each orifice in the upstream row. In addition, the backside of each of the upstream orifices was sharp edged, whereas, orifices in the remaining rows were rounded. This implies that hot combustion gases flowed into the first row and out the two downstream orifice rows. Since the cylindrical chamber does not have a static pressure gradient because of area change, wall friction is negligible, and the injector mass flux distribution is almost flat so no recirculation occurs. It can be assumed that the axial static pressure distribution is the result of the combustion process accelerating gas to high velocities over a short distance. It is estimated that the gas velocity into the first cavity's first orifice row is on the order of 10 ft/sec rather than 100 ft/sec since the damper was effective. The gas velocity past the damper orifices downstream of the first cavity were calculated to exceed 1300 ft/sec. Such a velocity is thought to decrease the absorption coefficient to less than 10%, whereas the first cavity gas velocities are low enough to sustain absorption coefficients exceeding 60%.

(23) Blackman, A. W., "Effect of Nonlinear Losses on the Design of Absorbers for Combination Instabilities," ARS Journal, November 1960, pp. 1022-1028.

# UNCLASSIFIED

UNCLASSIFIED

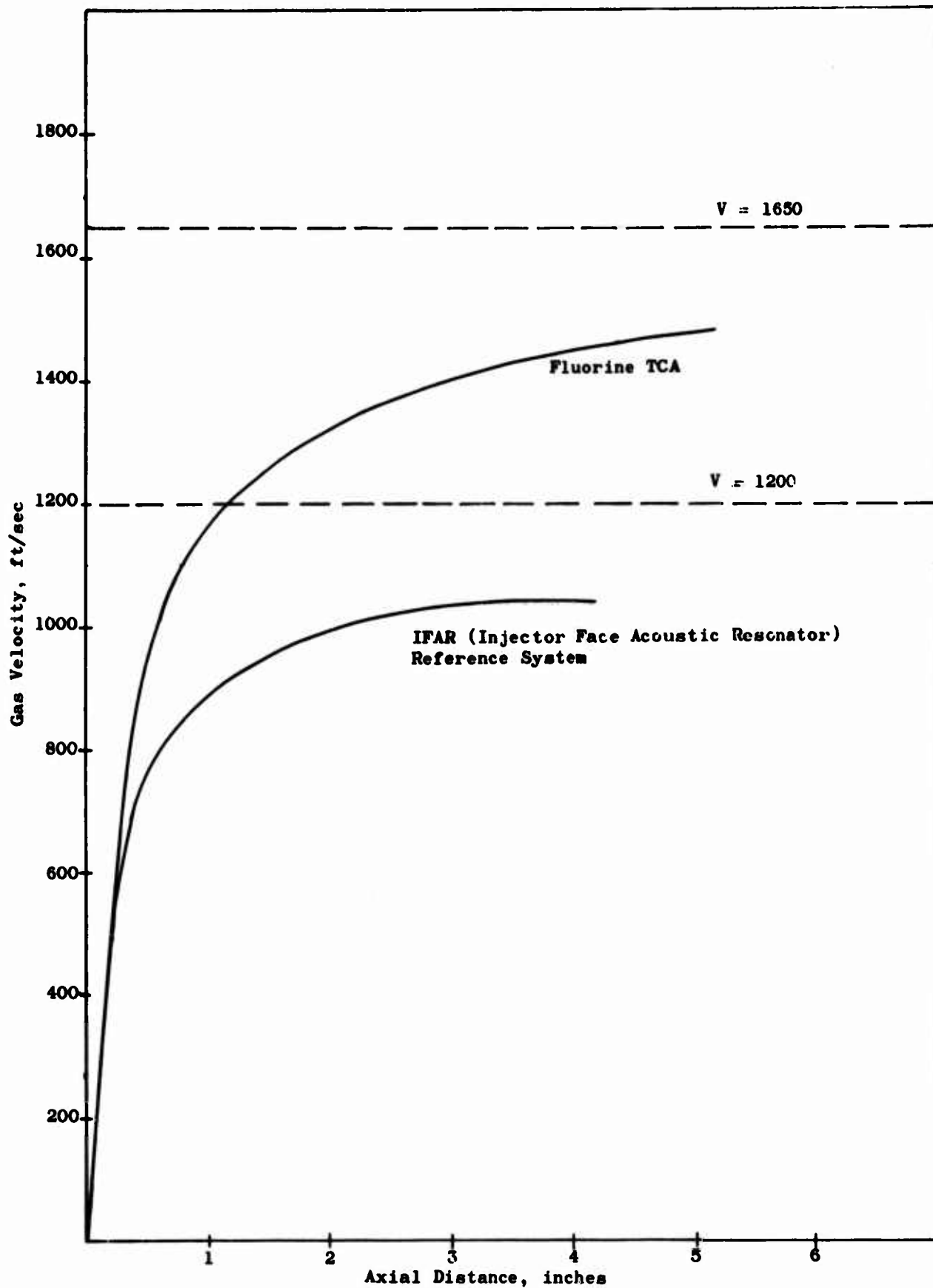


Figure 76. Theoretical Gas Velocity vs Chamber Length

UNCLASSIFIED

# UNCLASSIFIED

## 2. Methods of Injector Pattern Evaluation

The injector patterns for the fluorine thrust chamber assembly were compared upon the basis of the average active orifice size and the injection distribution factors. These two parameters were the major stability variables characterizing the seven different injector patterns fabricated and tested on this program.

The effect of the orifice diameter changes are summarized below in terms of the "sensitive frequency,"  $F$ , which would result from the various orifice sizes. This "sensitive frequency," is the one in which the injector provides the maximum amount of energy which may or may not coincide with chamber acoustic oscillation mode. The "sensitive" frequency is estimated using the relationship for the sensitive time lag,  $\tau$ , discussed in greater detail in Appendix II. Smith and Reardon<sup>(24)</sup> show the following relationship between the sensitive time lag,  $\tau$  (milliseconds), and the injector orifice size,  $d$  (inches), chamber Mach number,  $M$ , and the ratio of chamber pressure to the propellants critical pressure,  $P_c/P_{cr}$ ; for the fuel and oxidizer orifice:

$$\tau_{\text{fuel}} = 0.25 d_f^{1/2} / (M_c P_c / P_{\text{crf}})^{1/3} \quad \text{Equation (2)}$$

and

$$\tau_{\text{oxid}} = 0.21 d_{\text{ox}}^{1/2} / (M_c P_c / P_{\text{cro}})^{1/3} \quad \text{Equation (3)}$$

All of the parameters in the above equations are constant in the case in study, except for orifice sizes; therefore, the two correlating equations can be simplified by inserting the respective values as follows:  $M_c = 0.36$ ,  $P_c = 100$  psia,  $P_{\text{crf}} = 1600$  psi, and  $P_{\text{cro}} = 808$  psi.

Thus

$$\tau_f = 0.885 d_f^{1/2} \text{ (msec)}$$

and

$$\tau_{\text{ox}} = 0.595 d_{\text{ox}}^{1/2} \text{ (msec)}$$

The sensitive frequency can be determined by using the relationship:  $F = \frac{1}{2\tau}$  and is given in Table XI.

(24) Smith, A. J., Jr. and Reardon, F. H., The Sensitive Time Lag Theory and Its Application to Liquid Rocket Combustion Instability Problems, Vol I., AFRPL-TR-67-314, March 1968.

# UNCLASSIFIED

TABLE XI

## SUMMARY OF INJECTOR, ORIFICE, AND STABILITY DATA

S/N-Mod/No. of Element	Average Orifice Diameter and Number of Orifices		Estimated Sensitive Frequency (cps)		First Tangential Mode Injection Distribution Factor ( 1.0 more stable)	Experimental Stability Results
	Fuel	Oxid	Oxid	Fuel		
T <sup>2</sup> /215	0.025/480	0.050/215	3800	3600	0.93	Unstable in 1T Mode at 3500 cps
2-0/158	0.027/396	0.053/158	3600	3400	<1.00	Unstable in 1T Mode at 3500 cps
2-1/98	0.046/186	0.073/98	3100	2600	<1.00	Unstable in 1T Mode at 3500 cps
2-2/68	0.041/156	0.073/68	3100	2800	1.17	Stable
2-3/68	0.043/182	0.083/68	2900	2700	1.17	Stable
6/68	0.043*/210	0.078/68	3000	2700	1.17	Stable
7/344	0.020/688	0.0354/344	4400	4000	0.91	Stable with damper

\*Fuel film cooling neglected in averaging.

The results of a general combustion stability analytical investigation and the orifice size and number for each injector orifice pattern are shown in Table XI. The stability investigation evaluated injector patterns by "sensitive frequency" calculations based primarily on injection orifice sizes, and injected mass flux distribution over the injector face<sup>(25)</sup>. The first tangential mode was predicted to occur at a frequency of about 3500 cps. In testing, it was found to be the only acoustic mode that presented a significant stability problem. The application of this analysis is based upon the assumption that combustion takes place at the point of injection. The first tangential mode distribution factor shown in Table XI is defined as the inverse of the pressure sensitive coefficient ( $A_{\nu\eta}$ ). This makes the distribution factor directly proportional to the combustion stability effect of a given injection distribution. That is, a distribution factor of 1.0 defines a flat distribution, a distribution factor greater than 1.0 is in the direction of greater stability margin. The analytical results for the 68-element injector indicate that a distribution factor increase of 17% gave the desired stability characteristics.

(25) Reardon, F. H., McBride, J. M., and Smith, A. J., "Effect of Injection Distribution on Combustion Stability," AIAA Journal, Vol 4, No. 3, March 1966.

UNCLASSIFIED



UNCLASSIFIED

The 344-element injector, S/N 7, pattern injection distribution factor was adjusted to be as near as possible to that of the 215-element injector, S/N T<sup>2</sup>. This was done to assure that the S/N 7 injector would have stability characteristics that were similar to the S/N T<sup>2</sup> injector. The effect of orifice size upon the sensitive frequency of the two injectors (344- and 215-element) was not considered to be sufficiently large to cause a different acoustic mode of instability to occur. Both injectors were predicted to become unstable in the first tangential mode at approximately 3500 cps.

The most interesting injector pattern comparison is between the 98-element injector (S/N 2, Mod 1) and the 68-element injector (S/N 2, Mod 2 and Mod 3). It could have been possible to assume that the size of the orifice was the reason that the 68-element was stable and the 98-element was not. However, this was not possible because the S/N 2, Mod 2, 68-element injector was a simple modification of the S/N 2 Mod 1. The 30 doublets near the wall were plugged while the original 68 triplets of the core were left untouched. The fact that the remaining triplets were composed of two fuel and one oxidizer orifice was the reason that the average fuel orifice was actually a size smaller than the original 98-element injector.

### 3. Method of Damper Evaluation and Analytical Results

Three separate analytical techniques were used to evaluate acoustic liner design parameters. The analyses are discussed in more detail in Appendix II. The results of these analyses are presented here. The three analyses were as follows: the conventional absorption coefficient analysis of a two-dimensional Helmholtz array; the cylindrical damper analysis which accounts for the effect of the chamber wall resonator array on the frequency and damping rate of the combustion chambers acoustic modes; and the injector face acoustic resonator (IFAR) analysis which assumes all the resonators are near the face and accounts for their effect on acoustic mode frequency as well as the effect of the nozzles acoustic admittance.

The results of the absorption coefficient analytical evaluation of the nine-row, three-cavity acoustic damper design are shown on Figure No. 77 along with the cavity gas properties and cavity configuration. The cavity gas temperature range was assumed to be 2000°R to 4000°R, and a mean flow velocity past the damper of from 0 to 1050 ft/sec. With these assumptions and the structural limitations imposed, the configuration was selected as an optimum compromise.

The original test hardware was fabricated to this configuration except that the orifice diameter was reduced slightly to allow for modification by enlarging the orifice between tests. Using this approach, the costs of obtaining data over a range of open area would be minimized.

During the test phase of the program, involving both the uncooled chamber and the ablative unit, test evidence indicated that the three-row cavity was experiencing relatively high mean flows into the first row and

UNCLASSIFIED

UNCLASSIFIED

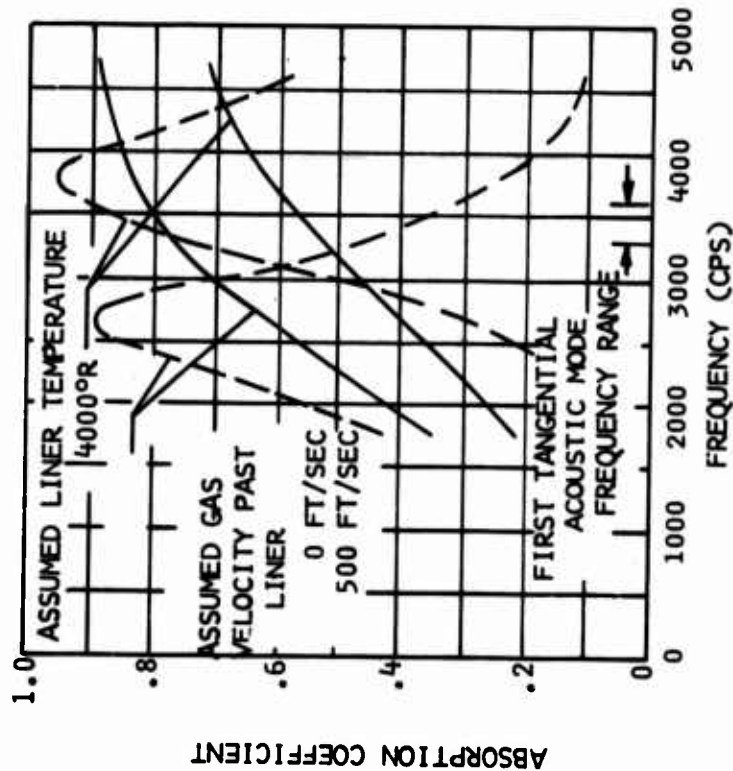
ASSUMED CHAMBER CONDITION

CHAMBER PRESSURE 100 PSIA  
 VELOCITY PAST LINER 500 FT/SEC  
 SOUND LEVEL 190 DB  
 FIRST TANGENTIAL MODE 3450 CPS

ASSUMED LINER CONDITION

TEMPERATURE °R 2000.  
 DENSITY. 16/FT<sup>3</sup> .075  
 VISCOSITY, LB/FT-SEC.  $328 \times 10^{-4}$   
 SPEED OF SOUND, FT/SEC 2660.

TEMPERATURE °R 4000.  
 DENSITY .0375  
 VISCOSITY, LB/FT-SEC.  $505 \times 10^{-4}$   
 SPEED OF SOUND, FT/SEC 3750.



ACOUSTIC LINER DIMENSIONS

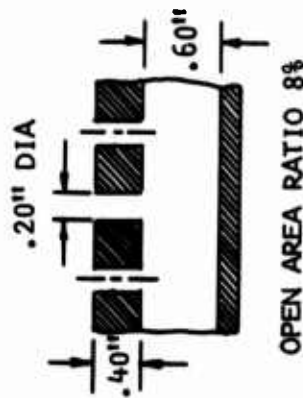


Figure 77. Liner Absorption Coefficient vs Frequency at 2000°R and 4000°R

UNCLASSIFIED

# UNCLASSIFIED

out of the third row. The excessively high temperatures ( $>4000^{\circ}\text{R}$ ) in the first cavity, as compared to downstream cavities, led to the noticeable erosion of the first row of orifices. However, the first cavity is known to potentially provide the most absorption. It was desirable to evaluate techniques of extending the chamber duration capability over that demonstrated with the graphite liner. It was decided to rework the entire damper in the steel chamber by plugging all of the nine rows and redrilling only the first cavity with one row of orifices whose total area was equal to that of the three rows previously used. This configuration would eliminate axial flow of gas in the liner cavity. This damper, which was designed for test purposes, then was evaluated with the absorption coefficient analysis at an assumed cavity gas temperature of  $4000^{\circ}\text{R}$  as was the later modification to two rows of large orifices which yielded twice the normal percentage of open area (approximately 16%). These absorption curves, along with their corresponding test results, are shown on Figure No. 78. Test results showed the one-row damper to be significantly cooler (approximately  $3000^{\circ}\text{R}$ ) than the other multi-row configurations as was expected since flow through the damper orifices was not possible.

Further analytical evaluation of the damper designs were performed as the analytical techniques were improved. The single resonator absorption coefficient approach was considered unsatisfactory, but was the only commonly-accepted method for establishing damper designs. However, over the past two years analyses have been performed which more realistically combine the damper and chamber as well as compare the damped and undamped chamber acoustics.

Typical results of the simplified cylindrical damper analysis of the three damper configurations are shown on Figure No. 79 for a cavity gas temperature of  $4000^{\circ}\text{R}$  and no flow past the orifices (no flow is considered in the analysis). The sound level incident on the damper is a significant factor and was considered by varying the non-linear resistance factor ( $\Delta_{n1}$ )<sup>(26)</sup><sup>(27)</sup> by two orders-of-magnitude where high values of  $\Delta_{n1}/d$  indicate high incident sound levels. The following is a summary of these results:

## FIRST TANGENTIAL MODE DECAY RATES

$\Delta_{n1}/d$	No Damper (rough wall)		$\sigma = 8\%$		$\sigma = 16\%$	
	Resonant Freq. cps	Decay Rate db/sec	Res F. cps	D.R. db/sec	R.F. cps	D.R. db/sec
0.22	3500	2500	2600	6000	2900	4000
2.2	3500	2500	2500	12000	2800	6000
22.0	3500	2500	1900	52000	2400	36000

(26) Blackman, A. W., op cit.

(27) A Study of Suppression of Combustion Oscillation with Mechanical Damping Devices, Pratt & Whitney PWA-FR-2596, 20 November 1967

UNCLASSIFIED

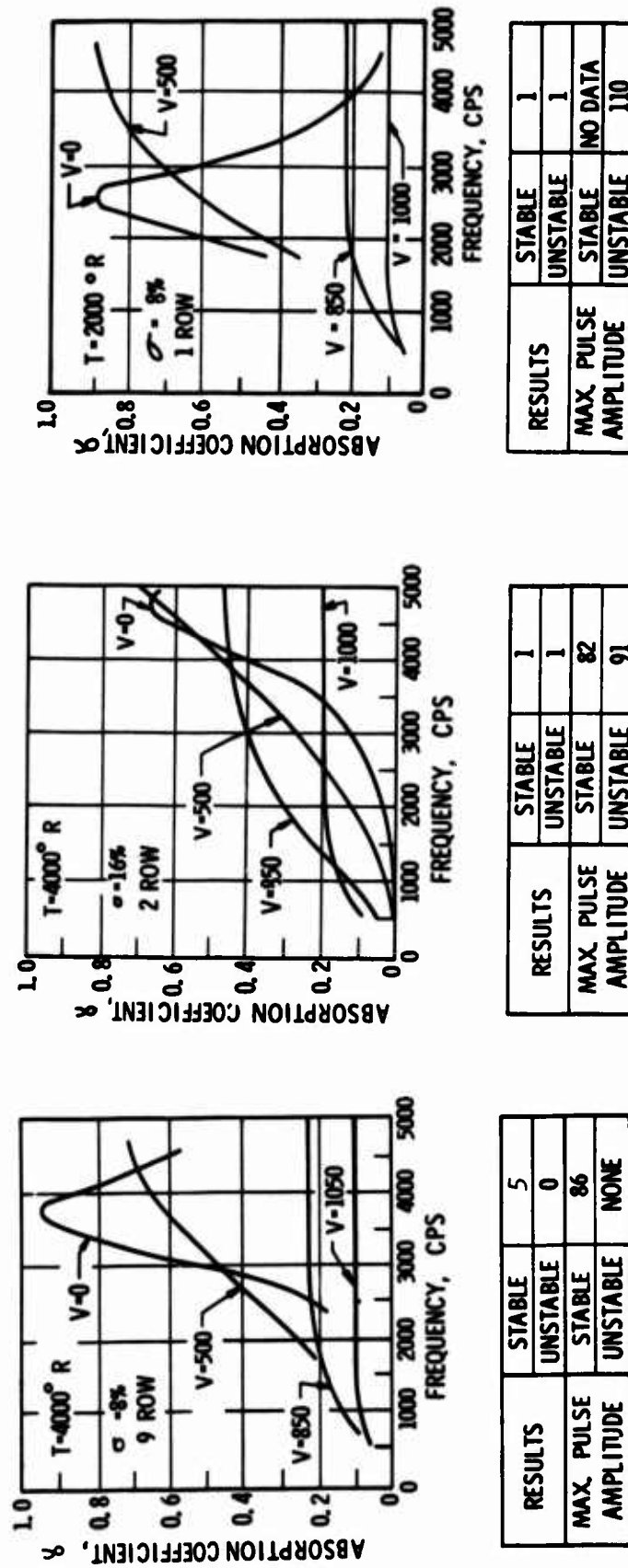


Figure 78. Absorption vs Frequency, Predicted and Actual

UNCLASSIFIED

UNCLASSIFIED

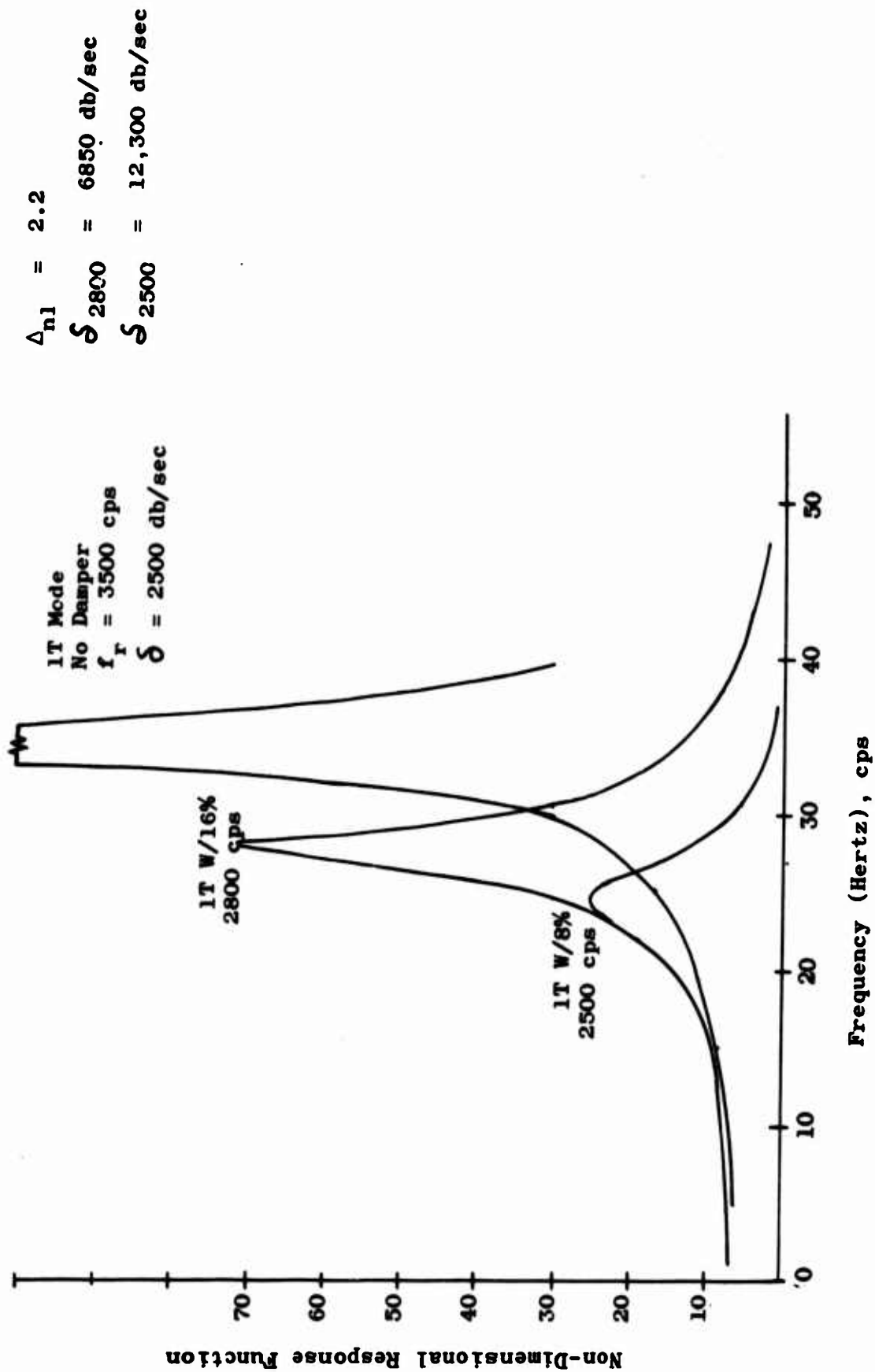


Figure 79. Cylindrical Acoustic Analysis

UNCLASSIFIED



# UNCLASSIFIED

The above results show the 8% open area damper to be most effective at all sound levels, both in depressing the first tangential mode resonant frequency and increasing its decay rate. However, this analysis is two-dimensional only and it does not consider the effect of partial chamber length dampers, nor pure or combined longitudinal acoustic modes. These results show the 8% and 16% designs are not significantly different at high sound levels (above 190 db), which produce an effective non-linear resistance factor of 22.0 or more. This analysis implies that at these levels, other acoustic modes would be more likely to occur because these are virtually eliminated.

The third and more comprehensive acoustic damper analysis, IFAR, (Injector Face Acoustic Resonator) was performed to help explain the experimental results of pulsed instability occurring at a frequency of from 3200 cps to 3700 cps. This analysis is founded in the sensitive time lag theory which is discussed in Appendix II. It assumes all of the damper to be in, or near the injector face. Also, it takes into account the mean flow acoustic nozzle admittance effects of the sonic nozzle. The output of this analysis is in the form of an  $n, \tau$  plot and can evaluate three-dimensional acoustic modes of the chamber. For this evaluation, primarily the first tangential mode and the first tangential mode combined with the first longitudinal were considered. The frequency depression results for the first tangential mode obtained were surprisingly like those of the two-dimensional cylindrical damper analysis. The quantitative and qualitative meaning of the  $n, \tau$  plot with dampers appears to be satisfactory; however, it will have to be evaluated further with other experimental correlations.

The following are the values of  $n_{min}$  and  $\tau$  at  $n_{min}$ , and the corresponding resonant frequency for the first tangential mode for the various incident sound levels as indicated by the non-linear resistance factors used.

## FIRST TANGENTIAL MODE $\tau$ 's AT $n_{min}$

$\Delta_{nl}/d$	No Damper			$\sigma = 8\%$			$\sigma = 16\%$		
	$f_{res}$ cps	$\tau_{res}$ msec	$n_{min}$ N.D.	$f_{res}$ cps	$\tau_{res}$ msec	$n_{min}$ N.D.	$f_{res}$ cps	$\tau_{res}$ msec	$n_{min}$ N.D.
0.22	3500	0.15	0.38	2100	0.31	11.7	2900	0.23	6.8
2.20	3500	0.15	0.38	1900	0.31	12.2	2500	0.24	7.0
22.00	3500	0.15	0.38	1600	0.33	16.5	2250	0.26	9.2

The data in the above table show the undamped chamber to have an  $n_{min}$  below the estimated operating range of  $0.82 = n = 0.68$ ; therefore, it can be expected to be spontaneously unstable because the  $\tau$  operating range falls within the acoustic mode neutral stability limit curve, as shown on Figure No. 80. The 8% and 16% open area  $n$  and  $\tau$  data shown on the above table indicate stable operation even with large pulses.

UNCLASSIFIED



UNCLASSIFIED

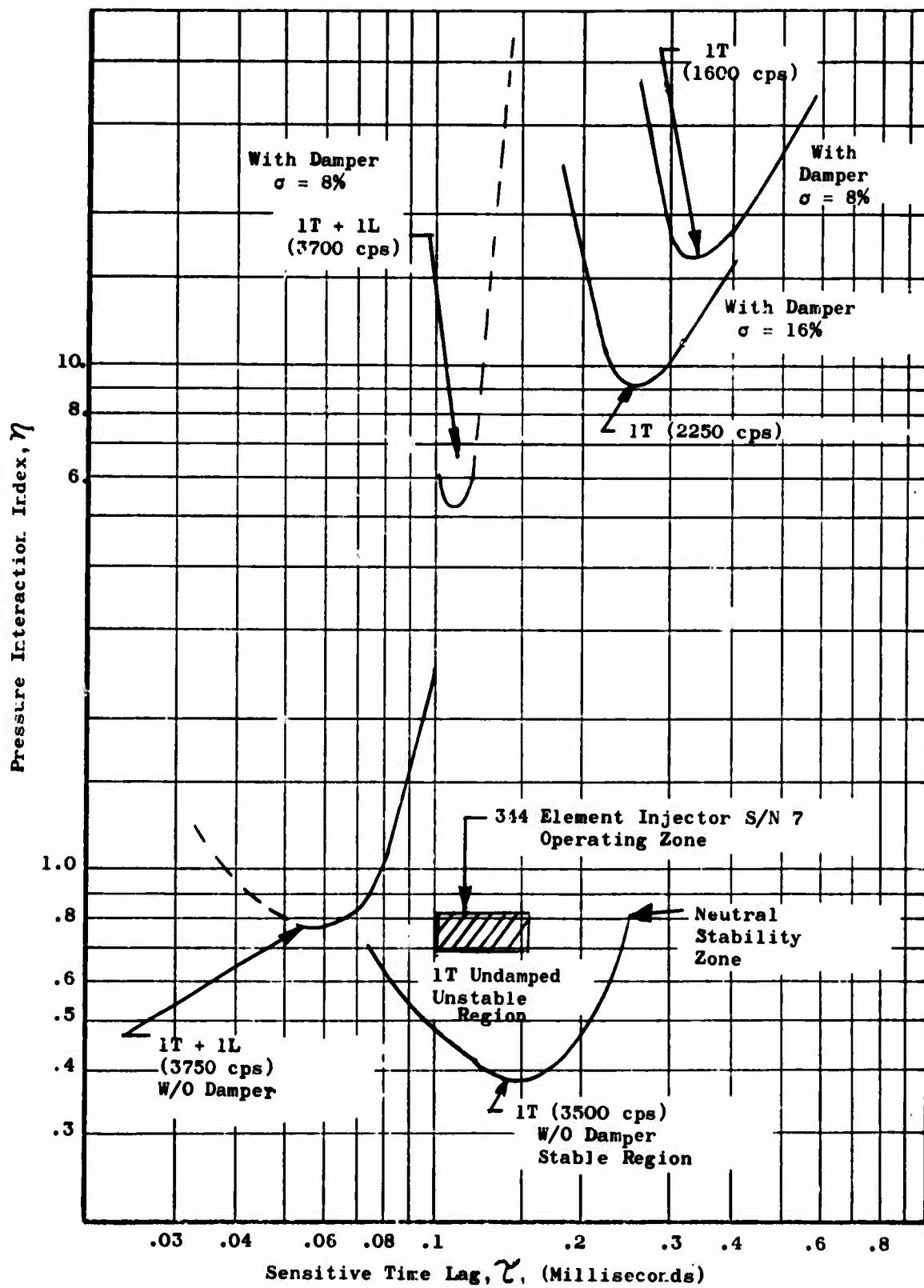


Figure 80. IFAR  $n/\tau$  Plot

UNCLASSIFIED

# UNCLASSIFIED

However, this result does not agree with the test results because the high frequency pressure transducer data clearly indicated a first tangential mode phase relationship around the chamber at the pulse gun plane. The phase data in the acoustic liner are complicated by phase changes caused by the liner resonance characteristics as a function of frequency. In view of the analysis predicting stable operation for the first tangential acoustic mode, one of three possibilities exist.

- The effect of the IFAR damper is overestimated in the analysis.
- The  $n$  and  $\tau$  linear theory has no validity for non-linear pulse effects.
- The acoustic mode observed was not a pure first tangential acoustic mode (1T) but rather it was the combined first tangential and first longitudinal mode (1T + 1L), the frequency of which is only slightly modified by the IFAR damper.

The testing and data analysis performed to date do not permit absolute verification of the third possibility; however, in all of the analyses that considered the combined chamber and damper acoustic modes, a noticeable depression of the pure first tangential mode was shown while displaying a less combined mode frequency depression. This pure first tangential mode frequency depression was not noticeable in the test data; therefore, it is possible that it was damped to the noise level and that the combined mode was suppressed to approximately the frequency originally observed for the pure first tangential mode in the undamped chamber.

This assumption was shown to have some validity in an analytical investigation of the combined (1T + 1L) mode, using the IFAR analysis. The results are as follows:

COMBINED (1T + 1L) MODE  $\tau$ 's AT  $n_{\min}$

$\Delta_{nl}/d$	No Damper			$\sigma = 8\% \text{ or } 16\%$		
	$f_{\text{res}}$ <u>cps</u>	$\tau_{\text{res}}$ <u>nsec</u>	$n_{\min}$ <u>N.D.</u>	$f_{\text{res}}$ <u>cps</u>	$\tau_{\text{res}}$ <u>msec</u>	$n_{\min}$ <u>N.D.</u>
0.22	3750	0.055	-	3600	0.12	3.5
2.20	3750	0.055	-	3600	0.12	4.0
22.0	3750	0.055	0.78	3700	0.11	5.1

The results for the 1T + 1L mode seem to resolve the question of what mode could occur, but they do not verify that it should be unstable because the  $n_{\min}$  values remain too high. The fact that the unstable mode had to be pulsed unstable (four out of four tests) indicates that it is probably stable to small linear perturbations while being unstable to large non-linear disturbances. The  $n$  and  $\tau$  theory is not quantitatively reliable as far as the

## CONFIDENTIAL

$n_{\min}$  values are concerned when large pulses are used. A pulse of 80% of the chamber pressure (100 psia) must be considered to be sufficiently large to be affected by non-linearities in combustion response.

(U) Although there is no indication of pure longitudinal instabilities occurring from the spectral analysis of stable and unstable tests, there is evidence of longitudinal modes occurring in the noise level of the stable tests. To verify their frequency and  $\tau$  values at  $n$  (minimum), they were analyzed using the IFAR damper analysis without a damper with the following results.

### LONGITUDINAL MODES AT $n_{\min}$

Mode	No Damper		
	$f_r$ cps	$\tau_r$ msec	$n_{\min}$ N.D.
1L	1650	0.031	1.03
2L	2600	0.019	1.29
3L	5200	0.010	1.27

### B. PERFORMANCE ANALYSIS

(U) Injector-chamber performance frequently is expressed as measured specific impulse or percentage of theoretical specific impulse. A higher measured value represents a superior performing injector when the two injectors are tested in identical thrust chambers under identical conditions. However, identical conditions for any two injector tests rarely exist; therefore, it is necessary that a performance evaluation technique be applied which clearly identifies the specific impulse effects for performance related variables so that a realistic assessment of the performance potential of an injector can be made.

(U) Such an analysis technique was used for all of the tests conducted in this program. The technique is known as the Performance Interaction Theory and it allows analytical determination of the component losses which affect the performance of a particular injector and enables scaling of these losses to any desired test condition and nozzle area ratio. Details of this technique are included in the method of analysis discussion.

(C) With the component losses for each injector test defined, a prediction of the altitude performance for each injector was completed. For these extrapolations, a hiperkinetic nozzle of 36.2 area ratio was used at a design chamber pressure of 100 psia and an injector mixture ratio, O/F, of 1.91. The results of these extrapolations indicated that a performance of 373 sec of specific impulse would be obtained using S/N 7 injector under the above stated design condition. This exceeded the contractually specified specific impulse of 370 sec. Table XII indicates the performance prediction at design conditions for each test mixture ratio and injector, respectively.

## CONFIDENTIAL

CONFIDENTIAL

TABLE XII

ALTITUDE HIPERKINETIC NOZZLE PERFORMANCE

ALTITUDE HIPERKINETIC NOZZLE

Pc = 100 Psia = 3

Test No.	Inj. SN	MR O/F	Is <sub>Theo</sub> Sec.	BL Sec.	CDL Sec.	MRD Sec.	FRL Sec.
1083-DO1-OM-001	72	1.71	405	7.3	4.3	1.2	
002	72	1.55	400.0	7.2	4.3	.9	
007	72	1.75	406	7.3	4.5	1.3	
003	2	1.57	400.5	7.2	4.5	0	
004	2	1.96	411.5	7.4	4.3	0	
005	2	1.87	409.5	7.4	4.4	0	
006	2	2.29	SHORT DURATION TEST - NO HIPERKINETIC EXTRAPOL				
008	2 Mod 1	1.77	407.0	7.3	4.5	0	
009	2 Mod 1	1.73	405.5	7.3	4.5	0	
010	2 Mod 1	1.75	406.0	7.3	4.5	0	
011	2 Mod 1	1.70	409.5	7.3	4.5	0	
012	2 Mod 2	2.01	412.5	7.4	4.4	0	
013	2 Mod 2	1.94	411.0	7.4	4.4	0	
014	2 Mod 2	2.26	LOW CHAMBER PRESSURE - NO HIPERKINETIC EXTRAPOL				
015	2 Mod 2	2.00	LOW CHAMBER PRESSURE - NO HIPERKINETIC EXTRAPOL				
016	2 Mod 2	1.83	LOW CHAMBER PRESSURE - NO HIPERKINETIC EXTRAPOL				
017	2 Mod 2	2.04	LOW CHAMBER PRESSURE - NO HIPERKINETIC EXTRAPOL				
018	2 Mod 3	1.91	410.5	7.4	4.3	.8	11.0
019	2 Mod 3	1.86	409	7.4	4.4	.6	11.0
020	2 Mod 3	1.85	409	7.4	4.4	.6	11.5
021	2 Mod 3	1.85	409	7.4	4.4	.6	11.5
022	2 Mod 3	1.86	409	7.4	4.1	.6	11.5
1083-DO2-OM-001	2 Mod 3	1.46	397.0	7.1	4.2	1.0	
002	2 Mod 3	DATA NEGATED DUE TO SKIRT FAILURE					
003	2 Mod 3	1.83	408.5	7.4	4.5	.7	
004	2 Mod 3	2.02	413.5	7.4	4.3	.7	
005	2 Mod 3	PREMATURE SHUTDOWN - DEFECTIVE CSM UNIT					
006	2 Mod 3	2.04	408.0	7.3	4.0	.7	
1186-XO1-OJ-001	2 Mod 3	1.57	400.5	7.2	4.4	.6	
002	2 Mod 3	1.67	404	7.3	4.5	.6	
1083-DO2-OM-023	6	1.79	407	7.3	4.4	2.1	14.5
007	6	1.91	410.5	7.4	4.3	2.7	15.5
1083-DO1-OM-024	7	3.10	377.5	6.8	4.3	0	3.0
025	7	2.20	416.0	7.5	4.5	0	21
1083-DO2-OM-008	7	1.70	404.5	7.3	4.5	0	14
009	7	2.03	413	7.4	4.5	0	16.5
010	7	1.97	412	7.4	4.5	0	15.5
1083-DO1-OM-026	7	1.82	408	7.3	4.5	0	14.5
027	7	1.98	412	7.4	4.5	0	16
028	7	1.99	412	7.4	4.5	0	16
029	7	2.18	415	7.5	4.5	0	20
030	7	2.03	413	7.4	4.5	0	16.5

CONFIDENTIAL

TABLE XII

## HYPERKINETIC NOZZLE PERFORMANCE EXTRAPOLATION

## HYPERKINETIC NOZZLE PERFORMANCE

$$P_c = 100 \text{ Psia} = 36.2$$

Enthalpy Defect					Mass Defect				
MRD Sec.	FRL Sec.	ERL Sec.	Is Sec.	%Is %v	FRL Sec.	ERL Sec.	ERE %	Is Sec.	%Is %v
1.2					22.5	27.5	92.1	342.3	85.6
.9					18.2	26.7	92.4	342.7	85.7
1.3					19.5	7.6	97.9	368.4	90.9
0					15.4	9.5	97.4	363.9	90.9
0					24.4	22.7	93.5	352.7	85.7
0					23.4	19.6	94.5	354.8	86.7
NO HIPERKINETIC EXTRAPOLATION					-	-	-	-	-
0					17.8	10.2	97.2	367.2	90.2
0					18.0	13.0	96.4	362.8	89.5
0					18.5	13.4	96.3	362.3	89.2
0					16.1	11.6	96.8	369.9	90.3
0					24.7	17.8	95.0	358.2	86.8
0					23.6	16.4	95.4	359.2	87.4
NO HIPERKINETIC EXTRAPOLATION					-	-	-	-	-
NO HIPERKINETIC EXTRAPOLATION					-	-	-	-	-
NO HIPERKINETIC EXTRAPOLATION					-	-	-	-	-
NO HIPERKINETIC EXTRAPOLATION					-	-	-	-	-
.8	11.0	34.5	353.3	86.1	28.9	18.0	95.7	351.3	85.6
.6	11.0	34.5	351.9	86.0	22.2	17.3	95.8	357.2	87.3
.6	11.5	34.5	351.4	85.9	21.6	17.4	95.7	357.6	87.4
.6	11.5	34.5	351.4	85.9	21.6	17.4	95.7	357.6	87.4
.6	11.5	34.5	351.4	85.9	22.3	18.5	95.5	356.1	87.1
1.0					15.2	19.3	95.1	350.2	88.2
.7					20.6	17.2	95.8	358.1	87.7
.7					23.9	24.5	94.1	352.7	85.3
IT									
.7					22.4	29.0	92.9	344.6	84.5
.6					16.3	16.7	95.8	355.3	88.7
.6					17.8	16.7	95.9	357.1	88.4
2.1	14.5	10.0	370.7	91.1	20.4	16.1	95.7	356.6	87.5
2.7	15.5	10.0	373.1	90.9	23.3	22.9	93.9	350.0	85.3
0	3.0	11.5	351.9	93.2	4.7	29.4	90.6	332.8	88.2
0	21	9.0	374.0	89.9	25.3	13.4	96.3	365.4	87.8
0	14	10.5	368.2	91.0	17.1	6.3	98.3	369.3	91.3
0	16.5	10.0	374.5	90.7	21.9	7.8	97.9	371.3	89.9
0	15.5	10.5	374.0	90.8	20.1	7.1	98.1	372.9	90.5
0	14.5	10.0	371.6	91.1	18.7	9.8	97.4	367.6	90.1
0	16	10.0	374.0	90.8	20.1	6.2	98.3	373.7	90.7
0	16	10.0	374.0	90.8	20.2	4.6	98.8	375.2	91.1
0	20	9.0	374.0	90.1	24.8	11.0	97.0	367.3	88.5
0	16.5	10.0	374.5	90.7	24.0	13.6	96.3	363.5	88.0

## UNCLASSIFIED

Following the design point (MR = 1.91) performance analysis, a perturbation study was completed to define the resulting specific impulse for variations in injector mixture ratio. Two types of O/F scaling were analyzed; Mass Defect and Enthalpy Defect.

In the mass defect technique injector energy release losses are equated to incomplete vaporization, wherein a portion of the injected propellant does not react and combust. As a result, the engine operates at a mixture ratio different from the propellant mixture ratio and at some combusted mass flow rate which is less than the total propellant flow rate. The model completely disregards the unvaporized mass flow in the nozzle expansion process. The mass has therefore disappeared from a performance standpoint.

The enthalpy defect method for scaling assumes that incomplete combustion reflects itself in reduced enthalpy development of the combustion products. This enthalpy reduction then defines a reduced temperature potential which reflects itself in a lower delivered impulse.

At the design point, the two methods yield a performance difference of 0.5 seconds of specific impulse with the enthalpy defect method evaluation being higher. To better understand the two scaling techniques and to define the one most applicable for this propellant combination, a specific study was conducted to evaluate the altitude performance of injector S/N 2, Mod 3, based upon both its sea-level and altitude testing. The results of these altitude predictions indicated the mass defect method not only gave more representative specific impulse values but tracked the test data over the full range of mixture ratios.

The ensuing discussion describes the method used in these analyses as well as the analyses themselves along with the factors affecting optimum performance of the final injector.

### 1. Method of Analysis

All test data were analyzed at test conditions and normalized to the design point operating conditions with an  $\epsilon = 36.2$  hyperkinetic nozzle using the ICRPG performance evaluation technique<sup>(28)</sup>. The performance of each injector was evaluated taking into account performance losses resulting from reaction kinetics, boundary layer flow, nozzle curvature and divergence, O/F maldistributions, and incomplete energy release.

#### a. Kinetic Loss

Kinetic losses account for the effect of finite reaction rates that do not permit equilibrium conditions to be maintained during the nozzle expansion process. Kinetic performance for the two conical and one hyperkinetic nozzle was calculated using a one-dimensional kinetic computer

(28) Performance Evaluation Methods for Liquid Propellant Rocket Thrust Chambers, ICRPG Working Group on Performance Standardization, CPIA Publication No. 132, November 1966.

UNCLASSIFIED



## UNCLASSIFIED

program<sup>(29)</sup>, wherein the non-equilibrium isentropic flow properties of the reacting gas expanding one-dimensionally are calculated<sup>(30)</sup>. Equilibrium constants for the reactions are those currently recommended. The theoretical kinetic performance in relationship to the theoretical shifting equilibrium is shown on Figure No. 81. The sharp departure of kinetic performance from shifting equilibrium above a mixture ratio of 1.8 is a result of the endothermic formation of  $H + F$  failing to recombine to the exothermic  $HF$  species.

### b. Boundary Layer, Loss, BLL

Boundary layer loss accounts for the thrust degradation resulting from viscous drag and heat transfer effects along the thrust chamber boundary. These losses were calculated using boundary layer charts from the ICRPG approved computer program for boundary layer loss<sup>(31)</sup>. From these charts, the momentum thickness and the displacement thickness of the boundary layer were obtained for the particular nozzle contour assumed boundary layer velocity profile and heat transfer wall conditions. This information, together with the general nozzle data permitted the drag loss in the boundary layer to be calculated. This drag then was converted to a specific impulse loss when it was divided by the measured weight flow. A divergence angle term in the boundary layer drag loss equation orients the thrust loss in the axial direction for the two-dimensional flow. These losses were calculated taking into account the cooling technique, wall temperature, and frictional characteristic for each test condition and nozzle area ratio extrapolation.

### c. Divergence Loss, CDL

This loss accounts for the non-axially directed momentum and other two-dimensional flow effects that reduce nozzle thrust and mass flow rate. The resulting nozzle divergence efficiency is stated as the relationship between two-dimensional and one-dimensional specific impulse. Therefore, this efficiency includes both the effects of non-axially directed momentum at the nozzle exit and the non-planar sonic surface (throat discharge coefficient) at the chamber throat.

### d. Mixture Ratio Distribution Loss, MRD

O/F maldistribution loss accounts for the effect of combustion gas O/F striations resulting from the injection process or from the use of film cooling. This loss in all  $LF_2/BA1014$  blend injectors was generated as the result of using fuel film cooling because actual injection was carefully designed for minimum gradient of O/F distribution across the face. The mixture ratio distribution loss is expressed by a summation of the mass weighted flow rate times the specific impulse of the particular stream tube originating at each element. These losses were calculated for each injector based upon a

(29) Axisymmetric Reacting Gas Nonequilibrium Performance Program, Contract NAS9-4358, TRW Report No. 02874-6004-R000, 8 March 1967

(30) CPIA Publication No. 132, op. cit.

(31) Ibid.

UNCLASSIFIED

CONFIDENTIAL

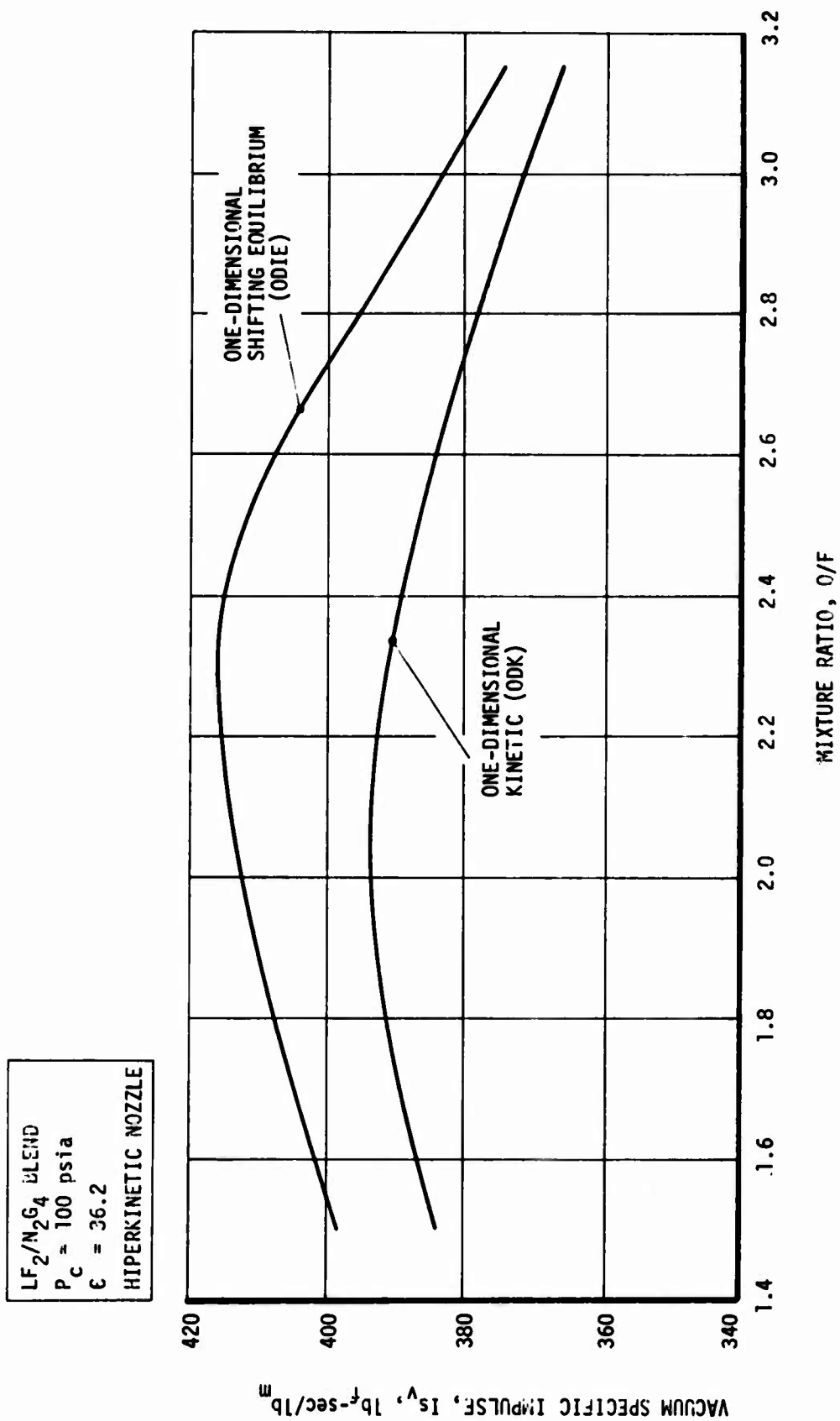


Figure 81. Kinetic and Shifting Equilibrium Comparison (u)

CONFIDENTIAL

# CONFIDENTIAL

2.77% fuel film cooling for S/N 2, Mod 3 injector and 9% fuel film cooling for S/N 6 injector.

## e. Energy Release Loss, ERL

This loss comes from incomplete or inefficient reaction of the propellants in the combustion chamber resulting from incomplete mixing, atomization, vaporization, and chemical reaction. The ICRPG method of scaling this loss to a new nozzle configuration is known to as the Reduced Enthalpy Technique. With this method, the low area ratio test data specific impulse is matched to the reduced enthalpy kinetic performance after boundary layer and divergence losses are accounted for. A ratio of 1%  $I_{sp}$  of energy release loss is equal to a 100 cal/gm reduction in the heat of formation ( $H_f$ ) for the propellants used in this program. This equivalence then can be expressed by:

$$ERL = I_{sp} \text{ (theo } H_f \text{ Ref.)} - I_{sp} \text{ (calc, } H_f \text{ effective)}$$

where:  $H_f$  is the reference value for the heat of formation at the combustion species.

$H_f$  effective is the effective value for the heat of formation for the resulting combustion performance.

The resulting reduced enthalpy value then is used to obtain kinetic performance at the high area ratio hiperkinetic nozzle conditions. However, when the data in this program were correlated, results indicated that an alternative method was superior for matching the altitude test data. This method is known as the Mass Defect Method, wherein the resulting energy release loss is described as a mass defect because of incomplete vaporization. In this case, the vaporization rate of the propellant governs the amount of reacted mass. Therefore, it can be considered that the vaporized mixture ratio determines the chemical composition of the gas and the percentage vaporized determines the amount in reaction. Using the Mass Defect Method, the energy release loss becomes:

$$ERL = I_{sp(O/F)} - I_{sp(O/F)_v} \times \frac{\dot{w}_v}{\dot{w}_t} \quad \text{Equation (4)}$$

When the percentage of vaporization for each propellant is known (based upon analytical calculations correlated with the test data), then the vaporized mixture ratio, vaporized theoretical impulse, and total vaporized ( $\dot{w}_v$ ) can be determined. This permits the energy release loss to be ascertained for the hiperkinetic nozzle conditions. With almost all of the injectors tested, it was found that oxidizer was fully vaporized and the unvaporized mass was entirely fuel.

CONFIDENTIAL

(This page is Unclassified)

# CONFIDENTIAL

## f. Performance Interaction

A performance interaction exists between the energy release and the kinetic losses which results in changes in the magnitude of kinetic loss for various values of energy release loss. Based upon the Enthalpy Defect technique, the lower enthalpy of combustion gas causes the subsequent kinetic loss to be lower. It can be considered that the same effect largely holds true for the Mass Defect model because all of the mass is not in kinetic reaction.

The over-all impulse calculation, accounting for each of the interaction methods, then results as the following for the extrapolated delivered impulse:

### Enthalpy Defect:

$$I_{sp_{vac}} = \sum_{i=1}^n \left\{ \left( \frac{\dot{w}_v}{\dot{w}_t} \right)_i I_{s_{ODK(HF_{effective})_i}} \right\} (\eta_{DIV} - BLL) \quad \text{Equation (5)}$$

NOTE: BLL is calculated two dimensionally and therefore is not multiplied by curvature - divergence efficiency, see Section VI,B,1,g.

### Mass Defect:

$$I_{sp_{vac}} = \sum_{i=1}^n \left\{ \left( \frac{\dot{w}_v}{\dot{w}_t} \right)_i I_{s_{ODK(O/F_v)_i}} \right\} (\eta_{DIV} - BLL) \quad \text{Equation (6)}$$

- where:
- $I_{sp_{vac}}$  = vacuum delivered impulse
  - $I_{s_{ODK(HF_{effective})_i}}$  = Kinetic impulse at reduced heat of formation for each of the stream tubes
  - $\eta_{DIV}$  = Divergence efficiency
  - BLL = Boundary layer loss
  - $I_{s_{ODK(O/F_v)_i}}$  = Kinetic impulse at vaporized mixture ratio for each stream tube
  - $\left( \frac{\dot{w}_v}{\dot{w}_t} \right)_i$  = percentage of vaporized flow rate in each stream tube

# CONFIDENTIAL

The summation of each mixture ratio stream tube weight with its percentage weight flow determines the effective specific impulse.

## 2. Sea-Level Test Results

(U) A complete loss analysis was conducted for all sea-level testing of injectors wherein a 1.65 area ratio nozzle was used. From this analysis, the vacuum specific impulse and its corresponding percentage of theoretical impulse were defined. A performance interaction theory loss analysis then provided definition of the component losses resulting from curvature-divergence, boundary layer flow, mixture ratio distribution, and nozzle kinetics. Once these values were known, the remaining loss, which results from incomplete energy release, was defined based upon the sum of the losses expressed as differences between actual and theoretical. From this value, the corresponding Mass Defect and Enthalpy Defects were developed for each of the injectors tested. Table XIII lists each of the losses for any test-injector combination together with relevant performance analysis data. The performance of each injector and the characteristics affecting the development of this performance are briefly summarized (in the chronological order of testing) in the ensuing sections.

### a. Injector S/N T<sup>2</sup>

(C) The 215-element injector, S/N T<sup>2</sup>, was tested three times with an uncooled steel chamber of 1.65 area ratio. All tests were of short duration, 2.7 sec or less, and were unsuitable for absolute performance determination. In tests of this short a duration, the initial flow consisted of low density/high temperature fluorine resulting from the uninsulated injector line through which it had to pass. Consequently, the fluorine downstream of the thrust chamber valve and flowmeters produced measured flow rates that differed from those through the injector orifices for durations of up to 2.0 sec. Therefore, performance data were taken instantaneously at the completion of each test and were based upon flowmeter measurements. Measured vacuum specific impulses ranged from 85% to 93% of vacuum theoretical specific impulse and indicated the unsteady conditions affecting the performance data. The predicted specific impulse, based upon vaporization analysis, for this injector was 266 sec or 86.5% of theoretical at an area ratio of 1.65.

### b. Injector S/N 2

(C) Injector S/N 2 represented the first in a series of four patterns having the same basic injector geometry. The original version was subjected to four tests (Tests No. 1083-D01-OM-003 through -006), all of which were of short duration (less than 2.0 sec). Excellent performance of 92.9% of theoretical vacuum impulse was indicated when tested at a 1.65 area ratio in an uncooled steel nozzle. Three tests were of 1.75 sec duration and therefore, not indicative of steady level performance. No vaporization analyses were made for this pattern because of the unacceptable stability characteristics of the injector. All pertinent data are summarized on Table XIII.

CONFIDENTIAL



TABLE XIII

## TEST RESULTS PERFORMANCE SUMMARY

## TEST DATA EVALUATION

Test No.	Inj. SN	Duration	Data Period Sec.		Nozzle	MR O/F	PC Psia	Pa Psia	Is <sub>TH</sub> sec
1083-DO1-OM-001	T <sub>2</sub>	2.024	0.900 to	1.900	Steel	1.71	111.3	1.65	306
002	T <sub>2</sub>	2.722	0.950 to	2.450	Steel	1.55	95.1	1.65	304
007	T <sub>2</sub>	1.534	1.000 to	1.400	Steel	1.75	97.7	1.65	306
003	2	2.027	0.926 to	2.027	Steel	1.57	93.6	1.65	304
004	2	1.765	0.800 to	1.050	Steel	1.96	101.2	1.65	307
005	2	1.695	0.900 to	1.620	Steel	1.87	97.0	1.65	307
006	2	1.358	0.900 to	1.290	Steel	2.29	97.1	1.65	306
008	2 Mod 1	1.833	1.200 to	1.700	Steel	1.77	102.9	1.65	306
009	2 Mod 1	3.987	3.487 to	3.987	Steel	1.73	111.0	1.65	306
010	2 Mod 1	3.047	2.500 to	2.900	Steel	1.75	112.3	1.65	306
011	2 Mod 1	1.596	1.096 to	1.446	Steel	1.70	124.5	1.65	305
012	2 Mod 2	2.014	1.514 to	2.014	Steel	2.01	98.1	1.65	307
013	2 Mod 2	4.023	3.423 to	3.923	Steel	1.94	98.3	1.65	307
014	2 Mod 2	4.019	3.519 to	4.019	Steel	2.26	68.4	1.65	306
015	2 Mod 2	4.987	4.487 to	4.987	Steel	2.00	72.9	1.65	307
016	2 Mod 2	4.987	4.489 to	4.989	Steel	1.83	73.2	1.65	307
017	2 Mod 2	6.033	5.533 to	6.033	Steel	2.04	72.5	1.65	307
018	2 Mod 3	8.417	7.916 to	8.416	Steel	1.91	101.8	1.65	307
019	2 Mod 3	39.349	32.500 to	37.500	Steel	1.86	100.7	1.65	307
020	2 Mod 3	50.326	42.500 to	47.500	Steel	1.85	101.7	1.65	307
021	2 Mod 3	48.863	42.500 to	47.500	Steel	1.85	101.0	1.65	307
022	2 Mod 3	49.884	42.500 to	47.500	Steel	1.86	101.0	1.65	307
1083-DO2-OM-001	2 Mod 3	8.544	2.000 to	8.544	Ablative	1.46	92.1	7.4	365
002	2 Mod 3	29.711	D A T A N E G A T E D D U E T O S K I R T F A I L						
003	2 Mod 3	194.700	194.000 to	194.500	Ablative	1.83	97.1	7.3	371
004	2 Mod 3	202.780	202.080 to	202.580	Ablative	2.02	100.7	9.1	381
005	2 Mod 3	.8	P R E M A T U R E S H U T D O W N - D E F E C T I V E -						
006	2 Mod 3	170.540	169.540 to	170.540	Ablative	2.04	97.5	7.3	373
1186-X01-OJ-001	2 Mod 3	10.120	5.060 to	8.120	Steel	1.57	100.5	1.65	304
002	2 Mod 3	14.230	13.730 to	14.230	Steel	1.67	102.6	1.65	306
1083-DO1-OM-023	6	5.072	4.572 to	5.072	Steel	1.79	95.5	1.65	306
1083-DO2-OM-007	6	36.620	12.00 to	19.000	Ablative	1.91	105.5	1.6	305
1083-DO1-OM-024	7	2.468	1.986 to	2.486	Steel	3.10	93.7	1.64	296
025	7	4.133	3.633 to	4.133	Steel	2.20	102.9	1.64	307
1083-DO2-OM-008	7	10.820	7.500 to	8.500	Ablative	1.70	95.6	1.61	306
009	7	50.490	49.490 to	50.490	Ablative	2.03	109.3	1.62	307
010	7	100.390	99.390 to	100.390	Ablative	1.97	106.7	1.64	307
1083-DO1-OM-026	7	2.200	1.700 to	2.200	Steel	1.82	96.5	1.65	306
027	7	2.486	1.986 to	2.486	Steel	1.98	104.3	1.65	307
028	7	2.250	1.646 to	2.146	Steel	1.99	103.0	1.65	307
029	7	2.300	1.659 to	2.159	Steel	2.18	102.5	1.65	307
030	7	3.980	3.480 to	3.930	Steel	2.03	101.9	1.65	307



TABLE XIII

## RESULTS PERFORMANCE SUMMARY

## TEST DATA EVALUATION

		Enthalpy Defect										Mass Defect		
FC Psia		Pa Psia	Is <sub>Theo</sub> sec.	Is <sub>vac</sub> sec.	% Is <sub>v</sub> %	BLL sec.	CDL sec.	MRD sec.	FRL sec.	ERL sec.	ERE %	FRL sec.	F <sub>1</sub> L sec.	ERE sec.
111.3	1.65	14.50	306.0	260.4	85.0	3.7	5.6	2.2	3.0	31.1	88.0	.7	33.4	87.2
95.1	1.65	14.67	304.0	257.5	84.7	3.7	5.3	2.1	3.0	32.4	87.4	.9	34.5	86.6
97.7	1.65	14.56	306.2	286.0	93.0	3.7	5.8	2.2	1.2	8.4	97.0	.8	8.8	96.9
93.6	1.65	14.60	304.0	283.4	92.9	3.7	5.8	0	1.3	10.8	96.1	1.2	10.9	96.2
101.2	1.65	14.73	307.5	275.6	89.3	3.7	5.6	0	1.6	22.0	92.0	1.3	22.3	91.9
97.0	1.65	14.69	307.2	276.8	89.7	3.7	5.6	0	1.4	20.8	92.4	1.1	21.1	92.4
97.1	1.65	14.67	306.5	247.3	80.4	3.7	5.0	0	4.0	47.5	80.7	1.7	49.8	79.9
102.9	1.65	14.65	306.5	285.6	92.8	3.7	5.8	0	1.3	11.1	96.1	.9	11.5	96.0
111.0	1.65	14.56	306.1	281.9	91.8	3.7	5.8	0	1.4	14.2	94.9	.8	14.8	94.7
112.3	1.65	14.63	306.3	281.4	91.5	3.7	5.7	0	1.4	15.1	94.6	.8	15.7	94.4
124.5	1.65	14.63	305.9	288.6	94.0	3.7	5.9	0	1.2	7.4	97.4	.7	7.9	97.3
98.1	1.65	14.58	307.5	279.7	90.6	3.7	5.7	0	1.4	18.1	93.5	1.4	18.1	93.5
98.3	1.65	14.58	307.5	280.0	90.7	3.7	5.7	0	1.3	17.8	93.6	1.2	17.9	93.6
68.4	1.65	14.49	306.7	257.8	83.8	3.7	5.3	0	3.0	37.7	85.3	1.7	39.0	84.9
72.9	1.65	14.49	307.5	270.7	87.7	3.7	5.5	0	2.2	26.5	90.2	1.3	27.4	89.9
73.2	1.65	14.50	307.0	274.7	89.1	3.7	5.1	0	1.6	22.9	91.6	1.0	23.5	91.4
72.5	1.65	14.50	307.5	274.3	88.9	3.7	5.0	0	1.6	23.9	91.2	1.4	24.1	91.2
101.8	1.65	14.59	307.3	274.3	89.2	3.0	6.1	1.0	1.6	21.5	93.1	1.2	21.9	92.9
100.7	1.65	14.59	307.0	278.3	90.6	3.0	6.1	1.0	1.2	17.2	94.4	1.1	17.5	94.3
101.7	1.65	14.55	307.0	278.3	90.6	3.0	6.1	1.0	1.2	17.2	94.4	1.0	17.6	94.3
101.0	1.65	14.54	307.0	278.2	90.6	3.0	6.1	1.0	1.2	17.3	94.3	1.0	17.7	94.2
101.0	1.65	14.56	307.0	277.0	90.2	3.0	6.1	1.0	1.4	18.3	94.1	1.1	18.8	94.0
92.1	7.4		365.0	317.8	87.1	5.1	16.7	1.0	NOT CALCULATED			3.8	20.6	94.3
TO SKIRT FAILURE														
97.1	7.3		371.5	323.9	87.2	2.0	17.1	.7	NOT CALCULATED			8.6	19.2	94.8
100.7	9.1		381.0	326.8	85.8	1.7	17.4	.7	NOT CALCULATED			11.9	22.5	94.0
- DEFECTIVE - CSM UNIT														
97.5	7.3		373.3	319.2	85.5	1.8	16.5	.7	NOT CALCULATED			9.5	26.6	93.0
100.5	1.65		304.0	277.2	91.1	3.0	6.0	.3	NOT CALCULATED			.3	17.2	94.4
102.6	1.65		306.0	279.0	91.1	3.0	6.0	.5	NOT CALCULATED			.6	17.0	94.4
95.5	1.65	14.56	306.7	274.9	89.6	3.7	5.6	3.9	1.3	18.3	93.9	1.0	18.6	93.8
105.5	1.6	14.73	305.2	263.4	86.3	2.2	13.4	4.15	2.0	20.0	92.9	1.2	20.8	93.2
93.7	1.64	14.65	296.6	268.0	90.8	3.7	6.0	0	3.0	14.3	94.7	2.1	15.2	94.3
102.9	1.64	14.62	307.0	285.3	93.0	3.8	6.1	0	1.4	9.9	96.5	1.6	9.7	96.6
95.6	1.61	1.65	306.0	283.4	93.1	3.0	12.1	0	1.1	4.6	98.4	1.0	4.7	98.3
109.3	1.62	.93	307.5	283.4	92.7	2.2	12.1	0	1.1	6.7	97.6	1.65	6.1	97.8
106.7	1.64	.81	307.5	286.8	93.5	1.2	11.0	0	1.1	6.4	97.8	1.55	5.9	97.9
96.5	1.65	14.53	306.8	285.5	93.0	3.8	6.1	0	1.2	10.2	96.4	1.0	10.4	96.4
104.3	1.65	14.53	307.5	290.0	94.3	3.8	6.1	0	1.1	6.5	97.8	1.3	6.3	97.8
103.0	1.65	14.54	307.5	291.1	94.6	3.8	6.1	0	1.1	5.4	98.1	1.3	5.2	98.2
102.5	1.65	14.53	307.0	286.3	93.2	3.8	6.1	0	1.1	9.7	96.6	1.6	9.2	96.8
101.9	1.65	14.52	307.5	282.8	91.9	3.8	6.1	0	1.2	13.6	95.2	1.4	13.4	95.3

## CONFIDENTIAL

### c. Injector S/N 2, Mod 1

(C) The basic S/N 2 injector pattern was modified to 98 elements to improve its stability. Four tests were conducted with this pattern and stable operation was demonstrated in one test (No. -009) only when a performance of 91.8% of vacuum theoretical specific impulse was generated. Test No. -010 became unstable after 2.5 sec; however, a comparable performance of 91.5% of theoretical vacuum specific impulse was exhibited. No vaporization analysis performance predictions were made for this injector. The consistency of the test data was sufficient to permit hiperkinetic nozzle altitude performance predictions to be made and these are subsequently summarized in Section VI,B,4.

### d. Injector S/N 2, Mod 2

(C) This injector was tested six times for durations of from 2 sec to 6 sec. In the initial two tests (Nos. 1083-D01-OM-012 and -013), a performance level of 90.6% and 90.7% of vacuum theoretical specific impulse were indicated, respectively. The recorded injector pressure drop was 95 psi and 70 psi in the oxidizer and fuel circuits, respectfully. Subsequent testing was accomplished at 70 psia chamber pressure to reduce the injector pressure drop to the specified requirement. In these tests, the exit pressure for the 1.65 area ratio nozzle was less than ambient at 11.5 psia, which introduced possible separation effects and increased kinetic losses. Measured performance for these tests varied from 85.8% to 89.2% of vacuum theoretical impulse and all tests were stable. Extrapolation to altitude data using the design chamber pressure tests is subsequently discussed in Section VI,B,4.

### e. Injector S/N 2, Mod 3

(C) Thirteen tests were conducted with injector S/N 2, Mod 3 for durations exceeding 8 sec in each test. Demonstrated performance was from 85.5% to 90.6% of theoretical vacuum specific impulse in all of the near-design mixture ratio tests (MR = 1.91). These tests (Nos. -018 through -022) were conducted with a water-cooled thrust chamber. Boundary layer losses were calculated commensurate with the wall temperatures of the cooled unit. The developed energy release loss of 17.5 sec yielded an energy release efficiency of 94.4%. Previous vaporization analysis had predicted 90.3% of theoretical vacuum specific impulse. The reduced performance of S/N 2, Mod 3 over that of S/N 2, Mod 2 was a direct result of the poorer atomization efficiency brought about by increasing the drop size of the larger elements in conjunction with the mixture ratio distribution loss caused by the 2.77% fuel film cooling. This increase in element orifice size was necessary to reduce the injector pressure drop to the contractually required values. Vaporization analysis of the test data indicated that the oxidizer was completely vaporized and the fuel 82.6% vaporized.

## CONFIDENTIAL

### f. Injector S/N 6

(C) To improve the compatibility of the S/N 2, Mod 3 injector pattern while maintaining its demonstrated stability of the injector, a new injector, S/N 6, was designed and tested. This design change included the relocation of long impinging triplets and the use of fuel film cooling to protect the chamber wall. Two tests were conducted with this injector for durations of 5 sec and 38 sec, respectively. The developed performance was 86.3% of theoretical vacuum specific impulse. Vaporization analysis had predicted an 87.6% specific impulse development. These results were in general agreement with those obtained from the S/N 2, Mod 3 testing, considering the 1% higher mixture ratio distribution loss caused by the 9% fuel film cooling. However, as a result of only two tests being conducted, there was a lower confidence level in the energy release loss evaluation.

### g. Injector S/N 7

(C) With the evolution of an acoustic resonator for stability improvement, a new injector design was tested with a high performance pattern of 344 elements. Previous low-thrust-per-element patterns had demonstrated a high incidence of instability which eliminated them from consideration. The 344-element injector offered three performance improvement characteristics over the previously tested injectors. Firstly, maximum propellant atomization and vaporization were obtained as a result of the smaller size of the injection orifice elements. Secondly, the pattern elements were oriented in such a manner so as to obtain maximum spray overlap and subsequent secondary mixing. Thirdly, the mixture ratio distribution loss across the face of the injector was zero because the fuel film cooling had been deleted.

(C) Ten tests were conducted with this injector, which demonstrated a 93.5% vacuum specific impulse performance at the design operating point of  $MR = 1.91$ . During the course of the testing program, tests were conducted over a mixture ratio range of 1.70 to 3.10 to fully define the operating characteristics. The 2% energy release loss shown on Table XIII was in close agreement with the vaporization model loss analysis, wherein an energy release loss was indicated. For energy release losses that are less than 2%, the performance analysis of an injector must include consideration of effects that are not normally considered to be important for injectors in the 5% energy release loss category. Therefore, a more detailed vaporization analysis is required. The BA1014 consists of 24% MMH (the highest volatility), 68%  $N_2H_4$  (intermediate volatility), and 9%  $H_2O$  (lowest volatility). As a result of the fractional distillation rate of BA1014, the water has the highest calculated liquid mass fraction at the throat. Therefore, the oxygen in the liquid  $H_2O$  is not available to react with the carbon from MMH to produce the desired CO. Also, the hydrogen from liquid  $H_2O$  cannot react with the F to form HF and the excess  $F_2$  dissociated to 2F. The reduction of combustion enthalpy from free radical formation and the gas phase mass defect resulting from the slower  $H_2O$  vaporization rate was calculated to result in a 1% inherent performance loss. Combining this effect with the nominal vaporization analysis indicates an efficiency level in close agreement with the experimental data.

CONFIDENTIAL

# CONFIDENTIAL

## 3. Altitude Test Results

(U) Six tests were conducted in the altitude chamber using nozzles with area ratios of 7.3 and 9.4, and the S/N 2, Mod 3 injector. These tests followed sea-level testing at an area ratio of 1.65. The same injector was tested with the two different area ratio nozzles; therefore, the data allowed highly valid verification of the altitude ERL and kinetic rate loss scaling techniques. As indicated in the method of analysis discussion, two energy release loss scaling techniques were available; the conventional method of incorporating enthalpy reduction for ERL scaling, and the mass defect scaling wherein energy release loss is evaluated by treating the lower than theoretical combustion as a vaporization loss.

(U) Both methods were used to evaluate the area ratio 1.65 data for scaling it to the 7.3 area ratio and 9.4 area ratio test conditions (Test Nos. -001 through -005). Predictions using both methods were made for the actual altitude test conditions. Table XIV summarizes the predictions while comparing them with the actual measured values.

(C) In Test No. -001, the measured performance was 317.8 sec of vacuum specific impulse. Predictions from the 1.65 area ratio sea-level tests indicated 305.9 sec of vacuum specific impulse using the enthalpy defect model for a difference of 11.9 sec or 3.75%. From the mass defect scaling technique, the prediction was for a vacuum specific impulse of 317.4 sec for a 0.4 sec difference or 0.125% error. The results from Tests No. -003, -004, and -006 largely show the same correlation with the mass defect prediction averaging less than 1% error. The enthalpy defect errors ranged from 1% to 4%.

(C) The slope characteristics of the large area ratio prediction is more important than the numerical solution. Figure No. 82 defines the Enthalpy Defect and Mass Defect scaling characteristics versus mixture ratio together with the actual test data. As can be seen, the mass defect scaling technique most nearly tracks the data curve, whereas the enthalpy defect intersects it. The optimum with mass defect occurs at a mixture ratio of approximately 1.8 while the enthalpy defect becomes optimum at a mixture ratio of 2.2. This characteristic shape of the two analytical curves is explained in the following manner.

(U) The Enthalpy Defect method expresses the energy release loss as a near constant percentage of theoretical, which gives the same shape but with a lower value. Slope variations between the two curves occur as a result of changes in the kinetics losses as a function of mixture ratio. Therefore, the resultant peak performance occurs at nearly the same mixture ratio as peak theoretical performance. The Mass Defect approach relates performance to a certain percentage of the kinetic performance based upon the vaporized mixture ratio and the percentage of vaporized mass. From the Mass Defect equation, it can be seen that the measured performance is most directly dependent upon the product of vaporized mass ( $\% w_v/w_t$ ) and vaporized kinetic performance ( $I_{sODK(O/F)v}$ ). With all of the injectors tested in this program, the resulting

CONFIDENTIAL

TABLE XIV

ALTITUDE TEST SUMMARY  
PREDICTIONS FROM SEA LEVEL TESTS

ENTHALPY AND MASS DEFECT TECHNIQUES

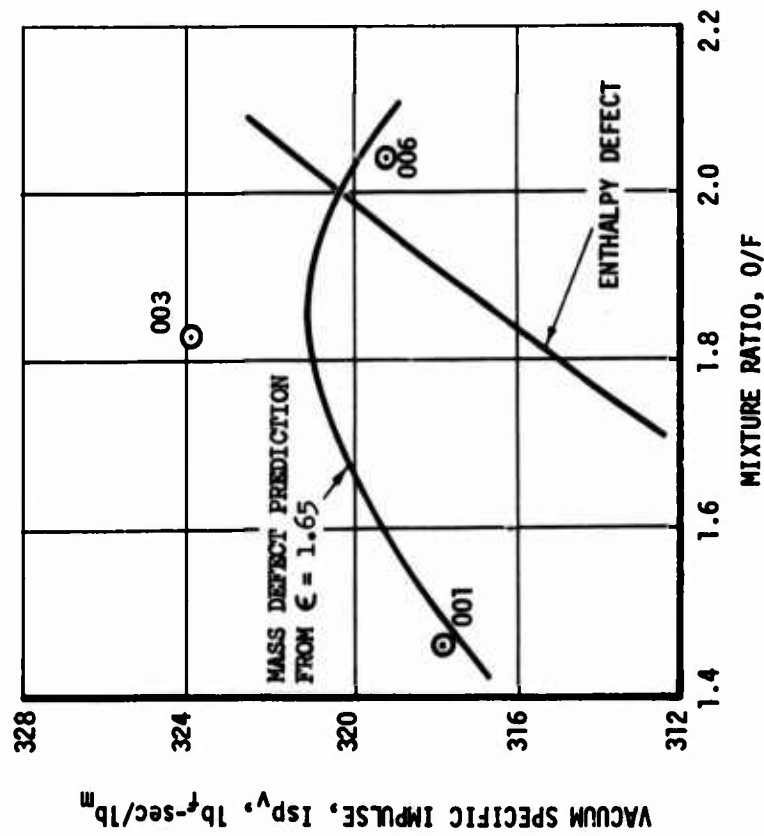
Test	Injector	MR O/F	$\epsilon$	$P_c$ psia	$I_{sTheo}$ Sec.	$I_{sMeas}$ Sec.	Enthalpy Defect			Mass Defect		
							$I_{spre}$	$\Delta$ Sec	$\Delta \%$	$I_{spre}$	$\Delta$ Sec	$\Delta \%$
1083-D02-OM-001	SN2-Mod 3	1.46	7.5	92.1	365.0	317.8	305.9	-11.9	-3.75	317.4	-0.4	-0.125%
1083-D02-OM-002	SN2-Mod 3	2.14	9.4	104.5	DATA NEGATED DUE TO SKIRT FAILURE							
1083-D02-OM-003	SN2-Mod 3	1.83	7.3	97.1	371.5	323.9	314.3	-9.6	-2.95	321.1	-2.8	-0.87
1083-D02-OM-004	SN2-Mod 3	2.02	9.1	100.7	381.0	326.8	322.6	-4.2	-1.3	325.3	-1.5	-0.46
1083-D02-OM-005	SN2-Mod 3	PREMATURE SHUTDOWN - DEFECTIVE CSM UNIT										
1083-D02-OM-006	SN2-Mod 3	2.04	7.3	97.5	373.3	319.2	322.2	+3.0	+0.94	319.8	+0.6	+0.19

CONFIDENTIAL



CONFIDENTIAL

LF<sub>2</sub>/N<sub>2</sub>H<sub>4</sub> BLEND  
 INJ. S/N 2 MOD 3  
 25° CONICAL NOZZLES  
 TEST SERIES: 1083-D02-OM-XXX



□ .....  $\epsilon = 9.1$  TEST DATA  
 ○ .....  $\epsilon = 7.3$  TEST DATA

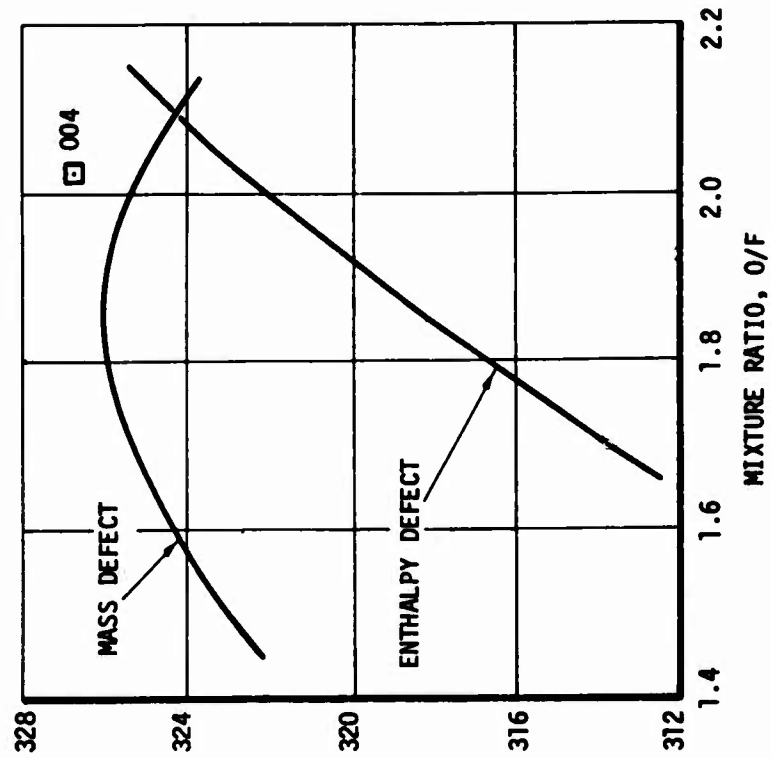


Figure 82. Comparison of Altitude Test Results with Predictions over a Range of Mixture Ratios (u)

CONFIDENTIAL



## CONFIDENTIAL

performance was fuel vaporization limited; therefore, the vaporized mixture ratio is more oxidizer-rich than the actual propellant mixture ratio. This characteristic has the tendency to move the resulting performance to a lower value because of the negative  $\Delta I_{sp}/\Delta O/F$  slope for mixture ratios greater than  $O/F \approx 1.9$  (see Figure No. 82). For these reasons, a sharper drop-off in specific impulse is evidenced on the oxidizer-rich side for the mass defect scaling than is for the enthalpy defect scaling.

(U) Excellent correlation in both absolute values of specific impulse and  $\Delta I_{sp}/\Delta O/F$  slope was obtained with Mass Defect scaling; therefore, the extrapolation to altitude performance primarily was accomplished using this technique. It should be noted that this correlation not only verifies the mass defect scaling criteria but also verifies the currently recommended kinetic rate constants. (32) Enthalpy defect extrapolations do not allow either of these verifications to be concluded.

#### 4. Design Condition Extrapolation

(U) Performance data obtained from all of the injector tests were evaluated at altitude conditions using the 36.2 area ratio hiperkinetic nozzle (see Appendix VIII) operated at 100 psia chamber pressure. The results are shown on Table XI and on Figure No. 83 at the test mixture ratios. Mass defect scaling is used in both instances and these analytical results are summarized by injector in the ensuing sections.

##### a. Injector S/N 7

(C) Contractually required performance was demonstrated with S/N 7 injector using Mass Defect ERL and kinetic loss extrapolations in four tests (Nos. 1083-D02-OM-009 and -010, Nos. 1083-D01-OM-027 and -028). A peak specific impulse of 375.2  $\text{lb}_f\text{-sec}/\text{lb}_m$  was demonstrated in Test No. -028 at a mixture ratio of 1.99. Extrapolating all of the test data over the mixture ratio range used in the testing (see Figure No. 83) indicated a design point (MR 1.91) performance of 372.7  $\text{lb}_f\text{-sec}/\text{lb}_m$ . Detailed losses for this condition are shown on Table XV, including a comparison with the S/N 2, Mod 3 injector. Peak performance is indicated at a mixture ratio of 1.96, although this possibly could be altered toward 1.91 if test data were available for mixture ratios of 1.8 through 1.9. The results of these tests are in close agreement with the original prediction of 373.0 sec for the 344-element injector.

(C) Performance decrease with increasing mixture ratio results from three effects; a reduction in theoretical performance, an increased kinetics loss, and a decreased fuel atomization at the lower velocities. Decreasing performance on the fuel-rich side primarily results from decreased theoretical performance. A comparison of performance extrapolation with the hiperkinetic nozzle for the two analysis methods is presented in Figure No. 84; however, based upon discussion, the enthalpy defect model is not favored.

---

(32) Ibid.

CONFIDENTIAL

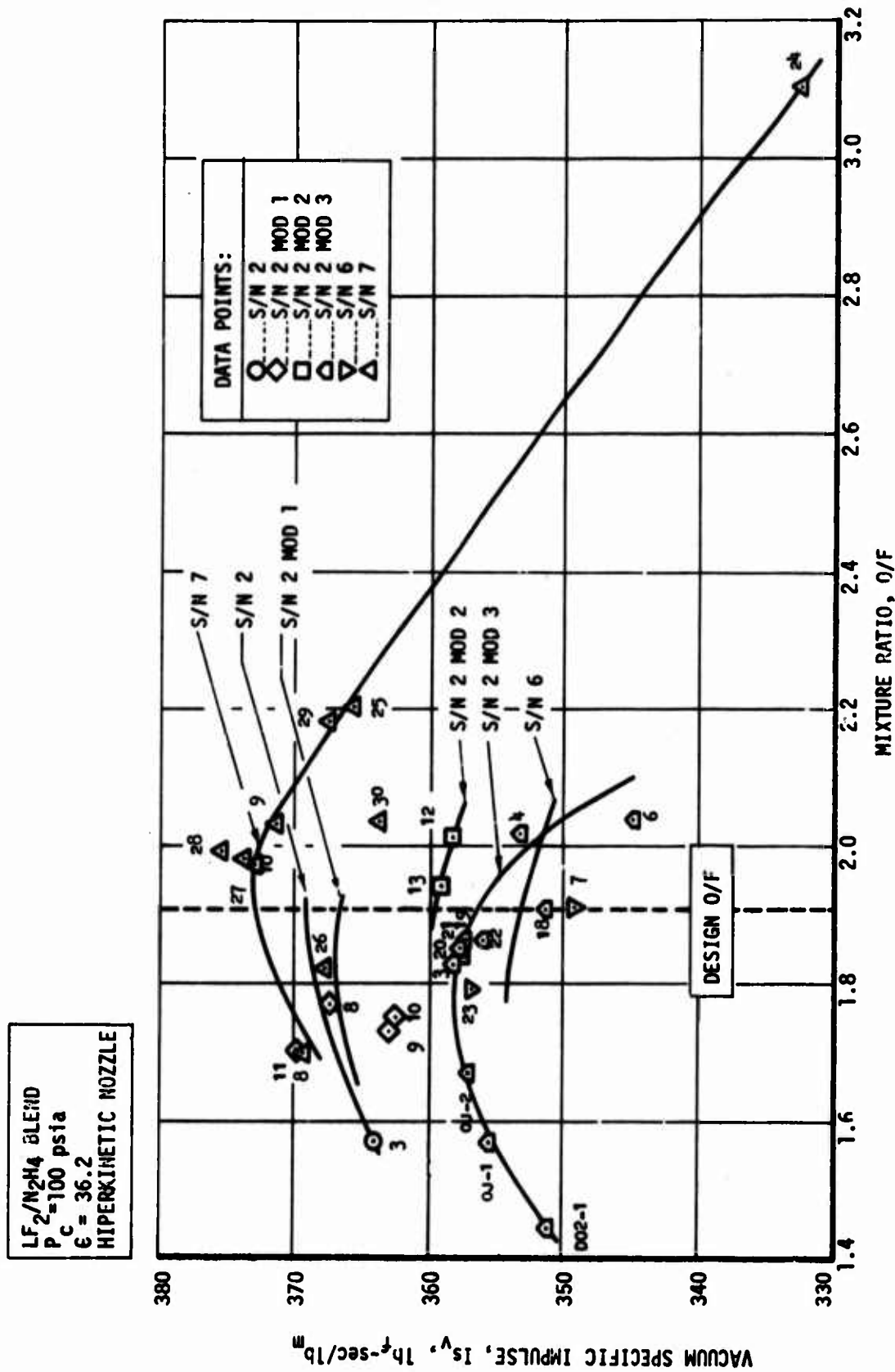


Figure 83. Performance Characteristics of Injectors Tested Using the Mass Defect Model and the 36.2 Hiperkinetic Nozzle (u)

CONFIDENTIAL

**CONFIDENTIAL**

**TABLE XV**

**PERFORMANCE COMPARISON BETWEEN S/N 7 AND S/N 2, MOD 3 INJECTORS**

**PERFORMANCE COMPARISON  
344 AND 68 ELEMENT INJECTORS**

$P_c = 100$  PSIA  
 $F_v = 7000$  lb  
 $O/F = 1.91$   
HIPERKINETIC NOZZLE

$\epsilon = 36.2$

	344 ELEMENTS SN-7		68 ELEMENTS SN-2 MOD 3	
<u>LOSS</u>	<u>%Isp</u>	<u>Sec.</u>	<u>%Isp</u>	<u>Sec.</u>
CURVATURE-DIVERGENCE	1.1	4.5	1.1	4.4
BOUNDARY LAYER	1.8	7.4	1.8	7.4
FINITE RATE	4.6	18.9	5.7	23.3
MIXTURE RATIO DISTRIBUTION	0.0	0.0	.2	.6
ENERGY RELEASE	1.7	7.0	4.5	18.6
$I_{sp}$ , vac, THEORETICAL	100	410.5	100	410.5
$I_{sp}$ , vac, DELIVERED	90.8	372.7	86.7	356.4

**CONFIDENTIAL**

CONFIDENTIAL

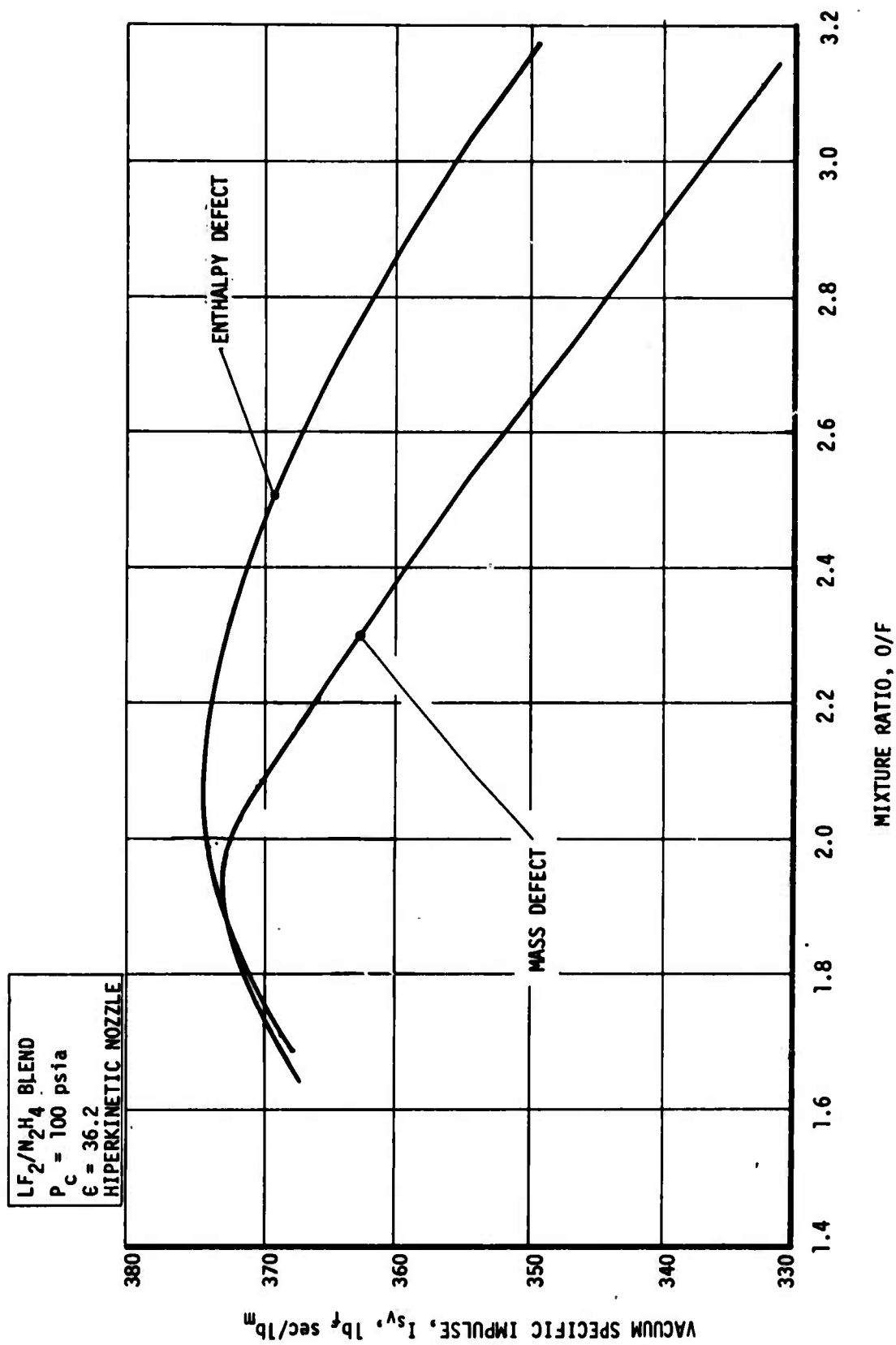


Figure 84. Comparison between Mass Defect and Enthalpy Defect Scaling Techniques for Injector S/N 7 (u)

CONFIDENTIAL

## CONFIDENTIAL

### b. Injector S/N 2, Mod 3

(C) Injector S/N 2, Mod 3 also was evaluated for hiperkinetic nozzle performance using both the Mass Defect and Enthalpy Defect modules. The Mass Defect results are shown on Figure No. 85. Mass Defect analysis indicated that maximum performance was obtained at a mixture ratio of 1.78 with 356.2  $\text{lb}_f\text{-sec}/\text{lb}_m$  vacuum specific impulse. At design point operation ( $\text{MR} = 1.91$ ) this value reduces to 355.3  $\text{lb}_f\text{-sec}/\text{lb}_m$ . The loss results at increasing mixture ratios are shown on Table XII. They indicate that the rapid drop-off in performance is attributable to high kinetic losses associated with high vaporized mixture ratios together with reductions in both fuel and oxidizer vaporization rates.

(C) Enthalpy Defect analysis indicated a specific impulse of 353.3 sec at the design mixture ratio of 1.91. As was the case with S/N 7 injector, mixture ratio becomes optimum at approximately 2.2 with this technique.

(C) S/N 2, Mod 3 injector generated a lower performance than S/N 7 because of the decreased vaporization resulting from the use of larger elements as well as the provision for 2.77% fuel film cooling. The oxidizer vaporization was calculated as being nearly complete at the throat (98%) with only 82.6% of the fuel being vaporized. This was corroborated by an energy release loss of 34.5  $\text{lb}_f\text{-sec}/\text{lb}_m$ , which was generated at a mixture ratio of 1.91 in Test No. 1083-D01-OM-018. A complete tabulation of all S/N 2, Mod 3 enthalpy and mass defect extrapolations was provided on Table XII.

### c. Injector S/N 6

(C) Hiperkinetic nozzle performance using S/N 6 injector was accomplished based upon the Mass Defect analysis and data from two tests (Nos. 1083-D01-OM-023 and 1083-D02-OM-007). Using the average percentage of fuel vaporization, the design point performance ( $\text{MR} = 1.91$ ) was calculated to be 353  $\text{lb}_f\text{-sec}/\text{lb}_m$  of vacuum specific impulse. The basic difference in performance between S/N 6 and S/N 2, Mod 3 results from the 6% increase in S/N 6 injector fuel film cooling.

### d. Injector S/N 2, Mod 2

(C) Of the six tests conducted with S/N 2, Mod 2 injector, only two were performed at the design chamber pressure. Evaluating these two tests at the design point yielded a vacuum hiperkinetic performance of 359.5  $\text{lb}_f\text{-sec}/\text{lb}_m$ . This higher performance as compared with S/N 2, Mod 3 injector, which had the same number of elements, results from the increased fuel vaporization attributable to higher injection velocities, smaller drop size (orifice), and the absence of fuel film cooling.

CONFIDENTIAL

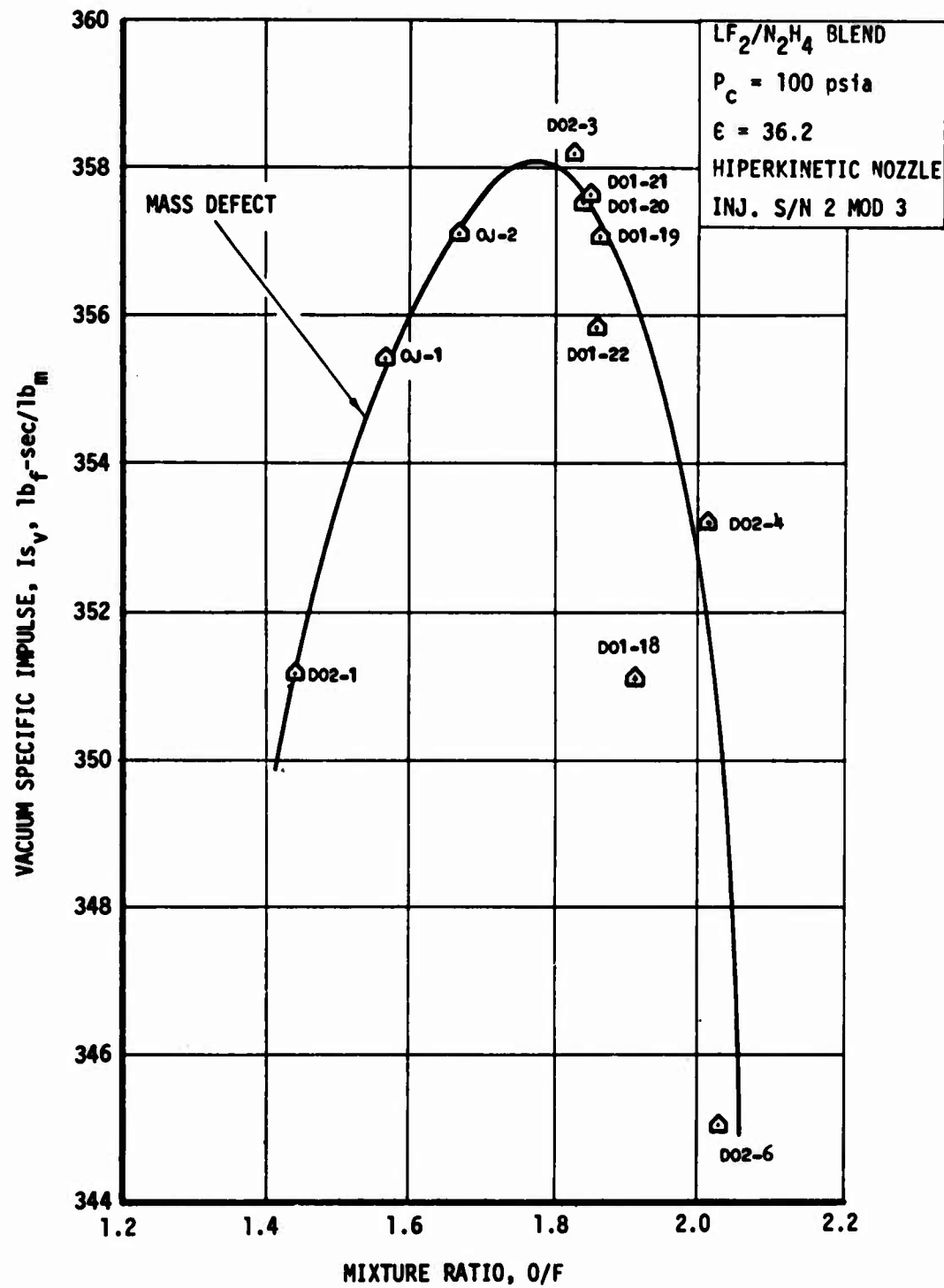


Figure 85. Mass Defect Scaling Techniques for Injector S/N 2, Mod 3 (u)

CONFIDENTIAL



## CONFIDENTIAL

### e. Injector S/N 2, Mod 1

(C) The performance data from the stable portions of four tests were used to evaluate the hiperkinetic performance of S/N 2, Mod 1 injector. The resulting design point performance was 366 lb<sub>m</sub>-sec/lb<sub>f</sub> at a mixture ratio of 1.91. The performance increase from S/N 2, Mod 2 was directly related to the improved atomization efficiency of the 98-element design as compared with the high velocity 68-elements of S/N 2, Mod 2. The limited test data did not permit complete extrapolation over the nominal mixture ratio range as shown on Figure No. 83. No Enthalpy Defect calculations were accomplished.

### f. Injector S/N 2

(C) Only one high confidence level test exists for injector S/N 2 (Test No. 1083-D01-OM-003). Design point extrapolation of this test indicated a hiperkinetic performance of 369 lb<sub>f</sub>-sec/lb<sub>m</sub>. This high performance is commensurate with the high vaporization efficiency associated with the 158-element design.

### g. Injector S/N 1<sup>2</sup>

(C) The very limited, short duration test data prevented design point extrapolation of the hiperkinetic performance of this injector. If Test No. 1083-D01-OM-001 is assumed to represent the nominal performance, a 368 lb<sub>f</sub>-sec/lb<sub>m</sub> vacuum hiperkinetic performance is obtained using the Mass Defect technique.

### h. Injector Performance Correlation

(U) The performance potential of all the injectors tested proved to be a direct result of the fuel atomization efficiency of these injectors as well as the amount of fuel film cooling. The fuel atomization efficiency is a direct result of the number of elements used because most of the elements were triplets of like design and injection velocity (same  $\Delta P$ ). Figure No. 86 indicates this comparison between all injectors and the number of elements used. A prediction line also is shown for this purpose; it was assumed that the elements are identical to the triplet elements of S/N 7 injector. The disparity between the prediction and the performance obtained for injectors having less than 100 elements is a direct result of other factors that have a significant affect when a small number of elements are used. These factors include impingement angle, the type of element, and the spray overlap characteristics. Therefore, it is indicated on Figure No. 86 that the number of elements is the overriding influence upon fuel vaporization efficiency. The number of elements needed to satisfy the contractually imposed performance also is shown.

CONFIDENTIAL

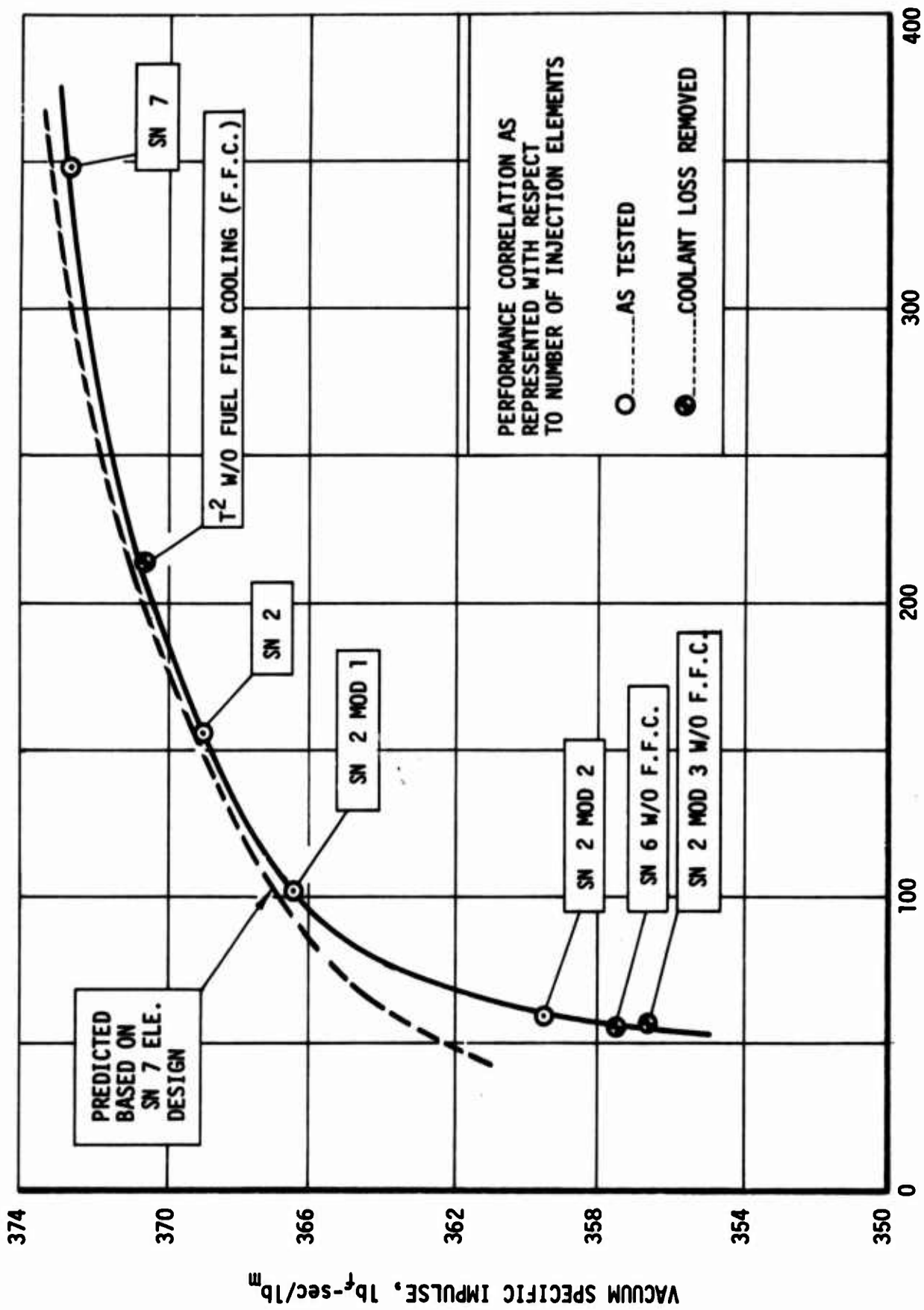


Figure 86. Performance vs Number of Elements (u)

CONFIDENTIAL

# CONFIDENTIAL

## 1. Optimum Injector Performance

Of all the injectors tested, optimum performance was essentially achieved with the design and demonstration of injector S/N 7. As can be seen on Figure No. 86, further improvements in the fuel atomization efficiency can be achieved by increasing the number elements beyond 344, but this will have a very small effect upon performance. Therefore, from a performance aspect, injector S/N 7 can be considered as an optimum design. However, the current S/N 7 design can be improved by design modifications to lower injector pressure drop and increase wall compatibility. In addition, system performance could be improved by a change in nozzle design. These considerations are dealt with independently, as follows:

### (1) Pressure Drop

The S/N 7 injector pressure drop exceeds the contractual requirements (75 psi  $\Delta P_f$  and 65 psi  $\Delta P_o$ ), which is 50 psi. Increasing the orifice size to satisfy pressure drop requirements while keeping 344 elements could result in a performance loss. Table XVI indicates the influence that the available design variables have upon performance. Although the momentum ratio and diameter ratio effects are in the proper direction, these effects relate to the non-critical propellant (oxidizer). The long chamber tends to complete oxidizer vaporization for all element constraints. Therefore, the fuel detrimental effects override the oxidizer influences. As a result, it is recommended that the number of elements be increased to correct the high pressure drop (at the same orifice sizes) unless the performance loss associated with the use of larger orifices is tolerable.

### (2) Wall Compatibility

The second area of improvement for the S/N 7 injector is the compatibility condition at the forward end of the chamber. Compatibility/performance analysis indicated that the chamber is attacked by the hot oxidizing atmosphere near the injector face in the resonator area. This condition prevails because the highly volatile oxidizer vaporizes readily while the fuel requires finite chamber length. This characteristic results in a high vaporized mixture ratio at the forward end of the chamber. Correction or minimization of this oxidizer-rich condition to alter it to a stoichiometric or reducing atmosphere can be accomplished by two mechanisms; barrier control and fuel film cooling. Barrier control appears to be the most feasible method. With this technique, the mixture ratio distribution across the injector is deliberately distorted to render the outboard elements fuel-rich and to obtain a reducing atmosphere over the entire chamber wall length. The core then becomes oxidizer-rich. The end product is a mixture ratio distribution loss with compatible boundary conditions. Based upon the result of S/N 6 testing, a 2 sec loss would be considered a maximum.

# CONFIDENTIAL

TABLE XVI

EFFECT OF DESIGN VARIABLES FOR REDUCING PRESSURE DROP UPON PERFORMANCE

PARAMETER		CURRENT SN 7	REVISED TO DESIGN $\Delta P$
PRESSURE DROP	OXID	66.0	50.0
	FUEL	75.0	50.0
VELOCITY FT/SEC	OXID	76.5	67.0
	FUEL	105.0	86.0
MOMENTUM RATIO	(O/F)	1.41	1.51
DIAMETER IN.	OXID	.0345	.0379
	FUEL	.020	.0245
DIAMETER RATIO	(O/F)	1.77	1.55
$\Delta V = (V_o - V_f \cos \theta)$		-11.5	-.6
ATOMIZATION			
DIAMETER EFFECT	OXID	OK	IMPROVED
	FUEL	OK	REDUCED
MOMENTUM RATIO	OXID	OK	IMPROVED
	FUEL	OK	REDUCED
MIXING			
ELEMENT MASS DISTRIBUTION		OK	IMPROVED
$\Delta V$ EFFECT		OK	REDUCED
VAPORIZATION	OXID	OK	OK
	FUEL	OK	REDUCED
PERFORMANCE		TEST VALUES	SLIGHTLY REDUCED ~ 1.0 SECOND

UNCLASSIFIED

The second method considered for improving compatibility is to inject fuel film cooling. A mixture ratio distribution loss results because of the lower performance of the monopropellant fuel together with the lower kinetic performance of the oxidizer-rich core. Performance losses of 3 sec are expected for the predicted required coolant flow of 6%.

(3) Nozzle Redesign

The hiperkinetic nozzle design was generated based upon existing kinetic rate constants and energy release efficiencies.<sup>(33)</sup> Therefore, making this nozzle optimum should be based upon the kinetic and energy release data for injector S/N 7. Designing this nozzle for maximum performance could provide a 1% increase in delivered performance.

---

(33) Pieper, J. L. and Anderson, G. E., LF<sub>2</sub>/N<sub>2</sub>H<sub>4</sub> Blend Optimum Nozzle Design Study, Aerojet-General Report TCER-9642:0079, 5 October 1967.

UNCLASSIFIED

# UNCLASSIFIED

## C. COMPATIBILITY

Compatibility between the injector and chamber is a function of the gas dynamic, thermal, and chemical environment at the chamber wall. This environment is established by the nature of the propellants and the specific design characteristics of the injector. Summarizing the compatibility characteristics of the injector patterns tested indicates that injector S/N 7 developed erosive characteristics at the chamber top, S/N 2, Mod 3 injector streaked axially along the chamber as well as eroding the top end of the chamber and S/N 6 injector showed no compatibility problems. For a thorough understanding of these test results, a complete analysis was conducted to establish a basis, from which the data could be interpreted. Following are brief descriptions of the models used for this analysis along with interpretations of test results for S/N 2, Mod 3, S/N 6, and S/N 7 injectors. The four other tested injectors (S/N T<sup>2</sup>, S/N 2, S/N 2, Mod 1, and S/N 2, Mod 2) are not discussed because these injectors demonstrated unstable or low performance characteristics and as a result, did not satisfy the program objectives.

### 1. Description of Compatibility Analytical Models

Two analytical techniques were used in evaluating the injector-chamber characteristics of S/N 2, Mod 3, S/N 6, and S/N 7 injectors with the graphite phenolic and fibrous graphite chambers. These models were designated as the gas dynamic model and the spray fan characterization model.

#### a. Gas Dynamic Model

The analytical gas dynamic model is based upon the stream tube theory. Each injector element is assigned a stream tube area proportioned to its energy release potential. The stream tubes, which are initially positioned over the elements, are relaxed to minimum stream tube interference locations. The stream tube interference or overlap generates a pressure potential for mass movement. This movement or "crosswind" is represented graphically by a vector joining the initial and relaxed locations.

For this study, the energy release potential of each element was characterized as a separate stream tube. The area of each stream tube is determined by multiplying the element to total flow rate ratio, the element temperature to lowest element temperature, times the injector face area. After each element was assigned a portion of the chamber flow area, based upon the portion of the total energy release of the element, the graphical gas dynamic potential was established. The gas dynamic movement next was attained by relaxing the stream tubes from their initial position to a position of minimum overlap. A vector connecting the centers of the initial and final position of each stream tube indicated the relative velocity of the stream tube. By considering the size of the stream tube and length of the velocity vector, the relative momentum of the stream tube was defined.

UNCLASSIFIED



# UNCLASSIFIED

## b. Spray Fan Characterization Model

This model was used to examine the resultant spray fan produced from impinging liquid jets. To accomplish this analysis, the mass flow was first determined for each element as a function of element hydraulic resistance. Next, the spray fan area of each element was assigned a value based upon the percentage of the total mass flow of each element times the total flow area. The characteristic spray shape was determined by the element configuration as illustrated on Figure No. 87(A). The mixture ratio within the spray was denoted by dividing the spray area into oxidizer-rich and fuel-rich zones using the method described on Figure No. 87(B). There is a delay time before the propellants vaporize and combust; therefore, the droplets from one spray pattern have time to intermix with droplets from adjacent patterns. This characteristic is shown on Figure No. 87(C). The percentage of the fuel-rich zones that are overlapped by oxidizer-rich zones was designated as the percentage of spray overlap.

## 2. Analysis of Test Results

The compatibility analysis of each injector tested consisted of two parts. First, a pre-test analysis was made defining the compatibility characterization of each pattern. This was followed by a complete evaluation of all visual information from the respective test firings. Each of these studies is delineated by injector, as follows.

### a. Injector S/N 2, Mod 3

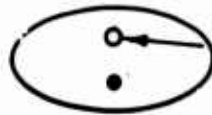
Gas dynamic analysis was made at two axial locations to account for the long and short impinging elements of the injector pattern. The first plane passed through the impingement point of the short impinging triplets and the second plane passed through the impingement point of the long impinging elements. At each axial position, the energy release calculations were based upon all the elements that actually contributed to the total energy release. After relaxing the stream tubes, the vectors, which represent the gas flow from initial to final position, were located on the pattern. Figure No. 88 (quadrants A and B) illustrates the total gas movement across the two planes. In Figure No. 88(B), the arrow head indicates the relaxation position of the first plane which also is the initial position of the second plane. To aid in the interpretation of the gas movement, three regions were selected to show hot gas flow paths that initiate in the pattern interior and extend to the chamber wall (see Figure No. 88(A)). The velocities are the highest (longest vectors) in these flow paths; therefore, the gas impact at the wall locations is the most severe. Creation of new stream tubes at the second plane (see Figure No. 88(B)) did not change the over-all gas dynamics across the injector other than providing a more uniform gas flow at the chamber wall.

The spray fan characterization was performed at the short impinging jet axial station. This position was selected upon the basis that the initial wall chemical environment primarily depended upon these elements.

UNCLASSIFIED

A. CHARACTERISTIC SPRAY SHAPES

DOUBLET:



OXIDIZER  
ORIFICE

TRIPLT:



FUEL ORIFICE

PENTAD:



BOUNDARY  
OF SPRAY

B. RELATIVE MIXTURE RATIO DISTRIBUTION

(E.G.) TRIPLT DIVIDED INTO FUEL AND OXIDIZER RICH  
AREAS BASED ON MIXTURE RATIO--

$$\text{i.e. } A_{\text{FUEL}} = \left[ \frac{(\text{WEIGHT FLOW FUEL})}{(\text{TOTAL WT. FLOW})} \right] A_{\text{ELEMENT}}$$

FUEL RICH AREA



OXIDIZER  
RICH AREA

C. SPRAY OVERLAP REPRESENTATION

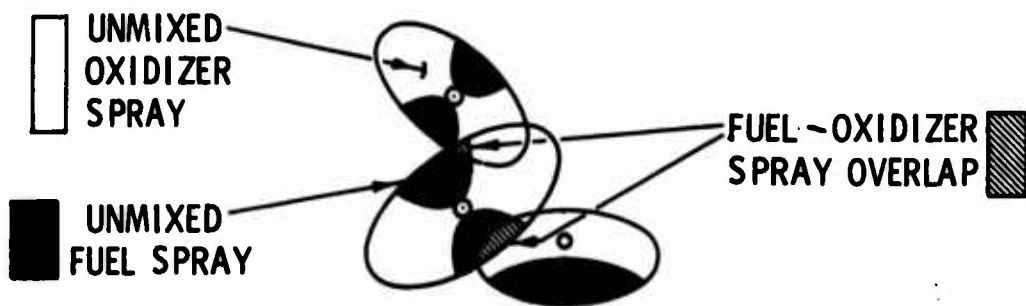


Figure 87. Spray Fan Characterization

UNCLASSIFIED

GAS DYNAMIC  
CHARACTERIZATION

COMPATIBILITY CHARACTERIZATION, INJECTOR SN 002, MOD 3

SPRAY FAN  
CHARACTERIZATION  
(AT PLANE OF SHORT  
IMPINGING ELEMENTS)

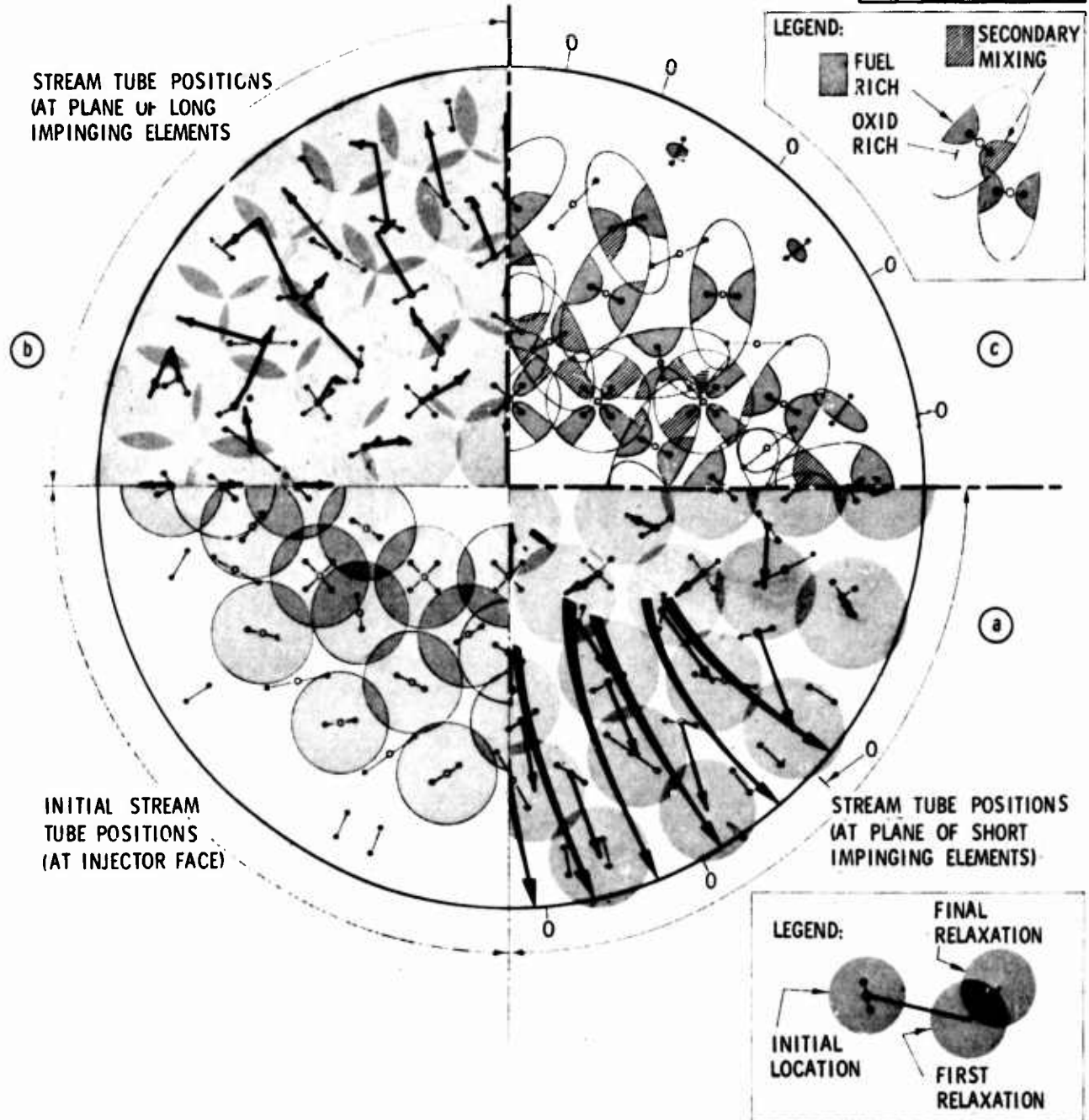


Figure 88. Compatibility Characterization, Injector S/N 2, Mod 3

UNCLASSIFIED

UNCLASSIFIED

Figure No. 88(C) illustrates the composite injector spray fan characterization. The hot gas flow paths from the gas dynamic analysis were overlayed to illustrate the type of chemical environment which will be driven to the chamber wall. From this figure, it is indicated that the main source of gas is from the oxidizer-rich lobes of the triplet spray fans on the oxidizer orifice of the long impingement elements. Wall locations where oxidizer will be present because of gas dynamics are denoted by the letter "O" on Figure No. 88(A and C). As can be seen, these oxidizer sources come from the outermost elements. The fans have oxidizer-rich zones which are not mixed with fuel from any adjacent element and are free to be forced to the chamber wall.

Test firing results were analyzed through examination of the heat mark patterns on the injector face and erosion on the chamber walls. Comparing the actual results with the compatibility predictions indicated that the expected compatibility environments at the injector face and at the chamber wall were qualitatively realized.

Figure No. 40 showed the injector face after 100 sec of test firing. The discoloration marks on the injector face were the result of the variation in local surface temperature and chemical composition at each location as well as the gas dynamic crosswinds which reflect the pressure variations across the face. Referring to Figure No. 80(A and C) for the relative velocities and chemical composition of the winds, it can be observed that most of the hot gas flow paths are clearly defined on the injector face. The darkest colors on the injector are the coolest in temperature. These dark areas are a result of low mixture ratio gasses recirculating in the vicinity. The decomposition of the fuel in these regions deposits a dark salt on the injector face.

In contrast, the lighter discolorations usually result from higher temperature gases and chemical reaction of the fluorine with the nickel injector. The resulting salt is a light greenish color. For this injector the higher mixture ratio gases are of a lower temperature than adiabatic flow temperature. This condition results due to the partial vaporization of the fuel near the face giving an even higher mixture ratio and subsequent lower combustion temperature. Therefore, the whitish areas indicate more of an oxidization condition than high temperature.

These high mixture ratio gases, do however, generate the gas dynamic wind movement. This condition results since the fluorine is nearly all vaporized while the fuel is not. Since the product of temperature (enthalpy) and vaporized flow describes the stream tube potential, then for the same temperature the high mixture ratio zones generate larger forces than the low mixture ratio zones. Therefore, the winds are from the low to high mixture ratio zones.

UNCLASSIFIED

## CONFIDENTIAL

The chamber wall, which is shown on Figure No. 89, was made from graphite-phenolic material. Oxidizer-rich gases flowing to the wall reacted exothermally with the resin. The chamber shown on Figure No. 91 was subjected to a total test duration of 150 sec. Those areas on the figure which appear to be light in color are plateau-like regions, the surface of which was not eroded. The darker areas surrounding the plateaus have eroded to a depth of 0.18-in. to 0.25-in. These eroded areas were the result of the oxidizer-rich gases impinging upon the chamber wall. The almost-virgin plateaus are areas in which fuel-rich gases impinged upon the wall. In most instances, the fuel-rich zones were in line with the peripheral fuel film coolant doublet. The oxidizer was carried to the wall by the radial outflow of gas from the central portion of the injector.

Figures No. 90 through No. 92 illustrate the regression rate of this pattern in a graphite phenolic chamber with an AGCarb throat subjected to 600 sec of accumulated test firing. The discrete circumferential erosion resulted from an oxidizer-rich environment emanating from the injector winds.

Over-all chamber wall compatibility could be improved with this pattern by reducing the oxidizer-rich flow paths. This is accomplished primarily by changing the long impinging triplets to short impinging triplets. The effect is twofold. First, the increased gas production near the face in previous void areas would reduce the amount of gas flow from the center of the injector pattern to the wall. Also, this concentration of gas close to the chamber wall would reduce the length of the vectors, which would lessen the gas impact velocity. Secondly, the secondary mixing between elements would be improved because of the inter-element spray fan overlap. This implies a shifting away from fuel-rich and oxidizer-rich zones to a system which would operate closer to the designated mixture ratio. This reduction in oxidizer-rich zones would lessen the amount of oxidizer available to react with the resin bonding material.

### b. Injector S/N 6

S/N 6 was a new injector. Its pattern was based upon that of the S/N 2, Mod 3 injector, differing as follows:

- film coolant orifices were located around the injector periphery
- the long impinging triplets were located toward the center of the pattern
- the outermost pentads were changed to triplets

Gas movement in the S/N 6 injector is graphically illustrated on Figure No. 93. However, these vectors were shorter and more uniform than those of S/N 2, Mod 3. This is evidenced by a comparison between Figures No. 88 and No. 93 (Quadrant A).

CONFIDENTIAL

(This page is Unclassified)



**CONFIDENTIAL**

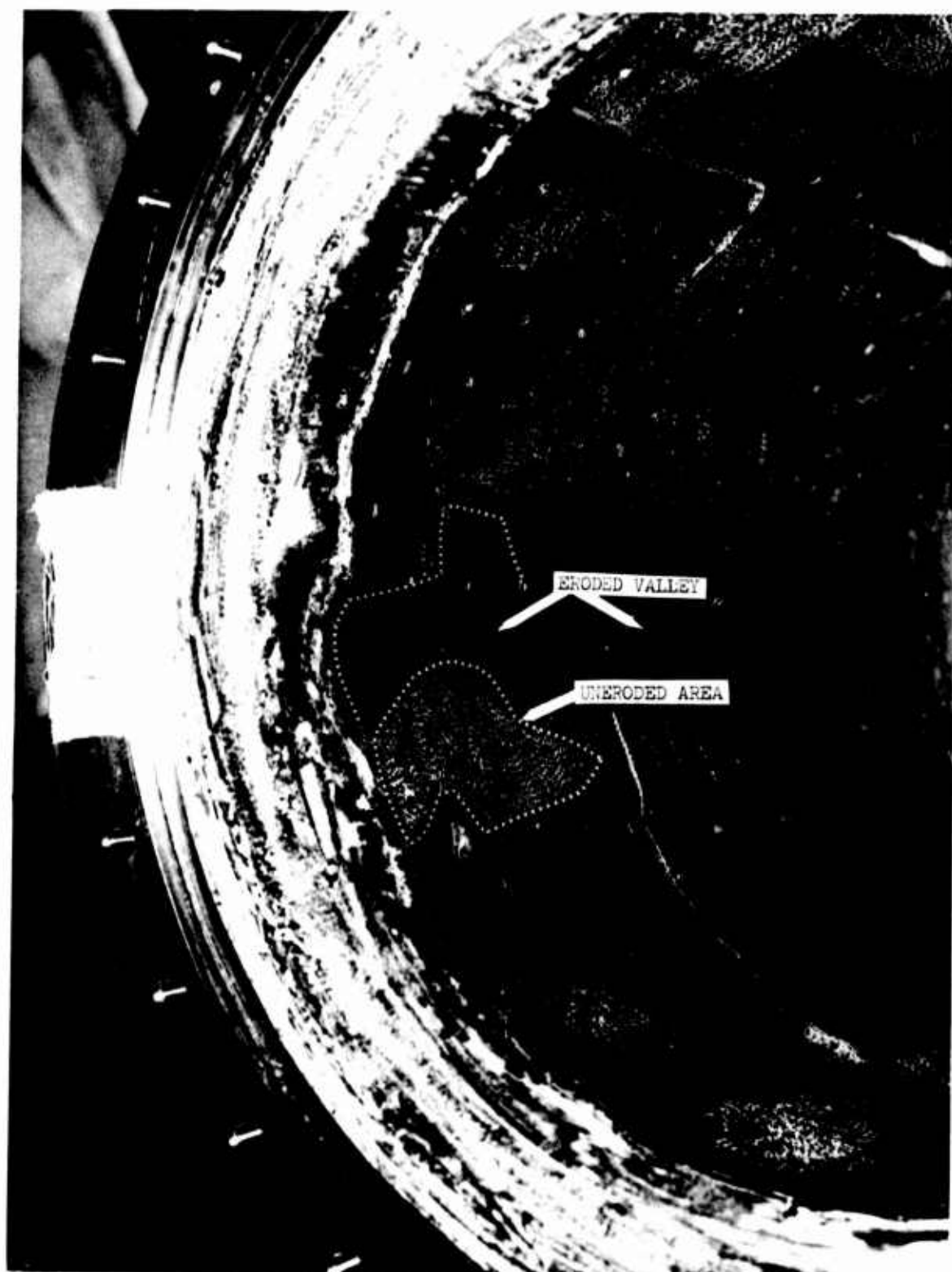


Figure 89. Graphite Phenolic Chamber after 50 sec of Testing  
with Injector S/N 2, Mod 3 (u)

Page 180

**CONFIDENTIAL**



**CONFIDENTIAL**

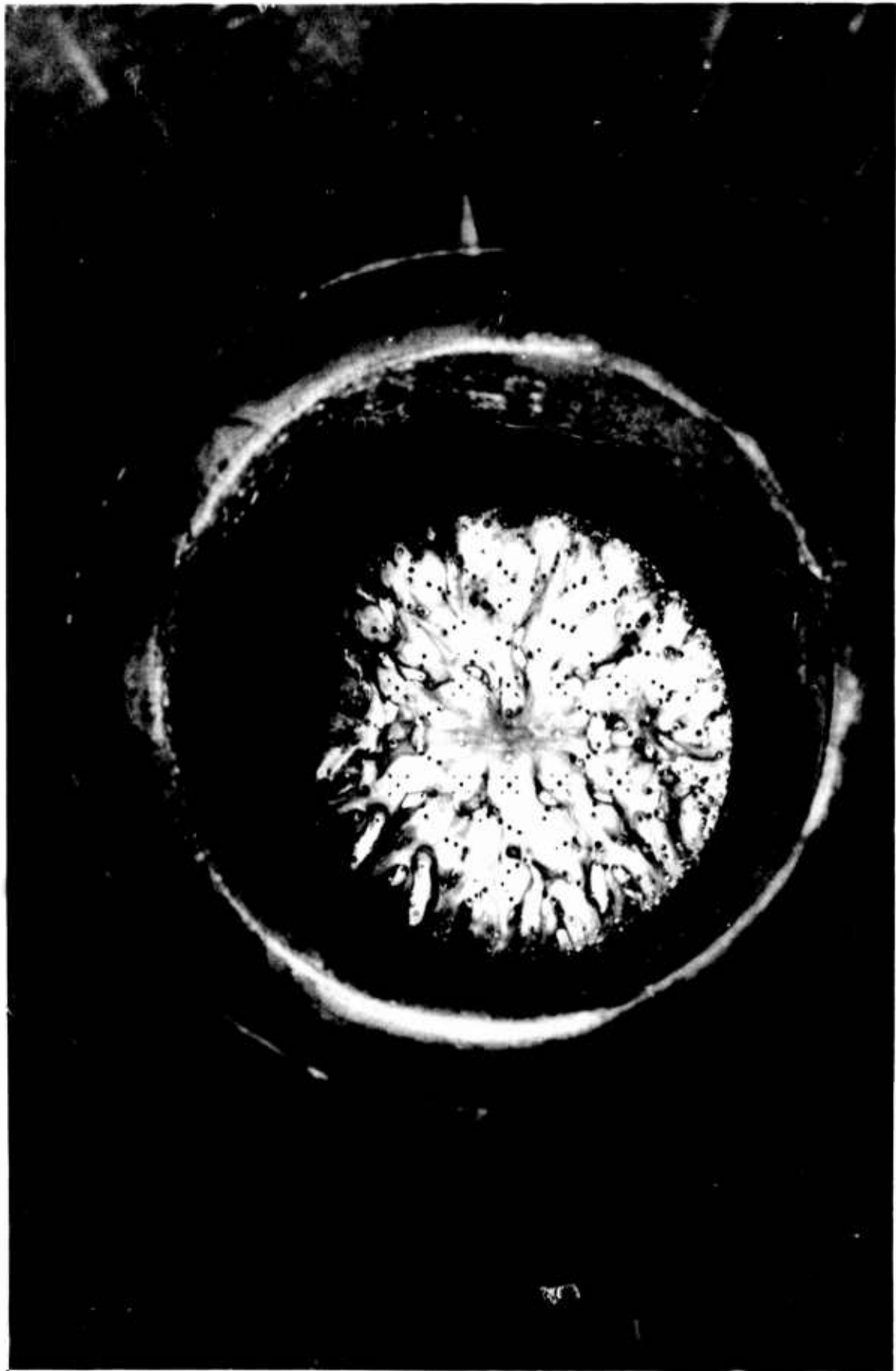


Figure 90. Graphite Phenolic Chamber after 202 sec of Testing with  
Injector S/N 2, Mod 3 (u)

**CONFIDENTIAL**

CONFIDENTIAL



Figure 91. End View of Graphite Phenolic Chamber Section Tested with Injector S/N 2, Mod 3 (u)

CONFIDENTIAL

**CONFIDENTIAL**



Figure 92. Axial Section of Graphite Phenolic Chamber Tested with Injector S/N 2, Mod 3 (u)

Page 183

**CONFIDENTIAL**

CONFIDENTIAL

COMPATIBILITY CHARACTERIZATION, INJECTOR SN 006

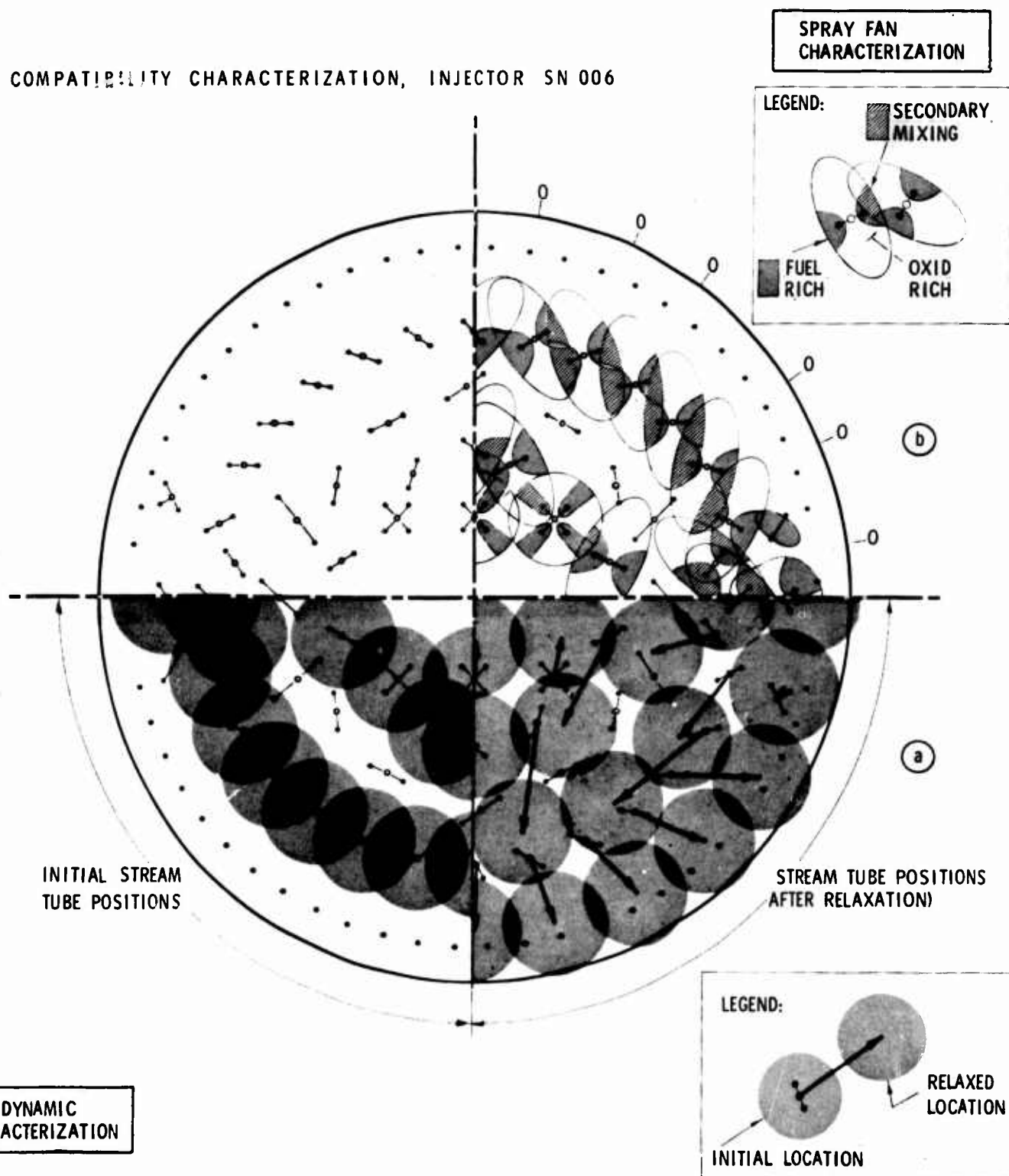


Figure 93. Compatibility Characterization, Injector S/N 6

CONFIDENTIAL

(This Page is Unclassified)

UNCLASSIFIED

The over-all chemical environment at the chamber wall was improved from that of the S/N 2, Mod 3 injector pattern. This resulted primarily from an increased spray fan overlap that occurred by changing the long impinging triplets to short impinging triplets. The increased spray fan overlap can be observed in Figure No. 93 (Quadrant B) as evidenced by the increased cross-hatched area. However, the spray overlap condition indicates that an oxidizer-rich zone exists about the outer boundary of the peripheral elements. The introduction of film cooling bars this oxidizer environment from reaching the wall by causing a reaction of the coolant with the oxidizer atmosphere as it moves toward the wall.

A 5 sec test firing in an uncooled steel chamber was accomplished to obtain performance and thermal data. The following test in ablative thrust chamber S/N 003 was terminated at 38 sec because of a blow-back into the altitude test cell. Post-test inspection showed the chamber liner was buckled at the throat. Examination of the surfaces of the liner in the chamber area and at the throat showed that there was little or no surface removal. There were no indications of streaking. The injector face following the 5 sec test is shown on Figure No. 94. The predicted flow of gas was from the oxidizer-rich zones in the lobes of the spray fans closest to the chamber wall (see Figure No. 93). The source and movement are confirmed by Figure No. 94, which shows the termination of the oxidizer fans at the film coolant injection points.

c. Injector S/N 7

This injector was designed for highest performance with good compatibility within the constraint of using the same manifold design as utilized for the prior injectors. Figure No. 95 illustrates the injector pattern and spray fan characterization for this injector. Several basic changes from the previous patterns were incorporated into the design. First, the number of elements were increased from 68 to 344 so that there would be increased vaporization of the propellants. From a performance viewpoint, this effectively increased the chemical reaction rate ensuring higher performance. The compatibility was enhanced because of less unreacted oxidizer. Secondly, 114 elements were placed near the chamber wall enabling a humped mass distribution close to the wall. This means that the combusting gases had a very short path to the wall so that this injector is excellent as regards gas dynamics. Also, the lower mass distribution in the pattern interior implies a pressure gradient from chamber wall to injector center, which again reduces the flow to the chamber wall. Lastly, within the manifold design constraints, all the elements were spray fan orientated for maximum overlap of oxidizer and fuel between adjacent elements. The chemical compatibility was predicted to be very good, as noted on Figure No. 95. The locations denoted by "O" indicate areas where oxidizer might be carried to the chamber wall from inboard elements. Streaks were predicted between the triplet elements at the wall which had the spray fans inclined to the wall. These erosion locations are marked as "A".

UNCLASSIFIED

UNCLASSIFIED

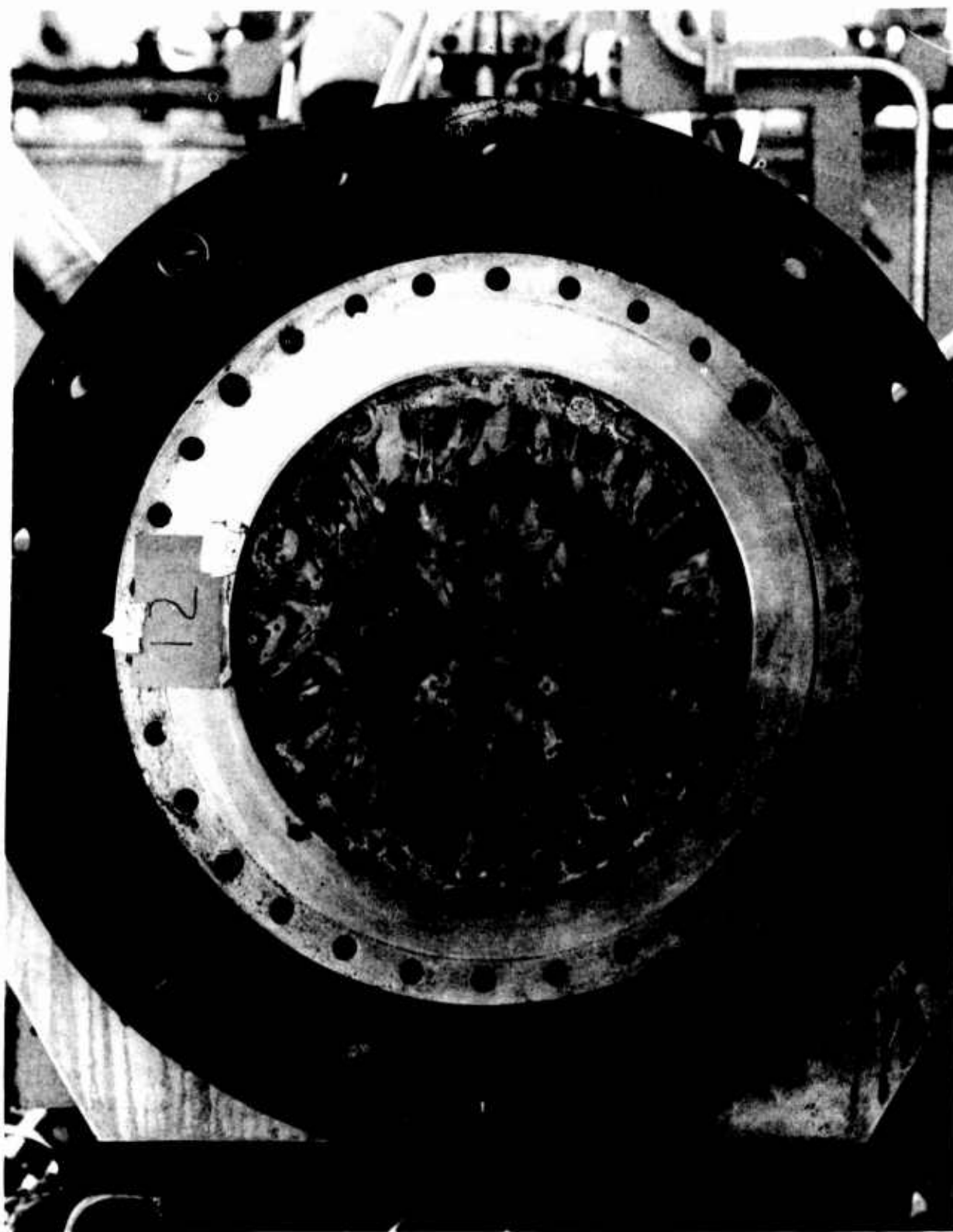


Figure 94. Injector S/N 6, Post-Test View

Page 186

UNCLASSIFIED



UNCLASSIFIED

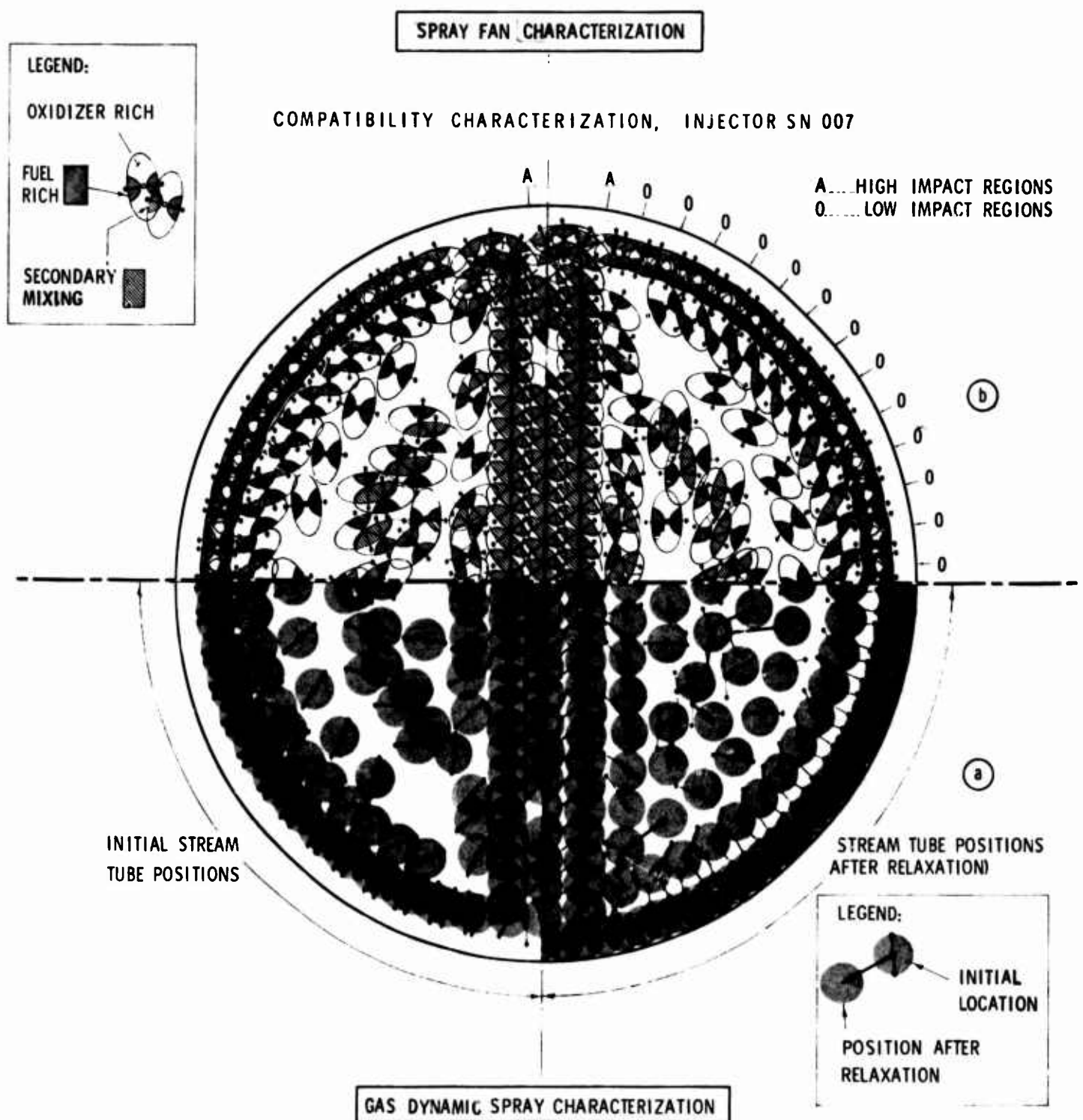


Figure 95. Compatibility Characterization, Injector S/N 7

UNCLASSIFIED

## UNCLASSIFIED

In all but one test of uncooled and ablative chambers, an acoustic resonator was used to ensure stability. The eroded areas that were observed after testing were all adjacent to the injector over the entire diameter of the acoustic resonator. The ablative portion of the chamber downstream of the resonator and the AGCarb-101 throat section was in excellent condition showing very minor erosion.

Post-test evaluation of the unit indicated that the injector produced a very uniform mixture ratio distribution in the outer triplet ring near the chamber wall and in the interior portion of the pattern. This can be seen by comparing Figure No. 95, the spray fan characterization, with the photograph of the fired injector, Figure No. 96. It should be noted that the areas which had a high degree of spray fan overlap produced an even discoloration on the injector face. The uneven mixture ratio in the non-spray fan overlapped areas produced the characteristic whitish and darkish streaks indicating oxidizer-rich and fuel-rich zones, with their respective winds.

Vaporization analysis of the fuel and oxidizer propellants for the injector/chamber system indicated that the region near the injector face was oxidizer-rich because of the more rapid vaporization of the fluorine. This means that the stream tube mixture ratio profile was oxidizer-rich near the injector and then proceeded toward stoichiometric as the gases moved axially down the chamber. This difference in vaporization rates was considered to be a cause of the erosion of the resonator. Inspection of the erosion characteristic on the steel resonator (see Figure No. 54) indicated a heavier erosion condition on the first row than on subsequent rows which also could have been the result of oxidizer reaction with the steel.

### 3. Optimum Comparability

Optimum compatibility characteristics were demonstrated in the convergent nozzle and the throat region of the thrust chamber used with injector S/N 7. Making the cylindrical section near the injector face at the acoustic resonator location optimum requires modifications to the injector.

The erosion of the orifices of the resonator appeared to have been caused by a combination of chemical and thermal effects. The chemical effect is the result of the oxidizer-rich condition while the thermal effect is indicated by discoloration of the steel chamber as well as by the response of the thermal sensors. Additionally, there could have been a gas dynamic effect caused by an increased reaction with chamber length as propellant vaporization approached completion. This could have resulted in higher dynamic pressures away from the injector face.

The thermal effect is not considered significant because the resonator wall material already has demonstrated its ability to sustain the thermal environment at the throat. The gas dynamic effect which might have resulted from the higher downstream dynamic pressure can be offset by designing the resonator in a one orifice row per cavity configuration. The oxidizer-rich condition requires correction.

UNCLASSIFIED

UNCLASSIFIED

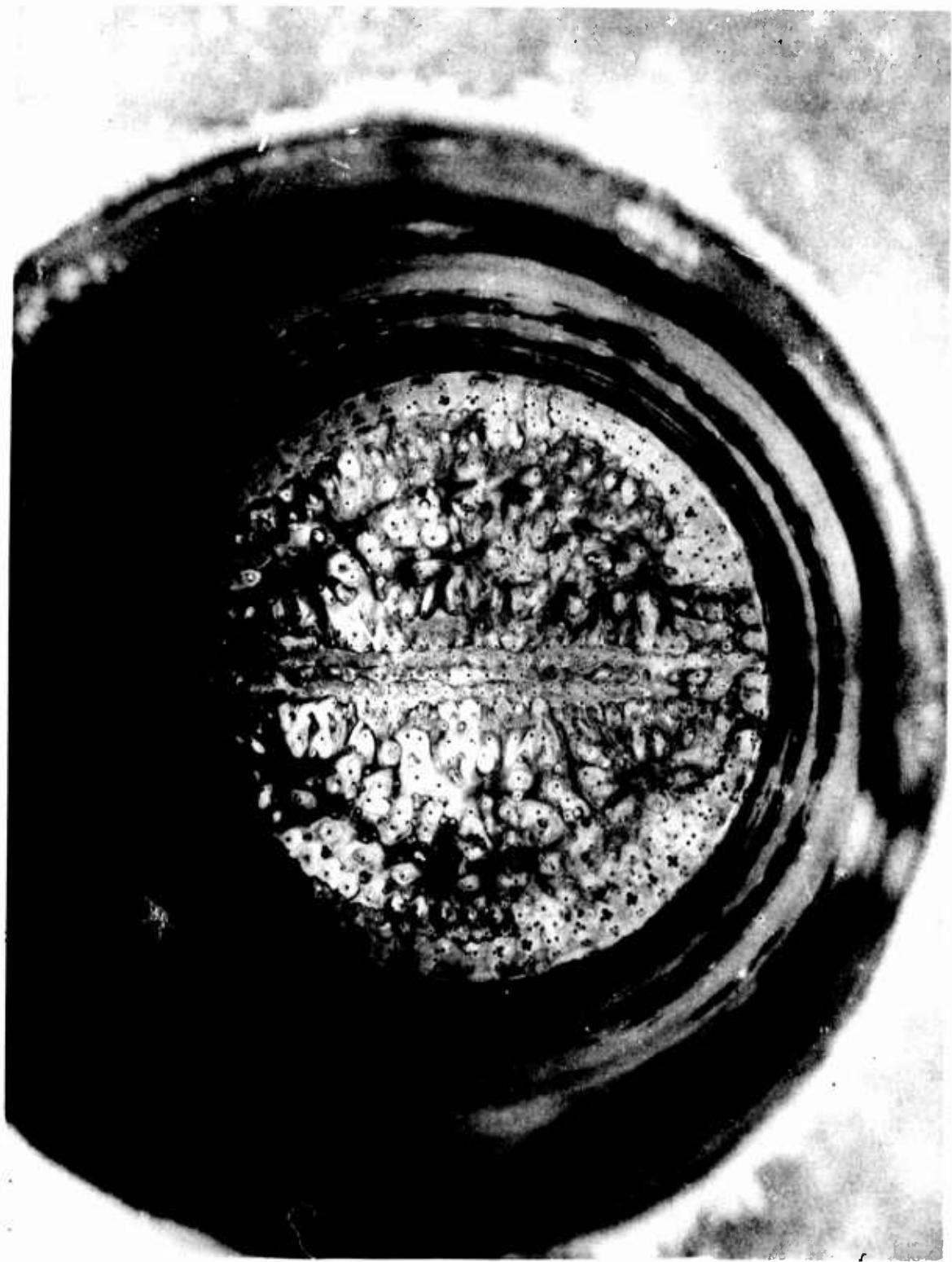


Figure 96. Injector S/N 7 after 5 sec of Testing

Page 189

UNCLASSIFIED

# UNCLASSIFIED

Two remedies appear to be feasible. One method utilizes fuel film coolant about the chamber periphery with injection located at the highest oxidizer gas dynamic environments, noted as "O" on Figure No. 95. Film coolant flow rate would be established at a level to provide a stoichiometric or reducing atmosphere for the initial section of the chamber. This method has the disadvantage of fuel film cooling performance degradations and offers the potential problem of excess fuel in the resonator cavities.

A preferred approach is to change the mixture ratio of the boundary triplets, thereby effecting a reducing atmosphere. This change would shift the core toward becoming more oxidizer-rich and would produce only a small performance degradation.

## D. THERMAL ANALYSIS

The thermal instrumentation proved to be adequate for providing the thermodynamic test data required from the testing. The injector face temperature measurements, in particular, represented a significant contribution to the understanding of injector heat transfer.

### 1. Uncooled Steel Chambers

The uncooled steel chamber temperature response data were useful primarily for determining convective boundary conditions along the chamber wall. These conditions varied most significantly with the mixture ratio distribution and combustion efficiency as well as with the injector pattern. Except for injector S/N 2, Mod 3, all of the injectors were fired with uncooled steel chambers which permits ready assessment of the injector effects upon chamber heat transfer.

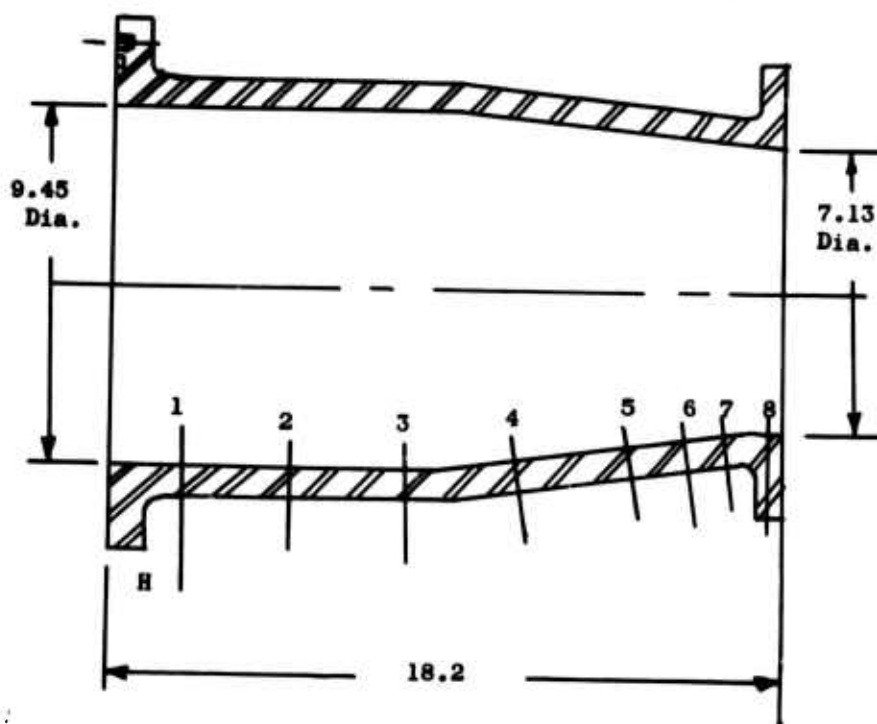
The instrumentation consisted of 29 thermocouples placed at eight axial positions. All were on the gas-side surface and from two to five thermocouples were located at each axial station. This instrumentation is shown on Figure No. 97 while typical chamber wall responses (recorded in Test 1083-D01-OM-023 with the injector S/N 6) at various axial locations are illustrated on Figure No. 98. These data clearly show the film cooling (9% fuel) effect at the upstream end of the chamber.

The following gas-side conditions were calculated as being at or immediately upstream from the throat (based upon the results from Tests No. -009, -013, -023, and -030 which were each in excess of 3 sec duration):

	<u>Injector S/N-Mod No.</u>			
	2-1 and 2-2	2-3	6	7
$h_g$ (Btu/in. <sup>2</sup> sec °F)	0.0006	0.00057	0.0006	0.0007
$T_r$ (°F)	6200	6200	6200	6500

UNCLASSIFIED

UNCLASSIFIED



Row No.	Angular Location	H Dim.	Ther. Symbol
1	180-Deg.	2.50	TC1-B
	240-Deg.	2.50	-C
	290-Deg.	2.50	-D
	330-Deg.	2.50	-E
2	120-Deg.	4.75	TC2-A
	180-Deg.	4.75	-B
	240-Deg.	4.75	-C
	290-Deg.	4.75	-D
	330-Deg.	4.75	-E
3	120-Deg.	8.00	TC3-A
	180-Deg.	8.00	-B
	240-Deg.	8.00	-C
	290-Deg.	8.00	-D
	330-Deg.	8.00	-E
4	180-Deg.	11.10	TC4-B
	240-Deg.	11.10	-C
	330-Deg.	11.10	-E
5	180-Deg.	14.10	TC5-B
	330-Deg.	14.10	-E
6	180-Deg.	15.60	TC6-B
	240-Deg.	15.60	-C
7	120-Deg.	16.60	TC7-A
	180-Deg.	16.60	-B
	240-Deg.	16.60	-C
	290-Deg.	16.60	-D
8	330-Deg.	16.60	-E
	120-Deg.	17.77	TCF-A
	240-Deg.	17.77	-C
	330-Deg.	17.77	-E

Figure 97. Location of Uncooled Steel Chamber Instrumentation

UNCLASSIFIED



UNCLASSIFIED

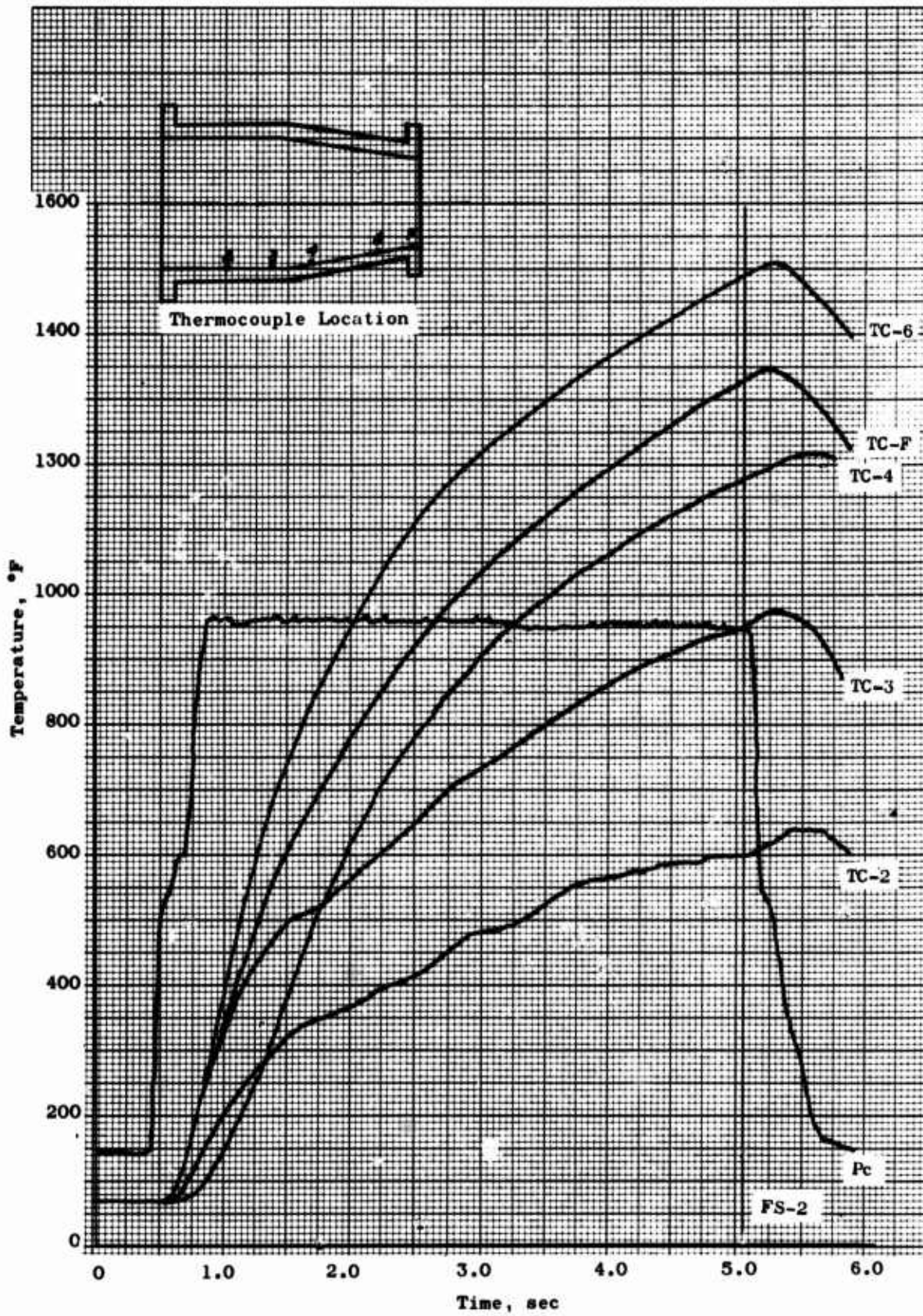


Figure 98. Typical Uncooled Steel Chamber Wall Responses with Injector S/N 6

UNCLASSIFIED



## UNCLASSIFIED

The injector S/N 2, Mod 3 data are calculated theoretically, using the simplified Bartz formulation for  $h_g$  and characteristic exhaust velocity performance for  $T_r$ . The other values were derived by matching the measured response to that predicted theoretically by a computer program for different assumed film coefficients and recovery temperatures based upon characteristic exhaust velocity efficiency. This method was not very accurate because the parameters were considered to be constant while in actuality they are not. Therefore, a relatively long firing period (3 + sec) was needed for the analytical studies to eliminate the effects of the initial variations. Consequently, a number of the uncooled steel chamber tests yielded little useful information for determining the gas-side boundary conditions. The data given represent the most severe gas-side convective conditions observed during the transients.

Without film cooling, the temperature response in the forward chamber section was much higher than that shown on Figure No. 98. The inferred boundary conditions agreed well with theoretical values based upon the simplified Bartz approach for the film coefficient and characteristic exhaust velocity efficiency for the recovery temperature. Typical values were  $5.3 \times 10^{-4}$  Btu/in.<sup>2</sup> °F for the film coefficient and 6200°F for the recovery temperature.

### 2. Cooled Chambers

Thermal instrumentation of the water-cooled chambers consisted of immersion thermocouples in the inlets and outlets of the chamber and nozzle sections. Both the graphite-lined and the ablative-lined thrust chambers had long transient responses; therefore, the limited resulting data was useful only for determining the transient over-all heat load. A valid direct comparison between the water-cooled chambers and the ablative chambers was not possible because of the effect of the water cooling; therefore, no analysis of the data was performed.

### 3. Ablative Chambers

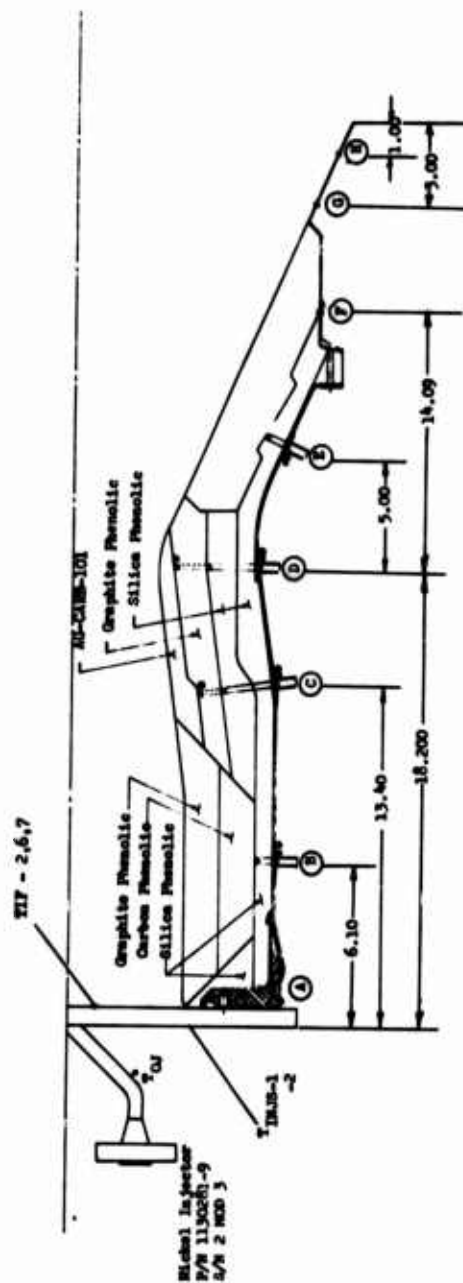
#### a. Chamber S/N 002

Ten test firings were made with the ablative chambers. Three of the tests were made with a chamber which contained an acoustic liner or resonator, to provide acoustic damping. Thermal instrumentation was provided at various axial and circumferential locations in the chamber wall, as shown on Figure No. 99. The first four test firings (Tests No. -001 through -004) were conducted with chamber S/N 002 and were analyzed to verify the analytical thermal model, calculated boundary conditions, and material properties.

In the analytical model, transient temperature profiles in a multiablative wall were calculated using four assumptions:

UNCLASSIFIED

THERMOCOUPLE POSITION									
A	B	C	D	E	F	G	H	I	J
TCS-0° TCS-120° TCS-240°	TAM-0° TAM-90° TCS-98°	TAM-0° TAM-90° TAM-120° TAM-150° TCS-105°	TAM-0° TAM-90° TAM-120° TAM-150° TCS-150° TCS-225°	TAM-0° TAM-90° TAM-120° TAM-150°	TAM-0° TAM-90° TAM-120° TAM-150°	TAM-0° TAM-90° TAM-120° TAM-150°	TAM-0° TAM-90° TAM-120° TAM-150°	TAM-0° TAM-90° TAM-120° TAM-150°	TAM-0° TAM-90° TAM-120° TAM-150°



\* THERMIST/THERMIST REF. TUM

6-2 LOCATED ON EXTERNAL SURFACE

Figure 99. Location of Thermal Instrumentation on Ablative Chamber  
S/N 002

## UNCLASSIFIED

- (1) One-dimensional radial heat conduction.
- (2) Charring of ablative materials using a char front model with a fixed charring temperature and heat of char.
- (3) No dimensional ablation.
- (4) No transpiration cooling effects caused by pyrolysis nor chemical reactions within the material or at the surface.

The gas-side convective heat transfer coefficient was based upon the simplified Bartz formulation and the recovery temperature on characteristic exhaust velocity efficiency. Gas-side radiation to the injector and out the exit was included along with backside radiation. The convective cooling introduced by the post-fire gaseous nitrogen purge also was considered.

Figure No. 100 shows both the analytical and the measured response for the four tests. In general, there was acceptable agreement between the predicted and actual results although the coast temperatures were less than predicted. This was probably the result of omitting the outgassing effects in the thermal model. Also, in the fourth firing, the measured temperature at the graphite phenolic/silica phenolic interface was higher than predicted. This was possibly the result of failing to account for dimensional ablation.

The final two tests with chamber S/N 002 were not analyzed using the thermal model. One test (No. -005) was of insufficient duration, while the other (No. -006) provided inadequate temperature response data because of a recorder malfunction.

### b. Chamber S/N 001

Ablative chamber S/N 001 was the same as chamber S/N 002 except for having three resonator cavities located at the upstream end of the chamber (see Figure No. 27). Instrumentation was limited to those thermocouples available prior to installation of the acoustic resonator; none were located close to the resonator. Since durability evaluation of the acoustic resonator assembly was the prime test objective, the limited temperature response data obtained was not analyzed.

### c. Chamber S/N 003

Chamber S/N 003 differed structurally from the other two chambers (see Figure No. 26). This chamber consisted of an AGCarb-101 liner extending the full length of the chamber, backed by carbon phenolic which in turn, was backed by a silica phenolic contained in a stainless steel shell. Interface temperatures were measured at several axial and circumferential locations in this chamber, which was fired only once (Test No. 007). The test was of insufficient duration and was not analyzed.

UNCLASSIFIED

UNCLASSIFIED

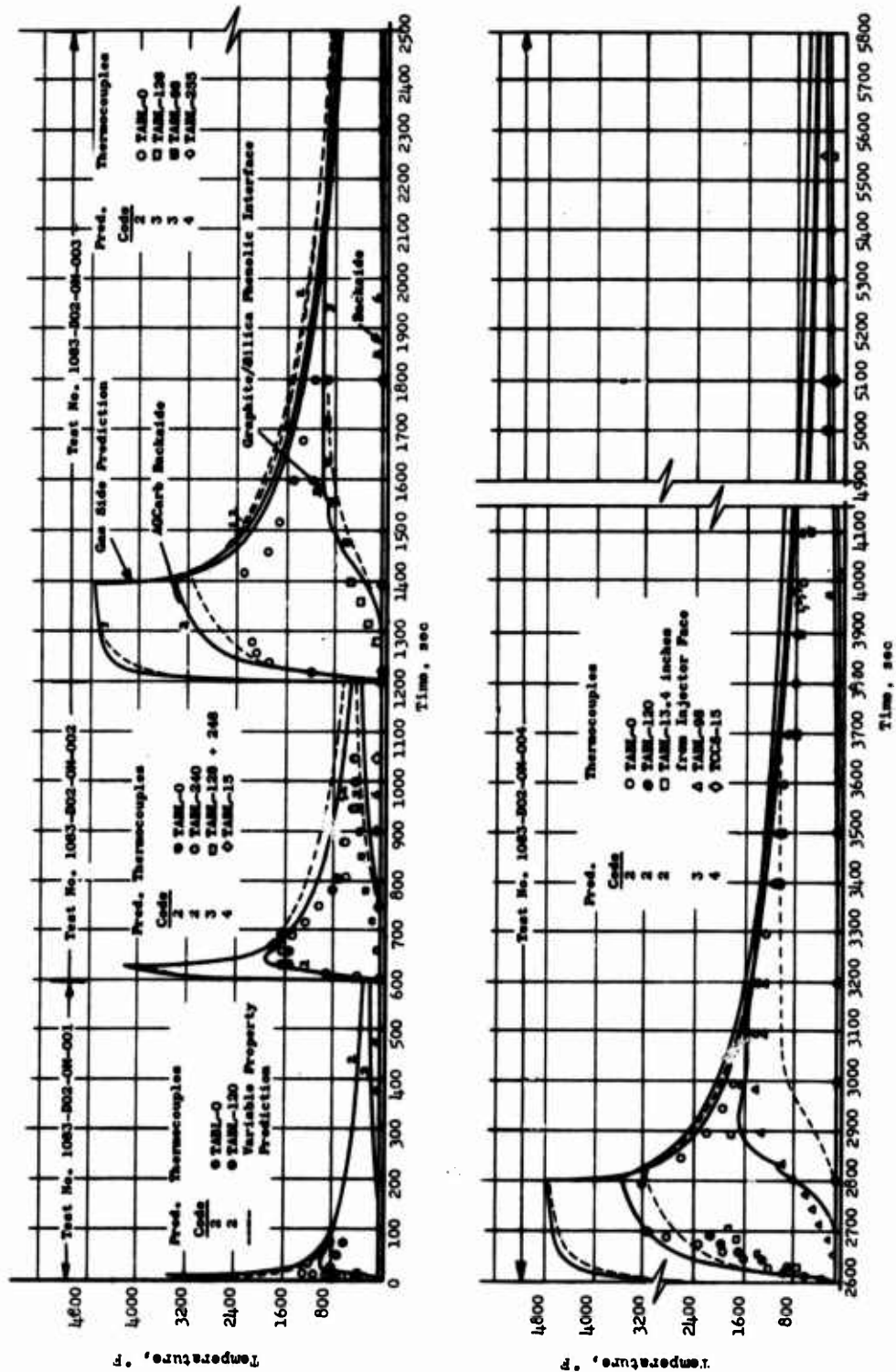


Figure 100. Analytical vs Measured Temperature Responses Tests No. -001 through -004

UNCLASSIFIED

# UNCLASSIFIED

## 4. Injectors

The thermal instrumentation for the injector was designed to obtain data concerning two potential problem areas. The first was that gas-side heat loads during firing could exceed coolant capabilities. The second was that the post-fire heat loads could raise the injector temperature to a point where restart became impossible because the fuel would most likely detonate. It was found that the latter concern seemed to be well-founded.

Injector instrumentation included thermocouples located on the gas-side of the injector face and on the outside of the backplate. The face instrumentation provided information regarding the unknowns pertaining to convective heating on the injector face. Figure No. 101 shows the typical placement of the thermocouples.

Figure No. 102 shows the temperature responses observed at three various points on the face of injector S/N 2, Mod 3 during a firing in a chamber with an ablative liner and water-cooled throat. Two of the three thermocouples reached a steady-state temperature of approximately 900°F while the remaining one attained approximately 700°F. The difference may be due to local effects caused by orifice pattern variations because the two high temperature locations had similar patterns while the low temperature location had a different pattern. The measured temperature levels also varied somewhat with chamber type; it was lower with the cooled chambers and higher with the uncooled ablative chambers (reflecting radiant heating of the face from the chamber walls).

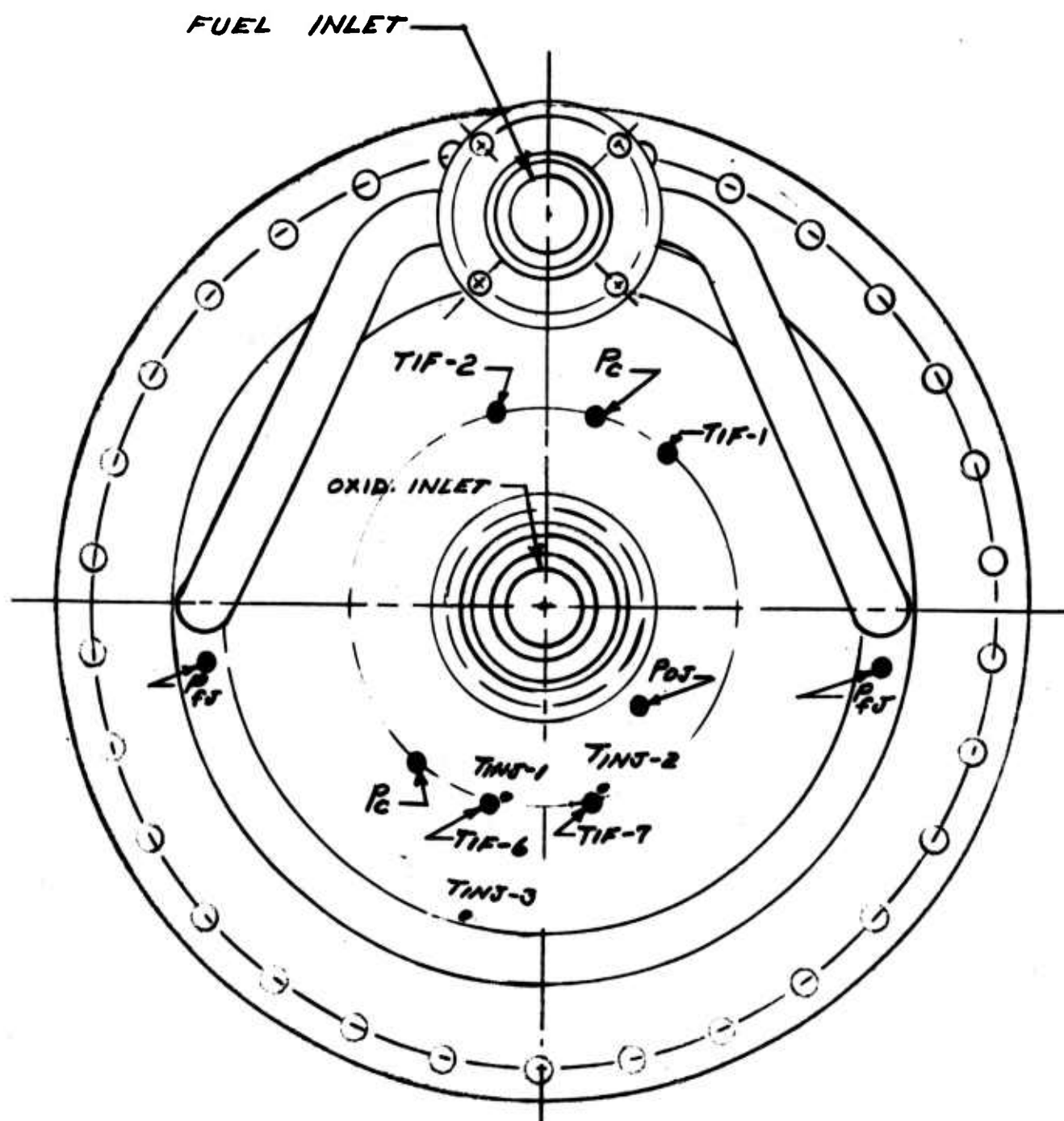
The face temperature data permit the following conclusions, which can be applied as basic guidelines for the thermal design of an injector:

- a. The convective film coefficient on the injector face, which was the greatest uncertainty in injector thermal design, was approximately 0.4 times that based upon the simplified Bartz correlation for the adjacent channel wall.
- b. Where applicable, a one-dimensional analysis between the gas-side and the coolant flow passages yielded reasonable results. In this case the linear length was taken to be the distance between the fuel channel and the midpoint on the surface between channels.
- c. Transient response times based on the one-dimensional approximation corresponded well with the measured response. Response times were fairly long; typically 5 or 6 sec.

The injector thermal design was based upon two-dimensional conduction studies to determine optimum channel spacing (described in Section IV,A,3). These studies were hindered by the uncertain gas-side boundary condition; however, a factor of 0.8 was considered conservative for the design work and subsequently demonstrated to be so.



UNCLASSIFIED



TIF	INJECTOR FACE TEMPERATURE
TINS	SURFACE TEMP. BACK COVER PLATE
P <sub>OJ</sub>	OXIDIZER MANIFOLD PRESSURE
P <sub>FJ</sub>	FUEL MANIFOLD PRESSURE
P <sub>C</sub>	CHAMBER PRESSURE

Figure 101. Injector Instrumentation

UNCLASSIFIED



UNCLASSIFIED

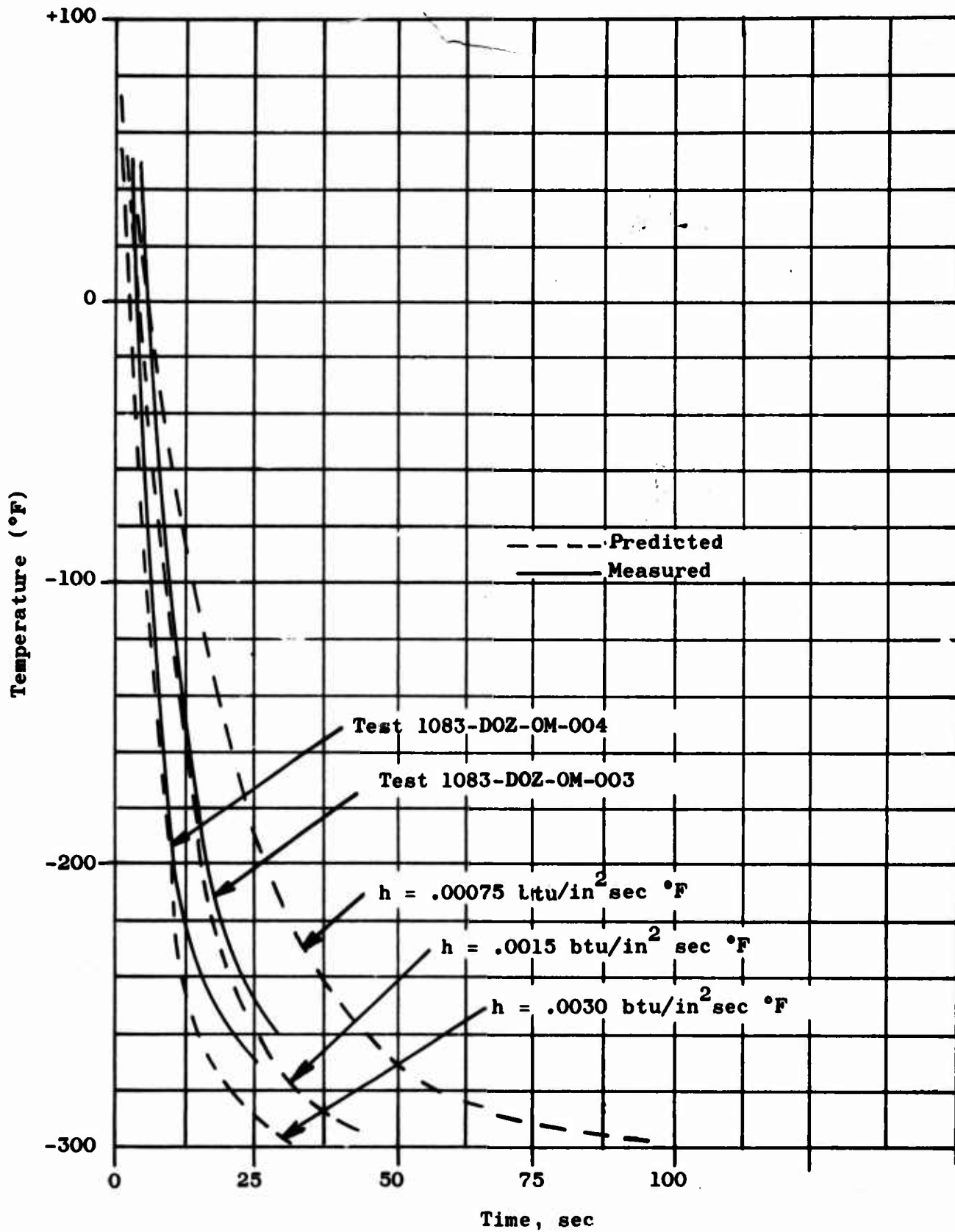


Figure 102. Comparison between Measured and Predicted Backplate Cooldown

UNCLASSIFIED

UNCLASSIFIED

Injector backplate instrumentation was useful for determining the convective cooling capability of the oxidizer during firing. That cooling capability influenced the face plate temperature and also provided a means of cooling the backplate and thermal accumulator (if utilized) for postfire heat sink purposes. The accumulator was a rechargeable heat sink designed to maintain postfire injector temperatures at levels low enough to permit restart without danger of fuel detonation. Figure No. 102 shows a comparison between the measured backplate cooldown during firing (at a point near the mid-radius of the plate where radial conduction effects were negligible) and the calculated response. These measured responses were from Tests No. -003 and -004 while the calculated response was based upon a one-dimensional treatment using a film coefficient of  $0.0015 \text{ Btu/in.}^2 \text{ sec } ^\circ\text{F}$ , which had been inferred from these as well as other test data. Calculated responses for values of half and twice of the indicated value also are shown. There is some variation in temperature response across the backplate caused by radial conduction effects. The mid-radius region was relatively free of these influences while the region between the posts connecting the front and back faces had a somewhat slower response. The region over the posts had an even slower response. The outer periphery, near the fuel manifold, remained at the fuel temperature throughout the firing.

#### 5. Simulant Thermal Accumulator

A simulant thermal accumulator, filled with 50 Pb/50 Sn solder instead of lithium, was tested in Test No. 007 for the purpose of confirming the oxidizer cooling capability with an actual accumulator located atop the injector. Solder has a thermal diffusivity that is approximately 25% different from that of lithium; therefore, it was considered to be an acceptable and economical substitute. Thermocouples were located near the solder-nickel backplate interface, at the mid-depth of the solder, and on the outer surface of the accumulator. The test duration (38.6 sec) was too short to allow much cooling of the solder, but the measured responses corresponded roughly to what would have been predicted for a lithium accumulator of proportional thickness. Such predictions and the measured responses are shown on Figure No. 103. The average lithium temperature was expected to drop from  $70^\circ\text{F}$  initially to  $-125^\circ\text{F}$  after 100 sec; the wetted backplate surface correspondingly was to drop to  $-265^\circ\text{F}$ . These values were considered to be sufficiently low starting points for absorbing post-fire heat loads.

#### E. STRUCTURAL ANALYSIS

Ablative chambers S/N 1 and S/N 2 performed satisfactory structurally except for the AGCarb-101 throat insert. Visual inspection of the inserts indicated that a longitudinal crack developed in the thicker portion of the insert. This crack appeared to be a result of high compressive hoop stress in the inner surface and progressed on a shear plane through the thickness. Upon the basis of the test results, the failures appeared to be marginal situations in that the inserts were operating at threshold stress levels. Little experimental data were available regarding the use of AGCarb-101 in this type of

UNCLASSIFIED

UNCLASSIFIED

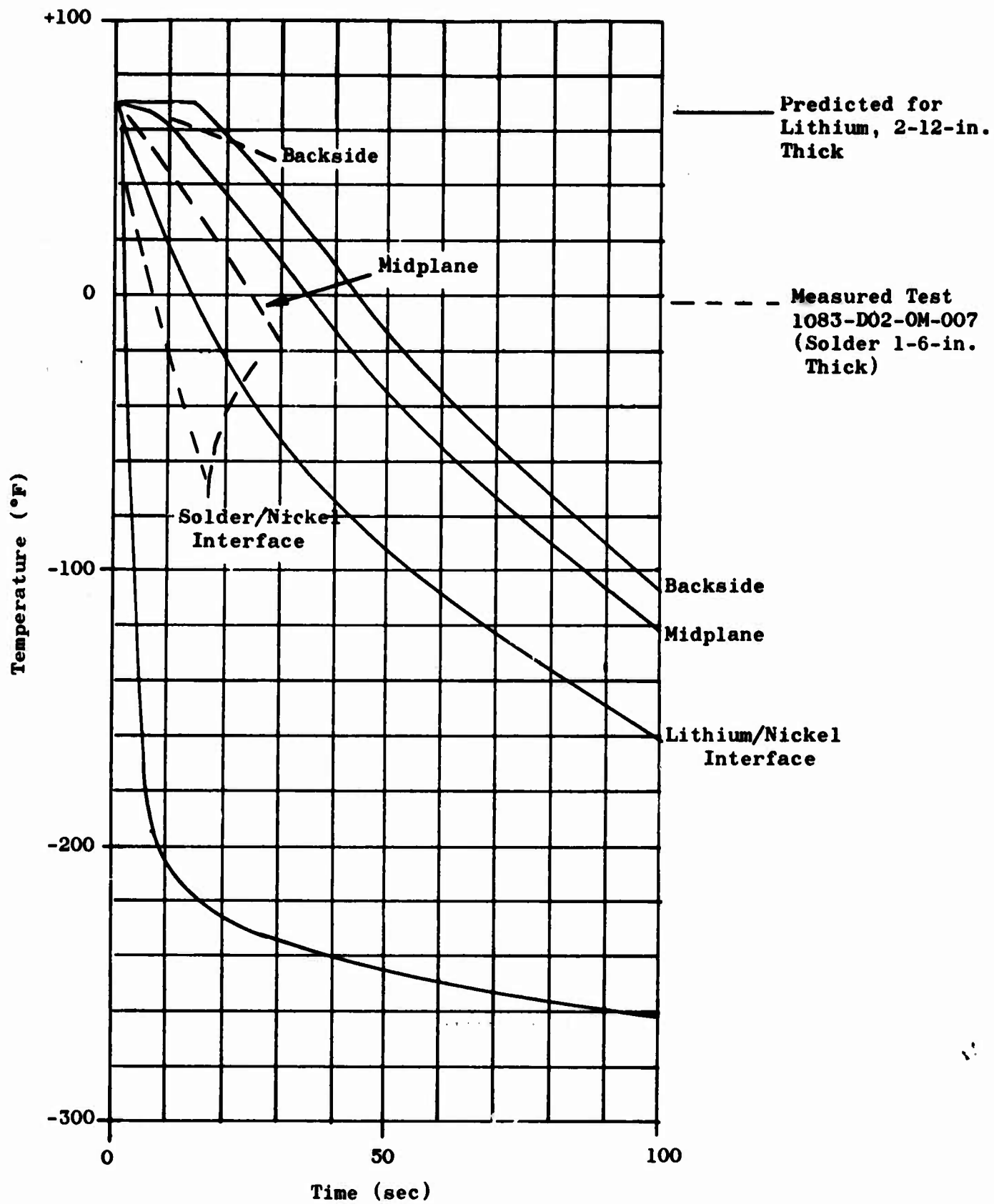


Figure 103. Predicted vs Measured Responses, Thermal Accumulator

UNCLASSIFIED

## UNCLASSIFIED

application; therefore, an analysis of the chamber was initiated to relate relative stress levels in the AGCarb-101 at various locations throughout the chambers. This analysis provided results which could be utilized for an improved chamber design as well as for other applications. Where possible, test temperature data was utilized. Ablative chamber S/N 3, with the full-length AGCarb-101 liner, failed during the first firing, which was terminated at 38.6 sec.

### 1. Method of Analysis

The analysis was conducted using the finite element method (Finite Element Program E11405) and took the bi-directional material properties of the AGCarb-101 into account. Previous analyses of these designs were not able to accommodate these bi-directional properties as the finite element method was not available.

#### a. Finite Element Program E11401

This finite element method is applied to the determination of displacements and stresses within plane or axisymmetric solids with linear or nonlinear material properties. The continuous body is replaced by a system of elements with triangular or quadrilateral cross-section. The elements are of arbitrary shapes and material properties; therefore, the procedure could be applied to structures comprised of many different materials of practically any symmetrical geometry.

In the finite element approximation of solids, the continuous structure is replaced by a system of elements which are interconnected at joints or nodal points. Equilibrium equations, in terms of unknown nodal point displacements, are developed at each nodal point. A solution of this set of equations constitutes a solution to the system.

The advantages of the finite element method, as compared to other numerical approaches, are numerous. The method is completely general with respect to geometry and material properties. Complex bodies comprised of many different materials are easily represented.

#### b. Finite Element Program E11405

The Finite Element Program E11405 is a modification of the E11401 program. The most significant of these modifications are:

- (1) All plasticity calculations are eliminated.
- (2) General cylindrical anisotropy has been included.

UNCLASSIFIED

# UNCLASSIFIED

## 2. Analysis Results

### a. Ablative Chamber S/N 001

Figure No. 104 shows the various materials and the temperatures utilized in the analysis. The chamber pressure was 100 psia. Figure No. 105 shows the distribution of hoop and axial compression stress on the gas-side surface along the AGCarb-101 throat insert. The hoop compressive stress is maximum (18,900 psi comp) just aft of the leading edge. In comparison, the maximum stress generated in the AGCarb-101 acoustical damper that did not fail was 16,700 psi compression. The results show that the stresses in the AGCarb-101 are a function of thickness as well as the stiffness of the back-up material. This is principally the result of the AGCarb-101 having a significantly higher expansion coefficient across the plies than along the plies.

Based upon the results of both the analysis and test firings, it is recommended that the AGCarb-101 compressive stress levels be maintained at or below 14,000 psi when the Table XVII material properties are utilized. This is lower than that experienced with the acoustical damper; however, the acoustical damper experienced considerable erosion which would decrease the stress level. If the stress is to be maintained below 14,000 compression in this chamber design, it would require that the thickness of the AGCarb-101 and the stiffness of the back-up material be adjusted. This could be readily accomplished within other design constraints (i.e., erosion and backside temperature).

### b. Ablative Chamber S/N 002

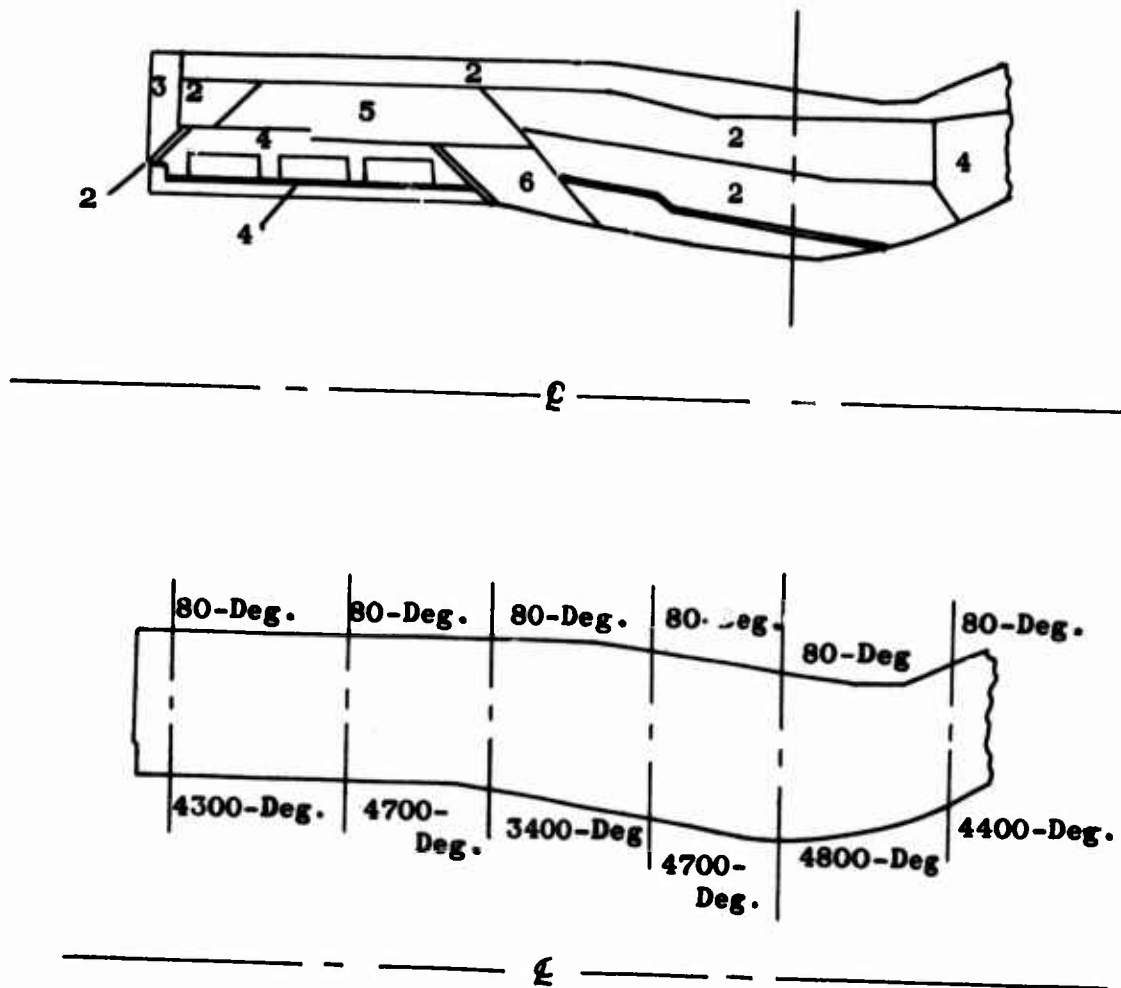
No post-test analysis was conducted for S/N 002 because the insert geometry was identical with S/N 001 and the temperature in the throat region was comparable. The differences in test time before failure indicated that the resultant stress levels were marginal, dependent upon temperature difference and material property variation. The S/N 001 recommendations also apply to S/N 002.

### c. Ablative Chamber S/N 003

A finite element analysis was not conducted for this chamber because of the similarity between the AGCarb-101 in the throat region with the throat region of S/N 001. However, stresses would be approximately 14,000 psi compression and would not peak at higher values like that of S/N 001 because of the absence of the thicker section. Failure analysis of S/N 003 was conducted and the conclusions are valid when considering the results of the finite element analysis of S/N 001. The differences in stresses principally are a result of the inability to previously accommodate for bi-directional material properties. This analysis indicated the following:

UNCLASSIFIED

UNCLASSIFIED



- ① AGCarb-101
- ② WBC 2230
- ③ 1018 Steel
- ④ WBC 8207
- ⑤ WBC 8217
- ⑥ FM 5064

Figure 104. Materials and Temperatures, Ablative Chamber S/N 001

UNCLASSIFIED



UNCLASSIFIED

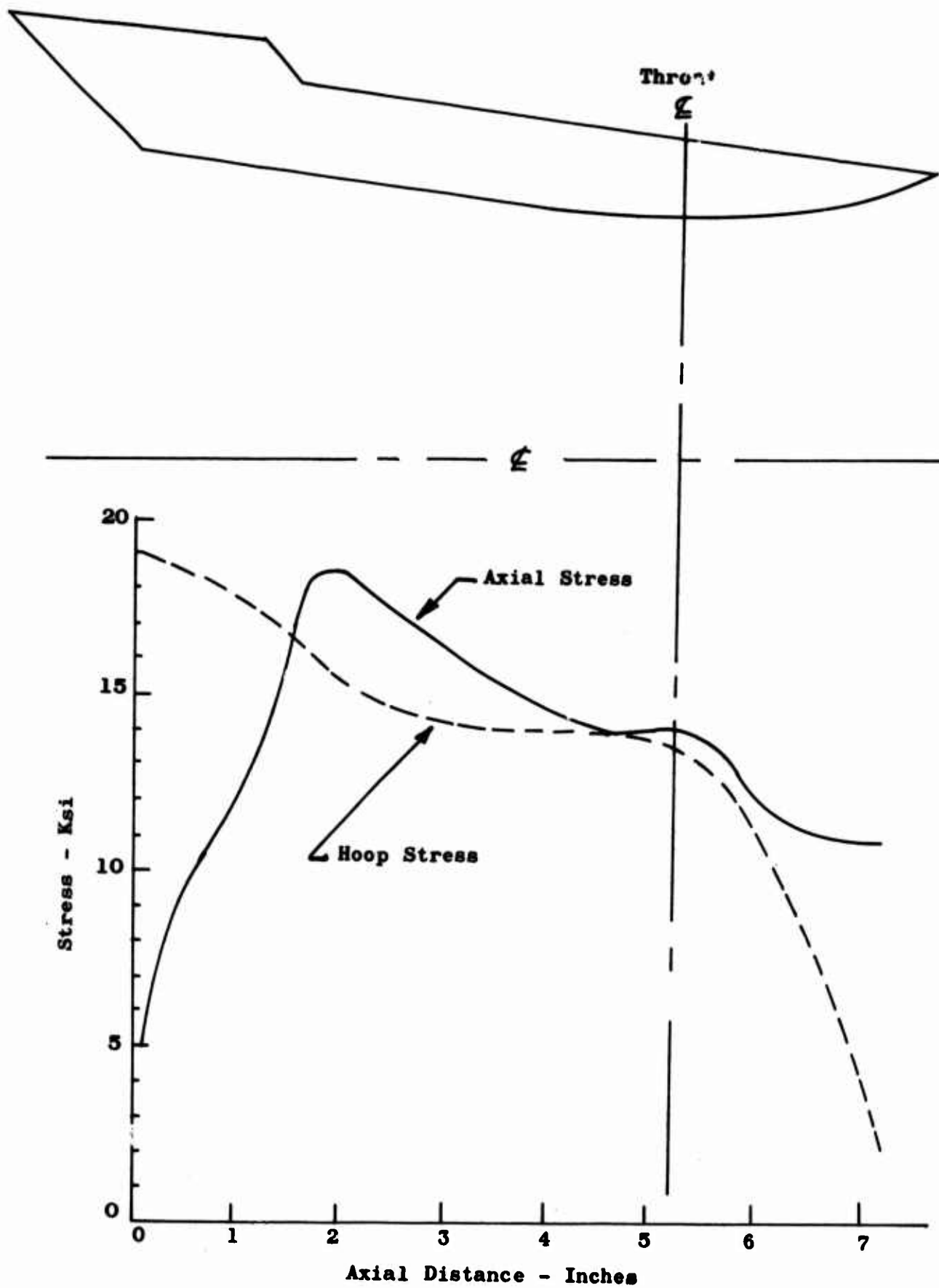


Figure 105. AGCarb-101 Throat Insert, Gas-Side Surface Stresses

UNCLASSIFIED

UNCLASSIFIED

TABLE XVII

AGCarb-101 MATERIAL PROPERTIES

Parallel to Plies

<u>Temperature °F</u>	<u>Modulus, lb/in.<sup>2</sup></u>	<u>Coefficient of Thermal Expansion in./in.-°F</u>
70	$1.7 \times 10^6$	$9 \times 10^{-7}$
1000	$1.7 \times 10^6$	$9 \times 10^{-7}$
3000	$1.8 \times 10^6$	$1.9 \times 10^{-6}$
4500	$1.85 \times 10^6$	$2.8 \times 10^{-6}$
6000	$1.9 \times 10^6$	$3.5 \times 10^{-6}$

Across Plies

<u>Temperature °F</u>	<u>Modulus, lb/in.<sup>2</sup></u>	<u>Coefficient of Thermal Expansion in./in.-°F</u>
70	$1.0 \times 10^6$	$2.8 \times 10^{-6}$
1000	$3.0 \times 10^6$	$3.6 \times 10^{-6}$
3000	$1.4 \times 10^6$	$4.6 \times 10^{-6}$
4500	$0.7 \times 10^6$	$4.6 \times 10^{-6}$
6000	$0.3 \times 10^6$	$4.6 \times 10^{-6}$

UNCLASSIFIED

## UNCLASSIFIED

(1) Failure was induced by hoop or circumferential compressive loads generated in the AGCarb-101 liner by restraining the liner against radial thermal growth.

(2) The hoop compressive stresses were calculated to be 5250 psi; however, as a result of the S/N 001 failure analysis, the stress level would most likely approach 14,000 psi compression. Based upon the results of the S/N 001 study, this stress level would be satisfactory. The liner failed as a result of the fold introduced in the manufacturing process. This fold provided a complete interlaminar shear plane through the thickness which was incapable of supporting the hoop compression.

(3) The axial movement of the ablative back-up (FM 5072 and FM 5067) was caused by the very hot (3000°F average) AGCarb-101 liner expanding longitudinally against the injector flange and forcing the ablative aft against the retaining ring. The axial load capacity of the retaining ring, bolts, and aft flange was less than the axial capacity of the AGCarb-101 liner (36,150 lb versus 114,400 lb). Therefore, the retaining ring offered very little resistance to the axial movement of the ablatives. The calculated axial movement of the ablative matched the 0.045-in. gap measured on the part after test. It was assumed that the steel shell had expanded away from the ablatives; therefore, it offered no radial restraint and only such axial restraint as that generated by the retaining ring.

(4) The axial movements of the ablatives and the axial load generated in the AGCarb-101 did not contribute to the actual failure of the liner. It was shown that considering friction, the shear capacity of the AGCarb-101/FM 5072 joint was greater than the maximum axial load that could be generated in the liner. Therefore, no relative axial motion occurred during the firing (other than differential expansion) and no additional radial loads were imposed.

(5) Failure of the liner was caused solely by the AGCarb-101 liner failing in shear along one of several apparent folds in the graphite fabric.

(6) If friction is disregarded ( $f = 0.25$  was assumed in Item 4 above), the axial load generated in the AGCarb-101 and reacted at the retainer would produce 10,700 psi compression (hoop) in the liner which is still within the allowable limits of a properly layed-up liner. Allowances should be made in future chambers to permit free longitudinal expansion of the AGCarb-101.

## UNCLASSIFIED

# UNCLASSIFIED

## SECTION VII

### FLIGHT CONFIGURATION

The design of a flightweight thrust chamber assembly, not including the thrust chamber valves, is illustrated on Figure No. 106. The design objective was to present a system having high performance with minimum weight, based upon a demonstrated dynamically stable, high performance injector, and an acoustically-damped ablative combustion chamber with demonstrated durability and long duration capabilities. Protection of the radiation-cooled columbium nozzle extension was based upon the Lunite 3 coating which was satisfactory during test evaluations.

Detail design requirements are the same as those presented in Section IV of this report.

#### A. DESCRIPTION

The basic configuration incorporates a modification of the injector body design used in the test program. The propellant inlet flanges are close-coupled to the body, thereby reducing axial length by 2.5-in. This was accomplished by replacing the split fuel inlet lines with a single entry torus similar to that used in the injector fuel circuit of the Titan first-stage engine.

High performance was assured with the 344-element pattern demonstrated in injector S/N 7. Injector-chamber compatibility was further improved with a reduced mixture ratio zone at the injector periphery. The design mixture ratio at the chamber wall is 1.0 and the effective mixture ratio 2.0 (based upon the reduced fuel vaporization rate).

The thermal accumulator consists of 2 lb of lithium which is enclosed in the cavity on the back of the injector, in a manner similar to that used to contain solder in injector S/N 6.

As seen on Figure No. 106, the ablative chamber design is a composite of chambers S/N 001 and S/N 002, which were evaluated in the testing. A single-cavity/single row acoustic resonator, similar to that tested in ablative chamber S/N 001, was placed as close as possible to the injector.

The fibrous graphite composite used at the throat and resonator is the same as that which was tested for 606 sec in chamber S/N 002. The orientation and selection of materials also are similar except that the total wall thickness was reduced to approximately 3.1-in. Additional allowances noted below for thermal growth in the design of the AGCarb-101 throat insert are used to reduce compressive loads to acceptable levels.

UNCLASSIFIED

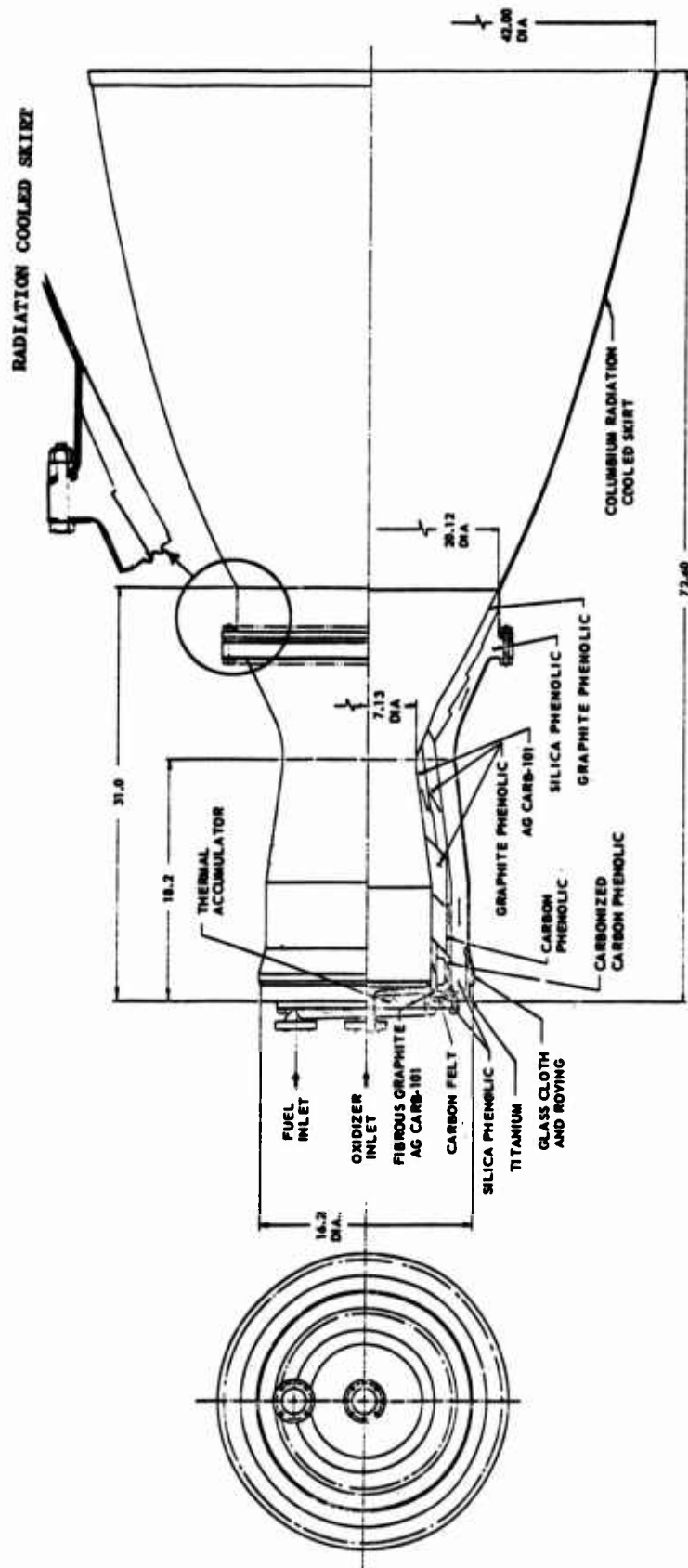


Figure 106. Conceptual Design of Flightweight Thrust Chamber Assembly

UNCLASSIFIED

# UNCLASSIFIED

- Minimum wall thickness
- Allowance for axial growth
- Axial segmentation

The Lunit 3 coated columbium nozzle extension is attached at the 7.5:1 area ratio station. The flange attachment design was based upon the proven Transtage design. The problem encountered while testing the nozzle extension, circumferential cracking in a sharp bend radii - discussed in Appendix VI, would be eliminated by reducing the bend angle and the resultant radius of curvature, (see Figure No. 106). Increasing the axial length of the nozzle by 2.5-in., the amount saved by close-coupling the injector inlet lines, permitted an exit area ratio increase to 39 without invalidating the over-all length requirement.

The component weights of the lightweight configuration thrust chamber assembly are shown below along with the weights of the hardware tested in this program.

<u>Component</u>	<u>Weight as Tested</u>	<u>Flightweight</u>
Injector	40.6	30.00
Thermal Accumulator	26.3 (solder)	2.0 (lithium)
Thrust Chamber	303.0 (S/N 002)	197.0
Nozzle Extension	<u>6.2 (9.4:1)</u>	<u>33.0</u>
TCA Weight	376.1 lb	262.0 lb

## B. THERMAL ANALYSIS OF ABLATIVE CHAMBER

The ablative chambers used for test purposes were thicker than required because of conservative design standards. Test experience indicates that these standards could be relaxed and that a flightweight chamber, using the same materials, could be approximately 1-1/4-in. thinner at the throat and approximately 35% lighter.

The chamber was designed by computer program, using a one-dimensional approximation to the heat conduction equation and treating the char process as a constant temperature, non-reversible phase change. Neither dimensional ablation and chemical interactions nor the effect of outgassing pyrolysis products, which could offer significant cooling during coast periods, was treated. Radiation to the injector face and to space via the nozzle exit and external surfaces from the gas-side was included. Convective boundary conditions of the gas-side were presumed to be the same as those inferred from steel chamber firings with injector S/N 7.

UNCLASSIFIED



# UNCLASSIFIED

Considerations in the design of the flightweight chamber include:

- Thickness reduction of the graphite phenolic because of its relatively high diffusivity.
- Thickness reduction of the silica phenolic because of its weight,
- Maintaining the existing thickness of the AGCarb-101 throat/insert for allowable thrust level decrease within specification.
- Limiting the silica phenolic temperature to 3000°F and preventing total charring until after the final burn.
- Holding the exterior temperature to 600°F.

Thicknesses of the several materials that comprised the tested and flightweight designs for the throat locations are:

<u>Material</u>	<u>Tested (in.)</u>	<u>Flightweight (in.)</u>
AGCarb-101	0.60	0.60
Graphite Phenolic	1.38	0.90
Silica Phenolic	2.17	1.48
Glass Overwrap	<u>0.12</u>	<u>0.12</u>
	4.27	3.10

Figure No. 107 shows the predicted temperature response for various points in the throat section of the flightweight design for the design duty cycle. The long first burn dictated the design of the chamber. A tremendous amount of heat was absorbed which was dissipated relatively slowly by radiation to space during the following coast so that after 240 min, the average chamber temperature was approximately 300°F. This high starting point for subsequent firings resulted in the back-side temperature being the limiting design factor rather than any internal temperature or depth of char in the silica phenolic.

## C. PERFORMANCE

Hiperkinetic nozzle performance tabulated in Section VI,B (Table XII) utilized a nozzle which was 51.9-in. long. Flightweight configuration design analysis indicated a nozzle length increase to 54.5-in. was feasible. The longer length allows a greater area ratio generation and subsequent performance improvement without the overriding penalty of high divergence losses.

UNCLASSIFIED

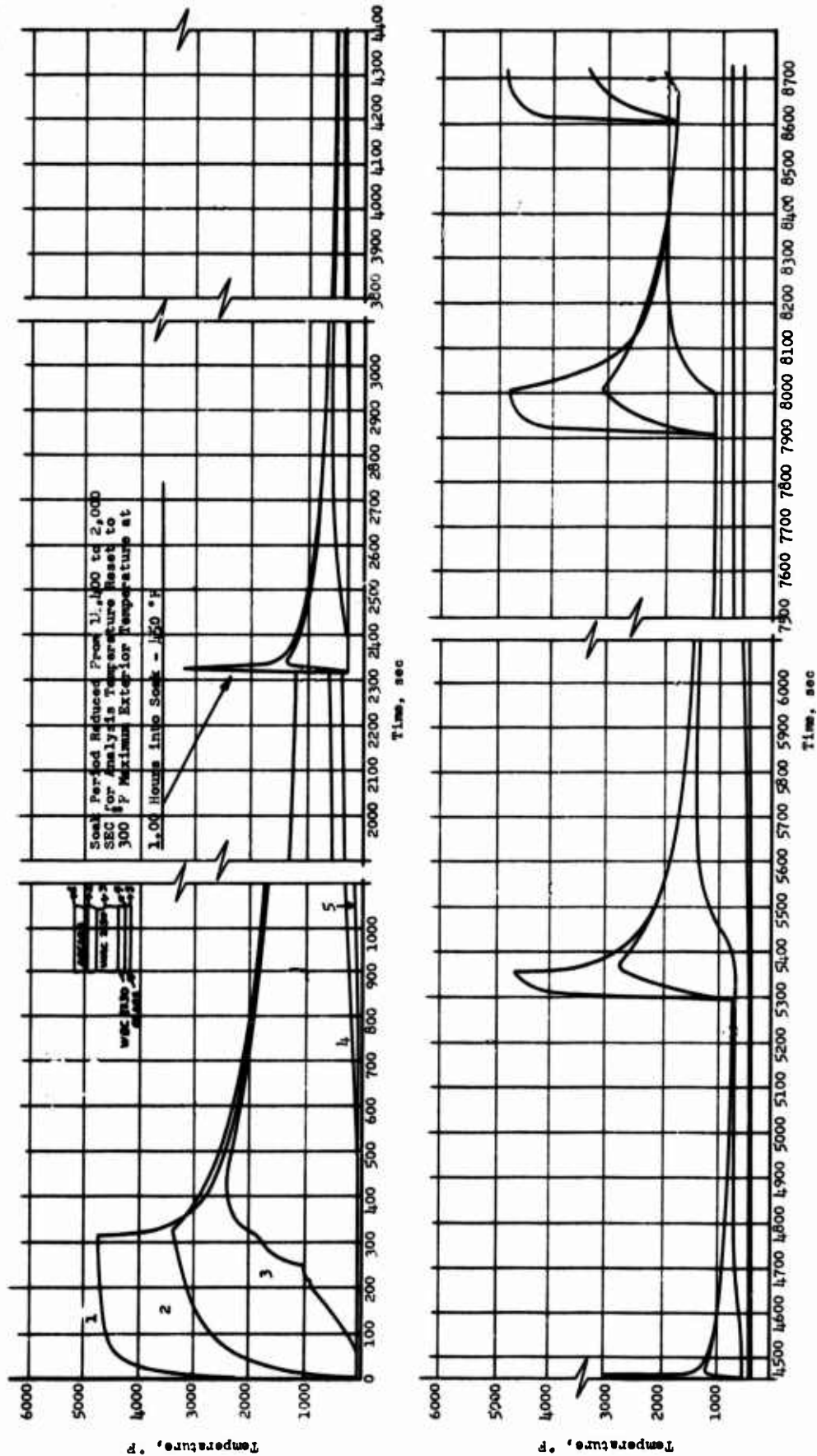


Figure 107. Predicted Throat Temperature for Design Duty Cycle

UNCLASSIFIED

**CONFIDENTIAL**

(U) Nozzle performance improvement analysis was conducted using previously-developed Rao optimum contour charts<sup>(34)</sup> and a nozzle area ratio increase to 39 was determined. Taking into account increases in theoretical impulse and friction loss together with a decrease in divergence loss resulted in a combined performance improvement of 1.2 sec.

(C) Using the new nozzle design, the lightweight configuration performance was defined at the optimum mixture ratio of 1.97 to be 374.6 sec.

---

(34) CPFA Publication No. 132, op. cit.

**CONFIDENTIAL**

**UNCLASSIFIED**

**APPENDICES**

**Page 214**

**UNCLASSIFIED**

UNCLASSIFIED

APPENDIX I

AEROJET-GENERAL SUBSCALE TESTING  
(PRE-PROPOSAL INVESTIGATION)

UNCLASSIFIED

# UNCLASSIFIED

## APPENDIX I

### AEROJET-GENERAL SUBSCALE TESTING (PRE-PROPOSAL INVESTIGATION)

#### A. INTRODUCTION

This Aerojet-General-sponsored subscale injector testing program was conducted as a pre-proposal effort to establish design criteria as well as to verify the element design selection.

#### B. PERFORMANCE RESULTS

One injector, with seventeen 12-lb-thrust-per-element triplet (F-O-F) elements, produced an average performance that was 94% of theoretical characteristic exhaust velocity ( $c^*$ ). The total impingement angle was 50-degrees and the impingement height was 0.25-in. Smooth start transients and stable steady-state operation were achieved in all tests. The orifice pressure drop and operating chamber pressure were approximately 50 psi and 115 psia, respectively, which was consistent with the full-scale design selected. The thrust chamber characteristic length ( $L^*$ ) was 26 in.

Two other injectors with impingement angles and distances that were identical to the above unit achieved an average performance of 92% of theoretical  $c^*$ . These units had thirteen 15-lb-thrust-per-element triplet elements. The operating characteristics of both these injectors were nearly identical.

A fourth injector with thirteen 15-lb-thrust-per-element triplets (F-O-F) also was tested. The elements on this unit had a total impingement angle of 30-degrees and an impingement distance of 0.5-in. The nominal performance of this unit was 94% of theoretical  $c^*$  and smooth operating characteristics also were achieved.

Based upon the results of this testing, it was concluded that triplet (F-O-F) elements would provide the necessary performance for the full-scale design. In addition, the use of either a 0.25-in. or a 0.50-in. impingement distance would be acceptable.

#### C. FUEL ORIFICE EROSION

The BA1014 fuel blend was developed<sup>(35)</sup> to provide a low freezing point fuel which would be suitable for the regenerative operation of a liquid fluorine engine. Published data as well as Aerojet experience indicated the occurrence of a phenomenon when the fuel is used with a 6061 aluminum alloy injector which results in a deterioration ("bellmouthing") of the fuel orifices at the discharge end. As cumulative test duration increases, this "bellmouthing" increases in depth, in turn, affecting the hydraulics of the fuel flow and resulting in a performance loss.

(35) Contract AF 04(611)-6353, "Research and Development to Advance State-of-the-Art of Fluorine High Energy Propulsion Systems," December 1960 - June 1961.

UNCLASSIFIED



## UNCLASSIFIED

The phenomenon has been observed with unlike-doublet, triplet, and like-doublet element designs at chamber pressures ranging from 100 psia to 350 psia and at cumulative test durations ranging from 10 to 100 sec. While it appears to be typical of the BA1014 fuel blend, there is some evidence that it also occurs with neat-hydrazine fuel. Existing literature indicates its occurrence on aluminum injectors operative with fuel blends such as MHF-3 and MHF-5; however, Aerojet-General tested a steel injector at 500 psia using ClF<sub>3</sub>/MHF-3 propellants and fuel orifice "bellmouthing" occurred at the end of 170 sec of testing. A similar design was fabricated from aluminum and tested with the same propellants. It also exhibited "bellmouthing" of the fuel orifices.

An Independent Research and Development Program was conducted by Aerojet-General in 1965(36), which provided an early demonstration of ablative thrust chambers with fluorine/hydrazine propellants. This effort was directed primarily toward a demonstration of ablatives used in 8000 lb thrust units at 100 psi for extended durations. The injectors used in this effort were fabricated from aluminum and their design was based upon successfully tested AFRPL units. One such injector, which was made from 6061 aluminum, is shown on Figure No. 108. It was tested for 118 sec at 100 psia using F<sub>2</sub>/BA1014 fuel and considerable fuel orifice erosion occurred.

The injector shown on Figure No. 109 is a single element pentad type, which was fabricated from 6061 aluminum and tested for 10 sec at 200 psia using F<sub>2</sub>/BA1014 propellants.(37) There is evidence of radial material flow as well as orifice "bellmouthing."

Figure No. 110 presents a like-on-like doublet element injector that was a scaled-down version of a 3500 lb thrust unit used by AFRPL for their in-house fluorine thrust chamber materials evaluation program.(38) It was tested for 57 sec at 200 psia using F<sub>2</sub>/BA1014 propellants and demonstrated a low performance level. The triplet (F-O-F) element injector shown on Figure No. 111 was the most successful injector design used in the referenced materials evaluation program. It demonstrated good performance during its 39.6 sec of testing at 200 psia using the F<sub>2</sub>/FA1014 propellant combination. Another injector tested in the same program is shown on Figure No. 112. This triplet unit was tested for 183.1 sec at 200 psia. Both show fuel orifice bellmouthing.

A stainless steel triplet type of injector was used in an Aerojet-General Independent Research and Development Program conducted during 1964.(39)

- (36) Aerojet-General IR&D, "Advanced Transtage Thrust Chamber," 1965
- (37) Fluorinated Oxidizer Thrust Chamber Materials Evaluation Program, Phase I, Contract AF 04(611)-10918, Report AFRPL-TR-66-77, 1966
- (38) Ibid.
- (39) Aerojet-General IR&D, "Advanced Transtage Fluorine Feasibility Program," 1964

## UNCLASSIFIED

UNCLASSIFIED

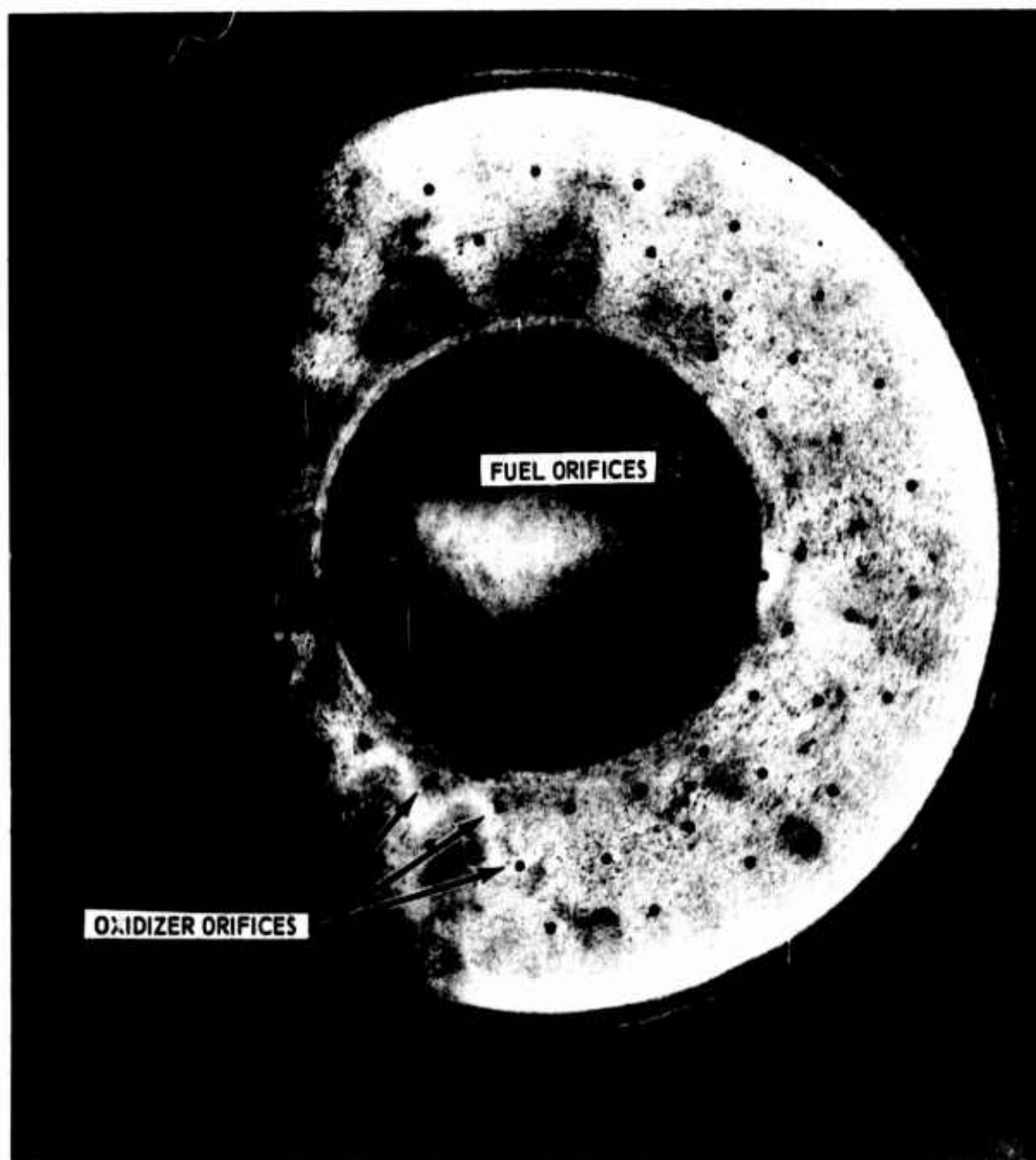


Figure 108. 8000 lb  $F_2$ /BA 1014 Injector

UNCLASSIFIED

UNCLASSIFIED

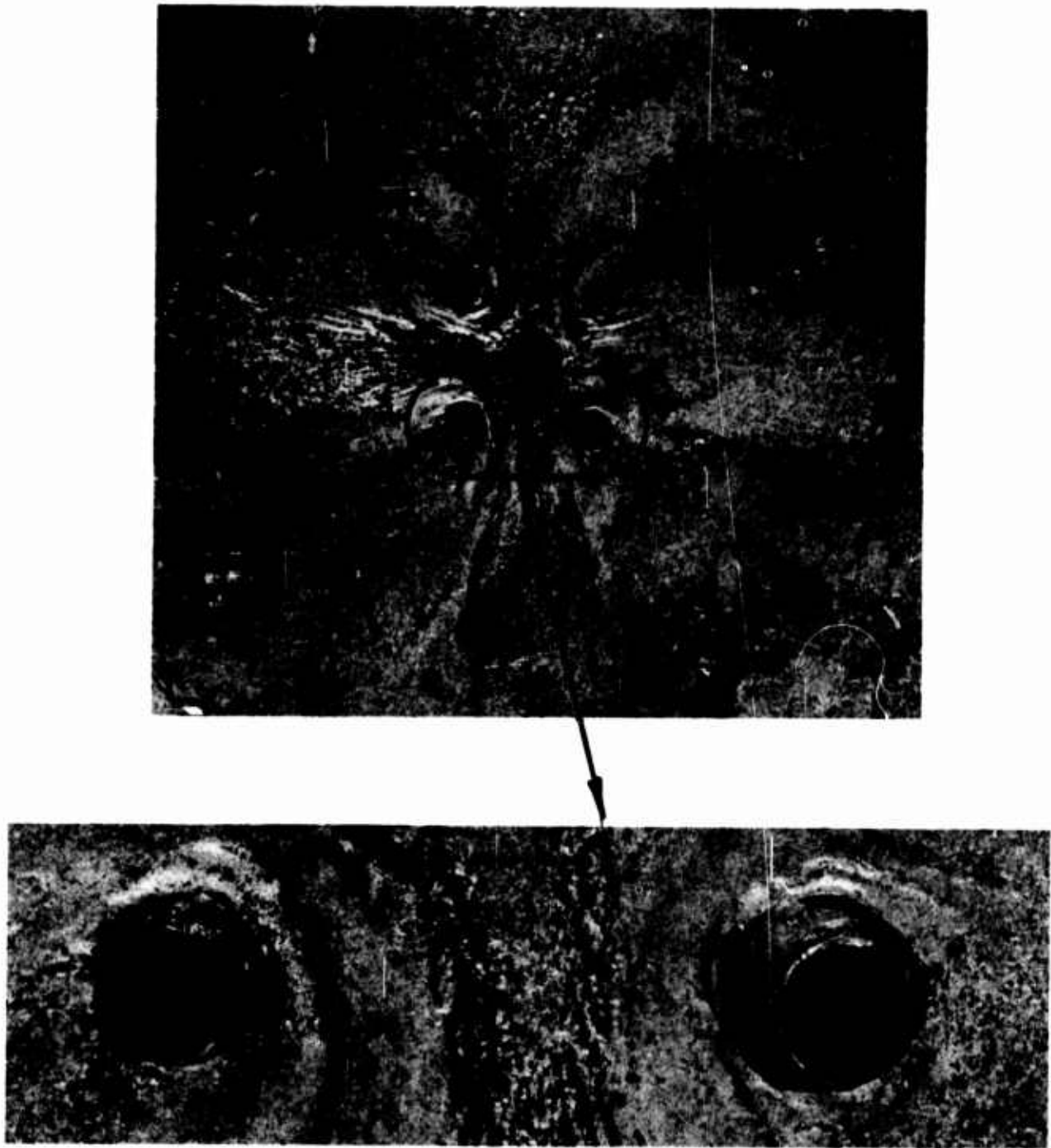


Figure 109. Single Element Pentad Injector

UNCLASSIFIED

UNCLASSIFIED

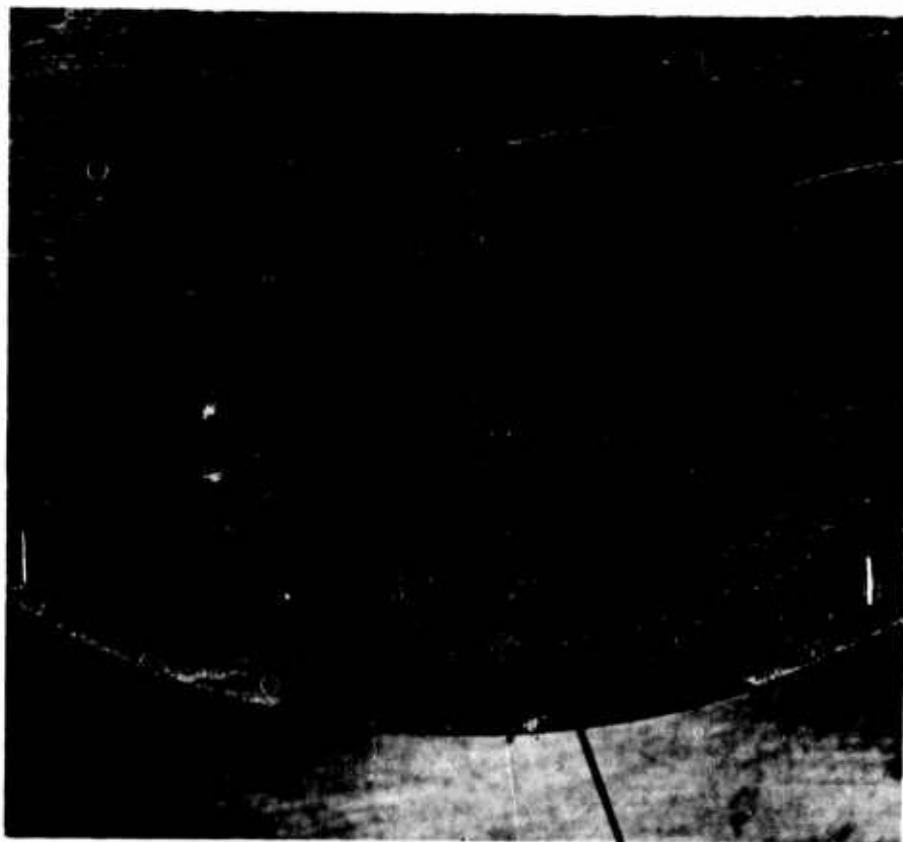


Figure 110. Like-on-Like Doublet Element

UNCLASSIFIED

UNCLASSIFIED

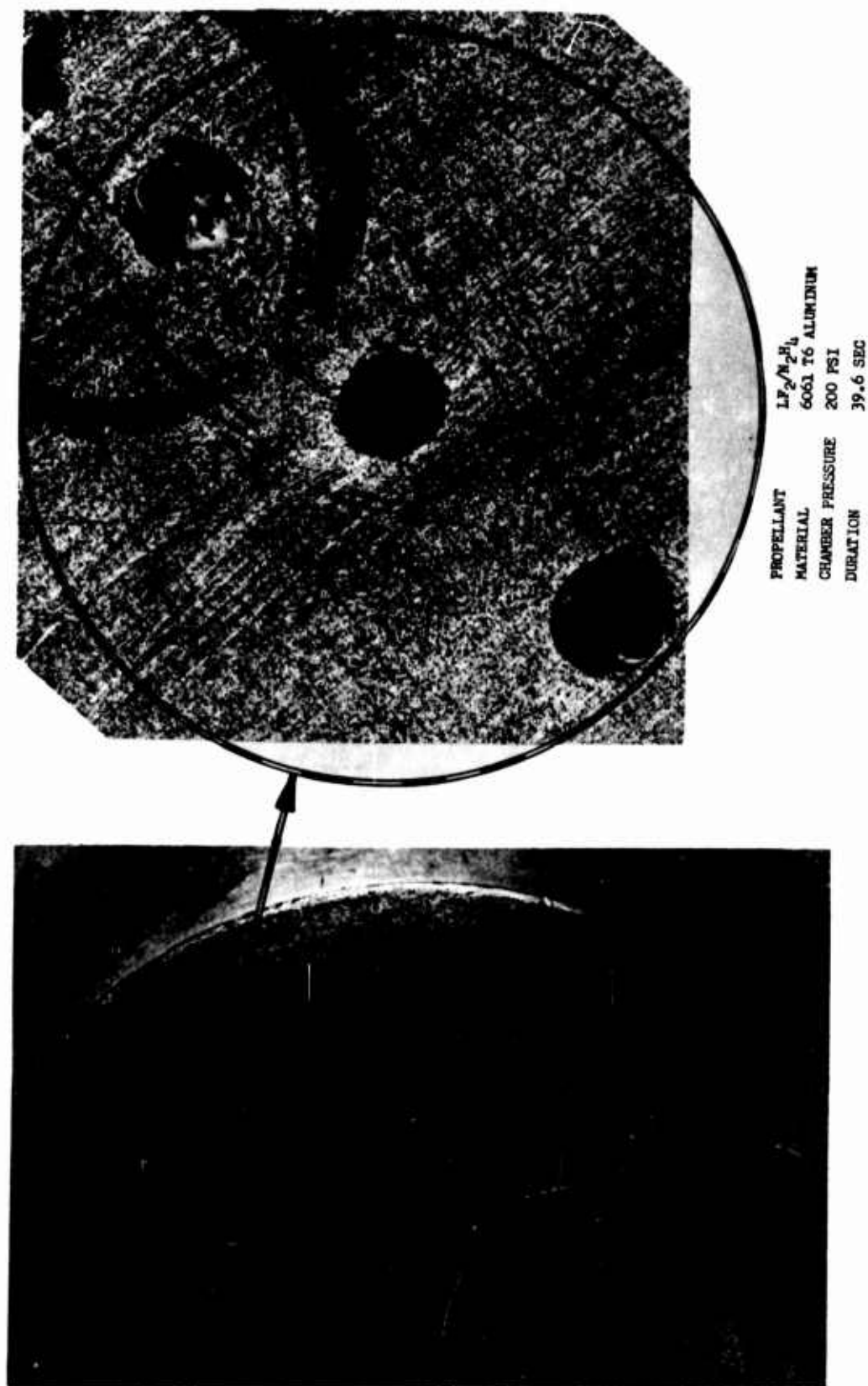


Figure 111. Four-Element Triplet Injector at 39 sec

UNCLASSIFIED

UNCLASSIFIED

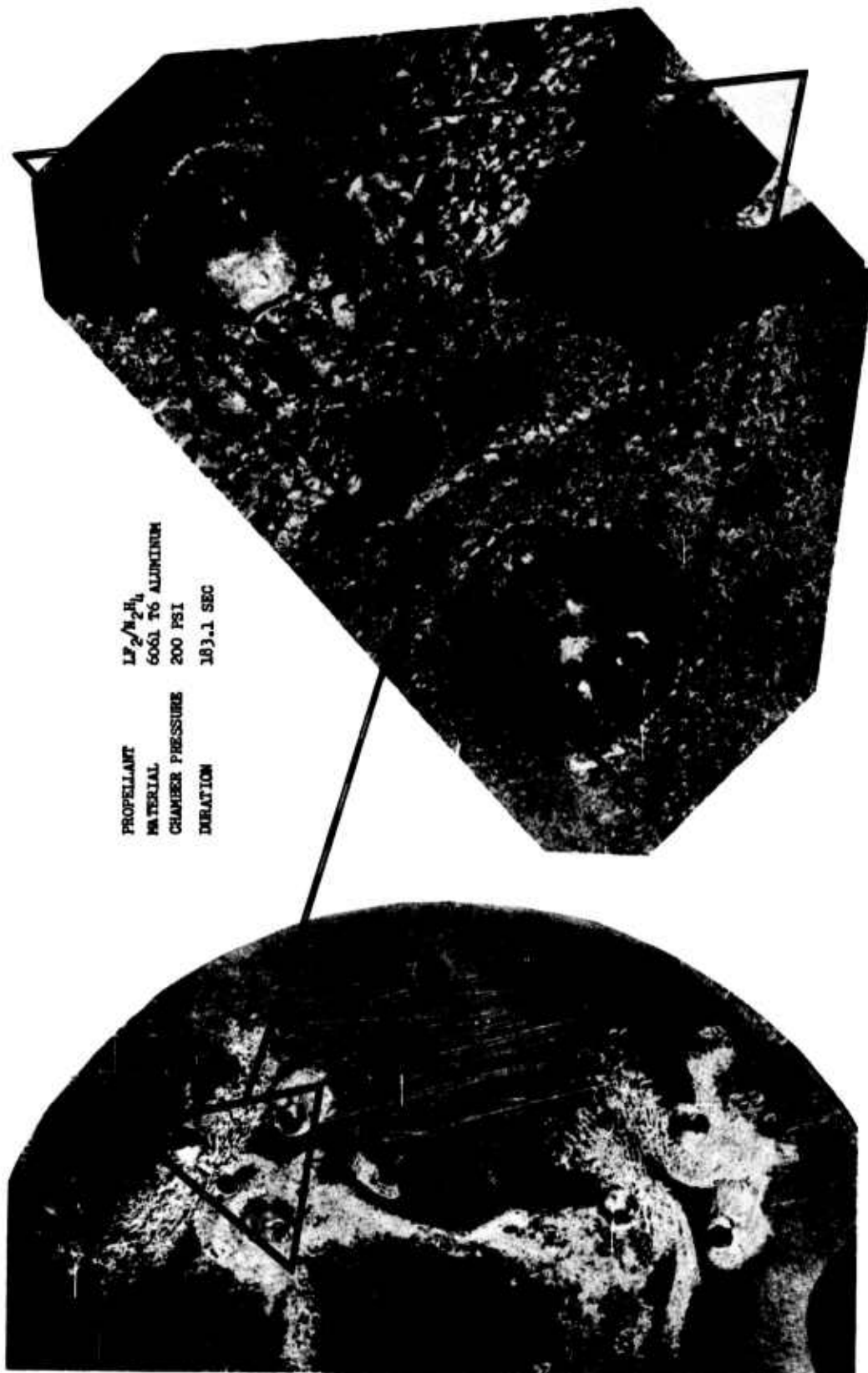


Figure 112. Four-Element Triplet Injector at 183 sec

UNCLASSIFIED



UNCLASSIFIED

This injector operated in a 750 lb thrust unit at 500 psia for an accumulated duration of 170 sec using ClF<sub>3</sub>/MHF-3 propellants. There was little evidence of orifice erosion at the center; however, there was noticeable erosion at the periphery where the radial gas flow was highest.

No known concerted analytical-experimental program existed for the purpose of identifying and resolving the "bellmouthing" phenomenon with aluminum and stainless steel injectors. There had been limited successes with some of the empirical solutions attempted, which included the addition of refractory and corrosion-resistant barrier materials on the injector face and in the fuel orifices.

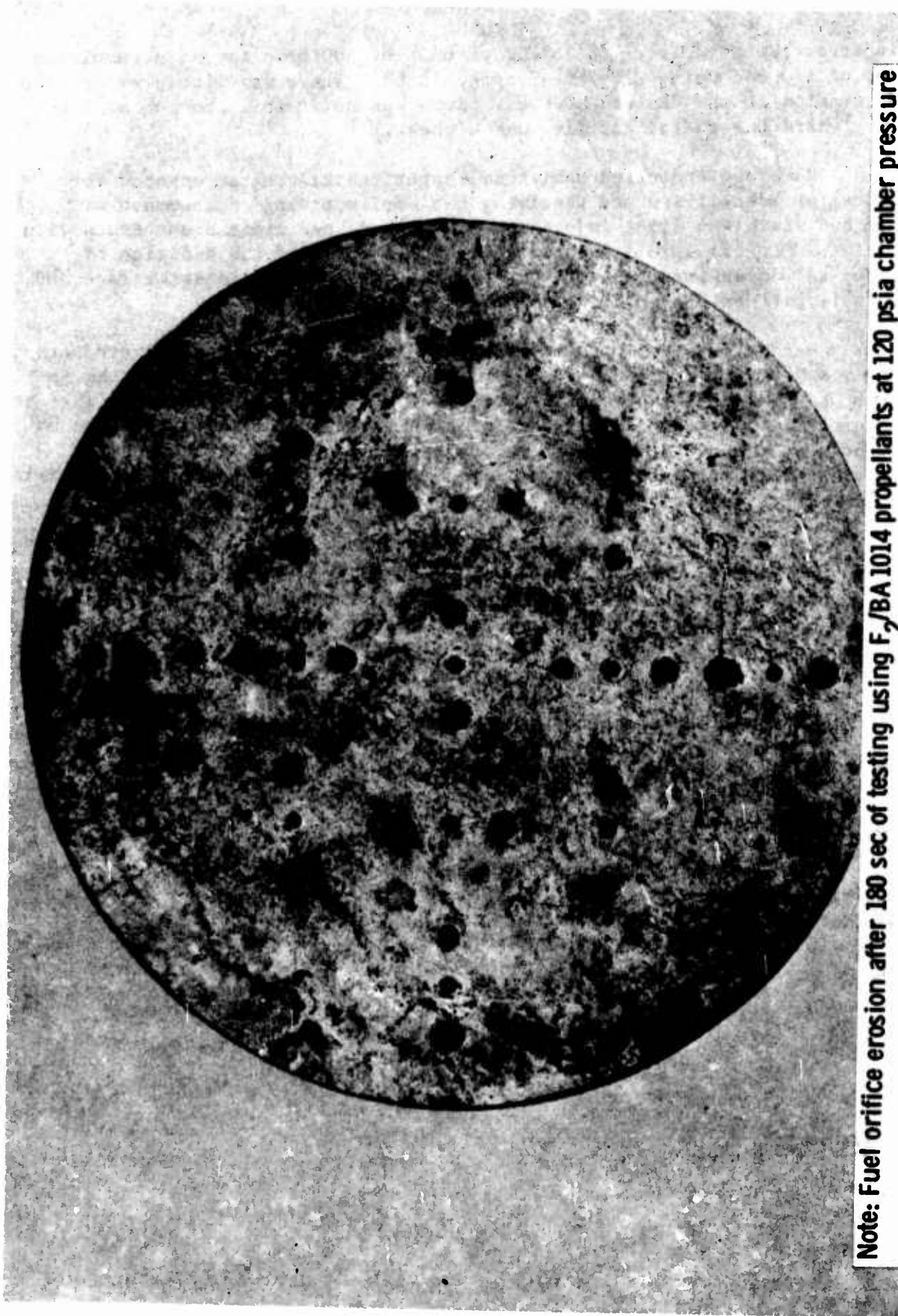
Aerojet-General conducted a subscale testing program wherein both aluminum and Nickel 200 injectors were subjected to long-duration testing in an attempt to resolve the potentially critical "bellmouthing" problem. The influence of the specific element design was eliminated from the evaluation by testing both nickel and aluminum injectors having identical patterns. The fuel-oxidizer-fuel triplet element was used in all of the units. The results from this testing were as follows:

- Gross orifice erosion was evident on both the aluminum injectors, which were tested for 180 sec and 185 sec of firing, respectively. A post-test view of one of the aluminum injectors is shown on Figure No. 113.
- Macroscopic examination of the two Nickel 200 injectors tested for 619 sec and 560 sec, respectively, failed to reveal any erosion. Some minor erosion was uncovered by microscopic examination; however, it was significant that this minor erosion did not cause any degradation in either performance or stability. One of these units is shown on Figure No. 114 after 610 sec of testing.

These results served as the basis for selecting Nickel 200 as the injector face material in conjunction with in-line triplet (F-O-F) injector elements for full-scale program use.

UNCLASSIFIED

UNCLASSIFIED



Note: Fuel orifice erosion after 180 sec of testing using F<sub>2</sub>/BA 1014 propellants at 120 psia chamber pressure

Figure 113. Post-Test View of Subscale Aluminum Injector

UNCLASSIFIED

UNCLASSIFIED

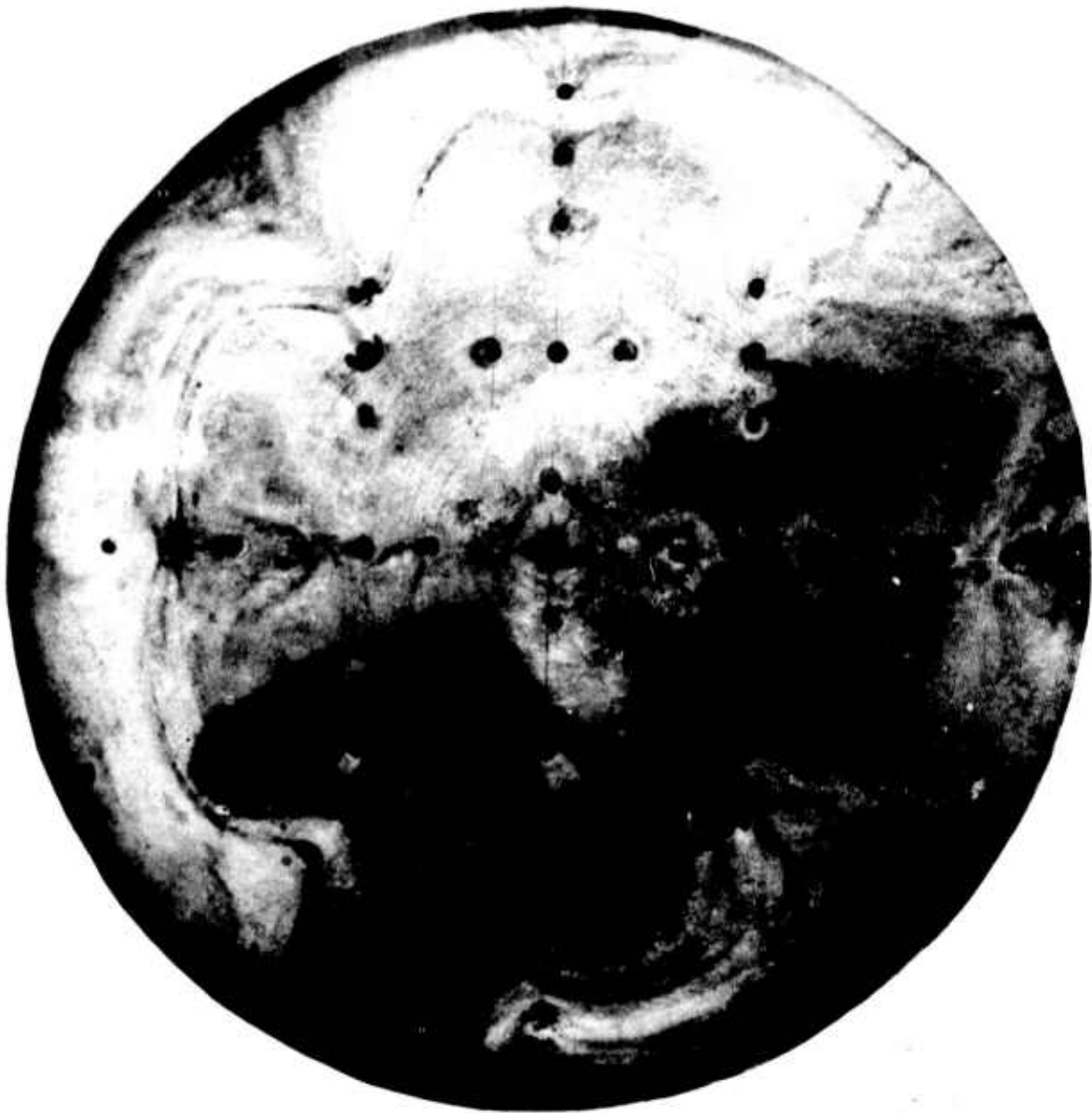


Figure 114. Subscale Nickel Injector after 619 sec of Testing

UNCLASSIFIED

UNCLASSIFIED

APPENDIX II

ACOUSTIC DAMPER ANALYSES, DESIGN, AND METHODS

UNCLASSIFIED

## UNCLASSIFIED

## APPENDIX II

## ACOUSTIC DAMPER ANALYSES, DESIGN, AND METHODS

## A. ACOUSTIC DAMPER ANALYSES AND DESIGN

1. Introduction

Currently, one of the most common analytical techniques for acoustic damper designs considers a two-dimensional array of individual Helmholtz resonators which are tuned to damp an acoustic mode of instability that has occurred in an undamped combustion chamber. One of the assumptions implied by this approach is that the addition of the acoustic damper to the chamber wall will not significantly change the resonant frequencies of the chamber acoustic modes. Such an assumption with the use of baffles was proven wrong in the GEMSIP program as a result of both hot fire and acoustic testing.

A similar result occurred during the company-sponsored Injector Face Acoustic Resonator Program, when an acoustic damper was added to the chamber, both in ambient acoustical tests and two independent mathematical analyses subsequently discussed in this appendix. The results of both these empirical and analytical efforts show that for a chamber similar to the one used in this program with a length to diameter ratio of approximately two, the first tangential mode frequency of the undamped chamber is within 8% of the frequency of the combined first tangential, first longitudinal mode (1T + 1L). Thus, when the acoustic damper is added to the chamber near the injector and tuned approximately for the first tangential acoustic mode frequency, it depresses the purely transverse first tangential mode to a significantly lower frequency while only slightly depressing the combined tangential and longitudinal mode. The combined mode has been found to be depressed only a few percent for the example cited here; therefore, it is possible that the combined mode might appear to be the pure first tangential mode because of the frequency and transverse pressure phase profile. The axial or longitudinal component of the pressure profile would be difficult to determine in a normal hot test firing situation without a rather elaborate high-frequency pressure transducer arrangement. This is the result of the distortion of the mode caused by the damper location and the nozzle admittance.

2. Discussion of Analysis Used

The acoustic damper analytical evaluation falls into two regimes:

a one-dimensional array of resonators, evaluated exclusive of the chamber,

a chamber with the acoustic damper included as an integral part.



# UNCLASSIFIED

The chamber with the acoustic damper included as an integral part has been further divided into the following two types:

cylindrical dampers which extend the full length of the chamber without mean flow,

dampers which are an integral part of the injector face at the chamber wall with mean flow nozzle effects.

The three dampers that were fabricated for this program are not exactly described by any of the above analyses. However, the nine-row three-cavity design was best described by the combination of the one dimensional array analysis and the full length cylindrical analysis. The latter analysis indicated some frequency shift and damping increase caused by the presence of the damper. The former analysis was used to obtain curves of absorption coefficient versus frequency for a sound level of 190 db and mean gas flow velocities of 0, 500 ft/sec, 850 ft/sec, and 1050 ft/sec past the damper orifices. Obviously, the actual absorption coefficient for such a damper covering only a portion of the chamber wall would be a function of many additional factors. However, single resonator analysis does provide somewhat of a qualitative measure with which to compare damper designs.

The one-row and two-row/one-cavity damper designs also were evaluated using a recently-developed Aerojet-General analysis, which is capable of evaluating a variety of acoustic dampers located at the injector face. This analysis is the most sophisticated of those mentioned because it accounts for the nozzle admittance with sonic flow at the throat. Further, it accounts for the combined transverse and longitudinal modes. The only disadvantage of this Injector Face Acoustic Resonator (IFAR) analysis is the one common to all the existing analyses; the actual value of orifice resistance is not known accurately for high sound levels, which results in a rather wide range of quantitative estimates for the performance of various dampers.

### 3. Historical Approach to Acoustic Damper Analysis

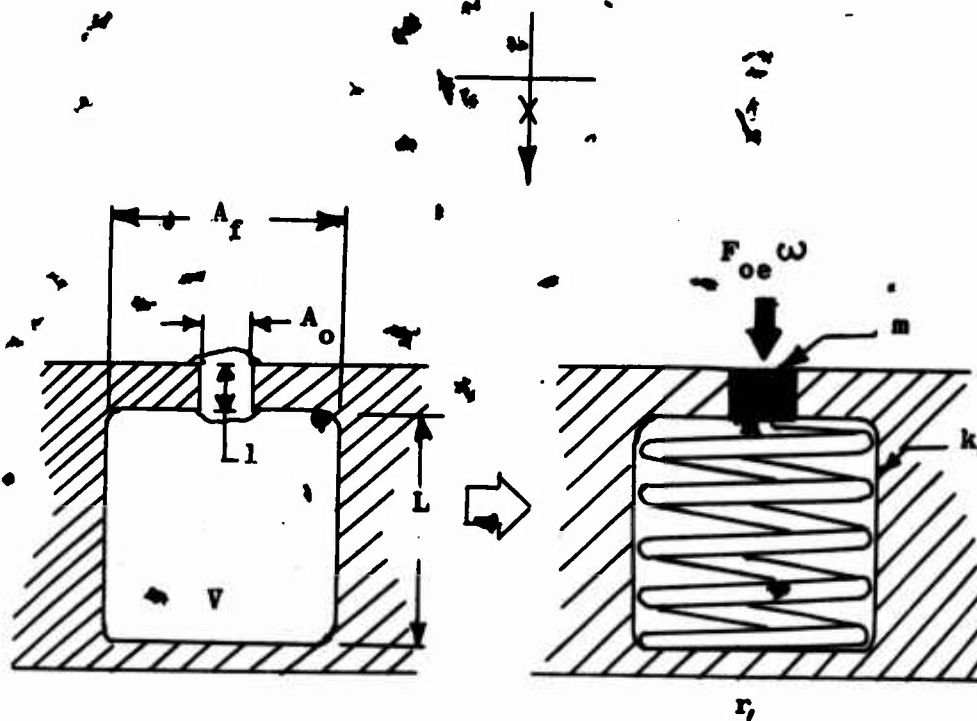
The simplified analysis of an air resonator made by Helmholtz almost a century ago still is used as a starting point for the evaluation of an acoustic liner design for a rocket engine. The common textbook method for describing this simplified analysis is with a mechanical or electrical analogy.

The mechanical analogy consists of a spring mass system as shown on Figure No. 115. The differential equation of the mechanical system with a periodic forcing function is:

$$m\ddot{x} + r\dot{x} + kx = F_0 e^{j\omega t}$$



UNCLASSIFIED



$A_f$  = Area of Face  
 $A_o$  = Area of Orifice  
 $V$  = Volume Cavity  
 $L$  = Backing Length  
 $l$  = Effective Length of Orifice Volume

$F_o$  = Force Function  
 $m$  = Mass  
 $r$  = Damping Constant  
 $k$  = Spring Constant  
 $\rho$  = Gas Density  
 $P$  = Gas Pressure  
 $c$  = Speed of Sound

Figure 115. Mechanical Analogy of Acoustic Resonator

UNCLASSIFIED

# UNCLASSIFIED

The damped natural frequency of such a system is given by

$$\omega_d = \sqrt{\frac{k}{m} - \left(\frac{r_1}{2m}\right)^2}$$

or if the damping is small, so that

$$\left(\frac{r_1}{2m}\right)^2 \ll \left(\frac{k}{m}\right)$$

then, the undamped natural frequency is given by:

$$\omega_n \approx \sqrt{\frac{k}{m}}$$

The natural frequency of the acoustic system can be related to the mechanical system just described by the following substitutions:

$$\text{mass} = m = \rho V_o = \rho A_o l$$

$$\text{spring constant} = K = A_o \frac{dp}{dx}$$

$$= -A_o^2 \frac{dp}{dV}$$

$$= c^2 A_o^2 / V$$

$$\text{forcing function} = F_o e^{j\omega t} = P A_o e^{j\omega t}$$

$$\text{damping constant} = r_1 = \rho \omega^2 A_o^2 / c 2\pi$$

This then gives the natural frequency of the acoustic resonator as

$$\omega = c \sqrt{\frac{A_o}{lV}}$$

where  $A_o$  represents the area of the orifice, and unsubscripted  $V$  represents the volume of the cavity.

## UNCLASSIFIED

Many assumptions were made to arrive at this simple formula for the resonant frequency; therefore, it is useful only for broad approximations of the resonant frequency of a given design. A correction that can be applied to improve the estimate relates to the relationship of the effective length of the orifice to its actual length. There are numerous versions of this length correction; however, typically, the values approximate three-fourths of the diameter of the orifice.

#### 4. Recent Modifications to the Historical Approach

In the preceding discussion it was assumed that the viscosity losses in the orifice are small when compared with the acoustic radiation losses. This assumption probably is the most unrealistic aspect of the preceding analysis. Actually, at high sound pressure levels and with small orifices, the viscosity losses are quite high and the radiation losses are no longer described by the equation for the acoustic resistance of an orifice opening into free space.<sup>(40)</sup>, <sup>(41)</sup>, <sup>(42)</sup> This acoustic resistance is better explained by incompressible gas dynamic parameters associated with turbulent incompressible gas flow caused by either direct or alternating air flow.<sup>(43)</sup>, <sup>(44)</sup>, <sup>(45)</sup>

As a result, it is recognized that the sound energy dissipating quality of a Helmholtz resonator is determined predominantly by the previously-ignored viscosity losses and by turbulence losses associated with high sound pressure levels. This loss mechanism is best described with a nonlinear acoustic resistance and has been empirically curve fitted for single resonators<sup>(46)</sup> and multiple resonators<sup>(47)</sup>. An attempt also has been made to model the nonlinear acoustic resistance losses theoretically.<sup>(48)</sup> The model assumes that the nonlinear losses result from the jet formation at the exit of the orifice (viz., while the resonator is expelling gas) and that all of the kinetic energy of this gas jet is lost by conversion to turbulence. This

- (40) Rayleigh, J. W. S., The Theory of Sound, Vol. II, Dover Publications
- (41) Morse, P. M., Vibration and Sound, second edition, McGraw-Hill Book Co., Inc., New York, 1948
- (42) Wood, A., Acoustics, Dover Publications
- (43) Ingard, V., "On the Theory and Design of Acoustic Resonators," Journal of the Acoustical Society of America, Vol. 25, No. 6, November 1953
- (44) Ingard, V. and Labate, S., "Acoustic Circulation Effects and the Non-linear Impedance of Orifices," Journal of the Acoustical Society of America, Vol. 22, March 1950
- (45) McAuliffe, C. E., "The Influence of High Speed Air Flow on the Behavior of Acoustical Elements," M. Sc. Thesis, Massachusetts Institute of Technology, 1950
- (46) Ingard, V., op. cit.
- (47) Blackman, A. W., op. cit., "Effect of Nonlinear Losses on the Design of Absorbers for Combustion Instabilities," ARS Journal, November 1960
- (48) Sirignano, W. A., et al, "Acoustic Liner Studies," ICRPG Third Combustion Conference, Vol. I, 17-21 October 1966

UNCLASSIFIED

UNCLASSIFIED

represents a nonlinear loss mechanism, because kinetic energy is proportional to the square of the velocity of the jet. The model very closely correlates the data obtained empirically. It deviates most at the very high sound pressure levels where little experimental data is available. This is to be expected because very high sound pressure levels are known to be highly nonlinear with respect to all of the acoustic loss mechanisms. The results obtained using this relatively simple theory also indicate that the empirical results used for previous rocket liner design applications are in error because the experiments have been performed using air at ambient conditions and were not corrected for viscosity, density, and frequency to the hot environment of an operating combustion chamber.

Having once resolved what the nonlinear losses are for an operating combustion chamber resulting from high sound levels, it is necessary to correct for the effects of mean gas flows past and/or through the liner. As indicated, this has been accomplished empirically.(49), (50) These effects are manifested as a decrease in the effective mass of the orifice and result in a significant increase in the resonant frequency of the resonator. The maximum shift observed is reported to be 63% of the resonant frequency obtained in a static environment. Some question still exists concerning the results obtained(51) because of the effect of flow past the resonator orifice and a saturation effect of the acoustic resistance resulting from mean flow turbulence effects as a function of frequency and velocity. Mechel(52) defined an acoustic resistance ratio which was experimentally shown to vary between 1.0 and 3.5 for a frequency of 400 Hertz. Currently, absorption coefficients are evaluated using 3.5 as an upper limit or using a simple curve-fit formula. However, the absorption coefficients obtained using these two methods clearly are not in agreement.

##### 5. Anomalies of Absorption Coefficient Approach

The evaluation of a particular acoustic liner design now can be made using the knowledge obtained from the empirical data of both theoretical models and a correct gas property scaling technique founded in the theoretical model. The best method for evaluating an acoustic liner design in a particular chamber is not necessarily the absorption coefficient method, which is emphasized in the technical literature. This method does not consider the system as a whole. Rather, it is based upon designing a liner independently of the combustion chamber and then incorporating it into the chamber wall. If

(49) Mechel, F., et al, Research on Sound Propagation in Sound Absorbent Ducts with Superimposed Air Streams, Report AMRL-TDR-62-140, Aerospace Medical Division, Wright-Patterson Air Force Base, Ohio December 1962

(50) McAuliffe, C. E., op. cit.

(51) Mechel, F., et al, op. cit.

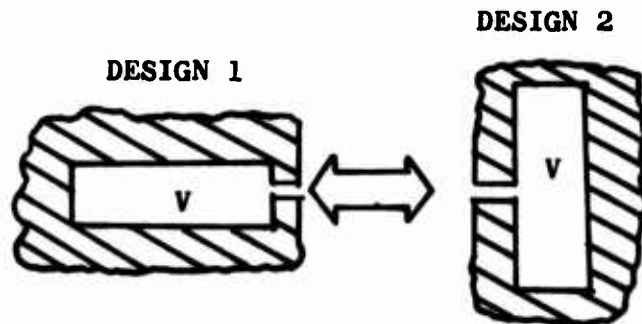
(52) Ibid.

UNCLASSIFIED

# UNCLASSIFIED

the liner is truly a large array of resonators making up a significant portion of the total chamber wall area, then it definitely should be evaluated as a complete system because its effect upon the system cannot be ignored. Conversely, if the liner is limited to a small area (i.e., around the injector) the absorption coefficient method does not give good design comparisons. A good example of the misleading results that can be obtained using the absorption coefficient method is shown with the following two designs:

	$\sigma$	$L$	$d$	$t_1$	SPL	$f_o$	$\alpha$
Design 1	0.25	0.625	0.2	0.0625	190	8000	0.34
Design 2	0.16	0.40	0.2	0.0625	190	8000	0.57



Note that the resonant frequencies,  $f_o$ , of the two designs are equal; the orifice thickness,  $t_1$ , diameter,  $d$ , and volume,  $V$ , of the resonator also are the same. The open area ratio,  $\sigma$ , and backing distance,  $L$ , are simply ratioed so as to yield the same resonant frequency. The pound pressure level, SPL, of the incident pressure oscillation is taken to be equal for the two designs as are all of the gas properties.

$$f = \frac{c}{2\pi} \sqrt{\frac{A_o}{Vl}} = \frac{c}{2\pi} \sqrt{\frac{A_o/A}{Ll}} = \frac{c}{2\pi} \sqrt{\frac{\sigma}{Ll}}$$

If the analytical assumptions are obeyed, then, the use of only one row of such an acoustic liner in a rocket chamber would result in identical absorption, but the calculated absorption coefficients differ by a factor of approximately two at resonance. Therefore, a more meaningful method for comparing two acoustic liner designs is needed. One such way for evaluating two different acoustic liner designs is an Aerojet-General computer program wherein the decay rate and frequency of the acoustic modes of a given combustion chamber are calculated with an acoustic resonator array over some percentage of its wall area. Thus, the best liner is the one that provides the most damping of the system as measured by its decay rate. However, an accurate determination of the acoustic resistance and reactance for a given sound level

and gas flow condition are still required. This method also takes into account the actual pressure distribution of the transverse acoustic modes of a cylindrical chamber.

#### 6. Generalized Liner Analysis

This analysis is one of the approaches considered for overcoming the indicated shortcomings of the one-dimension array resonator analysis. It specifically relates to transverse modes rather than the analysis of a separate one-dimensional resonator array.

The governing equations are written in cylindrical coordinates for both regions 1 and 2 as shown on Figure No. 116. Assuming radial flow through the liner holes, the one-dimensional wave equation can be written to relate the two regions. The acoustic equation in cylindrical coordinates was written for two regions; the region between the outer chamber wall and the liner as well as the region between the centerline of the chamber and the liner:

$$\frac{\partial^2 P}{\partial r^2} + \frac{1}{r} \frac{\partial P}{\partial r} + \frac{1}{r^2} \frac{\partial^2 P}{\partial \theta^2} + \frac{\omega^2}{c^2} P = 0 \quad \text{Eq. (7)}$$

If it is assumed the variables can be separated, the solution has the form  $P = R(r) \Theta(\theta)$ . Substituting this solution into Equation (7), the following ordinary differential equations are obtained:

$$\Theta' + \nu \Theta = 0 \quad \text{Eq. (8)}$$

$$r^2 R'' + r R' + \left( \frac{\omega^2}{c^2} r^2 - \nu^2 \right) R = 0 \quad \text{Eq. (9)}$$

The solutions to these equations are, respectively

$$\Theta = A \sin(\nu \theta) + B \cos(\nu \theta) \quad \text{Eq. (10)}$$

$$R = D J_{\nu} \left( \frac{\omega}{c} r \right) + E Y_{\nu} \left( \frac{\omega}{c} r \right) \quad \text{Eq. (11)}$$

The orifices between these two regions can be treated using the one-dimensional wave equation and a resistance connecting the orifices to the interior region. Radial volume flow and pressure must be matched at the



UNCLASSIFIED

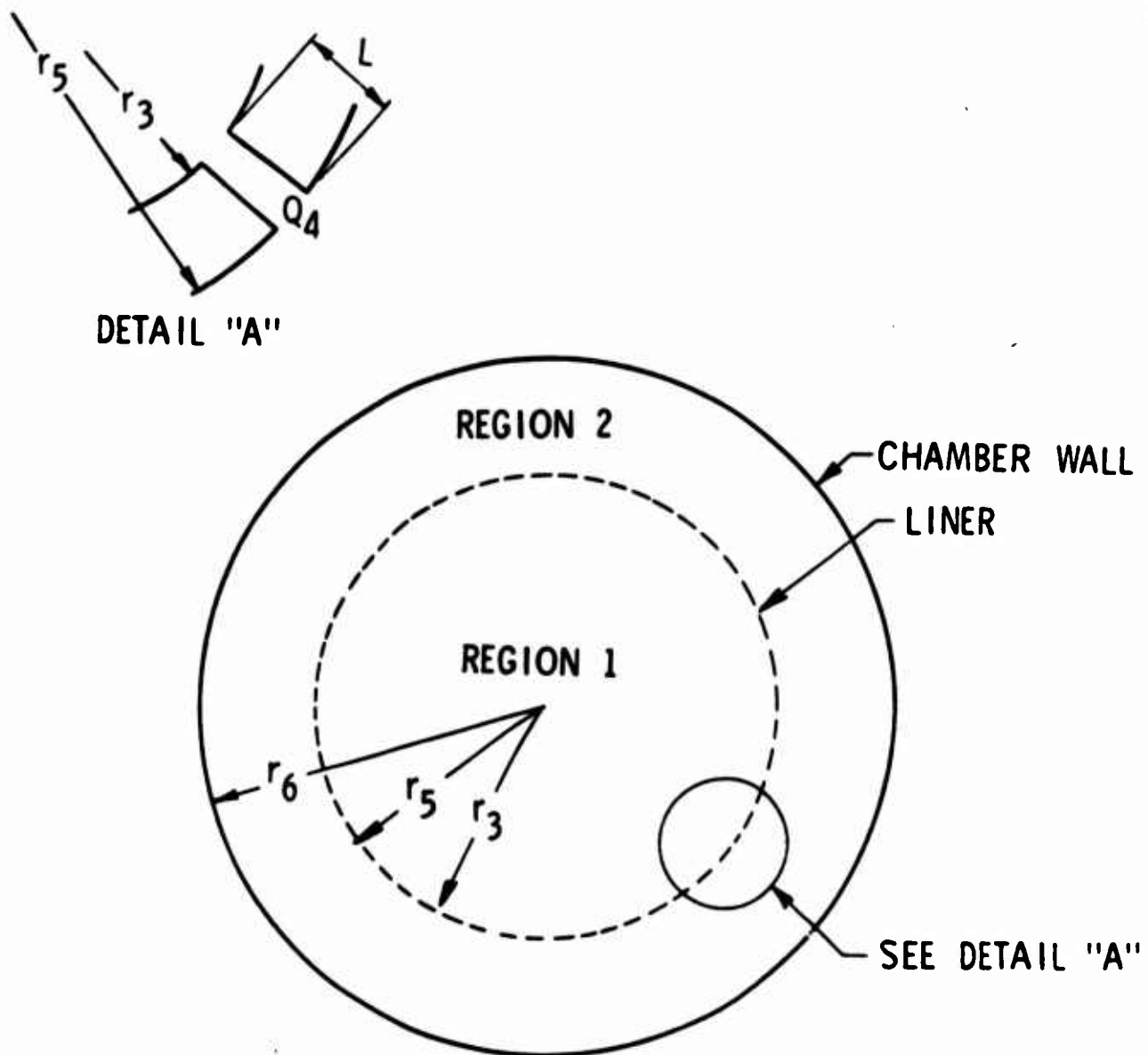


Figure 116. Liner Model

UNCLASSIFIED

UNCLASSIFIED

interface. The same conditions must apply to connect the orifices to the outer region. In addition, the radial velocity at the outer wall is zero and the pressure at the center of the chamber is finite.

The equations across the three regions as well as the matching and boundary conditions form a set of nine homogeneous algebraic equations. The characteristic equation of this system is obtained by equating the determinant of the matrix formed by the nine equations to zero. Integrating the differential equations by separation of variables and applying the boundary conditions lead to a set of simultaneous homogeneous equations, the coefficient determinant of which must vanish for a non-trivial solution to exist. The coefficients are transcendental functions; therefore, it is impractical to solve for the eigenvalues directly. The damping rate is obtained by plotting the amplitude of the inverse of the determinant as a function of frequency in the area of the characteristic equation zeros. Based upon these considerations, a computer program was developed to evaluate the determinant as a function of frequency. From the output of the program, it then is possible to determine the damping resulting from the liner by the frequency bandwidth at the half power point by using the following relationship:

$$\text{damping rate } (\delta) = 8.7 \pi \Delta f \text{ (db/sec)}$$

where  $\Delta f$  is the half-power frequency bandwidth of the response function.

The new resonant frequencies of the chamber cavity are as determined by plotting the inverted matrix with the resonant frequencies being at the maximum values of the inverted matrix (viz., the zeros of the characteristic equation).

Examples of the resulting output from the analysis are shown on Figures No. 117 and No. 118. The effect of incorporating an acoustic resonator in the chamber wall is illustrated on Figure No. 117. The resonator has a resonant frequency of 2800 hz and the chamber without the liner had a first tangential mode resonant frequency at approximately 3400 hz. With the addition of the resonators, the chamber cavity assembly resonant frequency is reduced to 2015 hz. The first tangential mode frequency depression observed here was investigated further and it was found to be a function of cavity temperature. The frequency depression of both the first and second tangential modes as a function of cavity temperature is shown on Figure No. 119. Figure No. 118 shows the analytical results for the same 9.45-in. diameter chamber with a rough chamber wall which had a resistance equivalent to that used for the resonator design discussed above. The results show only a small shift from the 3400 cps resonant frequency of the combustion chamber without a liner and a damping rate which is in the order of 20 db/sec lower than the resonant liner. These results should be used for comparison purposes only because the computing technique applied to obtain them has not been verified against the simplified model results as yet.

UNCLASSIFIED

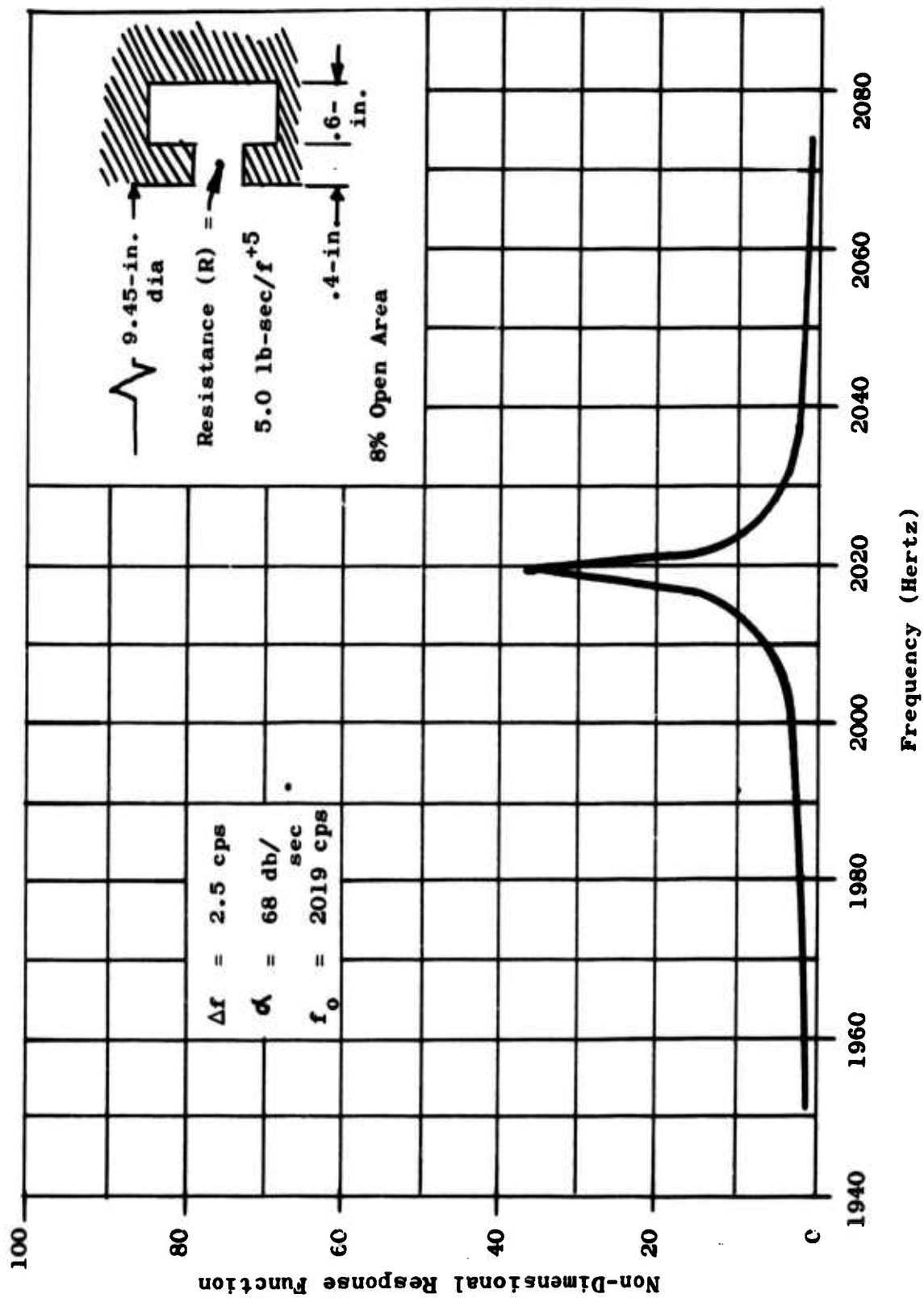


Figure 117. Non-Dimensional Chamber Response Function vs Frequency for a 2800 Hz

UNCLASSIFIED

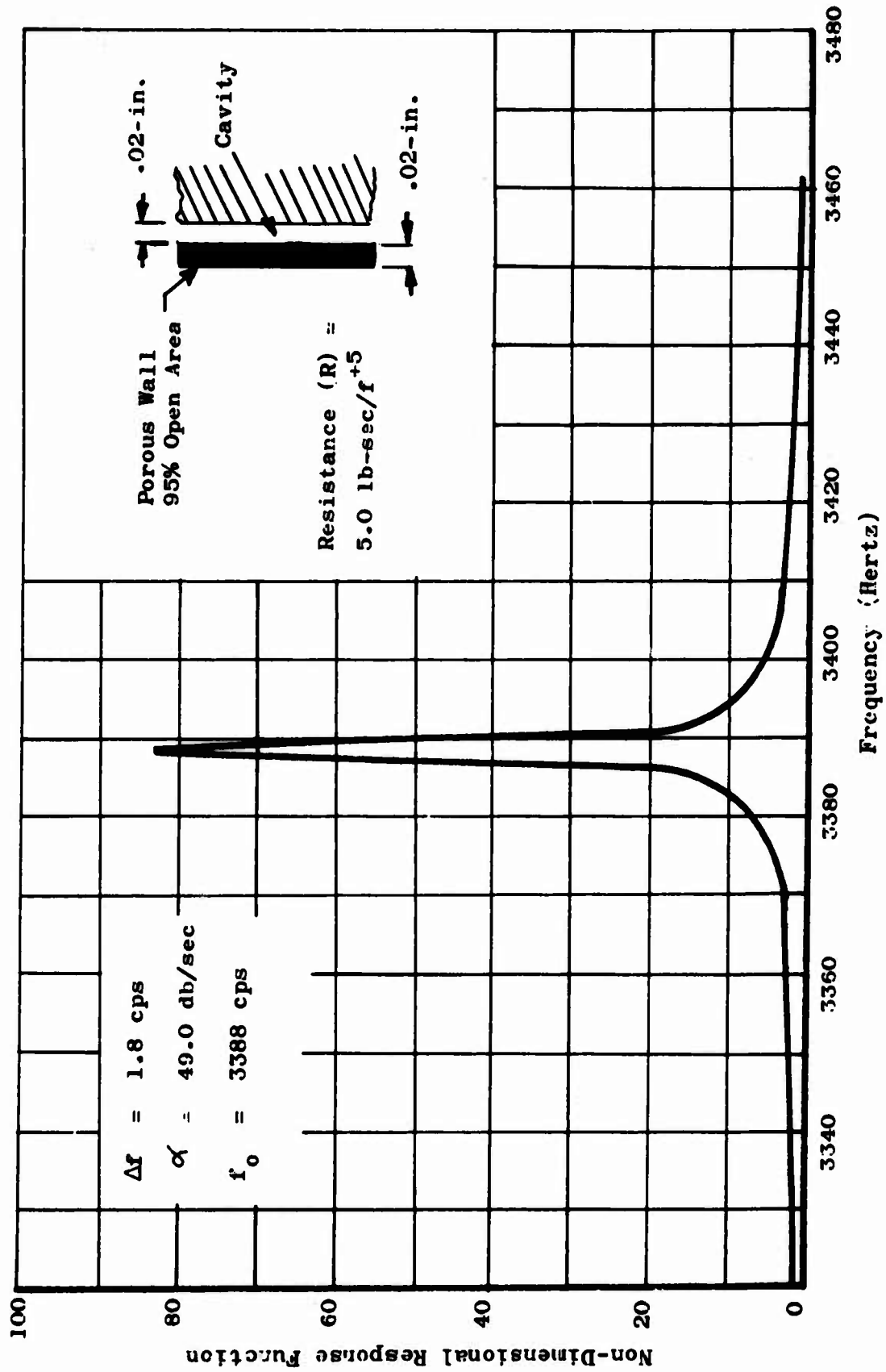


Figure 118. Non-Dimensional Chamber Response Function for a Rough 9.45-in. Chamber Wall

UNCLASSIFIED

UNCLASSIFIED

Chamber Diameter = 9.45-in.  
Liner Thickness = 0.4-in.  
Backing Distance = 0.6-in.  
Open Area Ratio = 0.08  
Orifice Diameter 2 0.20-0.25

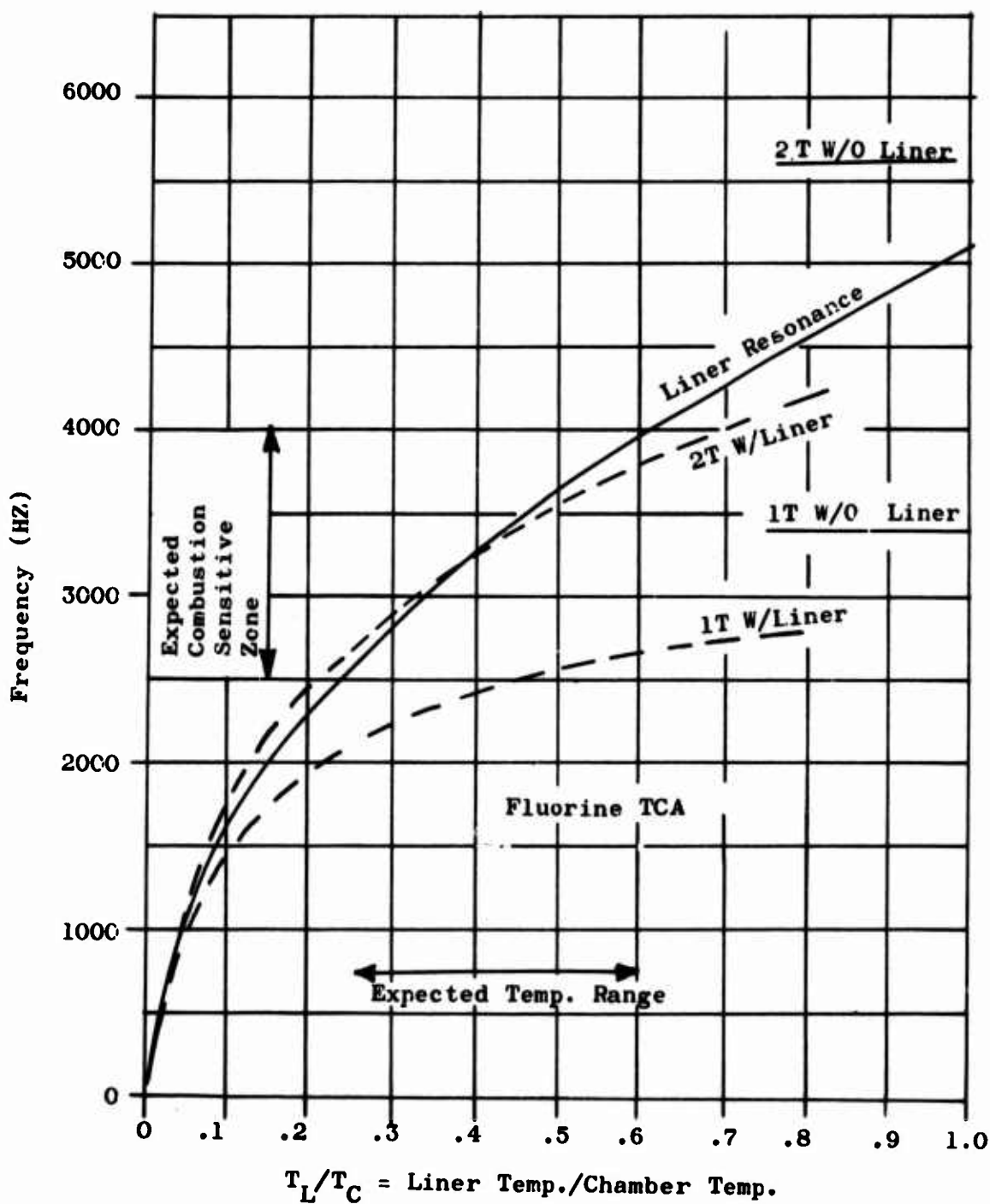


Figure 119. Frequency Depression of First and Second Tangential Modes as a Function of Cavity Temperature

UNCLASSIFIED

UNCLASSIFIED

It appears that the results obtained from the simplified analysis shown on Figure No. 79 are more reliable. The advantage of an analytical approach that treats the acoustic liner as an integral part of the combustion chamber is that it will predict the effect of the liner upon damping rate for each of the transverse modes and the change in the resonant frequencies of the system resulting from the introduction of the liner.

Because of the individual treatment of the backside cavity and the chamber cavity as well as the general treatment of the resonator neck, this analysis also can be used for what is generally referred to as a non-resonant liner. A modification of the Crocco-developed time-lag stability model(53), (54), (55) is used in the two previously discussed analyses. The modification consists of introducing the liner as a boundary condition at the chamber wall. The analysis is a linearized treatment of the combustion process using the small perturbation technique, which results in a prediction of the zones of instability as a function of two parameters ( $n$  and  $\tau$ ), where  $n$  is a gain parameter and  $\tau$  is a phase parameter.

The expected result of adding the liner is a shift in the stability zone to the right and upward as was shown on Figure No. 80, which means that the system would go from an unstable to stable combustion. The injector operating point was determined from empirical correlations of the type shown on Figures No. 120 and No. 121 which have been determined from an accumulation of data.

#### 7. IFAR Damper Analysis

In this analysis, it is assumed that the combustion is concentrated at the injector face. The acoustics of the chamber are described by the nozzle admittance, which is the relationship between perturbations in the axial and transverse velocity and pressure. Nozzle admittance depends upon the geometry of the nozzle, the frequency, and the mode being analyzed. The analysis is an extension of the liner  $n$ - $\tau$  theory developed by Crocco and others. This particular analysis is taken from Reardon(56), who deals with

- (53) Crocco, L. and Chang, S. I., Theory of Combustion Instability in Liquid Propellant Rocket Motors, AGARDograph No. 8, Butterworth's Scientific Publications, Ltd., London, 1956
- (54) Crocco, L., Grey, J., and Harrje, D. T., "Theory of Liquid Propellant Rocket Instability of Its Experimental Verification, ARS Journal, Vol. 30, No. 2, February 1960
- (55) Crocco, L., Harrje, D. T., and Reardon, F. H., "Transverse Combustion Instability in Liquid Propellant Rocket Motors," ARS Journal, Vol. 32, No. 3, March 1963
- (56) Reardon, F. H., An Investigation of Transverse Mode Combustion Instabilities in Liquid Propellant Rocket Motors, Princeton University Aeronautical Engineering Report No. 550, 1 June 1963

UNCLASSIFIED



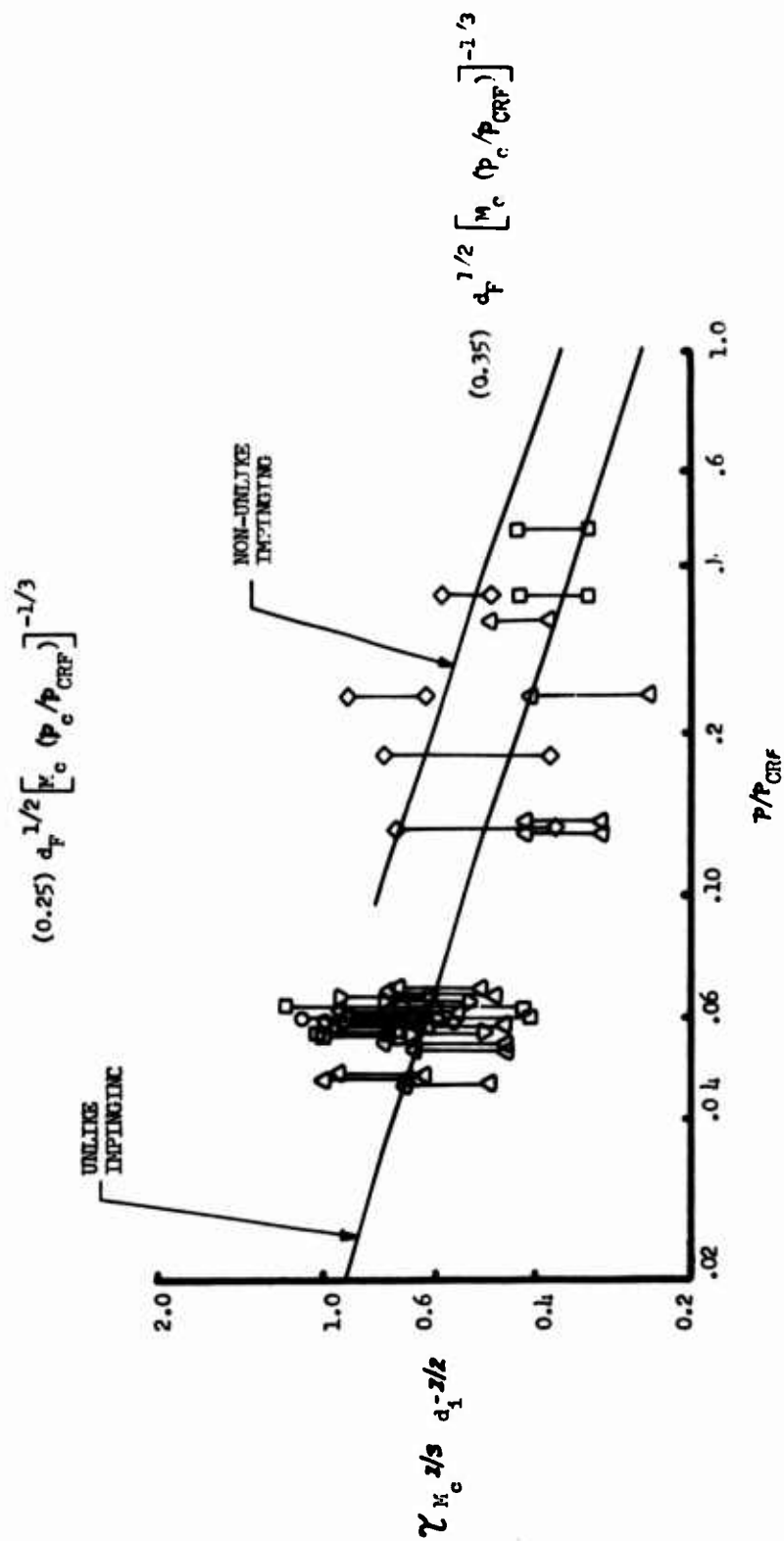


Figure 120. Fuel Controlling Stability Correlation, Hypergolic

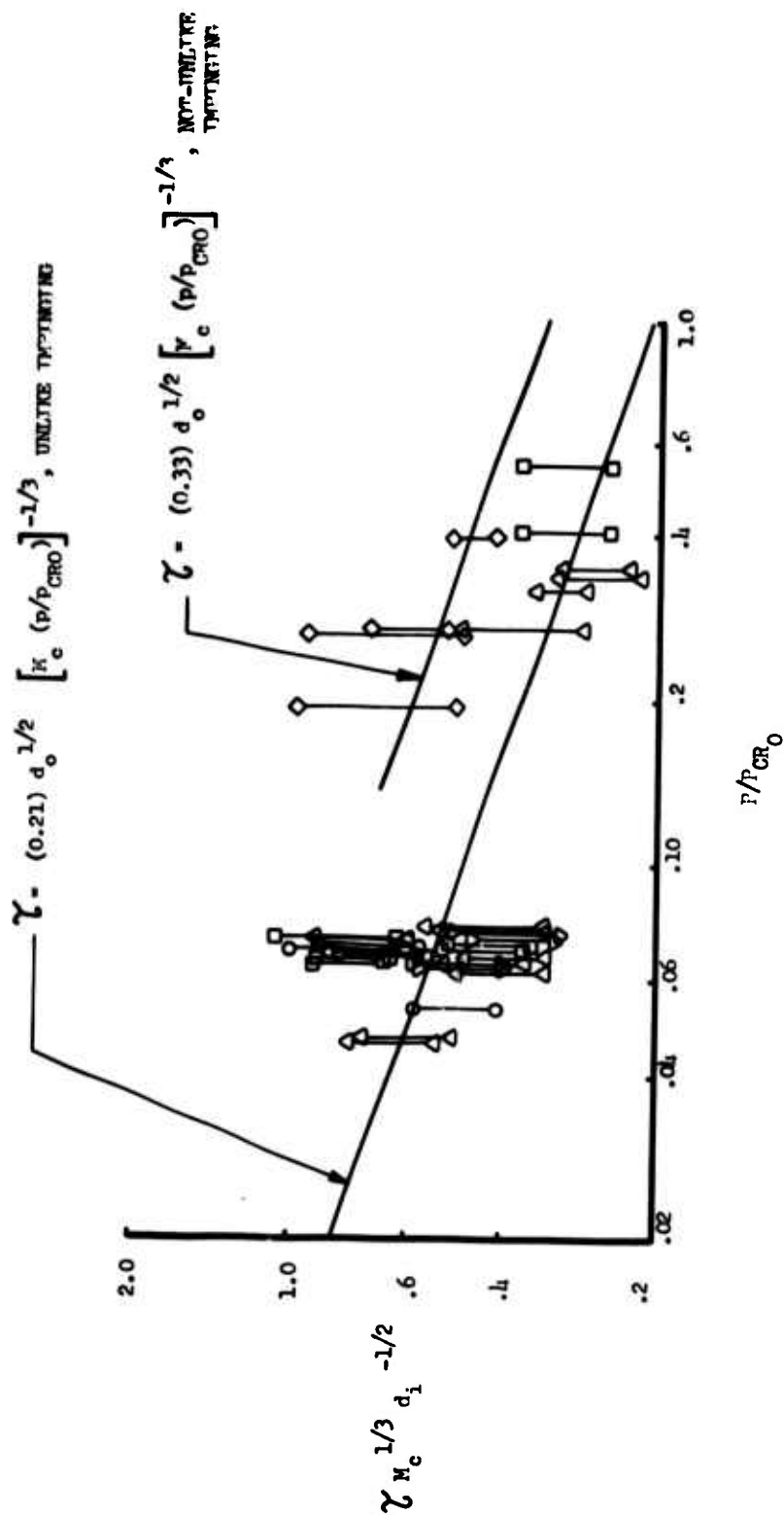


Figure 121. Oxidizer Controlling Stability Correlation, Hypersonic

the problem of non-uniform injection (i.e., injection density varies over the face of the injector). The same mathematical technique is applied in this analysis where the admittance of the face varies with position. In this case, the injection density is uniform, but at the outer edge of the injector there is a resonator which gives a different admittance in this region. The admittance of the resonator ( $Y_r$ ) was obtained from the literature<sup>(57)</sup>, except for the quarter wave tube which was obtained from another source.<sup>(58)</sup>

A similar analysis was accomplished to couple feed system oscillations to transverse mode acoustic oscillations in the combustion chamber.<sup>(59)</sup> After writing all dependent variables as a mean plus a perturbation ( $p = \bar{p} + p'$ ), the problem reduces to solving the acoustic equation for a cylinder (in this case, with zero length) with a nozzle at one end and an admittance that depends upon position on the other (injector) end.

For a cylinder, the most general expression for the solution of the acoustic equation

$$\nabla^2 p' + \Omega^2 p' = 0$$

is

$$p' = \sum_{h=1}^{\infty} \sum_{v=0}^{\infty} A_{vh} P_{vh}(z) R_{vh}(r) \Theta_v(\theta)$$

where

$$P(z) = A_{vh} \cosh \left[ (S_{vh}^2 - \Omega^2)^{1/2} z \right] + B_{vh} \sinh \left[ (S_{vh}^2 - \Omega^2)^{1/2} z \right]$$

$$R_{vh}(r) = J_v(S_{vh}r)$$

$$\Theta_v(\theta) = \cos v \theta$$

$$A_{vh} = \text{constants to be determined by the boundary conditions}$$

$$p' = \text{the perturbation in pressure}$$

(57) Blackman, A. W., op. cit.

(58) Beranek, L. L., Acoustics, McGraw-Hill Book Co., Inc., New York, 1954

(59) Waugh, R. C., et al, "A Mathematical Model for Transverse Mode Instability with Feed System Coupling for Titan IIIM," Presented at the Fifth ICRPG Combustion Conference, 1 October 1968

UNCLASSIFIED

$J_v$  = Bessel function of order  $v$

$S_{vh}$  and  $v$  = separation constants

$\Omega$  = the non-dimensional angular frequency,  $\omega r_c / c$

The axial velocity in the chamber is given by:

$$u' = \frac{1}{\gamma j \Omega} \sum_{h=1}^{\infty} \sum_{v=0}^{\infty} A_{vh} \frac{d P_{vh}(Z)}{dZ} R_{vh}(r) \Theta_v(\theta)$$

where  $\gamma$  is the ratio of specific heats.

The boundary condition at the injector is the sum of the generation rate of burned gas and the flow from the resonator matching the gas flow in the chamber.

$$(Y_r + Y_{nr}) p' = \bar{\rho} u' + \bar{u} \rho'$$

The symbol,  $\bar{u}$  is the chamber gas mean velocity near the injector and  $Y_{nr}$  is the combustion admittance. Using the momentum equation in the  $z$  direction and the isentropic relation between  $\rho'$  and  $p'$ , the above equation becomes

$$(Y_r + Y_{nr} - \frac{\bar{u}}{\gamma}) p' = - \frac{1}{\gamma j \Omega} \frac{dp'}{dZ}$$

All of the variables are non-dimensionalized. (60) Using these non-dimensional variables

$$\frac{p'}{\rho_r \gamma} \text{ and } \bar{\rho} = 1.$$

Then, using the assumed solution for  $R$  and  $\theta$  above, the equation becomes:

$$(Y_r + Y_{nr} - \frac{\bar{u}}{\gamma}) \sum_{h=1}^{\infty} \sum_{v=0}^{\infty} A_{vh} P_{vh} R_{vh} \Theta_v = \frac{1}{\gamma \Omega} \sum_{h=1}^{\infty} \sum_{v=0}^{\infty} A_{vh} \frac{dP_{vh}}{dZ} R_{vh} \Theta_v \quad \text{Eq. (12)}$$

(60) Reardon, F. H., op. cit.

UNCLASSIFIED

UNCLASSIFIED

The functions  $R$  and  $\Theta$  are orthogonal which allows solution for the coefficients  $A_{vh}$  in Equation (12).

$$\int_0^1 \int_0^{2\pi} R_{vh} H_v R_{pq} \Theta_q r dr d\theta = 0 \text{ if } v \neq q, h \neq p$$

$$= H_{pq} \text{ if } v = q, h = p$$

If both sides of Equation (12) are multiplied by  $R_{pq} \Theta_p$  and integrated, separate equations ( $q$  times  $p$ ) without summations result. For a 1T mode,  $v = 1$  and  $h = 1$ . For a 2T mode,  $v = 2$  and  $h = 1$ . These are the only modes considered in this analysis; therefore, only two of these equations need be retained: Using the solutions for  $R$  and  $\Theta$  given previously and recalling that the injector is at  $z = 0$ , for the 1T mode, Equation (12) becomes:

$$\frac{1}{\gamma \omega} (S_{11}^2 - \Omega^2)^{1/2} B_{11} H_{11} = A_{11} \iint Y_b R_{11}^2 \Theta_1^2 r dr d\theta + A_{11} (Y_{nt} - \frac{\bar{u}}{\gamma}) H_{11}$$

Eq. (13)

A similar equation can be obtained for the 2T mode.

For a given mode of oscillation, the boundary condition at the nozzle is determined by the nozzle admittance relation

$$\gamma U + \left( \frac{T_s}{\Omega} \right) P = 0$$

where  $U$  is the  $z$ -dependent factor in the axial velocity,

$$u' = U(z) R_{vh}(r) \Theta_v(\theta)$$

and  $T$  is an admittance coefficient which is obtained from an existing computer program.

From the momentum equations in the  $z$ -direction, it is found that

$$U = - \frac{1}{\gamma j \Omega} \frac{dP}{dz}$$

The nozzle admittance equation for the 1T mode then becomes

$$\frac{1}{\Omega} (S_{11}^2 - \Omega^2)^{1/2} B_{11} = - \frac{S_{11} T}{\Omega} A_{11}$$

Eq. (14)

UNCLASSIFIED

# UNCLASSIFIED

Equations (13) and (14) are two homogeneous equations in  $A_{11}$  and  $B_{11}$ . For these equations to have a solution, their determinant must be zero. The equation thus formed is the system characteristic equation, which characterizes the dynamics of the system and can be used to determine its stability. A  $n-\tau$  plot can be obtained from this equation.

To obtain the  $n-\tau$  plot, the factor  $\iint Y_r R^2 \frac{H_r^2}{d} dr d\theta$  must be evaluated.  $Y_r$  is zero in the center of the injector and is a function describing the resonator at the edge of the injector. The impedance of a Helmholtz resonator is given by  $\bar{\theta} + j\bar{\chi}$ , (61) where

$$\bar{\theta} = \frac{4}{\sigma \rho c} \left( \frac{\pi \mu \rho f}{g} \right)^{1/2} \left( 1 + \frac{t_1}{d} + \frac{\Delta_{nL}}{d} \right)$$

$$\bar{\chi} = \left( \frac{2\pi f_o l}{c \sigma} \right) \left( \frac{f}{f_o} - \frac{f_o}{f} \right)$$

where

- $\sigma$  = ratio of acoustic resonator orifice area to face area
- $\rho$  = gas density, lb-sec<sup>2</sup>/ft<sup>4</sup>
- $c$  = velocity of sound, fps
- $f$  = frequency, sec<sup>-1</sup>
- $\mu$  = gas viscosity, lb/sec-ft
- $g$  = gravitational constant, 32.2 fps<sup>2</sup>
- $t_1$  = acoustic resonator orifice thickness, ft
- $d$  = orifice diameter, ft
- $\Delta_{nL}$  = nonlinear correction factor, ft
- $f_o$  = resonant frequency, sec<sup>-1</sup>
- $l$  = effective length of orifice mass, ft

To obtain an expression for  $Y_r$ , the above expression is nondimensionalized in a manner consistent with the chamber non-dimensionalization. In addition,  $Y_r$  is an admittance per unit area. The area selected is somewhat arbitrary, except that it must be the same area used in the integral.

(61) Blackman, A. W., op. cit.



# UNCLASSIFIED

The impedance of the quarter wave tube also is  $\bar{\theta} + j\bar{\chi}$ , where

$$\bar{\chi} = -j \cos \left( \frac{2\pi f L}{c} \right)$$

$$\bar{\theta} = 0$$

$$L_Q = \text{length of tube}$$

## B. BASIS OF METHODS FOR STABILITY ANALYSIS

### 1. Description of Analytical Model

The method of analysis used to determine the stability characteristics of the various injectors is one developed by Mr. Crocco and his co-workers at Princeton University. (62)(63)(64)(65) Although there are some deficiencies in this theory (viz, it considers spontaneous or linear stability only and assumes a "black-box" approach to the combustion process), it was shown to be of considerable usefulness in the correlation of combustion stability behavior.

The theory is based upon the analysis of the stability of small perturbations from the mean operating conditions of the thrust chamber. For analytical simplicity, the gradual conversion of reactants to products in the liquid propellant combustion process is replaced by a step-function, thus defining a total combustion time lag associated with each element of propellant. It is assumed further that the combustion process is sensitive to changes in the local combustion chamber conditions (i.e., pressure, temperature, and gas velocity) only during the final portion of the total time lag. This portion is called the sensitive time lag and is denoted by  $\tau$ . The degree of sensitivity is measured by interaction indices. The pressure interaction index,  $n$ , measures the magnitude of the response of the combustion process to a pressure disturbance. The velocity interaction index,  $l$ , measures the response to a transverse gas-velocity perturbation. The velocity index is vectorial; therefore, it is most convenient to deal with its components,  $l_r$  and  $l_\theta$ , in the radial and tangential directions, respectively.

From the perturbed conservation equations for the flow with combustion in the thrust chamber, a characteristic equation is developed which establishes conditions for neutral stability (i.e., the conditions for which a small disturbance will neither grow nor decay). These "stability limit"

- (62) Crocco, L. and Cheng, S. I., op. cit., page 240
- (63) Crocco, L., Grey, J., and Harrje, D. T., op. cit., page 240
- (64) Crocco, L., Harrje, D. T., and Reardon, F. H., op. cit., page 240
- (65) Reardon, F. H., Crocco, L., and Harrje, D. T., "Velocity Effects in Transverse Mode Liquid Propellant Rocket Combustion Instability," to be published in AIAA Journal

# UNCLASSIFIED

UNCLASSIFIED

conditions are conveniently represented on the  $n, \tau$  plane. For the given thrust chamber geometry and operating conditions, there is a stability limit curve for each mode of high-frequency instability. The limit curves divide the  $n, \tau$  plane into stable and unstable regions. It is postulated that with each injector pattern, using a given propellant combination at a specific chamber pressure and mixture ratio, there are associated values of the sensitive time lag and interaction indices. If the point on the  $n, \tau$  plane for a given injector lies below the stability limit curve, the operation of the injector is expected to be stable. If the  $n, \tau$  point lies above the curve, oscillation combustion will result. Because the theory considers only small perturbation, the stability predictions refer to spontaneous instability only. For pulsed instability, only semi-quantitative results are obtainable.

The Sensitive Time Lag Theory has been used with good success in the correlation of experimental stability data from the experimental observations of combustion oscillations. Values of the stability parameters (the sensitive time lag and the interaction indices) can be inferred. The correlation of these stability parameters with injector design factors then can be used in the design of new injector patterns. Figures No. 120 and No. 121 showed the correlations for  $\tau$  that have been assembled to date. The latest correlations for the interaction index,  $n$ , show it to be essentially constant ( $0.68 \leq n \leq 0.82$ ) (Figure No. 122) for the type of injector being considered. Most of the patterns for which information is available are such as to have low values of the velocity index. For these reasons, only the pressure index is considered.

## 2. Analytical Assumptions

The approach taken in the stability analysis of the fluorine thrust chamber assembly injector was to assume that the F<sub>2</sub>/BA 1014 propellant combination would have a sensitive time lag,  $\tau$ , that would be approximately defined by correlations already established for the N<sub>2</sub>O<sub>4</sub>/A-50 propellant combination. Both fuel and oxidizer correlations were considered. Test results showed the fuel orifice size was the controlling factor. The similarity between A-50 and BA 1014 is demonstrated by the fact that they both contain a comparable amount of hydrazine, N<sub>2</sub>H<sub>4</sub>, (50% and 67%, respectively).

However, a review of published data and Aerojet-General experience with N<sub>2</sub>H<sub>4</sub> propellant indicated a possible risk of reduced stability margin as a result of the high percentage of hydrazine (N<sub>2</sub>H<sub>4</sub>) present in BA 1014. Hydrazine has a much more rapid pressure rise when it auto-ignites. These "pops" act as random perturbations in the chamber and are detrimental in that they may trigger high-amplitude oscillations in an otherwise stable combustion system. Although the presence of 24% MMH and 9% H<sub>2</sub>O makes the fuel more stable<sup>(66)</sup> than pure hydrazine, there is no experimental data available which indicates its relative stability.

(66) Weiss, R. R. and Klopotek, R. D., Experimental Evaluation of the Titan III Transtage Engine Combustion Stability Characteristics  
AFRPL-TR-66-51

UNCLASSIFIED

UNCLASSIFIED

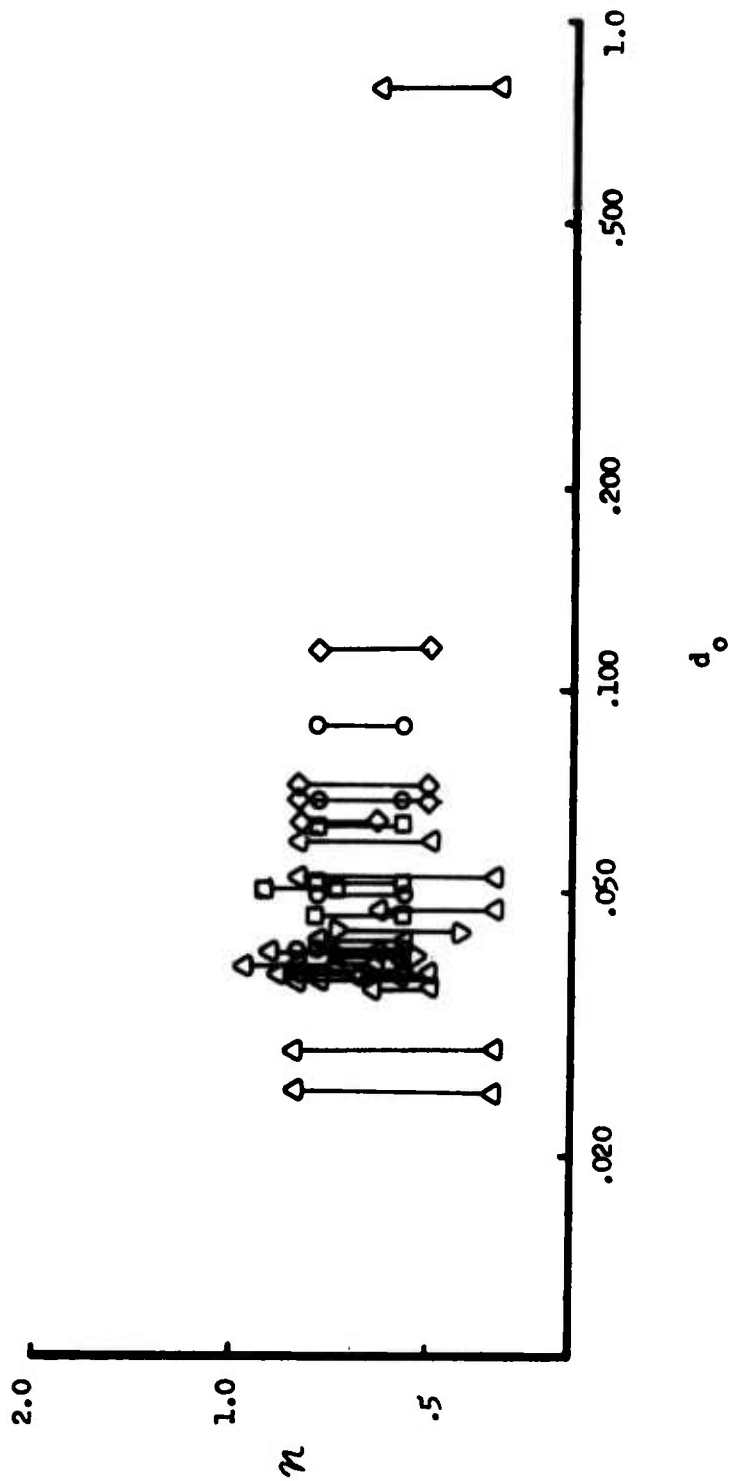


Figure 122. The Effect of Oxidizer Orifice Diameter upon  $n$ , Hypergolic

UNCLASSIFIED

UNCLASSIFIED

A review of currently available literature indicated the following:

- Injectors which were stable using MMH fuel have been unstable in the high frequency modes when operated with  $N_2H_4$ .
- There is no data available which indicates  $N_2H_4$  has been successfully demonstrated as a film coolant.

This and similar data lead some investigators<sup>(67)</sup> to conclude that the mono-propellant decomposition rate of  $N_2H_4$  is the initiator of the high-frequency instability. Fuel collects, decomposes, and the resultant "pop" initiates the instability. Random "pops" were not evident with injectors S/N 2 Mod 2, S/N 2 Mod 3, and S/N 7.

### 3. Injector Patterns

In reviewing injector performance, it is theoretically indicated that to improve performance, pattern changes should be made, wherein the number of injector elements are increased. Similarly, to improve compatibility, element orientation changes should be made which will provide a more uniform mixture ratio and reduced "winds" at the wall. This reduction in gas dynamic forces means shifting the elements closer to the edge of the injector.

However, in this program, it was found that both of these changes tended to destabilize the injector.

Empirical correlations indicated that the combustion stability operating zone primarily was determined by the fuel orifice sizes used. Chamber Mach number and chamber pressure also were factors but they were design constants and could be ignored for this comparison.

A preferential injection distribution effect is shown on a  $n$  and  $\tau$  plot, Figure No. 123, as an increase in the pressure interaction index,  $n$ , for the acoustic modes of the chamber. The injector operating zone correlations show that increased orifice sizes increased the stability of the 68-element injector. The test data indicated that it would be possible to increase the number of orifices while necessarily decreasing the orifice size, without significantly changing the stability if the stable injection distribution was maintained as shown on Figure No. 124. However, this conclusion only could be verified by testing.

(67) Ibid.

UNCLASSIFIED

UNCLASSIFIED

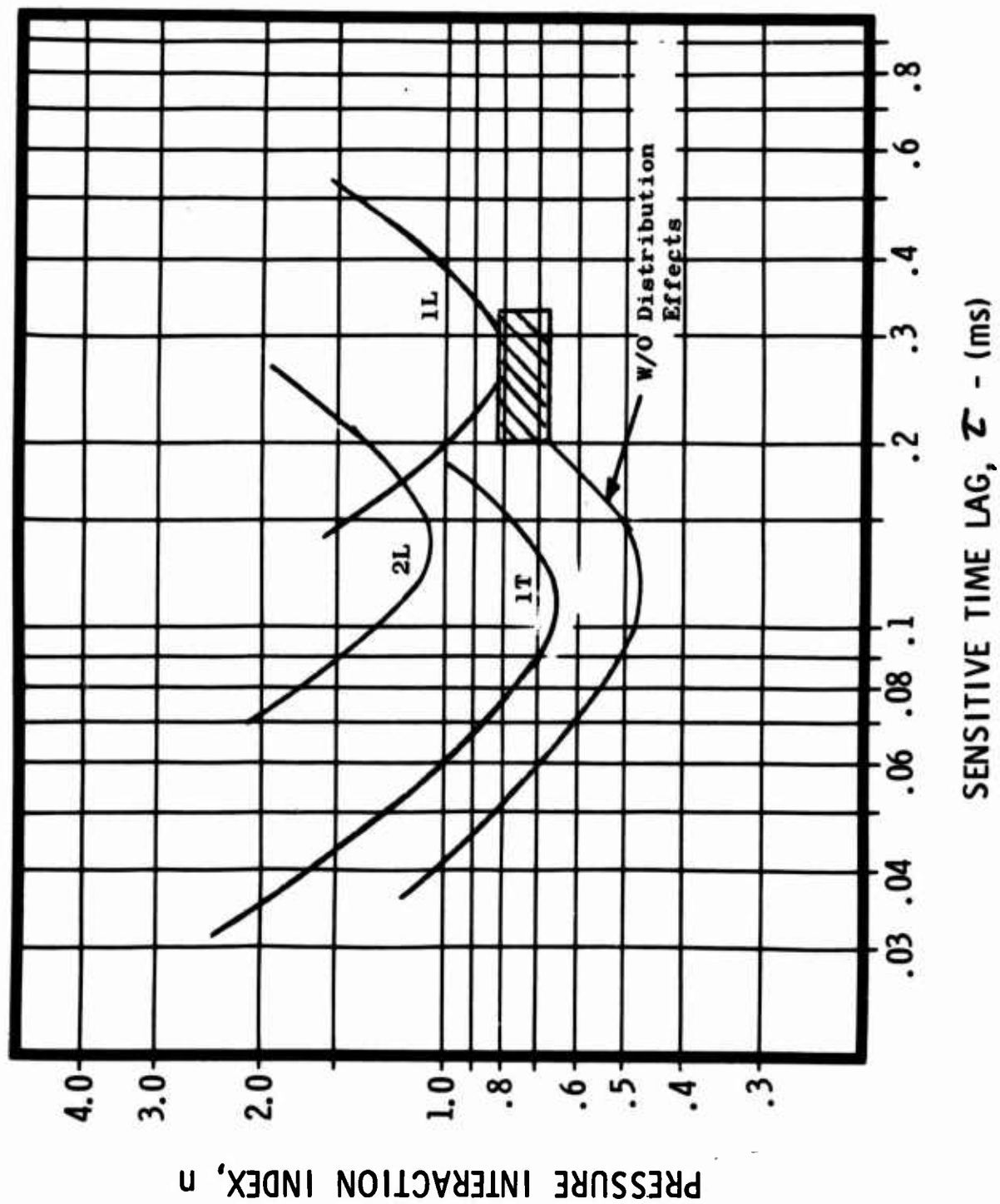


Figure 123. Injector S/N 2, Mod 3  $n/\tau$  Plot

UNCLASSIFIED

UNCLASSIFIED

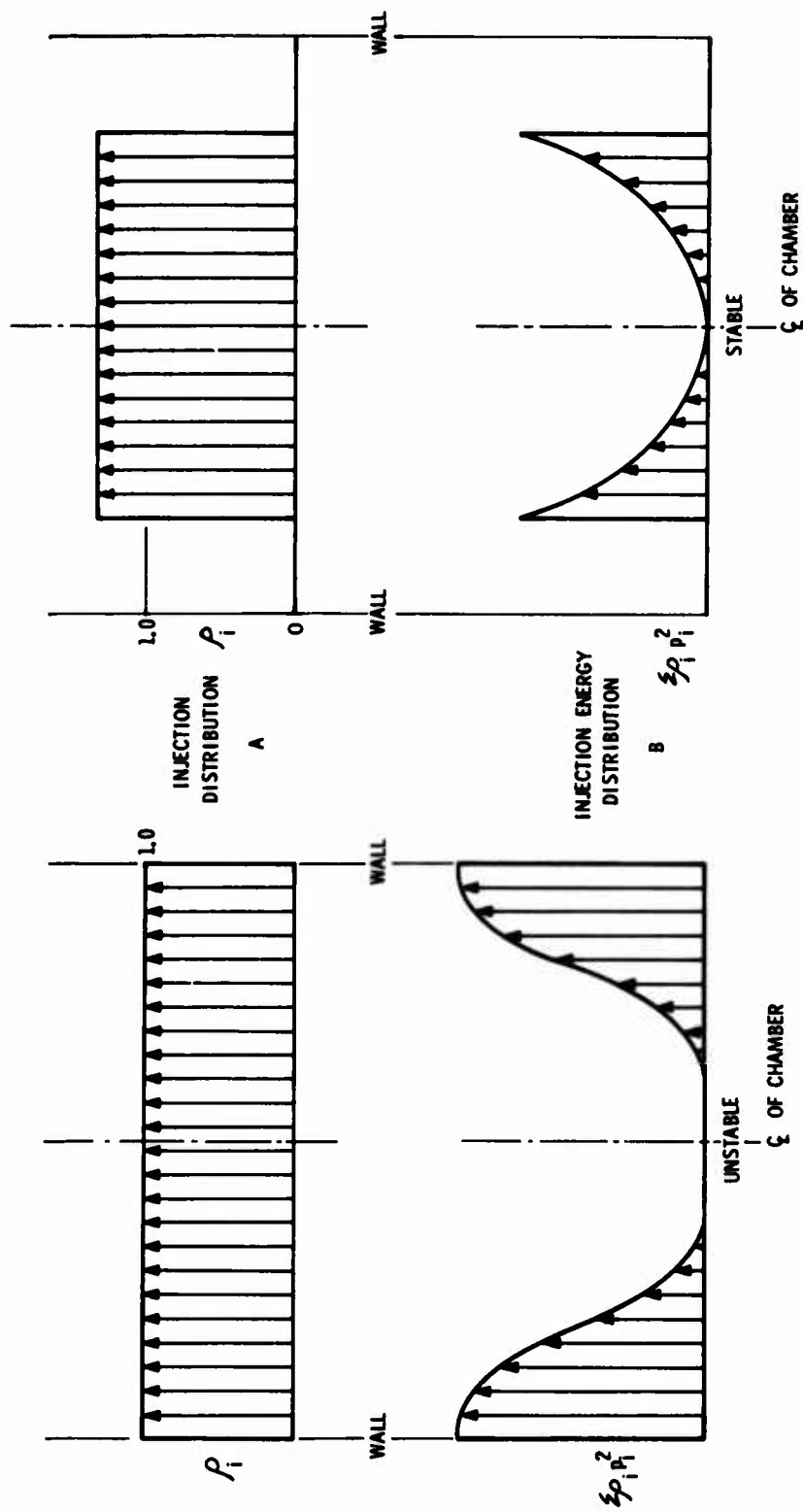


Figure 124. Effect of Injection Distribution Upon Stability

UNCLASSIFIED



UNCLASSIFIED

4. Results versus Predictions

The test results obtained in the fluorine thrust chamber assembly program are in agreement with the fuel orifice correlations. The test results indicate that the F<sub>2</sub>/BA 1014 propellant combination has combustion stability characteristics similar to the more common N<sub>2</sub>O<sub>4</sub>/A-50 combination. Subsequent to the analysis of the fluorine thrust chamber assembly stability, and making use of its test data, a new correlation for the sensitive combustion frequency was obtained which shows the only additional factor to be considered is the critical pressure of the propellants. This does not change the conclusions made because A-50 and BA 1014 both have critical pressures of approximately 1700 psia.

All the correlations used to predict stability yielded the same result, which was that the first tangential acoustic mode of the chamber at 3500 cps would be the most probable and would definitely occur in the case of the 215-element and 344-element injectors. Also, it possibly could occur in the 158-element and 98-element injectors.

The stability prediction for the 68-element injector was more involved because it made use of injection distribution as a means of combustion stabilizing the first tangential mode. The proof of the stabilizing influence of injection distribution is indicated by the stable operation of the 68-element injector with only the smaller orifices of the 98-element injector left after 30 rather large doublet orifices were welded shut at the injector perimeter.

UNCLASSIFIED

**UNCLASSIFIED**

**APPENDIX III**

**METHOD OF CONDUCTING A THERMAL DESIGN ANALYSIS**

**Page 254**

**UNCLASSIFIED**

# UNCLASSIFIED

## APPENDIX III

### METHOD OF CONDUCTING A THERMAL DESIGN ANALYSIS

#### A. INTRODUCTION

This appendix summarizes the basic approach to the thermal design of injector-ablative thrust chamber assembly and points out the problems to be avoided in such a task. The over-all design effort requires three separate, yet related thermal analyses: the ablative composite, the injector, and the total system (liner, injector, valves and environment). They are separate in the sense of being done one-at-a-time, but related by having physically common boundaries or boundary conditions. In addition, the thermal design analyses must be fully integrated with the structural analysis.

#### B. ABLATIVE CHAMBER ANALYSIS

Design criteria must include material selection, allowable temperature limits, char and erosion depths and system duty cycle. Other components of the system must also be considered, notably the injector which sustains postfire heat soakback from the chamber, and vehicle components which may limit exterior wall temperatures.

An ablative chamber analysis is predicated on knowing the material thermal properties and the gas-side boundary conditions. Quite often these factors are not well known. In particular, material properties are difficult to obtain, or are available only in a limited temperature range, usually near ambient conditions. The more sophisticated the analytical treatment, the more important it is to have accurate properties data, and seemingly the more scarce that information becomes. The simplified Bartz expression for film coefficient is usually adequate for gas-side boundary conditions; however, experimental values derived from instrumented uncooled steel chambers are preferable, especially when film cooling is significant.

The initial thermal analysis usually involves a one-dimensional radial study at several axial locations; one of these stations is almost always the throat, which has the most severe thermal conditions. Such studies are done by computer and a number of programs of varying sophistication are available. The simplest treat the char process as identical to a nonreversible phase change, at a constant char temperature and heat of char, that being a latent heat equivalent hiding all the sins of omission and commission in this approach. This type of program was used for the present design. Such a program may or may not account for surface erosion, internal convection by pyrolysis products, etc. Regardless of the shortcomings that may justifiably be ascribed to such programs, it can be said in their favor that they work, once the pseudo-property values are correctly interpreted.

UNCLASSIFIED

More sophisticated programs are gradually coming into popularity. These treat surface chemistry effects between the boundary layer gases, the liner reinforcement material, and the pyrolysis gases; they can account for multiple internal pyrolysis reactions, internal convection by the pyrolysis gases, surface erosion by chemical, mechanical, and thermal mechanisms, etc. For such programs too, correct interpretation of thermal properties is required, but on a much higher plane and in greater amounts than for the simpler programs. Thus there is still the limitation that the "answer" must be known before the problem can be solved.

The design process is essentially iterative. For a given duty cycle or firing duration, various material thicknesses are adjusted until various temperature and char depth requirements are met. Generally the process proceeds faster by starting with an excessively thick wall, and quite often only the longest firing duration of the duty cycle need be considered. A two dimensional analysis may be introduced if a truly optimum weight chamber is desired and if sufficient data exist to define the injector pattern influences.

#### C. INJECTOR ANALYSIS

While the chamber analysis is difficult by unknown material properties, the injector analysis is stymied by uncertain boundary conditions on the gas side and to a lesser degree on the coolant side. Factors which must be considered in injector thermal design, include the maximum face temperature, the burnout or ultimate heat flux of the coolant, and the bulk temperature rise and pressure drop of the coolant.

No theoretical correlation has been developed for the convective film coefficient on the injector face, presumably because of the complexity of the physical processes involved. Industry's approach is to treat the coefficient as being about equal to the Bartz coefficient on the adjacent chamber wall. Based on face thermocouple data, the face coefficient was found in this program to be about 0.4 times the Bartz coefficient.

The coolant side boundary condition is usually nucleat boiling for subcritical pressure coolants, and the prime consideration is the burnout heat flux. (For super-critical pressure coolants the consideration is the ultimate heat flux). While burnout data are readily available for most propellants, data scatter at the low velocities usually encountered in the injector manifold design is considerable, and it introduces some uncertainty into the analysis.

Depending on injector geometry, a simple one-dimensional conduction analysis may prove adequate for the thermal design purposes, or at least may provide quite conservative conclusions (after indicating the need for a two-dimensional analysis). The steady-state heat balance is made between the wetted surface of the coolant passage, which is taken to be at the coolant saturation temperature because of the nucleate boiling condition, and the combustion products; from this the gas-side surface temperature and heat flux can be found.

UNCLASSIFIED

UNCLASSIFIED

Excessive temperatures call for the coolant passages to be closer to the gas-side surface and more closely spaced; fluxes higher than the burnout heat flux (usually not physically possible without eventual material failure) require larger wall thicknesses between the face and the coolant passages, or more likely higher coolant velocities. In other words, alleviating a temperature problem worsens the flux problem, and vice versa.

The coolant bulk temperature rise can be determined by a simple heat balance. While the average rise for the total flow is usually small, the coolant in individual passages may be subject to overheating, by virtue of low flow rates or null velocity points. The rise in individual passages can be found from a series of heat balances to determine the rise between orifices, accounting for the correct weight flow in each section of the passage. Excessive bulk temperature rise in individual channels can be remedied by manifold design changes.

#### D. SYSTEM ANALYSIS

A given injector-chamber design may be thermally adequate for a given firing duration, and yet thermal problems may arise during coast periods. Injector heating after shutdown, due to radiation from the hot chamber surface as well as conduction via the flange, may be severe. Temperatures may be sufficient to cause auto ignition of the fuel or structural impairment. A thermal analysis of the entire system is necessary to avoid these hazards. A thermal network analyzer computer program is a suitable means of analysis. Such an analysis of the present design indicated that high injector temperatures would prevent refiring after short coast periods because of the danger of fuel detonation. Corrective design involved the addition of a rechargeable heat sink, termed a "thermal accumulator," to the injector back plate.

A related problem which should not be overlooked in the system analysis is postfire propellant valve overheating caused by chamber heat soakback. This was found not to be a problem during this program.

UNCLASSIFIED

UNCLASSIFIED

APPENDIX IV

FABRICATION CONTROL OF ABLATIVE CHAMBERS

Page 258

UNCLASSIFIED



# UNCLASSIFIED

## APPENDIX IV

### FABRICATION CONTROL, ABLATIVE CHAMBER

It is necessary that planned control be exercised of the many variables encountered during the fabrication of an ablative chamber if it is to satisfy the design requirements. Planned control includes knowledge and documentation of the supplier's Prepreg material properties, unless they are proprietary. The documented control of materials and fabrication processes provides:

- greater assurance that fabricated part will meet design requirements
- an increased potential of part reproducibility
- a basis for performance analysis

The following are some requirements and procedures that were applied in the fabrication of the ablative chambers tested in this program. The items listed were established for specific designs, but they are suitable as a base for developing similar controls of any ablative chamber design. (68)

- A fabrication plan defining the method of tape wrapping, assembly procedures, cure cycles, prepreg properties and tape wrapping parameters was established prior to fabrication. Parameters which were identified and recorded included the following:
  - Prepreg Properties
    - Percent resin flow
    - Percent volatiles
    - Degree of polymerization
    - Resin content
    - Tack
  - Tape Wrapping
    - As wrapped density
    - Percent debulk
    - Fabric reorientation
    - Roller pressure
    - Tape temperature
    - Billet temperature
    - Wrapping speed
- Resin content and resin advancement for each Prepreg were documented. Infra-Red Polymerization Index (IRPI) and acetone extraction were used to measure resin advancement.

(68) Evaluation of Characteristics Affecting Attainment of Optimum Properties of Ablative Plastics, Vol. II, Contract AF 04(611)-10933, Report AFRPL-TR-68-29, February 1968

UNCLASSIFIED

## UNCLASSIFIED

- Acetone extraction was limited to 0.5% or below per Federal Test Method Standards (FTMS) No. 406 method 7021 for cured components.
- Alcohol penetrant inspection per specification AGC 36417 was required.
- Cleanliness was in accord with specification AGC-46350, Level H. Components were protected from surface contamination during storage or delays.
- Graphite fabric from Union Carbide Co. was grade WCA.
- Crushing or damaging of the Prepreg tape during fabrication was prohibited. Folded or overlapping tape on the mandrel surface was minimized.
- At least two thermocouples were used to record part temperature during the entire cure cycle. All cure cycle data, vendor certification, and deviations were recorded.
- Components were cured on mandrels for three hours at  $300^{\circ}\text{F} \pm 10^{\circ}\text{F}$  and 200 psig minimum. The WB 2230 overwrap on chambers S/N 001 and 002 was cured at 100 psig and  $300^{\circ}\text{F} \pm 10$  for 3 hours.
- Tangential radiographic inspection of the component parts was required at 120-degree increments. Inclusion and separation of tape-wrapped plies were to be located, recorded, and reported. There were several small, 0.025-in. to 0.035-in. diameter, inclusions in the silica overwrap near throat station in both chambers S/N 001 and 002. Both chambers had indications of minor delaminations in the low temperature insulation, WB 2230, near the throat station. This was not considered serious. The AGCarb-101 throat insert in S/N 001 chamber contained a delamination just upstream of the throat which was exposed during final contour machining. The part was accepted. No inclusions or delaminations were detected in chamber S/N 003.
- Prior to each overwrap application, the surface to be wrapped was sanded, acetone-wiped, and a thin coat of MIL-R-9299 resin applied.
- The material initially used in the AGCarb-101 components for all three chambers, S/N's 001, 002 and 003, was graphite fabric reinforced phenolic laid up with bias cut tape. S/N 001 and 002 throat inserts were layed-up in a female mold. S/N 3 used a male mandrel. Although tape overlapping on the male mandrel and folds was minimized, the SN 3 liner had unexpected wrinkles. The oversized components were carbonized and graphitized. Oversize components were necessary to allow final machining after a 4 to 6% shrinkage during the graphitization process. The following are the specific gravities before and after processing:

UNCLASSIFIED

# UNCLASSIFIED

	<u>S/N 001</u>	<u>S/N 002</u>	<u>S/N 003</u>
Carbonizing Cycle			
Before	1.15	1.16	1.44
After	1.0	0.99	1.24
Graphitizing Cycle			
After	1.29	1.23	1.44

- The densities of the cured components and part fabric orientation are shown on Table XVIII.
- Joints at each end of the throat inserts were sealed with RTV60 silicone rubber. The mating surfaces were configured to provide a bearing contact area of 90% of that contact area. The joint gap did not exceed 0.015-in.
- The WB2230 was overwrapped with four layers of glass fabric, phenolic resin impregnated, specification AGC-44050, Type III.
- The impregnated glass fabric was overwrapped with four layers of glass filament roving (20 end), specification AGC-44205.
- The chamber assemblies were weighed to the nearest 0.5 lb. These weights were:
  - S/N 001 - 224.5 lb
  - S/N 002 - 303 lb
  - S/N 003 - 240 lb
- The thrust chambers were packaged per AGC-46387, Class 1. Caution was exercised to avoid standing chambers S/N 001 and S/N 002 on unprotected ends.
- Changes and deviations in processing were approved by the cognizant engineer. These included repair procedures on chamber S/N 002 for an undersize outer diameter surface at the downstream tip of the AGCarb-101 insert and the undersized chamber-nozzle extension flange.
- A 1-1/4-in. minimum length full section end ring from each component was supplied with the final assembly for material analysis.

UNCLASSIFIED

UNCLASSIFIED

TAB

COMPONENT DENSITIES AND

	DENSITY (GRAMS PER CUBIC CENTIMETER)			FABRIC ORIENTATION (DEGREES TO CENTERLINE UNLESS NOTED)			% RESIN FLOW	%
	S/N 001	S/N 002	S/N 003	S/N 001	S/N 002	S/N 003		
A. FM 5064, Forward Liner	1.45	1.42		45	45		9.86	
B. WB 8207, Aft Liner	-	1.38		20	20		6.68	
C. WB 8217, High Temperature Insulation, Chamber Section	1.37	1.41		0	0		9.86	
D. WB 8207, High Temperature Insulation Throat Insert Assy	1.37	1.39		45	45		6.23	
E. WB 2230, Low Temperature Insulation Throat Insert Assy	1.71	1.72		0 To Surface	0 To Surface		6.23	
F. WB 2230, Low Temperature Insulation Under Forward Flange	1.69	1.72		135	135		6.23	
G. WB 2230, Overwrap	1.70	1.71		0 To Surface	0 To Surface		6.23	
H. AGCarb-101 Throat Insert	1.29	1.23		5 To Surface	5 To Surface		0.7	
I. AGCarb-101 Liner			1.44	5 To Surface	5 To Surface	10 To Surface	4.5	
J. FM 5072, High Temperature Insulation			1.42			45	10.3	
K. FM 5067, Low Temperature Insulation			1.70			0 To Surface	11.2	

- (1) Extraction index, values in percentages
- (2) Based on roller pressure
- (3) Estimated - This is not acceptable as it produced excessive wrinkles in the cured component
- (4) Hand layup



S/N 001 & 002  
(S/N 002 Depicted)

TABLE XVIII

## DENSITIES AND FABRIC ORIENTATION

PREPREG PROPERTIES					TAPE WRAPPING CONDITIONS						
RESIN FLOW	% VOLATILES	DEGREE OF POLYMERIZATION INDEX	% RESIN CONSTANT	TACK, LBS	CALC. AS WRAPPED DENSITY, GMS/CC	PERCENT DEBULK	FABRIC REORIENTATION DEGREES TO CENTERLINE	ROLLER PRESSURE LBS PER IN. WIDTH	TAPE TEMP °F	BILLET TEMP °F	WRAPPING SPEED FT/MIN
9.86	3.1	.77	31.0	13	1.36	95	43	150	250	100	5.5
6.68	5.35	90.86 <sup>(1)</sup>	31.86	72	1.25	90	18	175-260	210	141	7-19
9.86	4.37	92.15 <sup>(1)</sup>	34.25	55	-	-	0	250	205	100	24
6.23	3.1	89.5 <sup>(1)</sup>	29.29	45	1.25	90	43	341	180	105	18-25
6.23	3.1	89.5 <sup>(1)</sup>	29.29	45	1.36	80	0 To Surface	250	200	120	17
6.23	3.1	89.5 <sup>(1)</sup>	29.29	45	1.53	89	133	186	210	110	3.3
6.23	3.1	89.5 <sup>(1)</sup>	29.29	45	1.54	90 <sup>(2)</sup>	0 To Surface	250	210	140	13.3
0.7	2.7	84	25.2	5	N/A <sup>(4)</sup>	N/A <sup>(4)</sup>	6	N/A <sup>(4)</sup>	N/A <sup>(4)</sup>	N/A <sup>(4)</sup>	N/A <sup>(4)</sup>
4.5	3.9	80	34.8	-	-	60 <sup>(3)</sup>	5-13	45	-	-	-
10.3	5.1	-	36.0	-	-	-	43	108	140	-	-
11.2	4.7	-	31.2	-	-	-	0 To Surface	N/A <sup>(4)</sup>	N/A <sup>(4)</sup>	N/A <sup>(4)</sup>	N/A <sup>(4)</sup>



S/N 003

UNCLASSIFIED

APPENDIX V

TEST FACILITIES AND TEST OPERATIONAL PROCEDURES

Page 263

UNCLASSIFIED



# UNCLASSIFIED

## APPENDIX V

### TEST FACILITIES AND TEST OPERATIONAL PROCEDURES

#### A. FACILITIES

All testing was accomplished in Aerojet-General's Test Area J at the Sacramento Facility. Either Test Stand J-2 or Test Stand J-4 was used depending upon the test objectives. Test Stand J-2 is a sea-level facility and Test Stand J-4 is a simulated altitude facility. Test Stand J-2 was limited by liquid fluorine tankage capacity to tests of approximately 50 sec duration. Simulated altitude duration capability of Test Stand J-4 exceeds 200 sec. Test Stand J-2 exhaust products were vented to the atmosphere while a water scrubber was used to control the exhaust products from Test Stand J-4.

All 30 tests with the uncooled steel chambers and the water-cooled chambers were conducted at Test Stand J-2. These tests included injector checkout, pulse, acoustic resonator, and initial compatibility. The 10 long duration, simulated altitude tests with ablative combustion chambers were conducted at Test Stand J-4.

##### 1. Test Facility J-2

Test Stand J-2, which is a flexure plate thrust stand mounted to a concrete base, is a horizontal firing position. It has a thrust measurement capability of up to 10,000 lb. Propellants are pressure-fed from a 50 gal, 1440 psig rated oxidizer tank and a 200 gal, 1400 psig fuel tank. The oxidizer tank has a liquid nitrogen jacket and is externally insulated with foamed-in-place insulation.

The liquid fluorine run line from the tank to the test stand is 1.5-in. diameter stainless steel pipe rated at 1320 psig. A liquid nitrogen jacket surrounded the run line up to an Annin start valve, which was cored to minimize the unjacketed line length feeding the injector. Foamed-in-place insulation was used at non-jacketed transition sections. The injector inlet lines downstream of the start valves were not insulated.

All joints in the oxidizer feed system were welded, except those at the flanges of the single turbine type flowmeter and the start valve.

The fuel was fed to the test stand through 1-in. diameter stainless steel pipe. There was a single fuel flowmeter flanged into place upstream of the propellant valve.

Helium was used to pressurize the oxidizer system. Gaseous nitrogen was used as the fuel pressurant.

A propellant line schematic of the Test Stand J-2 facility, showing the line lengths and instrumentation locations, is presented as Figure No. 125.

UNCLASSIFIED

UNCLASSIFIED

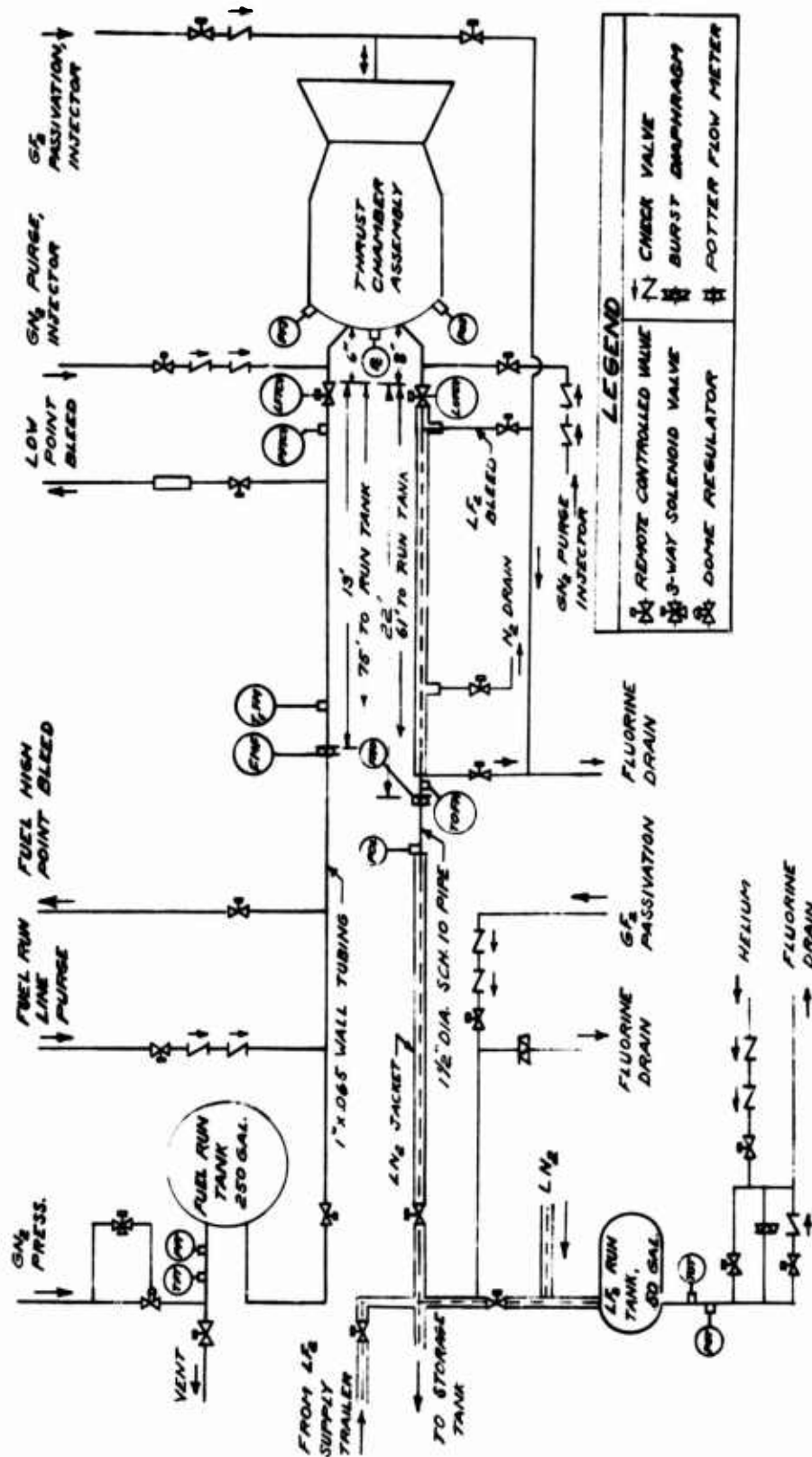


Figure 125. Test Stand J-2 Plumbing Schematic

UNCLASSIFIED

# UNCLASSIFIED

## 2. Test Facility J-4

Test Stand J-4 also is a horizontal firing position. The entire thrust frame is a flexure plate arrangement mounted in a 15 ft x 17 ft x 10 ft high altitude chamber which is connected into an array of stream ejectors capable of maintaining a 100,000 ft simulated altitude for 25 sec at 40,000 lb thrust or for 200 sec at the contractually specified 7000 lb thrust level. The over-all Test Stand J-4 complex is shown on Figure No. 126.

Both propellant tanks are 1000 gal units with a 2160 psig capability. A second 1000 gal oxidizer tank is used for storage purposes. The oxidizer tanks are triple-walled, stainless steel units which are liquid nitrogen and vacuum jacketed. Outlets are 2.0-in. in diameter. The 2.0-in. fuel and oxidizer feed lines from the tanks to the Annin stand valves were similar to those of Test Stand J-2 except that the oxidizer system had two turbine type flowmeters. A schematic of the Test Stand J-4 facility showing line lengths and instrumentation locations is presented in Figure No. 127.

### B. CLEANLINESS

The success of the test program was directly related to the cleanliness of all the circuitry exposed to  $LF_2$  prior to its entry into the facility and the injector. Strict adherence to the subsequently described cleaning procedure resulted in the accomplishment of 40 tests without experiencing a fire, line failure, or seal failure.

The basic procedures were successfully demonstrated during a previously conducted  $LF_2$  program.<sup>(69)</sup> The procedures were further simplified from the results of a literature search. The entire cleaning procedure consisted of basically two steps; removing foreign matter followed by passivation. This procedure was applied to the injector, pressure transducer lines, transducers, thermocouples, valves, and all of the other components subject to contact with  $LF_2$ . The run line was cleaned at the time that the facility was initially activated. When not in use, this run line was capped and pressurized with dry helium. Whenever a component was replaced or the continuity of the run line was disturbed, it was repassivated. The injector was recleaned and repassivated whenever it was removed from the test site.

Although it may appear that the passivation procedure could have been simplified without adverse effects the established procedure was highly successful. Since it was only a supporting consideration in the program, no effort was made to simplify it.

### 1. Initial Cleaning

The removal of alien matter from a part was accomplished with standard flushing and rinsing agents followed by purging and drying with hot gaseous nitrogen. The procedure was repeated until the cleanliness quality

(69) Aerojet-General IR&D, "Advanced Transtage Fluorine Feasibility Program," 1964

# UNCLASSIFIED

UNCLASSIFIED

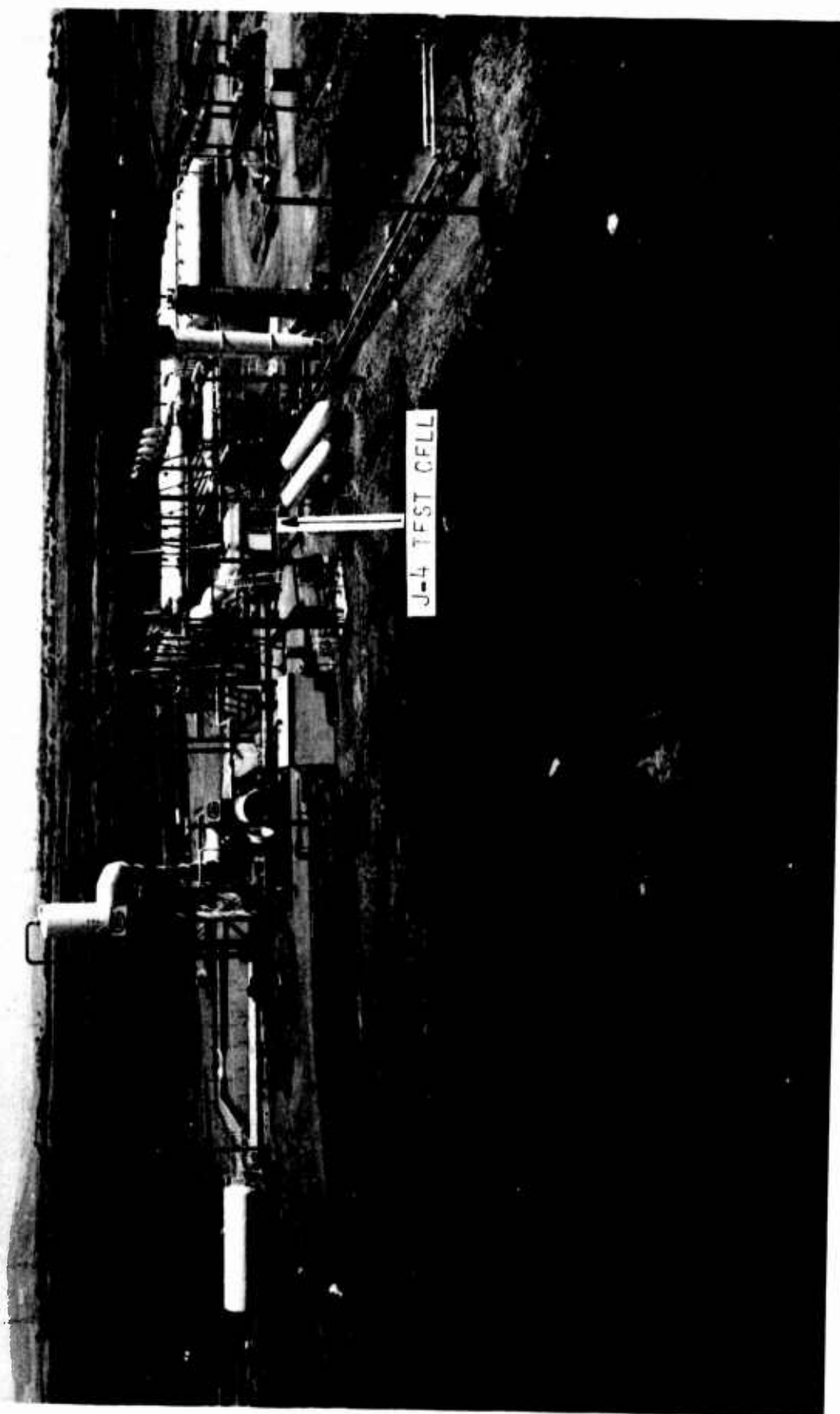


Figure 126. Test Stand J-4 Complex

UNCLASSIFIED

UNCLASSIFIED

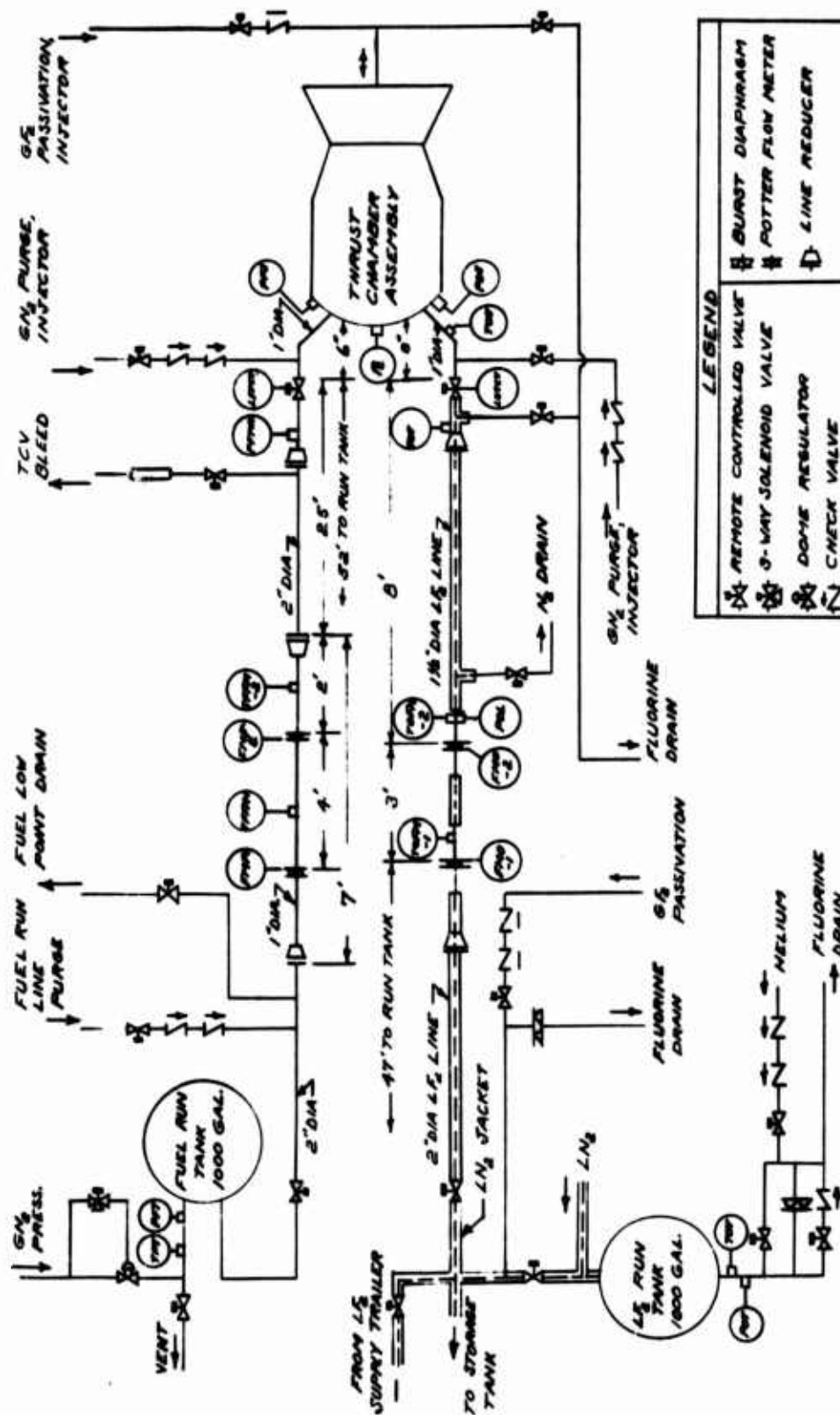


Figure 127. Test Stand J-4 Plumbing Schematic

UNCLASSIFIED

## UNCLASSIFIED

was equal to or better than that of Level E<sup>(70)</sup>. The components, including the injector, were processed under controlled environmental conditions, then it was sealed in a heavy plastic bag and the part remained packaged<sup>(71)</sup> until needed.

### 2. Passivation

The LF<sub>2</sub> run line components were passivated after installation. Passivation of the injector was more easily accomplished prior to its installation into the test stand. The workhorse steel combustion chamber with a closure plate on the exit end and blank flanges on the propellant inlet flanges provided a simple as well as effective pressure vessel for conducting the passivation treatment.

The following passivation procedure was almost identical for both the injector and test stand LF<sub>2</sub> run line:

- Evacuate the system with a GN<sub>2</sub> aspirator.
- Introduce the GF<sub>2</sub> slowly until the system pressure reached 5 to 10 psig. Hold system at this pressure for 15 min to 20 min.
- Increase the GF<sub>2</sub> pressure in the system to approximately 50 psig. Hold system at this pressure for 10 min to 15 min.
- Increase the GF<sub>2</sub> pressure in the system to approximate working level (80 psig to 100 psig for injector and approximately 250 psig for the run line). Hold system at this pressure for 3.5 hr to 4.0 hr.
- Vent the system and then lock with 5 psig GF<sub>2</sub>.

The pressure recorders were monitored during each hold period for any pressure change, particularly a rise which would indicate the reaction of fluorine with a contaminant.

### C. SAFETY

#### 1. Personnel Protection

Both test facilities, Test Stand J-2 and Test Stand J-4, were remotely operated from the control room during the LF<sub>2</sub> fill, bleed-in, firing, and post-fire purge operations. No personnel were permitted on the test stand

(70) Aerojet-General Process Specification - 46350C, "Levels of Cleanliness, Description of"

(71) Aerojet-General Process Specification - 46387, "Packaging Requirements and Product Environmental Capabilities"

UNCLASSIFIED



# UNCLASSIFIED

during the operations. The only manual stand operation was the connecting and opening of the Allied Chemical trailer fill and pressurization valves, which minimized personnel exposure under flow and pressure conditions.

Whenever it was necessary to change a valve or component in the pressurized  $\text{LF}_2$  system, the system was drained and purged by remote control. Following this, the repairs or replacements were made.

During any operation involving the flow of  $\text{LF}_2$ , all personnel were restricted from the entire J-Area and the number of personnel permitted in the control room was limited to the number of available emergency breathing air packs. An independent supply of breathing air also was provided for the control room to maintain a positive pressure.

Initial entry to the test stand vicinity following a test was limited to two personnel wearing full protective clothing and a Scott Air Pak. In addition, entry was restricted until the temperature of the external surface of the combustion chamber had dropped below  $200^\circ\text{F}$ .

Approximately 65% of the combustion products consisted of HF and F (see Table XIX) which were hazardous to animal and plant life. An investigation was made by Aerojet-General Industrial Hygiene personnel to determine what weather conditions would be suitable for testing and fluorine transfer to minimize these hazards. Their findings became operating guidelines in the form of a published checklist, which is summarized below.

## a. Fluorine Storage and Transfer

(1) Under no conditions would more than 5800 lb of  $\text{LF}_2$  be stored in one vessel. (Based upon effects resulting from total spillage.)

(2) Under no conditions would  $\text{LF}_2$  be transferred or the run tank pressurized if the mild irritation concentration of 30 PPM could extend beyond Aerojet-General controlled property.

TABLE XIX

### PRODUCTS OF COMBUSTION (SHIFTING EQUILIBRIUM)

Products of Combustion	MOL Fractions	
	Within Chamber	One Atmosphere
CO	0.0314	0.0331
$\text{H}_2$	0.0380	0.0474
H	0.1349	0.0793
FCN	0.0002	0.0002
HF	0.5732	0.6540
F	0.0577	0.1727
$\text{N}_2$	0.1632	0.1727
N	0.0004	0.00
$\text{C}_2\text{F}_2$	0.0001	0.0002
CN	0.0010	0.0008
MR	1.91	
$P_c$ (psia)	100	
T ( $^\circ\text{R}$ )	7347	

UNCLASSIFIED

# UNCLASSIFIED

The following shows the quantities of fluorine in pounds needed to produce less than 30 PPM average concentration with a minimum of 5 mph wind velocity:

Wind Direction (degrees)	Controlled Property (feet)	Maximum F <sub>2</sub> Release (pounds)	
		+2°F Inversion	0°F Neutral
160 through 230	9,000	2,290	5,375
030 through 160	11,000	4,030	9,430
230 through 030	15,250	10,000	23,520

## b. Test Firing

(1) Under no conditions would a test firing allow a concentration of 3 PPM to extend past Aerojet-General controlled properties. The following shows the quantities of fluorine in pounds needed to produce less than 3 PPM average concentration with a minimum of 5 mph wind velocity:

Wind Direction (degrees)	Controlled Property (feet)	Maximum F <sub>2</sub> Release (pounds)		
		+2°F Inversion	0°F Neutral	-0.26°F Lapse
160 through 230	9,000	115	135	294
030 through 160	11,000	202	236	514
230 through 030	15,250	484	563	1,224

(2) The Micrometeorologist assigned to the Industrial Hygiene Staff was notified 24 hr prior to the anticipated test time in accordance with prepared check lists, for a weather prediction. All tests were scheduled to take maximum advantage of the weather conditions.

(3) The Industrial Hygiene Staff installed a series of air sampling devices in downwind areas. These air sampling stations ranged between 2000 ft and 7000 ft from the test site at approximately one-half-degree intervals. They were instrumented prior to each test to adequately sample the air under the anticipated weather conditions and the quantity of fluorine involved.

(4) At 30 min prior to each test, the area was cleared of all personnel not involved with the test. The wind speed and direction were continuously recorded and the meteorological conditions were evaluated to determine whether favorable test conditions existed. Adverse weather conditions resulted in several test delays, the majority occurring during the winter months when rain, fog, and temperature inversions created unfavorable conditions.

## c. Check Lists

The following are the check lists with their designations and date of publications used during this program.

# UNCLASSIFIED

<u>Title</u>	<u>No. Designation</u> <u>ATP-TDO-</u>	<u>Date</u> <u>Published</u>
LF <sub>2</sub> Test Firing Area Clearance	J2-001C	26 Apr 67
Fluorine System Leak Check	J2-002A	9 Jan 67
Engineer Pre and Post-fire Checklist LF <sub>2</sub> TCA	J2-003B	11 Jul 67
Fluorine Fill Leadmans Check	J2-004A	27 Jan 67
Fluorine Fill Engineers Check	J2-005A	27 Jan 67
Fluorine System N <sub>2</sub> Hot Purge	J2-006A	25 Jan 67
*RTT's LF <sub>2</sub> TCA Assembly and Installation Check	J2-008B	11 Jul 67
Advance LF <sub>2</sub> Combustion Chamber Leak Check Checklist	J2-009A	25 Jan 67
RTT's Pre-fire Checklist	J2-010B	24 Jan 67
Advance LF <sub>2</sub> TCA Test Director's Checklist	J2-011B	21 Feb 67
RTT's Post-fire Checklist	J2-012A	24 Jan 67
Hardware GF <sub>2</sub> Passivation	J2-013C	26 Aug 67
Test Stand J-2 Propellant System Passivation	J2-014	9 Jan 67
RTT's Combustion Chamber Leak Check	J2-016	25 Jan 67
LF <sub>2</sub> Injector Receiving Inspection Checklist	J2-017	27 Jan 67
GF <sub>2</sub> Bottle Installation and/or Changeover	J2-018	31 Jan 67
Sequence Checklist (Uncooled TCA)	J2-019A	26 Aug 67
Engineer's Fluorine Transfer (J-4)	J2-1000	2 Oct 67
RTT's Passivation Preparation Checklist	J2-2000	29 Dec 66
Fluorine Pushback to Trailer	J2-2001	8 Mar 67
LF <sub>2</sub> Trailer Storage and Storage Emergency	J2-2002	13 Apr 67
RTT's LF <sub>2</sub> Storage and Emergency Checklist "E"	J2-2003	13 Apr 67
RTT's LF <sub>2</sub> Cooled TCA Assembly and Installation	J2-2004	11 Jul 67
RTT's Fluorine Transfer (J-4) Checklist	J2-2005	2 Oct 67
Pre-fire Electrical Advanced LF <sub>2</sub> -TCA Checklist	J2-4374A	10 Jan 67

\* Rocket Test Technician

# UNCLASSIFIED

## UNCLASSIFIED

### 2. Transfer of Fluorine

Gaseous fluorine (used for passivation) and liquid fluorine were received in "K" size cylinders holding 3 lb and LN<sub>2</sub> jacketed truck trailers having an approximate capacity of 5000 lb, respectively. The trailers were used as temporary storage vessels during the early injector evaluations at Test Stand J-2 because the run tank capacity was only 50 gal.

The altitude facility, Test Stand J-4, was activated in September 1967. It had two, triple-walled 1000 gal liquid nitrogen and vacuum-jacketed fluorine tanks used for storage and run. The Test Stand J-4 run tank was linked to the Test Stand J-2 run tank which permitted all off-loading directly into the 1000 gal run tank at Test Stand J-4. All movement of liquid fluorine was controlled remotely from the control room in accordance with above indicated standard published procedures.

### 3. Fluorine Disposal

Safety requirements dictated controlled disposal of all fluorine. All vents and bleeds were discharged into a remotely-located charcoal pit. Pre-test and post-test movement of waste fluorine was controlled from the central control room with the area clear of all personnel. The reaction products of carbon tetrafluoride were vented directly into the atmosphere.

The test stands and propellant facilities were protected from fire damage resulting from accidental fluorine spillage by either manual or remote-controlled water deluge systems and stand-by fire hoses. The deluge system provided a blanket of water fog over the facility which would control the resultant fire from a fluorine spill by reacting with the fluorine to form hydrogen fluoride and steam. However, there were no fluorine spills or fires throughout the program.

### 4. Exhaust Products Control

An exhaust scrubber was designed and incorporated into the Test Stand J-4 facility so that the scheduled long duration tests would not be as meteorologically dependent. Also, environmental pollution was minimized. The dilute hydrofluoric acid-water was directed into a 200,000 gal neoprene, rubber-lined concrete sump. The hydrofluoric acid was recirculated through a limestone reaction pit that provided the insoluble, relatively inert, calcium-fluoride as a solid waste for disposal. The water was recirculated until the fluoride concentration was reduced to less than 5 PPM. The water then was permitted to drain through the normal waste system.

The exhaust scrubber designed for the Test Stand J-2 facility is shown on Figure No. 128. It adversely affected thrust measurement and impeded hardware inspection; it was not used after the second test. The test durations at Test Stand J-2 were sufficiently short so that meteorological restrictions did not seriously hinder the test schedules.

UNCLASSIFIED

UNCLASSIFIED

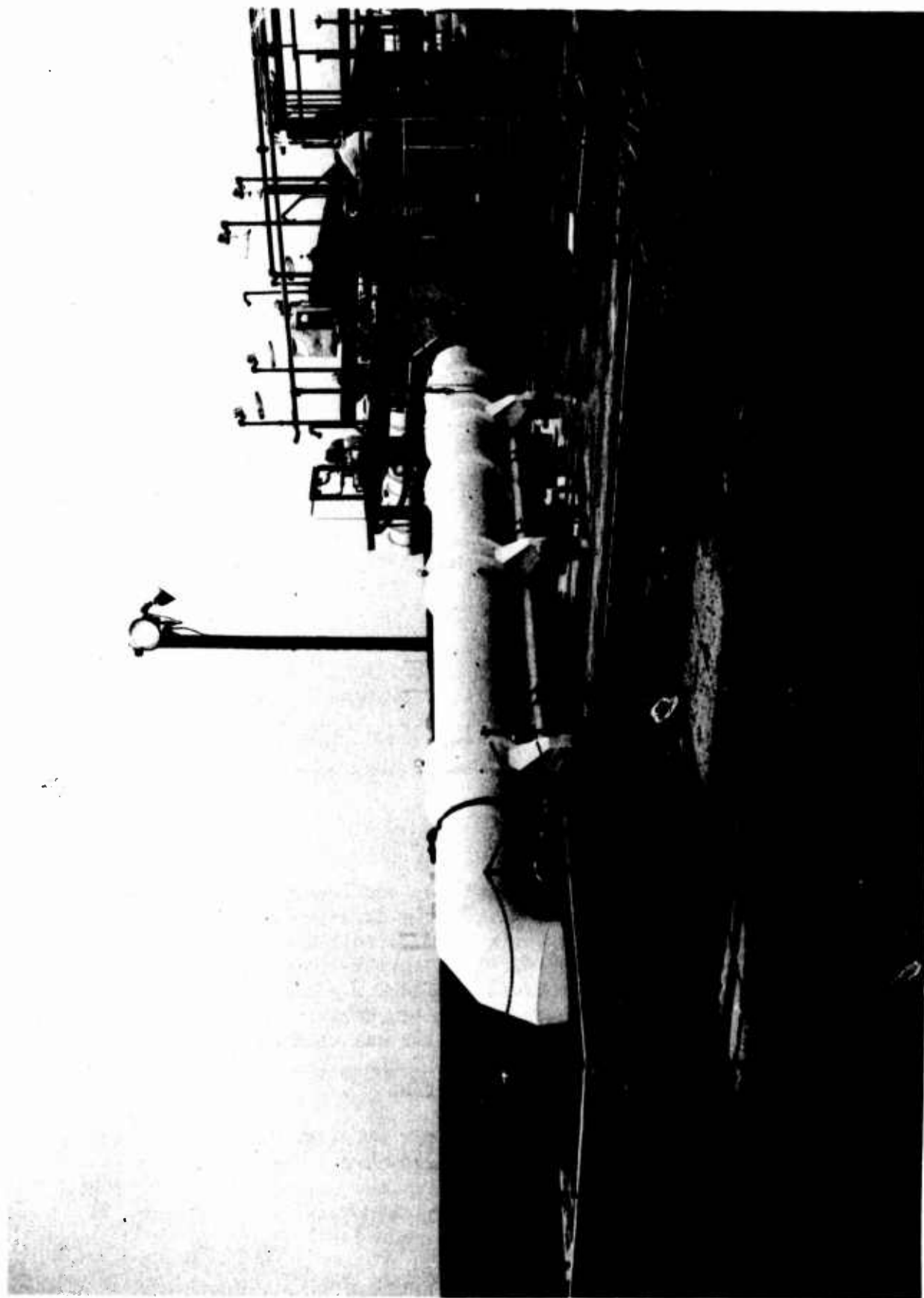


Figure 128. Test Stand J-2 Exhaust Scrubber

UNCLASSIFIED

# UNCLASSIFIED

## D. INSTRUMENTATION

The following is the basic instrumentation used during the program. The listed accuracy is based upon the manufacturer's quoted values and estimated values for calibration, electrical interconnections, and data reduction.

<u>Function</u>	<u>Sensing Unit</u>	<u>Range</u>	<u>Error (1% of Operating Point) Std Deviation Error</u>
Tank Pressures	Tabor Transducer	0-500 psig	$\pm 0.101$
Line Pressures	Tabor Transducer	0-500 psig	$\pm 0.101$
Injection Pressures	Tabor Transducer	0-500 psig	$\pm 0.101$
<u>Chamber Pressures</u>			
- Low-Frequency	Tabor Transducer	0-200 psig	$\pm 0.101$
- High-Frequency	Photocon	0-25 psi peak/peak	
Oxidizer Line Temp	Resistance Temperature Transducer	-265 to -425°F	$\pm 0.005$
Fuel Line Temperature	C A Thermocouple	0-2200°F	$\pm 0.96$
TCA Surface Temperature	C A Thermocouple	0-2200°F	$\pm 0.96$
Injector Face Temperature	C A Thermocouple	0-2200°F	$\pm 0.96$
<u>Ablative Chamber</u>			
<u>Imbedded Thermocouples</u>			
- Shallow Penetration	C A Thermocouple	0-2200°F	$\pm 0.96$
- Deep Penetration	Tungsten Rhenium Thermocouple	0-4200°F	$\pm 5.00$
Thrust	Baldwin Load Cell	0-10K	$\pm 0.105$
<u>Flowrates</u>			
- Fuel	Potter Flowmeter	0-15 lb/sec	$\pm 0.269$
- Oxidizer	Potter Flowmeter	0-20 lb/sec	$\pm 0.269$

The instrumentation locations in the test stand run lines are shown on Figures No. 125 and No. 127.

The model 5785A Potter flowmeter used in the fluorine line contained 440C stainless steel ball bearings. These flowmeters were completely satisfactory for fluorine service.

The Tabor pressure transducers installed in the fluorine lines were modified to incorporate Monel diaphragms rather than stainless steel to minimize the possibility of leaks.



## UNCLASSIFIED

Shielded thermocouples having a Monel sheath were used in the fluorine circuits.

Special temperature measuring probes were required to accurately determine the selected material interface temperatures of the full ablative chambers. There were no commercially-available thermocouples that could be used to meet all requirements. Specially designed Aerojet-General probes were developed. Silica and graphite phenolic interface temperatures were measured with a 0.005-in. diameter chromel-alumel wire encased in phenolic plugs, which had properties that were similar to the surrounding ablative material (see Figures No. 23 and No. 24). The small diameter wires were used to minimize stem conduction losses and to provide a fast response time. The sensing plug was spring-loaded to ensure continuous contact with the chamber material.

A high temperature sensing probe of similar design was used to measure the backside temperatures of the AGCarb-101 flame liner in the ablative chambers. Tungsten-rhenium was used as the thermocouple materials. Figure No. 129 shows an assembled unit and an exploded view of the components.

Injector face temperatures were measured with chromel-alumel thermocouples inserted in 0.0219-in. diameter holes drilled through the injector face from the back at the mid-radius support posts. The sensing junction was positioned flush with the injector face and silver-soldered into place. These thermocouples had a fast response and were sufficiently sensitive to detect the temperature increase associated with instability. Also, these thermocouples proved highly reliable and were used as one of the "kill" parameters during a hot test.

Two major problem areas were associated in the measurement of the temperature of the products of combustion in the resonating cavity of an acoustically-damped combustion chamber. First, there was the anticipated operating temperature which was in excess of 3000°F (chromel-alumel thermocouples with a stainless steel sheath in a resonating cavity indicated a rapid rise to approximately 2500°F before burning out). Secondly, there was the highly corrosive property of the fluorinated combustion products.

Fusible wires having different melting temperatures and the ability to withstand the corrosive fluorinated combustion products were used as temperature sensors in the resonating cavities. Stainless steel, platinum, and rhodium 0.010-in. diameter wire, having melting temperatures of approximately 2600°F, 3224°F, and 3571°F, respectively, were selected. One wire of each of the selected materials was mounted on the end of a 0.25-in. diameter steel rod to form the temperature sensor. Figures No. 56 and No. 57 showed the sensors after Tests -024 and -025. Three units were placed in each of the first and third (furthest from injector end) resonating cavities. An iridium/iridium 60 rhodium 40 thermocouple was placed in the cavity with each set of fusible wires for comparison. These thermocouples were calibrated to 3800°F. Test results indicated that the fusible wires provided satisfactory and useful data. This concept of sensing high temperature ranges proved to be very economical as well as productive.

## UNCLASSIFIED

UNCLASSIFIED

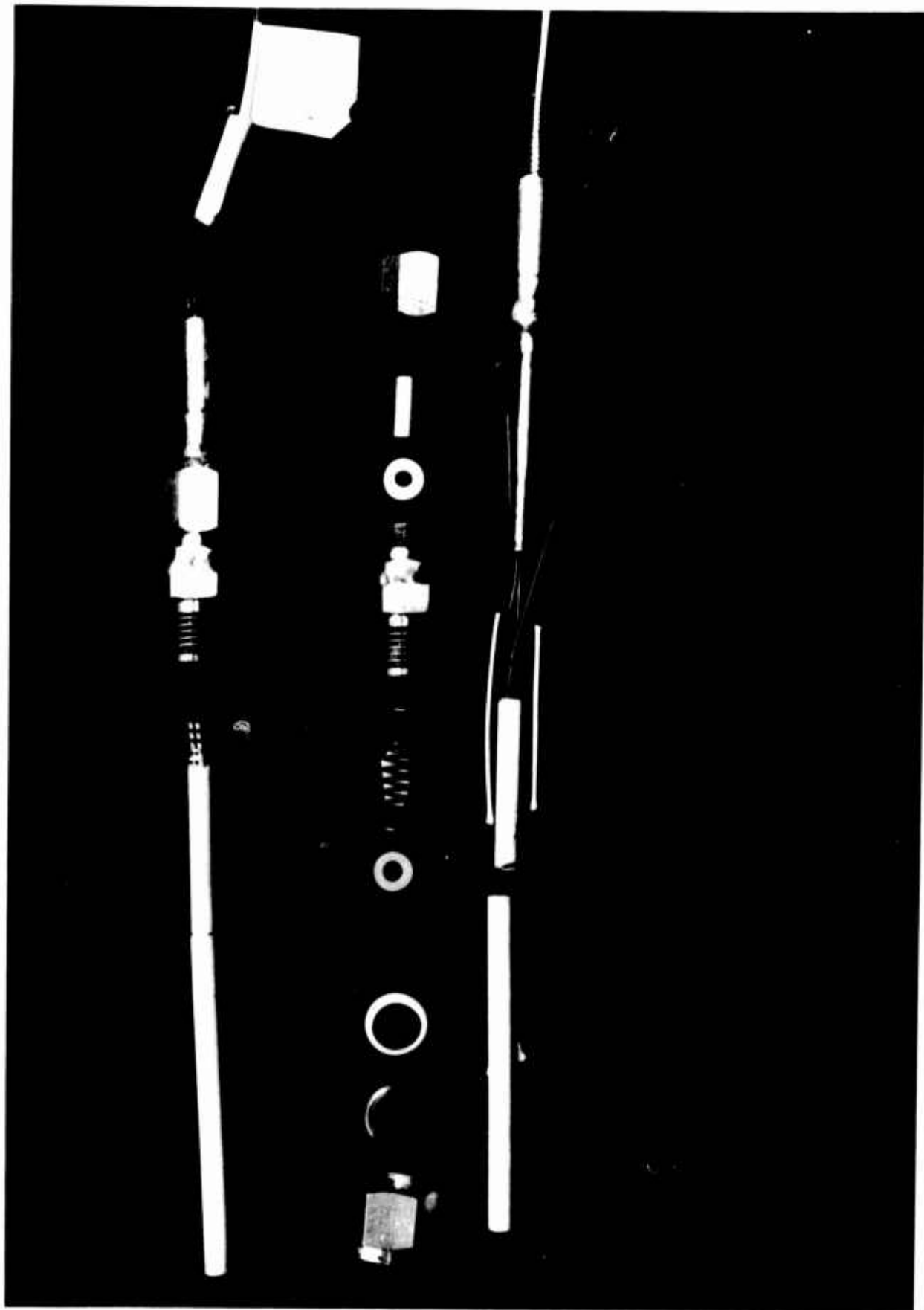


Figure 129. High Temperature Sensing Probe

UNCLASSIFIED

UNCLASSIFIED

E. TEST DATA ACQUISITION

1. Digital Test Data Acquisition and Processing

Raw commutated digital test data from J-Area was centrally recorded on magnetic tape within the Test Area IBM-360 computer system. The IBM-360 system simultaneously processed the test data through an engineering units time history listing and computer/plotter formatted tapes. Extended performance calculations then were developed with the IBM-360 system. Automatic plotters were used in conjunction with the IBM-360 computer system to provide a graphic presentation of recorded parameters and performance functions versus time. This was generally available within a few hours following the test. Digital Test Data Acquisition and Processing System has a confirmed 3 sigma channel accuracy of less than 0.1%.

2. Digital Data

The digital listing point frequency was varied from every recorded sample, 50 points-per-second, to one sample/sec which also varied within the test duration, depending upon the duration and/or area of interest.

The digital data was normally averaged over three time intervals.

UNCLASSIFIED

**UNCLASSIFIED**

**APPENDIX VI**

**METALLURGICAL EXAMINATION OF COLUMBIUM NOZZLE**  
**EXTENSION P/N 1131920-9**

**Page 279**

**UNCLASSIFIED**

# UNCLASSIFIED

## APPENDIX VI

### METALLURGICAL EXAMINATION OF COLUMBIUM NOZZLE EXTENSION P/N 1131920-9

#### A. SUMMARY

The nozzle extension, P/N 1131920-9, was fabricated from C103 columbium alloy. Then, it was divided into three sectors which were coated as follows:

- Lunite 2; an aluminide diffusion coating similar to the NAA-85 coating used on the columbium portion of the Apollo skirt.
- Lunite 3; a hafnium-tantalum coating (Both the Lunite 2 and 3, were applied by the Vac-Hyd Processing Corp.).
- A nickel aluminide ceramic plasma sprayed coating.

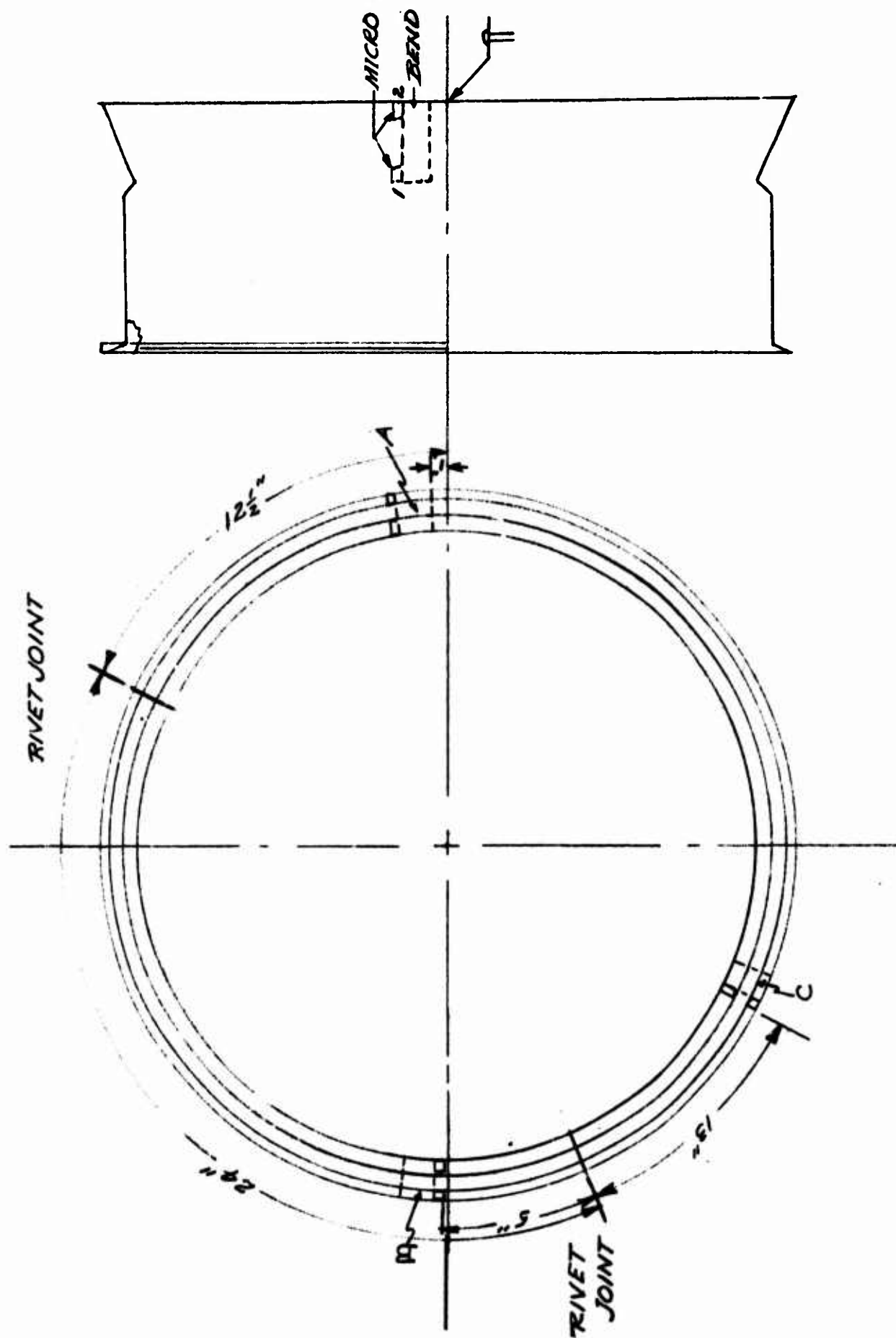
The nozzle extension was tested two times using thrust chamber S/N 002 and injector S/N 2 Mod 3. All tests were made in Test Stand J-4 and are summarized below.

<u>Test No.</u>	<u>Duration</u>	<u>Remarks</u>
002	29.7 sec	plasma sprayed portion of nozzle failed
004	202.8 sec	new nozzle sector riveted in place and coated with Lunite 2

Specimens taken from various locations of the test-fired nozzle extension (see Figure No. 130) were evaluated for coating performance. Results from guided bend tests, microhardness surveys, and metallographic examination revealed that the columbium alloy base material was not completely protected by the oxidation resistant coatings (Lunite 2 and 3). Both coatings spalled on the hot gas side and cracked on the chamber exterior; however, exterior cracks did not extend through the intermetallic coating interface. The Lunite 3 coating is considered suitable for a full-scale, full-duration nozzle extension.

UNCLASSIFIED

UNCLASSIFIED



NOT TO SCALE

Figure 130. Locations of Specimens

UNCLASSIFIED



## UNCLASSIFIED

### B. INVESTIGATION AND RESULTS

The nozzle extension was fabricated from C103 columbium alloy procured in accordance with Aerojet-General Specification 44141. It was instrumented using C/A thermocouples on the external surface. Test data from Test No. -004 indicated that the thermocouples detached from the skirt at the end of 40 sec of testing leaving a small gap between the skirt and the thermocouple. The junctions were not damaged and the temperature measurements after separation were in close agreement with predictions made for a surface acting as a radiation shield between a 2300°F body and a cold surface. Using this data, the steady-state skirt temperature was calculated to be between 2300°F and 2400°F.

Specimens from the nozzle extension (see Figure No. 130) were bend tested and microhardness determinations made.

#### 1. Bend Test

Three specimens (one from each area, A, B, and C of Figure No. 130) were subjected to a 105 degree guided bend test over a 2T to 6T (1/16-in. to 3/16-in.) radius. Examination of the specimens after bend tests showed cracks in the base material indicating localized embrittlement of the columbium alloy.

#### 2. Microhardness Traverse

Microhardness determinations were made of sections taken from each area. The results are shown on Table XX. A Knoop hardness number increase was noted on the surfaces of these specimens also indicating embrittlement of the columbium alloy.

#### 3. Metallographic Examination

Metallographic examination (Figures No. 131, No. 132 and No. 133) revealed cracking of the outside diameter coating, spalling of the inside diameter coating, and oxidation of the columbium alloy. The outside diameter cracking did not extend through the intermetallic bond region. Internal oxidation was more severe on the Lunit 2 coated specimens.

### C. DISCUSSION

Examination of the results indicates that the Lunit 2 and Lunit 3 coatings provided limited protection of the C103 columbium alloy base material against oxidation. This was shown by the cracking of some of the specimens during the 6T guided bend tests. The high hardness values were more typical on the hot surface side of the specimens. Metallographic examination of the two coatings (see Figures No. 131, No. 132, and No. 133) shows numerous cracks in the outside surface of the Lunit 3 coating. These cracks could have been the result of processing effects because the nozzle extension was reworked. They did not extend into the virgin material and were non-detrimental.

UNCLASSIFIED

UNCLASSIFIED

TABLE XX

MICROHARDNESS SURVEY OF  
VARIOUS AREAS OF NOZZLE EXTENSION, P/N 1131920-9

(KNOOP HARDNESS NUMBER)

Location	Specimen					
	A		B		C	
	1	2	1	2	1	2
Measured from outer surface						
0.001-in.	189	218	234	238	213	213
0.002-in.	216	215	201	204	213	203
0.003-in.	214	215	201	210	193	203
0.004-in.	204	202	194	191	194	203
Midway through wall	198	191	---	196	193	199
Measured from inner surface						
0.001-in.	488	406	353	295	360	259
0.002-in.	403	256	300	213	242	223
0.003-in.	262	194	290	206	200	206
0.004-in.	222	192	278	198	216	214
Aerojet-General Specification 44141					241 maximum	

UNCLASSIFIED

UNCLASSIFIED



a. Specimen C1



b. Specimen C2

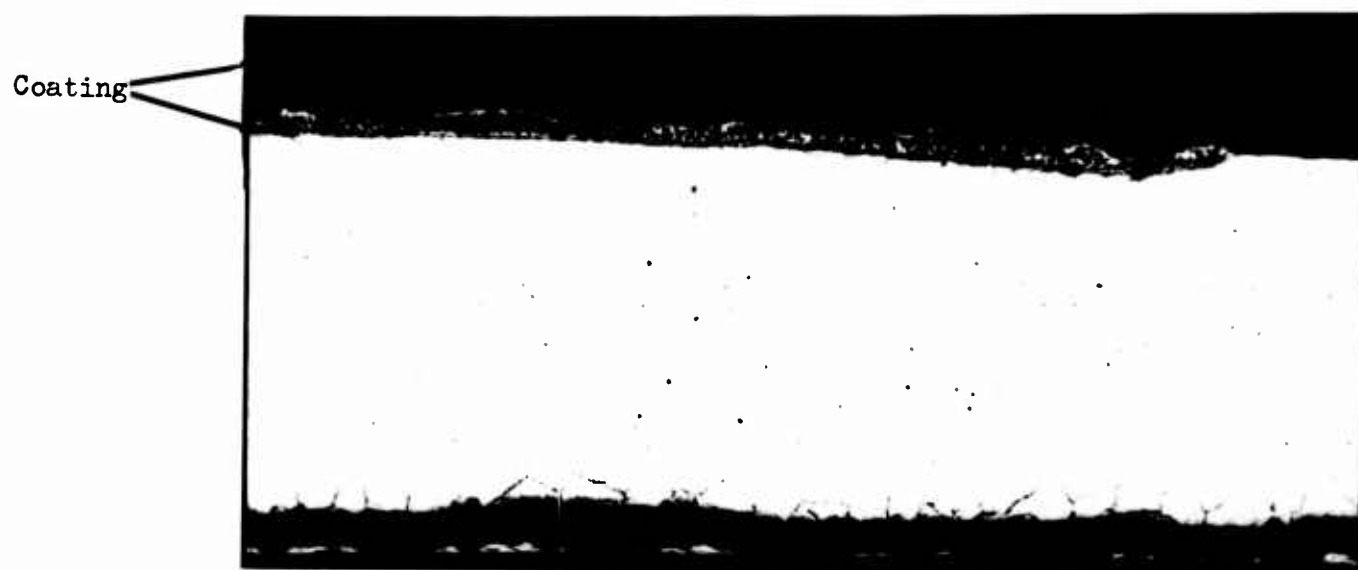
Mag: 100X

Etchant: Lactic Acid-HNO<sub>3</sub>-HF

Figure 131. Photomicrographs of "A" Specimens Taken from Nozzle Extension

UNCLASSIFIED

UNCLASSIFIED



a. Specimen B1



b. Specimen B2

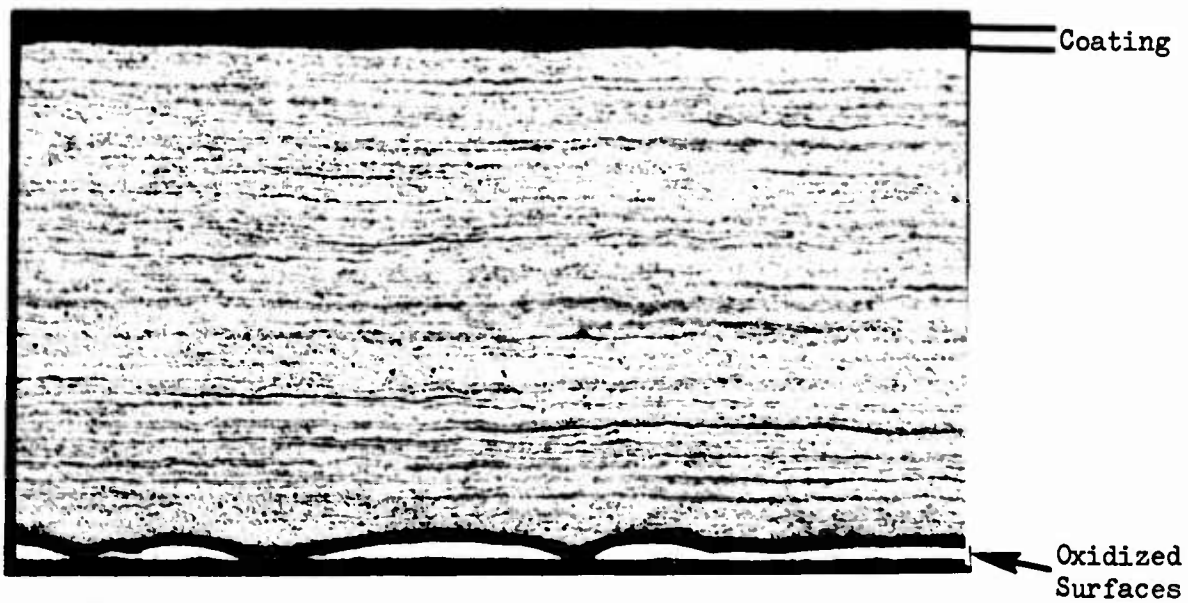
Mag: 100X

Etchant: Lactic Acid -  $\text{HNO}_3$  - HF

Figure 132. Photomicrographs of "B" Specimens Taken from Nozzle Extension

UNCLASSIFIED

UNCLASSIFIED



a. Specimen A1



b. Specimen A2

Mag: 100X

Etchant: Lactic Acid -  $\text{HNO}_3$  - HF

Figure 133. Photomicrographs of "C" Specimens Taken from Nozzle Extension

UNCLASSIFIED

## UNCLASSIFIED

Both the Lunite 2 and Lunite 3 coatings spalled on the nozzle interior (gas-side) surface. This is considered to be the result of high temperature and gas impingement. The Lunite 3 showed less spalling and oxidation.

The trailing edge of the nozzle indicated oxidation in excess of that on either the exterior or gas side surfaces. This appears to be the result of the difficulty in obtaining a good coating in this area as well as operation at higher temperature which was caused by the incidence of heat from two directions.

Apparently, there were differences in the original Lunite 2 coating on Specimen A and the new coating on the replacement nozzle sector, Specimen B. Table XIX shows that specimen B was less embrittled than A, which could be the result of the high temperature cure of the entire nozzle during its repair being adverse to the previously coated portion of the nozzle.

The Lunite 3 coated portion of the nozzle showed the least effect from its operation. The hardness test data on Table XIX shows that the outside surface did not exceed the specification maximum hardness of 241. The gas side surface was beyond the specification value for a depth of one mil.

A crack through the columbium at the forward end of the nozzle was noted. The lack of oxidation in this area indicates that the crack occurred after testing. Thermal gradients during thrust chamber cooldown appear to be the cause. The material thickness in this area was undersize.

### D. RECOMMENDATIONS

The cracking of the columbium was the result of localized thinning caused by the material being spun into the sharp corner at its forward end. An increase in the radius of curvature in this area should correct the condition.

Localized spalling of the coatings could be avoided by operating the nozzle at a reduced temperature. Consideration should be given to moving the attachment point aft.

Cracking of the Lunite 3 coating on the outside surface of the nozzle could result from the manner in which the nozzle was processed. Specimen panels should be evaluated prior to coating the next nozzle to determine the effects of processing parameters.

### E. CONCLUSIONS

It is concluded that the plasma sprayed nickel aluminide ceramic coating is completely inadequate. Its failure over the entire nozzle section in less than 30 sec indicates that the rate of attack upon the columbium was very high.

UNCLASSIFIED



**UNCLASSIFIED**

The Lunit 2 aluminide diffusion coating was proven adequate for the duration tested. However, the degree of oxidation shown indicates that it may not be adequate for the full duty cycle.

The Lunit 3 hafnium-tantalum coating is considered to be suitable for a full-length, full-duration nozzle. The surface cracking noted should be investigated because it could result in stress concentrations upon a full-length unit.

**UNCLASSIFIED**

**UNCLASSIFIED**

**APPENDIX VII**

**POST-TEST ANALYSES OF ABLATIVE CHAMBER S/N 002**

**Page 289**

**UNCLASSIFIED**

# UNCLASSIFIED

## APPENDIX VII

### POST-TEST ANALYSES OF ABLATIVE CHAMBER S/N 002

#### A. INTRODUCTION

Ablative chamber S/N 002, P/N 1131021-9, had an inside diameter of 9.45-in. in the cylindrical section tapering to a throat diameter of 7.13-in. and nominal exit area ratio of 7.5. The materials used are defined on Figure No. 134.

The chamber was designed to operate for a total duration of 600 sec but its actual duty cycle totaled 606.4 sec. The design and actual duty cycles are as follows:

<u>Firing Duration (sec)</u>		<u>Coast Period (min)</u>	
<u>Design</u>	<u>Actual</u>	<u>Design</u>	<u>Actual</u>
315	8.5	240	Complete Cooldown
9	29.7	35	
5	194.0	14	
61	202.8	41	
100	0.8	10	
110	170.6		

The design duty cycle was not accomplished as planned because of test stand limitations and the decision to inspect the chamber after each test.

All of the tests were conducted with the same 68-element pattern injector, S/N 2 Mod 3, which had approximately 2% fuel film cooling located in selected areas around the periphery. The chamber erosion characteristics, as related to the injector pattern, are shown on Figure No. 135. This pattern, which was recorded after the third test of the thrust chamber became more pronounced during subsequent tests. Examples of the non-uniform regression are shown in the subsequent photographs and regression measurements where angular locations are indicated correspond to Figure No. 135 with top center at 0-degrees (angle direction is clockwise on Figure No. 135 and counter-clockwise in all of the photographs).

UNCLASSIFIED

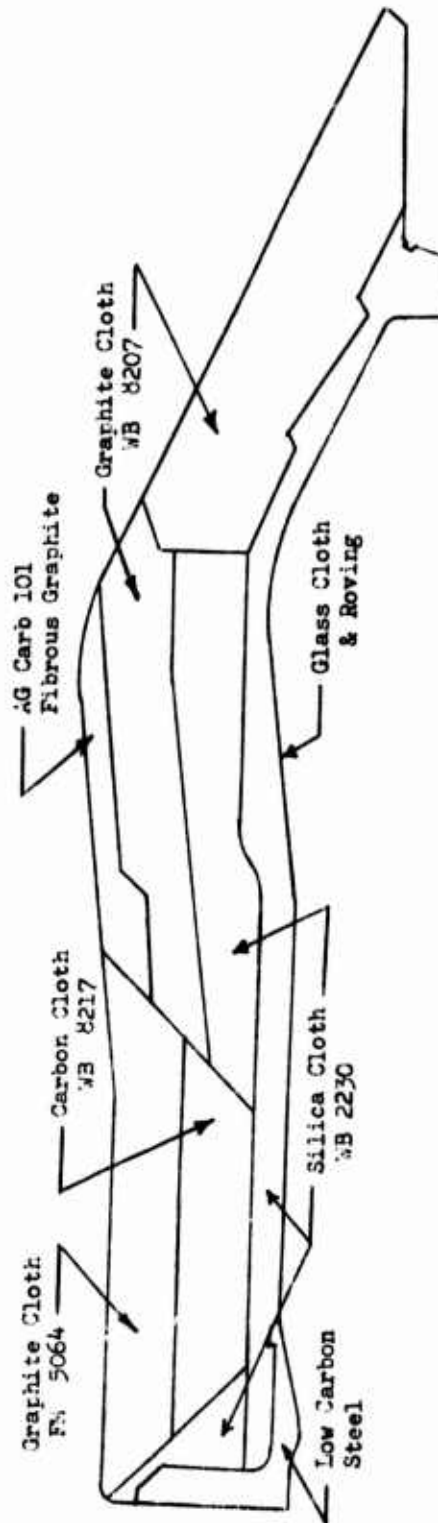
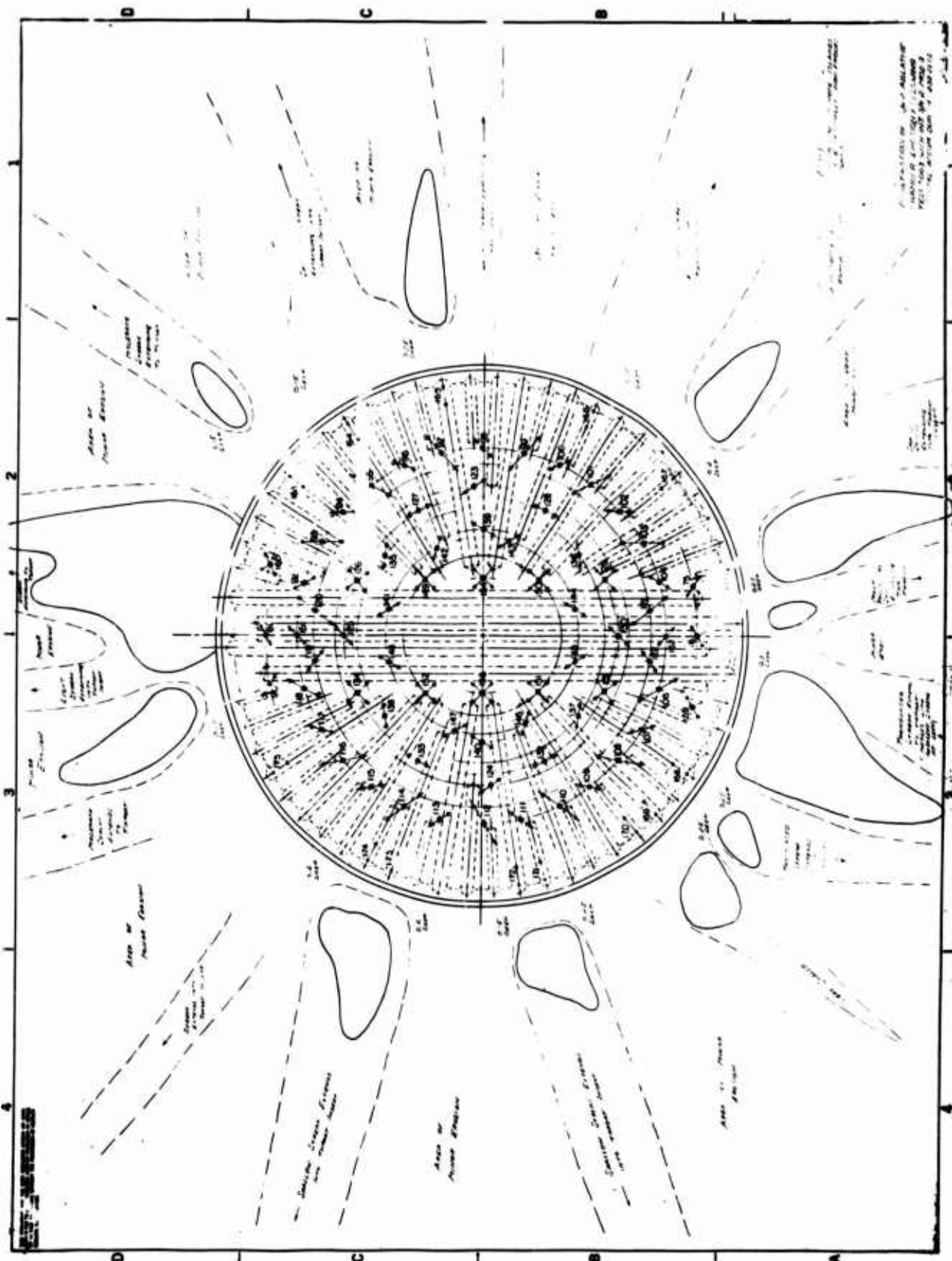


Figure 134. Ablative Thrust Chamber with Throat Insert, P/N 1131021-19

UNCLASSIFIED

**UNCLASSIFIED**



### Figure 135. Chamber Erosion Characteristics

**UNCLASSIFIED**

## CONFIDENTIAL

### B. SUMMARY

(U) The thrust chamber was sectioned and a post-test analysis was performed which included measurement of regression and char depths as well as an evaluation of the post-test condition of the materials.

(U) All of the materials performed well and the materials as well as fabrication processes are considered satisfactory for use in production hardware. Char depths indicate that an approximate 30% reduction in chamber wall thickness is possible for future designs.

(U) The pyrolytic deposition in the AGCarb-101 throat insert indicates a flow of decomposition gases from the back-up materials through the part. The permeability of the throat insert in this chamber, S/N 002, was relatively high because of its low pre-fire density of approximately  $1.22 \text{ gm/cm}^3$ .

### C. DISCUSSION

(U) The S/N 002 thrust chamber was measured to obtain inside diameter dimensions in the chamber and at the throat. It was weighed and then sectioned for further analysis. The results of this analysis follow.

#### 1. Dimensions and Weight

(C) Inside diameter measurements obtained prior to sectioning the chamber indicated the most severe streaking occurred in the 15-degree to 195-degree plane. Two streaks were approximately 0.50-in. deep on the radius. These streaks were located at each end of the full-length, drilled fuel manifolds of the injector (see Figure No. 135). The most severe streak, at the 195-degree location, extended through the AGCarb-101 material at the throat station where it is 0.6-in. thick. Other erosion streaks also extended to the throat area although they were not as deep.

(U) The post-fired chamber weighed 280.5 lb while in the pre-fire condition, it weighed 303 lb.

(U) The inside diameter measurements of the forward end of the chamber are as follows. They were taken with an ID micrometer prior to sectioning:

CONFIDENTIAL



# CONFIDENTIAL

	Orientation of ID Measurement (degrees)	Distance from Forward End of Chamber, in.				
		2.5	5.0	6.0	7.5	10.0
Pre-Fire Diameter, in.	0 - 360	9.450	9.450	9.450	9.450	8.960
Post-Fire ID Measurements, in.	0 - 180		10.105	10.287	10.273	9.965
	45 - 225	10.016		10.161		
	60 - 240	9.767	10.217		10.210	9.815
	90 - 270	9.721		9.995		
	120 - 300	9.832	10.080		10.236	9.785
	135 - 315	9.895		10.194		
	Average (*)	9.810	10.134	10.159	10.240	9.855
Average Regression Depth on Radius		0.180	0.342	0.354	0.395	0.447

(\*) This is an average of the measurements and does not completely reflect average regression depth because of large variations.

(C) The following regression data were taken from minimum and maximum throat diameter measurements:

Original (pre-test) throat diameter, in. = 7.135  
 Minimum (post-test) throat diameter, in. = 7.298  
 Maximum (post-test) throat diameter, in. = 8.035<sup>(\*\*)</sup>  
 Minimum total regression on radius, in. = 0.081  
     average regression rate, mils/sec = 0.13  
 Maximum total regression on radius, in. = 0.450,  
     average regression rate, mils/sec = 0.7

(\*\*) Measured at deepest point in throat corresponding to a 15-degree to 195-degree line looking aft through the throat centerline.

## 2. Visual Inspection

### a. Throat Profile

(C) The full-size throat profile is shown on Figure No. 136 which was taken from the forward end, looking aft. Maximum regression occurred at 11-degrees, 53.5-degrees, 196.5-degrees, and 246-degrees. The throat diameter measured at 15-degrees/195-degrees was 8.035-in. The minimum throat diameter, measured at 80-degrees to 260-degrees was 7.298-in. The difference, 0.368-in. on the radius, shows the pronounced effect of streaking as a result of the injector pattern. The streaking, which is shown on Figure No. 135 started just aft of the injector face and continued through the throat. The streak patterns diverged and were not always perfectly axial through the throat.

(C) Uncertain propellant flow characteristics during the combustion process make it difficult to ascribe the exact cause for the streaking. Both the  $H_2O$  in the fuel and the  $F_2$  are potential oxidizers of carbonaceous materials. The lower vaporization rate of the fuel plus the radial flow of oxidizer from the peripheral long impinging elements appear to identify the oxidizer as the primary cause.

### b. Full-Length Cross-Section

(U) A full length cross-section at 90-degrees is shown on Figure No. 137 (approximately one-third magnification). Char depths and degraded zones of the ablative materials can be seen. There were delaminations (normal for post-fired ablatives) in the graphite phenolic chamber liner and throat backup. The exit cone liner was comparatively free of delaminations; however, this liner charred completely through. Two of the three thermocouple plugs can also be seen in this photograph. The char depths behind the throat, and at the forward end are apparent. The char depths in the chamber section and exit cone are also shown on Figures No. 138 through 142.

### c. Profile of Maximum Regression

(U) There are two views of the heavy regression area at 195-degrees. Figure No. 138 shows this region looking aft. The top 6-in. of the chamber was removed prior to taking the photograph. In the forward area (not shown), the two heavy erosion streaks diverge from a single streak.

(U) Figure No. 139 shows the chamber surface from 90-degrees to 195-degrees. The photograph was taken from the aft end looking forward. The forward rings were replaced to show the erosion profile from the forward end of chamber through the throat. The delaminated portion of the throat insert is evident and extended to the back-up material except at the forward end of the insert. The AGCarb-101 was relatively thin in the delaminated area because of the heavy erosion; therefore, the stress was relieved by the delamination. In addition to the stress created by thermal expansion, there was a radial residual stress in the throat segment which sprung the wall toward the inside diameter upon sectioning.

**CONFIDENTIAL**

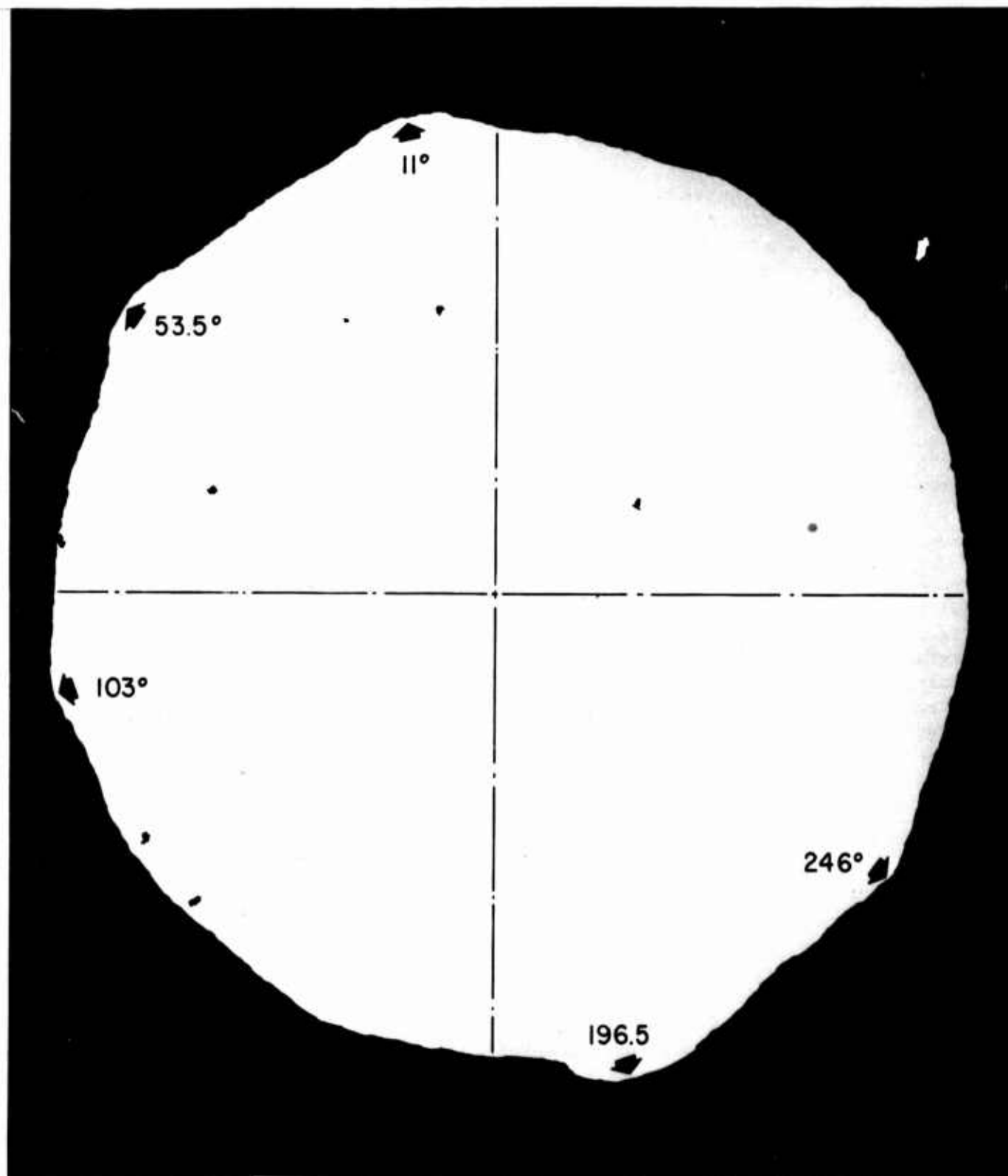


Figure 136. Throat Profile Showing Irregular Regression Pattern  
at Minimum Throat Diameter

Page 296

**CONFIDENTIAL**

**CONFIDENTIAL**



Figure 137. Cross-Section at 90-Degrees

**CONFIDENTIAL**

**CONFIDENTIAL**



Figure 138. Heavy Regression in Chamber and Throat Near 195-Degrees

Page 298

**CONFIDENTIAL**

**CONFIDENTIAL**



Figure 139. Regression Patterns in the 95-Degree to 195-Degree Segment

Page 299

**CONFIDENTIAL**



**CONFIDENTIAL**



Figure 140. Segment 195-Degrees to 270-Degrees

Page 300

**CONFIDENTIAL**

**CONFIDENTIAL**



Figure 141. Segment 270-Degrees to 45-Degrees

**CONFIDENTIAL**

**CONFIDENTIAL**

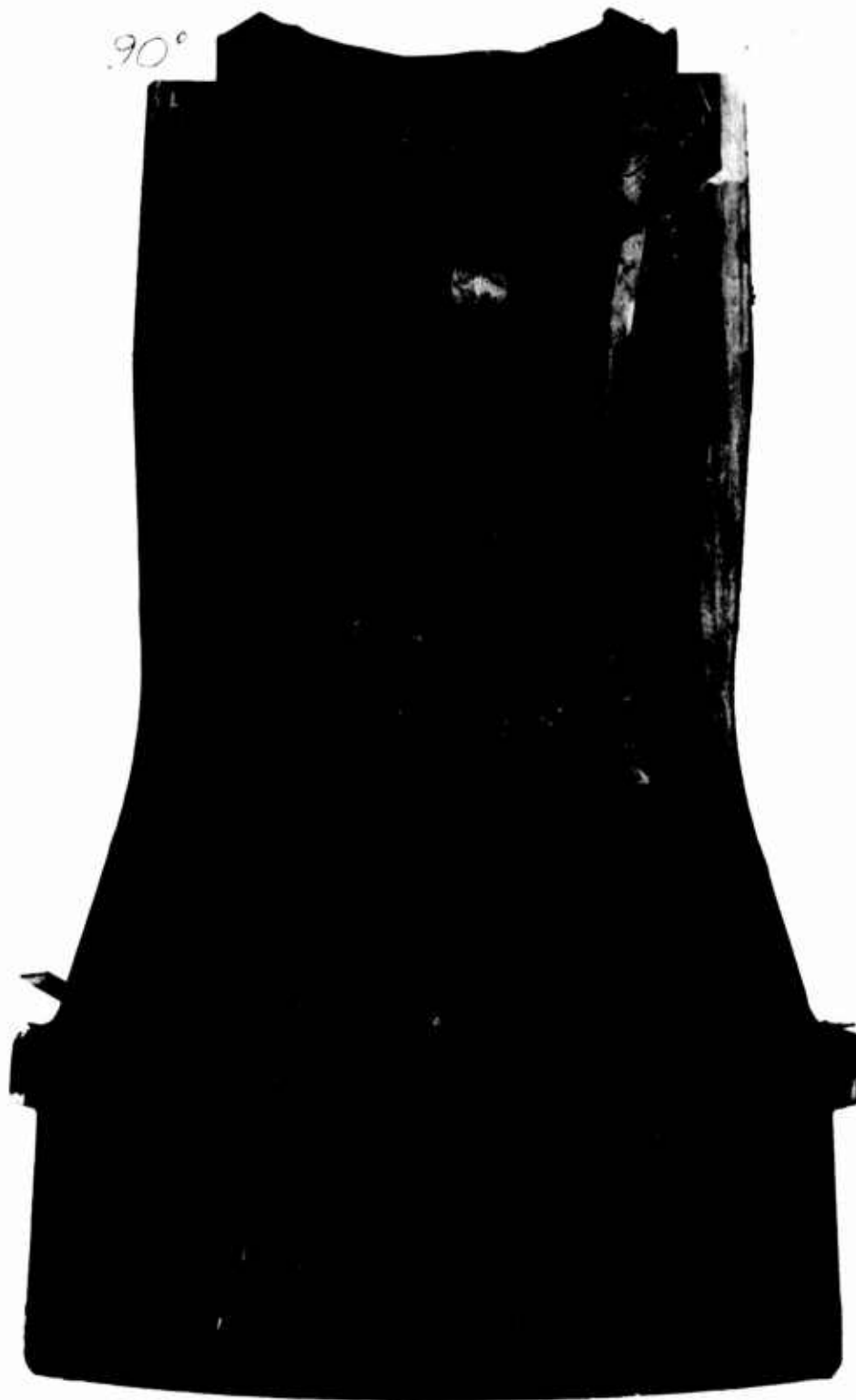


Figure 142. Segment 90-Degrees to 195-Degrees

**CONFIDENTIAL**

## CONFIDENTIAL

At the bottom right and center of Figure No. 139, there are two voids (below holes) at the exit cone/throat extension interface. One void area extended approximately 1-in. into the section at 195-degrees. There is no evidence of gas leakage behind the throat back-up. Furthermore, there is no internal material removal forward of these points. Therefore, it is concluded that the material removal occurred as a result of a concentration of decomposition gases escaping at the interface. The decomposition gases of phenolics contain potential oxidizing species as well as hydrocarbons<sup>(72)</sup>.

All voids or material loss at the material interface in the nozzle occurred in line with the heavily-eroded area. These areas possibly were hotter and exceeded threshold temperatures for oxidation attack by decomposition gases such as H<sub>2</sub>O and CO<sub>2</sub>. It also is possible that the faster temperature rise in the regions of high regression produced corresponding separations at the graphite cloth/silica cloth interface. The voids would produce a ready escape path for decomposition gases.

d. Segment 195-degrees to 270-degrees

The face of the 195-degrees to 270-degrees segment is shown on Figure No. 140. The material removal at the material interface in the nozzle is shown as well as the erratic surface profile resulting from injector streaking. The continuation of the void at the throat extension/exit cone interface at 195-degrees also can be seen.

e. Segment 270-degrees to 45-degrees

The face of the segment 270-degrees to 45-degrees is shown on Figure No. 141. Two voids, approximately 1-in. wide, and three smaller voids at the material interface in the nozzle can be seen. Heavy regression occurred at 15-degrees and 35-degrees.

f. Segment 90-degrees to 195-degrees

The face of the 90-degrees to 195-degrees segment is shown on Figure No. 142. The heavy regression and delaminated areas can be readily observed.

g. Radial Ring, Segment 6-in. from Forward End of Chamber

The specimen shown on Figure No. 143 extends from Stations 2.5-in. to 6.0-in. below the forward end of the chamber. It is viewed looking forward from the downstream end. The internal profile is at the forward end of the specimen. The aft internal contour is the line of demarcation between black and grey. It can be seen that the streaks are narrow and discrete

---

<sup>(72)</sup> Report AFRPL-TR-68-29, op. cit.

CONFIDENTIAL

(This Page is Unclassified)

CONFIDENTIAL

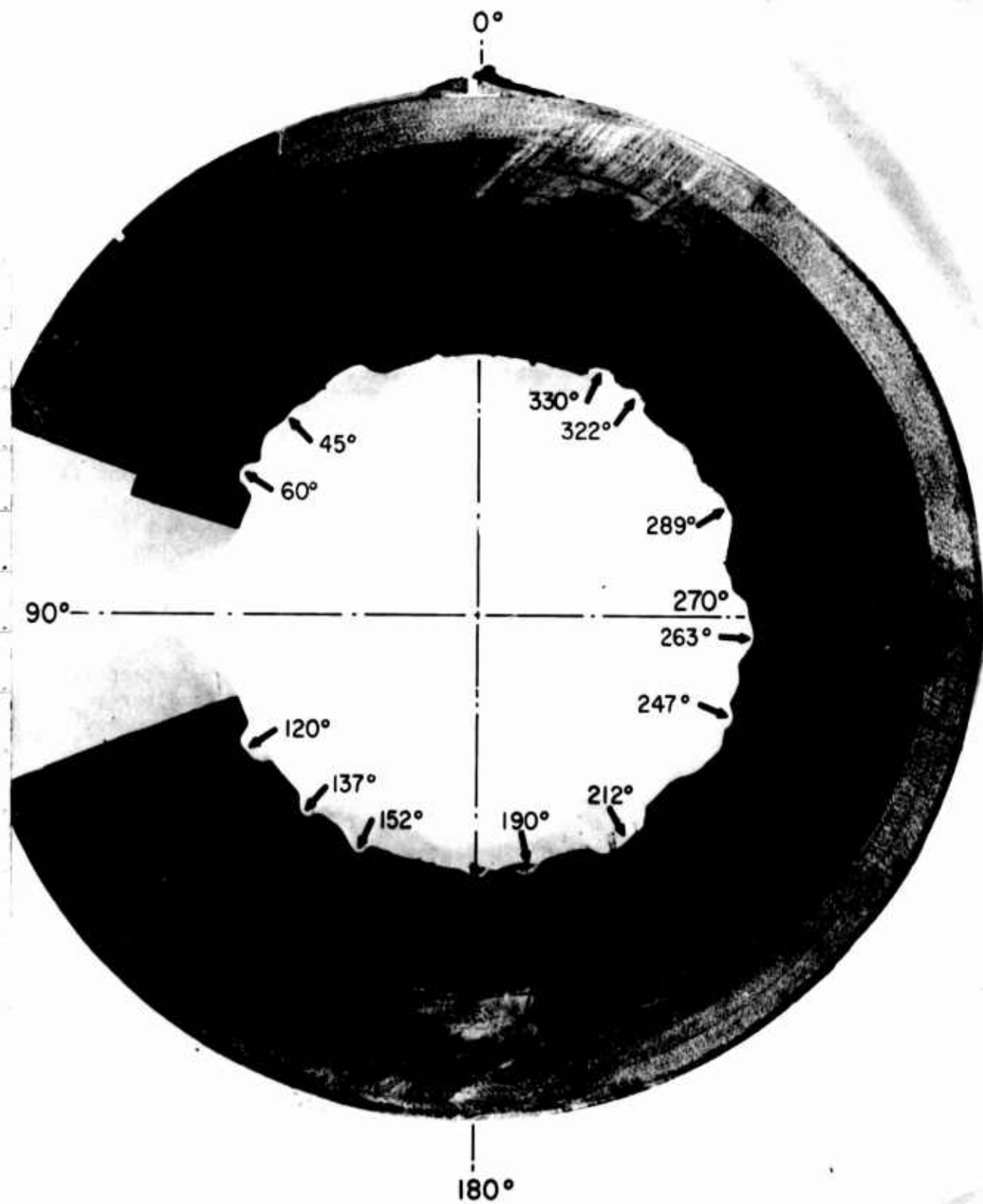


Figure 143. Radial Cross-Section 6-in. from Forward End

CONFIDENTIAL

## UNCLASSIFIED

at the forward end of the specimen while downstream, they tend to merge. Also shown is the circumferential displacement produced by the relief of stress in the chamber liner when sectioned. Char depth is generally uniform and extends into the liner back-up 0.400-in. to 0.500-in. The small wrinkles in the chamber liner overwrap are evidenced at the points of delamination in the overwrap.

### h. Photomicrographs of AGCarb-101 and Carbon/Phenolic Back-Up

Small sections of the throat and throat back-up were removed at a 45-degree angle for observation of the char structure. The source of the specimens is shown on Figure No. 144. The specimens were impregnated with epoxy, cured, and polished. They were observed at 500X magnification. Figure No. 145 is a photomicrograph of the throat back-up graphite phenolic, which is Specimen No. 3. Polarized light was used to ascertain if there was any pyrolytic graphite deposition in the char indicating exposure to temperatures in excess of 2000°F. There was no apparent deposition in the throat back-up char. The dark irregular shapes are ends of the fibers. The dark area extending at a 45-degree angle across the photograph is a separation in the char structure. The light areas are reflected light emitting from anisotropic material, other than pyrolytic graphite, because these areas do not have the characteristic cone shape shown on Figure No. 146. Pyrolytic graphite deposition on both sides of a separation in the throat material, AGCarb-101, is shown. The section was made at location No. 2 shown on Figure No. 144. The graphite fibers, which are the dark areas, were cut at an angle and appear to be elongated. The deposition thickness is approximately 0.00034-in. on the left and 0.00070-in. on the right side.

Figure No. 147 shows a pyrolytic graphite deposition thickness of 0.0007-in. from Specimen No. 2. A small section of the liner from LF<sub>2</sub> chamber S/N 003, P/N 1131377-7, also was prepared for observation at 5000X magnification. Figure No. 148 illustrates a typical area and separation. There was no pyrolytic deposition observable in the area examined.

### 3. Density Comparisons

The pre-fire density of the AGCarb-101 from S/N 002 was determined from a ring removed from the aft end of the component. The density varied from 1.20 grams/cc to 1.23 grams/cc. Deposition of pyrolytic carbon during hot tests increased the density of throat insert to 1.24 grams/cc.

The density of the char from the graphite phenolic throat back-up also was determined. The density was slightly higher than that for the flame surface char and approximated the density of charred material prepared at 1500°F in an inert atmosphere. The density was 1.21 to 1.22 grams/cc.<sup>(73)</sup>

(73) Evaluation of Characteristics Affecting Attainment of Optimum Properties of Ablative Plastics, Vol. I, Contract AF 04(611)-10933, AFRPL-TR-68-20, February 1968.



UNCLASSIFIED

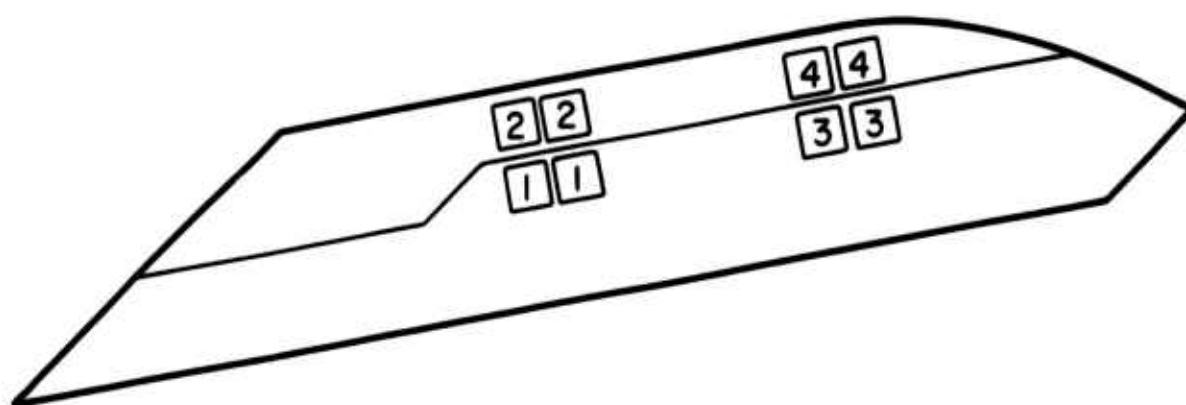
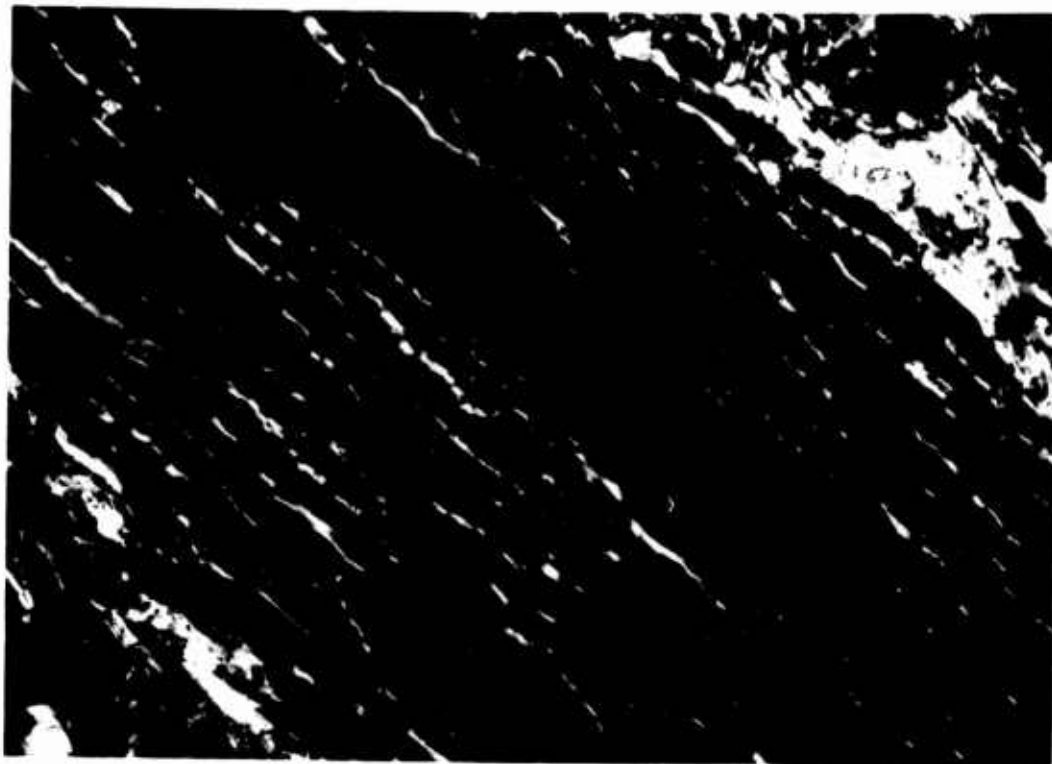


Figure 144. Throat and Throat Back-Up Showing Location of Density Specimens and Photomicrograph Specimens

UNCLASSIFIED

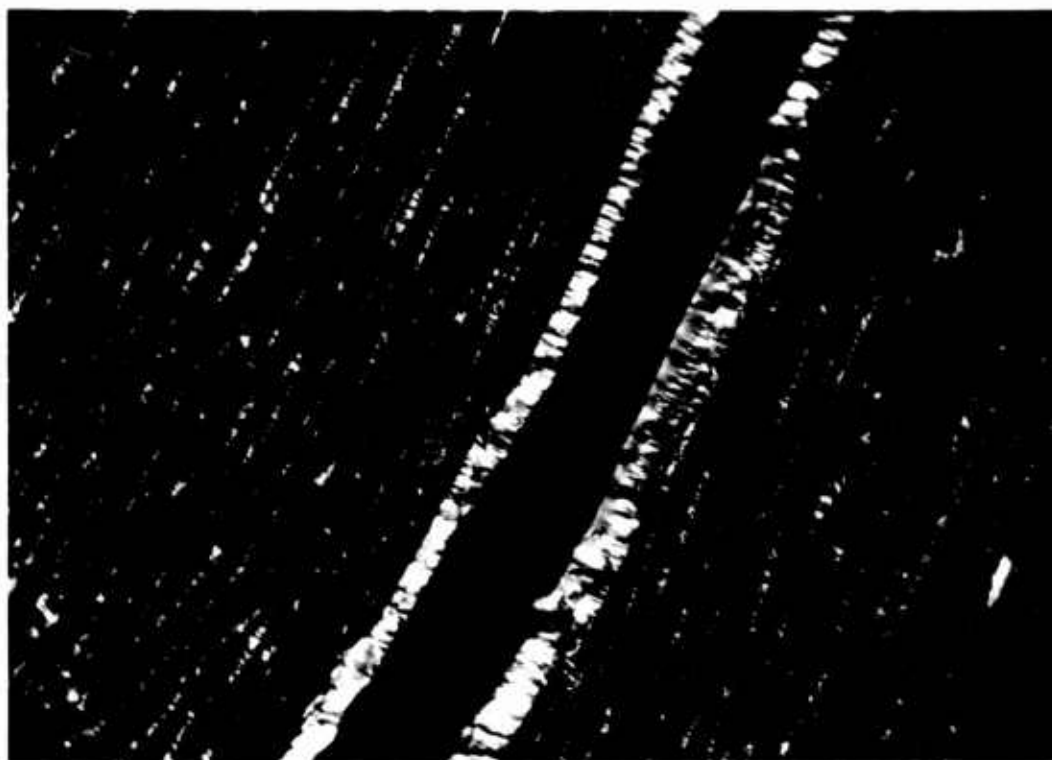
**UNCLASSIFIED**



**Figure 145. Photomicrograph of Throat Back-Up Char Structure Showing Separation**

**UNCLASSIFIED**

UNCLASSIFIED



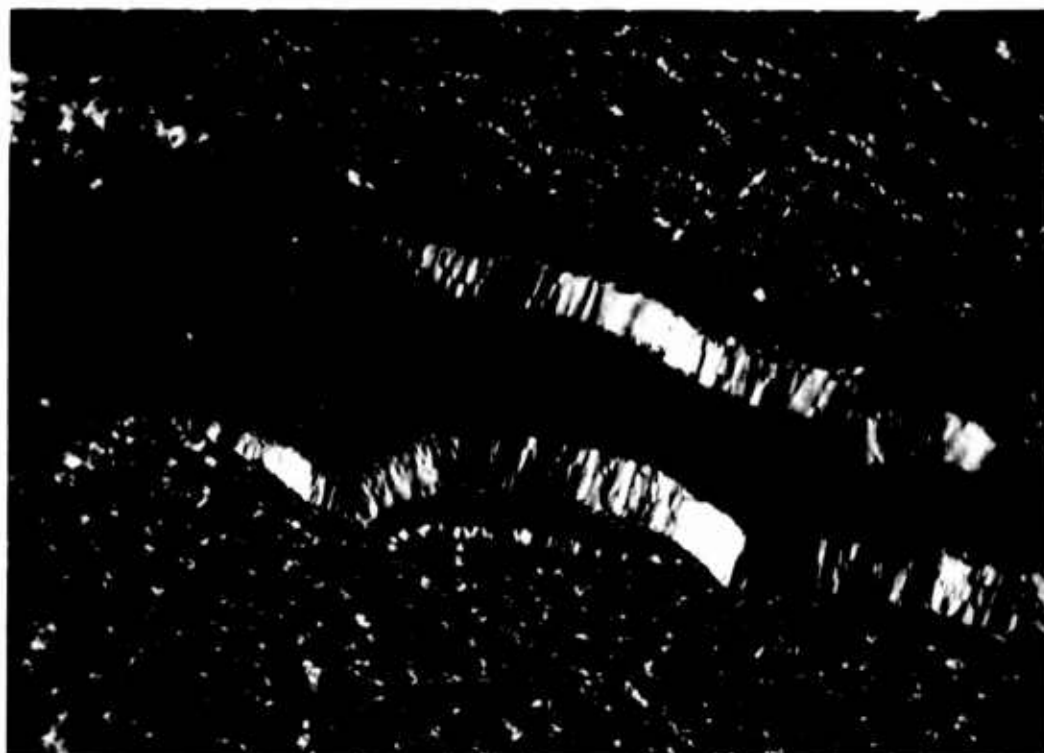
Pyrolytic Deposition Thickness:

Left Hand Layer = .00034"  
Right Hand Layer = .00070"

Figure 146. Photomicrograph of Throat AGCarb-101 Showing Pyrolytic Deposition in a Separation

UNCLASSIFIED

UNCLASSIFIED



Pyrolytic Deposition Thickness:

Left Hand Layer = .00066"  
Right Hand Layer = .00070"

Figure 147. Photomicrograph of Throat Showing Pyrolytic Deposition  
in a Separated Area

UNCLASSIFIED

**UNCLASSIFIED**

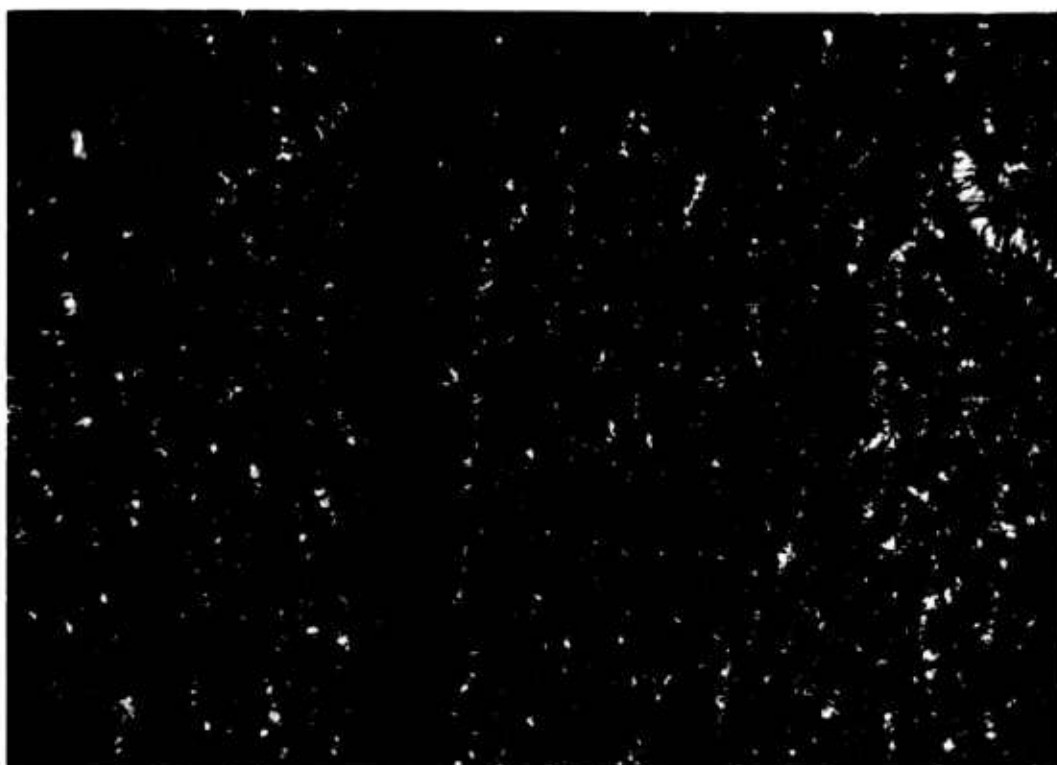


**Figure 148. Photomicrograph of AGCarb-101 Throat of Chamber S/N 003  
Showing Separation**

**UNCLASSIFIED**

## UNCLASSIFIED

### 4. Regression and Char Profile

A full-scale cross-section drawing was made from regression and char measurements at 90-degrees. Figure No. 149 is a reduced scale copy of this drawing. The regression profile was traced from the 90-degree cross-section measurements. The char depth was determined by measuring Barcol hardness. The char interface was established as the point where any hardness reading could be obtained. Completely charred material had 0 hardness on the Barcol Impressor scale. Partially-degraded carbon or silica phenolic had some hardness on the Barcol scale; therefore, the char line includes only the completely charred material.

The char thickness was rather uniform, as shown on the outline of Figure No. 149. The char depths indicate the chamber section was over-designed and the wall thickness could be reduced by approximately 30%. The graphite phenolic in the nozzle section, which is closer to minimum thickness than the chamber section, was charred to its interface with the silica phenolic insulation.

### 5. Decomposition Gas Effects

The decomposition gases created as the ablative material reaches 500°F or above must pass through the chamber wall into the gas stream at some location. The composition of the gases are water vapor oxides of carbon and hydrocarbons of various molecular weights. One of the hydrocarbon constituents is methane, which is cracked at temperatures ranging from 2000°F to 5000°F resulting in pyrolytic graphite being deposited on the surrounding material. Figure No. 147 shows a thickness of 0.0007-in. pyrolytic deposition in the AGCarb throat liner insert. This type of deposition was found throughout the wall of the AGCarb insert. Long-duration firings increase the amount of pyrolytic deposition because the total volume of methane passing through a pore increases with firing duration until the pore is restricted or filled.

Conversely, H<sub>2</sub>O also passes through the char layer and/or the AGCarb-101 insert. The H<sub>2</sub>O reacts with the carbon to produce CO or CO<sub>2</sub> resulting in carbon removal. The results of this phenomenon are shown on Figure No. 141. There are corroded areas at the material interface in the nozzle produced by oxidation. The holes were not observed until just prior to the last firing cycle. This indicates that a large volume of gases was venting through these holes causing them to erode and become larger during the last test. During earlier firings, the upstream gas escape paths were open. In other firings<sup>(74)</sup> holes have been formed in the liner materials. Although the pattern is random, it tends to cover the entire surface.

---

(74) Ablative Materials Evaluation in Fluorinated Oxidizer Environment,  
Contract AF 04(611)-9366, AFRPL-TR-65-138, 7 September 1965.



UNCLASSIFIED

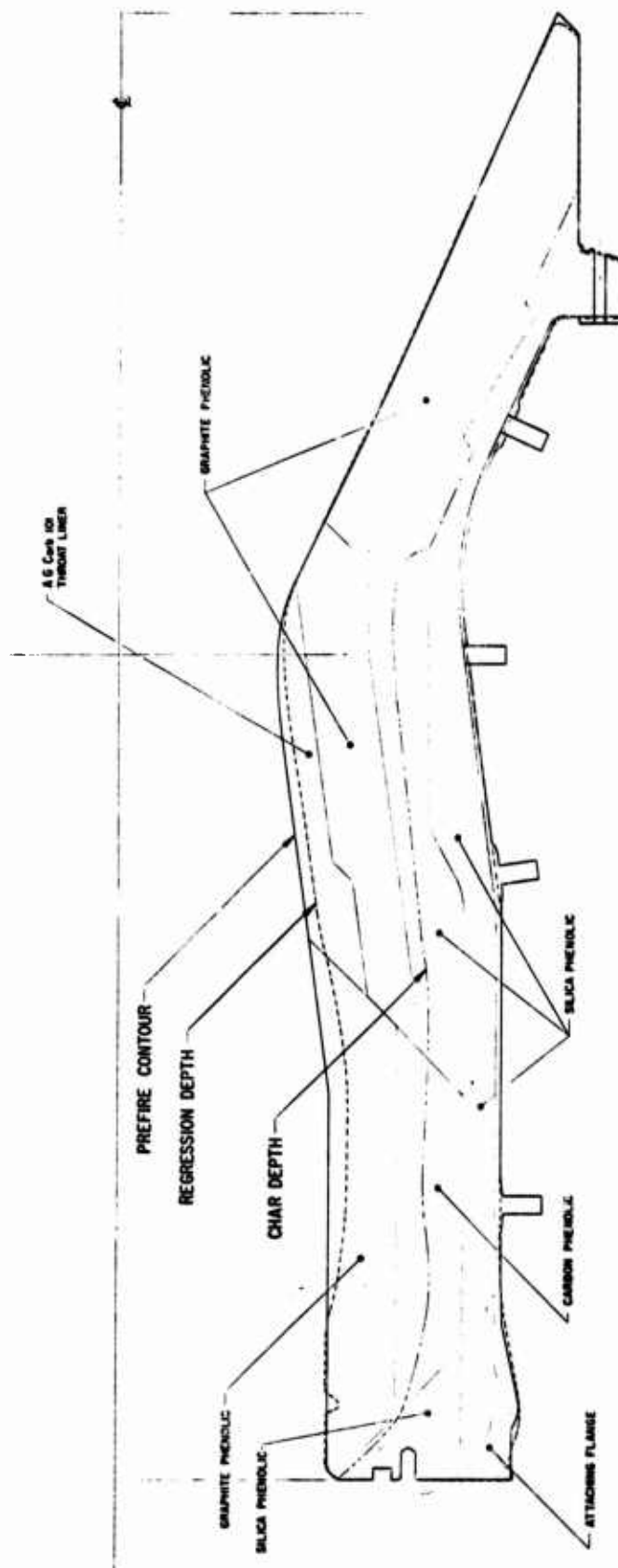


Figure 149. Regression and Char Profile for Chamber S/N 002 Taken at the 90-Degree Cross-Section

UNCLASSIFIED

UNCLASSIFIED

## 6. Performance of Materials

The flame surface materials used were graphite phenolic and a fibrous graphite composite, designated AGCarb-101. The throat material, AGCarb-101, was backed up by a graphite phenolic. The graphite phenolic in the chamber had a carbon phenolic overwrap. Silica phenolic was used as the overwrap for the full length of the chamber.

The test results indicate that the graphite or carbon phenolic/silica phenolic interface could have been closer to the flame surface in all locations. A practical upper temperature limit for silica phenolic is 3000°F.

Two types of graphite phenolic were used, FM 5064 in the chamber and WB 8207 in the exit cone and throat back-up. Both materials performed very well and could be used interchangeably. The WB 8207 was particularly characterized by the lack of delaminations while a few minor delaminations existed in the FM 5064. There were no anomalies observed in the performance of any of the back-up materials. The delaminations, which were observed after sectioning, are characteristic of post-fired ablative materials.

The AGCarb-101 used in the throat was lower density than that of the original chamber (Figure No. 21); however, it performed well. The high regression at 195-degrees did not prevent the attainment of the full 600 sec duration for the chamber. The fabrication technique using cut patterns in a female mold prevented wrinkles, which are potential areas of failure and high regression; however, delamination occurred. Autoclave pressure was used for debulking and curing. A 1000 psi hydroclave pressure would provide sufficient debulk to make the AGCarb-101 precursor density equivalent to a tape/wrap hydroclave process component. Wrinkles would be prevented by applying debulk and cure pressure to the inside diameter of the component.

The regression rate in streaked areas for the AGCarb-101 and graphite phenolic materials was higher than expected. The streaking produced non-uniform and high regression in localized areas. The regression next to the injector is attributed to the oxidizing molecules impinging upon the graphite chamber wall.

Based upon visual and microscopic evaluation, the material in the non-streaked areas was identical to the material which streaked. Non-uniformity in the materials, great enough to produce the large measured difference in regression, is inconceivable. If oxidizing specie in both propellants could be kept from impinging upon the chamber walls, little or no regression of the carbonaceous liner materials would be expected.

The pyrolytic deposition in the AGCarb-101 indicates that means for providing decomposition paths through the liner could be required in those liner materials having low permeability. Higher density AGCarb-101 would have resulted in a less permeable throat material.

UNCLASSIFIED

**UNCLASSIFIED**

**D. CONCLUSIONS**

All of the materials performed well. The thrust chamber performance indicates that the materials and the processes used for fabrication are satisfactory for production hardware. There is need for further improvement in the injector to reduce local streaking.

**UNCLASSIFIED**

**UNCLASSIFIED**

**APPENDIX VIII**

**HIPERKINETIC NOZZLE DESIGN,  $\text{LF}_2/\text{N}_2\text{H}_4$  BLEND**

**Page 315**

**UNCLASSIFIED**

# UNCLASSIFIED

## APPENDIX VIII

### HIPERKINETIC NOZZLE DESIGN, $LF_2/N_2H_4$ BLEND

#### A. SUMMARY

This appendix presents the results of an analytical study to determine the potential performance improvement obtainable by recontouring the  $LF_2/N_2H_4$  Blend Program nozzle in order to reduce the effects of finite reaction rates. Prior to this study, the nozzle configuration had a length of 49.5-in. and an area ratio of 33.5:1. For this study, the design constraint was to limit the nozzle length to 51.9-in.

The optimum high performing kinetic (hiperkinetic) nozzle design was determined by minimizing the combined performance effects of exit area ratio, curvature-divergence, boundary layer, and finite reaction rates. The best hiperkinetic nozzle was found to be a composite of two Rao nozzles. The first nozzle, which is used for the initial expansion ( $1 < \epsilon < 3$ ), is designed to reduce the kinetic loss. The second nozzle, which is attached to the first by a short transition radius, is designed to complete the expansion with a minimum divergence loss.

For the design constraints, two nozzles were designed and their performance determined. One nozzle was a conventional Rao optimum contour used to illustrate the performance improvement as a result of the increased length and area ratio, while the other was a hiperkinetic contour. The performance improvement of the two nozzles considered over the current  $\epsilon = 33.5$  design follows:

Nozzle Contour:	Rao Optimum	Hiperkinetic
Area Ratio:	36.2	36.2
Length (inches):	51.9	51.9
$I_{sp}$ Gain (%):	0.2	1.1

#### B. TECHNICAL DISCUSSION

##### 1. Method of Approach

High energy propellant systems, such as  $LF_2/N_2H_4$  blend, characteristically have high kinetic performance losses on the order of 4 to 8% of  $I_{sp}$ . Since the kinetic performance loss is based on rate phenomena, both the chemical reaction rates and the nozzle residence time will affect it. Nozzle residence time is the measure of the rate of gas expansion and thus is directly a function of the rate of change of area ratio with respect to axial length,  $\frac{d\epsilon}{dz}$ . Therefore, as the nozzle  $\frac{d\epsilon}{dz}$  is decreased, the residence time will increase and the kinetic performance loss will be lowered. However, a change

## UNCLASSIFIED

in  $\frac{dc}{dz}$  will also have an impact on other performance losses within a given set of design constraints. For example, with a fixed nozzle length, a decrease in  $\frac{dc}{dz}$  will result in a lower exit area ratio thus reducing the theoretically available performance. For a nozzle with fixed length and area ratio, an initial decrease in  $\frac{dc}{dz}$  will have to be accompanied by an increased  $\frac{dc}{dz}$  near the exit which will increase the nozzle curvature loss. Similarly, for a nozzle with fixed area ratio, a decrease in  $\frac{dc}{dz}$  will result in an increase in total nozzle length which will increase the boundary layer performance loss.

As a result of the interrelationship of nozzle contour, length, and expansion ratio, an optimum nozzle design can be found by minimizing the combined effects of exit area ratio, curvature-divergence, boundary layer and finite reaction rates. The effects of expansion ratio can be considered by utilizing Aerojet computer program No. 166. The curvature-divergence and boundary layer performance losses are calculated with computer programs 10003 and E25202, respectively. The kinetic performance loss is calculated by a sudden freezing procedure.<sup>(75)</sup>

### a. Potential Performance Improvement

The results of a kinetic analysis for the  $LF_2/N_2H_4$  blend propellant system at a chamber pressure of 100 psia and a mixture ratio of 1.91 are presented in Figure No. 150. This figure relates the effects of nozzle contour to the freezing parameter B and the nozzle pressure ratio. The regions of equilibrium and frozen flow are identified based on the results of the Rocketdyne F2-H2 analysis<sup>(76)</sup>. Note from Figure No. 150 that as the nozzle divergence wall angle is reduced, the freezing point is shifted to a higher pressure ratio or higher area ratio. This effect is, of course, expected because a reduction in the nozzle divergence angle results in a reduction in  $\frac{dc}{dz}$ . The effect of the freezing point location on performance is given in Figure No. 151. As the freezing pressure ratio increases, the kinetic performance loss decreases. Figure No. 151 also presents the one-dimensional relationship between the nozzle pressure ratio and expansion ratio. Returning for a moment to Figure No. 150, note that the current  $c = 33.5$  Rao optimum nozzle contour (dashed line) freezes at a  $P_c/P_s = 5.6$ , while a nozzle with a 15-degree expansion angle freezes at a  $P_c/P_s = 10.0$ . From Figure No. 151, this corresponds to a performance loss of approximately 4.1% and 2.6%, respectively. Thus, a 1.5% reduction in the kinetic performance loss could be realized simply by utilizing a 15-degree conical nozzle in place of the Rao optimum contour.

(75) Pieper, J. L., "Investigation of Finite Rate Performance Losses for Fluorine Based Propellants," TCER 9642:0078, Aerojet-General Corp., dated 14 August 1967.

(76) Ibid.



UNCLASSIFIED

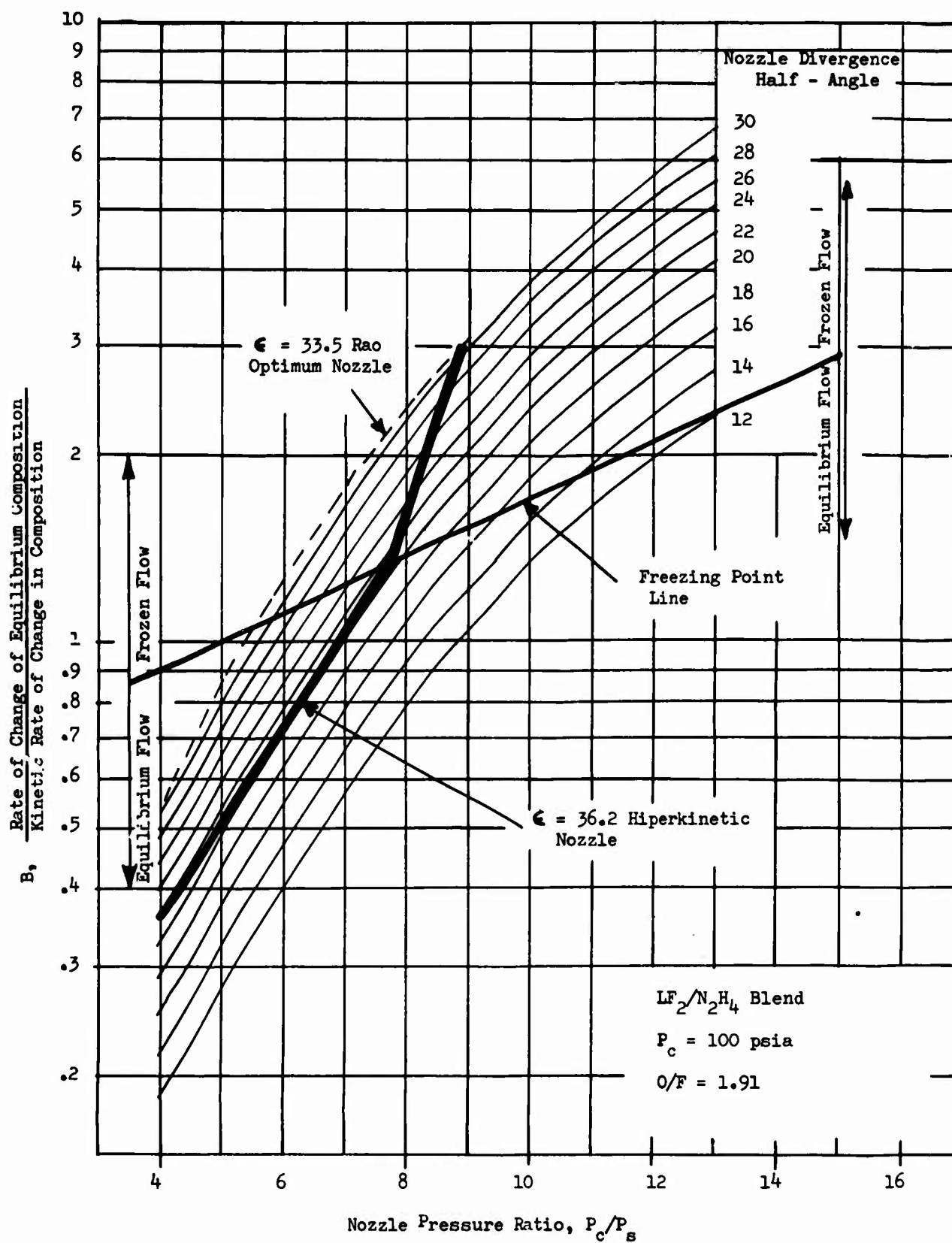


Figure 150. Effect of Nozzle Contour on the Freezing Point Location

UNCLASSIFIED

UNCLASSIFIED

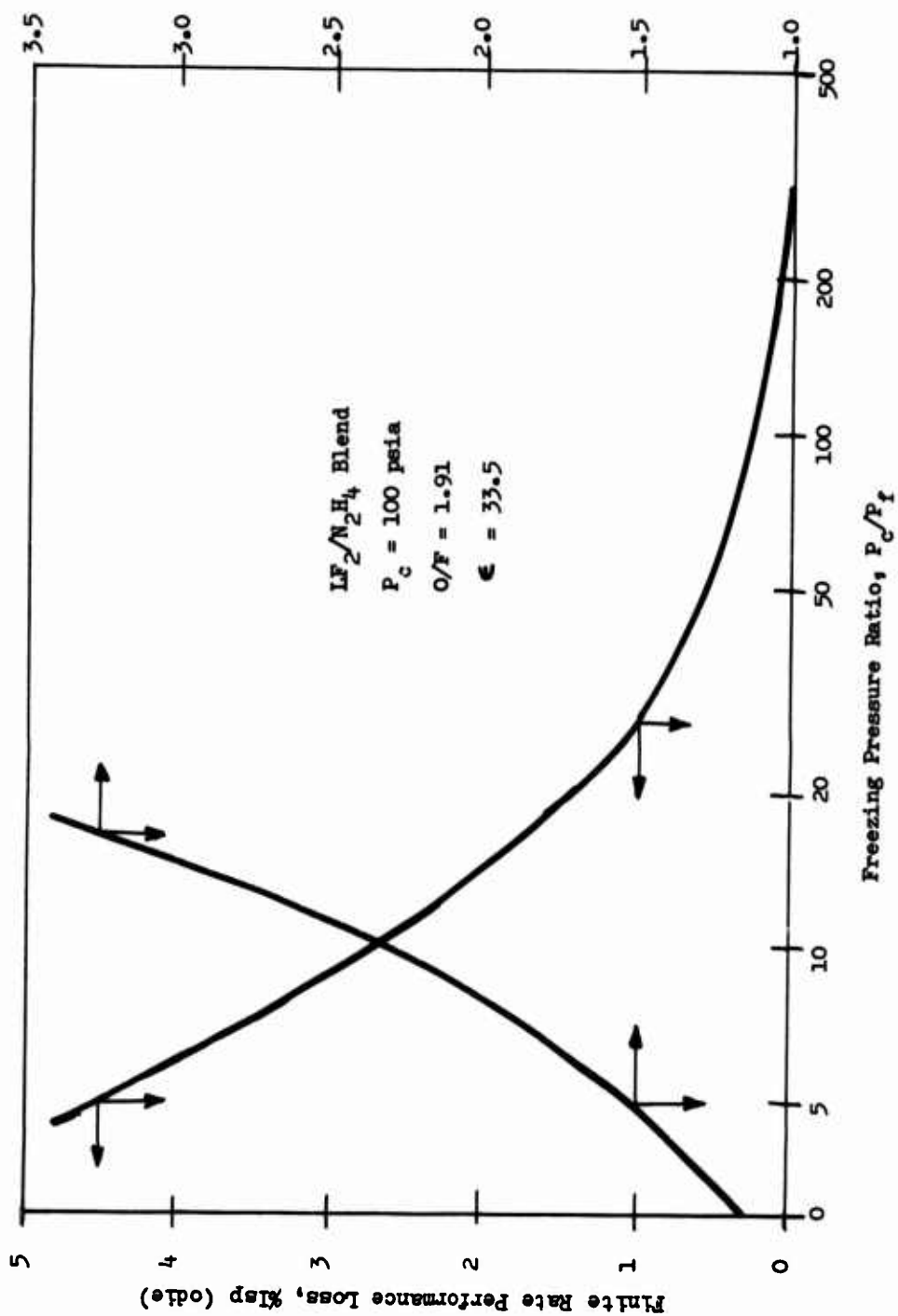


Figure 151. Effect of the Freezing Point Location on the Kinetic Performance Loss

UNCLASSIFIED

## UNCLASSIFIED

Of course, the net change in delivered performance would be a function of the design constraints and the effect of the nozzle contour change on the other performance losses.

### b. Method of Contour Adjustment

Considering only the kinetic performance loss, the nozzle contour which would provide the maximum  $\frac{dc}{dz}$  while still maintaining equilibrium flow would be the contour obtained by following the line separating the equilibrium and frozen flow regions in Figure No. 150. That is, at a pressure ratio of 5.8 ( $\epsilon = 1.65$ ) the nozzle wall angle  $\theta$  should be 30-degrees, at  $P_c/P_s = 8$  ( $\epsilon = 2.0$ )  $\theta = 20$ -degrees, at  $P_c/P_s = 10$  ( $\epsilon = 2.3$ )  $\theta = 15$ -degrees, etc. Such a contour, however, could produce shocks and thus significantly affect the expansion process and the reliability of the system. However, this does suggest that a high performance kinetic (hiperkinetic) nozzle should have a decreasing expansion rate during the initial expansion ( $1 < \epsilon < 3$ ) and then an increased expansion rate during the intermediate expansion, and finally a decreased expansion rate at the nozzle exit. A nozzle of this type is really a composite of two Rao nozzles. The first nozzle which is used for the initial expansion is designed to reduce the kinetic loss. The second nozzle, which is attached to the first by a short transition radius, is designed to complete the expansion with a minimum divergence loss. This procedure was utilized to obtain the hiperkinetic nozzle contour described in the following sections.

## 2. Analytical Results

### a. Design Constraints

The following design constraints were given for the design of a hiperkinetic nozzle for use on the  $LF_2/N_2H_4$  blend program:

Maximum Nozzle Axial Length (Throat to Exit)	= 51.9-in.
Maximum Exit Diameter	= 44.5-in.
Throat Diameter	= 7.135-in.

For these conditions, it appears that the nozzle length is the limiting constraint in determining the optimum nozzle contour. That is, a performance improvement could be realized by increasing the nozzle length beyond 51.9-in. while maintaining the other design constraints.

### b. Hiperkinetic Nozzle Contour

The first step in designing the hiperkinetic nozzle was to obtain the Rao optimum contour for the design constraints given above. This contour is required to provide a basis for obtaining the second expansion

UNCLASSIFIED

## UNCLASSIFIED

section of the hiperkinetic nozzle and estimating the performance improvement of the hiperkinetic nozzle. Next, a set of initial expansion contours with varying degrees of expansion rates was designed. Then the Rao optimum contour designed earlier was attached to the initial expansion contours by translating it in both a radial and axial direction. An approximate performance analysis which determined the combined performance effects of kinetics, divergence, and area ratio was made for each nozzle, from which the final nozzle contour was selected. A listing of the nozzle coordinates is presented in Table XXI. The hiperkinetic nozzle has an axial length of 51.9-in. and an expansion area ratio of 36.2:1.

### c. Performance Comparison

A performance analysis of the three nozzle configurations has been made in order to determine the performance gain of the hiperkinetic nozzle. The nozzle configurations included in this analysis were: the current  $\epsilon = 33.5$  Rao optimum contour; the  $\epsilon = 36.2$  hiperkinetic contour; and an  $\epsilon = 36.2$  Rao optimum contour. These results are presented in Table XXII. The  $I_{sp}$  (perf. injector) given in Table XXII is found by assuming a 100% energy release efficiency and a uniform propellant mixture ratio distribution. This comparison shows that a gain  $0.8 \text{ lb}_f\text{-sec/lb}_m$  of  $I_{sp}$  (0.2%) resulted from the increase in length and area ratio (33.5 to 36.2). Furthermore, a comparison of the performance of the two  $\epsilon = 36.2$  nozzles shows a  $3.5 \text{ lb}_f\text{-sec/lb}_m$  (0.85%) performance increase for the hiperkinetic nozzle contour over that of the conventional Rao optimum contour. As a result, a total performance increase of approximately 1.1% has been achieved by lengthening and recontouring the  $\text{LF}_2/\text{N}_2\text{H}_4$  blend nozzle.

### d. Effect of Design Constraints

On the basis of these results, an investigation was made to determine the approximate performance increase for an optimum hiperkinetic nozzle with an expansion area ratio of 43.6:1 with no length restriction. The results indicate that the optimum nozzle length on both cases would be 61.4 inches. The Rao optimum nozzle contour with  $\epsilon = 43.6$  is estimated to be  $4.1 \text{ lb}_f/\text{lb}_m$  (1%) higher performing than the  $\epsilon = 33.5$  Rao optimum nozzle. The  $\epsilon = 43.6$  hiperkinetic nozzle is estimated to be  $7.6 \text{ lb}_f\text{-sec/lb}_m$  or 1.85% higher performing than the  $\epsilon = 33.5$  nozzle.

UNCLASSIFIED

UNCLASSIFIED

TABLE XXI

HIPERKINETIC NOZZLE COORDINATES

<u>Axial Length</u> <u>in.</u>	<u>Radius</u> <u>in.</u>	<u>Angle</u> <u>Degrees</u>
0.	3.568	0.
0.012	3.568	1.000
0.025	3.568	2.000
0.037	3.569	3.000
0.050	3.570	4.000
0.062	3.571	5.000
0.075	3.572	6.000
0.087	3.573	7.000
0.099	3.575	8.000
0.112	3.577	9.000
0.128	3.579	10.000
0.136	3.581	11.000
0.148	3.584	12.000
0.161	3.586	13.000
0.173	3.589	14.000
0.185	3.592	15.000
0.197	3.596	16.000
0.209	3.599	17.000
0.221	3.603	18.000
0.232	3.607	19.000
0.244	3.611	20.000
0.256	3.615	21.000
0.267	3.620	22.000
0.267	3.620	22.002
0.335	3.647	22.026
0.470	3.702	22.062
0.605	3.757	22.071
0.741	3.812	22.075
0.877	3.867	22.073
1.014	3.922	22.054
1.150	3.978	22.020
1.288	4.033	21.981
1.425	4.089	21.934
1.563	4.144	21.867
1.701	4.199	21.797
1.840	4.255	21.721
1.979	4.310	21.626
2.119	4.365	21.528
2.259	4.420	21.423
2.399	4.475	21.304
2.540	4.530	21.183
2.682	4.585	21.052

UNCLASSIFIED

UNCLASSIFIED

TABLE XXI (cont.)

HIPERKINETIC NOZZLE COORDINATES

<u>Axial Length</u> <u>in.</u>	<u>Radius</u> <u>in.</u>	<u>Angle</u> <u>Degrees</u>
2.824	4.639	20.914
2.966	4.693	20.771
3.109	4.748	20.619
3.253	4.801	20.465
3.398	4.855	20.302
3.543	4.908	20.136
3.688	4.962	19.964
3.690	4.963	20.000
3.749	4.985	21.000
3.807	5.008	22.000
3.864	5.032	23.000
3.921	5.056	24.000
3.978	5.082	25.000
4.034	5.109	26.000
4.090	5.137	27.000
4.145	5.166	28.000
4.200	5.195	29.000
4.254	5.226	30.000
4.308	5.258	31.000
4.334	5.274	31.491
4.956	5.655	31.577
6.175	6.401	31.227
7.420	7.145	30.464
8.703	7.886	29.500
10.028	8.620	28.442
11.401	9.347	27.337
12.824	10.065	26.222
14.297	10.773	25.103
15.827	11.471	23.977
17.413	12.158	22.899
19.056	12.833	21.835
20.758	13.497	20.815
22.519	14.149	19.822
24.341	14.788	18.860
26.221	15.413	17.939
28.163	16.025	17.035
30.166	16.622	16.176
32.231	17.204	15.338
34.359	17.771	14.529
36.551	18.323	13.748
38.804	18.858	12.988
41.122	19.377	12.260

UNCLASSIFIED



UNCLASSIFIED

TABLE XXI (cont.)

HIPERKINETIC NOZZLE COORDINATES

<u>Axial Length</u> <u>in.</u>	<u>Radius</u> <u>in.</u>	<u>Angle</u> <u>Degrees</u>
43.504	19.878	11.546
45.955	20.362	10.862
48.449	20.829	10.200
51.900	21.450	9.800

UNCLASSIFIED

# CONFIDENTIAL

TABLE XXII

COMPARISON OF THE  $\text{LF}_2/\text{N}_2\text{H}_4$  BLEND PROGRAM NOZZLE DESIGN

$$P_c = 100 \text{ psia } O/F = 1.91$$

Nozzle Control	<u>Rao Optimum</u>	<u>Rao Optimum</u>	<u>Hiperkinetic</u>
Area Ratio	33.5	36.2	36.2
Nozzle Length	49.503	51.900	51.900
$I_{sp}$ (ODIE)	408.7	410.0	410.0
C-D Loss, sec	5.0	5.2	5.3
B.L. Loss, sec	7.2	7.4	7.4
Kinetic Loss, sec	16.8	16.9	13.3
$I_{sp}$ (100% ERE)	379.7	380.5	384.0

CONFIDENTIAL

# CONFIDENTIAL

## BIBLIOGRAPHY

1. Beranek, L. L., Acoustics, McGraw-Hill Book Co., Inc., New York, 1954
2. Crocco, L. and Cheng, S. I., Theory of Combustion Instability in Liquid Propellant Rocket Motors, AGARDograph No. 8, Butterworth's Scientific Publications, Ltd., London, 1956
3. Mechel, F., et al, Research on Sound Propagation in Sound Absorbent Ducts with Superimposed Air Streams, Report AMRL-TDR-62-140, Aerospace Medical Division, Wright-Patterson Air Force Base, Ohio, December 1962
4. Morse, P. M., Vibration and Sound, second edition, McGraw-Hill Book Co., Inc., New York, 1948
5. Pieper, J. L. and Anderson, G. E., LF<sub>2</sub>/N<sub>2</sub>H<sub>4</sub> Blend Optimum Nozzle Design Study, Aerojet-General Report TCER-9642:0079, 5 October 1967
6. Rayleigh, J. W. S., The Theory of Sound, Vol. II, Dover Publications
7. Reardon, F. H., An Investigation of Transverse Mode Combustion Instabilities in Liquid Propellant Rocket Motors, Princeton University Aeronautical Engineering Report No. 550, 1 June 1963
8. Smith, A. J., Jr. and Reardon, F. H., The Sensitive Time Lag Theory and its Application to Liquid Rocket Combustion Instability Problems, Vol. I, AFRPL-TR-67-314, March 1968
9. Weiss, R. R. and Klopotek, R. D., Experimental Evaluation of the Titan III Transtage Engine Combustion Stability Characteristics, AFRPL-TR-66-51, 1966
10. Wood, A., Acoustics, Dover Publications
11. A Study of Suppression of Combustion Oscillations with Mechanical Damping Devices, Pratt & Whitney PWA-FR-2596, 20 November 1967
12. Ablative Materials Evaluation in Fluorinated Oxidizer Environment, Contract AF 04(611)-9366, Report AFRPL-TR-65-138, September 1965
13. Axisymmetric Reacting Gas Nonequilibrium Performance Program, Contract NAS 9-4358, TRW Report 02874-6004-R000, 8 March 1967
14. Chemical Reaction Between Plastic Composite Materials and Propellant Exhaust Products, Aeronautical Systems Division, Atlantic Research Corp., Technical Documentary Report No. ASD-TDR-63-737, August 1963
15. Coatings for Regenerative Engines, Second Monthly Research Contract Status Report, NAS 3-7955, 15 September 1966

CONFIDENTIAL

(This page is Unclassified)

# UNCLASSIFIED

16. Evaluation of Characteristics Affecting Attainment of Optimum Properties of Ablative Plastics, Vol. I, Contract AF 04(611)-10933, Report AFRPL-TR-68-20, February 1968
17. Evaluation of Characteristics Affecting Attainment of Optimum Properties of Ablative Plastics, Vol. II, Contract AF 04(611)-10933, Report AFRPL-TR-68-29, February 1968
18. Feasibility of Uncooled Thrust Chamber and Nozzle Designs, Publication C-1432, Aeronutronics Division, Ford Motor Co., 30 October 1961
19. Fluorinated Oxidizer Thrust Chamber Materials Evaluation Program, Phase I, Contract AF 04(611)-10918, Report AFRPL-TR-66-77, 1966
20. Fluorinated Oxidizer Thrust Chamber Materials Evaluation Program, Phase II, Contract AF 04(611)-10918, Report AFRPL-TR-66-322, 1966
21. Performance Evaluation Methods for Liquid Propellant Rocket Thrust Chambers, ICRPG Working Group on Performance Standardization, CPIA Publication No. 132, November 1966
22. Blackman, A. W., "Effect of Nonlinear Losses on the Design of Absorbers for Combustion Instabilities," ARS Journal, November 1960
23. Crocco, L., Grey, J., and Harrje, D. T., "Theory of Liquid Propellant Rocket Instability of its Experimental Verification," ARS Journal, Vol. 30, No. 2, February 1960
24. Crocco, L., Harrje, D. T., and Reardon, F. H., "Transverse Combustion Instability in Liquid Propellant Rocket Motors," ARS Journal, Vol. 32, No. 3, March 1963
25. Ingard, V., "On the Theory and Design of Acoustic Resonators," Journal of the Acoustical Society of America, Vol. 25, No. 6, November 1953
26. Ingard, V. and Labate, S., "Acoustic Circulation Effects and the Nonlinear Impedance of Orifices," Journal of the Acoustical Society of America, Vol. 22, March 1950
27. McAuliffe, C. E., "The Influence of High Speed Air Flow on the Behavior of Acoustical Elements," M. Sc. Thesis, Massachusetts Institute of Technology, 1950
28. Reardon, F. H., Crocco, L., and Harrje, D. T., "Velocity Effects in Transverse Mode Liquid Propellant Rocket Combustion Instability," to be published in AIAA Journal
29. Reardon, F. H., McBride, J. M., and Smith, A. J., "Effect of Injection Distribution on Combustion Stability," AIAA Journal, Vol. 4, No. 3, March 1966

UNCLASSIFIED

UNCLASSIFIED

30. Sirignano, W. A., et al, "Acoustic Liner Studies," ICRPG Third Combustion Conference, Vol. I, 17-21 October 1966
31. Waugh, R. C., et al, "A Mathematical Model for Transverse Mode Instability with Feed System Coupling for Titan IIIM," Presented at the Fifth ICRPG Combustion Conference, 1 October 1968

UNCLASSIFIED

Unclassified

Security Classification

DOCUMENT CONTROL DATA - R&D		
(Security classification of title, body of abstract and indexing annotation must be entered when the overall report is classified)		
1. ORIGINATING ACTIVITY (Corporate author)		2a. REPORT SECURITY CLASSIFICATION
Aerojet-General Corp. Sacramento, Calif.		Confidential
		2b. GROUP
		4
3. REPORT TITLE		
Development and Demonstration of Ablative Thrust Chamber Assemblies Using $LF_2/N_2H_4$ Blend Propellants (U)		
4. DESCRIPTIVE NOTES (Type of report and inclusive dates)		
Final Report 1 September 1966 through 19 August 1968		
5. AUTHOR(S) (Last name, first name, initial)		
Schindler, Robert C. Kiser, Harold V.		
6. REPORT DATE	7a. TOTAL NO. OF PAGES	7b. NO. OF REFS
January 1969	328	76
8a. CONTRACT OR GRANT NO.	9a. ORIGINATOR'S REPORT NUMBER(S)	
F04611-67-C-0003	AGC 9400-14	
a. PROJECT NO.		
c.	9b. OTHER REPORT NO(S) (Any other numbers that may be assigned to this report)	
d.	None	
10. AVAILABILITY/LIMITATION NOTICES		
In addition to security requirements which must be met, this document is subject to special export controls and each transmittal to foreign governments or foreign nationals may be made only with prior approval of AFRPL (RPPR/STINEO) Edwards, California 93523.		
11. SUPPLEMENTARY NOTES		12. SPONSORING MILITARY ACTIVITY
		Air Force Rocket Propulsion Laboratory Research and Technology Division Air Force Systems Command, Edwards, California
13. ABSTRACT		
See next page		

DD FORM 1473

1 JAN 64

Page 329

UNCLASSIFIED

Unclassified

Security Classification



# UNCLASSIFIED

## ABSTRACT

The "Development and Demonstration of Ablative Thrust Chamber Assemblies Using  $\text{LF}_2/\text{N}_2\text{H}_4$  Blend Propellants," Contract F04611-67-C-0003, was a comprehensive exploratory development effort which included the design, fabrication, and testing of injectors, ablative thrust chambers, and a radiation-cooled-divergent nozzle extension. It was conducted in three phases over a 25 month period. The design study was accomplished in Phase I while Phases II and III consisted of evaluations of thrust chamber assemblies which utilized non-damped and acoustically-damped injectors, respectively.

A single injector body configuration was used through the program. It incorporated triplet-type elements in a flat-faced, nickel body without baffles. Injector durability was demonstrated with a single unit which accumulated over 846 sec of testing. It was determined that maximum performance could be achieved with stable operation by using acoustic resonators built into the chamber wall.

Two different composite ablative chamber configurations were evaluated. One had a precharred fibrous graphite throat insert with uncharred ablative materials both upstream and downstream of the throat. The other had a precharred fibrous graphite liner which extended from the injector to a station downstream of the throat. The latter configuration failed during testing as a result of local buckling of the liner. A throat insert design unit was tested six times at vacuum conditions for a total duration of 605 sec. An acoustic resonator was incorporated in a second throat insert chamber configuration and tested three times for a duration of 160 sec.

A radiation-cooled columbium nozzle was tested at vacuum conditions for an accumulated duration of 233 sec. This nozzle was used to evaluate three different thermal barrier coatings.

The forty tests conducted in the program provided verification of the analytical methods applied in the chamber design, supplemented existing technology and provided previously unavailable materials information. This demonstration of the two ablative chamber designs provided ample evidence that adequate technology is available to develop space engines using an interhalogen oxidizer.

UNCLASSIFIED

Unclassified  
Security Classification

14. KEY WORDS	LINK A		LINK B		LINK C	
	ROLE	WT	ROLE	WT	ROLE	WT
INJECTOR DEVELOPMENT ABLATIVE CHAMBER DEVELOPMENT WITH AND WITHOUT ACOUSTIC RESONATORS PERFORMANCE, COMPATIBILITY AND STABILITY EVALUATION HIPERKINETIC NOZZLE DESIGN						

## INSTRUCTIONS

1. **ORIGINATING ACTIVITY:** Enter the name and address of the contractor, subcontractor, grantee, Department of Defense activity or other organization (corporate author) issuing the report.
- 2a. **REPORT SECURITY CLASSIFICATION:** Enter the overall security classification of the report. Indicate whether "Restricted Data" is included. Marking is to be in accordance with appropriate security regulations.
- 2b. **GROUP:** Automatic downgrading is specified in DoD Directive 5200.10 and Armed Forces Industrial Manual. Enter the group number. Also, when applicable, show that optional markings have been used for Group 3 and Group 4 as authorized.
3. **REPORT TITLE:** Enter the complete report title in all capital letters. Titles in all cases should be unclassified. If a meaningful title cannot be selected without classification, show title classification in all capitals in parentheses immediately following the title.
4. **DESCRIPTIVE NOTES:** If appropriate, enter the type of report, e.g., interim, progress, summary, annual, or final. Give the inclusive dates when a specific reporting period is covered.
5. **AUTHOR(S):** Enter the name(s) of author(s) as shown on or in the report. Enter last name, first name, middle initial. If military, show rank and branch of service. The name of the principal author is an absolute minimum requirement.
6. **REPORT DATE:** Enter the date of the report as day, month, year; or month, year. If more than one date appears on the report, use date of publication.
- 7a. **TOTAL NUMBER OF PAGES:** The total page count should follow normal pagination procedures, i.e., enter the number of pages containing information.
- 7b. **NUMBER OF REFERENCES:** Enter the total number of references cited in the report.
- 8a. **CONTRACT OR GRANT NUMBER:** If appropriate, enter the applicable number of the contract or grant under which the report was written.
- 8b, 8c, & 8d. **PROJECT NUMBER:** Enter the appropriate military department identification, such as project number, subproject number, system numbers, task number, etc.
- 9a. **ORIGINATOR'S REPORT NUMBER(S):** Enter the official report number by which the document will be identified and controlled by the originating activity. This number must be unique to this report.
- 9b. **OTHER REPORT NUMBER(S):** If the report has been assigned any other report numbers (either by the originator or by the sponsor), also enter this number(s).
10. **AVAILABILITY/LIMITATION NOTICES:** Enter any limitations on further dissemination of the report, other than those

imposed by security classification, using standard statements such as:

- (1) "Qualified requesters may obtain copies of this report from DDC."
- (2) "Foreign announcement and dissemination of this report by DDC is not authorized."
- (3) "U. S. Government agencies may obtain copies of this report directly from DDC. Other qualified DDC users shall request through \_\_\_\_\_."
- (4) "U. S. military agencies may obtain copies of this report directly from DDC. Other qualified users shall request through \_\_\_\_\_."
- (5) "All distribution of this report is controlled. Qualified DDC users shall request through \_\_\_\_\_."

If the report has been furnished to the Office of Technical Services, Department of Commerce, for sale to the public, indicate this fact and enter the price, if known.

11. **SUPPLEMENTARY NOTES:** Use for additional explanatory notes.

12. **SPONSORING MILITARY ACTIVITY:** Enter the name of the departmental project office or laboratory sponsoring (paying for) the research and development. Include address.

13. **ABSTRACT:** Enter an abstract giving a brief and factual summary of the document indicative of the report, even though it may also appear elsewhere in the body of the technical report. If additional space is required, a continuation sheet shall be attached.

It is highly desirable that the abstract of classified reports be unclassified. Each paragraph of the abstract shall end with an indication of the military security classification of the information in the paragraph, represented as (TS), (S), (C), or (U).

There is no limitation on the length of the abstract. However, the suggested length is from 150 to 225 words.

14. **KEY WORDS:** Key words are technically meaningful terms or short phrases that characterize a report and may be used as index entries for cataloging the report. Key words must be selected so that no security classification is required. Identifiers, such as equipment model designation, trade name, military project code name, geographic location, may be used as key words but will be followed by an indication of technical context. The assignment of links, rules, and weights is optional.

GPO 886-561

Unclassified  
Security Classification

UNCLASSIFIED